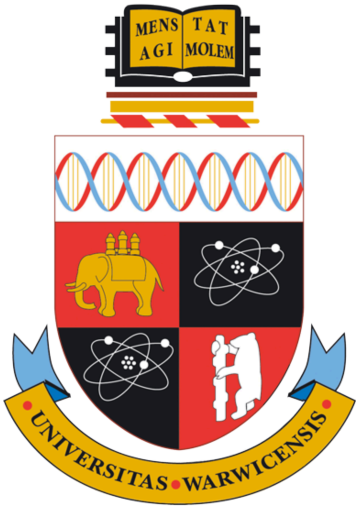

Quantifying biased agonism of adenosine and calcitonin-like receptors

by

Ian James Winfield

A thesis submitted to the University of Warwick

for the degree of

Doctor of Philosophy

Medical Research Council: Doctoral Training Center

September 2017

‘Per Ardua Ad Astra’

Contents

List of Figures

List of Tables

Abbreviations and Acronyms

A_1R	Adenosine A_1 receptor
A_{2A}R	Adenosine A_{2A} receptor
A_{2B}R	Adenosine A_{2B} receptor
A_3R	Adenosine A_3 receptor
AC	Adenylate cyclase
AM	Adrenomedullin
AM2	Adrenomedullin 2
AMY	Amylin
AR	Adenosine receptor
AT_1	Angiotensin II type 1 receptor
ATP	Adenosine triphosphate
BSA	Bovine serum albumin
CAM	Constitutively active mutant
cAMP	Cyclic adenosine monophosphate
CCPA	2-Chloro-N^6-cyclopentyladenosine
CFTR	Cystic fibrosis transmembrane conductance regulator
cGMP	Cyclic guanine monophosphate
CGRP	Calcitonin gene-related peptide
CLR	Calcitonin-like receptor
Cmpd	Compound
CRF	Corticotrophin-releasing factor
CT	Calcitonin
CTC	Cubic ternary complex
CTR	Calcitonin receptor
CVD	Cardiovascular disease
DAG	Diacylglycerol
DMEM	Dulbecco's modified Eagle's medium
DMSO	Dimethyl sulphoxide
DPP-IV	Dipeptidyl peptidase-IV
E. coli	*Escherichia coli*

EC_{50}	Concentration of stimulating agonist at 50% maximal response
ECL	Extracellular loop
E_{max}	Maximal observed response
EPAC	Exchange factor directly activated by cAMP
ER	Endoplasmic reticulum
ERK	Extracellular signal-regulated kinase
ETC	Extended ternary complex
FBS	Fetal bovine serum
GAP	GTPase activating proteins
GDP	Guanosine diphosphate
GEF	Guanine nucleotide exchange factors
GIP	Gastric inhibitory peptide
GIRK	G protein-coupled inwardly-rectifying K^+ channels
GLP-1	Glucagon-like peptide-1
GPCR	G protein-coupled receptor
GTP	Guanosine triphosphate
H8	Helix 8
HBSS	Hank's balanced salt solution
HTT	Mutant huntingtin protein
HUVEC	Human umbilical vein endothelial cell
IBMX	3-isobutyl-1-methylxanthine
$_{i}Ca^{2+}$	Intracellular Ca^{2+}
ICL	Intracellular loop
IP_3	Inositol 1,4,5-triphosphate
JNK	Janus kinase
Ka	Ligand's intrinsic affinity for its receptor
LB	Luria broth
LR	Ligand-receptor
MAPK	Mitogen-activated protein kinase
MAPKK	Mitogen-activated protein kinase kinase
MAPKKK	Mitogen-activated protein kinase kinase kinase
NECA	5'-N-Ethylcarboxamidoadenosine

PBS	Phosphate-buffered saline
PDE	Phosphodiesterase
PEI	Polyethylenimine
PIP_2	Phosphatidylinositol 4,5-bisphosphate
PKA	Protein kinase A
PKB	Protein kinase B
PKC	Protein kinase C
PLC	Phospholipase C
PMA	Phorbol 12-myristate 13-acetate
PTX	Pertussis toxin
R	Inactive receptor
R^*	Active receptor
RAMP	Receptor activity-modifying protein
RGS	Regulator of G protein signalling
RO	Reverse osmotically
RTK	Receptor tyrosine kinase
SD-URA	Synthetic dropout media lacking uracil
SR	Sarcoplasmic reticulum
τ	Ligand's intrinsic efficacy
TM	Transmembrane
TR-FRET	Time-resolved fluorescence energy transfer
TZQ	Triazoloquinazoline
WT	Wild type
YE	Yeast extract

Acknowledgements

This work, and the entirety of my Ph.D, would not have been possible without the help and guidance of several people. Primarily, I would like to extend my gratitude to Dr. Graham Ladds, my supervisor, who has guided and supported me throughout the entirety of the last 4 years, allowing me to grow into a better, more rounded scientist. Every member of Graham's laboratory, past and present, has also helped me, in one way or another. I would especially like to acknowledge: Kerry Barkan and Sarah Routledge, whom I have worked alongside throughout my Ph.D; Matt Harris and Ashley Clark, who have helped with various experiments, and made the lab a fun place to work; Eugenia Frattini, who assisted with A_1R and A_3R investigations, and Sabrina Carvalho, who performed the initial work investigating test $A_{2A}R$ compounds, and is someone who always knows how to make me laugh. Additionally, Professors Chris Reynolds and David Poyner have been instrumental in aiding with my work on the CLR, as well as Heptares therapeutics who kindly helped with the CLR ICL1 investigation. I would also like to extend my thanks to the Department of Pharmacology, University of Cambridge, for allowing me to work there, and who accepted me as one of their own. Finally, I would like to extend my greatest appreciation to the Medical Research Council who have funded my research and thus allowed me to undertake this Ph.D; without their funding I would not have been able to achieve this long held ambition.

Declaration of authorship

I, Ian James Winfield, declare that this thesis, titled: 'Quantifying signalling bias of adenosine and calcitonin-like receptors', and the work presented in it are my own. This thesis is submitted to the University of Warwick in support of my application for the degree of Doctor of Philosophy. It has been composed by myself and has not been submitted in any previous application for any degree. I confirm that:

- The work presented (including data generated and data analysis) was carried out by myself, except the cases outlined below:
    - Generation of CLR ICL1 mutants, which was performed by Heptares therapeutics
    - Quantification of CLR ICL1 mutant cell surface expression data (Figure 5.7, Table 5.3), which was performed by Heptares therapeutics

- Where I have quoted the work of others, the source is always given. With the exception of such quotations, this thesis is entirely my own work.

- Where this thesis is based on work done by myself jointly with others, I have made clear exactly what was done by others, and what I have contributed myself.

Parts of this thesis have been published by myself:

- Knight *et al*, 2016. *J. Med. Chem.* (59):947-964 –Appendix 1
- Weston *et al*, 2016. *J. Biol. Chem.* (42):21925-21944 – Appendix 2

Signed:_____

Dated:_____

Abstract

G protein-coupled receptors (GPCRs) elicit an ability to activate multiple downstream signalling pathways. It is becoming evident that for many GPCRs, agonists are able to activate several of these pathways, each to differing extents; a phenomenon termed pathway bias, or biased agonism.

Here, work is presented quantifying biased agonism for the: adenosine A_1 and A_{2A} receptors, as well as the calcitonin-like receptor (CLR). For the adenosine receptors, novel selective, and non-selective, agonists are identified and characterised. Further, the extent of biased agonism is determined for A_1R agonists with respect to their abilities to positively and negatively regulate cAMP production, mobilise intracellular Ca^{2+} and activate ERK1/2. The activity of triazoloquinazoline compounds against the A_{2A}R is validated, identifying 3 to be selective. Further investigations into the ability of triazoloquinazolines to mediate cAMP production and ERK1/2 activation uncovers each tested agonist to be biased towards activating ERK1/2, at the A_{2A}R. A characterisation of the effects of receptor activity modifying proteins (RAMPs) upon signalling from the CLR is presented: quantifying the extent of biased agonism, with respect to the ability of RAMP-CLR heterodimers to: mediate cAMP production and inhibition, as well as mobilise intracellular Ca^{2+}, uncovering this to be a $G\alpha_{q/11}$-mediated process. Further, through applying a saturation mutagenesis approach to the CLR, a potential interaction is identified between intracellular loop 1 (ICL1) and helix 8, which is broken upon receptor activation, further identifying ICL1 to be a region of the CLR responsible for influencing G protein specificity.

Ultimately, these findings relating to both adenosine and CLR-based receptors uncovers further evidence of biased agonism at GPCRs, which may have potential implications upon improving the efficacy and safety profiles of novel pharmaceutics targeting these clinically relevant GPCRs.

Chapter 1
Introduction

1.1 Cellular signalling

In multicellular organisms, cells need to able to communicate to one another, resulting in complex modifications in either cellular behaviour, or gene expression. These can be brought about due to changes in the organism's external environment, or in its own internal biochemistry. Such responses are governed by many differing types of stimuli, including, but not limited to: physical, such as touch, heat, light and pressure; or chemical, such as: neurotransmitters, lipids, nucleotides or peptides. For lipophilic signalling molecules, or ligands, these are able to directly cross the plasma membrane and affect their changes. Examples of such molecules include retinoids (derivatives of vitamin A), thyroid hormones, and sex hormones, such as testosterone and oestrogen. Each of these different ligand types will result in differing effects upon the target cell. These are brought about through binding to, what, in 1905, James Langley called the "receptive substance" (Langley, 1905), now more commonly termed 'receptors'. However, many ligands are lipophobic, and thus are unable to directly cross the plasma membrane. Therefore, they are unable to interact with receptors located within the cell, unlike lipophilic molecules. Thus, to respond to these ligands, cells developed transmembrane (TM) receptors, residing within the plasma membrane, providing a conduit through which extracellular stimuli can transduce their signal, bringing about intracellular effects.

Many different subtypes of TM-receptors exist, but the largest by far consist of G protein-coupled receptors (GPCRs). The human genome project identified 23,000 distinct genes (Venter *et al*, 2001), of which over 800 were identified as potentially coding for GPCRs (Fredriksson *et al*, 2003). Thus, >0.03% of our DNA encodes for this group of receptors. As

large a family as they are, they also bind, and respond to, an equally diverse array of ligands. Examples of these include photons, ions, proteins, lipids, nucleotides and sugars (Fredriksson *et al*, 2003). Each of these differing ligand types, bind distinct receptor subgroups, all of which are able to result in a wide range of intracellular effects, ranging from: gene expression changes and the regulation of enzymes, to the secretion of further signalling molecules. It is GPCRs that will form the focus of the research presented within this thesis.

1.2 G protein-coupled receptors

The large diversity in GPCR subtypes, ligands, and elicited responses underlies how important they are in regulating correct cellular function. Thus, perturbation, or malfunction, of these signalling pathways can have dire consequences. This is indicated by the fact that GPCRs are implicated in a wide array of pathological states including, but not limited to: cardiovascular disease, cancer, diabetes mellitus, migraine, hypertension, addiction and various neurological diseases such as Huntington's, schizophrenia, Alzheimer's and Parkinson's (Bristow, 2000, Hack and Christie, 2003, Sloop *et al*, 2005, Hill, 2006, Ohta *et al*, 2006, Mehta and Griendling, 2007, Morelli *et al*, 2007, Branca *et al*, 2014, Lee and Chern, 2014, Villar-Menéndez *et al*, 2014, Walker *et al*, 2015). Due to their implications in such a wide array of diseases, GPCRs are currently the target of an estimated 30% of prescription drugs (Correll and McKittrick, 2014). Thus, a greater understanding of the function of this family of receptors will allow us to gain a more in-depth knowledge of their roles played in various pathologies, and have implications upon therapeutic intervention strategies.

1.2.1 GPCR families

Despite the wide diversity of receptor subtypes, all are grouped into one of six families, A-F, based upon similarities in: structure, function and

ligand binding (Krishnan *et al*, 2012) (Table 1.1). Of these, family A is the largest group, consisting of 719 distinct GPCRs, of which 87 currently have no known ligand, referred to as 'orphan' receptors (Davenport *et al*, 2013). They are commonly called the 'rhodopsin-like' receptors, due to similarity to the prototypical GPCR, rhodopsin (Palczewski *et al*, 2000). They are so diverse that they have been further split into 19 subgroups (A1-19), based upon phylogenetic analysis (Joost and Methner, 2002). Examples of family A GPCRs include the: opioid, vasopressin, purinergic, cannabinoid, dopamine, adenosine and adrenergic receptors. The family as a whole, binds, and responds, to a diverse array of ligand types, such as purines, neurotransmitters, odorants and photons. Due to their diversity, members of this family of receptors have been implicated in many human pathological states such as: cancer, various neurodegenerative diseases, addiction and cardiovascular disease (Bristow, 2000, Hack and Christie, 2003, Morelli *et al*, 2007, Allard *et al*, 2016). Thus, family A GPCRs have been of great interest to the pharmaceutical industry, in the treatment of human diseases.

The second group of GPCRs, the secretin-like, or family B, GPCRs are a much smaller group than family A, consisting of 15 distinct receptors, only found to be expressed in animals. They are also a much less understood group than their family A counterparts. This is surprising, given they are implicated in many human disease states, including: diabetes, bone disorders, cardiovascular disease, migraine and various inflammatory diseases. They respond to a series of peptide hormones, ranging in size from 20-50 amino acids, via an extra large, extracellular N-terminus (Fredriksson *et al*, 2003). Such peptides include: glucagon, glucagon-like peptide-1 (GLP-1), corticotrophin-releasing factor (CRF), calcitonin (CT), calcitonin gene-related peptide (CGRP), amylin (AMY), adrenomedullin (AM) and adrenomedullin 2 (AM2), all of which play important metabolic and physiological roles within man.

Family C GPCRs, the 'metabotropic glutamate receptors', bind ligands such as Ca^{2+} ions and glutamate. Members of this group include the

calcium-sensing receptor, $GABA_B$ and taste receptors. It is these first three families that are found in mammals, with families D and E being absent. Family D receptors are the fungal mating-pheromone receptors, whilst those in family E represent various cyclic adenosine monophosphate (cAMP) receptors. The final group, family F, is present in mammals and includes the frizzled/smoothened receptors. These play key roles in influencing cell proliferation and differentiation in response to binding secreted glycoproteins, Wnts.

Table 1.1: G protein-coupled receptor families.

Family	Type
A	Rhodopsin-like receptors
B	Secretin-like receptors
C	Metabotropic glutamate receptors
D	Fungal mating-pheromone receptors
E	Cyclic AMP receptors
F	Frizzled/Smoothened receptors

1.2.2 GPCR structure

GPCRs are expressed in every known eukaryotic organism (Krishnan *et al*, 2012), and regardless of the families to which they belong, they all share the same gross macro-structure. This consists of an extracellular N-terminus, 7 TM α-helical domains: each joined by a series of intra- and extracellular loops (ICL/ECL), ending in an intracellular C-terminus (Figure 1.1).

The N-terminus, along with the ECLs, play roles in ligand recognition and binding (Olah *et al*, 1994, Avlani *et al*, 2007), whilst ICLs have roles in mediating downstream signalling, through interaction with other proteins (Bockaert and Pin, 1999, Ballesteros *et al*, 2001). The C-terminal domain of a GPCR commonly forms an 8^{th} helix, which aligns with the plasma

membrane (Wess *et al*, 2008, Conner *et al*, 2008), and is a region that has been shown to be bound by proteins responsible for desensitisation and further signalling (Lohse *et al*, 1990, Gurevich *et al*, 1995).

The seven TM domains are the most highly conserved domains of all GPCRs (also known as 7-TM receptors). Upon ligand binding, and activation, a series of structural rearrangements occur within the TM bundle. This results in a conformational change from the 'inactive' to 'active' state. The 'inactive' state is maintained, in many GPCRs, by an ionic lock, a D/ERY motif, in TM3. This motif interacts with a glutamic acid residue, located in TM6, and serves to 'lock' the receptor in its 'inactive' state. Upon transition to the active state, this 'lock' is 'broken', resulting in a twisting of TM3, away from TM6, by ~30°. As a consequence, the ICLs further move, allowing interaction with signalling machinery (Bockaert and Pin, 1999, Ballesteros *et al*, 2001), such as heterotrimeric guanine nucleotide-binding proteins (G proteins).

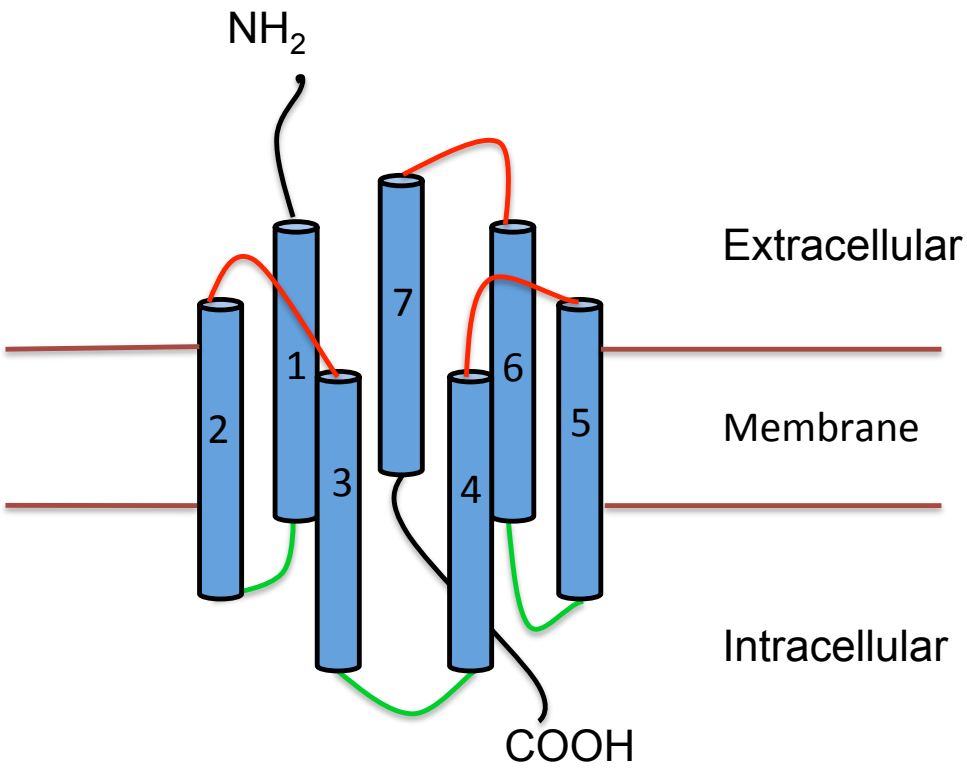

Figure 1.1: G protein-coupled receptor basic structure.

A GPCR consists of 7 transmembrane (TM) domains (Blue), joined together by 3 extracellular loops (ECLs) (Red), and 3 intracellular loops (ICLs) (Green), with an extracellular N-terminus, and intracellular C-terminus.

1.3 GPCR signal transduction

1.3.1 G protein activation

The main mechanisms through which GPCRs transduce signals are via heterotrimeric G proteins. These belong to a large superfamily, which also include monomeric G proteins. They all function as 'binary switches': whilst in an 'inactive' state, they are bound to guanosine diphosphate (GDP), becoming 'active' upon binding guanosine triphosphate (GTP) (Figure 1.2). This GDP/GTP binding is conferred by a conserved G domain of ~20 kDa (Lambright *et al*, 1994). The switch from a GDP to GTP-bound state can occur spontaneously, due to higher cellular concentrations of GTP. However, it can also be accelerated by guanine nucleotide exchange factors (GEFs) (Figure 1.2). This is achieved by the

GEF inducing changes within the G protein: reducing its affinity for GDP, leading to its exchange for GTP. Once active, a G protein can also transition back to an 'inactive', GDP-bound state. This is facilitated either by: the G protein's own intrinsic GTPase activity, or the action of GTPase activating proteins (GAPs) (Randazzo and Kahn, 1994, Bos *et al*, 2007) (Figure 1.2).

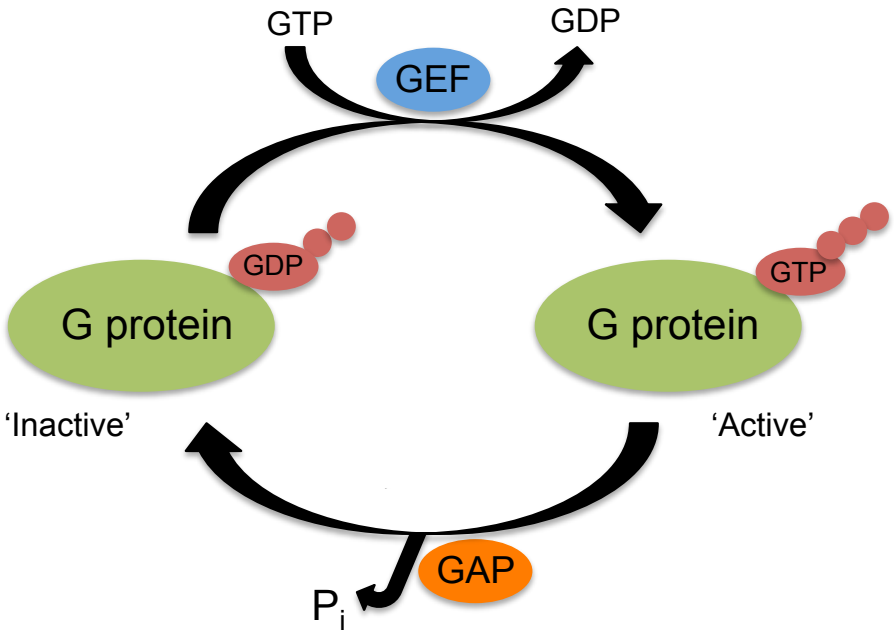

Figure 1.2: Activation cycle of G proteins.

In a GDP-bound state, a G protein is inactive; however, through the action of guanine exchange factors (GEFs), their conversion to an active, GTP-bound state, is catalysed. Reversion to an inactive state occurs through a G protein's own intrinsic GTPase activity, which can be accelerated by the action of GTPase-activating proteins (GAPs).

1.3.2 Heterotrimeric G proteins

Heterotrimeric G proteins consist of a Gα subunit associated with a dimer of Gβ and Gγ subunits (Hepler and Gilman, 1992), which couple to GPCRs. The Gα subunit consists of two domains, a nucleotide-binding domain and helical domain, whilst the Gβ subunit consists of seven repeated WD motifs, which arrange to form a propeller-like structure

(Sondek *et al*, 1996). The Gγ subunit is smaller than Gβ and is unstable in the absence of an associated Gβ subunit, hence these are found associated as a Gβγ dimer.

Upon ligand-induced transition from 'inactive' to the 'active' state, a GPCR is able to promote the release of GDP from Gα, allowing exchange for GTP. In this manner, a GPCR serves to function as a GEF for Gα proteins. Upon activation, Gα dissociates from the Gβγ dimer due to loss of a hydrophobic binding pocket required for their association (Lambright *et al*, 1994). Transduction of the ligand-associated signal is therefore passed through a GPCR into a cell, and its intracellular effects mediated by either the active Gα or Gβγ dimer.

1.3.2.1 Gα-dependent signalling

The Gα subunit typically defines the heterotrimeric G protein, and often governs the response mediated by a given GPCR (Wettschureck and Offermanns, 2005). There are 17 differing Gα proteins, grouped into four families: $G\alpha_s$, $G\alpha_{i,}$ $G\alpha_q$ and $G\alpha_{12}$, based upon their intracellular targets and effects (Table 1.2).

Table 1.2: Gα families.

Gα family	Members	Effects
$G\alpha_s$	$G\alpha_s$ and $G\alpha_{olf}$	Stimulates adenylate cyclase
$G\alpha_i$	$G\alpha_{i1}$, $G\alpha_{i2}$, $G\alpha_{i3}$, $G\alpha_{oa,}$ $G\alpha_{ob,}$ $G\alpha_z$, $G\alpha_t$, $G\alpha_{gust}$	Inhibits adenylate cyclase
$G\alpha_q$	$G\alpha_q$, $G\alpha_{11}$, $G\alpha_{14}$, $G\alpha_{15}$, $G\alpha_{16}$	Stimulates activity of phospholipase C-β
$G\alpha_{12}$	$G\alpha_{12}$ and $G\alpha_{13}$	Modulates Rho family G proteins

Where GPCR activation leads to signalling mediated via the $G\alpha_s$ family of G proteins, activation of adenylate cyclase (AC) occurs (Figure 1.3). AC serves to catalyse the conversion of adenosine triphosphate (ATP) to

cAMP. This in turn activates protein kinase A (PKA), through the binding of four cAMP molecules to its regulatory subunit, allowing dissociation from the, now active, catalytic subunit (Huang and Taylor, 1998). PKA then mediates further transduction of the ligand-induced signal, via the phosphorylation of further target proteins (Iwami *et al*, 1995). This can result in effects such as promoting glycolysis in the liver and skeletal muscle (Rui, 2014), regulating the cystic fibrosis transmembrane conductance regulator (CFTR) (Chappe *et al*, 2005), vasodilation through action in smooth muscle cells (Yang *et al*, 2008), and enhancing lipolysis in adipocytes (Tansey *et al*, 2003).

Activation of $G\alpha_{i/o}$ directly opposes the action of $G\alpha_s$: serving to inhibit the action of AC (Figure 1.3), thereby reducing cellular concentrations of cAMP. Further to this, $G\alpha_{i/o}$ proteins have also been shown to be able to activate phospholipase C (PLC), and G protein-coupled inwardly-rectifying K^+ channels (GIRKs) (Peleg *et al*, 2002, Lei *et al*, 2003, Lüscher and Slesinger, 2010). The $G\alpha_{i1/2/3}$ and $G\alpha_{oa/b}$ members of this family are sensitive to pertussis toxin (PTX) from *Bordetella pertussis*. PTX serves to ADP-ribosylate the C-terminus of these G proteins, preventing their interaction with a GPCR (West *et al*, 1985).

The $G\alpha_q$ family of G proteins all serve to stimulate the activity of PLC isoforms (Birnbaumer *et al*, 1990) (Figure 1.3). Once activated, PLC is able to cleave phosphatidylinositol 4,5-bisphopshate (PIP_2), to inositol 1,4,5-triphosphate (IP_3) and diacylglycerol (DAG). IP_3 is then able to bind directly to IP_3 receptors, located on both the endoplasmic and sarcoplasmic reticulums (ER and SR, respectively) (Shah *et al,* 2015). Activation of these receptors results in the release of free Ca^{2+} ions into the cell (Figure 1.3), having effects upon: muscle contraction and vasoconstriction, secretion of neurotransmitters and other signalling peptides, such as insulin (Seino and Shibasaki 2005). The final group of Gα proteins, $G\alpha_{12}$, serve to regulate the activity of Rho family GTPases (Figure 1.3), which serve to modulate the cell's actin cytoskeleton (Perez and Rinćon, 2010).

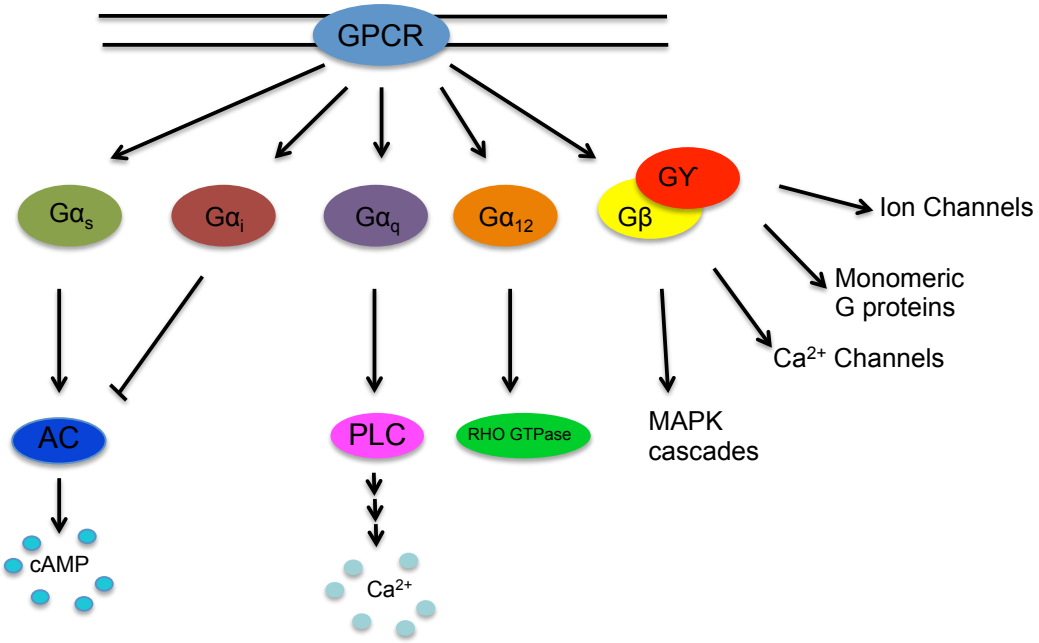

Figure 1.3: GPCR-mediated G protein-dependent signalling pathways.

GPCRs can activate several G protein-dependent pathways: activation of $G\alpha_s$ (Green) results in adenylate cyclase (AC – Dark blue) activation and cAMP production, whilst $G\alpha_i$ activation (Brown) inhibits AC activity. Activation of: $G\alpha_q$ (Purple) results in PLC-dependent release of Ca^{2+} from ER stores, $G\alpha_{12}$ (Orange) leads to actin cytoskeleton regulation via the action of RHO GTPases. Gβγ can also signal, leading to a multitude of downstream signalling events (Yellow/Red).

1.3.2.2 Gβγ-dependent signalling

Each of the Gα proteins interacts with an associated Gβγ dimer. There are 5 Gβ proteins, and a further 12 Gγ subunits, in mammals (Gautam *et al*, 1998, McCudden *et al*, 2005). These dimers, which are released upon Gα activation, are also able to propagate signals in their own right. Such signal propagation includes: opening GIRK channels (Logothetis *et al*, 1987, Huang *et al*, 1995, He *et al*, 2002) and Ca^{2+} channels (Herlitze *et al*, 1996), regulation of various kinases, such as: extracellular signal-regulated kinases (ERK), and janus kinases (JNK) (McCudden *et al*, 2005), as well as regulating monomeric G proteins (Clapham and Neer, 1997) (Figure 1.3).

1.3.3 G protein-independent signalling

As well as utilising G proteins as a conduit to transduce extracellular signals, GPCRs are also able to signal in manners independent of G proteins. The most common, and well-known, method is via β-arrestin recruitment. This group of proteins was initially thought to 'arrest' GPCR signalling, but have subsequently been implicated in acting as scaffolds for the recruitment, and activation, of other signalling proteins. The most characterised of these are the mitogen activated protein kinases (MAPKs), particularly ERK1/2 (Shenoy and Lefkowitz, 2005 and 2011). In this instance, the activated GPCR is phosphorylated, at its C-terminus, by G protein-coupled receptor kinases (GRKs). This allows recruitment of β-arrestins, to the C-terminus (Lefkowitz, 2005), in turn, facilitating recruitment of the MAPK kinase kinase (MAPKKK), Raf-1. This serves to phosphorylate the MAPK kinase (MAPKK), MEK-1, which subsequently phosphorylates the MAPKs, ERK1/2 (Pierce *et al*, 2001). Activation of the MAPK pathway can have effects upon cells, such as: cell cycle arrest, cytokine secretion, promoting proliferation and inducing apoptosis (Kranenburg and Moolenaar, 2001, Pierce *et al*, 2001). As well as coupling MAPK activation to GPCRs, β-arrestins have also been observed to regulate phosphodiesterases (PDEs), thereby influencing G protein-dependent signalling pathways (DeFea, 2011).

1.4 Regulation of GPCR signal transduction

As cells have developed methods to detect signals from their external environment, they are also in need of a way to 'turn off' these signals. Upon ligand activation of a given GPCR, a number of signalling cascades will be initiated, to effect the desired changes required by a cell. Without a method to halt these signals, they will continue to function indefinitely, perhaps with detrimental effects upon the cell or organism. Thus, cells have evolved mechanisms to return the levels of secondary messengers or phosphorylated proteins, to resting, basal, levels.

1.4.1 Regulating GPCR signalling via ligand depletion

One method, by which cells can prevent their continual response to a stimulus, is to remove it. This is elegantly illustrated by two family B receptors, the: GLP-1, and gastric inhibitory peptide (GIP) receptors. These respond to 2 peptide hormones, secreted by pancreatic β-cells, in response to the ingestion of food (Baggio and Drucker, 2007). Activation by these hormones, of their associated receptor, results in the secretion of insulin. In order to prevent prolonged stimulation and over production of insulin, cells express an enzyme, dipeptidyl peptidase–IV (DPP-IV), upon their surface (Mentlein *et al*, 1993), which rapidly cleaves both GLP-1 and GIP to inactive metabolites (Kieffer *et al*, 1995). Through degradation of these hormones, the cells prevent overexpression of insulin (Yabe and Seino, 2011), and serve to help maintain blood glucose homeostasis.

1.4.2 Receptor internalisation

Another method of regulating signalling, and returning a cell to its basal state, prior to receptor activation, is via internalisation of the GPCR. Ligand-bound, active receptors become the target for GRKs, which phosphorylate serine and threonine residues located with ICL3 and the C-terminus (Figure 1.4). The phosphorylated C-terminus facilitates interaction with β-arrestins (Lefkowitz, 2005) (Figure 1.4). There are four arrestins: 1-4, with 2 and 3 also referred to as β-arrestins 1 and 2, respectively (Shenoy and Lefkowitz, 2011). Each of these 4 proteins share a similar structure, consisting of 12 polar residues flanked by an N- and C-terminus (Hirsch *et al*. 1999). Upon binding a GPCR's phosphorylated C-terminus, the β-arrestin's own C-terminus becomes exposed. This serves to inhibit further G protein-mediated signalling, and serves to facilitate internalisation of the receptor, via clathrin-mediated endocytosis (Figure 1.4). This is brought about by direct interaction of the arrestin with clathrin (Krupnick *et al*, 1997, Kang *et al*, 2009), or the

clathrin adaptor protein, AP-2 (Figure 1.4) (Laporte *et al*, 1999, 2000, Kim and Benovic, 2002, Schmid *et al*, 2006, Burtey *et al*, 2007). The internalised receptor can then either be: recycled back to the cell surface, or targeted for degradation (Figure 1.4) (Marchese *et al*, 2008, Correll and McKittrick, 2014). Indeed, it has been observed that some GPCRs, notably the β_2-adrenergic receptor, can continue to signal whilst located within the endosome (Vilardaga *et al*, 2014).

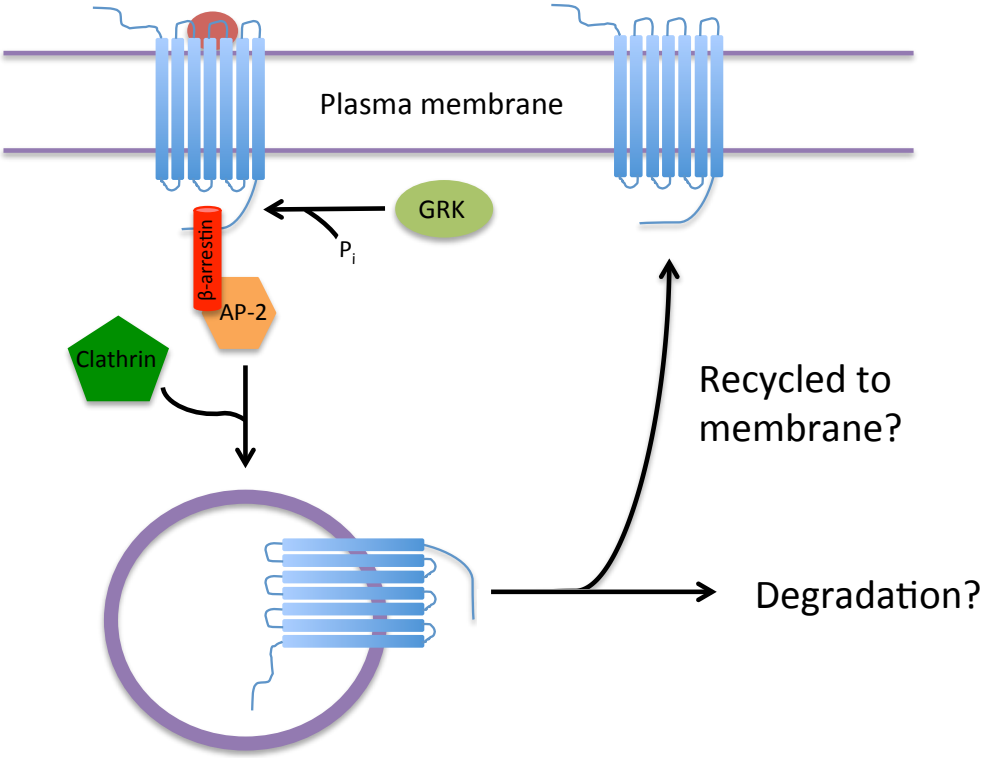

Figure 1.4: β-arrestins can mediate internalisation of active GPCRs.

Once activated by a ligand, the C-terminus of a GPCR can be phosphorylated by GRKs. This results in recruitment of β-arrestin to the C-terminus. β-arrestin then facilitates the further recruitment of the clathrin adapter protein, AP-2, resulting in clathrin-mediated endocytosis of the GPCR. Once internalised, the receptor can either be targeted for degradation, or recycled back to the plasma membrane.

Some GPCRs can also be internalised in a β-arrestin-independent manner. For example: the PAR-2 receptor can itself, directly interact with AP-2, and thus clathrin, resulting in internalisation (Paing *et al*, 2004). Other GPCRs, such as the M3 muscarinic receptor, are also able to be

internalised using clathrin-independent mechanisms (Scarselli and Donaldson, 2009).

1.4.3 Receptor phosphorylation

As well as being phosphorylated by GRKs, numerous other enzymes are also able to phosphorylate GPCRs, in a regulatory manner. This can occur via the action of downstream enzymes, activated through the receptor, in a negative feedback manner. One such example is that of PKA, which is able to phosphorylate ICL3 and the C-terminus of the β_2-adrenergic receptor (Benovic *et al*, 1985), preventing signalling by sterically inhibiting its interaction with a G protein (Benovic *et al*, 1985, Lefkowitz *et al*, 1990). Similarly, the angiotensin II type 1 receptor (AT_1), which couples to $G\alpha_q$, activates protein kinase C (PKC), resulting in the subsequent phosphorylation of AT_1's C-terminus. The β_2-adrenergic receptor has also been observed to be phosphorylated by receptor tyrosine kinases (RTKs) (Karoor and Malbon, 1996, Karoor *et al*, 1998), and Akt/protein kinase B (PKB) (Doronin *et al*, 2002).

1.4.4 Regulation of G protein-dependent signalling

Whilst a GPCR functions as a GEF, to facilitate the activation of various G proteins, a cell requires a method to terminate this signalling. This is able to occur due to the intrinsic GTPase activity of the G protein, converting the bound GTP, back to GDP, thereby inactivating Gα. GDP-bound Gα is then able to re-associate with its Gβγ, reforming the heterotrimer, also serving to halt, Gβγ-mediated signalling. This process can be catalysed by regulator of G protein signalling (RGS) proteins (Dohlman *et al*, 1995). These serve to increase the rate of GTP hydrolysis, thereby speeding G protein inactivation.

Where cAMP production has been facilitated via the action of $G\alpha_s$, simply inhibiting the G protein will not 'turn off' signalling. Reverting $G\alpha_s$ to a

GDP-bound state will prevent further activation of AC, but cAMP levels will remain elevated. To deal with this, cells express PDEs. These catalyse the degradation of phosphodiester bonds in cyclic secondary messengers, such as cAMP and cyclic guanine monophosphate (cGMP). They are therefore able to regulate both the amplitude and duration of a response, as well as spatial regulation, through containment of signalling to specified 'microdomains', particularly for cAMP-mediated signalling (Rich *et al*, 2001, 2007, Zaccolo and Pozzan, 2002, Terrin *et al*, 2006, Oliveira *et al*, 2010, Mika *et al*, 2012).

1.5 GPCR pharmacology

1.5.1 Classification of agonists and their action

Many differing ligands bind GPCRs, inducing conformational changes, resulting in the activation of downstream signalling pathways. When a ligand brings about this response, it is termed an agonist (Table 1.3). Each differing GPCR will only respond to a specific set of agonists, serving to give the global GPCR system specificity, thereby preventing aberrant signalling. Some receptors will only be activated by a single, endogenous, agonist, such as the: adenosine, β_2-adrenergic, dopamine, glucagon and muscarinic receptors (Table 1.3), whilst others, such as the calcitonin-like and opioid receptors can be activated by multiple agonists (Table 1.3). To date there are around 150 orphan GPCRs (Davenport *et al*, 2013). Of the GPCRs with known ligands, only ~10% are targeted by existing therapeutic drugs (Garland, 2013).

Table 1.3: Endogenous GPCR ligands.

GPCR	Endogenous ligand
Adenosine receptors	Adenosine
β_2-adrenergic receptor	Adrenaline
Calcitonin-like receptor	CGRP, Adrenomedullin, Adrenomedullin 2
Dopamine receptors	Dopamine
Glucagon receptor	Glucagon
Muscarinic receptors	Acetylcholine
Opioid receptors	Opioids (dynorphins, endorphins, nociceptin)

Regardless of which ligand acts as an agonist at a given GPCR, they will fall into one of three classes, based upon their action. Agonists can be classified as either: full, partial, or inverse. Both full and partial agonists will increase the level of a measured response as the concentration of stimulating agonist is increased (dose-dependency) (Figure 1.5). Full agonists, will generate the maximal response (E_{max}), for a given pathway, at a given receptor (Figure 1.5). A single GPCR may have multiple full agonists. On the other hand, partial agonists will bring about a response, but with a lower E_{max} than that observed for a full agonist (Figure 1.5). In contrast, an inverse agonist is one that binds a receptor, resulting in a decrease in activity, in a dose-dependent manner (Figure 1.5).

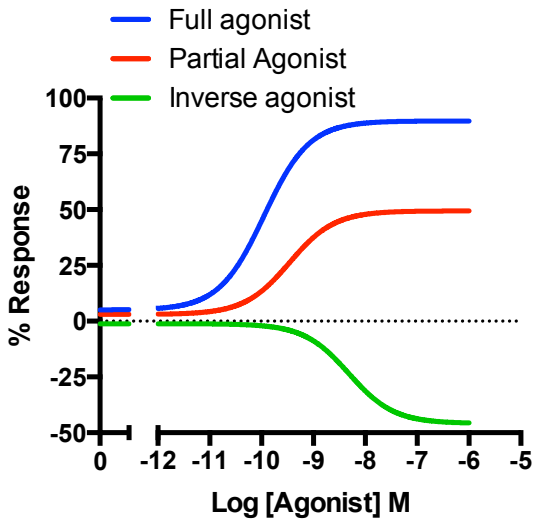

Figure 1.5: The different effects of ligands acting as agonists.

Agonists can exert differing effects upon a GPCR. Activation brought about by a full agonist will generate the maximal, largest, response observed for that receptor (E_{max}). Partial agonists will still result in receptor activation, but the maximal response will be lower than that observed for a full agonist. Inverse agonists, on the other hand, cause a receptor with constitutive activity, to transit to an inactive state, thereby reducing activity at higher agonist concentrations.

Another measure of how an agonist activates a GPCR is its potency (EC_{50}). This essentially displays how 'well' an agonist activates a GPCR. It is defined as the concentration of drug required to affect half maximal response (Figure 1.6). Thus, where a drug induces 100% response, the EC_{50} would be the concentration required to affect a 50% response. Thus, agonists may be defined as being more, or less, potent compared to others. This is particularly important clinically, where a higher potency requires a lower dose of drug to be administered.

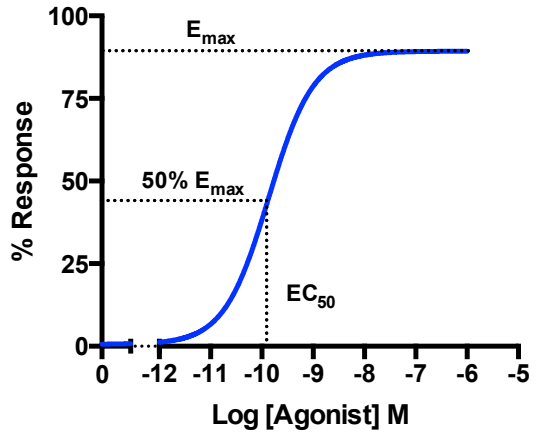

Figure 1.6: The concentration at 50% of maximal response defines potency.

The potency (EC_{50}) of an agonist is defined as the concentration of agonist, that affects a response equal to 50% of the maximal response observed.

1.5.2 Two-state receptor model

The phenomena whereby agonists can have differing effects, with respect to both E_{max} and EC_{50}, can be explained by the two-state receptor model (Kenakin, 2004) (Figure 1.7). This predicts that receptors exist in two distinct states: the inactive (R), and the agonist-bound active (R^*) states. Agonists thus serve to move the equilibrium of the receptor system towards the active R^* state, whilst inverse agonists reverse this, shifting equilibrium towards the R state (Kenakin, 2004), (Figure 1.7). Thereby, it can be envisaged that full agonists (Figure 1.5) shift the extent of equilibrium further towards a system with full R^*, whilst partial agonists (Figure 1.5) result in a lesser shift. Potency can also be envisaged as how 'effective' an agonist is at mediating this transition: those more effective being the more potent agonists.

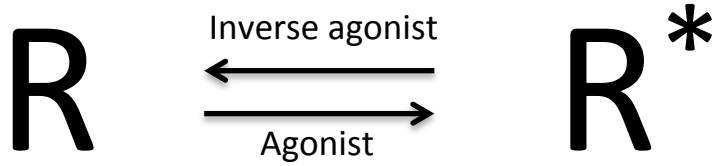

Figure 1.7: Two-state model of receptor activation.

The two-state model of receptor activation predicts that receptors exist in one of two states: the inactive (R), and the ligand-bound, active (R*) state. Inverse agonists thus push the equilibrium towards a predominantly R state, whilst agonists shift equilibrium to the R^* state. (Adapted from Kenakin, 2004)

1.5.3 Constitutively active receptors

Some receptors spontaneously exist in an R^* state, in the absence of a stimulating agonist, thus exhibiting constitutive activity. Such receptors are inherently able to activate downstream signalling pathways, as was first observed for the β_2-adrenergic receptor in 1984 (Cerione *et al*, 1984). However, upon agonist binding, their equilibrium is further shifted towards the R^* state, resulting in an amplification of their signalling output. Such receptors exist naturally, but can also arise due to mutation, causing constitutively active mutants (CAMs). Naturally occurring CAMs have been implicated in pathological states such as hyperthyroidism and retinitis pigmentosa (Hwa *et al*, 1997). Indeed, loss of constitutive activity can also lead to a pathological state (Srinivasan *et al*, 2004). CAM GPCRs can also be artificially generated; mimicking the active receptor (Ladds *et al*, 2005a), providing a system whereby the structure of the active state can be investigated (Kobilka and Deupi, 2007).

1.5.4 GPCR dimerisation

GPCRs are predominantly considered to exist as distinct monomeric units, however some have been show to form higher order oligomers. These may be homodimers, such as for the β_2-adrenergic receptor

(Lohse, 2010), or heterodimers between two different GPCRs, this being observed for both adenosine and dopamine receptors (Franco *et al*, 2000). Such dimers have been seen to form due to interactions between the TM domains of the different receptors involved (Milligan *et al*, 2007, Rivero-Müller *et al*, 2013). Dimerisation, or indeed oligomerisation, can have various implications for the GPCRs involved. Indeed, it can impact upon receptor trafficking from the ER to the cell surface (Reviewed by Milligan, 2009), as well as ligand binding and activation, whereby one protomer allosterically influences the other (Rozenfeld and Devi, 2010, Hill *et al*, 2014). This can potentially pose challenges for the development of novel pharmaceuticals targeting GPCRs that undergo dimerisation.

1.6 Biased agonism of GPCRs

GPCRs regulate, and govern, a complex system of signalling pathways, in response to agonist-induced activation. The ultimate outcomes from a single GPCR are both varied and diverse. We have seen how agonists can have differing effects upon a single signalling pathway. This can manifest as full or partial responses (Figure 1.5), and differing potencies of the stimulating agonist. Thus, for two agonists of the same receptor, activating the same single pathway, two differing magnitudes of response can be observed. This is complex enough for some receptors, such as the neurotensin receptor, which can only bind and activate a single pathway ($G\alpha_i$ in this instance) (Mustain *et al*, 2011). However, many GPCRs express an ability to activate a network of multiple, yet distinct, signalling pathways, both G protein-dependent (Figure 1.3) and independent (Koole *et al*, 2010, Weston *et al*, 2014, 2016, Knight *et al*, 2016). It is therefore clear that multiple, diverse responses can occur through the activation of a single GPCR. This is further complicated by the fact that some receptors bind, and are activated by, multiple endogenous ligands (Table 1.3). Thus, a single GPCR can be activated by different ligands, which activate multiple signalling pathways to differing extents. The difference between these ligands' ability to activate

different pathways is a phenomenon termed: biased agonism, functional selectivity, pathway or signalling bias (Figure 1.8).

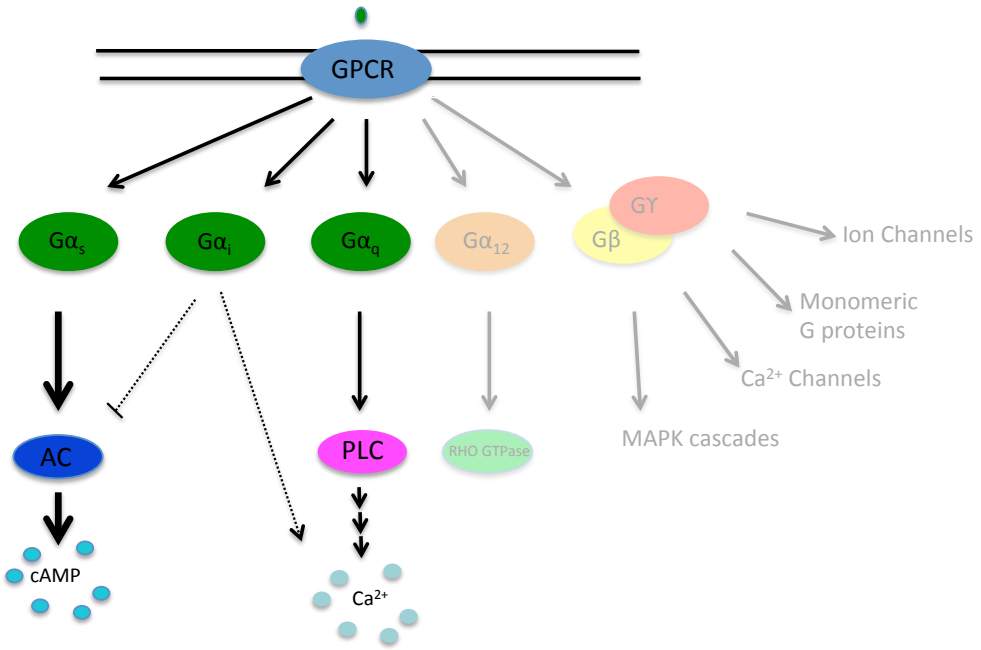

Figure 1.8: Biased agonism results in agonist-induced activation of specific pathways.

Activation of a GPCR by a given agonist will, potentially, result in activation of multiple downstream signalling pathways. These may also be activated to differing extents. Here, the agonist results in receptor-mediated activation of three G protein-dependent pathways: $G\alpha_s$, $G\alpha_i$, and $G\alpha_q$. A large response is mediated via $G\alpha_s$ (indicated by a thick, bold arrow), resulting in downstream cAMP production. An intermediate Ca^{2+} response is mediated by $G\alpha_q$ activation, whilst a weak $G\alpha_i$ response is also activated (indicated by a dotted line). In terms of biased agonism, this agonist would therefore be biased towards cAMP production, over all pathways, and biased towards Ca^{2+} mobilisation over cAMP inhibition.

Despite much research into quantifying the extent of pathway bias at GPCRs, little is understood about how this phenomenon occurs, at both a structural and functional level. Multiple structures have been observed for each of the receptors, for which crystal structures have been resolved (Wacker *et al*, 2013, Fenalti *et al*, 2014). Indeed, differing structures have been found for the β_2-adrenergic receptor, dependent upon the bound ligand (Swaminath *et al*, 2004, 2005). These different structures, and the fact that GPCRs exhibit pathway bias, has lead to the postulation that ligands stabilise different receptor conformations, allowing activation of specific pathways (Violin *et al*, 2014), something not accounted for by the two state model of receptor activation (Figure 1.7) (Kenakin, 2004).

A classical example of pathway bias is that of the μ-opioid receptor. This receptor plays key roles in our feeling of pain. As such, it is the target of many analgesics, perhaps the most well known of which being morphine. This brings about its analgesic effects through the activation of $G\alpha_{12}$-mediated signalling (Pradhan *et al*, 2010, 2012). Chronic dosing of morphine however, results in increased tolerance, reducing morphine's efficacy as an analgesic (Dumas and Pollack, 2008). Complications further associated with this include: respiratory suppression, constipation and addiction (Rawal and Wattwil, 1984, Ammon-Treiber and Höllt, 2005 Huang *et al*, 2017). This was shown, by Raehal and colleagues, to be due to morphine-induced, μ-opioid receptor-dependent activation of β-arrestin 2 signalling (Raehal *et al*, 2005). Thus, pathway bias can have direct implications upon drug efficacy and safety. Indeed, drugs have subsequently been developed that preferentially activate $G\alpha_{12}$-mediated signalling, over β-arrestin 2 signalling, at the μ-opioid receptor (Chen *et al*, 2013, DeWire *et al*, 2013).

1.6.1 Quantifying biased agonism

Qualitative analysis of bias for a ligand between two activating pathways can be determined through the comparison of dose-response curves for measured responses at each pathway. However, this does not provide a quantitative measure of the extent of bias towards one pathway, over the other. In order to achieve this, several methods have been developed which utilise data obtained via secondary messenger assays (Reviewed by Rajagopal *et al*, 2011).

The most commonly used methods of quantifying biased agonism rely on fitting data with the operational model of pharmacological agonism (Black and Leff, 1983). This model revolutionised the field of receptor pharmacology and hence, signalling bias. The model allows the calculation of two parameters that perfectly describe an agonist's ability to activate a receptor, and transduce a signal. These are: Ka, the ligand's

intrinsic affinity for its receptor, and log τ, its *intrinsic* efficacy. The model states that a ligand binds a receptor, with an affinity, Ka, forming a ligand-receptor (LR) complex (Figure 1.9). This is then able to transduce the ligand's signal with a transduction coefficient, K_E (Figure 1.9). The efficiency of this signal is thus a function of the number of LR complexes formed, and therefore dependent upon the number of free receptors, R, available to bind ligand. Hence, the efficacy of a ligand, log τ, is a function of the number of LR complexes and K_E. Alternatively, log τ is given by $\frac{[LR]}{K_E}$. Evaluation of this at steady-state yields:

$$Response = Basal + \frac{E_{max} - Basal \cdot \tau \cdot [Agonist]}{\tau \cdot [Agonist] + ([Agonist] + Ka)} \qquad \textbf{Equation 1.1}$$

whereby 'Response' is the level of response generated for a given concentration of stimulating agonist, 'E_{max}' is the maximal response observed upon activation, whilst 'Basal' is the level of response observed in the absence of an agonist.

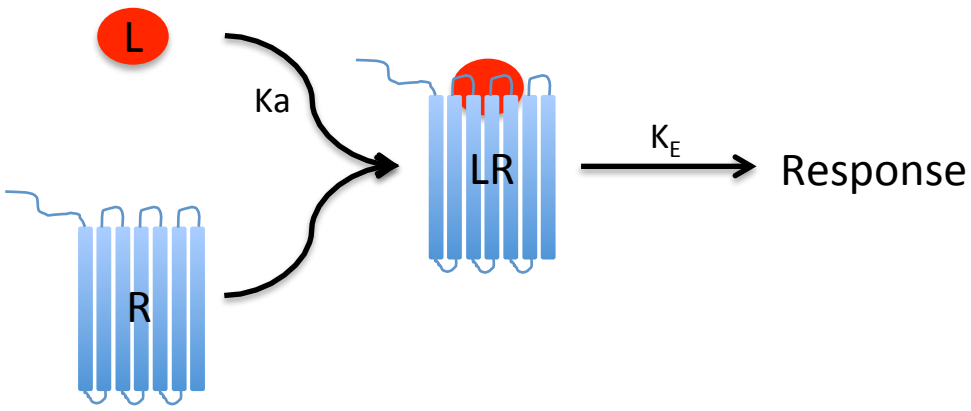

Figure 1.9: Summary of the operational model of pharmacological agonism.

A ligand (L), binds a receptor (R), with an affinity (Ka), forming an active ligand-receptor (LR) complex. This is then able to transduce a response with a signal transduction coefficient (K_E).

In this model (Equation 1.1), efficacy, τ, and *intrinsic* affinity, Ka, are related to the potency of an agonist (EC_{50}) by the following equation:

$$EC_{50} = \frac{Ka}{1+\tau} \qquad \textbf{Equation 1.2}$$

Having calculated log τ and Ka, a transduction coefficient can then be calculated as the ratio between these two parameters (τ/Ka). Through calculating the degree of change in the transduction coefficient (Δ τ/Ka) for a given ligand between different signalling pathways, biased agonism can be quantified (Figure 1.10) (Baltos *et al*, 2016, Qin *et al*, 2017). This thesis will specifically investigate, and quantify, the extent of biased agonism at 2 family A GPCRs, the adenosine A_1 and A_{2A} receptors, as well as a family B GPCR, the calcitonin-like receptor (CLR).

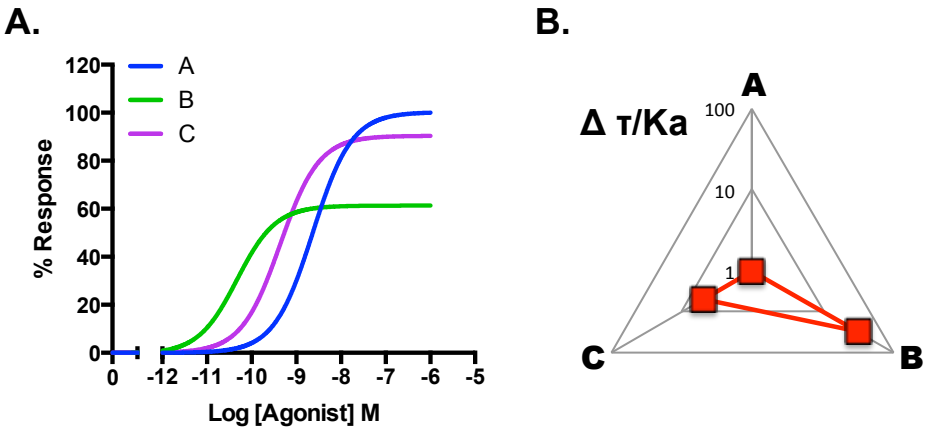

Figure 1.10: Quantification of bias for an example agonist activating three signalling pathways.

Representative data obtained from fitting the operational model of pharmacological agonism (Black and Leff, 1983) to an agonist activating three signalling pathways: A, B and C (A), can be utilised to create a web of bias (B) that displays the extent of the agonist's bias (Δ τ/Ka) to activating each pathway. Here we observe the agonist to be heavily biased towards activating pathway B over A and C, whilst being least biased towards activating pathway A.

1.7 Adenosine receptors

The adenosine receptors (AR) are a small sub-group of family A GPCRs, consisting of four members: The A_1R, $A_{2A}R$, $A_{2B}R$ and the A_3R (Fredholm *et al*, 2011). All four of these receptors bind to, and are activated by, the purinergic nucleoside, adenosine. They are widely expressed within the

human body, residing in such tissues as the: lung, colon, brain, liver, cardiac tissue, and both the central and peripheral nervous systems (Jacobson and Gao, 2006, Cheong *et al*, 2013). Due to this wide ranging pattern of expression, they have been implicated in many human diseases including, but not limited to: Alzheimer's, Parkinson's, Huntington's, cardiovascular disease, cancer, sleep disorders and inflammation (Chen *et al*, 2007, Fredholm *et al*, 2005, Dale and Frenguelli 2009, Sharma *et al*, 2010, Sachdeva and Gupta, 2013, Allard *et al*, 2016).

1.7.1 The adenosine A_1 receptor

The adenosine A_1 receptor (A_1R) is a predominantly $G\alpha_{i/o}$-coupled receptor, activation of which serves to inhibit the activity of adenylate cyclase, thereby lowering cellular cAMP levels. In contrast to this, it has also been observed to couple to $G\alpha_s$, resulting in the production of cAMP (Cordeaux *et al*, 2000 and 2004). Thus, the A_1R displays an ability to activate two, diametrically opposing, signalling pathways. Indeed, Stewart *et al* managed to show that the A_1R mediates cAMP inhibition, via specific coupling to $G\alpha_{i1}$, $G\alpha_{i3}$, $G\alpha_o$ (Stewart *et al*, 2009). It has further been shown to couple to GPA1/$G\alpha_z$ in yeast (Knight *et al*, 2016). Aside from its ability to modulate cAMP levels within a cell, the A_1R is also able to mediate the mobilisation of intracellular Ca^{2+} (Dickenson and Hill, 1993), in a PTX-sensitive manner (Gao and Jacobson, 2016). Thus suggesting that A_1R-mediated Ca^{2+} release occurs in a $G\alpha_{i/o}$-dependent manner. PTX-treatment has also been observed to be efficient in ablating A_1R-mediated ERK1/2 activation (Gao and Jacobson, 2016, Hussain *et al*, 2007), suggesting that, unlike the β_2-adrenergic receptor (Shenoy *et al*, 2006), this occurs in a β-arrestin-independent manner. Interestingly, activation of ERK1/2 signalling by the A_1R has been seen to be cytoprotective in CHO-K1 cells (Baltos *et al*, 2016). Further, the A_1R has an ability to modulate the activity of K^+ channels, particularly in the cardiovascular system (Belardinelli *et al*, 1995). Due to these signalling

properties, activation of the A_1R has been found to be, primarily, cardio-protective. This is particularly true in ischemia-reperfusion, where pre-treatment with an A_1R agonist, prior to reperfusion, has beneficial effects (Zhao *et al,* 1994, Hochhauser *et al*, 2007).

Due to its effects upon the cardiovascular system, many drugs target the A_1R. However, with such a diversity of activated pathways, in response to a single endogenous ligand (that activates all four ARs), it is unsurprising that many pharmaceuticals targeting the A_1R fail in clinical trials (Massie *et al*, 2010). In an attempt to address this, several groups have attempted to develop agonists that are selective for the A_1R, over other ARs (Hutchinson *et al*, 1999, Ashton *et al*, 2007, Franchetti *et al*, 2009, Nell and Albrecht-Küpper*,* 2009, Petrelli *et al*, 2015). Many of the compounds developed, that target the A_1R, actually fail due to poor patient compliance, due to the consumption of caffeine (Robeiro and Sebastiao, 2010). A large proportion of people drink tea or coffee on a regular basis, both of which contain caffeine, an antagonist of the A_1R. This binds to ARs, as would adenosine, but does not result in activation. Thus, caffeine serves to reduce the response observed for a given dose of drug targeting ARs. However, there is still a demand for the discovery of selective A_1R compounds. Indeed, the crystal structure of the A_1R has identified structural, and conformational, differences between ECL2 of the A_1R, compared to the $A_{2A}R$, as well as a wider extracellular cavity and the existence of a second ligand-binding pocket (Glukhova *et al*, 2017). It is believed that these differences may govern ligand selectivity for the A_1R, over the $A_{2A}R$.

1.7.2 The adenosine A_{2A} receptor

The structure of the adenosine A_{2A} receptor ($A_{2A}R$) was the first of the ARs to be solved, with structures for both unbound, and ligand-bound forms (Lebon *et al*, 2011, Xu *et al*, 2011). It is a $G\alpha_s$-coupled receptor, serving to activate adenylate cyclase, thereby elevating cellular levels of

cAMP. Unlike the other ARs, the $A_{2A}R$ is well known for having high levels of constitutive activity (Ibrisimovic *et al*, 2012, Bertheleme *et al*, 2013). Additionally, in the striatum, $A_{2A}R$-mediated activation of adenylate cyclase has been observed via $G\alpha_{olf}$ (Kull *et al*, 2000). However, it has also been shown to be able to dimerise with the A_1R (Ciruela *et al*, 2006. Ferré *et al*, 2008), allowing $A_{2A}R$ activation to result in the subsequent activation of $G\alpha_{i/o}$ (Casadó *et al*, 2010). In addition, the $A_{2A}R$ is also able to form heterodimers with: dopamine D_2 (Kamiya *et al*, 2003, Fuxe *et al*, 2005) and D_3 receptors (Torvinen *et al*, 2005), cannabinoid CB_1 receptor (Ferré *et al*, 2009) and glutamate $mGluR_5$ (Zezula and Freissmuth, 2008), as well as forming a CB_1R-$A_{2A}R$-D_2R heterotrimer (Marcellino *et al*, 2008).

As with other ARs, the $A_{2A}R$ is widely expressed within the human body, but is particularly abundant within the striatum and olfactory bulb of the CNS (Lynge and Hellsten, 2000), as well as platelets (Dionisotti *et al*, 1996), heart, lungs and kidney (Peterfreund *et al*, 1996). In addition to its diverse expression, the $A_{2A}R$ has been implicated in many pathological states, and physiological processes including: hypotension, tachycardia, inflammation, angiogenesis, immunosuppression and cancer, as well as many neurological diseases such as: drug addiction, Huntington's, Parkinson's and schizophrenia (Shin *et al*, 2000, Hack and Christie, 2003, Sullivan, 2003, Dhalla *et al*, 2006, Ohta *et al*, 2006, Morelli *et al*, 2007, Ahmad *et al*, 2009, Lee and Chern, 2014, Villar-Menéndez *et al*, 2014, Allard *et al*, 2016). Indeed, due to its importance in human physiology and pathology, there have been many ligands developed that show selectivity for the $A_{2A}R$, over other ARs (Ongini *et al*, 2001, Baraldi *et al*, 2002, 2003, Christalli *et al*, 2003, Weiss *et al*, 2003).

1.7.3 The adenosine A_{2B} receptor

Of the ARs, the adenosine A_{2B} receptor ($A_{2B}R$) is, perhaps, the least studied and understood (Jacobson, 2009). It couples to $G\alpha_s$ elevating

cAMP levels, via adenylate cyclase activation. Coupling to $G\alpha_q$ has also been reported (Linden *et al*, 1999), as has activation of ERK1/2 (Hasakó *et al*, 2009). Unlike the other ARs, the $A_{2B}R$ only appears to be activated under high levels of adenosine, available in times of physiological stress and pathology (Hasakó *et al*, 2009). This being particularly true within tumours, where $A_{2B}R$ activation has been shown to promote metastasis (Desmet *et al*, 2013, Ntantie *et al*, 2013, Mittal *et al*, 2016). $A_{2B}R$ activation has also been found to have immunosuppressive effects (Hasakó *et al*, 2009, Morello and Miele, 2014), as well as promoting angiogenesis (Sorrentino *et al*, 2015). Due to these effects, targeting the $A_{2B}R$ has so far proved beneficial in mouse models of cancer (Cekic *et al*, 2012, Iannone *et al*, 2013, Wei *et al*, 2013, Mittal *et al*, 2016).

1.7.4 The adenosine A_3 receptor

The adenosine A_3 receptor (A_3R) is a $G\alpha_{i/o}$-coupled GPCR, activation of which results in a lowering of cellular cAMP levels. The A_3R has also been observed to mediate Ca^{2+} release (Fossetta *et al*, 2003) in a PTX-sensitive, G protein-dependent manner (Shneyvays *et al*, 2004). In addition, ERK1/2 activation can arise from A_3R-mediated signalling, also in a PTX-sensitive manner (Schulte and Fredholm, 2000, Hammarberg *et al*, 2003). To date there is no known crystal structure of the A_3R, however, several homology models have been generated (Cheong *et al*, 2013).

The A_3R has been found to be specifically expressed within the CNS, in cell types such as: glial cells (Ochaion *et al*, 2009), peripheral (Ru *et al*, 2011) and central neurons (Zhang *et al*, 2010), in addition to both the brain and spinal cord (Borea *et al*, 2015, Haeusler *et al*, 2015). As such it has become a target in the treatment of pain. Indeed, agonists targeting the A_3R have been shown to have analgesic actions (Janes *et al*, 2016), and may provide one method of treating pain without targeting the μ-opioid receptors.

1.8 The calcitonin receptor family

The CLR is a family B GPCR, which, as its name suggests, is closely related to the calcitonin receptor (CTR). They both respond to a series of peptide hormones, namely: calcitonin (CT, 32 amino acids), amylin (AMY, 37 amino acids), α and β calcitonin gene-related peptide (CGRP, 37 amino acids), adrenomedullin (AM, 52 amino acids) and adrenomedullin 2/Intermedin (AM2/IM, 53 amino acids). All of these ligands share a similar secondary structure, consisting of: an amidated C-termius, an α-helical region, and a N-terminus consisting of a six amino-acid ring structure (seven for CT) (Poyner *et al*, 2002). This homology at the secondary structure level is surprising considering that they display low homology at the amino acid level (Poyner *et al*, 2002). Of these agonists, all five have been identified as being able to activate the CTR, whilst only CGRP, AM and AM2 are able to activate the CLR (Albrandt *et al,* 1995, Armour *et al,* 1999, Leuthauser *et al*, 2000, Poyner *et al*, 2002, Kuwasako *et al*, 2003, 2004, Chang *et al,* 2004, Roh *et al*, 2004, Takei *et al,* 2004, Hay *et al*, 2005, Wunder *et al*, 2008, Qi *et al*, 2011, Bailey *et al*, 2012, Gingell *et al*, 2014). Of those agonists activating the CLR, CGRP and AM have been identified as being potent vasodilators, as well as being implicated in cardiovascular disease (Woolley and Conner, 2013). CGRP has also been observed to play key roles within migraine (Russo, 2015). However, to date little is known about the role of AM2 within the body. In order for these agonists to exert their effects they need to bind, and activate, the CLR, however, unlike all other GPCRs, the CLR is unable to traffic to the cell surface on its own. In order for surface expression to be achieved the CLR requires association of one of three molecular chaperone proteins called receptor activity-modifying proteins (RAMPs) (McLatchie *et al*, 1998). Formation of a RAMP-CLR heterodimer results in trafficking to the cell surface and also has implications upon downstream signalling observed from the CLR in response to CGRP, AM and AM2.

1.9 Receptor activity-modifying proteins

Receptor activity-modifying proteins (RAMPs) were initially identified, by Foord and colleagues, in attempts to clone the calcitonin-like receptor (CLR) (McLatchie *et al*, 1998). RAMPs are type 1 single span membrane proteins, that exist in three distinct isoforms in humans (although 5 exist in *Takifugu obscurus* (Nag *et al*, 2006)): RAMP1 (148 amino acids), RAMP2 (174 amino acids) and RAMP3 (148 amino acids). All three human RAMPs display similar α-helical structures, despite only sharing ~30% amino acid homology (Udawela *et al*, 2004).

To date, RAMP expression has been found in nearly all tissues that have been studied (McLatchie *et al*, 1998, Husmann *et al*, 2000, Sexton *et al,* 2001). Particularly high expression has been observed in: the cardiovascular system and skeletal muscle, RAMP1 in the pancreas, and RAMPs 2 and 3 in the lungs (McLatchie *et al*, 1998). They have also been shown to be expressed in tissues where no known RAMP interacting partner has been found, suggesting that they play a crucial role in the modulation of GPCR-mediated signalling, and may have, as yet, unknown functions. Whilst little is currently known about how RAMP levels are regulated, several studies have shown changes in RAMP expression within the cardiovascular system in various pathological states (Totsune *et al*, 2000, Cueille *et al*, 2002, Qi *et al*, 2003), indicating that RAMPs potentially provide one mechanism by which cells are able to respond to physiological stress.

1.9.1 RAMP-GPCR interactions

RAMPs were initially identified as interacting with the CLR (McLatchie *et al*, 1998). Since then, much research has been carried out into identifying new RAMP-GPCR interactions. Such receptors are predominantly found within family B, but interacting receptors have also been identified in families A and C. These interactions are summarised in Table 1.4.

Table 1.4: Known RAMP interacting GPCRs.

GPCR	Family	Interacting RAMP	Refs
GPR30	A	RAMP 3	Lenhart *et al*, 2013, Broselid *et al*, 2014
CLR	B	RAMPs 1, 2 and 3	McLatchie *et al*, 1998, Weston *et al*, 2016
CTR	B	RAMPs 1, 2 and 3	Poyner *et al*, 2002, Morfis *et al*, 2008
CRF1R	B	RAMP 2	Wootten *et al*, 2013
Glucagon	B	RAMP 2	Weston *et al*, 2014, 2015
PTH1	B	RAMP 2	Christopoulos *et al*, 2003
PTH2	B	RAMP 3	Christopoulos *et al*, 2003
Secretin	B	RAMP 3	Harikumar *et al*, 2009
VPAC1	B	RAMPs 1, 2 and 3	Christopoulos *et al*, 2003
VPAC2	B	RAMPs 1, 2 and 3	Wootten *et al*, 2013
CaSR	C	RAMPs 1 and 3	Huang and Miller, 2007, Desi *et al*, 2014.

1.9.2 The role of RAMPs in receptor trafficking and internalisation

It was initially identified that RAMPs play roles in receptor glycosylation, as well as regulating trafficking to the plasma membrane; indeed, CLR can only reach the cell surface in conjunction with RAMPs (McLatchie *et al*, 1998). However, more recently, it has been found that receptors, which can be functionally expressed without an associating RAMP, can also interact (Poyner *et al*, 2002, Christopoulos *et al*, 2003, Morfis *et al*, 2008, Harikumar *et al*, 2009, Wootten *et al*, 2013, Weston *et al*, 2014, 2015). Thus, RAMPs are not absolutely required to allow their GPCR partner to be trafficked to the cell surface. However, RAMPs require interaction with an associating GPCR for their own expression at the cell surface (Sexton *et al*, 2009). Once a RAMP-GPCR oligomer has formed, in the ER/Golgi apparatus, it is thought that they stay associated for the life of the receptor (Kuwasako *et al*, 2000, Hilairet *et al*, 2001a, 2001b). As this is a non-dynamic process, it further shows that RAMPs do not exist purely for receptor trafficking or localisation. In addition to roles in trafficking, it has also been identified that they may play roles in influencing receptor internalisation; however, little is know about this process (Kuwasako *et al*, 2006).

1.9.3 The effects of RAMPs upon receptor pharmacology

One of the most interesting aspects of RAMP-GPCR interactions is that they have an ability to modulate the pharmacology of their associated GPCR. Indeed, these interactions can have such dramatic effects that they form distinct receptor phenotypes, dependent upon the interacting RAMP. In some instances, RAMP association can lead to the loss of ligand-receptor interaction, for example RAMP2 abolishes GLP-1 interaction with the GCGR (Weston *et al*, 2015). RAMPs can also induce changes in both: ligand affinity and potency (Reviewed by Hong *et al*, 2012), as well as modulating G protein coupling (Udawela *et al*, 2006a).

These effects have been mapped to the individual domains of the RAMPs; whereby the N-terminus has implications for ligand binding, with the C-terminal domain influencing receptor 'output' (Udawela *et al*, 2006a). Further, the transmembrane domain has been implicated in forming interactions with the GPCR (Udawela *et al*, 2006b).

All these effects exerted by RAMPs upon GPCRs provide cells with a mechanism whereby they can modulate the pharmacology of the receptors they express, allowing differing effects to be exerted by one receptor subtype. Thus, there is growing interest in the possibility that many family B GPCRs may be modulated by RAMPs, and that these interactions may alter signalling induced by various ligands, thereby further contributing to pathway bias at these receptors.

1.9.4 The effects of RAMP-CLR interactions

The CLR on its own is unable to traffic to the cell surface, and cannot bind any known ligand. However, upon association with any of the three RAMPs, a functional receptor is formed (McLatchie *et al*, 1998). This association results in the formation of three distinct receptor phenotypes, each of which can be activated by CGRP, AM and AM2. Dimerisation between RAMP1 and the CLR forms the CGRP receptor (CGRPR); RAMP2-CLR, the adrenomedullin (AM_1) receptor; and RAMP3-CLR, the adrenomedullin 2 (AM_2) receptor (Figure 1.11) (McLatchie *et al*, 1998, Poyner *et al*, 2002). To date, it is not know if these RAMP-CLR heterodimers can bind the other calcitonin family peptides, namely CT or amylin.

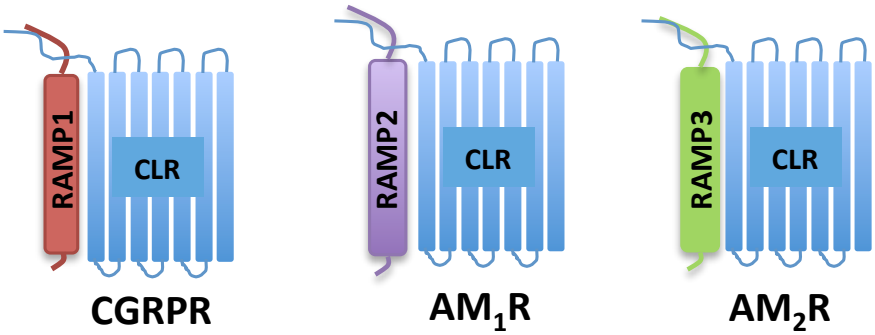

Figure 1.11: RAMP-CLR heterodimers form distinct receptor phenotypes.

The CLR is able to interact with all three RAMPs. RAMP1-CLR forms the CGRP receptor, with CGRP being the cognate ligand. RAMP2-CLR forms the AM_1 receptor, with AM being the cognate ligand. RAMP3-CLR forms the AM_2 receptor, with AM also being the cognate ligand.

All RAMP-CLR dimers display an ability to couple to $G\alpha_s$, resulting in the downstream production of cAMP, in response to either CGRP, AM or AM2 (Poyner *et al*, 2002, Hay *et al*, 2003, Hong *et al*, 2012, Weston *et al*, 2016). In addition, some evidence exists for a $G\alpha_{i/o}$ component for the CLR-based receptors, when stimulated with CGRP, as indicated by PTX-sensitivity in several investigations (Kim, 1991, Wiley *et al*, 1992, Main *et al*, 1998, Disa *et al*, 2000). This has also been observed for AM stimulation (Kuwasako *et al*, 2010). Despite this evidence, little follow up work has been undertaken to confirm signalling via $G\alpha_{i/o}$. There is also evidence to suggest that RAMP-CLR heteromers can signal via $G\alpha_{q/11}$ (Hay *et al*, 2003, Dickerson, 2010), as well as activating ERK1/2 (Yu *et al*, 2009, Wang *et al*, 2009), although this has not been fully described.

Study of CLR, and CTR, pharmacology has predominantly utilised a subset of the aforementioned ligands against each receptor. However, considering the similarity between each of the six ligands, and the promiscuity of the ligands at each receptor subset (CTR or CLR-based), it would not be surprising if those ligands traditionally associated with CLR-based receptors would activate the CT receptors, and vice-versa. To date, only one study has looked at these ligands upon all receptors; however, this only focused upon CT, CGRP, AM and AM2. This identified

that all four ligands were able to bind to, and activate, the CT receptors with varying potencies (Hay *et al*, 2005).

Differing RAMP associations have effects upon CLR pharmacology. The predominant effect observed in published literature is that the differing RAMPs modulate the potency of CGRP, AM and AM2 upon the CLR, in terms of $G\alpha_s$-mediated signalling (Table 1.5). In the case of the RAMP1-CLR, CGRP is seen to be the most potent ligand, with AM and AM2 being approximately equipotent, thus CGRP is termed the cognate ligand for this receptor. Whilst for RAMP2-CLR heteromers, a general rank order of potency of AM > AM2 > CGRP, is observed, which is similar to that seen with RAMP3. Thus, for RAMP2/3-CLR complexes, AM is the cognate ligand.

As can be seen, the RAMPs greatly modulate CLR-mediated signalling. However, the above data is all obtained from experiments measuring cAMP production. To date, little focus has been paid to other pathways. Thus, there is the potential for unexplored bias at these receptors to be uncovered: something that this thesis aims to address. An in-depth investigation of this nature will allow us to quantify bias, which may ultimately aid in the design of drugs targeting specific CLR-activated pathways.

Table 1.5: pEC_{50}[a] of the calcitonin peptide family of ligands upon RAMP-CLR heteromers.

Ligand	CLR-based receptor		
	RAMP1-CLR[1,2-7]	**RAMP2-CLR**[1,4,7]	**RAMP3-CLR**[1, 2-6]
CT	ND	ND	ND
Amylin	ND	ND	ND
αCGRP	9.5-10.1	6.4-7.7	6.8-8.0
AM	8.0-9.8	8.8-9.9	8.0-9.9
AM2	8.0-9.1	7.5-8.3	8.7-10.1

[a] Negative logarithm of agonist concentration producing half-maximal response
ND – Not determined

References; [1]Hay *et al*, 2005, [2]Qi *et al*, 2011, [3]Roh *et al*, 2004, [4]Takei *et al*, 2004, [5]Chang *et al*, 2004, [6]Wunder *et al*, 2008, [7]Poyner *et al*, 2002.

1.10 Aims

This work aims to investigate and quantify biased agonism for both adenosine receptors, and the calcitonin-like receptor. In terms of adenosine receptors, this will focus upon the **A_1R** and **A_{2A}R**, whilst work upon the **CLR** will focus upon all three RAMP-CLR heteromers.

Work focusing on the adenosine receptors relates directly to projects involved in developing novel, selective agonists, to each receptor. With this I aim to:

- Quantify the extent of biased agonism for A_1R-selective agonists
- Identify A_{2A}R-selective agonists
- Quantify biased agonism of A_{2A}R-selective agonists

Work relating to the CLR will aim to investigate the effects of RAMPs upon:

- CLR-mediated cAMP production
- CLR-mediated $G\alpha_{i/o}$ activation
- CLR-mediated mobilisation of intracellular Ca^{2+} and determine its underlying mechanism
- Biased agonism

Investigative work will als be performed to attempt to uncover the role of ICL1 in RAMP1-CLR-mediated signalling and activation.

Chapter 2
Materials and Methods

2.1 Materials

2.1.1 General laboratory reagents

All general laboratory reagents were supplied by Sigma-Aldrich (Poole, Dorset, UK) and of analytical grade, unless specifically stated. YM-254890 was supplied by Alpha Laboratories (Hampshire, UK). Ionomycin and Rolipram were purchased from Cayman chemicals (Michigan, USA).

2.1.2 Ligands

Human (h) α-CGRP, hAM, hAM2 (1-47) were purchased from Bachem (Bubendorf, Switzerland) and dissolved in dH_2O to 1 mM, containing 0.1% bovine serum albumin (BSA). Ionomycin was dissolved in ethanol to produce 10 mM stocks. Phorbol 12-myristate 13-acetate and forskolin were prepared in dimethyl sulphoxide (DMSO), to 10 mM. 5'-N-Ethylcarboxamidoadenosine (NECA), adenosine, 2-Chloro-N^6-cyclopentyladenosine (CCPA), and CGS21680 were purchased from Tocris Bioscience (Wiltshire, UK) and made to 10 mM in DMSO or dH_2O (for adenosine). All compounds tested against the A_1R (Cmpd prefix) were synthesised by Dr. J. Hemmings (University Bern, Switzerland), whilst those with a TZQ prefix were purchased from Ambinter (Orleans, France), and made to 10 mM stocks in DMSO.

2.1.3 Bacterial strains

Plasmid amplification was performed using DH5α *Escherichia coli* (*E. coli*) from Stratagene (Cambridge, UK). DH5α genotype: *supE44 hsdR17 endA96 thi-1 relA1 recA1 gyrA96.*

2.1.4 Growth media

S. cerevisiae strains were routinely grown in either yeast extract (YE) media (Table 2.1), or synthetic dropout media lacking uracil (SD-URA) (Table 2.2). Plates were prepared as per liquid media with the addition of 15 g/l select agar. All media were made through dissolving the required reagents in reverse osmotically (RO) filtered water, and autoclaved prior to first use.

Dulbecco's modified Eagle's medium/F-12 (DMEM/F-12) and HAM's F-12 were supplied by Life Technologies (Paisely, UK) and supplemented with 10% heat inactivated fetal bovine serum (FBS), purchased from Sigma-Aldrich (Poole, Dorset, UK).

Table 2.1: Yeast extract media (YE) (per litre).

Yeast extract	5 g
Glucose	30 g

Table 2.2: Synthetic dropout media (SD) (per litre).

Yeast nitrogen base (without amino acids)	6.7 g
Glucose	20 g
Amino acid mix (Table 2.3)	1.5 g
Selection amino acid mix (Table 2.4)	0.5 g

Table 2.3: Amino acid mix.

L-alanine	2 g
L-arginine	2 g
L-asparagine	2 g
L-cysteine	2 g
L-glutamine	2 g
L-glutamate	2 g
L-glycine	2 g
L-isoleucine	2 g
L-lysine	2 g
L-phenylalanine	2 g
L-proline	2 g
L-serine	2 g
L-threonine	2 g
L-tryptophan	2 g
L-tyrosine	2 g
L-valine	2 g
Myo-inositol	2 g
Para-amino benzoic acid	0.4g

Table 2.4: Select amino acid mix.

Adenine	2 g
L-histidine	2 g
L-leucine	4 g
L-methionine	2 g

2.1.5 *Saccharomyces cerevisiae* strains

Standard nomenclature has been used throughout this thesis to describe the genotypes of *S. cerevisiae* strains used (Table 2.5). Gene deletions are denoted *gpa1Δ*, in the case of deletion of the *gpa1* locus. Gene replacement is shown as *gpa1Δ*::*ADE2*, indicating that *gpa1* has been deleted and replaced with *ADE2*. Whilst replacement using G418 resistance is indicated: *ste2*::$G418^R$.

In order to utilise *S. cerevisiae* for the study of GPCR signalling, their endogenous GPCR, STE2, is deleted. The *gpa1* locus is also deleted, preventing expression of GPA1 (the yeast Gα protein). This is then replaced with genes encoding yeast-human chimeric G proteins that have the final 5 C-terminal amino acids of human Gα proteins transplanted onto GPA1 (Brown *et al,* 2000). To allow measurement of receptor activation, the pheromone response gene, *fus1*, promoter has been linked to *his3* and *lacZ.* Thus, receptor activation leads to increased expression of *his3* (encoding imidazoleglycerol-phosphate dehydratase, required for histidine biosynthesis), as well as *lacZ,* resulting in increased expression of *β*-galactosidase (Brown *et al*, 2000). Output from this system can therefore be measured as growth in media lacking histidine, or via a *β*-galactosidase assay.

To increase output in *β*-galactosidase assays, cell-cycle arrest in response to pheromone has been inhibited via the deletion of *far1*. *far1* encodes FAR1, a cyclin-dependent kinase interacting protein, which leads to cell-cycle arrest (Tyers and Futcher, 1993). In order to further increase sensitivity, the gene encoding endogenous RGS proteins (SST2) has also been deleted (Brown *et al*. 2000).

S.cerevisiae are able to undergo mating type switching (between MATa and MATα). In order to prevent cells switching to MATα (which express another GPCR, STE3), all cells are *MATaΔ*. To allow selection for cells

expressing both the required GPCR, and chimeric G protein, all strains have *his3*, *trp1* and *ura3* deleted, as well as the gene encoding arginine permease (*can1)*, thereby preventing amino acid uptake (Brown *et al*, 2000). This allows amino acids to be used as nutritional selectors.

To enable expression of the adenosine A_1, A_{2A} or A_{2B} receptors, *ADORA1*, *ADORA2A*, or *ADORA2B,* respectively, have been integrated at the *ura3* loci, utilising p426-GPD (Knight *et al*, 2016, Appendix 1).

Table 2.5: *Saccharomyces cerevisiae* strains.

Strain	Genotype	Source
SC13	*MATa his3 leu2 trp1 ura3 can1 gpa1Δ::ADE2 fus1::FUS1-HIS3 LEU2::FUS1-lacZ far1Δ::ura3Δ sst2Δ::ura3Δ ste2Δ::G418^R TRP::GPA1/$G_{αi1/2(5)}$ URA3::ADORA1*	Knight *et al*, 2016
SC217	*MATa his3 leu2 trp1 ura3 can1 gpa1Δ::ADE2 fus1::FUS1-HIS3 LEU2::FUS1-lacZ far1Δ::ura3Δ sst2Δ::ura3Δ ste2Δ::G418^R TRP::GPA1/$G_{αs(5)}$ URA3::ADORA2A*	Knight *et al*, 2016
SC224	*MATa his3 leu2 trp1 ura3 can1 gpa1Δ::ADE2 fus1::FUS1-HIS3 LEU2::FUS1-lacZ far1Δ::ura3Δ sst2Δ::ura3Δ ste2Δ::G418^R TRP::GPA1/$G_{αs(5)}$ URA3::ADORA2B*	Knight *et al*, 2016

2.1.6 Plasmids and expression vectors

Plasmids and expression vectors used within this thesis are displayed in Table 2.6. Whilst CLR ICL1 mutants, pIRES-RAMP1-SNAP-CLR (X), are displayed in Table 2.7, where X represents each substitution within the table.

Table 2.6: Plasmids used within this thesis.

Plasmid	Source
pcDNA3.1-GFP	S. Allen
pcDNA3.1-cMyc-CLR-GFP	M. Bouvier
pcDNA3.1-HA-CLR	H. Watkins
pcDNA3.1-A_1R	cDNA resource centre
pcDNA3.1-A_{2A}R	cDNA resource centre
pcDNA3.1-FLAG-RAMP1	Wootten *et al*, 2013
pcDNA3.1-FLAG-RAMP2	Wootten *et al*, 2013
pcDNA3.1-FLAG-RAMP3	Wootten *et al*, 2013
pIRES-RAMP1-SNAP-CLR(WT)	Heptares therapeutics

Table 2.7: CLR ICL1 mutant vectors generated by Heptares therapeutics.

Substitution	WT Residue							
	Y165	**F166**	**K167**	**S168**	**L169**	**S170**	**C171**	**Q172**
A	Y165A	F166A	K167A	S168A	L169A	S170A	C171A	Q172A
C	Y165C	F166C	-	S168C	L169C	S170C	-	Q172C
E	Y165E	F166E	K167E	S168E	L169E	S179E	C171E	Q172E
F	Y165F	-	K167F	S168F	L169F	S170F	C171F	Q172F
G	Y165G	F166G	K167G	S168G	L169G	S170G	C171G	Q172G
H	Y165H	F166H	K167H	S168H	L169H	S170H	C171H	Q172H
I	Y165I	-	K167I	S1768I	L169I	S170I	C171I	Q172I
M	Y165M	F166M	K167M	S168M	L169M	S170M	C171M	Q172M
Q	Y165Q	-	K167Q	S168Q	L169Q	-	C171Q	-
R	Y165R	F166R	K167R	S168R	L169R	S170R	C171R	Q172R
W	Y165W	F166W	K167W	S168W	L169W	S170W	C171W	Q172W

pIRES-RAMP1-SNAP-CLR(X) – where X represents either wild type CLR, or each mutant shown.
- indicates mutant not generated.

2.2 Methods

2.2.1 E. coli transformation

Competent DH5α *E. coli* were transformed by addition of 100-1000 ng DNA to 100 µl of cells, kept on ice for 5 minutes, followed by heat shock for 2 minutes at 37°C, and then placed on ice for a further 5 minutes. 100 µl Luria broth (LB) was then added and cells allowed to recover for 30-60 minutes at 37°C with constant agitation, before growth in liquid LB or on LB-agar plates containing either ampicillin (100 mg/ml) or kanamycin (50 mg/ml), as appropriate.

2.2.2 Plasmid amplification and purification

All plasmids used in this study were prepared through transformation of *E. coli*, followed by growth in 5-100 ml liquid LB cultures containing antibiotics, as required, overnight at 37°C with constant agitation. DNA was then purified using either a QIAprep maxiprep or miniprep kit (Qiagen, Manchester, UK), as per manufacturers protocols, with DNA eluted and resuspended in dH_2O.

2.2.3 Double stranded DNA sequencing

Prior to first use in experiments, all DNA was sequenced with oligonucleotides binding specific regions of the vector to confirm that the plasmid contained the correct insert, and that no mutations had been introduced. This was performed using Sanger sequencing outsourced to either GATC biotech (Constance, Germany) or the Department of Biochemistry (University of Cambridge, UK).

2.2.4 *Saccharomyces cerevisiae* culture

All *S. cerevisiae* stocks were stored at -80°C. Upon first use, an aliquot was plated onto the required media, and incubated at 30°C for 16-24 hours. Cells were then re-streaked onto fresh plates and grown as previously. These were then stored at 4°C for up to one week. Prior to assay, 10 ml cultures were inoculated in SD-URA media, and grown for 16 hours, at 30°C with constant agitation.

2.2.5 β-galactosidase assays

S. cerevisiae cells strain expressing adenosine receptors were grown as described and *β*-galactosidase activity determined in a similar manner to Hoffman *et al* (Hoffman *et al,* 2002). On the day of assay, cultures were diluted 1:10 in SD-URA media, and grown for 8 hours. These cultures were then further diluted 1:100 and seeded onto 96 wells plates, and stimulated with a range of ligand concentrations (100 µM – 10 pM) for 16 hours, at 30°C. 20 µl of cells were then added to 250 µl Z buffer (Table 2.8), and incubated at 30°C for 90 minutes. The reaction was then terminated by addition of 50 µl 2M Na_2CO_3. *β*-galactosidase activity was determined using a mithras LB940 plate reader, reading OD_{430}.

Table 2.8: Z-buffer

Na_2HPO_4	60 mM
NaH_2PO_4	42 mM
KCl	10 mM
$MgSO_4$	1 mM
β-mercaptoethanol	50 mM
Chloroform	0.5% (v/v)
SDS	0.005% (w/v)
o-nitophenyl-D-galactopyranoside	0.067% (w/v)

In order to account for variable cell number, measurements were also taken to determine cell density at OD_{620}. β-galactosidase activity was thus calculated as:

$$Activity = \frac{OD_{430} - OD_{620}}{OD_{620}}$$

2.2.6 Mammalian cell culture and transfection

HEK 293 cells, gifted by Prof. C. Taylor (University of Cambridge, UK), were grown in DMEM/F-12 supplemented with 10% FBS, at 37°C in a humidified atmosphere containing 5% CO_2. CHO-K1 cells, gifted by Dr E. St. John Smith (University of Cambridge, UK), were cultured in Ham's F-12 nutrient mix, supplemented with 10% FBS, in the same conditions as HEK 293 cells. CHO-K1 cells stably expressing the A_3R (CHO-A_3R) were kindly donated by Dr. K-N. Klotz (University of Wuerzburg, Germany), and grown as per CHO-K1 cells.

24 hours prior to transfection, cells were seeded onto 24 well plates. All cells were transfected with 250 ng total DNA, utilising either Fugene6 (Roche), or polyethylenimine (PEI), at a 1:3 (w/v) DNA:Fugene/PEI ratio. Where required, a 1:1 pcDNA3.1-FLAG-RAMP:pcDNA3.1-cMyc-CLR-GFP, or pcDNA3.1-HA-CLR, ratio was utilised. Cells were then grown for 24-48 hours prior to assay and, where appropriate, treated with 200 ng/ml pertussis toxin (PTX) 16 hours before assaying, in order to uncouple $G\alpha_{i/o}$ subunits from the GPCRs, through ADP-ribosylation of the C-terminus of the G proteins (West *et al*, 1985).

2.2.7 Generating a CHO-K1 cell line stably expressing the A_1R

CHO-K1 cells, transfected with pcDNA3.1-A_1R, were cultured in 24 well plates in Ham's F-12 nutrient mix, supplemented with 10% FBS, and 800 µg/ml G418 (Sigma-Aldrich, Dorset, UK), in order to select for transfected

cells. G418-containing media was replaced every 48 hours. Wells that attained 100% confluency were sub-cultured into 24 well plates, at a ratio of 1:4 (Cell suspension: Ham's F-12 media). Cells were then grown to 80% confluency and tested for their ability to inhibit forskolin-mediated cAMP production, in response to NECA stimulation. Responding cells were further cultured in the presence of 800 µg/ml G418, and frozen stocks made by gradually freezing to -80°C in FBS + 10% DMSO, before being stored in the vapour phase of liquid nitrogen.

2.2.8 cAMP accumulation assays

Transfected cells were brought to single cell suspension using a solution of trypsin containing 0.05% EDTA. Cells were then washed with phosphate-buffered saline (PBS), followed by resuspension in stimulation buffer (PBS containing 0.1% BSA, and either 0.5 mM 3-isobutyl-1-methylxanthine (IBMX) or 25 µM rolipram). Assays were then performed using a LANCE® cAMP detection kit (PerkinElmer, Boston, MA), as per manufacturer's protocol, with 2000 cells per well of a 384-well white optiplate (PerkinElmer, Boston, MA), stimulated with a range of ligand concentrations (1 pM – 1 mM) for 8 minutes, and cAMP levels measured using a Mithras LB 940 multimode microplate reader (Berthold technologies, Germany) (excitation: 340 nm, emission: 665 nm). Where receptors that couple to $G\alpha_{i/o}$ (A_1R and A_3R) were assayed, cells were co-stimulated with ligand and 10 µM forskolin (to stimulate cAMP production), for 30 minutes. All assays were run in conjunction with a standard curve and a dose-response curve for forskolin. Where appropriate, cells were treated overnight with 200 ng/ml PTX to inhibit $G\alpha_{i/o}$-mediated signalling.

The LANCE® kit is a time-resolved fluorescence energy transfer (TR-FRET) immunoassay, that utilises Alexa Fluro® 647-labelled cAMP specific antibodies. A complex of biotin-cAMP and europium-labelled streptavidin compete with cAMP produced by cells, for binding to this

antibody (Figure 2.1). In the absence of free cAMP, excitation at 340 nm causes an energy transfer from the biotin-europium complex to the Alexa dye, resulting in an emission at 665 nm (Figure 2.1). Thus, in the presence of cAMP produced by cells, a reduction in signal intensity at 665 nm is observed (Figure 2.1). The use of PDE inhibitors in assays serves to prevent the breakdown of cAMP, thereby increasing the range of signal observed. For assays involving adenosine receptors, rolipram, a selective PDE 4 inhibitor, was used, whilst all other assays utilised IBMX, a pan-PDE inhibitor.

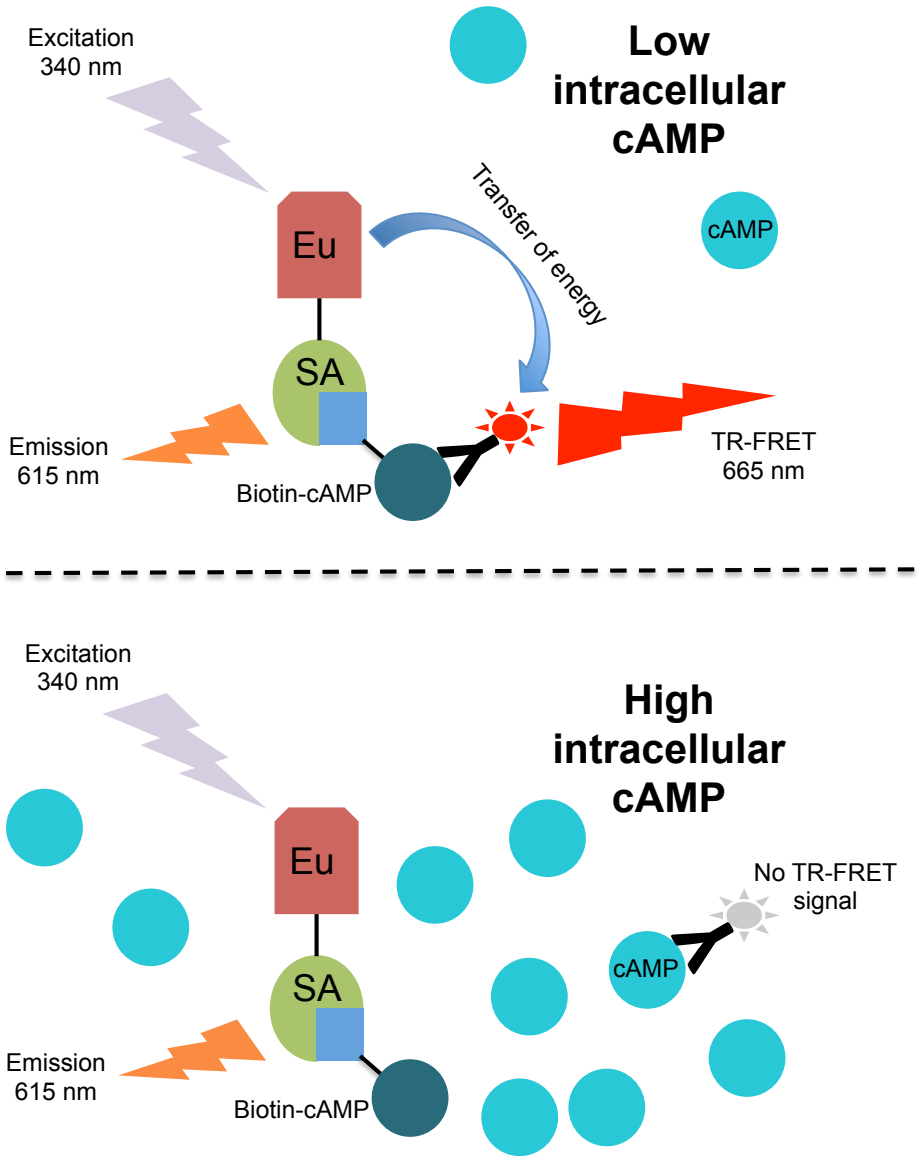

Figure 2.1: LANCE® cAMP accumulation assay.

Alexa Fluro® 647-labelled cAMP specific antibodies compete for binding to free cAMP, or a complex of europium (Eu)-labelled streptavadin (SA) and biotin-cAMP. Upon excitation at 340 nm, the Eu-SA fluoresces at 615 nm. In the presence of low intracellular cAMP levels, there is an energy transfer from this complex to the Alexa Fluro® 647 antibody, exciting it, resulting in a TR-FRET emission at 665 nM. In the presence of high intracellular cAMP levels, the Alexa Fluro® 647 binds free cAMP, preventing TR-FRET occurring, resulting in a decreased emission at 665 nm.

2.2.9 Intracellular calcium mobilisation assays

Transfected cells were seeded onto a black, clear bottomed, 96 well plates and grown for 24 hours, until confluent. The media was then removed and cells washed with Hank's balanced salt solution (HBSS), followed by addition of 50 µl of 10 µM Fluo-4/AM (Invitrogen, Paisely, UK) containing 2.5 mM probenecid, in order to prevent dye leakage. These were then incubated at room temperature for 1 hour, and washed a further 3 times in HBSS. Prior to assaying, HBSS was replaced with 100 µl Ca^{2+}-free HBSS, and the plate transferred to a Mithras LB 940 multimode microplate reader. Agonist injection occurred robotically and fluorescence reading occurred immediately (excitation: 485 nm, emission: 535 nm) at intervals of 0.5 s for 120 s. Where appropriate, cells were either pre-treated with 200 ng/ml PTX for 16-18 hours, or 100 nM YM-254890 for 30 min, to inhibit either $G\alpha_{i/o}$- or $G\alpha_{q/11}$-mediated signalling, respectively. All assays contained at least a single well that was stimulated with 100 µM ionomycin, to account for day-to-day cell variability, and differential dye loading between experiments.

2.2.10 ERK1/2 assays

ERK1/2 phosphorylation was measured using a Phospho-ERK1/2 (Thr202/Tyr 204) kit (Cisbio, Codolet, France). Transfected cells were serum starved overnight prior to assaying for ERK1/2 activation, in an attempt to lower basal pERK1/2 levels, and gain a larger signalling window. These cells were then harvested using trypsin as described, followed by the addition of an equal volume of serum-free media. Cells were then washed in HBSS, followed by seeding 35,000 cells per well, of a white 384-well optiplate (PerkinElmer, Boston, MA). These were then stimulated for 5 minutes, with ligands ranging from 1 µM – 1 pM. Cells were then lysed using lysis buffer containing Triton™ X-100 (0.25% w/w) and sodium orthovanadate (0.25% w/w), for 30 min. Finally, a mixture of pERK1/2 d2 and pERK1/2 cryptate antibodies (vol/vol) were added and

incubated in the dark for 2 hours, at room temperature. Plates were then read using a Mithras LB 940 multimode microplate reader (excitation: 340 nm, emission: 665 nm and 620 nm). ERK1/2 phosphorylation is then expressed as a ratio between the signals observed at 665 nm and 620 nm. On all assays, a phorbol 12-myristate 13-acetate (PMA) dose-response curve (100 μM – 100 pM) is also generated to allow for day-to-day variability of cells.

2.2.11 Molecular and structural analysis of GPCRs

Structures of the GCGR (PDB – 5XEZ (Zhang *et al*, 2017)) and the GLP-1R (PDB – 5VEX (Song *et al*, 2017), 5VAI (Zhang *et al*, 2017)) were analysed using the PyMOL molecular graphics system v1.7.4.5 (Schrödinger, LLC), whilst structural alignments of ICL1 and helix 8 were performed using gpcrdb.org.

2.2.12 Data analysis

Data obtained from all experiments was analysed using GraphPad Prism 6.0e (San Diego, CA). For cAMP assays, values were converted to cAMP concentrations, through interpolation to a standard curve run in parallel to the assay. For intracellular calcium mobilisation assays, maximum fluorescence intensity was calculated using 5 point smoothing and corrected for background fluorescence. Whilst for ERK1/2 assays, fluorescence ratios were calculated as described. These values were then utilised for construction of concentration-response curves. To allow for the stochastic nature of biological systems, all concentration-response curves were normalised to either: 100 μM forskolin (cAMP assays), 10 μM ionomycin (calcium mobilisation assays) or 100 μM PMA (pERK1/2 assays). All data were fitted using a three-parameter logistic equation (Equation 2.1) to obtain pEC_{50}, and E_{max} values.

Equation 2.1: Three-parameter logistic equation

$$Y = Basal + \frac{(E_{max} - Basal)}{1 + 10^{(\log EC_{50} - x)}}$$

Equation 2.2: Operational model of pharmacological agonism (Black and Leff, 1983)

$$Response = Basal + \frac{E_{max} - Basal \cdot \tau \cdot [Agonist]}{\tau \cdot [Agonist] + ([Agonist] + Ka)}$$

Where necessary, the operational model of pharmacological agonism (Equation 2.2) (Black and Leff, 1983) was implemented to calculate Log τ (efficacy) and the equilibrium dissociation constant (pKa). These were then utilised to quantify signalling bias through calculating the transduction ratio (τ/Ka). To determine signalling bias, relative to a given pathway, the change in transduction ratios for a given pathway was calculated relative to a reference pathway (Baltos *et al*, 2016) (Equation 2.3).

Equation 2.3: Relative bias

$$\Delta Log\left(\frac{\tau}{Ka}\right) = Log\left(\frac{\tau}{Ka}\right)_{Pathway} - Log\left(\frac{\tau}{Ka}\right)_{Ref.Pathway}$$

To allow for system-dependent effects upon the responses observed, values were calculated relative to the cognate ligand (Figueroa *et al*, 2009) in each instance (Equation 2.4): CGRP for RAMP1-CLR, AM for RAMP2/3-CLR, and NECA for the A_1R, or CGS21680 for the $A_{2A}R$.

Equation 2.4: Transduction ratio

$$\Delta\Delta Log\left(\frac{\tau}{K_a}\right) = \Delta Log\left(\frac{\tau}{K_a}\right)_{ligand} - \Delta Log\left(\frac{\tau}{K_a}\right)_{cognate\ ligand}$$

This can then be expressed as a bias factor (Baltos *et al*, 2016) (Equation 2.5).

Equation 2.5: Bias factor

$$Bias\ factor = 10^{\Delta\Delta Log\left(\frac{\tau}{Ka}\right)}$$

Statistical significance was calculated using a: one-way ANOVA with either a Bonferroni's correction, or Dunnet's post-test; or a Student's t-test, as appropriate, $p < 0.05$ was considered significant.

Chapter 3
Characterising adenosine receptor pharmacology

3.1 Introduction

The adenosine receptor (AR) family consists of four distinct receptor subtypes, the: A_1R, $A_{2A}R$, $A_{2B}R$ and A_3R (Fredholm *et al*, 2011), all belonging to the rhodopsin-like family: family A. Each of the different subtypes bind, and respond to, the purinergic nucleoside, adenosine, resulting in differing effects upon a cell. The A_1R and A_3R are both predominantly coupled to inhibitory $G\alpha_{i/o}$ proteins, serving to inhibit the activity of adenylate cyclase and subsequently lower intracellular levels of cAMP. Opposing the action of these receptors are the $A_{2A}R$ and $A_{2B}R$, which both predominantly couple to $G\alpha_s$, resulting in increased adenylate cyclase activity upon receptor activation. The ARs have been observed to be expressed in a wide variety of tissue types including, but not limited to, the central and peripheral nervous system, the colon, liver and lungs, as well as cardiac tissue (Jacobson and Gao, 2006, Cheong *et al*, 2013). The roles played by all four AR subtypes are as equally diverse as their expression patterns, with AR activity being implicated in pathological states such as Alzheimer's, Parkinson's, Huntington's and various cardiovascular diseases, as well as cancer, sleep disorders and inflammation (Fredholm *et al*, 2005, Chen *et al*, 2007, Dale and Frenguelli, 2009, Sharma *et al*, 2010, Sachdeva and Gupta, 2013, Allard *et al*, 2016). With the ARs having such a diverse range of expression, and playing roles in so many disease states, there is a need to develop pharmaceuticals that will allow intervention and potential treatment. In order to do this it is necessary to develop compounds that are selective for a single AR subtype, and to quantify the extent of pathway bias observed by these compounds, in order to be able to produce drugs with

reduced side-effects and improved safety profiles. Therefore, the work presented in this chapter pertains to the development and characterisation of agonists for the A_1R and the $A_{2A}R$.

3.2 Identifying a suitable cell line for investigating adenosine receptors

It is essential to perform investigations into AR pharmacology in a system that has a null background, with regards to endogenous AR expression. It was initially proposed to utilise HEK 293 cells: thus, to test for endogenous responses to AR agonists, HEK 293 cells, transfected with pcDNA3.1-GFP, were stimulated with NECA (concentrations ranging 100 μM – 100 pM) and cAMP accumulation measured (Figure 3.1A). This indicated that HEK 293 cells endogenously express a receptor(s) that leads to the activation of adenylate cyclase, in response to NECA stimulation. As a consequence, it was not possible to utilise HEK 293 cells in experiments pertaining to AR pharmacology. Thus, CHO-K1 cells were analysed to determine if they would provide an appropriate, AR-null, background. As with HEK 293 cells, pcDNA3.1-GFP-transfected CHO-K1 cells were stimulated with NECA and cAMP accumulation measured. No increase in cAMP, above basal levels, was observed (Figure 3.1B), and as such there could be confidence that these cells do not endogenously express a functional $G\alpha_s$-coupled receptor that responds to NECA. It was further sought to determine if CHO-K1 cells expressed any functional $G\alpha_{i/o}$-coupled receptors that may respond to NECA. To achieve this cells were co-stimulated with both NECA and 1 μM forskolin. The forskolin served to promote cAMP production, via activation of adenylate cyclase, which would then be inhibited by NECA, if any $G\alpha_{i/o}$-coupled adenosine receptors were being expressed. Upon NECA stimulation no reduction in intracellular cAMP levels was observed (Figure 3.1B), thus there was confidence that there would be no observable endogenous responses in assays when stimulating with AR agonists. Hence, all experiments pertaining to AR pharmacology were performed using CHO-K1 cells.

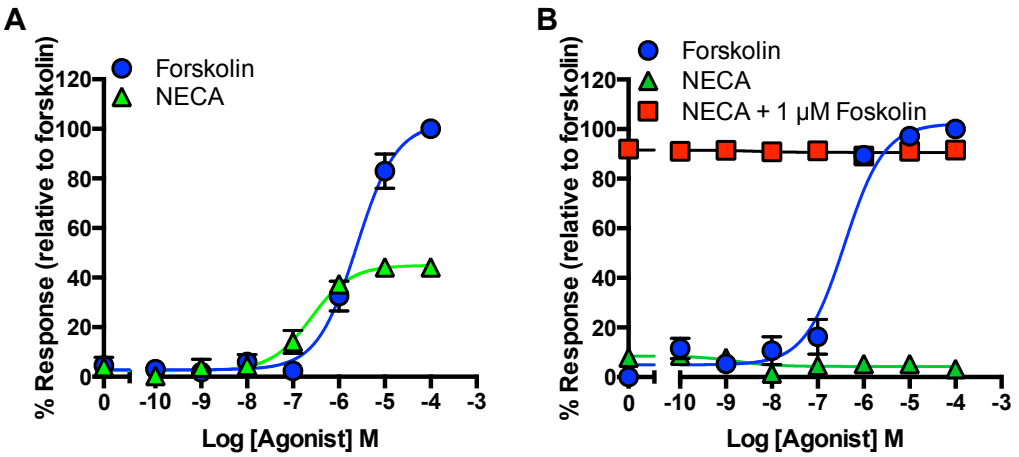

Figure 3.1: HEK 293 cells endogenously express adenosine receptors, which are absent in CHO-K1 cells.

Treatment of HEK 293 cells with NECA results in elevation of intracellular cAMP (A). CHO-K1 cells treated with NECA, or co-stimulated with NECA and 1 µM forskolin, failed to generate a response. Data represented as a percentage of the cAMP produced upon treatment with 100 µM forskolin, ± SEM, of 3 replicates.

3.3 Adenosine A_1 receptor

The work pertaining to characterising A_1R agonists in this chapter initially arose due to a collaborative project between Professor M. Lochner (University of Bern, Switzerland) and ourselves. The focus of this project was to develop novel AR agonists, with an aim to produce agonists displaying selectivity for the A_1R. This was achieved by utilising the structures of NECA and adenosine upon which to design new compounds. Novel compounds were then synthesised by creating a series of N^6-bicyclic and N^6-(2-hydroxy)-cyclopentyl derivatives of adenosine and NECA (Figure 3.2). A previous PhD student in our laboratory screened these compounds in yeast expressing either the A_1R (SC13, Table 2.5), A_{2A}R (SC217, Table 2.5), or the A_{2B}R (SC224, Table 2.5). This identified compounds (Cmpds) 20 and 21, to be non-selective, acting as agonists against all three ARs tested, whilst Cmpds 5, 6, 16 and 18 displayed selectivity for the A_1R over the other AR subtypes investigated (Knight *et al*, 2016). This work, however, lacked any investigation into the action of these compounds upon the A_3R as, to date, there are no published accounts of the A_3R being functionally

expressed in yeast. Thus, in order to characterise the compounds action upon this receptor CHO-K1 cells were utilised, that stably express the A_3R, and cAMP inhibition measured in response to stimulation with compounds. Further, it was also sought to investigate the action of agonists upon the A_1R in mammalian cells; thus, CHO-K1 cells stably expressing the A_1R were also utilised, again measuring cAMP inhibition. This served to give a comparator to which A_3R results could be compared. These findings were subsequently published in the Journal of Medicinal Chemistry (Knight *et al*, 2016, Appendix 1). Within this chapter, data pertaining to the action of these compounds upon the A_1R and A_3R is presented, with respect to their ability to mediate cAMP inhibition. Further, a more in-depth, pharmacological characterisation of the action of these agonists at the A_1R, is provided.

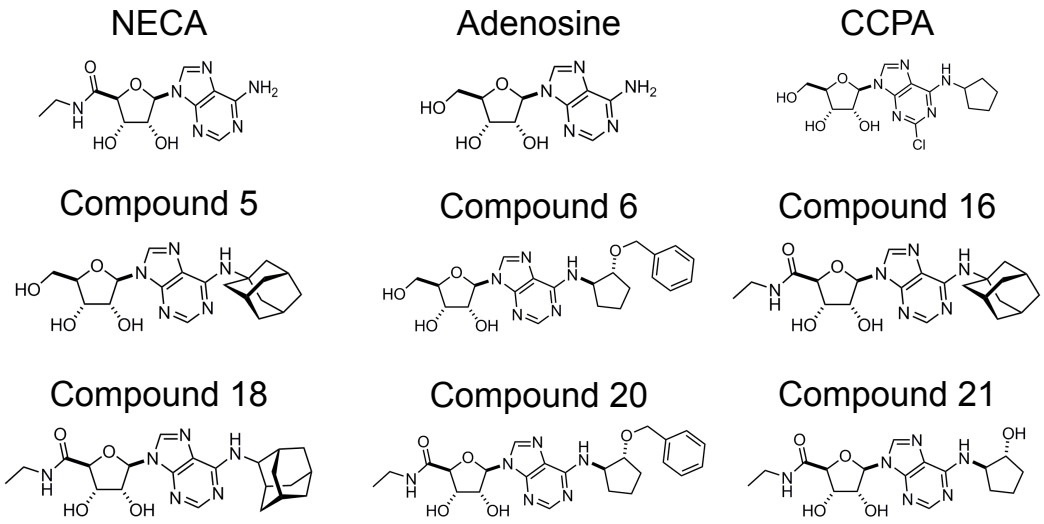

Figure 3.2: Structures of known adenosine A_1R agonists.

Structures for prototypical agonists: NECA, adenosine and CCPA are shown, as well as atypical agonists: Compounds 5, 6, 16, 18, 20, 21. Compounds 5, 6, 16 and 18 having formerly displayed A_1R selectivity at < 1 μM (Knight *et al*, 2016, Appendix 1).

3.3.1 Identifying A_1R selectivity, over the A_3R

Having previously established the selectivity profiles of the compounds between the A_1R, $A_{2A}R$ and $A_{2B}R$ in yeast (Knight *et al*, 2016, Appendix 1), their efficacy against the A_3R was also tested. In order to achieve this, CHO-K1 cells stably expressing the A_3R, were utilised. In order to measure a $G\alpha_{i/o}$-mediated response, whereby the activity of adenylate cyclase is inhibited, cells first need to be stimulated to produce cAMP. To achieve this, cells were stimulated with 1 μM forskolin, in order to activate adenylate cyclase, and co-stimulated with each agonist (Figure 3.2) in order to identify if it was possible to observe agonist-induced inhibition of the forskolin-mediated cAMP production. This identified that all three prototypical agonists, NECA, adenosine and CCPA, are agonists of the A_3R (Figure 3.3, Table 3.1). Of these, NECA and adenosine appeared the most potent agonists (pEC_{50}: 9.31±0.2, 8.94±0.2, respectively), with CCPA being less potent (pEC_{50}: 7.95±0.1); however, all were full agonists (Figure 3.3, Table 3.1). Stimulation with atypical agonists failed to generate any response for Cmpds 5, 6, 16 or 18 (Figure 3.3, Table 3.1). In contrast, Cmpds 20 and 21 displayed an ability to inhibit forskolin-stimulated cAMP production, in an A_3R-dependent manner, with Cmpd 21 being equipotent to NECA (pEC_{50}: 8.64±0.1), and Cmpd 20 displaying a greatly reduced potency (pEC_{50}: 6.57±0.2) (Figure 3.3, Table 3.1). Therefore, this identified that Cmpds 20 and 21 are agonists of the A_3R; taken in conjunction with our data previously obtained from yeast (Knight *et al*, 2016, Appendix 1), thus 2 non-selective AR agonists (Cmpds 20 and 21), and 4 A_1R-selective agonists (Cmpds 5, 6, 16 and 18) have been developed (Knight *et al*, 2016, Appendix 1).

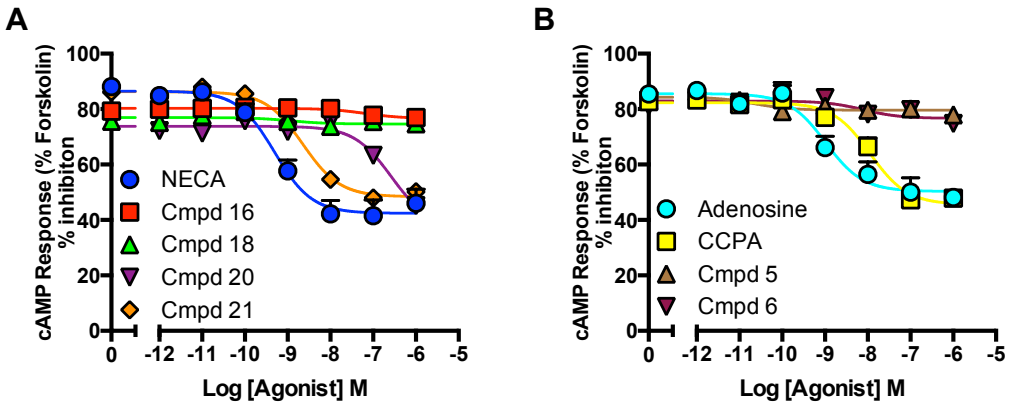

Figure 3.3: Prototypical agonists, Compounds 20 and 21, mediate A_3R-dependent cAMP inhibition.

CHO-K1, stably expressing the A_3R, stimulated with NECA-based compounds (A) and adenosine-based compounds (B), display an ability to inhibit cAMP production stimulated with 1 μM forskolin, only in response to NECA, adenosine, CCPA, Cmpd 20 and 21. Data represented as the percentage cAMP response relative to that observed upon stimulation with 1 μM forskolin, ± SEM, of 5-8 replicates.

Table 3.1: Potency (pEC_{50}) and range of response for cAMP inhibition in CHO-K1 cells stably expressing the A_3R, upon stimulation with prototypical and atypical adenosine receptor agonists.

	pIC_{50}[a]	Range[b]	n
NECA	9.31±0.2	44.09±3.0	8
Adenosine	8.94±0.2	38.67±2.5	5
CCPA	7.95±0.1**	36.74±2.3	8
Cmpd 5	NR	NR	8
Cmpd 6	NR	NR	6
Cmpd 16	NR	NR	6
Cmpd 18	NR	NR	6
Cmpd 20	6.57±0.2***	37.65±4.0	5
Cmpd 21	8.64±0.1	37.87±1.2	5

Data ± SEM of n individual replicates.
[a] Negative logarithm of agonist concentration producing half-maximal response.
[b] Range of response measured as a percentage reduction in response obtained for stimulation with 10 μM forskolin.
NR – No response.
Statistical difference between each agonist and NECA was calculated using a one-way ANOVA with Dunnet's post-test (**, $p < 0.01$, ***, $p < 0.001$).

In order to investigate the agonistic action of the compounds upon the A_1R in a mammalian system, the CHO-K1 cells previously identified as lacking expression of any functional AR subtypes (Figure 3.1B) were utilised. From these a CHO-K1 cell line stably expressing the A_1R (CHO-K1-A_1R) was generated, in which cAMP inhibition was subsequently measured, using the same method as with CHO-K1-A_3R cells. Upon stimulation with the prototypical adenosine agonists (NECA, adenosine and CCPA), it was possible to observe robust inhibition of forskolin-mediated cAMP production (Figure 3.4, Table 3.2), with all three agonists displaying similar potencies to NECA (pEC_{50}: 9.65 ± 0.2), and all being full agonists. In comparison, of the NECA-based compounds (Cmpds 16, 18, 20 and 21), all were observed to be full agonists, with responses ranging from -51.22%±3.8 to -63.75%±3.5 inhibition of 10 μM forskolin-

stimulated cAMP production (Figure 3.4A, Table 3.2). However, whilst Cmpds 16, 18 and 21 display a reduced potency relative to NECA, Cmpd 20 is equipotent to NECA (Figure 3.4A, Table 3.2). Fitting the operational model of pharmacological agonism (Black and Leff, 1983) to this data allows calculation of the *intrinsic* affinity (pKa) and efficacy (Log τ) for the agonists. Analysis of these pKa values identified a similar pattern to the observed response range, whereby Cmpd 20 has an equal pKa to NECA, in comparison to Cmpds 16, 18 and 21 which all have greatly reduced pKa values (Table 3.2). Of the adenosine-based compounds (Cmpds 5 and 6), it was observed that both are full agonists with a response range of -56.03%±6.3 and -68.16%±2.8, respectively (Figure 3.4B, Table 3.2). However, Cmpd 5 displays a ~3600 fold reduction in potency relative to adenosine, whilst Cmpd 6 displays a ~20 fold reduction, relative to adenosine (Figure 3.4B, Table 3.2). This order of potencies again matches that observed for pKa values, whereby Cmpd 5 displays a greatly reduced pKa, compared to a slight reduction for Cmpd 6 (Table 3.2). There is also an apparent correlation between E_{max} (response range in this instance) and each agonist's efficacy (Log τ). This was observed for both prototypical and atypical agonists, none of which display any statistical difference to NECA, with regards to either response range or efficacy (Log τ) (Table 3.2).

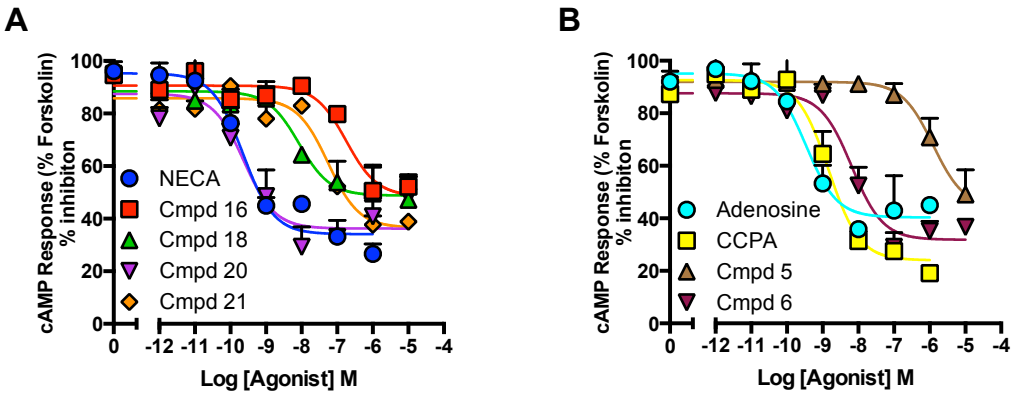

Figure 3.4: Prototypical and atypical agonists mediate a reduction in intracellular cAMP in an A_1R-dependent manner.

CHO-K1 cells stably expressing the A_1R, stimulated with NECA-based compounds (A) and adenosine-based compounds (B), display an ability to inhibit cAMP production stimulated with 1 μM forskolin. Data represented as the percentage cAMP response relative to that observed upon stimulation with 1 μM forskolin, ± SEM, of 4 replicates.

Table 3.2: Potency (pEC_{50}), affinity (pKa) and efficacy (Log τ) values for cAMP inhibition, upon agonist stimulation in CHO-K1 cells stably expressing the A_1R.

	pIC_{50}[a]	Range[b]	pKa[c]	Logτ[d]	n
NECA	9.65±0.2	-65.89±4.0	9.20±0.2	0.25±0.08	4
Adenosine	9.47±0.2	-59.65±3.6	9.02±0.2	0.11±0.07	4
CCPA	8.83±0.2	-75.97±4.3	8.23±0.2	0.45±0.1	4
Cmpd 5	5.91±0.2***	-56.03±6.3	5.57±0.3***	0.04±0.1	4
Cmpd 6	8.18±0.1**	-68.16±2.8	7.81±0.2**	0.27±0.07	4
Cmpd 16	6.75±0.3***	-51.48±4.6	6.47±0.3***	-0.06±0.09	4
Cmpd 18	8.07±0.4***	-51.22±3.8	7.81±0.4**	-0.09±0.08*	4
Cmpd 20	9.62±0.2	-63.75±3.5	9.24±0.3	0.15±0.08	4
Cmpd 21	7.25±0.2***	-63.41±3.8	6.89±0.2***	0.13±0.08	4

Data ± SEM of n individual replicates.
[a] Negative logarithm of agonist concentration producing half-maximal response.
[b] Range of response measured as a percentage reduction in response obtained for stimulation with 10 μM forskolin.
[c] Negative logarithm of the equilibrium dissociation constant, as determined using the operational model of agonism (Black and Leff, 1983).
[d] Coupling efficiency parameter as determined using the operational model of agonism (Black and Leff, 1983).
Statistical difference between each agonist and NECA was calculated using a one-way ANOVA with Dunnet's post-test (*, $p < 0.05$, **, $p < 0.01$, ***, $p < 0.001$)

3.3.2 A_1R agonists promote $G\alpha_s$-mediated cAMP production

Having identified that the A_1R agonists are able to activate the canonical $G\alpha_{i/o}$ pathway, and elicit responses whereby the A_1R serves to reduce intracellular cAMP levels, it was decided to attempt to identify through which specific $G\alpha_{i/o}$ these agonists mediated their responses. In order to do this it was planned to transfect CHO-K1-A_1R cells with plasmids containing PTX insensitive $G\alpha_{i/o}$ proteins. These cells would then be treated with 200 ng/ml PTX, for 16-18 hours, to ADP-ribosylate the C-termini of $G\alpha_i$, in order to uncouple them from GPCRs (West *et al*, 1985). This would ablate activity from the endogenous inhibitory pathway, which the compounds activate (Figure 3.4, Table 3.2). Following this, cells would be stimulated with each prototypical or atypical agonist, and inhibition of cAMP accumulation measured, in order to identify specific $G\alpha_{i/o}$ couplings. However, upon performing control experiments with cells which had not been transfected with vectors containing the PTX insensitive G proteins, it was identified that all agonists were able to induce elevations in cAMP above basal levels. From this it was observed that none of the compounds displayed any statistical difference to NECA, in terms of potency (Figure 3.5, Table 3.3). The same trend was also observed for the pKa values obtained for each agonist (Table 3.3). In terms of maximal signalling, Cmpds 5 and 18 appear as partial agonists (E_{max}: 36.10%±5.4 and 34.82%±2.4), relative to NECA, with Cmpd 18 also displaying a reduced efficacy (Figure 3.5, Table 3.3). What was thus observed is that the A_1R displays an ability to mediate the production of cAMP, presumably in a $G\alpha_s$-dependent manner. This opposing action to its canonical $G\alpha_{i/o}$ pathway is, however, only observed at higher agonist concentrations. Indeed, the agonist concentrations required to activate this pathway are near identical to those whereby a reduction in inhibition of forskolin-mediated cAMP production is observed (Figure 3.5C-D). This is particularly apparent for Cmpd 20, when fitted with a biphasic dose-response curve (Figure 3.5C), where an upward inflection occurs at

agonist concentrations >100 nM. This curve has a higher 'goodness of fit' value, R^2, compared to when fitted with the standard 3-parameter logistic equation (0.810 vs 0.783, $p < 0.001$), implying that Cmpd 20, at least, does indeed display a biphasic response. For all the other compounds, the 3-parameter logistic equation gave a better fit, suggesting that over the concentration range which the cAMP inhibition assays were performed, the compounds do not show a high enough level of cAMP production to show true biphasic responses. At this point it still remains unclear whether the production of cAMP occurs at these higher concentrations; due to the level of receptor or G protein expression, it is indeed possible that at a higher receptor number, other A_1Rs, not coupled to $G\alpha_{i/o}$, are then able to couple to $G\alpha_{s}$. It is also feasible that the receptors sit in 'pools' or micro-domains, whereby individual groups of A_1R are differentially coupled to differing G proteins, and that the $G\alpha_{i/o}$ 'pool' is the larger, more dominant, thereby overcoming any response mediated via a smaller $G\alpha_s$-coupled 'pool'.

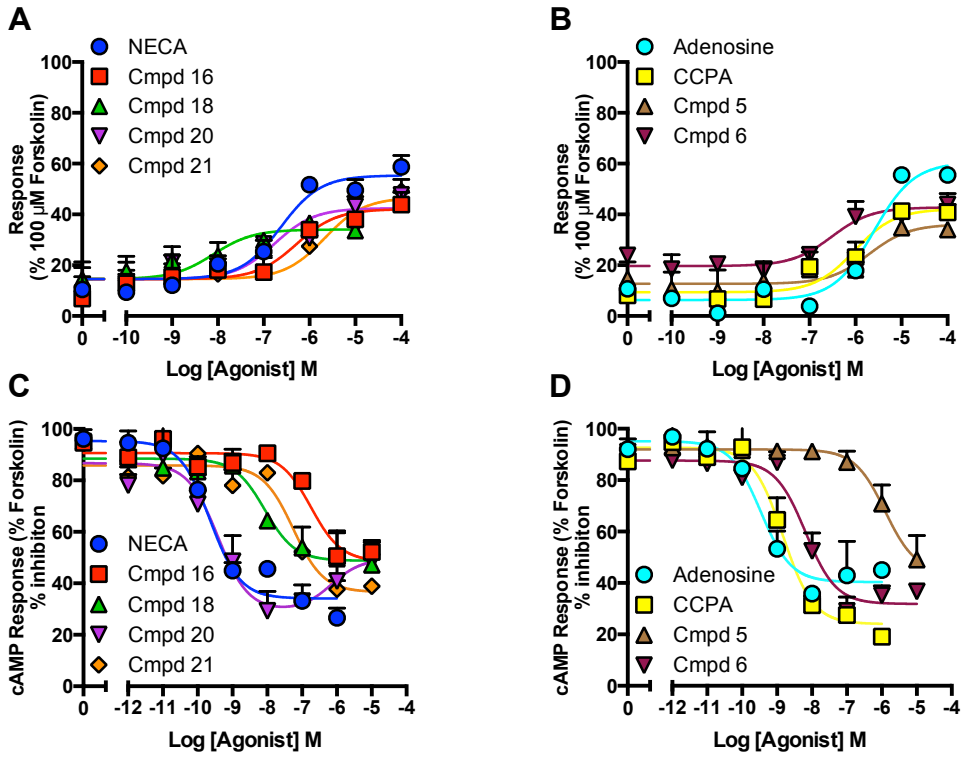

Figure 3.5: A_1R agonists display an ability to elevate intracellular cAMP levels in PTX-treated cells.

CHO-K1 cells stably expressing the A_1R, treated with 200 ng/ml PTX, for 16-18 hours, display an ability to produce cAMP when stimulated with NECA-based (A) and adenosine-based compounds (B). Data represented relative to cAMP levels observed with 100 µM forskolin, ± SEM, of 2-4 replicates. To allow comparison between A_1R-mediated cAMP production and $G\alpha_{i/o}$ activation, cAMP inhibition data, fitted with biphasic dose-response curves, is presented for NECA-based (C) and adenosine-based compounds (D); this indicates that only Cmpd 20 displays a truly biphasic response. Data represented as the percentage cAMP response relative to that observed upon stimulation with 1 µM forskolin, ± SEM, of 4 replicates.

Table 3.3: Potency (pEC_{50}), affinity (pKa) and efficacy (Log τ) values for cAMP production, upon agonist stimulation in CHO-K1 cells stably expressing the A_1R, pre-treated with 200 ng/ml PTX, for 16-18 hours.

	pEC_{50}[a]	E_{max}[b]	pKa[c]	Logτ[d]	n
NECA	6.72±0.2	55.20±2.8	6.35±0.3	-0.039±0.09	4
Adenosine	5.60±0.2	60.49±3.9	5.23±0.2	0.14±0.07	4
CCPA	6.02±0.2	42.13±3.2	5.82±0.3	-0.25±0.07	4
Cmpd 5	5.71±0.5	36.10±5.4*	5.57±0.5	-0.44±0.1	4
Cmpd 6	6.52±0.4	42.78±2.7	6.37±0.4	-0.39±0.08	4
Cmpd 16	6.35±0.3	41.93±3.3	6.12±0.3	-0.32±0.08	4
Cmpd 18	7.64±0.5	34.82±2.4*	7.99±0.4	-0.53±0.09*	4
Cmpd 20	6.21±0.3	45.43±4.0	6.59±0.3	-0.31±0.08	4
Cmpd 21	5.67±0.4	46.67±5.3	5.47±0.3	-0.22±0.09	4

Data ± SEM of n individual replicates.
[a] Negative logarithm of agonist concentration producing half-maximal response.
[b] Maximal response observed upon agonist stimulation, as a percentage of that observed upon stimulation with 10 μM forskolin.
[c] Negative logarithm of the equilibrium dissociation constant, as determined using the operational model of agonism (Black and Leff, 1983).
[d] Coupling efficiency parameter as determined using the operational model of agonism (Black and Leff, 1983).
Statistical difference between each agonist and NECA was calculated using a one-way ANOVA with Dunnet's post-test (*, $p < 0.05$, **, $p < 0.01$, ***, $p < 0.001$).

3.3.3 Intracellular calcium mobilisation at the A_1R

In order to investigate the ability of both prototypical and atypical agonists to mediate the mobilisation of intracellular Ca^{2+} ($_iCa^{2+}$), CHO-K1-A_1R cells, which had been loaded with FLUO-4/AM, were utilised. If agonist stimulation results in mobilisation of $_iCa^{2+}$, an increase in fluorescence, at 506 nm, would be observed, upon Ca^{2+} binding FLUO-4, when excited at 494 nm (Gee *et al*, 2000). In each experiment, stimulation with 100 μM ATP was used as a control to confirm both: sufficient loading of the dye, and the ability of the cells to mobilise $_iCa^{2+}$. All assays were run in Ca^{2+}-free HBSS, in order to prevent Ca^{2+} influx via the opening of cell surface calcium channels.

Initially, the prototypical adenosine receptor agonists NECA, adenosine and CCPA were tested, with all three displaying an ability to mediate the mobilisation of $_iCa^{2+}$, in a dose-dependent manner (Figures 3.6A-C). Immediately post-injection, a rapid increase in $_iCa^{2+}$ mobilisation was observed (as an increase in fluorescence), for both NECA and adenosine, at agonist concentrations ranging 10 nM to 1 μM (Figures 3.6A-B). For adenosine, no response was observed when cells were stimulated with less than 10 nM. However, with NECA, small responses were recorded at concentrations as low as 10 pM, but responses were seen to be slower than those at higher agonist concentrations (Figure 3.6A). With CCPA stimulation, rapid $_iCa^{2+}$ mobilisation was observed for 1 μM, whilst 100 nM and 10 nM generated smaller responses that were slower than those observed at 1 μM (Figure 3.6C).

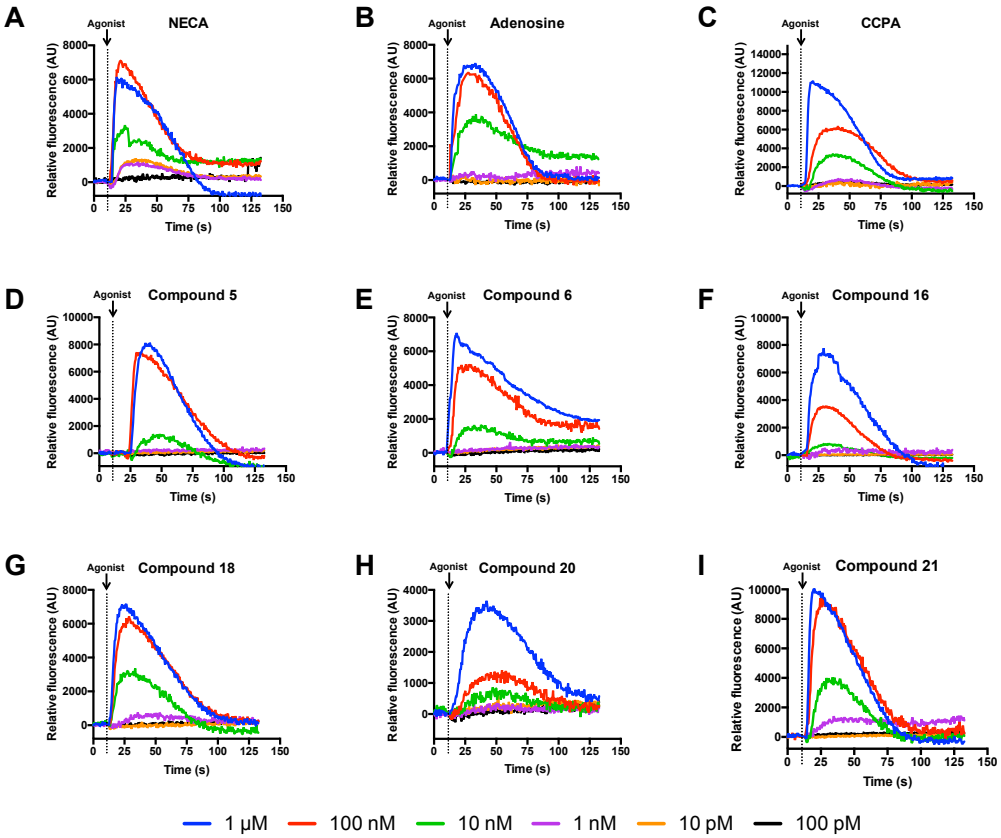

Figure 3.6: A_1R agonists display an ability to mobilise $_i Ca^{2+}$ in CHO-K1 cells.

CHO-K1 cells stably expressing the A_1R, loaded with FLUO-4/AM in Ca^{2+}-free HBSS, were stimulated with both NECA-based (A) and adenosine-based (B) compounds, identifying that all agonists are able to lead to mobilisation of $_i Ca^{2+}$. Data shown as the fluorescence relative to that prior to agonist injection, with the dotted line indicated point of agonist injection. Traces representative of the average response obtained from 3-5 replicates.

Having confirmed the ability of the cells to mobilise $_i Ca^{2+}$, in an A_1R-dependent manner, in response to prototypical agonists, the effects of the atypical agonists were further investigated. Utilising the same approach as with the prototypical agonists, it was observed that all 6 compounds being tested were able to elevate $_i Ca^{2+}$ (Figure 3.6D-I). For all compounds, a rapid increase in fluorescence upon agonist stimulation was evident, except for Cmpd 20, which generated a slower increase compared to the others (Figure 3.6D-I). Stimulation with 100 nM also resulted in rapid increases in $_i Ca^{2+}$ mobilisation for all compounds, with the exception of Cmpd 20 (Figure 3.6D-I), whilst 10 nM generated a slower response, except for Cmpd 18, which elicited a response as rapid as those seen at 1 µM and 100 nM (Figure 3.6D-I). At concentrations below 10 nM, only Cmpds 18 and 21 were able to generate a response,

which occurs at 1 nM, with no compound displaying agonistic activity at <10 pM (Figure 3.6D-I).

It is clear that each of the compounds tested display an ability to mobilise $_{i}Ca^{2+}$. However, to characterise this pharmacologically, the calcium traces obtained (Figure 3.6) were converted to dose-response curves in order to allow calculation of pEC_{50} and E_{max}. In order to account for the variability of cells on differing days, and subsequently differing passage numbers, as well as differential dye loading between experiments, this data is required to be presented relative to a control agonist. Thus, 100 μM ATP was utilised as a control, to which all data was normalised. The response of each different agonist concentration, at the time point when 1 μM generated the maximal response, was then plotted as a dose-response curve (Figure 3.7). This identified that, of the prototypical agonists, NECA and adenosine are the most potent mediators of $_{i}Ca^{2+}$ mobilisation (pEC_{50}: 8.20±0.1 and 8.08±0.1, respectively) with both being full agonists (E_{max}: 102.6%±3.0 and 99.38%±3.5, respectively) (Figure 3.7, Table 3.4). These observations regarding NECA's ability to mediate mobilisation of $_{i}Ca^{2+}$ closely match previously reported data, obtained from CHO cells (Gao and Jacobson, 2016). Interestingly, in comparison to cAMP data (Figures 3.4 and 3.5, Tables 3.2 and 3.3), CCPA is greatly reduced in potency, relative to both NECA and adenosine (pEC_{50}: 6.94±0.1), and is also observed to be a partial agonist (E_{max}: 79.02%±6.4) (Figure 3.7, Table 3.4). Indeed, CCPA is one of the least potent mediators of $_{i}Ca^{2+}$ mobilisation, as is Cmpd 20 (pEC_{50}: 6.65±0.2), which is also a partial agonist (E_{max}: 68.84%±9.0) (Figure 3.7, Table 3.4).

Of the atypical agonists, only Cmpds 18 and 21 are as equally potent as NECA (pEC_{50}: 8.03±0.1 and 7.92±0.1, respectively); however, Cmpd 18 is a partial agonist (E_{max}: 67.02%±2.4), whilst Cmpd 21 is a full agonist (E_{max}: 96.13%±5.7) (Figure 3.7A, Table 3.4). Cmpd 16 is also observed to be a full agonist (E_{max}: 99.61%±6.1), but displays a ~15 fold reduction in potency, compared to NECA (pEC_{50}: 7.02±0.1) (Figure 3.7A, Table 3.4). Of the adenosine-based compounds (Cmpds 5 and 6), both are full

agonists (E_{max}: 88.79%±4.8 and 97.95%±2.9, respectively) with reduced potencies relative to NECA (pEC_{50}: 7.60±0.1 and 7.36±0.1, respectively) (Figure 3.7B, Table 3.4). It is interesting to note, that in contrast to data pertaining to the effects of the agonists upon cAMP production, there is no correlation between pKa and Log τ, to potency and E_{max} (Table 3.4). In terms of pKa, none of the agonists display any statistical difference to NECA, whilst for Log τ, only Cmpd 18 displays any reduction (Table 3.4).

It has thus been observed that the A_1R is able to mediate mobilisation of $_i Ca^{2+}$ in response to the cognate agonist, adenosine, as well as NECA and the synthetic A_1R selective agonist, CCPA. It has also been identified that by utilising NECA and adenosine as scaffolds, upon which to design new A_1R agonists, each agonist still displays an ability to bring about the mobilisation of $_i Ca^{2+}$. Some of the developed compounds displayed responses similar to NECA, such as Cmpd 21, whereas others were less potent than NECA, but still full agonists, in the case of Cmpds 5, 6, and 16. Some compounds have also been produced that are equipotent to NECA but are partial agonists, such as Cmpd 18.

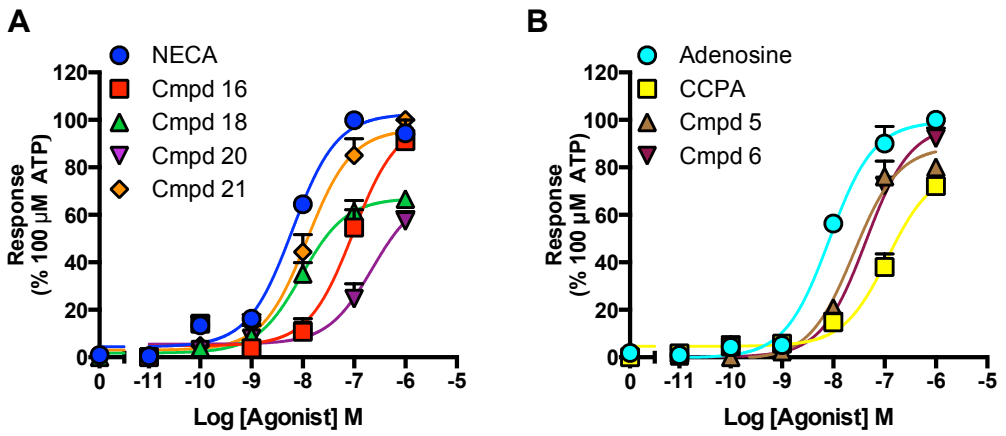

Figure 3.7: A_1R agonists display differential efficacies when mobilising $_i Ca^{2+}$.

Calcium trace data (Figure 3.5) was converted to dose-response curves by plotting the value of each concentration, at the time point that gives the maximal response at 1 µM of agonist. Data represented as the percentage of the maximal response observed with 100 µM ATP, ± SEM, of 3-5 replicates.

Table 3.4: Potency (pEC_{50}), affinity (pKa) and efficacy (Log τ) values for agonist-induced mobilisation of $_{i}Ca^{2+}$ in CHO-K1 cells stably expressing the A_1R.

	pEC_{50}[a]	E_{max}[b]	pKa	Logτ[d]	n
NECA	8.20±0.1	102.6±3.0	6.58±0.6	1.61±0.6	7
Adenosine	8.08±0.1	99.38±3.5	6.81±0.3	1.25±0.3	4
CCPA	6.94±0.1***	79.20±6.4**	6.35±0.2	0.46±0.1	5
Cmpd 5	7.60±0.1**	88.79±4.8	6.79±0.2	0.74±0.1	4
Cmpd 6	7.36±0.1***	97.95±2.9	6.19±0.2	1.14±0.2	6
Cmpd 16	7.02±0.1***	99.61±6.1	5.75±0.6	1.25±0.5	4
Cmpd 18	8.03±0.1	67.02±2.4***	7.59±0.1	0.24±0.04*	4
Cmpd 20	6.65±0.2***	68.84±9.0***	6.21±0.3	0.24±0.2	5
Cmpd 21	7.92±0.1	96.13±5.7	6.86±0.4	1.02±0.3	5

Data ± SEM of n individual replicates.
[a] Negative logarithm of agonist concentration producing half-maximal response.
[b] Maximal response observed upon agonist stimulation, as a percentage of that observed upon stimulation with 100 μM ATP.
[c] Negative logarithm of the equilibrium dissociation constant, as determined using the operational model of agonism (Black and Leff, 1983).
[d] Coupling efficiency parameter as determined using the operational model of agonism (Black and Leff, 1983).
Statistical difference between each agonist and NECA was calculated using a one-way ANOVA with Dunnet's post-test (*, $p < 0.05$, **, $p < 0.01$, ***, $p < 0.001$).

3.3.4 ERK1/2 activation by the A_1R

In order to measure the ability of both the prototypical and atypical agonists to mediate the activation of ERK1/2, CHO-K1-A_1R cells were serum-starved overnight in an attempt to reduce basal levels of ERK phosphorylation, potentially brought about by the action of growth factors within the growth media which these cells were cultured in. Through measuring the total amount of phospho-ERK generated in response to agonist stimulation, it was observed that of the prototypical agonists (NECA, adenosine and CCPA), all are full, potent agonists with a pEC_{50} of ~8.6 (Figure 3.8, Table 3.5). In comparison, of the atypical agonists, only Cmpds 6 and 21 display equipotency to NECA (pEC_{50}: 8.70±0.3 and 8.27±0.2, respectively), however both are partial agonists (E_{max}: 23.05%±1.5 and 21.02%±1.5, respectively) (Figure 3.8, Table 3.5). In contrast, one agonist, Cmpd 20, displays a ~6.5 fold increase in potency, relative to NECA, but is also a partial agonist (E_{max}: 17.32%±1.3) (Figure 3.8A, Table 3.5). Of the remaining atypical agonists, all display a reduced potency, relative to NECA, and all are partials, except Cmpd 16, which is a full agonist (E_{max}: 52.99%±4.1) (Figure 3.8, Table 3.5). Thus, a rank order of potency for all agonists of Cmpd 20 > CCPA = Adenosine = NECA > Cmpd 6 > Cmpd 21 > Cmpd 18 = Cmpd 16 > Cmpd 5 was observed (Figure 3.8, Table 3.5). As with other assay data in this thesis, there was a strong correlation between E_{max} and the efficacy (Log τ) for each agonist; however, only Cmpd 5 displays a reduced pKa, whilst Cmpd 20 displays an increased pKa, relative to NECA (Table 3.5). Therefore, by changing the various functional groups of NECA and adenosine on the atypical agonist, it has been possible to produce a series of compounds that are partial agonists, in terms of ERK1/2 activation, and one, Cmpd 16, which is a full agonist (Figure 3.8, Table 3.5).

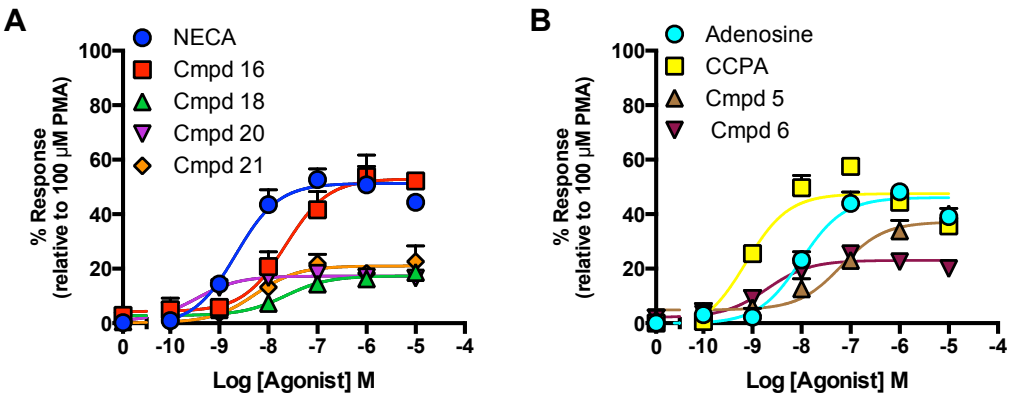

Figure 3.8: A_1R agonists display an ability to activate ERK1/2 in CHO-K1 cells.

Serum-starved CHO-K1 cells, stably expressing the A_1R, were stimulated with both NECA-based (A) and adenosine-based (B) compounds, identifying that all agonists are able to result in phosphorylation of ERK1/2. Data represented as the percentage of the maximal response observed with 100 µM PMA stimulation, ± SEM, of 3-5 replicates.

Table 3.5: Potency (pEC_{50}), affinity (pKa) and efficacy (Log τ) values for ERK1/2 activation in CHO-K1 cells stably expressing the A_1R.

	pEC_{50}[a]	E_{max}[b]	pKa[c]	Logτ[d]	n
NECA	8.66±0.2	51.34±2.5	8.30±0.1	0.014±0.03	5
Adenosine	8.01±0.1	46.11±2.2	7.71±0.1	-0.079±0.04	4
CCPA	9.12±0.2	47.53±2.9	8.75±0.2	-0.053±0.04	3
Cmpd 5	7.19±0.2***	37.14±2.6**	7.27±0.2*	-0.28±0.05*	4
Cmpd 6	8.70±0.3	23.05±1.5***	8.64±0.3	-0.55±0.06***	3
Cmpd 16	7.65±0.2**	52.99±4.1	7.42±0.1	0.032±0.14	4
Cmpd 18	7.65±0.2**	17.33±1.1***	7.75±0.5	-0.72±0.09***	3
Cmpd 20	9.47±0.2*	17.32±1.3***	9.34±0.4*	-0.71±0.07***	3
Cmpd 21	8.27±0.2	21.02±1.5***	8.09±0.4	-0.60±0.07***	3

Data ± SEM of n individual replicates.
[a] Negative logarithm of agonist concentration producing half-maximal response.
[b] Maximal response observed upon agonist stimulation, as a percentage of that observed upon stimulation with 100 μM PMA.
[c] Negative logarithm of the equilibrium dissociation constant, as determined using the operational model of agonism (Black and Leff, 1983).
[d] Coupling efficiency parameter as determined using the operational model of agonism (Black and Leff, 1983).
Statistical difference between each agonist and NECA was calculated using a one-way ANOVA with Dunnet's post-test (*, $p < 0.05$, **, $p < 0.01$, ***, $p < 0.001$).

3.3.5 Quantifying biased agonism at the A_1R

This work has identified that the A_1R is able to activate its canonical signalling pathway: activation of $G\alpha_{i/o}$, bringing about an inhibition of the activity of adenylate cyclase, serving to lower intracellular cAMP levels (Figure 3.4, Table 3.2). Further, the A_1R has been observed to mediate: the activation of a pathway leading to stimulation of adenylate cyclase, thereby elevating intracellular cAMP, presumably in a $G\alpha_s$–dependent manner (Figure 3.5, Table 3.3), as well as the ability to mobilise $_iCa^{2+}$ (Figures 3.6 and 3.7, Table 3.4) and activate ERK1/2 (Figure 3.8, Table 3.5). All of the agonists tested in this chapter, both prototypical and atypical, were able to activate these pathways to differing extents. There is, therefore, a degree of inherent biased agonism at the A_1R. In order to quantify this, all data was fitted with the operational model of pharmacological agonism (Black and Leff, 1983), and transduction coefficients (Log τ/Ka) calculated. These were then analysed for the degree of change between each differing pathway (Δ τ/Ka), for each agonist studied (Figure 3.9). This identified that all agonists are more biased towards the inhibition of cAMP production, than its stimulation, with Cmpd 18 exhibiting only a slight bias towards inhibition. Of all agonists, it is the natural cognate agonist, adenosine, which displays the greatest extent of bias towards the canonical, inhibitory pathway (Figure 3.9). Cmpd 21 displays the greatest extent of bias towards the mobilisation of $_iCa^{2+}$ (Figure 3.9). In terms of ERK1/2 activation bias, CCPA is most heavily biased agonist towards this pathway, being as equally biased towards the inhibition of cAMP production (Figure 3.9). It is interesting to observe that the pathway opposing the canonical $G\alpha_{i/o}$ pathway, cAMP production, is the one to which all agonists display the lowest level of bias towards (Figure 3.9).

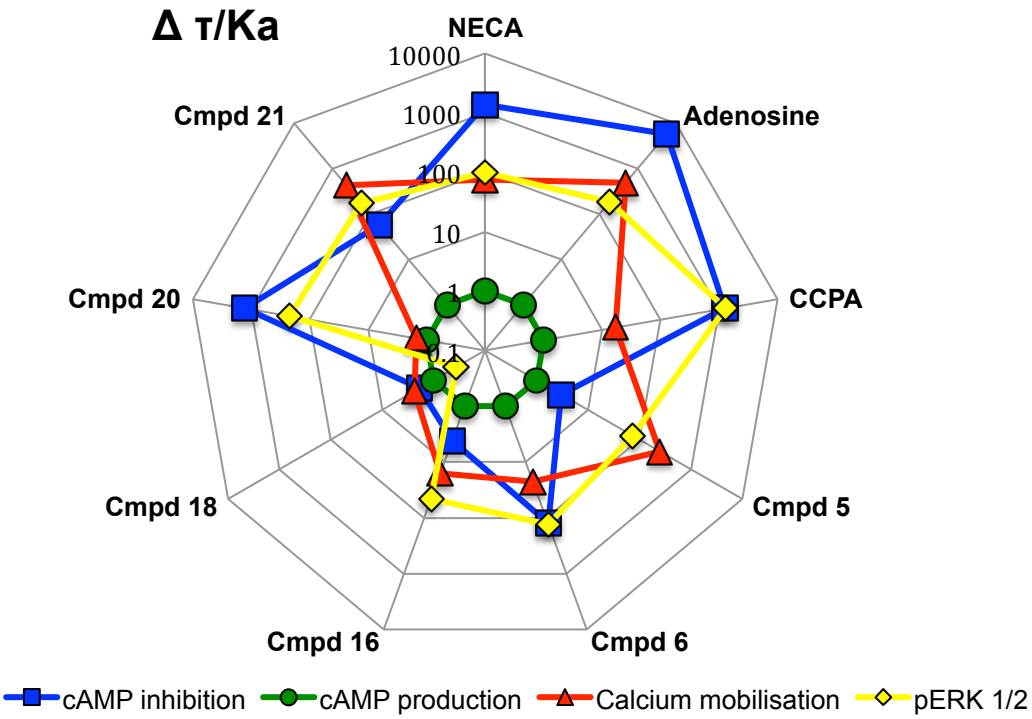

Figure 3.9: Pathway bias plot (Δ τ/Ka) for prototypical and atypical A_1R agonists.

Quantification of pathway bias (Δ τ/Ka) between: cAMP inhibition, cAMP production, $_{i}Ca^{2+}$ mobilisation and ERK1/2 activation, for both prototypical and atypical A_1R agonists. Bias is shown relative to the ability of each agonist to stimulate cAMP production.

It is also possible to quantitate bias relative to a reference ligand (ΔΔ τ/Ka), NECA in this instance. This serves to present the quantification of bias in a system-independent manner, which should be translatable to other systems (Kenakin *et al*, 2012). Through calculating relative bias, NECA is perceived to display no bias towards any of the four pathways studied (Figure 3.10), thus the extent of bias for other agonists is now apparent, relative to NECA. This indicates that adenosine is more biased towards the: inhibition of cAMP, mobilisation of $_{i}Ca^{2+}$, and ERK1/2 activation than NECA. CCPA is more biased towards ERK1/2 activation than NECA, more so than any of the other agonists studied (Figure 3.10). However, CCPA is also less biased towards the mobilisation of $_{i}Ca^{2+}$, but is equally biased towards both cAMP production and inhibition (Figure

3.10). Cmpd 5 displays a greater relative bias towards $_{i}Ca^{2+}$ mobilisation, but also displays a greatly reduced bias towards the inhibition of cAMP production, relative to NECA (Figure 3.10). Indeed, all of the atypical agonists are least biased towards signalling via $G\alpha_{i/o}$, over any other pathway, relative to NECA, except for Cmpd 20 (Figure 3.10). Cmpd 6 is as equally biased as NECA towards the activation of ERK1/2 and the production of cAMP, whilst being slightly less biased towards $_{i}Ca^{2+}$ mobilisation and cAMP inhibition, with Cmpd 16 displaying a similar pattern of bias (Figure 3.10). Cmpd 18 is the only agonist that displays relative bias toward the production of cAMP over all other pathways, it being equivalent to NECA, whilst being less biased towards ERK1/2 activation and cAMP inhibition than NECA (Figure 3.10). Cmpd 20 appears equally biased as NECA towards both the inhibition and production of cAMP production, whilst also displaying a slightly greater level of bias towards ERK1/2 activation, and also displaying a much lower level of bias towards $_{i}Ca^{2+}$ mobilisation (Figure 3.10). Cmpd 21 is more biased toward $_{i}Ca^{2+}$ signalling and ERK1/2 activation than NECA, as well as being less biased than NECA towards the inhibition of cAMP production, as with all atypical agonists (barring Cmpd 20) (Figure 3.10).

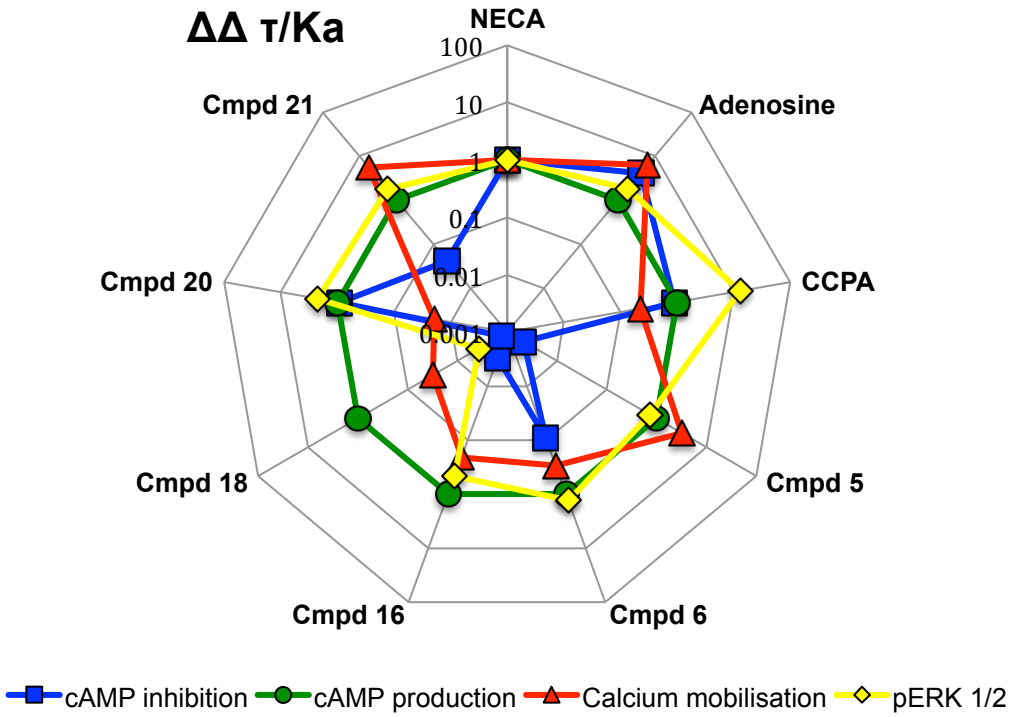

Figure 3.10: Relative bias plot (ΔΔ τ/Ka) for both prototypical and atypical A_1R agonists.

Quantification of relative pathway bias (ΔΔ τ/Ka) between: cAMP inhibition, cAMP production, $_iCa^{2+}$ mobilisation and ERK1/2 activation, for both prototypical and atypical A_1R agonists. Bias is shown relative to a reference pathway (cAMP production) and the reference agonist (NECA).

3.4 Adenosine A_{2A} receptor

The work in the following sections of this chapter pertains to a collaborative project between Leen Kalash, a member of Dr. A. Bender's research group (University of Cambridge, UK), and ourselves. In this project, Dr. Bender's group were searching for multi-target, dual $A_{2A}R$ agonists and phosphodiesterase (PDE) 10A inhibitors. The rationale for this is that agonism of the $A_{2A}R$ will promote cAMP production, in a $G\alpha_s$-dependent manner, whilst inhibition of PDE10A will prevent the subsequent breakdown of cAMP by the cell. They utilised an *in silico* approach to identify compounds that fit these criteria. This identified a series of known PDE10A inhibitors, triazoloquinazolines (Kehler *et al*, 2011), which displayed suitable docking scores to the $A_{2A}R$. We then sought to pharmacologically validate these results, and characterise the identified compounds *in vitro*. In order to maintain integrity of this validation of the *in silico* findings all work was performed while blinded as to the structures of the compounds.

3.4.1 Identifying novel $A_{2A}R$ selective agonists

In order to confirm the *in silico* results obtained by our collaborators, it was required to confirm two points: 1) the compounds are agonists of the $A_{2A}R$, and 2) the compounds are selective for the $A_{2A}R$ over other ARs. In order to achieve this, the GlaxoSmithKline yeast-screening platform (Brown *et al*, 2000) was initially utilised. The advantage of this model over immortalised mammalian cells is that yeast provides a cheap and fast growing organism to culture. They can be readily grown in cheap media, and are easy to genetically manipulate. A major advantage for the study of GPCRs is that they provide a 'clean' background upon which to study a GPCR of interest, with limited 'cross talk' between signalling pathways (Ladds *et al*, 2005b). The main advantage of this limited interplay is that one pathway can be manipulated, to study a drug of interest, without the other modulating the observed response. In contrast, mammalian cells

display a complex network of interconnected signalling pathways, providing great difficulty in elucidating the effect of an agonist upon a specific pathway. They also provide a system whereby agonist selectivity can rapidly be assessed, as each constructed strain will only express a single GPCR subtype.

Human GPCRs can be transformed into yeast cells, expressing chimeric yeast-human G proteins. These chimeras consist of the yeast homologue of Gα, GPA1, with the final 5 C-terminal amino acids being replaced with those of each individual human Gα subunit (GPA1/Gα) (Brown *et al*, 2000). This is sufficient to allow the chimeric G protein to interact with the GPCR. Upon receptor activation, GPA1/Gα is able to mediate the activation of the yeast mating response gene, FUS1 (Brown *et al*, 2000). The promoter of FUS1 is linked to *LacZ* (Brown *et al*, 2000), allowing GPCR activation to be measured via conventional β-galactosidase assays. This system was previously utilised to investigate the A_1R, $A_{2A}R$ and $A_{2B}R$ (Knight *et al*, 2016, Appendix 1). Here, this system is again utilised for the screening of test triazoloquinazoline compounds, identified from our collaborators' *in silico* screen.

NECA and test triazoloquinazoline compounds 1-5 (TZQ 1-5) were applied to yeast cells expressing the: A_1R and GPA1/$G\alpha_{i1/2}$ (SC13, Table 2.5), $A_{2A}R$ and GPA1/$G\alpha_s$ (SC13, Table 2.5), or the $A_{2B}R$ and GPA1/$G\alpha_s$ (SC224, Table 2.5). β-galactosidase activity was measured to determine agonistic activity, as well as selectivity for the $A_{2A}R$ (Figure 3.11). Initially, the ability of NECA to activate each AR in the yeast strains was tested. NECA stimulation of yeast expressing the A_1R resulted in a potent response (pEC_{50} 5.87±0.1), as did stimulation of the $A_{2A}R$ (pEC_{50}: 5.50±0.2) (Figure 3.11A, Table 3.6). In contrast, NECA-mediated activation of the $A_{2B}R$ generated a weak response (pEC_{50}: 4.14±0.1) (Figure 3.11A, Table 3.6), which is consistent with previous studies using this strain (Knight *et al,* 2016, Appendix 1).

Upon stimulating the yeast strains expressing the three ARs with TZQ 1, it was only possible to observe a response at the $A_{2A}R$. This identified TZQ 1 to be slightly less potent than NECA (pEC_{50}: 5.4±0.3), as well as being a partial agonist (E_{max}: 63.68%±6.5) (Figure 3.11B, Table 3.6). Testing the actions of TZQs 2 and 3 also identified that these compounds only acted as agonists upon the $A_{2A}R$, with TZQ 2 displaying an increased potency (pEC_{50}: 5.98±0.4) relative to NECA, and TZQ 3 being equipotent to NECA (Figure 3.11C-D, Table 3.6). As with TZQ 1, TZQs 2 and 3 were observed to be partial agonists, with TZQ 3 generating the smallest response (E_{max}: 45.90%±8.3) (Figure 3.11C-D, Table 3.6)

Contrasting with TZQ 1-3, TZQ 4 displayed an ability to act as an agonist of all three ARs under investigation, being most potent upon the $A_{2A}R$ (pEC_{50}: 6.14±0.5) (Figure 3.11E, Table 3.6). A rank order of potency, between the three receptors, of $A_{2A}R$ > A_1R > $A_{2B}R$ was observed; however, like TZQ 1-3, TZQ 4 was also a partial agonist of all three receptors (Figure 3.11E, Table 3.6). Upon testing TZQ 5 against each AR, only limited activity was observed, with the largest response being observed through activation of the A_1R (E_{max}: 12.94%±3.9); however, TZQ 5 was identified as being more potent than NECA at both the A_1R and $A_{2A}R$ (pEC_{50}: 7.39±1.2 and 8.20±0.8, respectively) (Figure 3.11F, Table 3.6). This data thus confirms that TZQ 1-5 are agonists of the $A_{2A}R$, whilst TZQ 1-3 display no efficacy at the A_1R or $A_{2B}R$. TZQ 1-3 are, therefore, selective agonists for the $A_{2A}R$ over the A_1R and $A_{2B}R$.

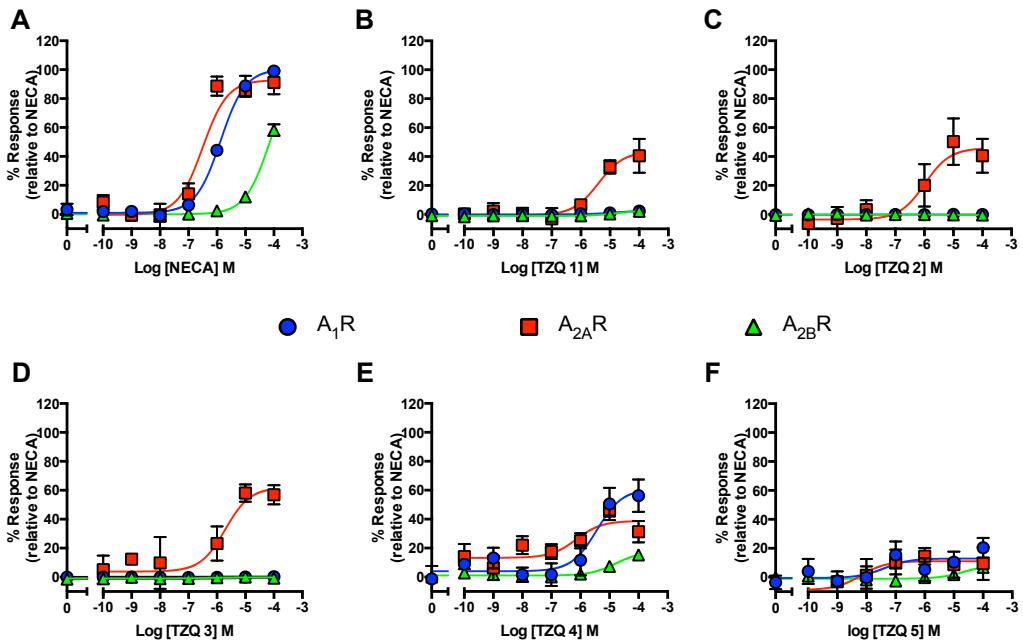

Figure 3.11: Triazoloquinazolines display agonistic activity against adenosine receptors in yeast.

Dose-response curves for NECA and TZQ 1-5 were constructed in yeast strains expressing either the: A_1R and GPA1/$G\alpha_{i1/2}$, $A_{2A}R$ and GPA1/$G\alpha_s$, or $A_{2B}R$ with GPA1/$G\alpha_s$. Reporter gene activity was determined using β-galactosidase assays, following 16 hour stimulation with either: NECA (A), TZQ 1 (B), TZQ 2 (C), TZQ 3 (D), TZQ 4 (E) or TZQ 5 (F). All data represented as the percentage response relative to NECA stimulation for each given receptor, ± SEM, of 5 replicates.

Table 3.6: Potency (pEC_{50}) and E_{max} values for triazoloquinazoline stimulation of adenosine A_1, A_{2A} and A_{2B} receptors in yeast expressing GPA1/$G\alpha_{i1/2}$ or GPA1/$G\alpha_s$

	A_1R - GPA1/$G\alpha_{i1/2}$			$A_{2A}R$ - GPA1/$G\alpha_s$			$A_{2B}R$ - GPA1/$G\alpha_s$		
	pEC_{50}[a]	E_{max}[b]	n	pEC_{50}[a]	E_{max}[b]	n	pEC_{50}[a]	E_{max}[b]	n
NECA	5.87±0.1	100.40±3.2	5	5.50±0.2	92.84±5.1	5	4.14±0.1	99.76±13.2	5
TZQ 1	NR	NR	5	5.40±0.3*	63.68±6.5**	5	NR	NR	5
TZQ 2	NR	NR	5	5.98±0.4*	45.90±8.3***	5	NR	NR	5
TZQ 3	NR	NR	5	5.71±0.4	61.94±9.9**	5	NR	NR	5
TZQ 4	5.44±0.3	60.88±9.0**	5	6.14±0.5	38.78±5.3**	5	4.79±0.2	17.62±2.5***	5
TZQ 5	7.39±1.2**	12.94±3.9**	5	8.20±0.8***	11.09±3.9***	5	6.64±0.3	8.66±2.2***	5

Data ± SEM of n individual replicates.
[a] Negative logarithm of agonist concentration producing half-maximal response.
[b] Maximal response observed upon agonist stimulation, as a percentage of that observed upon stimulation with 100 μM NECA.
NR – No response.
Statistical difference between each agonist and NECA was calculated using a one-way ANOVA with Dunnet's post-test (*, $p < 0.05$, **, $p < 0.01$, ***, $p < 0.001$).

In order to determine if TZQ 1-3 are wholly selective for the $A_{2A}R$ over all AR subtypes, it was required to test for activity against the A_3R. However, to date, no reports of successful expression of functional A_3R in yeast have been published. Thus, in order to test the A_3R, CHO-K1 cells stably expressing the human A_3R were utilised, and each compound tested for its ability to inhibit 1 μM forskolin-mediated cAMP production. Upon stimulation with NECA, it was possible to observe a reduction in forskolin-mediated cAMP production of 34.35%±2.2, with a pEC_{50} of 9.75±0.1 (Figure 3.12, Table 3.7). When stimulated with the triazoloquinazoline compounds, no inhibition was observed for TZQs 1, 2, 3 or 5; however, TZQ 4 displayed agonistic activity, with a pEC_{50} of 9.45±0.2 and a 16.59%±1.1 inhibition of forskolin-mediated cAMP production (Figure 3.12, Table 3.7).

From the experiments performed in yeast upon the A_1R, $A_{2A}R$ and $A_{2B}R$, and in CHO-K1 cells upon the A_3R, it is possible to confirm that all five triazoloquinazolines are $A_{2A}R$ agonists; TZQ 4 and 5 are also A_1R and $A_{2B}R$ agonists, with TZQ 4 also being an agonist of the A_3R. Thus, this work identified one non-selective AR agonist (TZQ 4), one that is selective for the A_1, A_{2A} and A_{2B} receptors over the A_3R (TZQ 5), and three (TZQ 1-3) that are selective for the $A_{2A}R$ over all other AR subtypes.

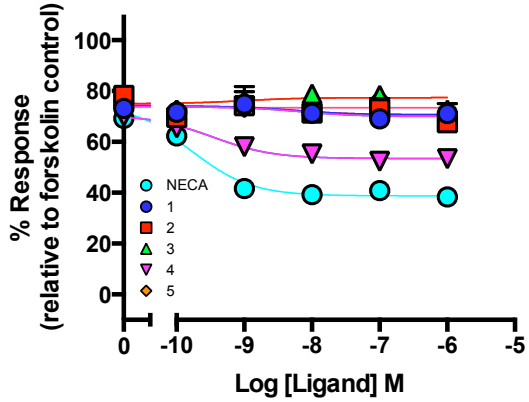

Figure 3.12: Triazoloquinazolines display limited agonistic activity at the A_3R.

CHO-K1 cells stably expressing the A_3R were co-stimulated with 1 μM forskolin, to promote cAMP production, as well as either NECA or TZQ 1-5. Data represented as the percentage response relative to 100 μM forskolin, ± SEM, of 5 replicates.

Table 3.7: Potency (pEC_{50}) and range of response for cAMP inhibition in CHO-K1 cells stably expressing the A_3R, upon stimulation with NECA and TZQ 1-5.

	pEC_{50}[a]	Range	n
NECA	9.75±0.1	-34.35±2.2	5
TZQ 1	NR	NR	5
TZQ 2	NR	NR	5
TZQ 3	NR	NR	5
TZQ 4	9.45±0.2	-16.59±1.1**	5
TZQ 5	NR	NR	5

Data ± SEM of n individual replicates.
[a] Negative logarithm of agonist concentration producing half-maximal response.
[b] Range of response measured as a percentage reduction in response obtained for stimulation with 10 μM forskolin.
NR – No response.
Statistical difference between each agonist and NECA was calculated using a one-way ANOVA with Dunnet's post-test (**, $p < 0.01$).

3.4.2 Triazoloquinazolines as $A_{2A}R$ agonists in mammalian cells

Having confirmed the activity of the triazoloquinazolines upon the $A_{2A}R$ in yeast, these findings were further validated in mammalian cells. In order to do this, CHO-K1 cells were utilised, due to their lack of an endogenous response to the non-selective adenosine agonist, NECA (Figure 3.1). In order to achieve this, cells were transfected with pcDNA3.1-$A_{2A}R$ and stimulated with a selective $A_{2A}R$ agonist, CGS21680, as a reference ligand, as well as with each triazoloquinazoline. The data obtained for CGS21680 however, resulted in a more linear relationship than the fitting of a dose-response curve suggests (Figure 3.1.3); this is potentially a result of averaging each data point before fitting a dose-response curve, rather than creating an average of each curve for each individual replicate. Upon stimulation with each TZQ compound it was apparent that each are indeed $A_{2A}R$ agonists, except TZQ 5, which displayed no activity

up to 1 μM (Figure 3.13, Table 3.8). As TZQ 5 showed a very limited response in yeast (Figure 3.11F, Table 3.6), and none in CHO-K1 cells, it presumably suggests that the small response observed (only at 1 μM) in yeast is more of an effect of stochastic noise, rather than true agonistic activity. For TZQ 1-4, it was apparent that all responses are more potent in CHO-K1 cells than in yeast, by ~3-150 fold (Figure 3.13 and 3.11, Table 3.6 and 3.8). Of the selective TZQ compounds, it was identified that TZQ 1 and 2 are the most potent (pEC_{50}: 7.60±0.2 and 7.21±0.4, respectively), with TZQ 3 displaying a reduced potency (pEC_{50}: 6.35±0.5) (Figure 3.13, Table 3.8). All of these compounds are less potent than the known $A_{2A}R$ agonist, CGS21680 (pEC_{50}: 9.16±0.2), with TZQ 4 displaying the smallest reduction (pEC_{50}: 8.73±0.8) (Figure 3.13, Table 3.8). In terms of maximal signalling, all TZQ compounds are partial agonists relative to CGS21680, with TZQ 1 generating the largest response (E_{max}: 73.23%±6.7) (Figure 3.13, Table 3.8). Analysis of the efficacy (Log τ) and pKa values obtained through fitting the operational model of pharmacological agonism (Black and Leff, 1983) to cAMP data appears to display correlations between E_{max} and Log τ, as well as pEC_{50} and pKa. However, whilst pKa and Log τ appear to be reduced relative to CGS21680, this only seems to be statistically significant for the pKa of TZQ 3. By testing the triazoloquinazolines in mammalian CHO-K1 cells, it was possible confirm the findings in yeast, and confirm that the compounds are indeed agonists of the $A_{2A}R$.

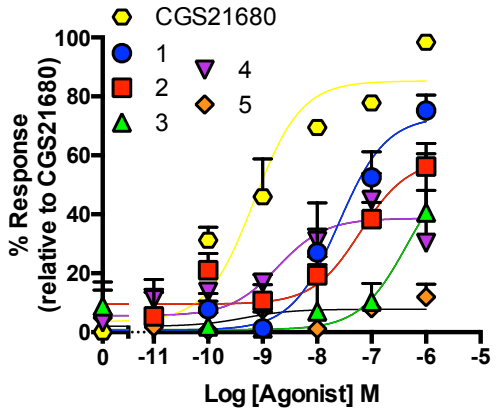

Figure 3.13: Triazoloquinazolines display agonistic activity at the $A_{2A}R$.

CHO-K1 cells transfected with pcDNA3.1-$A_{2A}R$ were stimulated with either CGS21680 or TZQ 1-5, and cAMP accumulation measured. Data represented as the percentage response relative to 1 μM CGS21680 stimulation, ± SEM, of 5 replicates.

Table 3.8: Potency (pEC_{50}), affinity (pKa) and efficacy (Log τ) values for cAMP production upon agonist stimulation in CHO-K1 cells transfected with pcDNA3.1-$A_{2A}R$.

	pEC_{50}[a]	E_{max}[b]	pKa[c]	Logτ[d]	n
CGS21680	9.16±0.2	85.25±6.4	8.93±0.2	-0.15±0.07	5
TZQ 1	7.60±0.2**	73.23±6.7**	7.41±0.2	-0.24±0.06	5
TZQ 2	7.21±0.4**	58.56±10.0**	7.08±0.4	-0.46±0.4	5
TZQ 3	6.35±0.5***	36.10±5.4***	6.21±0.6***	-0.39±0.3	5
TZQ 4	8.73±0.8*	38.61±7.3***	8.65±0.8	-0.69±0.1	5
TZQ 5	ND	ND	ND	ND	5

Data ± SEM of n individual replicates.
[a] Negative logarithm of agonist concentration producing half-maximal response.
[b] Maximal response observed upon agonist stimulation, as a percentage of that observed upon stimulation with 1 μM CGS21680.
[c] Negative logarithm of the equilibrium dissociation constant, as determined using the operational model of agonism (Black and Leff, 1983).
[d] Coupling efficiency parameter as determined using the operational model of agonism (Black and Leff, 1983).
ND – Not Determined, full dose-response curve not feasible.
Statistical difference between each agonist and NECA was calculated using a one-way ANOVA with Dunnet's post-test (*, $p < 0.05$, **, $p < 0.01$, ***, $p < 0.001$).

3.4.3 ERK1/2 activation at the $A_{2A}R$

In order to investigate if the $A_{2A}R$ agonists are able to mediate activation of ERK1/2 in an $A_{2A}R$-dependent manner, CHO-K1 cells transfected with pcDNA3.1-$A_{2A}R$ were again utilised. These were serum-starved overnight to reduce basal ERK1/2 phosphorylation, followed by stimulation with either CGS21680 or TZQ 1-5. This identified that each agonist is able to promote ERK1/2 phosphorylation, except TZQ 5 (Figure 3.14, Table 3.9). It was observed that CGS21680 is the most potent activator of ERK1/2 signalling (pEC_{50}: 9.06±0.2), with TZQ 1, 2 and 4 displaying pEC_{50}s in the nM range (8.14±0.3, 8.55±0.2, and 8.53±0.2, respectively) (Figure 3.14, Table 3.9). In comparison to CGS21680, it was also observed that TZQ 1, 2 and 4 are partial agonists, with TZQ 2 generating the largest response (E_{max}: 76.65%±3.8) (Figure 3.14, Table 3.9). Whilst TZQ 3 displayed an ability to promote ERK1/2 activation, in an $A_{2A}R$-dependent manner, this was only observed with agonist concentrations in the μM range (Figure 3.14, Table 3.9). Thus, it was not possible to fit a full dose-response curve to the data for TZQ 3. This work has thus identified that all of the TZQ compounds are able to mediate ERK1/2 activation to differing extents.

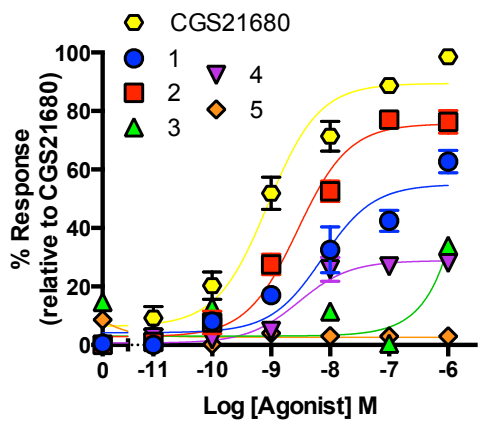

Figure 3.14: Triazoloquinazolines activate ERK1/2 signalling in an $A_{2A}R$-dependent manner.

CHO-K1 cells transfected with pcDNA3.1-$A_{2A}R$ were stimulated with either CGS21680 or TZQ 1-5, and phosphorylation of ERK1/2 measured. Data represented as the percentage response relative to 1 μM CGS21680 stimulation, ± SEM, of 3 replicates.

Table 3.9: Potency (pEC_{50}), affinity (pKa) and efficacy (Log τ) values for ERK1/2 activation, upon agonist stimulation in CHO-K1 cells transfected with pcDNA3.1-$A_{2A}R$.

	pEC_{50}[a]	E_{max}[b]	pKa[c]	Logτ[d]	n
CGS21680	9.06±0.2	89.42±5.4	8.60±0.1	0.21±0.05	3
TZQ 1	8.14±0.3**	54.94±6.2**	7.83±0.2*	-0.22±0.07**	3
TZQ 2	8.55±0.2*	75.65±3.8*	8.20±0.1	0.05±0.04	3
TZQ 3	ND	ND	ND	ND	3
TZQ 4	8.53±0.2*	28.83±1.9***	8.42±0.2	-0.59±0.05***	3
TZQ 5	NR	NR	NR	NR	3

Data ± SEM of n individual replicates.
[a] Negative logarithm of agonist concentration producing half-maximal response.
[b] Maximal response observed upon agonist stimulation, as a percentage of that observed upon stimulation with 100 μM PMA.
[c] Negative logarithm of the equilibrium dissociation constant, as determined using the operational model of agonism (Black and Leff, 1983).
[d] Coupling efficiency parameter as determined using the operational model of agonism (Black and Leff, 1983).
ND – Not Determined, full dose-response curve not feasible.
NR – No response.
Statistical difference between each agonist and NECA was calculated using a one-way ANOVA with Dunnet's post-test (*, $p < 0.05$, **, $p < 0.01$, ***, $p < 0.001$).

3.4.4 Quantifying biased agonism of the $A_{2A}R$

The work upon the $A_{2A}R$ has identified that the five triazoloquinazolines tested all exhibit agonistic activity, except TZQ 5, at two distinct $A_{2A}R$-mediated signalling pathways, cAMP production and ERK1/2 activation. As has been observed, the responses for each ligand at each given pathway differ (Figures 3.13 and 3.14, Tables 3.8 and 3.9). There is, thus, an inherent level of biased agonism exhibited by the agonists. In order to quantify this, the same approach as for the A_1R agonists was utilised (Figures 3.9 and 3.10). This identified that all of the compounds tested, including CGS21680, display biased agonism towards activating ERK1/2-mediated signalling pathways, with TZQ 2 displaying the greatest extent of bias (Figure 3.15A). Calculation of this relative to the reference ligand, CGS21680, also displayed the same trend (Figure 3.15B). As TZQ 3 only mediated ERK1/2 activation at 1 μM, and did not generate a full dose-response curve, it was not possible to fit the operational model of pharmacological agonism (Black and Leff, 1983). This also meant that it was not possible to calculate any parameters for pKa or Log τ, and as such pathway bias could not be quantitated; however, it is clear that TZQ 3 is biased towards cAMP production, as it exhibits greater activity in cAMP accumulation assays (Figure 3.13, Table 3.8) than in ERK1/2 assays (Figure 3.14, Table 3.9). This work has thus identified a series of chemical compounds that display agonistic activity against the $A_{2A}R$, some of which are selective, and display biased agonism towards activating ERK1/2 over $G\alpha_s$-mediated cAMP production.

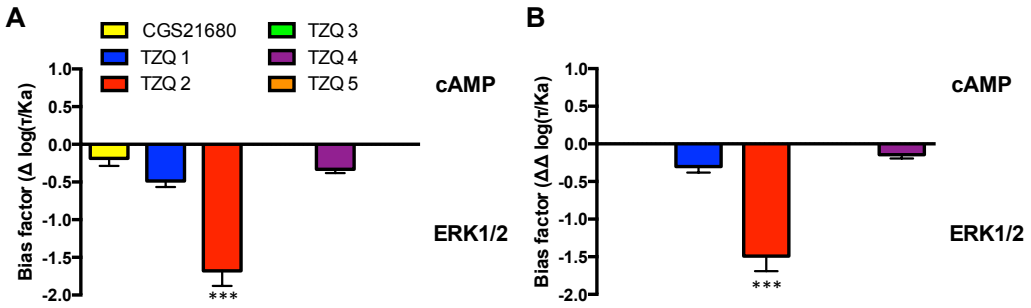

Figure 3.15: Bias plots for triazoloquinazolines between cAMP modulation and ERK1/2 activation.

Quantification of biased agonism, Δ Log (τ/Ka) (A), and relative pathway bias, ΔΔ log (τ/Ka) (B), between: cAMP modulation and ERK1/2 activation, for CGS21680 and Triazoloquinazolines (TZQ) 1-5. Significance was calculated using a one-way ANOVA with Bonferroni's correction (*** $p < 0.001$). Data represented ± SEM.

3.5 Summary

The work in this chapter has highlighted how diverse signalling from ARs actually is: it was possible to observe the ability of the A_1R to activate its canonical $G\alpha_{i/o}$ pathway (Figure 3.4, Table 3.2), as well as the opposing $G\alpha_s$ pathway (Figure 3.5, Table 3.3). In addition, mobilisation of $_iCa^{2+}$ (Figures 3.6 and 3.7, Table 3.4), and activation of ERK1/2 (Figure 3.8, Table 3.5) was also observed. Activation of all such pathways was apparent for the cognate ligands, NECA and adenosine, as well as the commercially available, AR agonist, CCPA. This phenomenon had also been observed for the selective and non-selective A_1R agonists, which had been developed, based upon NECA and adenosine scaffolds (Figure 3.2). Through modulating the functional groups of NECA and adenosine to those in the A_1R compounds (Figure 3.2), it is apparent how activity against the A_1R is maintained, and in the case of Cmpds 5, 6, 16 and 18, how A_1R selectivity is gained (Knight *et al*, 2016, Appendix 1). In addition, modulating the functional groups in these compounds has given each a distinct pattern of bias (Figure 3.9 and 3.10): with some being more biased towards mobilisation of $_iCa^{2+}$ over all other pathways (Cmpds 5 and 21), some being most biased towards cAMP production (Cmpds 16 and 18), and one being more biased to the activation of ERK1/2 over all other pathways (Cmpd 20). Having developed and characterised these compounds, with respect to their ability to activate different signalling

pathways at the A_1R, it will now be possible to, potentially, utilise these compounds to probe differing active conformations of the A_1R. They may also be of use for the promotion of cell survival, as A_1R activation has been observed to be cytoprotective *in vitro* (Baltos *et al*, 2016).

In addition to the pharmacology of the A_1R, the $A_{2A}R$ has also been investigated. Along with collaborators in Dr. Bender's group, we have identified a series of existing compounds, triazoloquinazolines, which have previously been identified as PDE10A inhibitors (Kehler *et al*, 2011) that are also $A_{2A}R$ agonists (Figure 3.11 and 3.13, Tables 3.6 and 3.8). For some of these, TZQ 1-3, it was possible to successfully identify selectivity for the $A_{2A}R$, over other AR subtypes (Figures 3.11-13, Tables 3.6-8). Having identified selective and non-selective $A_{2A}R$ agonists, for cAMP accumulation, their ability to activate ERK1/2 signalling was also investigated. This identified that CGS21680 is able to bring about activation of ERK1/2 as are TZQ 1, 2 and 4, with TZQ 3 generating a weak response at 1 μM (Figure 3.14, Table 3.9). Analysis of the bias profile for these compounds indicated that all $A_{2A}R$ agonists tested display bias towards signalling via ERK1/2 pathways, over cAMP production (Figure 3.15). This may potentially prove beneficial in the treatment of various neurodegenerative diseases, as ERK1/2 activation by ARs has been seen to promote cell survival and proliferation (Jacques-Silva *et al*, 2004, Migita *et al*, 2008, Baltos *et al*, 2016).

Chapter 4

The effects of RAMPs upon CLR pharmacology

4.1 Introduction

The calcitonin-like receptor (CLR) is a family B GPCR, closely related to the calcitonin receptor; on its own it is non-functional, being unable to traffic to the cell surface. In order to allow cell surface expression, the CLR requires the association of one of three molecular chaperone proteins, receptor activity modifying proteins (RAMPs) 1, 2 or 3 (McLatchie *et al*, 1998). Association of both CLR and RAMP is essential for surface expression of both proteins (McLatchie *et al*, 1998). Each RAMP-CLR heterodimer forms a distinct receptor phenotype: RAMP1-CLR forms the calcitonin gene-related peptide (CGRP) receptor, RAMP2-CLR the adrenomedullin 1 (AM_1) receptor, and RAMP3-CLR the adrenomedullin 2 (AM_2) receptor. Each of these three heterodimers bind, and respond, to three peptide hormones: CGRP, AM and AM2 (or intermedin). Each of these peptides act as agonists against each RAMP-CLR heterodimer, with differing potencies (Poyner *et* al, 2002, Hong *et al*, 2012). Activation of all of the CLR-based receptors has been shown to result in raising intracellular cAMP levels, in a $G\alpha_s$-dependent manner (McLatchie *et al*, 1998, Poyner *et al*, 2002, Chang *et al*, 2004, Roh *et al*, 2004, Takei *et al*, 2004, Hay *et al*, 2005, Wunder *et al*, 2008). Each receptor has also been observed to activate other signalling pathways, including $G\alpha_{i/o}$ (Kim, 1991, Wiley *et al*, 1992, Main *et al*, 1998, Disa *et al*, 2000, Kuwasako *et al*, 2010). However, to date little work has been performed to elucidate the full signalling repertoire associated with the CLR, and how RAMPs modulate this. Previous work in our laboratory, performed by Dr. C. Weston (University of Warwick, UK), investigated the individual G protein couplings of the CLR using the yeast screening

system. Through this she identified the ability of each RAMP-CLR heterodimer to signal via GPA1/$G\alpha_s$, GPA1/$G\alpha_{i1/2}$ and GPA1/$G\alpha_q$, in response to all three agonists: CGRP, AM and AM2 (Weston *et al*, 2016, Appendix 2). This work also informed upon potential biased agonism at the CLR, as the observed responses at each pathway were both agonist- and RAMP-dependent. In this chapter the ability of CGRP, AM and AM2 to activate each RAMP-CLR heterodimer in a mammalian system, HEK 293 cells, is characterised. This is investigated with regards to their ability to activate $G\alpha_s$-mediated signalling, $G\alpha_{i/o}$ signalling, and intracellular calcium ($_iCa^{2+}$) mobilisation. Having characterised their signalling properties at these three pathways, the extent of biased agonism for each agonist is quantified, at each RAMP-CLR heterodimer. These findings were reported in the Journal of Biological Chemistry in 2016 (Weston *et al*, 2016, Appendix 2).

4.2 HEK 293 cells - a model for studying RAMP-CLR pharmacology

In order to be able to study family B GPCRs, such as the CLR, in mammalian cells lines, it is necessary to establish that the cells do not endogenously express the receptor of interest, nor RAMPs. Dr. C. Weston had previously identified a HEK 293 cell line that did not express functional RAMPs (Weston *et al*, 2015), thus it was sought to further identify if they expressed functional CLR. To determine this HEK 293 cells were transfected with pcDNA-FLAG-RAMP1, 2, or 3, and cAMP accumulation measured, in response to stimulation with CGRP, AM or AM2, due to the well-known ability of the CLR to couple to $G\alpha_s$ proteins (McLatchie et al, 1998, Poyner *et* al. 2002, Chang *et al*, 2004, Roh *et al*, 2004, Takei *et* al, 2004, Hay *et al*, 2005, Wunder *et al*, 2008). Agonist stimulation did not result in any observable increase above basal cAMP levels, whilst stimulation with 100 μM forskolin indicates the cells' ability to produce cAMP (Figure 4.1). Thus, our HEK 293 cell line does not only lack expression of functional RAMPs, but also functional CLR. This

simple characterisation allowed the identification of the HEK 293 cell line to be suitable for the purposes of RAMP-CLR studies.

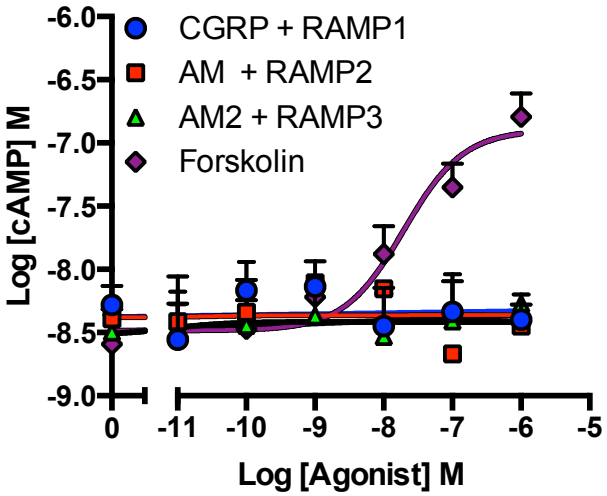

Figure 4.1: HEK 293 cells do not express RAMPs.

Transfection of cells with pcDNA3.1-FLAG-RAMP 1, 2, or 3 followed by stimulation with CGRP, AM or AM2 resulted in no increase in cAMP levels, above basal. Stimulation with 100 μM forskolin indicates the ability of these cells to produce cAMP. Data represented as total cAMP per cell, ± SEM.

4.3 Investigating $G\alpha_s$-mediated signalling of the CLR

In order to investigate the commonly characterised $G\alpha_s$-mediated signalling pathway of the CLR, HEK 293 cells were co-transfected with a 1:1 ratio of pcDNA3.1-FLAG-RAMP and pcDNA3.1-cMyc-CLR-GFP. Successful transfection, and expression of both RAMP and CLR, from these plasmids, would result in the formation of RAMP-CLR heterodimers. Thus, upon stimulation with CGRP, AM or AM2, for each RAMP-CLR complex, it should be possible to observe an increase in intracellular cAMP levels. In order to measure this the LANCE® cAMP accumulation kit was utilised. The ability of these three agonists to activate the CLR in terms of cAMP production is well characterised (McLatchie et al, 1998, Poyner *et al*, 2002, Chang *et al*, 2004, Roh *et al*, 2004, Takei *et* al, 2004, Hay *et al*, 2005, Wunder *et al*, 2008). By further investigating CLR-mediated cAMP production it is possible to establish that functional RAMP-CLR dimers can be formed in the system of study. It is also necessary to characterise their functional ability due to the variance in cellular background of these HEK 293 cells relative to those

previously used, as this has been shown to have distinct effects upon the response observed (Weston *et al*, 2016, Appendix 2). Upon co-transfection with pcDNA3.1-FLAG-RAMP1 and pcDNA3.1-cMyc-CLR-GFP, followed by stimulation with CGRP, AM and AM2, it was observed that all three agonists elicit a response (Figure 4.2A, Table 4.1), with a rank order of potency of: CGRP > AM = AM2 (pEC_{50}: 9.81±0.20, 7.92±0.19, 7.93±0.24, respectively). In addition, all three agonists were observed to be full agonists, generating maximal responses of approximately 45% (relative to 100 μM forskolin). In contrast, RAMP2-CLR heterodimers exhibit a different response, where the rank order of potency is AM > CGRP > AM2 (pEC_{50}: 10.35±0.13, 8.97±0.24, 7.48±0.23, respectively), with CGRP and AM2 being partial agonists (E_{max}: 37.2%±2.4, 34.1%±4.0, respectively), relative to AM (E_{max}: 55.0%±1.7) (Figure 4.2B, Table 4.1). For RAMP3-CLR it was observed that AM2 displays an increased potency compared to that observed with RAMP1 or 2, whilst CGRP displays a reduction in potency, giving a rank order of potency of: AM = AM2 > CGRP (pEC_{50}: 8.86±0.14, 9.14±0.22, 7.75±0.30, respectively) (Figure 4.2C, Table 4.1). As with RAMP2-CLR, both CGRP and AM2 are partial agonists (E_{max}: 22.3%±2.1, 21.9%±0.22, respectively) relative to AM (E_{max}: 32.1%±1.6) (Figure 4.2C, Table 4.1).

Analysis of this data, through utilising the operational model of pharmacological agonism (Black and Leff, 1983), clearly shows how RAMPs significantly alter the action of each agonist upon the CLR. Investigating the effect of RAMPs upon the intrinsic affinity (pKa) of each agonist identified that for RAMP1-CLR, CGRP has the highest pKa, with AM and AM2 having equal values (Table 4.1). This correlates with the orders of potency for these agonists. Whilst each agonist is equally efficacious (Log τ) (Figure 4.2D, Table 4.1), this suggests that it is the affinity of each agonist for the RAMP1-CLR complex that is the main determinant of potency. At RAMP2-CLR complexes it was observed that AM displays the highest affinity, followed by CGRP, with AM2 having the lowest pKa (Table 4.1). This again closely correlates with what is observed in terms of potency order (Figure 4.2B, Table 4.1). Interestingly,

efficacy follows the same trend observed for the E_{max} of each agonist, where CGRP and AM2 are both partial agonists; they also display a much lower efficacy than AM (Table 4.1). This again correlates with the RAMP1-CLR data, whereby pKa appears to influence potency, but also suggests that efficacy determines E_{max}. This pattern is also apparent for RAMP3-CLR, where pKa follows rank order of potency (Table 4.1), and CGRP and AM2 both have equal lower efficacies than AM, which is a full agonist (Table 4.1).

Characterising the ability of CGRP, AM and AM2 to mediate an increase in intracellular cAMP has identified that the CLR can be stimulated by all three agonists in the presence of each RAMP. This work has further identified that RAMPs modulate the ability of each agonist to stimulate the CLR, bringing about an increase in intracellular cAMP, in a $G\alpha_s$-dependent manner.

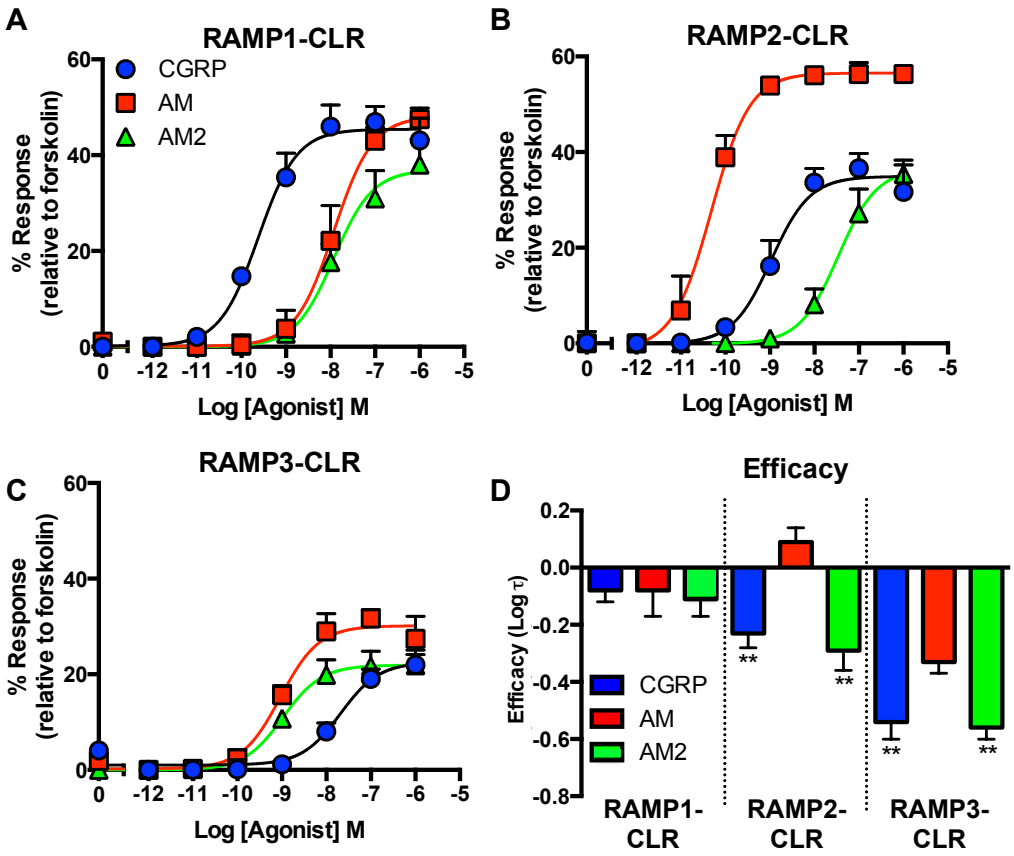

Figure 4.2: RAMPs modulate the ability of CGRP, AM and AM2 to elevate intracellular cAMP levels in a CLR-dependent manner.

cAMP accumulation was measured in HEK 293 cells transfected with pcDNA3.1-FLAG-RAMP 1 (n = 11) (A), -RAMP 2 (n = 8) (B) or -RAMP 3 (n = 9) (C) in conjunction with pcDNA3.1-cMyc-CLR-GFP, upon stimulation with CGRP, AM or AM2 for 30 minutes. Data are expressed relative to stimulation with 100 μM forskolin, ± SEM. D – Bar chart displaying the efficacy (Log τ) values for each ligand stimulating each RAMP-CLR heterodimer. Significance was calculated using a one-way ANOVA with Bonferroni's correction (** $p < 0.01$). Data represented ± SEM.

Table 4.1: Potency (pEC_{50}), affinity (pKa) and coupling efficacy (Log τ) values for cAMP production at each RAMP-CLR heterodimer.

	RAMP1-CLR			RAMP2-CLR			RAMP3-CLR		
	CGRP	**AM**	**AM2**	**CGRP**	**AM**	**AM2**	**CGRP**	**AM**	**AM2**
pEC_{50}[a]	9.81±0.20	7.92±0.19**	7.93±0.24**	8.97±0.24***	10.35±0.13	7.48±0.23***	7.75±0.3**	8.86±0.14	9.14±0.22
E_{max}[b]	45.0±2.2	45.2±3.7	43.6±4.2	37.2±2.4**	55.0±1.7	34.1±4.0**	22.3±2.1**	32.1±1.6	21.9±1.7**
pKa[c]	9.60±0.18	7.64±0.28**	7.76±0.20**	8.71±0.2	9.95±0.23	7.16±0.24	7.64±0.26	8.50±0.19	9.00±0.18*
Logτ[d]	-0.08±0.04	-0.08±0.09	-0.11±0.06	-0.23±0.05*	0.09±0.05	-0.29±0.07**	-0.54±0.06*	-0.33±0.04	-0.56±0.04*
n	11	11	11	8	8	8	9	9	9

Data ± SEM of n individual replicates.
[a] Negative logarithm of agonist concentration producing half-maximal response.
[b] Maximal response observed upon agonist stimulation, as a percentage of that observed upon stimulation with 10 μM forskolin.
[c] Negative logarithm of the equilibrium dissociation constant, as determined using the operational model of agonism (Black and Leff, 1983).
[d] Coupling efficacy parameter as determined using the operational model of agonism (Black and Leff, 1983).
Statistical significance compared to the cognate agonist for each receptor heterodimer (RAMP1-CLR, CGRP; RAMP2/3-CLR, AM) was determined by one-way ANOVA with Dunnett's post-test (*, $p < 0.05$, **, $p < 0.01$, ***, $p < 0.001$, ****, $p < 0.0001$).

4.4 Investigating $G\alpha_{i/o}$-mediated signalling of the CLR

It is well known that the activity of adenylate cyclase can be modulated via both $G\alpha_s$ and $G\alpha_{i/o}$ (Milde *et al*, 2013), having positive and negative effects upon the levels of intracellular cAMP, respectively. Thus, a GPCR that potentially couples to both will elicit a perceived $G\alpha_s$ response that is actually a summation of both pathways. Where increases in cAMP are measured, they will be 'dampened' by the opposing action of $G\alpha_{i/o}$, potentially in terms of both maximal signalling (E_{max}) and potency (pEC_{50}). Therefore, in order to uncover any potential couplings to $G\alpha_{i/o}$, it is first necessary to inhibit its action, and look for a subsequent increase in either E_{max} or pEC_{50}. This can be achieved via pre-treatment of cells with PTX, which ADP-ribosylates the C-termini of $G\alpha_{i/o}$, serving to uncouple them from GPCRs (West *et al*, 1985).

Whilst many groups have looked at the ability of the CLR to elevate intracellular cAMP, no extensive characterisation of their coupling to inhibitory G proteins has been undertaken. To address this, HEK 293 cells were co-transfected with pcDNA3.1-FLAG-RAMP and pcDNA3.1-cMyc-CLR-GFP and treated with 200 ng/ml PTX, for 16-18 hours, to inhibit the action of $G\alpha_{i/o}$ proteins. In order to confirm that any differences observed are due to true biological effects, mock-transfected cells (expressing pcDNA3.1-GFP) were treated with PTX, and the effect of forskolin upon cAMP levels was measured and compared to untreated cells. It was observed that pre-treatment with PTX had no effect (Figure 4.3). Thus, there can be confidence that any effects observed are not due to PTX affecting other signalling components.

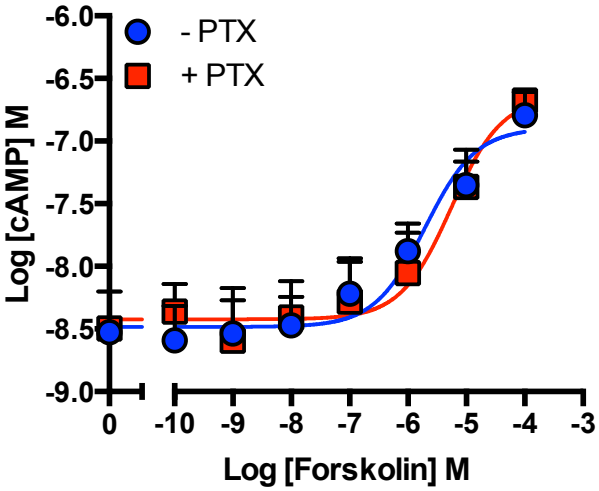

Figure 4.3: Pre-treatment with pertussis toxin does not affect cAMP production in HEK 293 cells.

Pre-treatment of HEK 293 cells, for 16-18 hours, with 200 ng/ml pertussis toxin (PTX) did not affect their ability to produce cAMP in response to forskolin stimulation, relative to untreated cells. Data ± SEM, of 3 replicates.

Having confirmed that PTX had no toxic effects on HEK 293 cells' ability to signal, cells co-expressing RAMP-CLR heterodimers were treated, and their ability to produce cAMP compared to untreated cells, upon stimulation with CGRP, AM and AM2. In PTX-treated cells, transfected with pcDNA3.1-FLAG-RAMP1 and pcDNA3.1-cMyc-CLR-GFP, stimulated with CGRP, no difference in cAMP accumulation was observed, relative to untreated cells (Figure 4.4A). This was also apparent for the pKa and efficacy values (Table 4.2). However, upon challenge with AM an increase in maximal signalling was observed, whilst with AM2 an increase in both E_{max} and potency were observed (Figure 4.4A). These increases in maximal level of signalling are also concurrent with increases in efficacy of the agonists (Table 4.2). An increase in pKa was observed for AM2 upon PTX pre-treatment, however this was not significant. The effects upon AM and AM2 responses are indicative of removal of an inhibitory $G\alpha_{i/o}$ signalling component. In contrast, the lack of an effect of PTX upon CGRP signalling indicates that this agonist is unable to mediate signalling in a $G\alpha_{i/o}$-dependent manner from RAMP1-CLR heterodimers.

In cells transfected with pcDNA3.1-FLAG-RAMP2 and pcDNA3.1-cMyc-CLR-GFP, it was possible to observe increases in E_{max} upon PTX pre-

treatment for stimulation with both CGRP and AM2, with an associated increase in potency (Figure 4.4B). In contrast, AM displayed no difference to untreated cells (Figure 4.4B). These increases in E_{max} are again concurrent with an increased efficacy (Table 4.2). Interestingly, whilst AM2 displays an expected increased pKa, CGRP also showed a small increase, without an increase in pEC_{50} (Table 4.2). These results indicate a lack of ability of AM to signal in a $G\alpha_{i/o}$-dependent manner in the presence of RAMP2, whilst both CGRP and AM2 are able to signal via this pathway. A similar pattern is observed in PTX pre-treated cells co-transfected with pcDNA3.1-FLAG-RAMP3 and pcDNA3.1-cMyc-CLR-GFP, with AM stimulation displaying no discernable difference relative to untreated cells (Figure 4.4C, Table 4.2). CGRP displayed coupling to $G\alpha_{i/o}$, with an increased E_{max} and potency, concurrent with an associated increase in pKa. An increased efficacy was also observed, however this was not significant (Figure 4.4C, Table 4.2). AM2 also displayed PTX-sensitivity with an increase in both E_{max} and efficacy (Figure 4.4C, Table 4.2).

This data thus indicates that the CLR has the ability to couple to $G\alpha_{i/o}$ in the presence of all three RAMPs. Interestingly, this appears to be both agonist- and RAMP-dependent, with the cognate agonist for each RAMP-CLR complex (CGRP for RAMP1-CLR; AM for RAMP2, 3-CLR) being insensitive to PTX. This indicates that not only do RAMPs modulate the ability of each agonist to bring about elevations in cAMP, but that they also serve to modulate G protein-coupling.

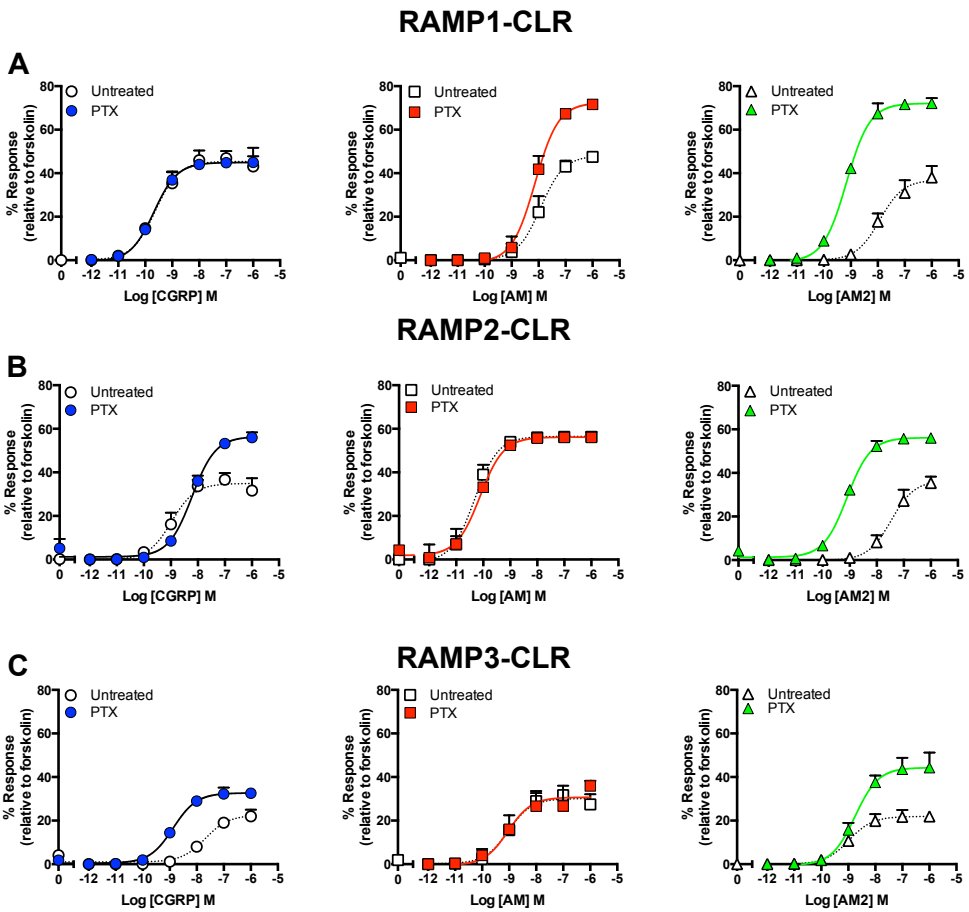

Figure 4.4: RAMP-CLR heterodimers display PTX-sensitivity in response to stimulation with CGRP, AM and AM2.

cAMP accumulation was measured in HEK 293 cells pre-treated, for 16-18 hours, with 200 ng/ml PTX, transfected with pcDNA3.1-FLAG-RAMP 1 (n = 6) (A), -RAMP 2 (n = 6) (B) or -RAMP 3 (n = 6) (C) in conjunction with pcDNA3.1-cMyc-CLR-GFP, upon stimulation with CGRP, AM or AM2 for 30 minutes. Data are expressed relative to stimulation with 100 μM forskolin, ± SEM.

Table 4.2: Potency (pEC_{50}), affinity (pKa) and coupling efficacy (Log τ) values for cAMP production at each RAMP-CLR heterodimer in PTX pre-treated and untreated HEK 293 cells.

	Untreated					Treated				
RAMP1	**pEC_{50}[a]**	**E_{max}[b]**	**pKa[c]**	**Logτ[d]**	**n**	**pEC_{50}[a]**	**E_{max}[b]**	**pKa[c]**	**Logτ[d]**	**n**
CGRP	9.66±0.2	47.07±2.2	9.43±0.2	-0.11±0.04	9	9.65±0.2	44.95±2.2	9.33±0.3	-0.11±0.07	6
AM	7.93±0.2	48.06±2.5	7.67±0.2	-0.09±0.05	9	8.14±0.07	72.17±1.7***	7.66±0.2	0.36±0.1**	6
AM2	7.93±0.2	46.10±4.1	7.70±0.2	-0.11±0.07	9	9.15±0.1*	72.15±2.4***	8.56±0.3	0.40±0.1**	6
RAMP2	**pEC_{50}[a]**	**E_{max}[b]**	**pKa[c]**	**Logτ[d]**	**n**	**pEC_{50}[a]**	**E_{max}[b]**	**pKa[c]**	**Logτ[d]**	**n**
CGRP	9.00±0.2	36.97±2.4	8.82±0.2	-0.27±0.05	9	8.25±0.4	56.27±1.4***	7.92±0.2*	0.1±0.06**	6
AM	10.35±0.1	56.33±1.6	10.00±0.1	0.07±0.02	9	10.16±0.07	56.07±1.1	9.83±0.2	0.07±0.02	6
AM2	7.46±0.2	36.61±3.5	7.24±0.2	-0.29±0.07	9	9.13±0.1**	56.05±2.2***	8.84±0.2**	0.1±0.06*	6
RAMP3	**pEC_{50}[a]**	**E_{max}[b]**	**pKa[c]**	**Logτ[d]**	**n**	**pEC_{50}[a]**	**E_{max}[b]**	**pKa[c]**	**Logτ[d]**	**n**
CGRP	7.75±0.3	22.38±2.6	7.64±0.3	-0.54±0.07	8	8.90±0.1*	32.61±1.5*	8.74±0.2*	-0.29±0.06	7
AM	8.98±0.2	32.00±1.5	8.83±0.1	-0.33±0.03	8	9.10±0.2	35.95±2.2	8.94±0.2	-0.34±0.05	7
AM2	9.10±0.2	21.92±1.7	9.08±0.2	-0.51±0.06	8	8.74±0.2	44.35±2.7****	8.43±0.1*	-0.07±0.07***	7

Data ± SEM of n individual replicates.
[a] Negative logarithm of agonist concentration producing half-maximal response.
[b] Maximal response observed upon agonist stimulation, as a percentage of that observed upon stimulation with 10 μM forskolin.
[c] Negative logarithm of the equilibrium dissociation constant, as determined using the operational model of agonism (Black and Leff, 1983).
[d] Coupling efficacy parameter as determined using the operational model of agonism (Black and Leff, 1983).
Statistical difference between PTX pre-treated and untreated was determined using Student's t-test (*, $p < 0.05$, **, $p < 0.01$, ***, $p < 0.001$, ****, $p < 0.0001$).

4.5 Investigating CLR-mediated $_{i}Ca^{2+}$ mobilisation

It has long been known that activation of many GPCRs can result in the mobilisation of $_{i}Ca^{2+}$ (Carroll and Peralta, 1998, Yatani *et al*, 1999, Xu and Xie, 2009, Koole *et al*, 2010, Gao and Jacobson, 2016, Hager *et al*, 2017)**;** there is thus interest in establishing whether this also occurs at the CLR. From the work of Dr. C. Weston, we had observed functional coupling of RAMP-CLR heterodimers to GPA1/$G\alpha_q$, in yeast (Weston *et al*, 2016, Appendix 2). To validate this, the aim was to determine if the CLR can mobilise $_{i}Ca^{2+}$ in response to CGRP, AM or AM2 stimulation, and also if this process is modulated by RAMPs. In order to do this the same HEK 293 cells as for cAMP assays were utilised, co-transfected with pcDNA3.1-HA-CLR and each FLAG-RAMP construct (pcDNA3.1-FLAG-RAMP1, 2, or 3). These were then loaded with the calcium dye FLUO-4/AM, which fluoresces (excitation: 494 nm, emission: 506 nm) upon binding Ca^{2+} (Gee *et al*, 2000). In each experiment, stimulation with 10 μM ionomycin was utilised to establish sufficient dye loading, as well as the ability of the cells to mobilise $_{i}Ca^{2+}$. The observed response was normalised to that obtained from 10 μM ionomycin stimulation, in order to account for variations in dye loading and $_{i}Ca^{2+}$ content on each day. Each experiment was performed in Ca^{2+}-free HBSS, thus only mobilisation of $_{i}Ca^{2+}$ is measured, and not entry via cell surface channels.

4.5.1 RAMP1-CLR-mediated $_{i}Ca^{2+}$ mobilisation

HEK 293 cells co-transfected with pcDNA3.1-HA-CLR and pcDNA3.1-FLAG-RAMP1 were assayed for responses to CGRP, AM and AM2 (Figure 4.5A-D, Table 4.3). Upon stimulation with each agonist, an increase in fluorescence was observed, reaching peak intensity before decaying, with the maximal observed intensity being dose-dependent (Figure 4.5A-C). The post-stimulation peak and decay indicates that only $_{i}Ca^{2+}$ is being measured; if extracellular entry were observed, a sustained phase following peak intensity would be predicted. Converting this data to

dose-response curves (Figure 4.5D) allows calculation of the potency of each agonist (Table 4.3), whereby a rank order of potency of CGRP >> AM > AM2 (pEC_{50}: 9.52±0.2, 7.87±0.3, 6.76±0.2, respectively) was observed. This data also identified that AM and AM2 are partial agonists (E_{max}: 33.94%±4.7, 25.05%±2.4, respectively), whilst CGRP is a full agonist (E_{max}: 73.84%±2.7). Analysis of the efficacy (Log τ) values for these three agonists at RAMP1-CLR heterodimers (Figure 4.5E, Table 4.3) reveals a rank order of efficacy of CGRP >> AM > AM2, matching the same trends observed for agonist potency. Interestingly, as with cAMP accumulation, it was observed that the cognate agonist to RAMP1-CLR, CGRP, is the most potent and efficacious agonist at mobilising $_{i}Ca^{2+}$.

Table 4.3: Potency (pEC_{50}), affinity (pKa) and coupling efficacy (Log τ) values for $_{i}Ca^{2+}$ mobilisation at each RAMP-CLR heterodimer in PTX pre-treated and untreated HEK 293 cells.

RAMP1	Untreated					Treated				
	pEC_{50}[a]	E_{max}[b]	pKa[c]	Logτ[d]	n	pEC_{50}[a]	E_{max}[b]	pKa[c]	Logτ[d]	n
CGRP	9.52±0.2	73.84±2.7	8.91±0.2	0.45±0.07	5	8.93±0.2	74.29±3.9	8.30±0.2	0.45±0.07	5
AM	7.87±0.3	33.94±4.7	7.72±0.3	-0.30±0.08	5	7.92±0.2	42.56±3.5	7.67±0.3	-0.13±0.07	5
AM2	6.76±0.2	25.05±2.4	6.66±0.1	-0.48±0.03	5	7.01±0.1	22.44±0.9	6.90±0.1	-0.54±0.03	5
RAMP2	**Untreated**					**Treated**				
	pEC_{50}[a]	E_{max}[b]	pKa[c]	Logτ[d]	n	pEC_{50}[a]	E_{max}[b]	pKa[c]	Logτ[d]	n
CGRP	7.71±0.1	62.42±4.0	7.06±0.1	0.53±0.1	5	7.67±0.2	62.7±4.6	7.29±0.3	0.21±0.1	5
AM	7.86±0.1	63.00±2.8	7.51±0.1	0.21±0.04	5	7.88±0.1	63.07±1.8	7.45±0.1	0.20±0.1	5
AM2	7.41±0.4	44.41±7.1	7.17±0.3	-0.10±0.1	5	7.41±0.3	41.88±5.7	7.12±0.6	-0.13±0.2	5
RAMP3	**Untreated**					**Treated**				
	pEC_{50}[a]	E_{max}[b]	pKa[c]	Logτ[d]	n	pEC_{50}[a]	E_{max}[b]	pKa[c]	Logτ[d]	n
CGRP	7.15±0.2	90.26±9.8	6.14±0.5	0.96±0.4	5	7.20±0.3	85.07±9.5	6.83±0.5	0.35±0.3	5
AM	8.12±0.3	56.59±7.0	7.75±0.2	0.12±0.08	5	8.44±0.1	52.64±1.6	8.11±0.2	0.045±0.08	5
AM2	8.21±0.3	19.17±2.8	8.77±0.3	-0.72±0.07	5	8.07±0.3	22.12±2.3	7.99±0.3	-0.56±0.07	5

Data ± SEM of n individual replicates.
[a] Negative logarithm of agonist concentration producing half-maximal response.
[b] Maximal response observed upon agonist stimulation, as a percentage of that observed upon stimulation with 10 μM forskolin.
[c] Negative logarithm of the equilibrium dissociation constant, as determined using the operational model of agonism (Black and Leff, 1983).
[d] Coupling efficacy parameter as determined using the operational model of agonism (Black and Leff, 1983).
Statistical difference between PTX pre-treated and untreated cells was determined using Student's t-test (*, $p < 0.05$, **, $p < 0.01$, ***, $p < 0.001$, ****, $p < 0.0001$).

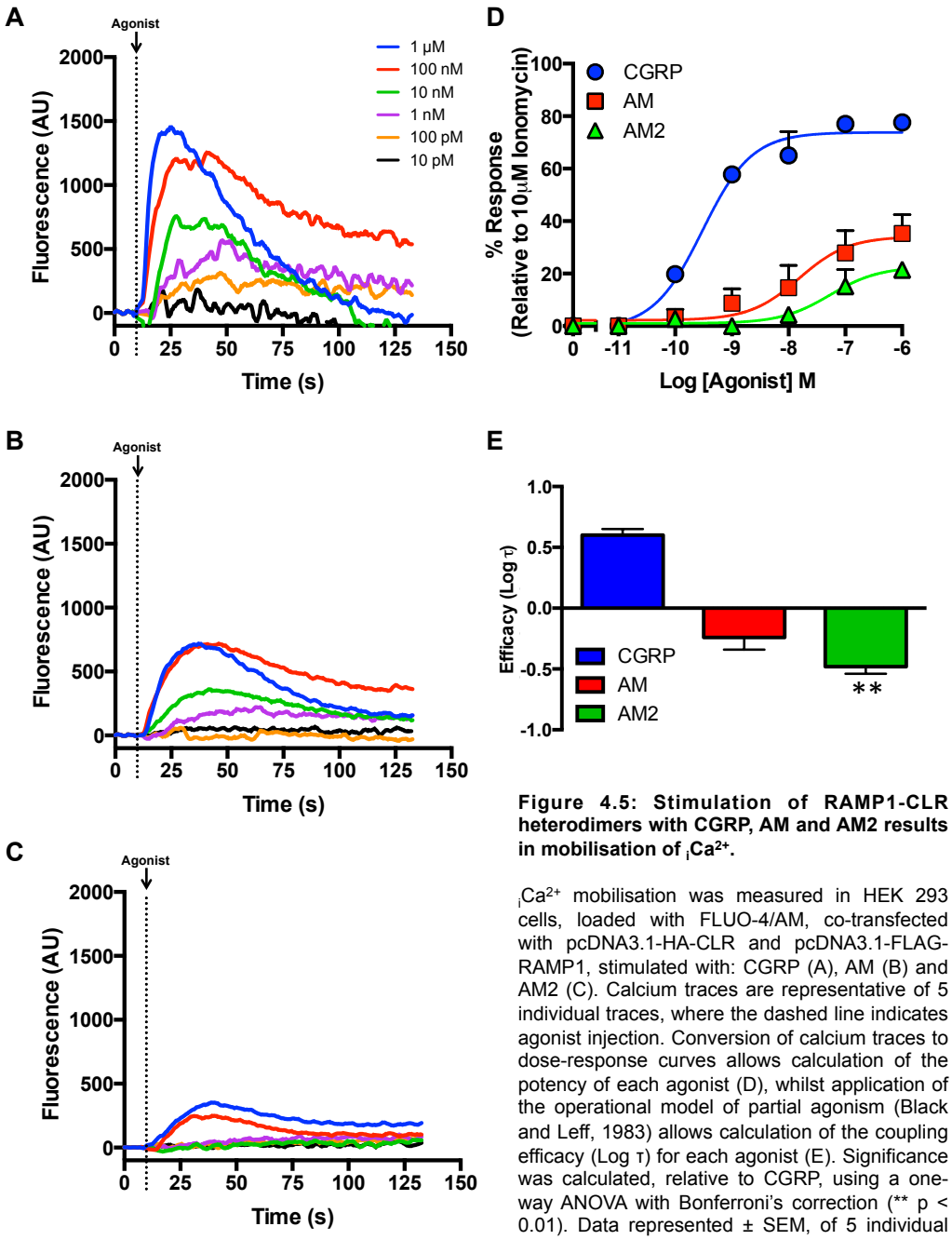

Figure 4.5: Stimulation of RAMP1-CLR heterodimers with CGRP, AM and AM2 results in mobilisation of $_{i}Ca^{2+}$.

$_{i}Ca^{2+}$ mobilisation was measured in HEK 293 cells, loaded with FLUO-4/AM, co-transfected with pcDNA3.1-HA-CLR and pcDNA3.1-FLAG-RAMP1, stimulated with: CGRP (A), AM (B) and AM2 (C). Calcium traces are representative of 5 individual traces, where the dashed line indicates agonist injection. Conversion of calcium traces to dose-response curves allows calculation of the potency of each agonist (D), whilst application of the operational model of partial agonism (Black and Leff, 1983) allows calculation of the coupling efficacy (Log τ) for each agonist (E). Significance was calculated, relative to CGRP, using a one-way ANOVA with Bonferroni's correction (** $p < 0.01$). Data represented ± SEM, of 5 individual replicates.

In order to elucidate the mechanism whereby CGRP, AM and AM2 mediate $_{i}Ca^{2+}$ mobilisation via RAMP1-CLR, HEK 293 cells co-transfected with pcDNA3.1-FLAG-RAMP1 and pcDNA3.1-HA-CLR, were pre-treated with 200 ng/ml PTX, for 16-18 hours, to determine if the $G\alpha_{i/o}$ signalling component previously uncovered (Figure 4.4) plays any role. Cells treated in this manner were then assayed for the mobilisation of $_{i}Ca^{2+}$ as previously. Through doing this it was still possible to observe

$_{i}Ca^{2+}$ mobilisation, upon stimulation with each agonist, which decreased in a dose-dependent manner (Figure 4.6A-C). Conversion of the raw traces observed for changes in fluorescence intensity, to dose-response curves for CGRP, AM and AM2 indicated no differences relative to untreated cells (Figures 4.6D-F, Table 4.3). Thus, it was concluded that the mobilisation of $_{i}Ca^{2+}$ mediated via RAMP1-CLR heterodimers occurs in a PTX-insensitive manner, and not via the action of $G\alpha_{i/o}$ proteins.

Having established the ability of the CLR to mediate $_{i}Ca^{2+}$ mobilisation, when in association with RAMP1, and that this is not mediated in a PTX-sensitive manner, it was further investigated if the classic mediator of Ca^{2+} release, $G\alpha_{q}$, was the facilitator. In order to investigate this, a selective $G\alpha_{q/11/14}$ inhibitor, YM-254890 (Takasaki *et al*, 2004) was utilised. Pre-treatment of cells with this inhibitor, at 100 nM for 30 minutes, was sufficient to ablate $_{i}Ca^{2+}$ mobilisation upon stimulation with CGRP, AM or AM2 (Figures 4.7A-F). Whilst it was possible to observe some increases in fluorescence intensity upon agonist stimulation (Figure 4.7 A-B), most of these responses were maintained, and did not decay following reaching peak intensity. As there is no extracellular Ca^{2+} in the assays, it is not believed that these responses represent mobilisation of $_{i}Ca^{2+}$, or that they may be partial release where G protein activation has not been fully inhibited. Alternatively, it is plausible that $_{i}Ca^{2+}$ mobilisation driven by exchange factor directly activated by cAMP (EPAC) could be occurring. Thus, it is apparent that RAMP1-CLR-mediated mobilisation of $_{i}Ca^{2+}$ can be stimulated via CGRP, AM and AM2, and this occurs in a $G\alpha_{q/11/14}$-dependent manner.

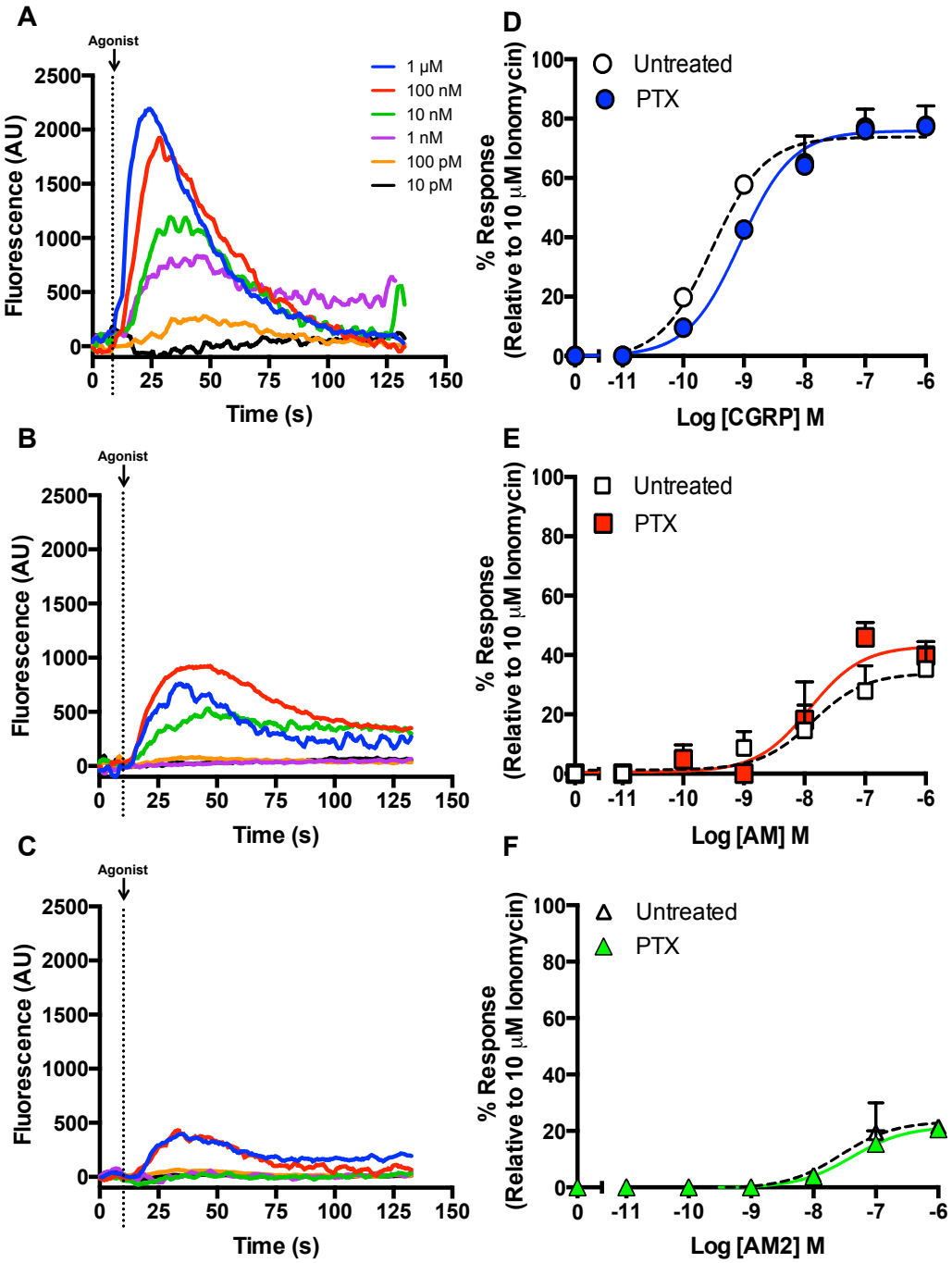

Figure 4.6: RAMP1-CLR-mediated $_{i}Ca^{2+}$ mobilisation is insensitive to PTX pre-treatment.

HEK 293 cells transfected with both pcDNA3.1-HA-CLR and pcDNA3.1-FLAG-RAMP1, were pre-treated with 200 ng/ml PTX for 16-18 hours, and stimulated with: CGRP (A), AM (B) and AM2 (C), and $_{i}Ca^{2+}$ mobilisation measured. Calcium traces are representative of 5 individual traces, where the dashed line indicates agonist injection. Conversion of calcium traces to dose-response curves allows the effects of PTX, relative to untreated cells, to be observed (D-F). Data represented ± SEM, of 5 individual replicates.

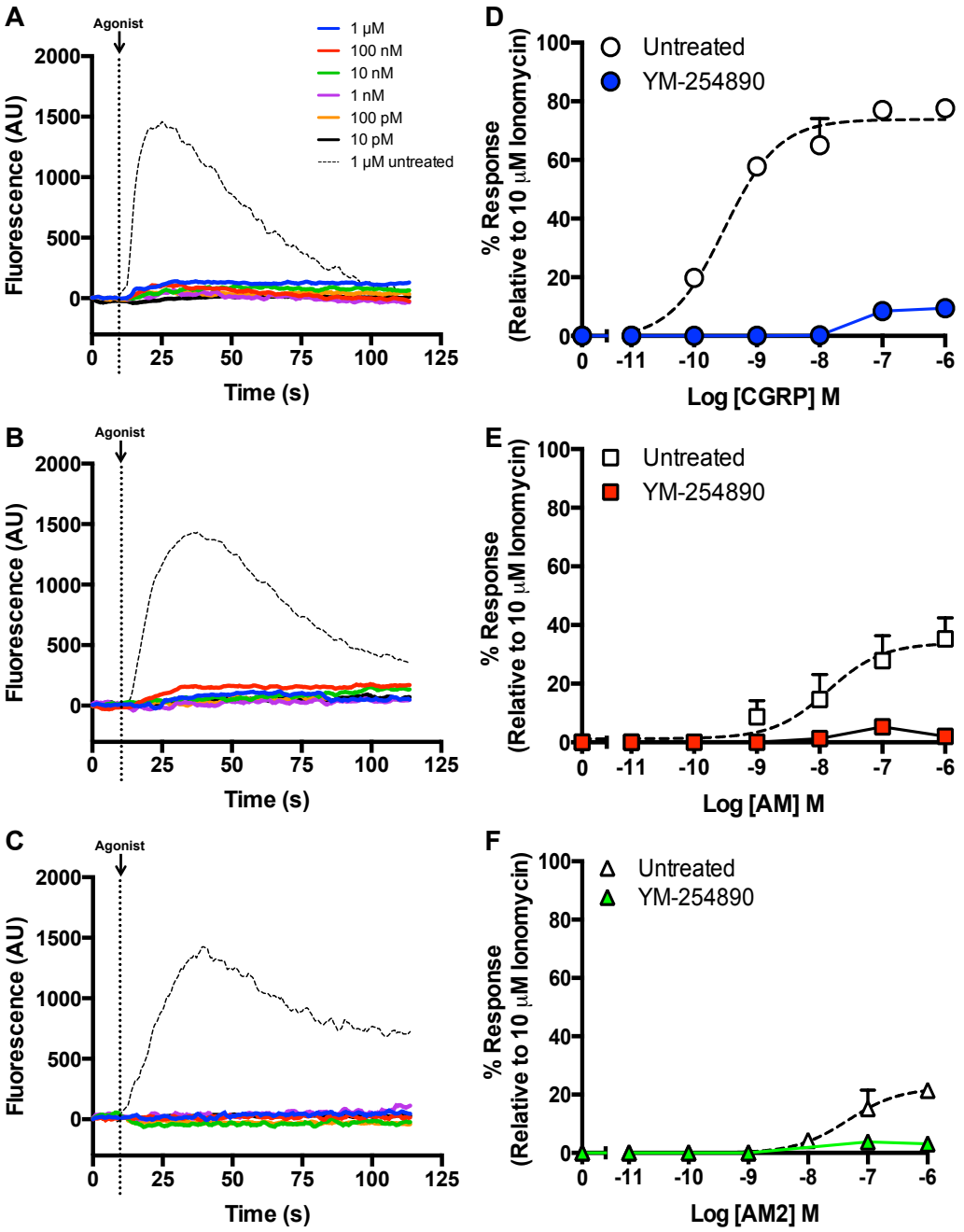

Figure 4.7: RAMP1-CLR-mediated $_{i}Ca^{2+}$ mobilisation is sensitive to YM-254890 pre-treatment.

HEK 293 cells co-transfected with pcDNA3.1-HA-CLR and pcDNA3.1-FLAG-RAMP1, were pre-treated with 100 nM YM-254890, for 30 minutes, to inhibit $G\alpha_{q/11/14}$, and stimulated with: CGRP (A), AM (B) or AM2 (C), and $_{i}Ca^{2+}$ mobilisation measured. Calcium traces are representative of 5 individual traces, where the dashed line indicates agonist injection. Conversion of calcium traces to dose-response curves shows how YM-254890 treatment has significantly reduced $_{i}Ca^{2+}$ mobilisation relative to untreated cells (D-F). Data represented ± SEM, of 5 individual replicates.

4.5.2 RAMP2-CLR-mediated $_{i}Ca^{2+}$ mobilisation

In order to determine the effect of RAMP2 upon CLR-mediated $_{i}Ca^{2+}$ mobilisation, the same method as for RAMP1-CLR was utilised. As previously, it was possible to obtain increases in FLUO-4 fluorescence, for all three agonists, which reached a peak post-injection maximal intensity, before decaying back towards resting $_{i}Ca^{2+}$ levels (Figure 4.8A-C). Conversion of the raw fluorescence values to dose-response curves (Figure 4.8D) identified a rank order of potency of CGRP = AM > AM2 (pEC_{50}: 7.71±0.1, 7.86±01, 7.41±0.4, respectively), with the same trend being observed for the efficacy (Log τ) values (Figure 4.8E, Table 4.3). Interestingly, it is now observed that CGRP and AM are full agonists (E_{max}: 62.42±4.0, 63.00±2.8, respectively), with AM2 being a partial (E_{max}: 44.41%±7.1). Whilst CGRP is observed to be a potent agonist at RAMP2-CLR heterodimers, it displays a lower potency relative to the response observed at RAMP1-CLR, with the cognate agonist AM now being more potent and displaying a much higher efficacy (Figure 4.8E, Table 4.3).

Having elucidated the mechanism of $_{i}Ca^{2+}$ mobilisation from RAMP1-CLR, there was interest to see if this occurs in the same manner for RAMP2-CLR. Thus, the same approach was utilised, using PTX pre-treatment to inhibit any potential $G\alpha_{i/o}$ signalling component, and observe the effects of this upon $_{i}Ca^{2+}$ mobilisation. As with untreated cells, it was still possible to observe $_{i}Ca^{2+}$ mobilisation upon stimulation with CGRP, AM and AM2, in a dose-dependent manner (Figure 4.9A-C). As before, analysis of dose-response curves created from the initial calcium traces (Figure 4.9D-F) indicated that mobilisation of $_{i}Ca^{2+}$ via RAMP2-CLR heterodimers occurs in a PTX-insensitive manner (Table 4.3), and is thus not brought about via $G\alpha_{i/o}$ proteins.

Having established that, like RAMP1-CLR, RAMP2-CLR is still able to mediate $_{i}Ca^{2+}$ mobilisation in a manner independent of $G\alpha_{i/o}$, the action of $G\alpha_{q/11/14}$ was investigated. Treatment of cells with 100 nM YM-254890, for

30 minutes, was sufficient to ablate all calcium release, except for when stimulated in the micromolar range for CGRP and AM (Figure 4.10A-C). This may be due to the higher efficacy observed for these agonists in the presence of RAMP2, indicating that the dose of YM-254890 used was, potentially, not sufficient to inhibit all $G\alpha_{q/11/14}$ signalling, or alternatively this could again be EPAC-mediated $_{i}Ca^{2+}$ mobilisation. However, the observed inhibition is sufficient to indicate that for all three agonists, there is effectively no signalling in comparison to untreated cells (Figure 4.10E-F). Thus, as with RAMP1-CLR, RAMP2-CLR-mediated $_{i}Ca^{2+}$ mobilisation occurs in a $G\alpha_{q/11/14}$-dependent manner.

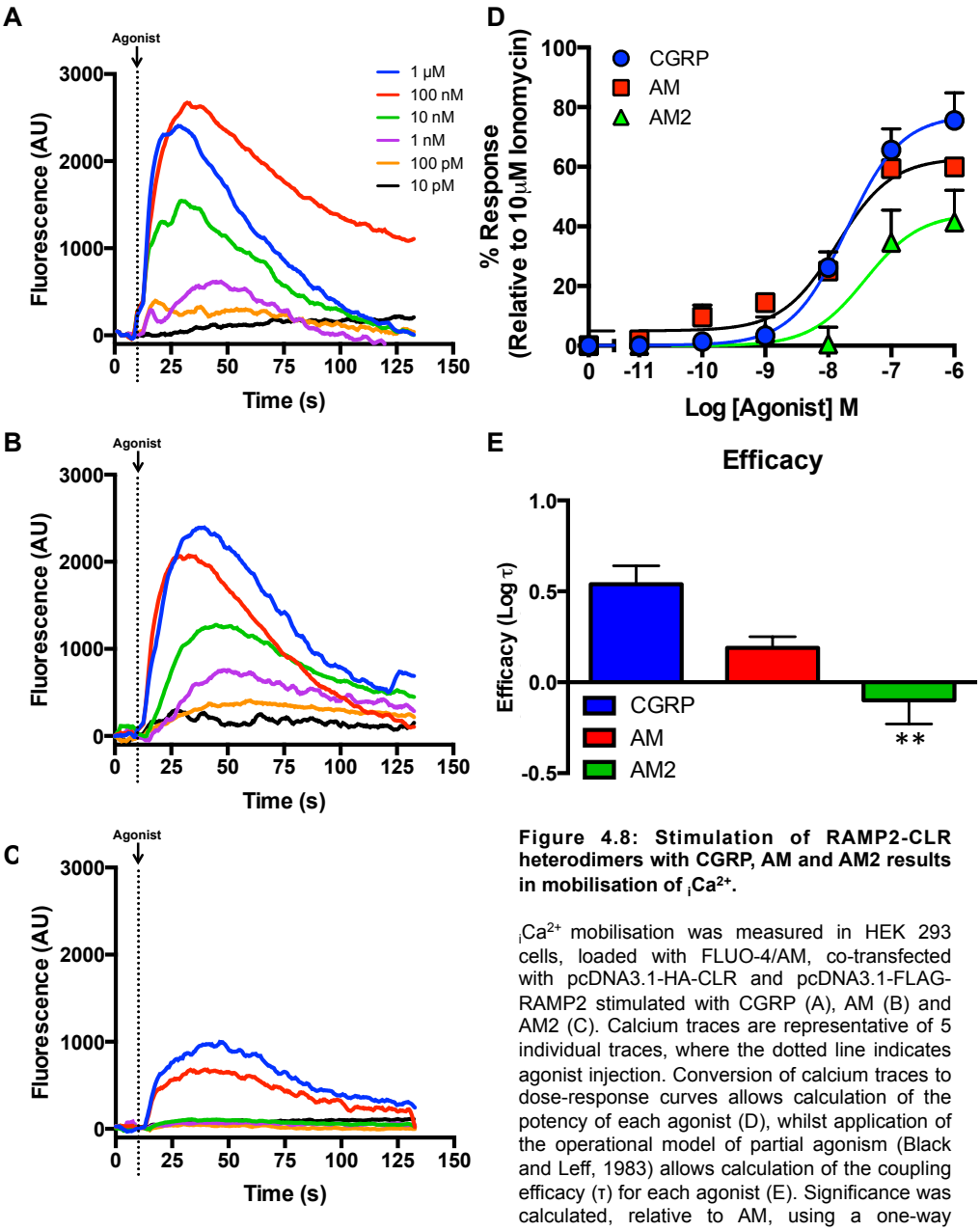

Figure 4.8: Stimulation of RAMP2-CLR heterodimers with CGRP, AM and AM2 results in mobilisation of $_{i}Ca^{2+}$.

$_{i}Ca^{2+}$ mobilisation was measured in HEK 293 cells, loaded with FLUO-4/AM, co-transfected with pcDNA3.1-HA-CLR and pcDNA3.1-FLAG-RAMP2 stimulated with CGRP (A), AM (B) and AM2 (C). Calcium traces are representative of 5 individual traces, where the dotted line indicates agonist injection. Conversion of calcium traces to dose-response curves allows calculation of the potency of each agonist (D), whilst application of the operational model of partial agonism (Black and Leff, 1983) allows calculation of the coupling efficacy (τ) for each agonist (E). Significance was calculated, relative to AM, using a one-way ANOVA with Bonferroni's correction (** $p < 0.01$) Data represented ± SEM, of 5 individual replicates.

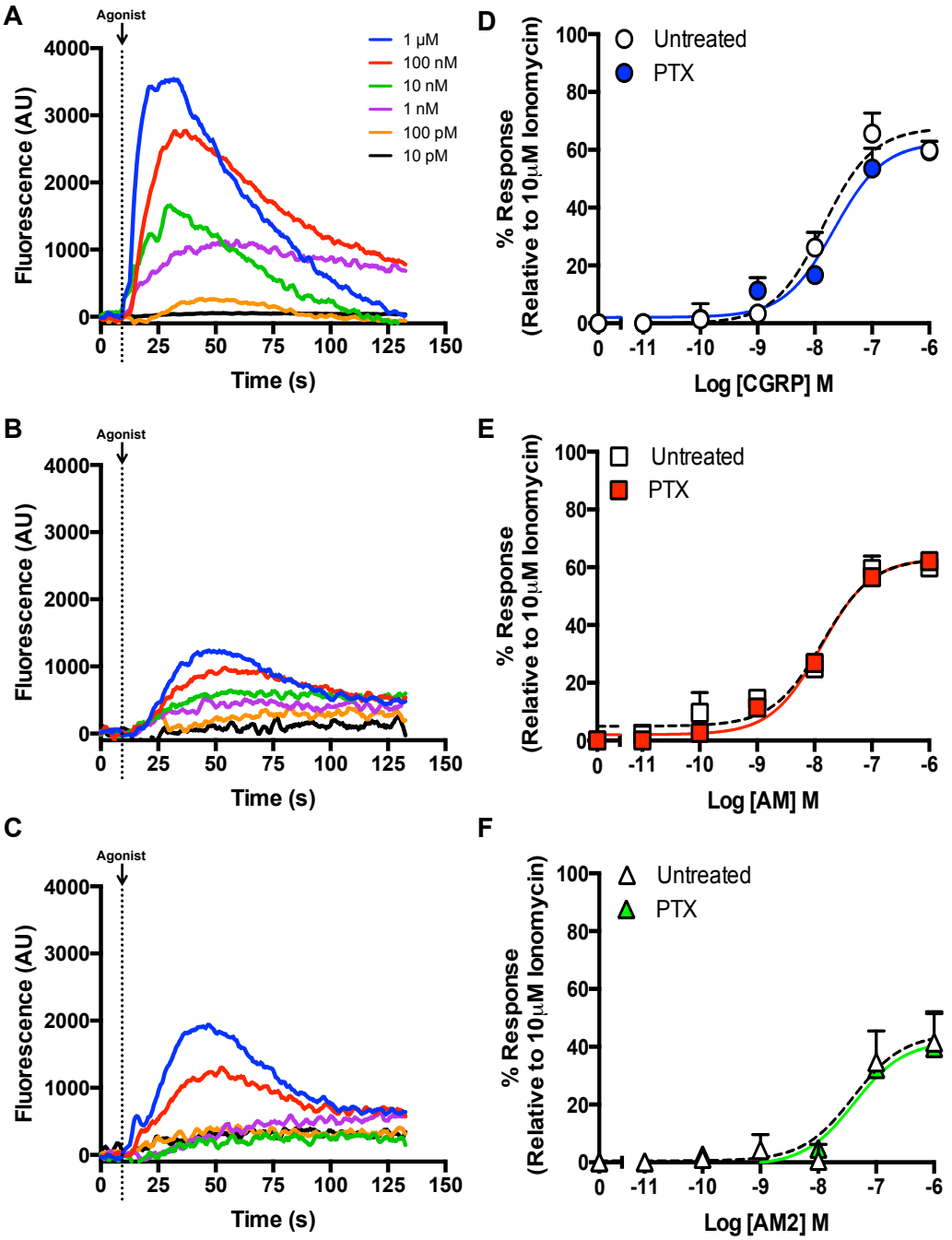

Figure 4.9: RAMP2-CLR-mediated $_{i}Ca^{2+}$ mobilisation is insensitive to PTX pre-treatment.

HEK 293 cells co-transfected with pcDNA3.1-HA-CLR and pcDNA3.1-FLAG-RAMP2, were pre-treated with 200 ng/ml PTX for 16-18 hours, and stimulated with: CGRP (A), AM (B) and AM2 (C) and $_{i}Ca^{2+}$ mobilisation measured. Calcium traces are representative of 5 individual traces, where the dotted line indicates lagonist injection. Conversion of calcium traces to dose-response curves allows the effects of PTX, relative to untreated cells, to be observed (D-F). Data represented ± SEM, of 5 individual replicates.

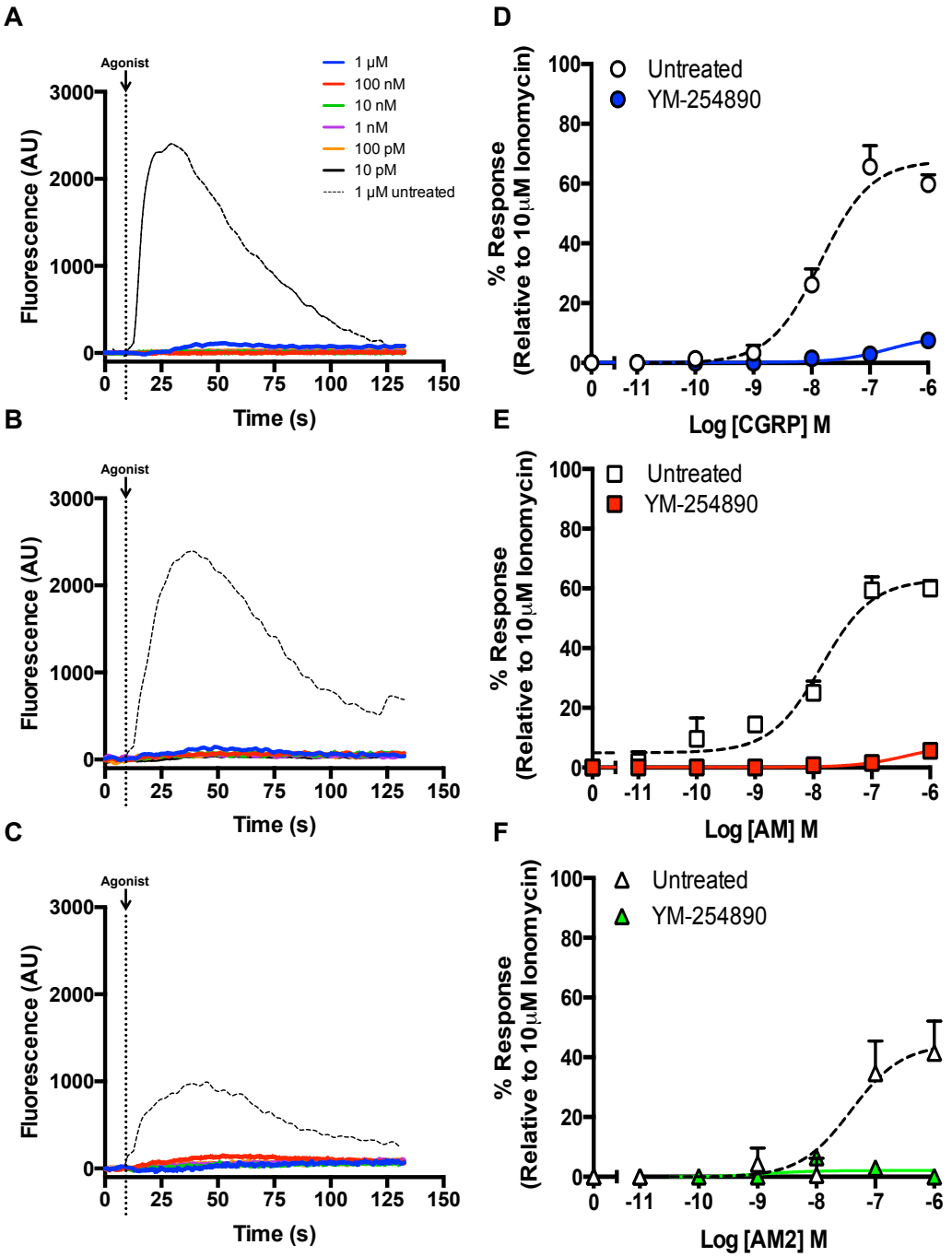

Figure 4.10: RAMP2-CLR-mediated $_{i}Ca^{2+}$ mobilisation is sensitive to YM-254890 pre-treatment.

HEK 293 cells co-transfected with pcDNA3.1-HA-CLR and pcDNA3.1-FLAG-RAMP2, were pre-treated with 100 nM YM-254890, for 30 minutes, to inhibit $G\alpha_{q/11/14}$, and stimulated with: CGRP (A), AM (B) or AM2 (C), and $_{i}Ca^{2+}$ mobilisation measured. Calcium traces are representative of 5 individual traces, where the dotted line indicates agonist injection. Conversion of calcium traces to dose-response curves shows how YM-254890 treatment has significantly reduced $_{i}Ca^{2+}$ mobilisation relative to untreated cells (D-F). Data represented ± SEM, of 5 individual replicates.

4.5.3 RAMP3-CLR-mediated $_{i}Ca^{2+}$ mobilisation

HEK 293 cells, co-transfected with pcDNA3.1-FLAG-RAMP3 and pcDNA3.1-HA-CLR, were stimulated with CGRP, AM and AM2, in order to determine the effect of RAMP3 upon CLR-mediated $_{i}Ca^{2+}$ mobilisation. The same observations as in previous CLR calcium experiments were made, with an increase in fluorescence intensity upon agonist injection, which reached a peak maximal level before decaying towards basal levels (Figure 4.11A-C). Analysis of this data revealed a rank order of potency of: AM2 = AM > CGRP (pEC_{50}: 8.21±0.3, 8.12±0.3, 7.15±0.2, respectively) (Figure 4.11D, Table 4.3). It was also observed that CGRP remained a full agonist (E_{max}: 90.26±9.8), with AM and AM2 being partial agonists (E_{max}: 56.59%±7.0, 19.17%±2.8, respectively) (Figure 4.11D, Table 4.3). Through calculation of the efficacy values of each agonist a rank order of: CGRP > AM > AM2 (Figure 4.11E, Table 4.3) was observed. The low efficacy for AM2 correlates with it being a partial agonist, whilst the higher value for CGRP is presumably due to its higher E_{max} (Figure 4.11D, Table 4.3).

As with RAMPs 1 and 2, pre-treatment with PTX still allowed $_{i}Ca^{2+}$ mobilisation, in response to all three agonists, in a dose-dependent manner (Figure 4.12A-C), with no observable difference to untreated cells (Figure 4.12D-F, Table 4.3). In contrast, treatment of cells with 100 nM YM-254890, for 30 minutes, was again able to ablate all $_{i}Ca^{2+}$ mobilisation, in response to all agonists (except CGRP at the micromolar level) (Figure 4.13 A-F). It is thus possible to conclude that RAMP3-CLR heterodimers mediate $_{i}Ca^{2+}$ mobilisation via the action of $G\alpha_{q/11/14}$ proteins, and that all three RAMP-CLR complexes utilise this transduction pathway to elevate $_{i}Ca^{2+}$ levels.

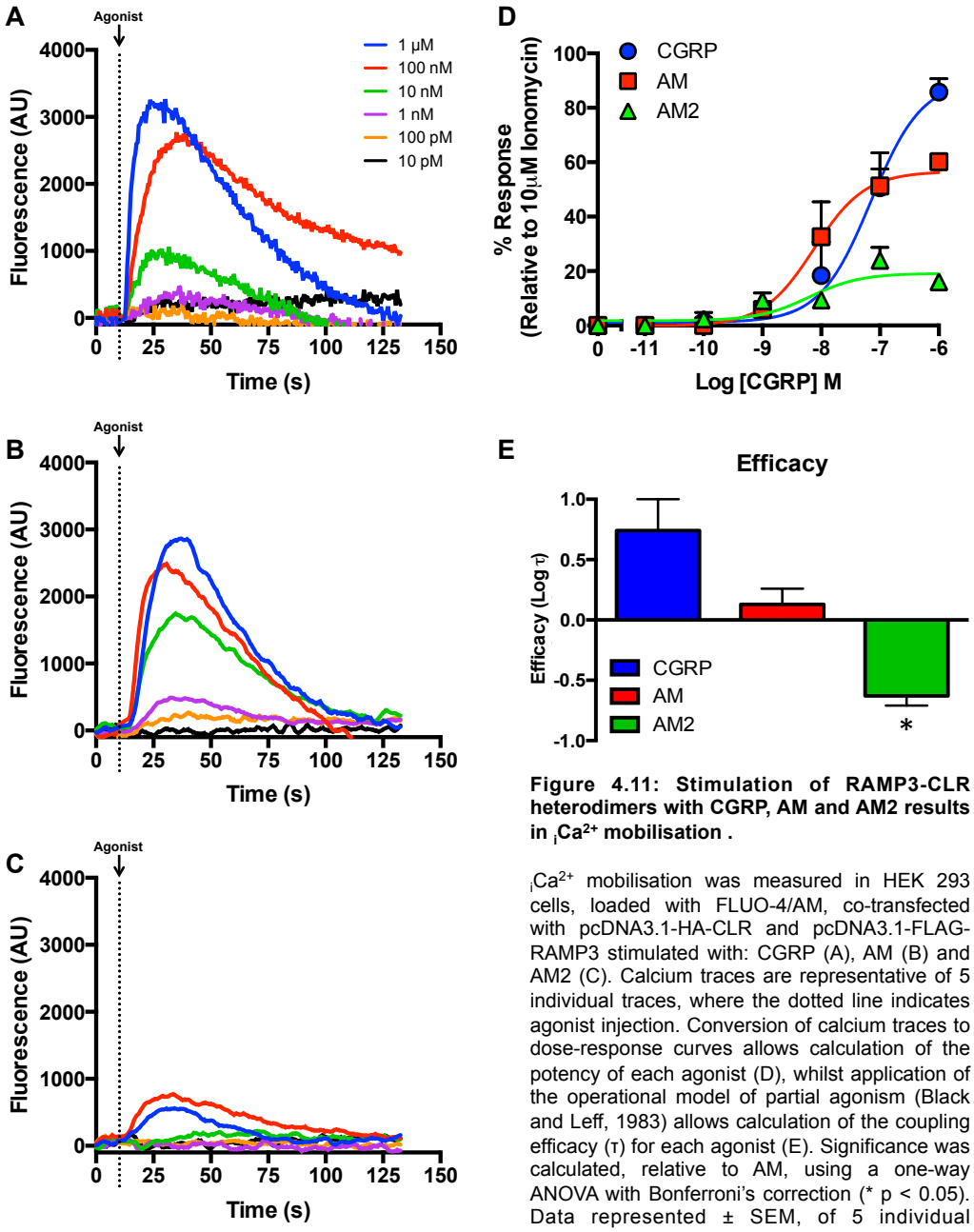

Figure 4.11: Stimulation of RAMP3-CLR heterodimers with CGRP, AM and AM2 results in $_{i}Ca^{2+}$ mobilisation .

$_{i}Ca^{2+}$ mobilisation was measured in HEK 293 cells, loaded with FLUO-4/AM, co-transfected with pcDNA3.1-HA-CLR and pcDNA3.1-FLAG-RAMP3 stimulated with: CGRP (A), AM (B) and AM2 (C). Calcium traces are representative of 5 individual traces, where the dotted line indicates agonist injection. Conversion of calcium traces to dose-response curves allows calculation of the potency of each agonist (D), whilst application of the operational model of partial agonism (Black and Leff, 1983) allows calculation of the coupling efficacy (τ) for each agonist (E). Significance was calculated, relative to AM, using a one-way ANOVA with Bonferroni's correction (* $p < 0.05$). Data represented ± SEM, of 5 individual replicates.

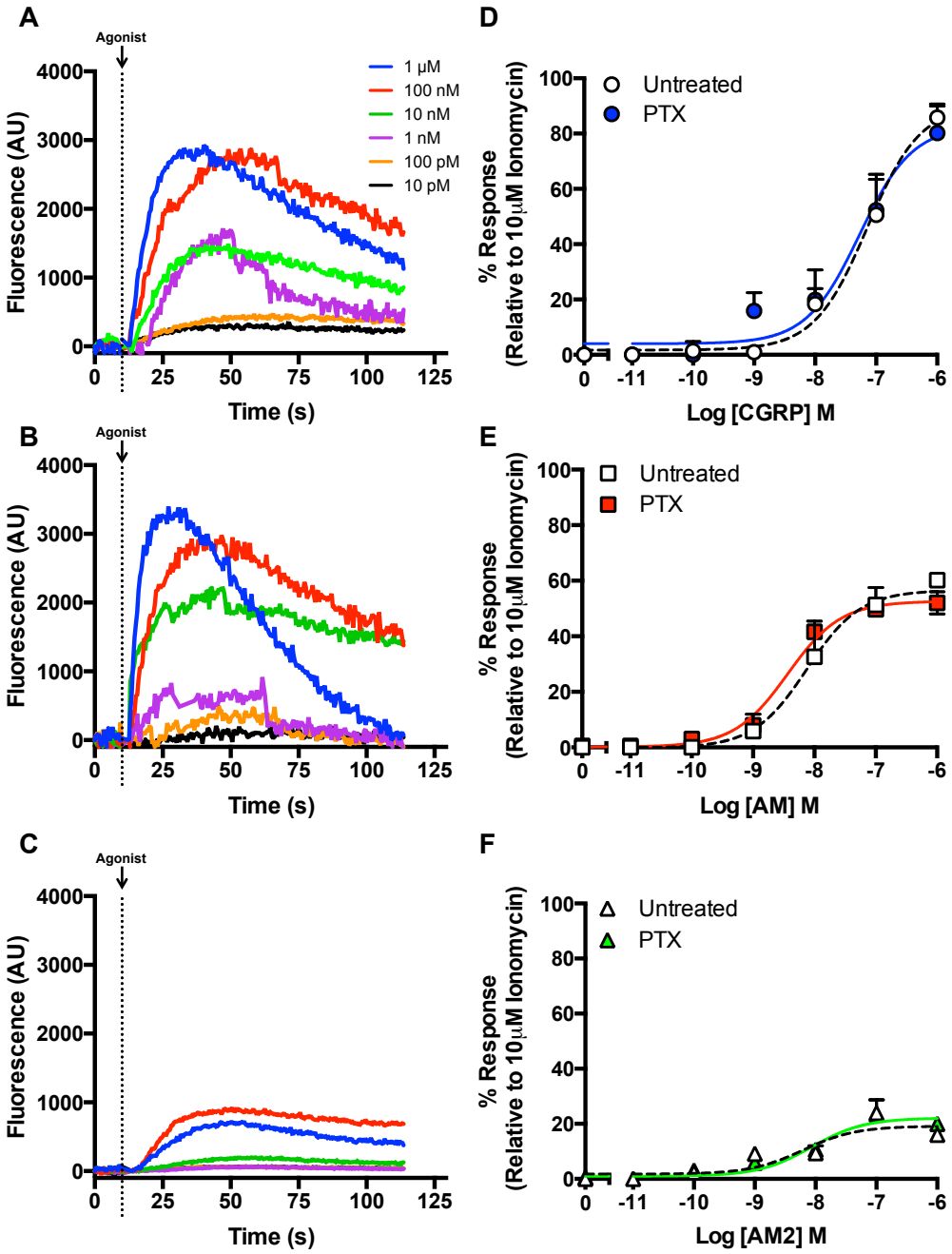

Figure 4.12: RAMP3-CLR-mediated $_{i}Ca^{2+}$ mobilisation is insensitive to PTX pre-treatment.

HEK 293 cells co-transfected with pcDNA3.1-HA-CLR and pcDNA3.1-FLAG-RAMP3, were pre-treated with 200 ng/ml PTX for 16-18 hours, and stimulated with: CGRP (A), AM (B) and AM2 (C) and $_{i}Ca^{2+}$ mobilisation measured. Calcium traces are representative of 5 individual traces, where the dotted line indicates agonist injection. Conversion of calcium traces to dose-response curves allows the effects of PTX, relative to untreated cells, to be observed (D-F). Data represented ± SEM, of 5 individual replicates.

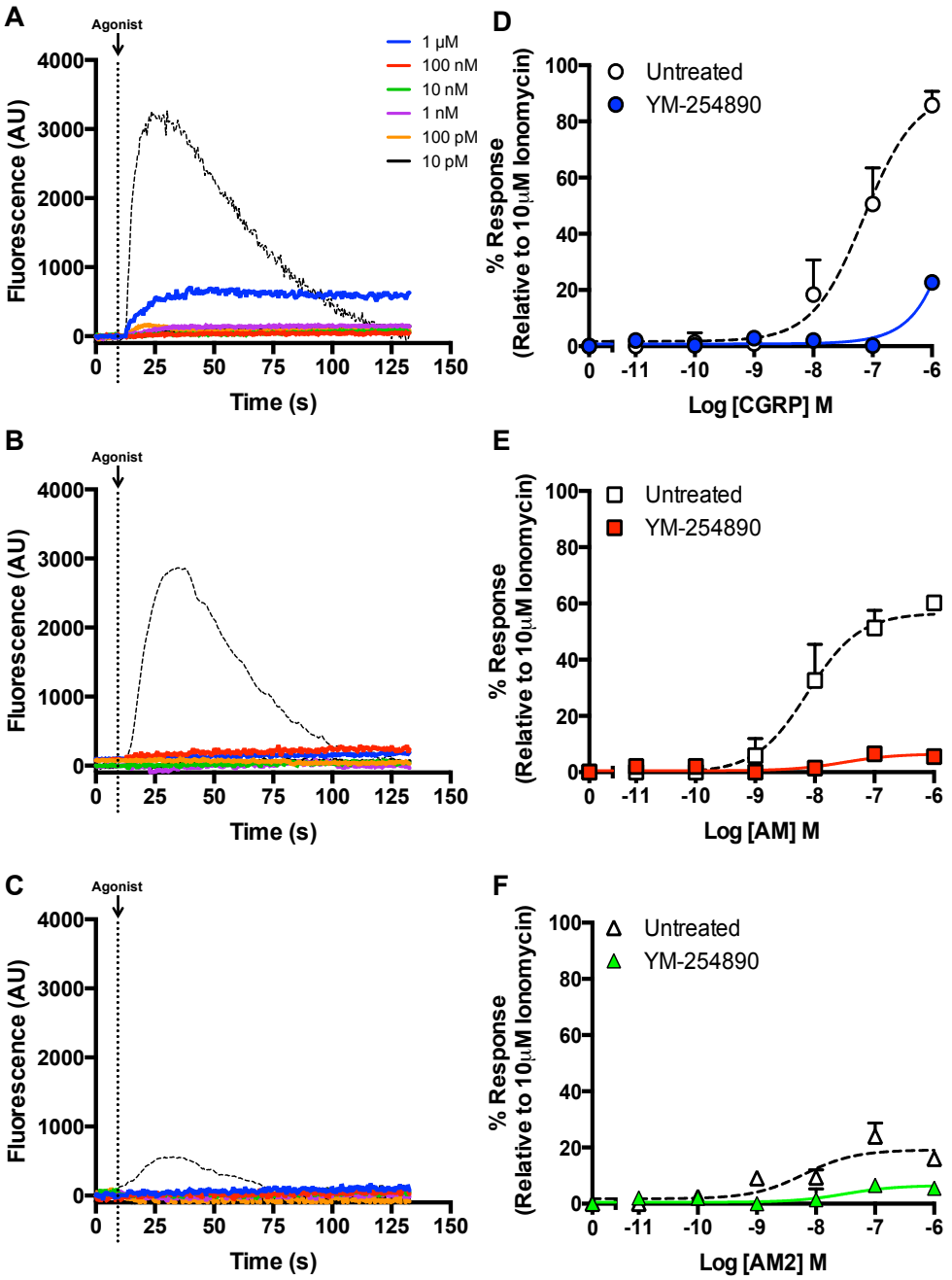

Figure 4.13: RAMP3-CLR-mediated $_{i}Ca^{2+}$ mobilisation is sensitive to YM-254890 pre-treatment.

HEK 293 cells co-transfected with pcDNA3.1-HA-CLR and pcDNA3.1-FLAG-RAMP3, were pre-treated with 100 nM YM-254890, for 30 minutes, to inhibit $G\alpha_{q/11/14}$, and stimulated with: CGRP (A), AM (B) or AM2 (C), and $_{i}Ca^{2+}$ mobilisation measured. Calcium traces are representative of 5 individual traces, where the dotted line indicates agonist injection. Conversion of calcium traces to dose-response curves shows how YM-254890 treatment has significantly reduced $_{i}Ca^{2+}$ mobilisation relative to untreated cells (D-F). Data represented ± SEM, of 5 individual replicates.

4.6 Quantification of biased agonsim at RAMP-CLR heterodimers

The preceding data has identified that each RAMP-CLR complex displays an ability to: elevate cAMP levels, couple to $G\alpha_{i/o}$ proteins and mobilise $_{i}Ca^{2+}$, in a $G\alpha_{q/11/14}$-dependent manner. It has been observe that each RAMP has an ability to modulate the response to CGRP, AM and AM2 at each given pathway, and that the responses to a single agonist, at a given RAMP-CLR heterodimer, are different. There is, therefore, a degree of inherent pathway bias. In order to quantitate this, the operational model of agonism (Black and Leff, 1983) was utilised. From which it is possible obtain the coupling efficacy parameter (Log τ) and the intrinsic affinity parameter (pKa) (Tables 4.1, 4.2 and 4.3); using these allows calculation of the transduction coefficient (Log τ/Ka). The change in transduction coefficient between two given pathways (Δ Log (τ/Ka)) serves to give a measure of the extent of bias. In the case of the RAMP-CLR system, it is possible to calculate the extent of bias between mobilisation of $_{i}Ca^{2+}$ and cAMP modulation.

As has been show, the CLR is able to couple to both $G\alpha_{s}$ and $G\alpha_{i/o}$ proteins (Figures 4.2 and 4.4). Therefore, where cAMP accumulation assays are performed in the absence of PTX pre-treatment, the combined effect of both signalling pathways are being studied. Thus, it is only possible to determine the extent of bias between $_{i}Ca^{2+}$ mobilisation and cAMP modulation as a whole. Therefore, it is possible to identify that all three agonists exert bias towards cAMP modulation over $_{i}Ca^{2+}$ mobilisation at RAMP1-CLR heterodimers, with CGRP and AM2 being the most heavily biased (Figure 4.14A). In contrast, with RAMP2-CLR, AM displays a highly elevated bias towards cAMP modulation, whilst AM2 is now weakly biased towards the mobilisation of $_{i}Ca^{2+}$, with CGRP displaying a similar extent of bias as at RAMP1-CLR (Figure 4.14A). In the case of RAMP3-CLR heterodimers, it is observed that CGRP is a calcium-biased agonist, with both AM and AM2 being biased towards

signalling via cAMP, with AM being less biased than AM2 (Figure 4.14A). Comparing this to data obtained from PTX pre-treated cells (essentially a 'pure' $G\alpha_s$ versus $G\alpha_q$ system), a different extent of bias is obtained. With RAMP1-CLR, it is observed that, essentially, all three agonists are still biased towards cAMP modulation, but AM and AM2 are more heavily biased than in untreated cells (Figure 4.14B). This is unsurprising as PTX pre-treatment served to potentiate the effect of both AM and AM2 in cAMP accumulation assays, through removing the inhibitory effect of $G\alpha_{i/o}$ (Figure 4.4A). With RAMP2-CLR, a switch in bias towards cAMP modulation for AM2 occurs, which now displays a similar level to that observed for AM (Figure 4.13B). Whilst with RAMP3-CLR, all three agonists display a similar extent of bias towards cAMP modulation (Figure 4.13B). It is therefore evident that CGRP, AM and AM2 have differing bias profiles at the CLR, which are heavily modulated by each of the three RAMPs.

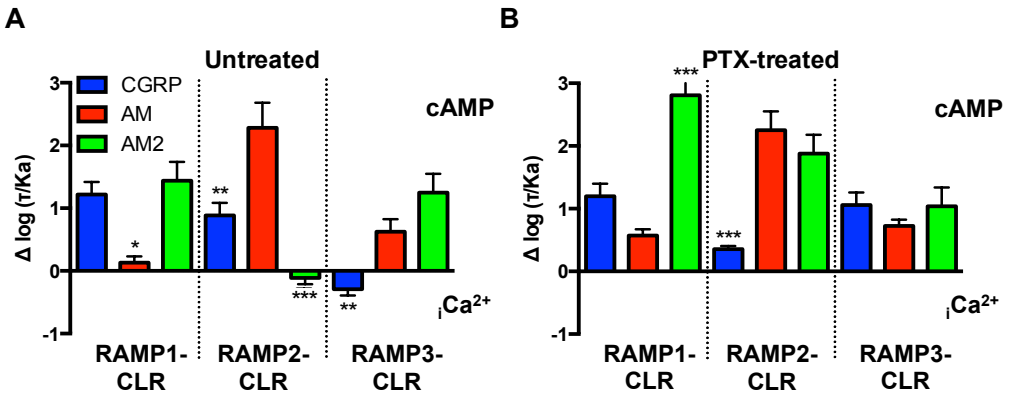

Figure 4.14: CGRP, AM and AM2 display differing bias profiles dependent upon which RAMP is present and upon PTX-treatment.

Quantification of pathway bias (Δ Log(τ/Ka)) between cAMP modulation and $_i Ca^{2+}$ mobilisation, for both untreated (A) and PTX-treated (B) HEK 293 cells. Coupling efficacy (Log τ) and intrinsic affinity (pKa) parameters calculated through implementation of the operational model of agonism (Black and Leff, 1983). Significance was calculated using a one-way ANOVA with Bonferroni's correction (* $p < 0.05$, ** $p < 0.01$ *** $p < 0.001$). Data represented ± SEM.

Pathway bias can also be calculated relative to a given agonist (ΔΔ Log (τ/Ka)), commonly the cognate agonist. This allows quantification of bias in a system-independent manner. As a given response will be perceived to change depending upon the system in which it is studied, the change will be relative to that observed for the reference agonist. This method

therefore allows a quantification of bias that transcends all systems, and is thus comparable between data obtained via other methods (Kenakin *et al*, 2012). Applying this approach to the data in this chapter, using the cognate agonist of each RAMP-CLR heterodimer (RAMP1-CLR, CGRP; RAMP 2 and 3- CLR, AM), it is possible to determine the bias of each agonist, relative to the reference agonist. In the absence of PTX, AM is biased towards $_{i}Ca^{2+}$ mobilisation in the presence of RAMP1-CLR heterodimers, whilst AM2 is biased towards cAMP modulation (Figure 4.15A). For RAMP2-CLR, it was observe that both CGRP and AM2 are heavily calcium biased (Figure 4.15A). In the case of RAMP3-CLR, CGRP is biased towards $_{i}Ca^{2+}$ mobilisation, whereas AM2 predominantly signals via cAMP modulation (Figure 4.15A). A similar trend is observed in cells treated with PTX, but the extent of bias is modulated by the loss of $G\alpha_{i/o}$ coupling. With RAMP1-CLR, AM has a reduced bias towards $_{i}Ca^{2+}$ mobilisation, and AM2 has an increased extent of cAMP bias (Figure 4.15B). With RAMP2-CLR, a dramatic reduction in the extent of AM2's bias towards $_{i}Ca^{2+}$ mobilisation is apparent, whilst with RAMP3-CLR, CGRP switches towards being cAMP biased over $_{i}Ca^{2+}$ (Figure 4.15B).

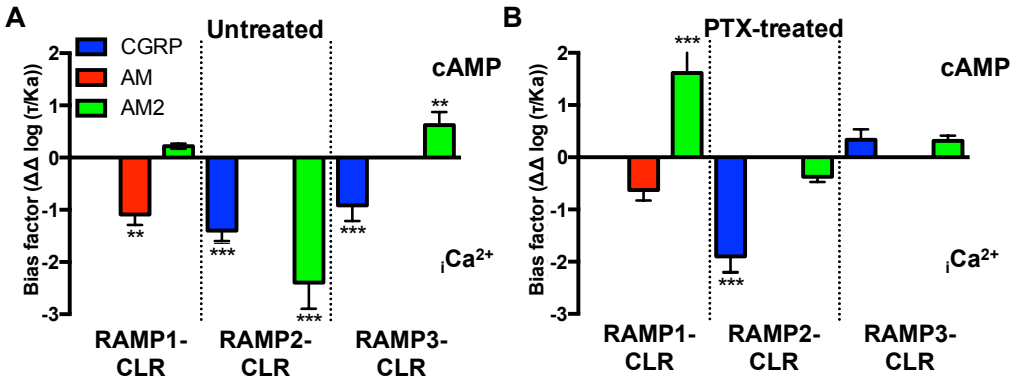

Figure 4.15: Relative bias plots for RAMP-CLR heterodimers.

Quantification of relative pathway bias (ΔΔ log (τ/K_a)) between cAMP modulation and $_{i}Ca^{2+}$ mobilisation, for both untreated (A) and PTX-treated (B) HEK 293 cells. Plots are relative to the cognate agonists at each RAMP-CLR heterodimer: RAMP1-CLR, CGRP; RAMP2 and 3-CLR, AM. Coupling efficacy (log τ) and intrinsic affinity (pKa) parameters calculated through implementation of the operational model of agonism (Black and Leff, 1983). Significance was calculated using a one-way ANOVA with Bonferroni's correction (* $p < 0.05$, ** $p < 0.01$ *** $p < 0.001$). Data represented ± SEM.

Comparing these bias observations in HEK 293 cells to that obtained for identical experiments performed in HEK 293S cells (Figure 4.16) (Weston *et al*, 2016, Appendix 2), a similar pattern of bias is obtained to that observed in PTX-treated HEK 293 cells (Figure 4.14B, 4.15B). This data suggests there is no $G\alpha_{i/o}$ signalling component in HEK 293S cells. Indeed, cAMP accumulation was found to be PTX-insensitive for all ligand-RAMP-CLR combinations (Weston *et al*, 2016, Appendix 2). Thus, there are cell type specific effects upon CLR-mediated signalling. Characterising the relative expression levels of different Gα proteins identified that HEK 293S cells exhibit a much lower expression level of $G\alpha_{i1}$ and $G\alpha_{i2}$ (Weston *et al*, 2016, Appendix 2), suggesting that the PTX-sensitivity observed in HEK 293 cells is due to effects upon inhibition of either of these two $G\alpha_i$ proteins.

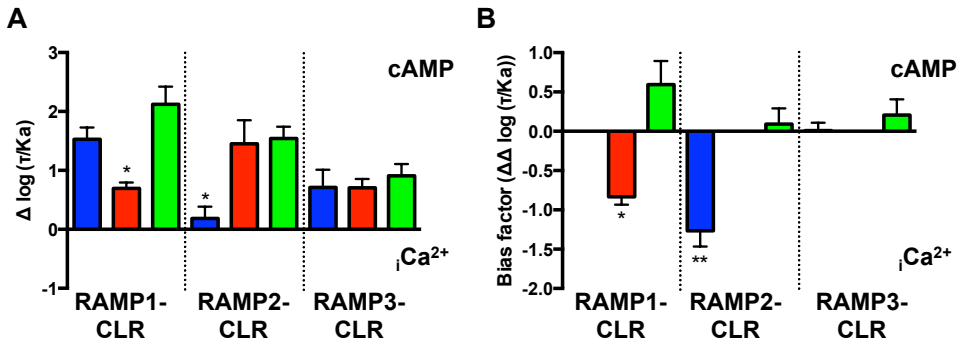

Figure 4.16: Bias plots for RAMP-CLR heterodimers expressed in HEK 293S cells.

Quantification of pathway bias (Δ log (τ/Ka) (A), and relative pathway bias (ΔΔ log (τ/Ka) (B) between cAMP modulation and $_iCa^{2+}$ mobilisation, in HEK 293S cells. ΔΔ log (τ/Ka) plots (B) are relative to the cognate agonist at each RAMP-CLR heterodimer: RAMP1-CLR, CGRP; RAMP2 and 3-CLR, AM. Coupling efficacy (τ) and intrinsic affinity (Ka) parameters calculated through implementation of the operational model of agonism (Black and Leff, 1983). Significance was calculated using a one-way ANOVA with Bonferroni's correction (* $p < 0.05$, ** $p < 0.01$ *** $p < 0.001$). Data represented ± SEM.

4.7 Summary

The work in this chapter has provided an in-depth pharmacological analysis of the CLR, and the effects and roles played by RAMPs. It has highlighted the ability of the CLR to couple to, and signal via, $G\alpha_s$, a process which is stimulated via all three agonists: CGRP, AM and AM2. In contrast, $G\alpha_{i/o}$ activation has also been identified (via PTX pre-treatment leading to a potentiation of cAMP accumulation), which occurs

for all agonists, but never the cognate agonist at each RAMP-CLR heterodimer (RAMP1-CLR, CGRP; RAMP 2- and 3-CLR, AM). Thus, not only do RAMPs differentially modulate the coupling to diametrically opposing G proteins at the CLR, but they also modulate, both positively and negatively, the responses observed for stimulation with a given agonist. This chapter has also further highlighted how each RAMP-CLR complex is able to bring about the mobilisation of $_{i}Ca^{2+}$, in a $G\alpha_{q/11/14}$-dependent manner. It is therefore possible to begin to understand how treatment of cells expressing a single RAMP-CLR heterodimer, with a given agonist, may bring about diametrically opposing effects, as well as activation of other signalling pathways. If cells expressing more than one RAMP isoform are treated with an agonist, it is therefore feasible that any response observed would be an amalgamation of that observed for each RAMP-CLR in isolation. It is also plausible that each RAMP may have differing affinities for the CLR, or traffic the CLR to greater or lesser extents. In this instance, unravelling the response and associating it to a given receptor phenotype would be a complex task. Thus, by using cells transfected with the CLR in conjunction with each RAMP, it was possible to pharmacologically characterise the extent of G protein-mediated signalling for three pathways, as well as quantitate the extent of RAMP-engendered pathway bias at the CLR. This data has shown that at RAMP1-CLR, CGRP and AM2 predominantly activate cAMP signalling pathways, whilst AM displays little difference between both cAMP and calcium signalling (Figure 4.17A). In contrast, at RAMP2-CLR, AM predominantly activates cAMP-mediated signalling, whilst AM2 is mainly activating $_{i}Ca^{2+}$ mobilisation. Interestingly, CGRP displays slightly greater activity towards cAMP production, but is the least ‘active’ of the three agonists (Figure 4.17B). With RAMP3-CLR, the cognate agonist, AM, predominantly signals via cAMP, as does AM2, whilst CGRP mainly mobilises $_{i}Ca^{2+}$ (Figure 4.17C).

In order to determine how RAMPs modulate the extent of biased agonism observed at the CLR, for each agonist, Professor C. Reynolds (University of Essex, UK) utilised molecular modelling simulations of the CLR in

complex with an associated RAMP. This identified that the RAMP C-terminus is closely associated with helix 8, the intracellular portions of TM6 and 7, as well as the C-terminus of $G\alpha_s$, but that there are no direct agonist-RAMP interactions (Weston *et al*, 2016, Appendix 2). These simulations provide one potential mechanism whereby RAMPs may modulate receptor activity: either by direct interaction with the associated Gα, or allosterically influencing the orientations of TM6/7 and helix 8.

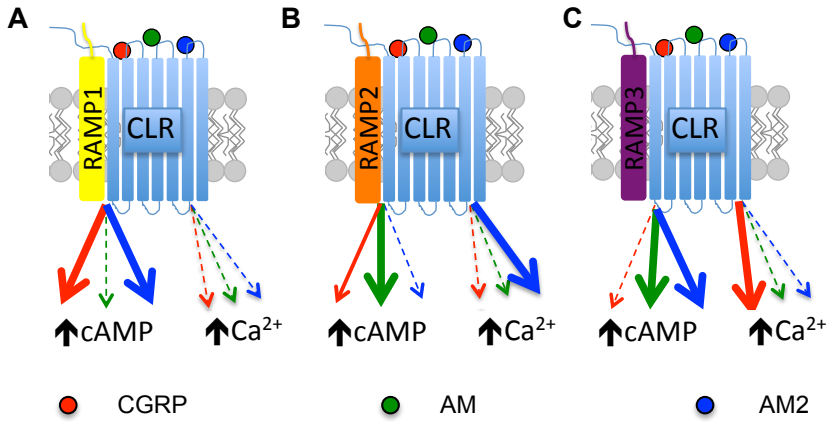

Figure 4.17: Extent of pathway activation at the CLR is dependent upon both agonist and RAMP.

Schematic representation of the extent of pathway bias observed at RAMP1-CLR (A), RAMP2-CLR (B) and RAMP3-CLR (C). The thickness of each line indicates the extent of bias observed for that ligand towards the indicated pathway, Thicker lines being more biased, dashed lines indicating a lesser extent of bias towards the indicated pathway.

Overall, it can be appreciated how upon association with a single GPCR, the CLR, the three RAMPs are able to bring about three distinct pharmacological phenotypes. Each of these three 'receptors' are able to respond to the same three agonists, and activate the same pathways, but in a RAMP-specific manner. Thus, any consideration of the activity of CGRP, AM, or AM2, or any clinically used mimetics, needs to be considered with close attention paid to both the target tissue, and RAMP expression in target cells. In addition, the expression of RAMPs and CLR in other tissues, and the potential activation of other signalling pathways, needs to be considered. Thus, with a fuller understanding of the roles played by RAMPs, and their effects upon biased agonism at the CLR, there is potential to develop more effective, and safer, therapeutic intervention strategies, in the many pathological states where the CLR is known to play a role.

Chapter 5
Intracellular loop 1 of the CLR influences biased agonism

5.1 Introduction

The largest and most understood group of GPCRs are those within family A, the rhodopsin-like receptors. For this group, numerous crystal structures exist; whilst these are also available for family B GPCRs, they are either not in active conformations, or incomplete. In contrast, those that exist for family A receptors come either bound to G proteins or nanobodies that mimic a G protein (Kruse *et al*, 2013, Huang *et al*, 2015, van Eps *et al*, 2015, Carpenter *et al*, 2016, Stauss *et al*, 2016). Beyond G proteins, a structure also exists for a β-arrestin-bound rhodopsin (Kang *et al*, 2015). From these structures, we now have an understanding of how agonist binding/retinal isomerisation leads to movement of transmembrane (TM) domains 2 and 3 away from one another. This thus has implications upon intracellular loops (ICL) 2 and 3 moving, in turn allowing the C-terminus of the G protein to interact directly with the GPCR. This knowledge, however, does not explain how GPCRs selectively couple to differing G proteins, or how they preferentially couple to one G protein over another, nor how differing agonists modulate this. Thus, we have little understanding of how biased agonism occurs at a molecular level. This is even less understood for family B receptors, where existing structures for the glucagon (Siu *et al*, 2013, Zhang *et al*, 2017) and corticotropin-releasing factor (CRF) (Hollenstein *et al*, 2013) receptors are in inactive forms, whilst the glucagon-like peptide-1 (GLP-1) receptor has structures solved in complex with either a bound allosteric modulator (Song *et al*, 2017), agonist (Jazayeri *et al*, 2017), or G protein (Zhang *et al*, 2017). What we do know is that amino acids at the junctions

of ICL1 and the base of TM2 work in conjunction with TM3 to form a G protein-binding pocket (Vohra *et al*, 2013, Wootten *et al*, 2016).

To date, this region, particularly ICL1, has been little studied in family B GPCRs; however, it has been observed that mutating this region has effects upon cell surface expression (Bentrop *et al*, 1997, Wess, 1998). Thus, we can be confident that ICL1 at least plays key structural roles within these receptors. In the existing G protein-bound crystal structure of the GLP-1R, ICL1 does not itself directly interact with Gα (Zhang *et al*, 2017). It has, however, been shown to be an important region required for receptor activation in more than 10 family A and B GPCRs (Hirata *et al*, 1994, Thomas III *et al*, 1995, Wu *et al*, 1997, Liu and Wu, 2003, Yu *et al*, 2005, Kleinau *et al*, 2010). It has also been observed that differing agonists lead to distinct conformational changes within ICL1 (West *et al*, 2011). Indeed, within the μ-opioid receptor these changes precede the movements of TM 5 and 6, suggesting that they are an early event in receptor activation, occurring soon after agonist binding (Sounier *et al*, 2015), and that this may be a highly conserved phenomenon (Shihoya *et al*, 2016). Within family B, two GPCRs, CRF and the calcitonin receptor, also exist as isoforms containing an insert within ICL1. For the calcitonin receptor, this has been seen to result in reduced $G\alpha_q$-mediated signalling, with little effect upon $G\alpha_s$ signalling (Furness *et al*, 2012). Thus, evidence exists to suggest that ICL1 may play key roles in receptor activation and G protein-mediated signalling, and, therefore, may have profound effects upon biased agonism.

This chapter attempts to characterise ICL1, of the CLR, and gain an understanding of its function and possible roles played in influencing biased agonism. To achieve this, a saturation mutagenesis approach was utilised, investigating the effects of substituting all residues within ICL1 (Y165-Q172) (Figure 5.1), to various other residues. For each substitution cAMP production was measured, in response to CGRP stimulation, where each mutant CLR is co-expressed with RAMP1 in HEK 293 cells. In terms of alanine substitutions further characterisation is provided, with

respect to the ability of each mutant to mediate mobilisation of $_{i}Ca^{2+}$ and activate ERK1/2. This data is then utilised in the quantification of biased agonism, subsequently uncovering a role of ICL1 in influencing G protein specificity of the CLR, and hence, bias.

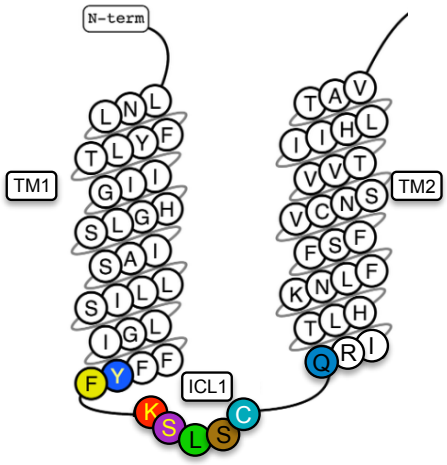

Figure 5.1: Mutated residues in intracellular loop 1 of CLR.

Location of the residues at the base of transmembrane domain (TM) 1, within intracellular loop (ICL 1), and the base of TM 2, which have been mutated in our saturation mutagenesis study. Coloured residues indicate those mutated, white shows those left as in wild type. Figure adapted from gpcrdb.org.

This chapter represents a large collaborative effort between: Professors D. Poyner and C. Reynolds, Heptares therapeutics (who generated expression constructs for each mutant, and quantified cell surface expression (Figure 5.7, Table 5.3)), and ourselves. It is currently part of a wider, ongoing study into the roles of ICL1 within the: CLR, CRF receptors, GCGR and the $A_{2A}R$.

5.2 ICL1 of family B GPCRs potentially interacts with helix 8

In silico molecular modelling studies, performed by Professor C. Reynolds (University of Essex, UK), identified a potential series of contacts between ICL1 and helix 8 (H8) of family B GPCRs. Structural alignment of the ICL1 region of family B GPCRs reveals that there is a high level of structural homology within this region (Figure 5.2). Positively charged residues are generally conserved at the 3rd position (position 167, relative to the CLR), except for the GCGR, which has a serine (Figure 5.2). In addition, leucine/isoleucine is conserved at the 5th position (position 169 relative to the CLR), with a cysteine being absolutely conserved at the 7th position (position 171, relative to CLR), as well as an arginine at the base of TM2 (position 173, relative to the CLR) (Figure 5.2). Interestingly, the CLR, CTR and both CRF1 and 2 receptors, appear to display a slightly differing primary structure to the rest of family B. Whilst most receptors contain a second positively charged residue at position 168, these four receptors contain a serine. Additionally, the CLR and CTR contain either a serine or glycine at position 170, whilst all other family B GPCRs contain positively charged residues (histidines, except for the CRF receptors which contain arginines) (Figure 5.2). At position 172 (relative to the CLR), the CRF receptors and the growth-hormone-releasing hormone receptor contain non-polar residues, whilst the CLR, CTR and the rest of family B contain polar residues at this position (Figure 5.2).

Receptor	Position (As for CLR)								
	165	166	167	168	169	170	171	172	173
CLR	Y	F	K	S	L	S	C	Q	R
CT	F	F	R	S	L	G	C	Q	R
CRF1	R	L	R	S	I	R	C	L	R
CRF2	A	L	R	S	I	R	C	L	R
GHRH	A	L	R	R	L	H	C	P	R
GIP	L	F	R	R	L	H	C	T	R
GLP-1	G	F	R	H	L	H	C	T	R
GLP-2	F	L	R	K	L	H	C	T	R
GCGR	G	L	S	K	L	H	C	T	R
Secretin	A	F	R	R	L	H	C	T	R
PTH1	Y	F	R	R	L	H	C	T	R
PTH2	Y	F	R	R	L	H	C	T	R
PAC1	R	F	R	K	L	H	C	T	R
VPAC1	L	F	R	K	L	H	C	T	R
VPAC2	L	F	R	K	L	H	C	T	R

Figure 5.2: Alignment of ICL1 for all family B GPCRs.

Alignment of equivalent residues to CLR ICL1 (Y165-Q172) for all family B GPCRs. Residue numbering is shown as for CLR. Alignment performed in gpcrdb.org.

Receptor	Position (As for CLR)								
	388	387	388	389	390	391	392	393	394
CLR	N	G	E	V	Q	A	I	L	R
CT	N	N	E	V	Q	T	T	V	K
CRF1	N	S	E	V	R	S	A	I	R
CRF2	N	G	E	V	R	S	A	V	R
GHRH	N	Q	E	V	R	T	E	I	S
GIP	N	K	E	V	Q	S	E	I	R
GLP-1	N	N	E	V	Q	L	E	F	R
GLP-2	N	G	E	V	K	A	E	L	R
GCGR	N	K	E	V	Q	S	E	L	R
Secretin	N	G	E	V	Q	L	E	V	Q
PTH1	N	G	E	V	Q	A	E	I	K
PTH2	N	G	E	V	Q	A	E	V	K
PAC1	N	G	E	V	Q	A	E	I	K
VPAC1	N	G	E	V	Q	A	E	L	R
VPAC2	N	S	E	V	Q	C	E	L	K

Figure 5.3: Alignment for helix 8 of all family B GPCRs.

Alignment of equivalent residues to CLR helix 8 for all family B GPCRs. Residue numbering is shown as for CLR. Alignment performed using gpcrdb.org.

Alignment of H8 for family B reveals that two glutamic acid residues (positions 388 and 392, relative to the CLR), and a valine (position 389, relative to the CLR) are conserved (Figure 5.3). However, in the CLR, CTR and CRF receptors, the second glutamic acid is not present (Figure 5.3). Analysing the structures of the inactive GCGR and GLP-1R identifies the possibility for charge-charge interactions between positively charged residues at the start of ICL1 and the base of TM2, with the negatively charged glutamic acids on H8. In the GCGR, this may occur between S167/K168 and E410, as well as between R173 at the base of TM2 and E406 (Figure 5.4A). Likewise, in the inactive GLP-1R the same phenomenon has the potential to occur by an area of positive charge formed by R170 and H171, creating a charge-charge interaction with E412, whilst R176 (equivalent to R173 in the GCGR) may also form an

interaction with E408 (Figure 5.4B). Similar interactions, between ICL1 and H8, to those observed in the GCGR and GLP-1R, may also potentially occur in other family B GPCRs due to the high level of conservation of positively charged residues at the equivalent positions of 167/168 and 173, in the CLR (Figure 5.2), as well as the conservation of glutamic acids within H8 (Figure 5.3). However, as the CLR, CTR and CRFRs lack a second positive charge at positions 168 (Figure 5.2), as well as a second glutamic acid in H8 (Figure 5.3), it is possible that in these receptors there is only a single ICL1-H8 interaction, between an arginine at the base of TM2 and the first glutamic acid in H8. Therefore, the CLR, CTR, and CRF receptors potentially form a second group, which function differently to the majority of family B GPCRs.

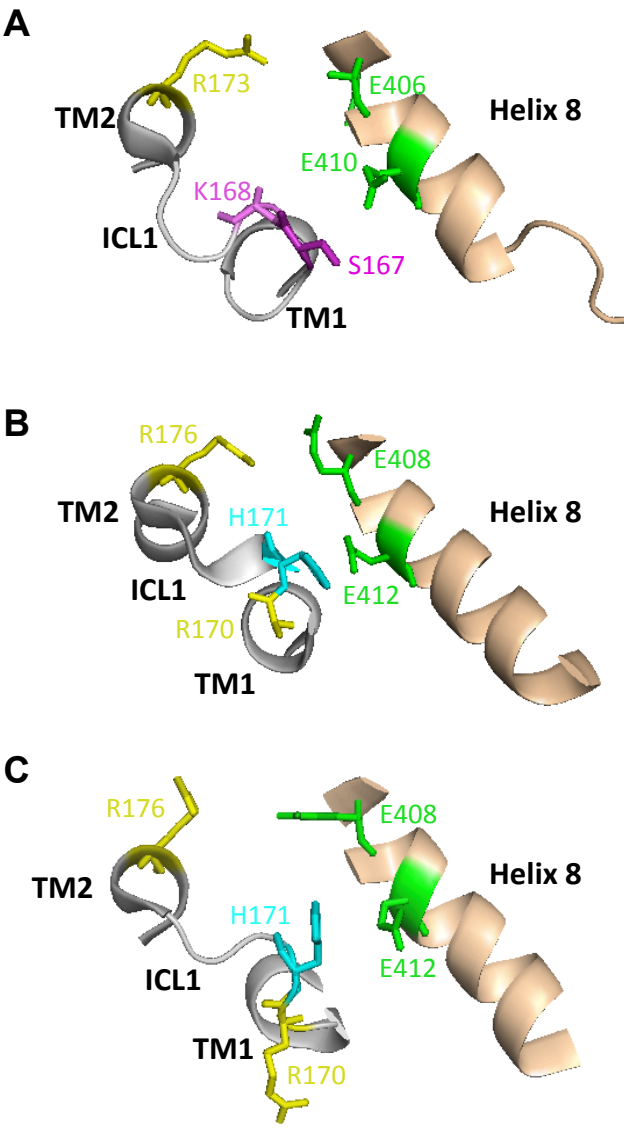

Figure 5.4: Intracellular loop 1 of the glucagon and glucagon-like peptide-1 receptors may form interactions with helix 8, which are broken upon activation.

Within the inactive glucagon receptor (GCGR) crystal structure (PDB – 5XEZ, Zhang *et al*, 2017) (A) ICL1 may form interactions with helix 8 (H8) between S167/K168 and E410, as well as R173 and E406. Similar interactions are observed within the glucagon-like peptide-1 receptor (GLP-1R) (PDB - 5VEX, Song *et al*, 2017) (B), where R170/H171 may form an area of positive charge, creating a charge-charge interaction with E412, whilst R176 may also interact with E408. These interactions appear to be lost in the active GLP-1R (PDB – 5VAI, Zhang *et al*, 2017) (C). Upon activation, R170 and H171 appear to rotate away from H8, whilst E412 rotates towards the orientation of H8. Additionally, R176 rotates away from E408, which in turn rotates to orientate itself pointing towards transmembrane (TM) bundle 2. The movements of these resides correspond with an opening of the space between ICL1 and H8.

Comparison of the inactive GLP-1R structure to that in the active state reveals that upon activation, R170 rotates to point away from the centre of the receptor and H8, whilst H171 rotates back away from H8 (Figure 5.4C). The movement of these two residues is concurrent with a rotation of E412 inwards, towards H8 (Figure 5.4C). Likewise, R176 rotates to point away from the intra-ICL1-H8 space, whilst E408 moves to point towards TM2. These observations indicate that ICL1-H8 interactions may break upon receptor activation. The breaking of these interactions results in ICL1 and H8 moving apart, as observed in GLP-1R crystal structures, where the orientation of the TM1-ICL1-TM2 axis is altered relative to the inactive state, and also positioned further away from H8 (Figure 5.4B-C).

In order to provide *in vitro* validation of an ICL1-H8 interaction, a saturation mutagenesis approach was utilised, mutating each residue within ICL1, Y165-Q172 (Figure 5.1), in turn, to either: alanine, arginine, cysteine, glutamic acid, glutamine, glycine, histidine, isoleucine, methionine, phenylalanine, or tryptophan. Each of these mutant CLRs were co-transfected with RAMP1, into HEK 293 cells, utilising a bis-cistronic vector, containing both RAMP1 and SNAP-CLR, pIRES-RAMP1-SNAP-CLR (WT or Y165-Q172X). In order to characterise the effects of these substitutions, the ability of each mutant to mediate the production of cAMP in response to CGRP stimulation was measured, as performed previously for RAMP-CLR experiments (Chapter 4). CGRP was utilised as the stimulating agonist, due to its inability to mediate $G\alpha_{i/o}$ signalling (Figure 4.4, Table 4.2). Thus, measuring cAMP production has the potential to study the CLR's ability to solely couple to, and activate, $G\alpha_s$.

An initial screen of all these mutants (performed in duplicate, with 1 replicate per experiment) (Figure 5.5, Table 5.1-2) identified a series of key substitutions as providing interesting biochemical and biophysical properties. Through mutating the residues within the ICL1 region (Y165-Q172), it was possible to observe both increases and decreases in the potency of CGRP, as well as decreases in E_{max} (Figure 5.5, Tables 5.1-2). Glutamic acid substitution resulted in large reductions in functionality for most residues within ICL1 (Figure 5.5, Table 5.2). In contrast, glycine substitution, which is generally deleterious, was observed, for some residues, to have minimal effects upon potency or E_{max}, whilst others displayed a greatly reduced E_{max} (Figure 5.5, Tables 5.1-2). Indeed, glycine substitution of L169 resulted in an increased potency of CGRP, relative to WT CLR, which was also apparent for S168R (Figure 5.5, Table 5.1). Substitution of residues towards the end of ICL1 (S170-Q172) with isoleucine resulted in severely reduced E_{max}s (Figure 5.5, Table 5.2). Due to the observations from this initial scan, these mutants were further investigated. As the initial analysis revealed that substitution of S168 with a positively charged arginine resulted in a gain-of-function, the effect of histidine substitution, upon ICL1, was also further investigated. Each of

these sets of mutants are characterised in terms of their ability to mediate the production of cAMP whilst, in order to investigate the effects of ICL1 upon biased agonism, the alanine mutants were utilised to perform a more wide ranging investigation into their ability to mediate: the production of cAMP, $_{i}Ca^{2+}$ mobilisation, and activation of ERK1/2 signalling. The extent of bias between each pathway for each alanine mutant was then quantified.

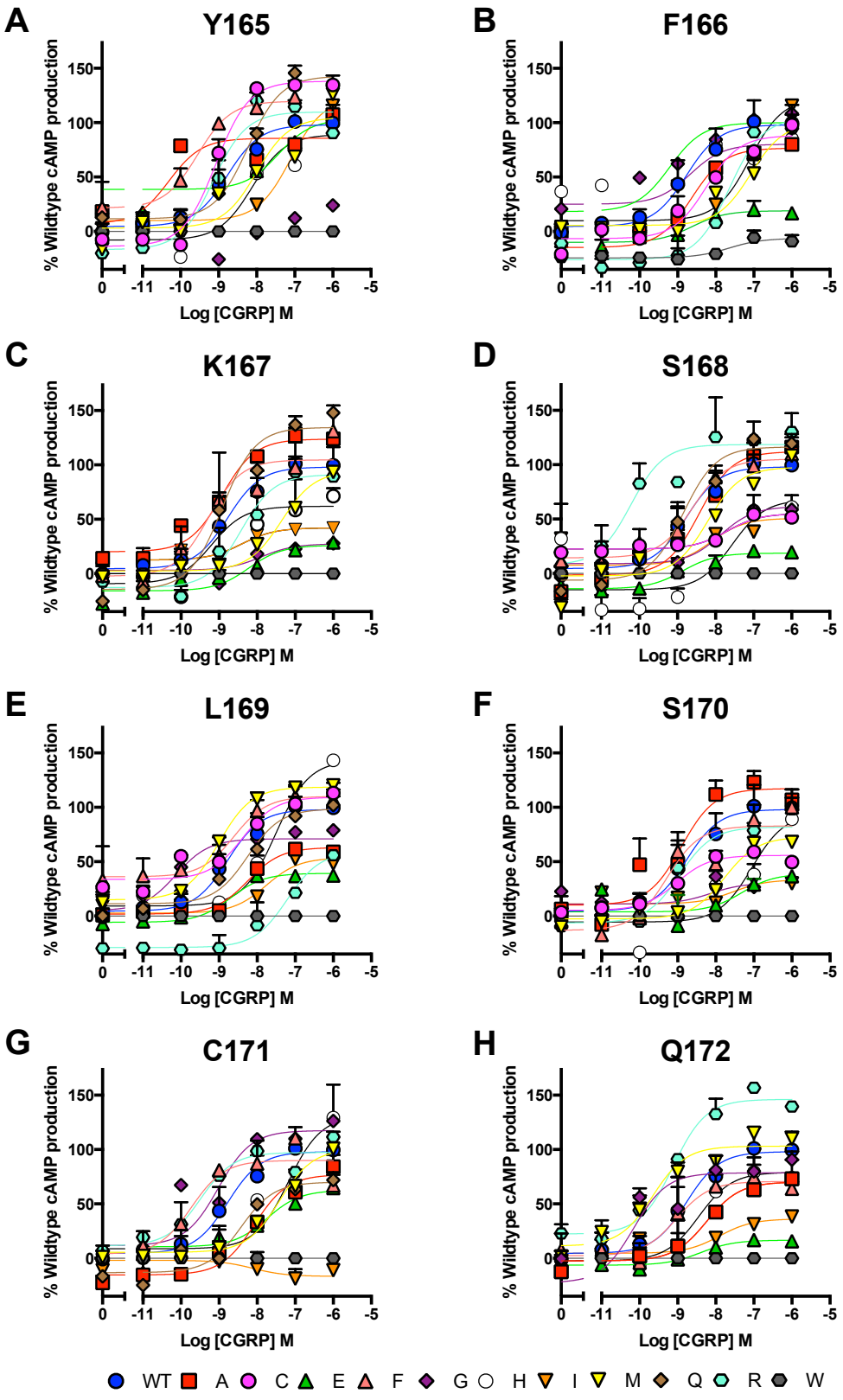

Figure 5.5: Saturation mutagenesis of intracellular loop 1.

Saturation mutagenesis of each residue across intracellular loop 1 (ICL1): Y165 (A), F166 (B), K167 (C), S168 (D), L169 (E), S170 (F), C171 (G), Q172 (H), reveals differential effects upon cAMP production, when each mutant is co-expressed with RAMP1, in HEK 293 cells, and stimulated with CGRP. Data represented as the percentage cAMP production relative to wild type (WT) CLR, ± SEM, of 2 replicates.

Table 5.1: Potency (pEC_{50}[a]) values for cAMP production in HEK 293 cells, transfected with each CLR ICL1 mutant (pIRES-RAMP1-SNAP-CLR (WT, Y165-Q172X)), upon CGRP stimulation.

Substitution	WT Residue							
	Y165	**F166**	**K167**	**S168**	**L169**	**S170**	**C171**	**Q172**
WT	8.78±0.3							
A	10.31±0.5	8.63±0.3	8.92±0.4	8.43±0.2	8.24±0.1	8.91±0.3	8.08±0.2	8.24±0.3
C	9.07±0.1	8.25±0.2	-	7.71±0.4	8.39±0.2	9.04±0.1	-	8.24±0.3
E	7.43±1.1	8.62±0.4	8.22±0.4	8.87±0.3	8.69±0.2	7.32±0.9	7.74±0.2	8.40±0.3
F	9.55±0.3	-	9.29±0.4	8.62±0.3	8.61±0.4	9.29±0.3	9.02±0.5	9.03±0.5
G	-	9.21±0.4	7.90±0.8	7.87±0.4	10.13±0.3*	8.14±1.9	9.73±0.3	10.20±0.4*
H	8.12±0.4	8.67±0.8	9.20±0.7	7.57±0.6	7.51±0.1*	7.05±0.3*	7.19±0.3*	8.45±0.3
I	7.11±0.4	-	8.41±0.9	8.12±0.9	7.76±0.3	7.55±0.9	8.12±1.1	7.91±0.5
M	8.01±0.3	7.18±0.5	7.36±0.3	8.21±0.3	9.02±0.1	7.78±0.1	7.41±0.4	9.66±0.2
Q	8.23±0.1	-	8.92±0.2	8.86±0.2	8.25±0.3	-	8.43±0.3	8.43±0.3
R	9.14±0.3	7.65±0.2	8.43±0.2	10.23±0.4*	7.21±0.2*	8.95±0.2	9.49±0.2	9.13±0.1
W	NR	NR	NR	NR	NR	NR	NR	NR

Data ± SEM, of 2 replicates

[a] Negative logarithm of agonist concentration producing half-maximal response.

NR – No response

- indicates mutant not generated

Statistical difference between each mutant and wild type CLR was calculated using a one-way ANOVA with Dunnet's post-test (*, $p < 0.05$).

Table 5.2: E_{max}[a] values for cAMP production in HEK 293 cells, transfected with each CLR ICL1 mutant (pIRES-RAMP1-SNAP-CLR (WT, Y165-Q172X)), upon CGRP stimulation.

Substitution	WT Residue							
	Y165	**F166**	**K167**	**S168**	**L169**	**S170**	**C171**	**Q172**
WT	98.04±9.8							
A	85.7±8.5	76.7±7.7	123.7±4.4	112.1±6.6	63.1±3.7	117.2±11.1	76.9±6.7	70.1±7.9
C	138.1±5.8	88.3±7.0	-	55.1±6.0	109.3±6.4	55.8±2.3	-	71.1±8.1
E	103.3±31.5	19.0±4.1*	26.0±6.4*	18.7±3.8*	39.3±2.4*	38.9±14.8	62.6±4.7	16.7±2.2*
F	119.7±10.7	-	104.6±12.7	105.1±9.4	110.0±8.7	82.8±9.9	89.9±9.4	70.6±10.3
G	-	100.0±9.3	27.4±8.4*	61.6±9.5	71.0±5.8	30.5±16.5	117.5±18.0	78.5±10.2
H	89.1±16.3	80.2±14.3	61.9±12.7	67.9±21.0	143.2±7.4	94.5±19.4	131.1±20.2	79.0±8.5
I	123.0±22.8	-	42.1±9.9	50.7±15.2	53.6±5.9	33.4±8.6*	-16.7±7.5*	36.2±7.8*
M	104.7±12.0	120.3±24.1	94.3±5.6	97.7±10.0	118.6±2.9	72.7±5.4	100.4±6.1	103.1±6.3
Q	142.8±6.9	-	134.5±8.0	116.3±8.1	98.6±8.2	-	70.0±9.2	70.0±9.1
R	109.8±10.4	104.4±8.8	91.1±7.6	118.6±9.9	59.3±10.0	81.9±5.9	97.3±4.6	146.2±5.0
W	NR	NR	NR	NR	NR	NR	NR	NR

Data ± SEM, of 2 replicates

[a] Maximal response observed upon CGRP stimulation, as a percentage of that observed for wild type CLR.

NR – No response

- Indicates mutant not generated

Statistical difference between each mutant and wild type CLR was calculated using a one-way ANOVA with Dunnet's post-test (*, $p < 0.05$).

In order to provide an explanation of the effects observed for each substitution, the biochemical/physical properties of the substituted amino acid were compared to those in the WT receptor, as well as to the structure of ICL1. Unfortunately, no crystal structures exist for the CLR; thus, our findings are compared to the existing structures of the GCGR in an inactive form (Zhang *et al*, 2017), as well as the GLP1-R in both inactive (Song *et al*, 2017) and active forms (Zhang *et al*, 2017). Thus, these serve as models upon which to base our understanding of the CLR.

Analysis of the ICL1 region in the crystal structure for inactive GCGR (Zhang *et al*, 2017) indicates that there is some structural similarity to that observed for the inactive GLP-1R (Song *et al*, 2017), with the backbone shape of ICL1 following broadly similar patterns (Figure 5.6A-B). Indeed, glycine and threonine residues found at the base of TM1 and TM2 display similar spatial orientations within both receptors, with them both being relatively packed into the bases of each TM bundle. Comparison of ICL1 in the inactive (Figure 5.6B) and active (Figure 5.6C) GLP-1R reveals that this region undergoes a large conformational change upon activation. Residues F169, H171 and H173 undergo large movements, whilst L172 and C174 are observed to slightly rotate (Figure 5.6B-C). In contrast, residues G165 and T175 remain in the same spatial orientations in both active and inactive conformations (Figure 5.6B-C), suggesting that these residues may play important structural roles around the bases of the TMs and ICL1.

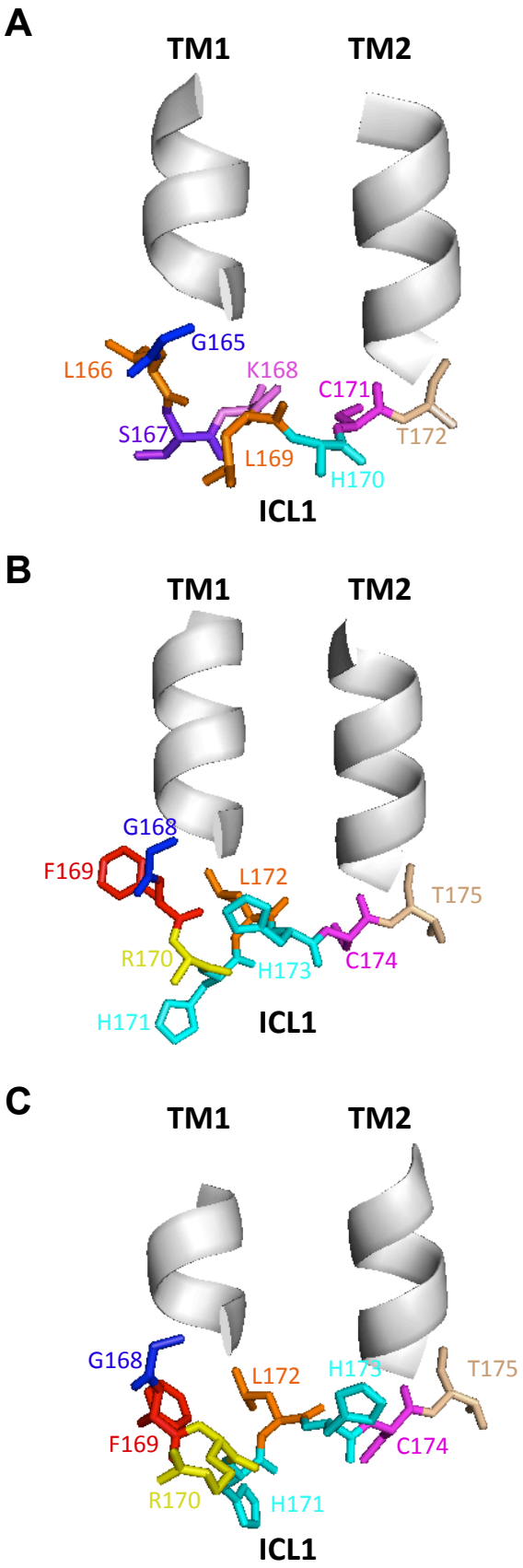

Figure 5.6: Structures of intracellular loop 1 in the glucagon and glucagon-like peptide-1 receptors.

Structures are shown for the intracellular loop 1 (ICL1) region of the inactive glucagon receptor (PDB – 5XEZ, Zhang *et al*, 2017) (A) and glucagon-like peptide-1 receptor (GLP-1R) (PDB - 5VEX, Song *et al*, 2017) (B), as well as active GLP-1R (PDB – 5VAI, Zhang *et al*, 2017) (C). Comparison of inactive (B) and active (C) GLP-1R indicates the large extent of movement observed within the ICL1 region, that occurs upon receptor activation, particularly for residues F169, R170, H171, H173 and C171. Residues G168 and T175 appear to show little movement between inactive (B) and active (C) GLP-1R, and also appear in similar orientations within the inactive glucagon receptor. Transmembrane (TM) bundles are displayed in a grey colour as helices, whilst the residues within ICL1 are differentially coloured according to residue.

5.3 Cell surface expression of CLR ICL1 mutants

As mutation of the ICL1 region has previously been reported to influence cell surface expression of GPCRs (Bentrop *et al*, 1997, Wess *et al*, 1998), each mutant was transfected into HEK 293 cells, and ELISAs utilised to quantify the SNAP signal obtained for each mutant, relative to that of wild type (WT) CLR. This work was performed by Heptares therapeutics as part of our collaborative efforts with them.

Initial quantification of cell surface expression (n = 1) revealed that each mutation had differing effects upon CLR's expression, with some increasing expression (Y165A, S168E and C171I), and others greatly reducing it, as low as 4.35% for L169R (Figure 5.7, Table 5.3). The greatest reductions in expression, observed upon alanine substitution, were apparent for K167A, L169A, C171A and Q172A, with Y165A and F166A displaying increased expressions of ~150% and ~107%, respectively, relative to WT CLR (Figure 5.7, Table 5.3). Whilst substituting for glutamic acid results in reduced expression for residues: Y165-K167E and L169-Q172E, S168E displayed an elevated expression of ~126%, relative to WT (Figure 5.7, Table 5.3). A similar pattern to glutamic acid substitution for the final 4 amino acids is also observed for glycine substitutions, with L169-Q172 exhibiting the greatest reductions (Figure 5.7, Table 5.3). F166G and K167G are more greatly affected than the equivalent glutamic acid substitutions, with expressions of ~51% and ~62%, relative to WT, respectively (Figure 5.7, Table 5.3). However, Y165G is better tolerated than Y165E with expression being ~83% that of WT, whilst S168G displays an elevated expression of ~110% of WT (Figure 5.7, Table 5.3). In terms of mutation to histidine, F166H is well tolerated with an expression of ~103% (relative to WT), and Y165H, S170 and C171 displaying reductions in expression of only ~15-23% of WT (Figure 5.7, Table 5.3). However, histidine substitution causes reductions of ~60-68% for K167-L169H, and a dramatically reduced expression for Q172H to only 10.05%, relative to WT (Figure 5.7, Table 5.3). K167,

S170 and Q172 display the greatest reductions in surface expression upon isoleucine substitution, with reductions of ~64-77%. (Figure 5.7, Table 5.3) S168I and L169I appear similarly affected, with cell surface expressions of ~58% and ~57%, respectively, and Y165I being expressed similarly to WT (~108%), whilst C171I has an increase to ~139%, relative to WT CLR. (Figure 5.7, Table 5.3). Mutation to arginine has little effect upon the expression of Y165R (~103% relative to WT) and K167R (~94% relative to WT). In contrast, arginine substitution appeared to reduce expression for: F166R (~26% relative to WT), S168R (~66% relative to WT), S170R (~73% relative to WT), C171R (~45% relative to WT) and Q172R (~64% relative to WT) (Figure 5.7, Table 5.3). L169R appears to display the greatest reduction in surface expression, being only ~4% that of WT (Figure 5.7, Table 5.3). It is therefore clear that the differential substitution of each residue in the region of ICL1 (Y165-Q172) can have drastic consequences upon the cell surface expression of the CLR. This tends to result in decreases of > 50% when these mutations are at positions L169 and Q172, suggesting that these residues may play an important role in influencing the cell surface expression of the CLR.

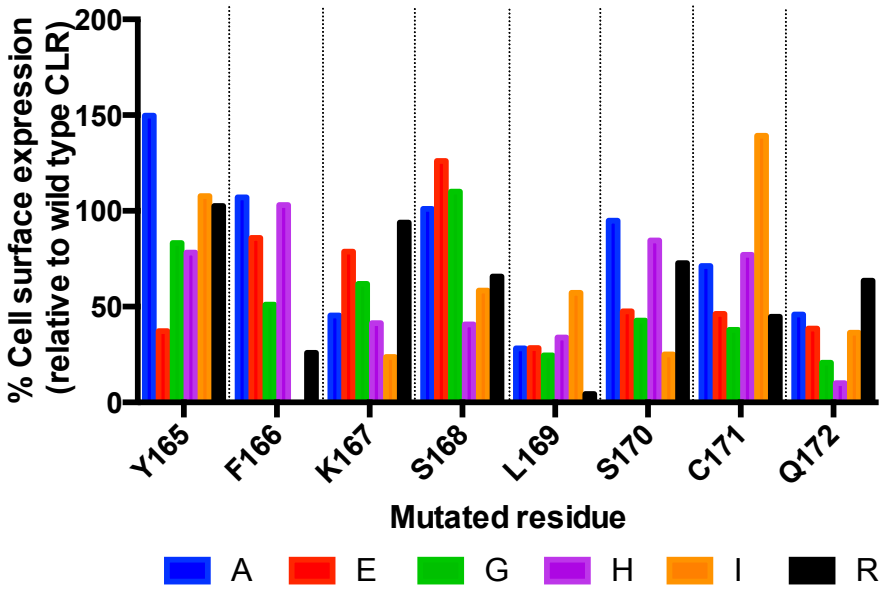

Figure 5.7: Cell surface expression of CLR ICL1 mutants.

Cell surface expression of CLR ICL1 mutants determined, upon co-expression with RAMP 1, in HEK 293 cells. Quantified using SNAP-tagged CLR ELISAs. Data expressed relative to expression of wild type RAMP1-CLR. Work performed by Heptares therapeutics.

Table 5.3: Cell surface expression data for SNAP-CLR ICL1 mutants (pIRES-RAMP1-SNAP-CLR (WT, Y165-Q172 A/E/G/H/I/R)), expressed in HEK 293 cells, as determined via ELISA.

WT residue	Mutation					
	A	**E**	**G**	**H**	**I**	**R**
Y165	149.81	37.18	83.25	78.25	107.68	102.64
F166	107.07	85.93	51.05	103.08	-	25.87
K167	45.38	78.71	61.84	41.45	23.68	93.91
S168	101.01	126.02	110.10	40.80	58.38	65.80
L169	28.27	28.45	24.61	33.94	57.27	4.35
S170	94.87	47.64	42.82	84.61	25.07	72.67
C171	71.23	46.18	37.85	77.03	139.29	44.68
Q172	45.91	38.63	20.82	10.05	36.35	63.63

Data represented as percentage expression of wild type CLR, of 1 replicate.

5.4 Effects of ICL1 glutamic acid mutations upon cAMP production

In order to investigate the effect of introducing negative charges within ICL1, each residue was mutated, in turn, to glutamic acid. This identified that loss of the hydrophobic properties at Y165 could be tolerated by replacement with a negative charge (Y165E), with signalling being comparable to WT (Figure 5.8A, Table 5.4), despite Y165E having a relative expression of only 37% (Figure 5.7, Table 5.3). In contrast, replacing each of the other residues (F166-Q172) with glutamic acid had deleterious effects upon the CLR's ability to signal (Figure 5.8B-H, Table 5.4). These effects may be, in part, explained for L169-Q172 by accompanying reductions in cell surface expression of ~52-72% (Figure 5.7, Table 5.3). This indicates that a negative charge cannot be tolerated at any point across ICL1. Replacement of the aromatic, polar phenylalanine at position 166 results in a ~15 fold reduction in potency, and a ~68% reduction in E_{max} (Figure 5.8B, Table 5.4). Replacement of the positive charge at K167 with a negative one is also detrimental, with similar effects to F166E, and a reduction in maximal signalling of ~62% being apparent (Figure 5.8C, Table 5.4). This indicates that K167 may possibly serve a similar function to S167 in the GCGR (Figure 5.4A), and R170/H171 in the GLP-1R (Figure 5.4B), in forming an interaction with negatively charged residues on H8. As there is only one glutamic acid in H8 of the CLR (Figure 5.3), K167 may potentially form an interaction with E388. In addition, substitution of all the remaining polar residues, S168-Q172, with a negatively charged glutamic acid results in a reduction in potency for S168E and S170-C171E, with S170E displaying the largest reduction, of ~50 fold, relative to WT (Figure 5.8D-H, Table 5.4). These effects are also concurrent with large reductions in E_{max} for all residues (Figure 5.8D-H, Table 5.4). This data may suggest that negative charges across the ICL1 region may all result in charge-charge repulsion with the negative charge on E388. Interestingly, Q172E actually displays an increased potency, but also the greatest reduction in E_{max} of ~76%

(Figure 5.8H, Table 5.4), which may be due to effects upon TM2/ICL2. It is thus observed that the CLR is unable to tolerate substitution with glutamic acid for residues F166-Q172, and that negative charges in this region greatly reduce the CLR's ability to mediate activation of $G\alpha_s$. The only position where this can be tolerated is Y165. The equivalent residues to Y165 in the GCGR (G165) and GLP-1R (G168) are relatively packed into the base of TM1 (Figure 5.6A-C); this could also be true of the CLR. Thus, Y165 appears to play a minor role in signalling.

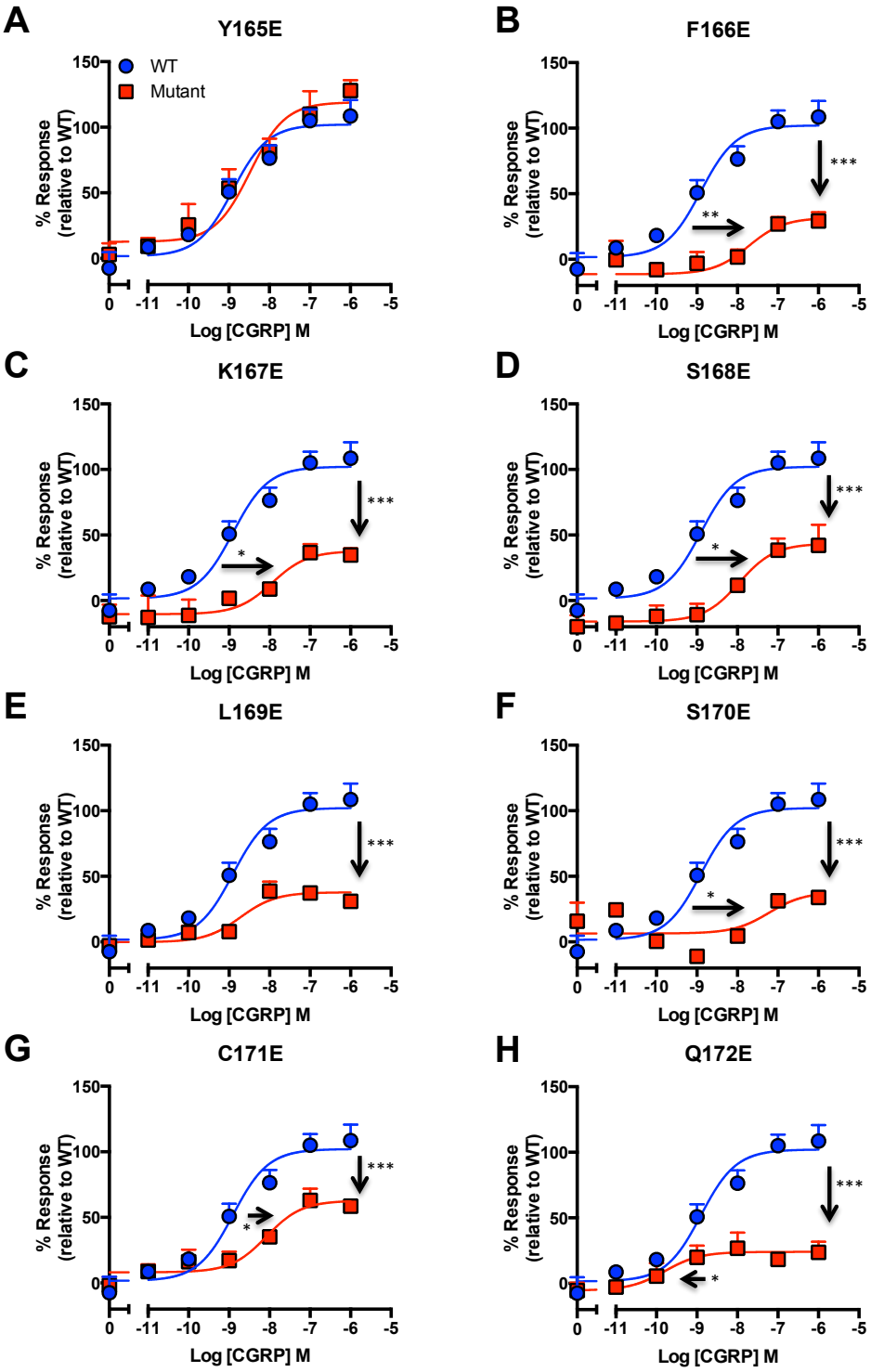

Figure 5.8: Glutamic acid scan of ICL1 (Y165-Q172) of CLR.

cAMP accumulation was measured, upon CGRP stimulation, in HEK 293 cells transfected with pIRES-RAMP1-SNAP-CLR for either WT CLR ● (n = 10), or each mutant (n = 6) ■ :Y165E (A), F166E (B), K167E (C), S168E (D), L169E (E), S170E (F), C171E (G), Q172E (H). Data are expressed relative to levels of cAMP produced by wild type CLR, ± SEM, of n replicates. Arrows indicate changes in pEC_{50} or E_{max}. Significance was calculated using a one-way ANOVA with Dunnet's post-test (*, $p < 0.05$, **, $p < 0.01$, ***, $p < 0.001$).

Table 5.4: Potency (pEC_{50}) and E_{max} values for cAMP production in HEK 293 cells transfected with pIRES-RAMP1-SNAP-CLR (WT, Y165-Q172E), upon CGRP stimulation.

	pEC_{50}[a]	E_{max}[b]	n
WT	8.90±0.2	102.1±6.4	10
Y165E	8.48±0.2	119.1±8.5	6
F166E	7.72±0.3**	31.7±6.1***	6
K167E	7.93±0.3*	37.8±6.0***	6
S168E	7.96±0.3*	43.5±7.2***	6
L169E	8.72±0.3	37.8±4.2***	6
S170E	7.22±0.8*	37.9±12.3***	6
C171E	8.08±0.2*	62.8±5.6***	6
Q172E	9.80±0.6*	24.1±5.0***	6

Data ± SEM of n individual replicates.
[a] Negative logarithm of agonist concentration producing half-maximal response.
[b] Maximal response observed upon CGRP stimulation, as a percentage of that observed for wild type CLR.
Statistical difference between each mutant and wild type CLR was calculated using a one-way ANOVA with Dunnet's post-test (*, $p < 0.05$, **, $p < 0.01$, ***, $p < 0.001$).

5.5 Effects of ICL1 glycine mutations upon cAMP production

Having determined that negative charges are not tolerated, a glycine scan of this region was also performed. This would remove all side chain chemistry, whilst also introducing flexibility within the backbone structure of ICL1. Thus, by conferring increased flexibility at each position, it is possible to highlight how crucial the positioning of each residue is to CLR's functionality. Unlike Y165E (Figure 5.8A, Table 5.4), substitution for glycine at this position is poorly tolerated, with reductions in both potency and E_{max} (Figure 5.9A, Table 5.5). This may suggest that Y165 plays a key role in packing against TM1, and in holding ICL1 in an optimal conformation for G protein activation. Indeed, with the GLP-1R, the equivalent residue, G168, remains in a relatively similar position in both inactive and active conformations (Figure 5.6B-C). Therefore, through mutating Y165 to glycine, greater flexibility at this position has been conferred, perhaps affecting the orientation of ICL1. In contrast, F166G is well tolerated, with signalling being similar to WT (Figure 5.9B, Table 5.5). However, near total abolition of activity for K167G is observed, with signalling reduced to ~28% that of WT (Figure 5.9C, Table 5.5). This could, perhaps, be due to loss of the positive charge at this position in WT CLR, which appears to be required, in other family B GPCRs, for interaction with H8 (Figure 5.4A-B). In stark contrast, L169G, whilst having a reduced E_{max}, actually has an increased potency of ~26 fold over WT (Figure 5.9E, Table 5.5), despite a great reduction in cell surface expression of ~75% (Figure 5.7, Table 5.3). This suggests that loss of rigidity here makes it easier for the CLR to adopt an active confirmation, upon CGRP binding. Indeed, in the GLP-1R the equivalent residue, L172, appears to undergo little movement between inactive and active states (Figure 5.6 B-C). As with K167G, glycine substitution at S170 has a dramatic effect upon signalling, resulting in total abolition of activity (Figure 5.9F, Table 5.5). This occurs despite S170G being expressed at levels ~40% that of WT (Figure 5.7, Table 5.3), a level of expression

which has previously still resulted in CGRP-mediated cAMP production. Thus, it appears that the positioning of the polar side chain of S170 is critical for correct CLR function. In the GLP-1R, the equivalent residue of S170 is H173, which appears to undergo a large rotation away from TM1, towards TM2 (Figure 5.6B-C). Whilst this residue appears to play no role in interacting with H8, its conservation in all family B GPCRs, except the CLR, CT and CRF receptors, suggests its function is critical. These residues may therefore play some role in regulating downstream signalling, after ICL1 and H8 have moved apart during receptor activation. Unlike all other substitutions, C171G and Q172G are extremely well tolerated with regards to E_{max}, also displaying an increased potency relative to WT (Figure 5.9G-H, Table 5.5). The fact that these two substitutions are so well tolerated is in spite of the fact that C171G has an expression of 37.85%, and Q172G 20.82%, relative to WT (Figure 5.7, Table 5.3). Thus, it appears that C171 and Q172 may actually serve to hold the CLR in an inactive conformation. Through conferring flexibility at these two positions, it is possible that a constraining interaction has been removed, allowing for an easier transition from an inactive to active conformation, hence resulting in an increase in CGRP's potency. Indeed, in the GLP-1R the equivalent residues to C171 and Q172 (C174 and T175) appear to be fairly immobile, with only C174 displaying a small amount of movement, between inactive and active states (Figure 5.6B-C). It may therefore be possible that these residues, in family B GPCRs, serve as 'anchor points' between ICL1 and TM2. T175 appears to be packed into the base of TM2 in the GLP-1R, much like G168 (Figure 5.6B-C). Therefore, Q172 may also be similarly positioned in the CLR. Overall, glycine scanning has identified that: Y165, C171 and Q172 may play roles in the positioning of ICL1, whilst K167 and S170 are required to be held in specific positions for optimal activity.

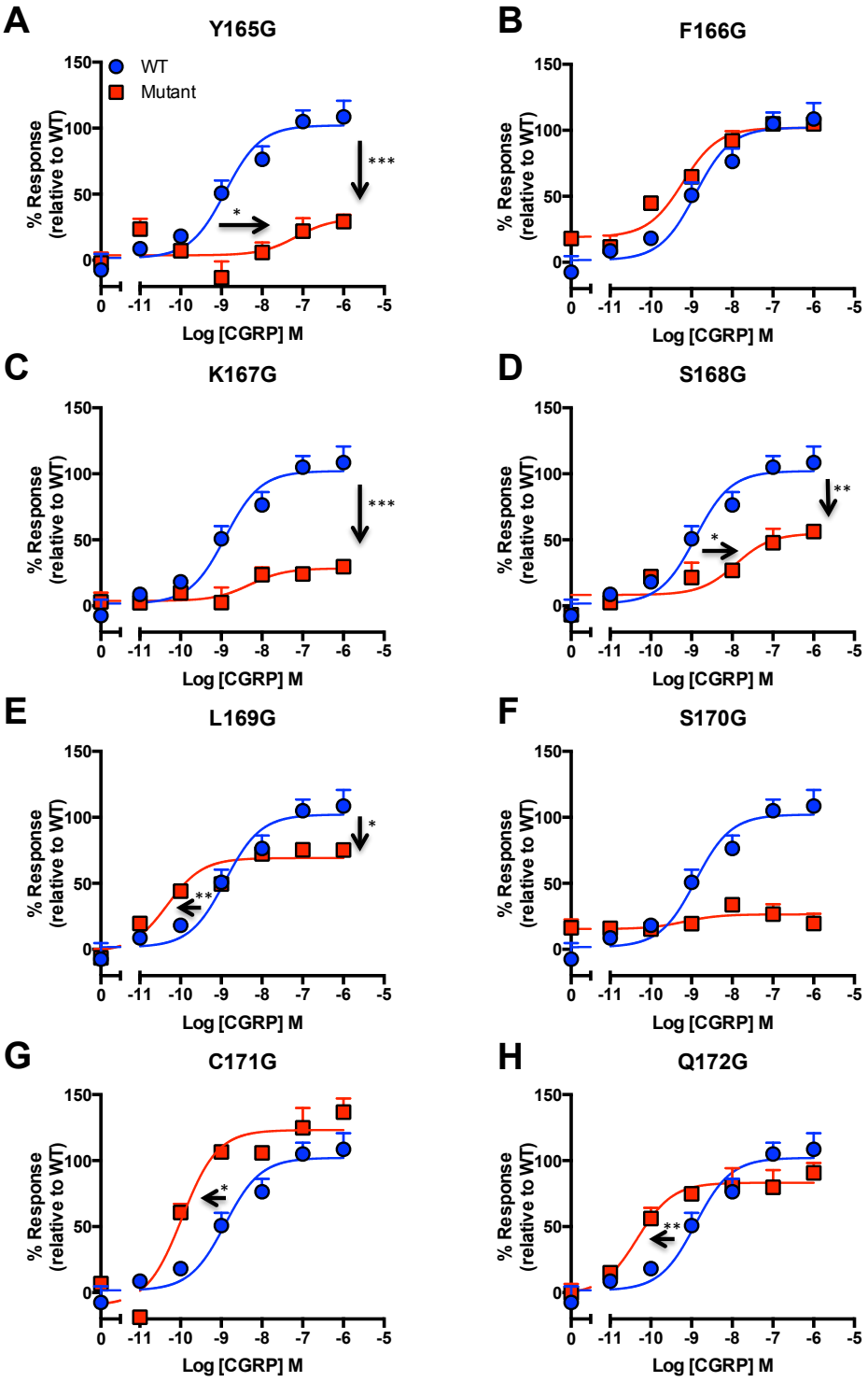

Figure 5.9: Glycine scan of ICL1 (Y165-Q172) of CLR.

cAMP accumulation was measured, upon CGRP stimulation, in HEK 293 cells transfected with pIRES-RAMP1-SNAP-CLR for either WT CLR (n = 10) ●, or each mutant (n = 3) ■ :Y165G (A), F166G (B), K167G (C), S168G (D), L169G (E), S170G (F), C171G (G), Q172G (H). Data are expressed relative to levels of cAMP produced by wild type CLR, ± SEM, of n replicates. Arrows indicate changes in pEC_{50} or E_{max}. Significance was calculated using a one-way ANOVA with Dunnet's post-test (*, $p < 0.05$, **, $p < 0.01$, ***, $p < 0.001$).

Table 5.5: Potency (pEC_{50}) and E_{max} values for cAMP production in HEK 293 cells transfected with pIRES-RAMP1-SNAP-CLR (WT, Y165-Q172G), upon CGRP stimulation.

	pEC_{50}[a]	E_{max}[b]	n
WT	8.90±0.2	102.1±6.4	10
Y165G	7.16±0.9*	31.7±13.4***	3
F166G	9.21±0.2	101.9±4.3	3
K167G	8.30±0.5	28.3±4.2***	3
S168G	7.91±0.4*	54.8±7.6**	3
L169G	10.32±0.2**	69.2±3.7*	3
S170G	NR	NR	3
C171G	9.96±0.2*	123.2±7.0	3
Q172G	10.33±0.2**	83.3±4.3	3

Data ± SEM of n individual replicates.
[a] Negative logarithm of agonist concentration producing half-maximal response.
[b] Maximal response observed upon CGRP stimulation, as a percentage of that observed for wild type CLR.
NR – No response.
Statistical difference between each mutant and wild type CLR was calculated using a one-way ANOVA with Dunnet's post-test (*, $p < 0.05$, **, $p < 0.01$, ***, $p < 0.001$).

5.6 Effects of ICL1 histidine mutations upon cAMP production

Having investigated the effects of glutamic acid and glycine scanning of ICL1 upon the CLR, a histidine scan was also performed to investigate how positive charges affected CGRP-mediated, CLR-dependent cAMP production. Unlike substitution with negatively charged glutamic acid, positively charged histidine is fairly well tolerated. As with glutamic acid substitution at Y165 (Figure 5.8A, Table 5.4), histidine is well tolerated, with only a small reduction in E_{max} being apparent (Figure 5.10A, Table 5.6). This further implies that Y165 is relatively packed into the base of TM1, acting as a linker between TM1 and ICL1. A similar trend is observed for residues: F166 and K167 (reduction in E_{max} observed), whilst S168 displays a reduction in potency (Figures 5.10B-D, Table 5.6). The fact that replacing a positively charge lysine (K167), with a positively charged histidine has no effect upon potency, and only a small effect upon E_{max}, implies that histidine can potentially still form the same interactions that K167 does in the WT CLR. Substitution of S168 for histidine creates an analogous situation to WT GLP-1R, which has a histidine at the equivalent position as CLR (Figure 5.2). The fact that this has little effect implies that a serine, in the CLR, is able to perform similar functions to this histidine in the GLP-1R, a residue that undergoes a large rotation upon activation (Figure 5.6B-C). In contrast, histidine substitution at L169 results in an ~14 fold reduction in potency, relative to WT, with no concurrent effect upon E_{max} (Figure 5.10E, Table 5.6). For the remaining residues at the end of ICL1, S170-Q172, histidine substitution appears to have little effect, with slight reductions in E_{max} being observed for S170H and Q172H, along with a concurrent reduction in potency for Q172H (Figure 5.10F-G, Table 5.6). In fact, lack of any larger effects upon Q172H's ability to signal is surprising, given that it is only expressed to 10% that of WT CLR (Figure 5.7, Table 5.3). This indicates the great level of receptor reserve for RAMP1-CLR, and that the pharmacological effects observed in these studies may not be solely due to reductions in receptor

expression. Overall, this data indicates that positive charges are fairly well tolerated within ICL1, having minimal impact upon signalling activity except for L169H, which displays a reduced potency, apparent whenever a charge is introduced at position 169. In the GLP-1R, the equivalent of L169, L172, appears to undergo little movement between inactive and active conformations (Figure 5.6B-C). The fact that this residue is universally conserved amongst family B GPCRs (albeit with CRF having isoleucines in this position), and often found between two positively charged residues, may suggest it serves to prevent a large area of positive charge being formed, or preventing charge-charge repulsion between the flanking residues. By introducing a histidine at position 169 in the CLR, a secondary charge-charge interaction with E388 in H8 may be formed, thereby making it harder for an ICL1-H8 interaction to be broken upon activation (hence the reduction in potency of CGRP for this mutant).

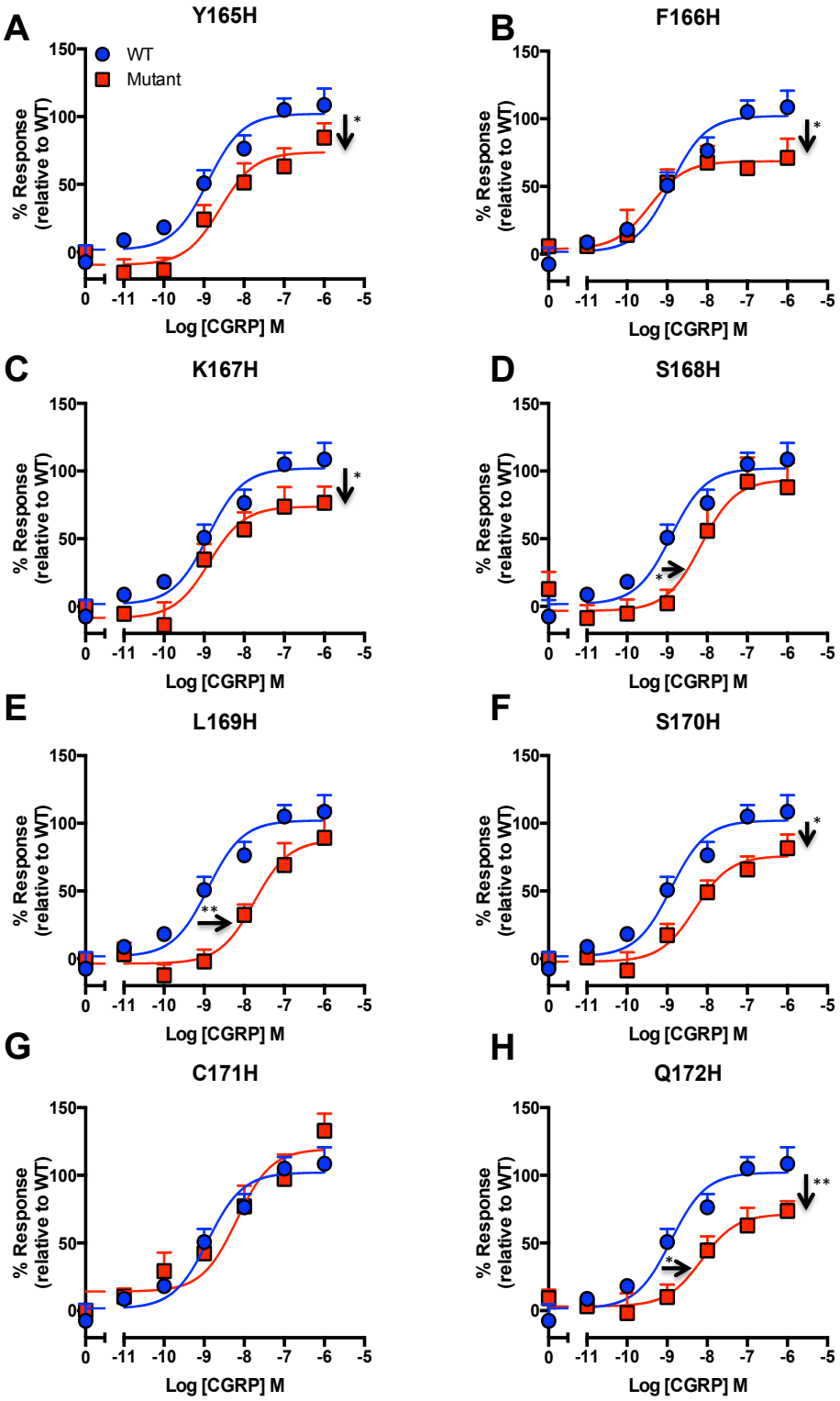

Figure 5.10: Histidine scan of ICL1 (Y165-Q172) of CLR.

cAMP accumulation was measured, upon CGRP stimulation, in HEK 293 cells transfected with pIRES-RAMP1-SNAP-CLR for either WT CLR (n = 10) ●, or each mutant ■: Y165H (n = 6) (A), F166H (n = 3) (B), K167H (n = 6) (C), S168H (n = 6) (D), L169H (n = 5) (E), S170H (n = 6) (F), C171H (n = 4) (G), Q172H (n = 6) (H). Data are expressed relative to levels of cAMP produced by wild type CLR, ± SEM, of n replicates. Arrows indicate changes in pEC_{50} or E_{max}. Significance was calculated using a one-way ANOVA with Dunnet's post-test (*, $p < 0.05$, **, $p < 0.01$).

Table 5.6: Potency (pEC_{50}) and E_{max} values for cAMP production in HEK 293 cells transfected with pIRES-RAMP1-SNAP-CLR (WT, Y165-Q172H), upon CGRP stimulation.

	pEC_{50}[a]	E_{max}[b]	n
WT	8.90±0.2	102.1±6.4	10
Y165H	8.59±0.3	73.7±7.5*	6
F166H	9.42±0.3	68.6±5.7*	3
K167H	8.87±0.3	73.8±7.6*	6
S168H	8.16±0.2*	93.6±11.3	6
L169H	7.75±0.3**	87.7±10.7	5
S170H	8.30±0.2	76.0±6.6*	6
C171H	8.19±0.3	119.4±10.3	4
Q172H	8.14±0.3*	71.4±7.6**	6

Data ± SEM of n individual replicates.
[a] Negative logarithm of agonist concentration producing half-maximal response.
[b] Maximal response observed upon CGRP stimulation, as a percentage of that observed for wild type CLR.
Statistical difference between each mutant and wild type CLR was calculated using a one-way ANOVA with Dunnet's post-test (*, $p < 0.05$, **, $p < 0.01$).

5.7 Effects of ICL1 isoleucine mutations upon cAMP production

Scanning ICL1 with isoleucine (Y165I, K167-Q172I) identified that at most positions, a branched, hydrophobic side chain is not well tolerated. However, as with most previous substitutions, isoleucine substitution of Y165 is tolerated with signalling being comparable to WT CLR (Figure 5.11A, Table 5.7). This further suggests that Y165 plays a role in helping to correctly position ICL1, rather than providing biochemical properties required for function. Isoleucine substitution of K167 results in a reduction in E_{max} by ~60% (Figure 5.11B, Table 5.7), perhaps due to loss of a seemingly essential positive charge at this position. A similar reduction in E_{max} is also observed for S168I, with no apparent effect on potency (Figure 5.11C, Table 5.7), whilst L169I substitution results in a ~21 fold reduction in potency, and in E_{max} of ~45% (Figure 5.11D, Table 5.7). The equivalent residue in GLP-1R (L172) appears to move little between active and inactive conformations (Figure 5.6B-C), suggesting that the positioning of this residue is critical. Therefore, changing the chirality of the WT residue alters its position, resulting in a loss of function. Interestingly, in the CRF receptors an isoleucine is present in this position (Figure 5.2), suggesting the possibility of a slightly different role for this residue within these two GPCRs. The reductions in E_{max} for K167-L169I may also be explained by each of these mutant receptors having reductions in cell surface expression of 42-76% (Figure 5.7, Table 5.3). Substitution of the uncharged, polar residues S170 and Q172 to non-polar isoleucine results in total abolition of functionality for S170I, and a large reduction in E_{max} for Q172I (Figure 5.11E-G, Table 5.7). Whilst this may be explained by S170I and Q172I having greatly reduced cell surface expressions (Figure 5.7, Table 5.3), they are expressed at levels equal to, or greater than, K167I, which is still functional. Thus, these effects may be due to biochemical/biophysical determinants, rather than solely due to expression levels. In the case of Q172I this may be due to effects upon the positioning of ICL1, as the equivalent residue in the

GLP-1R shows little difference in orientation between inactive and active conformations (Figure 5.6B-C), but may also be due to effects upon TM2 and/or ICL2. For C171I, CGRP is observed to act as an inverse agonist, with a reduction in signalling of ~17%, relative to unstimulated cells (Figure 5.11F, Table 5.7). This could potentially be due to non-specific coupling to differing G proteins (potentially $G\alpha_{i/o}$), due to a greatly increased expression (Figure 5.7, Table 5.3), or stabilising a more inactive receptor conformation. Alternatively, an isoleucine at this position may promote coupling to $G\alpha_{i/o}$, thereby resulting in a reduction in AC activity, mediated via some level of constitutive activity of the CLR. The data obtained from isoleucine scanning has thus identified how important the chirality of L169 is, and the crucial roles played by the polar residues towards the end of ICL1 (S170-Q172).

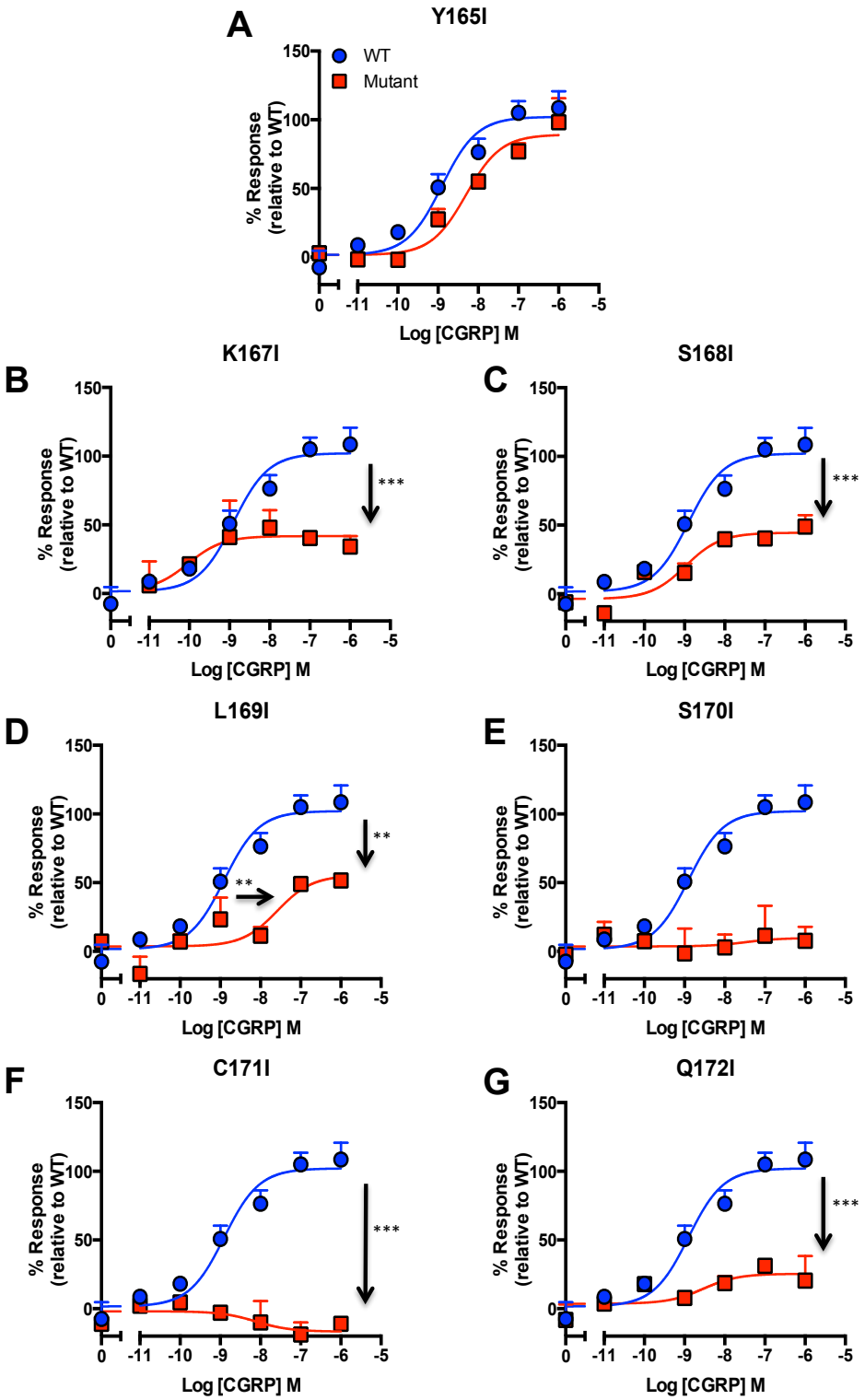

Figure 5.11: Isoleucine scan of ICL1 (Y165-Q172) of CLR.

cAMP accumulation was measured, upon CGRP stimulation, in HEK 293 cells transfected with pIRES-RAMP1-SNAP-CLR for either WT CLR (n = 10) ● , or each mutant (n = 3) ■ : Y165I (A), K167I (B), S168I (C), L169I (D), S170I (E), C171I (F), Q172I (G). Data are expressed relative to levels of cAMP produced by wild type CLR, ± SEM, of n replicates. Arrows indicate changes in pEC_{50} or E_{max}. Significance was calculated using a one-way ANOVA with Dunnet's post-test (*, $p < 0.05$, **, $p < 0.01$, ***, $p < 0.001$).

Table 5.7: Potency (pEC_{50}) and E_{max} values for cAMP production in HEK 293 cells transfected with pIRES-RAMP1-SNAP-CLR (WT, Y165I, K167-Q172I), upon CGRP stimulation.

	pEC_{50}[a]	E_{max}[b]	n
WT	8.90±0.2	102.1±6.4	10
Y165I	8.30±0.2	89.2±6.5	3
K167I	10.03±0.8	41.8±7.6***	3
S168I	8.97±0.3	44.5±4.9***	3
L169I	7.58±0.5*	55.4±11.0**	3
S170I	NR	NR	3
C171I	8.12±1.1	-16.7±7.5***	3
Q172I	8.54±0.9	25.4±6.6***	3

Data ± SEM of n individual replicates.
[a] Negative logarithm of agonist concentration producing half-maximal response.
[b] Maximal response observed upon CGRP stimulation, as a percentage of that observed for wild type CLR.
NR – No response.
Statistical difference between each mutant and wild type CLR was calculated using a one-way ANOVA with Dunnet's post-test (*, $p < 0.05$, **, $p < 0.01$, ***, $p < 0.001$).

5.8 Effects of ICL1 arginine mutations upon cAMP production

As substituting each residue in ICL1 with a positively charged histidine was well tolerated by the CLR, it was sought to further investigate the effect of other positive charges, through arginine scanning. As with histidine substitutions for Y165-K167 (Figure 5.10A-C, Table 5.6), substitution with arginine displayed little effect in terms of both potency and maximal signalling, with only F166R displaying a slight reduction in potency (Figure 5.12A-C, Table 5.8). However, substitution of S168, to arginine, results in a large increase, of ~29 fold, in potency, over WT, with no detrimental effects upon E_{max} (Figure 5.12D, Table 5.8). This substitution represents the largest gain-of-function observed of all the mutations studied, suggesting that a positively charged, highly branched side chain is actually beneficial, and improves CLR activity, compared to the WT serine, at this position. Through substituting S168 for an arginine the CLR has been made more like the consensus for family B, with a positive charge at this position (Figure 5.2). Indeed, the CRF receptors contain an arginine at this position (Figure 5.2). The fact that a gain-of-function is now observed implies that a beneficial interaction with downstream signalling proteins may have been generated. This may be with Gβ, as H171 in the GLP-1R, the equivalent residue to S168, has been observed to directly interact with D312 of Gβ via an electrostatic interaction (Zhang *et al*, 2017). Therefore, through introducing a positive charge at this position in the CLR (S168R), which is absent in the WT receptor, an ICL1-Gβ interaction may be promoted, resulting in potentiation of CGRP-mediated signalling at the CLR. Arginine substitution of L169 results in a large reduction in E_{max} by ~55% (Figure 5.12E, Table 5.8). It is surprising that L169R is able to function, as it has a surface expression of only 4.35%, relative to WT (Figure 5.7, Table 5.3). Along with Q172H having an expression of ~10% (Figure 5.7, Table 5.3), this data again highlights the large extent of receptor reserve in this system, and indicates that effects observed are not solely due to reducing

receptor number. In contrast to L169R, arginine substitutions at positions S170-Q172 appeared to have little effect, with Q172R displaying a slight increase in E_{max} (Figure 5.12F-H, Table 5.8). Therefore, as with histidine substitutions (Figure 5.10, Table 5.6), ICL1 appears, again, to be tolerant to positive charges inferred by arginine. Indeed, these even prove beneficial, and confer a gain of function, when at position 168, potentially through promoting interactions with associating G proteins.

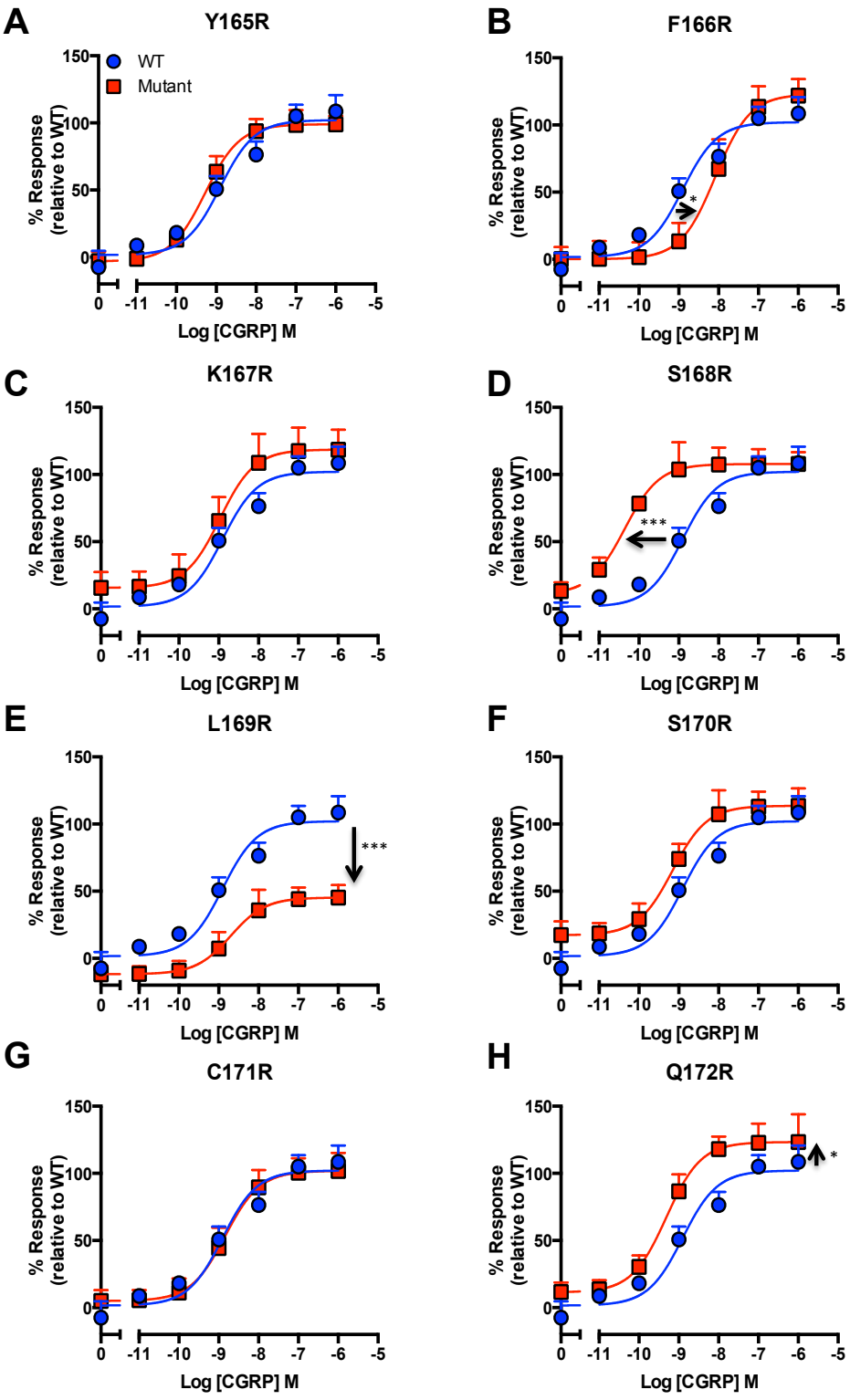

Figure 5.12: Arginine scan of ICL1 (Y165-Q172) of CLR.

cAMP accumulation was measured, upon CGRP stimulation, in HEK 293 cells transfected with pIRES-RAMP1-SNAP-CLR for either WT CLR (n = 10) ● , or each mutant ■ : Y165R (n = 6) (A), F166R (n = 6) (B), K167R (n = 6) (C), S168R (n = 6) (D), L169R (n = 6) (E), S170R (n = 6) (F), C171R (n = 8) (G), Q172R (n = 8) (H). Data are expressed relative to levels of cAMP produced by wild type CLR, ± SEM, of n replicates. Arrows indicate changes in pEC_{50} or E_{max}. Significance was calculated using a one-way ANOVA with Dunnet's post-test (*, $p < 0.05$, **, $p < 0.01$, ***, $p < 0.001$).

Table 5.8: Potency (pEC_{50}) and E_{max} values for cAMP production in HEK 293 cells transfected with pIRES-RAMP1-SNAP-CLR (WT, Y165-Q172R), upon CGRP stimulation.

	pEC_{50}[a]	E_{max}[b]	n
WT	8.90±0.2	102.1±6.4	10
Y165R	9.28±0.2	99.01±4.8	6
F166R	8.08±0.2*	122.9±11.1	6
K167R	8.97±0.3	118.6±9.9	6
S168R	10.36±0.3***	107.8±5.7	6
L169R	8.70±0.3	45.3±6.9***	6
S170R	9.16±0.2	113.6±7.2	6
C171R	8.84±0.2	101.9±7.4	8
Q172R	9.31±0.2	123.3±7.2*	8

Data ± SEM of n individual replicates.
[a] Negative logarithm of agonist concentration producing half-maximal response.
[b] Maximal response observed upon CGRP stimulation, as a percentage of that observed for wild type CLR.
Statistical difference between each mutant and wild type CLR was calculated using a one-way ANOVA with Dunnet's post-test (*, $p < 0.05$, **, $p < 0.01$, ***, $p < 0.001$).

5.9 Effects of ICL1 alanine mutations upon cAMP, $_{i}Ca^{2+}$ and ERK1/2 signalling

Through performing an alanine scan it was identified that substituting residues Y165, K167 and S168, to alanine, has minimal effects upon CGRP-mediated cAMP production from the CLR, in terms of potency and maximal signalling, relative to WT (Figure 5.13A, C and D, Table 5.9). This lack of effect for K167A is despite a reduction in cell surface expression of ~55%, relative to WT (Figure 5.7, Table 5.3). Substituting the remaining residues has differing effects, depending upon the residue mutated. F166A displays a reduction in potency of ~6 fold, relative to WT, and a reduced E_{max} (Figure 5.13B, Table 5.9). This suggests that loss of a bulky aromatic side chain at this position is detrimental in terms of the level of response mediated upon agonist stimulation. Substitution of L169 for alanine has a similar effect to F166A, with a ~3 fold reduction in potency (not statistically significant), as well as an associated reduction in E_{max} (Figure 5.13E, Table 5.9). These reductions may be due to a reduced cell surface expression (Figure 5.7, Table 5.3). This data suggests that at position 169, a relatively large, non-polar R group is required for optimal, maximal, signalling, and that substitution for a small, non-polar R group is detrimental. Substitution of a polar R group at position 170 for a non-polar one (S170A) has no effect upon potency, but slightly increases E_{max} (Figure 5.13F, Table 5.9). In contrast, loss of a polar R group at position 171 (C171A) results in a reduced potency, with little effect on E_{max} (Figure 5.13G, Table 5.9). As with S170A, loss of a large, polar R group at position 172 (Q172A) results in a decrease in potency (not statistically significant), with an associated reduction in E_{max} (Figure 5.13H, Table 5.9). As with L169A, this may, in part, be due to a reduction in cell surface expression, of ~54% that of WT CLR.

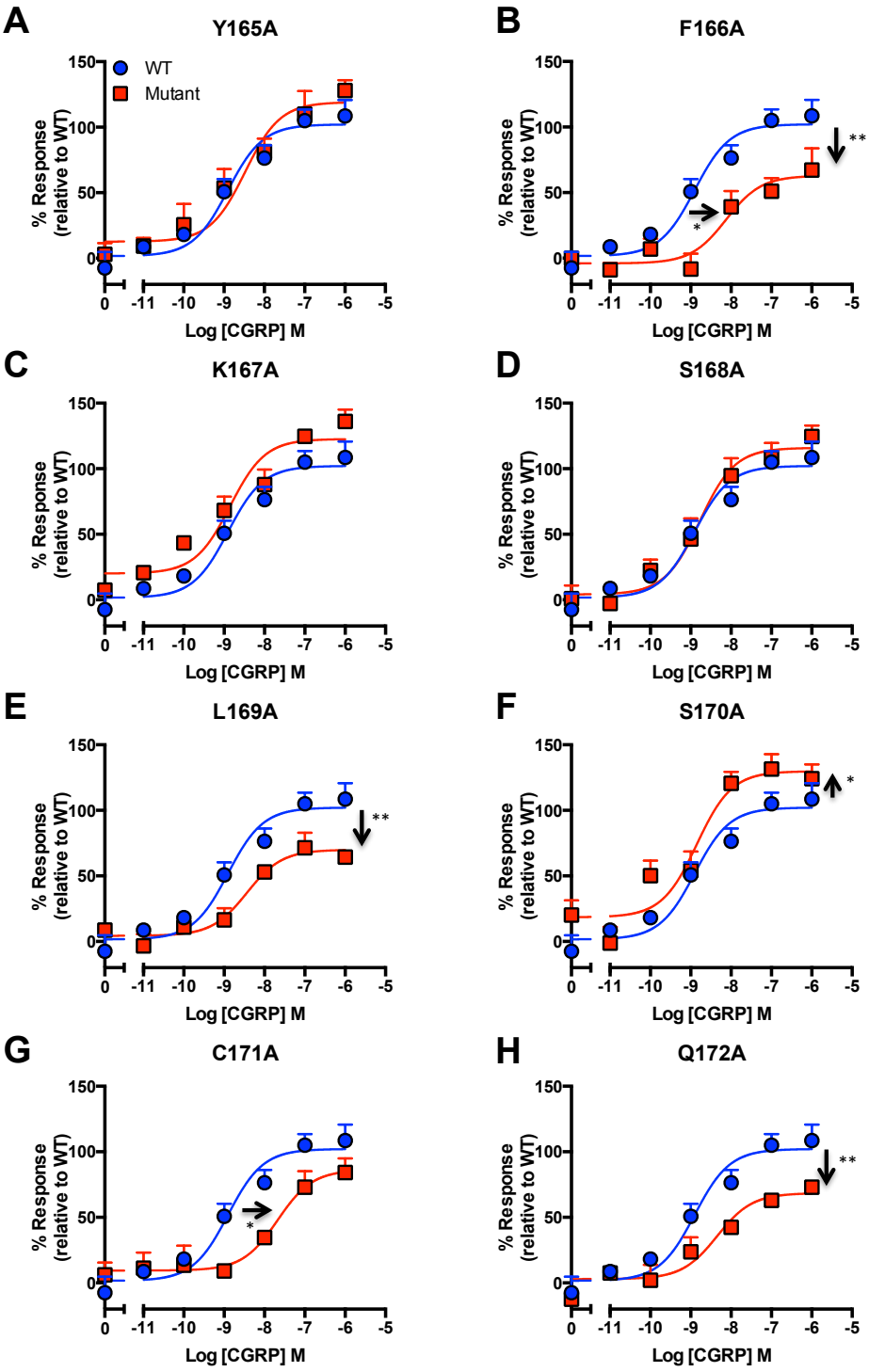

Figure 5.13: Alanine scan of ICL1 (Y165-Q172) of CLR.

cAMP accumulation was measured, upon CGRP stimulation, in HEK 293 cells transfected with pIRES-RAMP1-SNAP-CLR for either WT CLR ● (n = 10), or each mutant (n = 6) ■ : Y165A (A), F166A (B), K167A (C), S168A (D), L169A (E), S170A (F), C171A (G), Q172A (H). Data are expressed relative to levels of cAMP produced by wild type CLR, ± SEM, of n replicates. Arrows indicate changes in pEC_{50} or E_{max}. Significance was calculated using a one-way ANOVA with Dunnet's post-test (*, $p < 0.05$, **, $p < 0.01$).

Table 5.9: Potency (pEC_{50}), affinity (pKa) and coupling efficacy (Log τ) values for cAMP production in HEK 293 cells, transfected with pIRES-RAMP1-SNAP-CLR (WT, Y165-Q172A), upon CGRP stimulation.

	pEC_{50}[a]	E_{max}[b]	pKa[c]	Logτ[d]	n
WT	8.90±0.2	102.1±6.4	8.69±0.2	-0.19±0.02	10
Y165A	8.48±0.2	119.1±8.5	8.81±0.2	-0.000087±0.03***	6
F166A	8.12±0.3*	62.9±8.2**	8.54±0.3	-0.42±0.02***	6
K167A	8.85±0.2	122.6±6.6	8.72±0.2	-0.14±0.02	6
S168A	8.78±0.2	115.9±7.9	8.17±0.2	-0.11±0.04	6
L169A	8.44±0.2	69.9±6.2**	8.13±0.3	-0.50±0.03***	6
S170A	8.85±0.2	129.8±8.3*	8.00±0.2*	-0.082±0.03**	6
C171A	7.68±0.4*	86.2±10.5	7.57±0.3**	-0.35±0.03***	8
Q172A	8.35±0.2	68.5±5.7**	8.09±0.3	-0.42±0.02***	8

Data ± SEM of n individual replicates.
[a] Negative logarithm of agonist concentration producing half-maximal response.
[b] Maximal response observed upon CGRP stimulation, as a percentage of that observed for wild type CLR.
[c] Negative logarithm of the equilibrium dissociation constant, as determined using the operational model of agonism (Black and Leff, 1983).
[d] Coupling efficacy parameter as determined using the operational model of agonism (Black and Leff, 1983).
Statistical difference between each mutant and wild type CLR was calculated using a one-way ANOVA with Dunnet's post-test (*, $p < 0.05$, **, $p < 0.01$, ***, $p < 0.001$).

Having previously identified the ability of RAMP1-CLR heterodimers to be able to mobilise $_{i}Ca^{2+}$, in response to CGRP stimulation, in a $G\alpha_{q/11}$-dependent manner (Figure 4.5, Table 4.3), the effects of alanine substitutions upon this signalling pathway were further investigated. In order to achieve this, each alanine mutant was transfected into HEK 293 cells loaded with FLUO-4/AM and $_{i}Ca^{2+}$ mobilisation measured, in response to CGRP stimulation. Through characterising RAMP1-WT CLR (pIRES-RAMP1-SNAP-CLR (WT)), it was identified that 10-100 nM CGRP is able to generate equally large responses, with 1 nM and 100 pM producing intermediate responses, with no $_{i}Ca^{2+}$ being mobilised at < 10

pM (Figure 5.14A). In contrast, for Y165A it was observed that 1-100 nM CGRP is able to mediate large, robust responses, but at < 1 nM, no response is observed (Figure 5.14B). Mutating F166 and K167 to alanine had little effect upon CGRP-mediated mobilisation of $_{i}Ca^{2+}$, with similar responses to WT CLR being observed (Figure 5.14C-D). In contrast, mutating residues S168-Q172 to alanine had profound effects upon $_{i}Ca^{2+}$ mobilisation. It was possible to observe reductions in the maximal fluorescence intensity observed for each stimulating CGRP concentration, as well as those that are able to mediate mobilisation of $_{i}Ca^{2+}$ (Figure 5.14E-J). For S168, it was observed that 1-100 nM CGRP stimulation results in $_{i}Ca^{2+}$ mobilisation (Figure 5.14E). In contrast, 1 nM CGRP had no effect upon L169-Q172, whilst 10 nM generated much smaller responses compared to Y165-K167 (Figure 5.13). It was thus identified that residues at the base of (Y165), and close to (F166-K167), TM1 are more tolerant to alanine substitution than those across ICL1 (S168-C171) and at the base of TM2 (Q172A), with respect to mobilising $_{i}Ca^{2+}$.

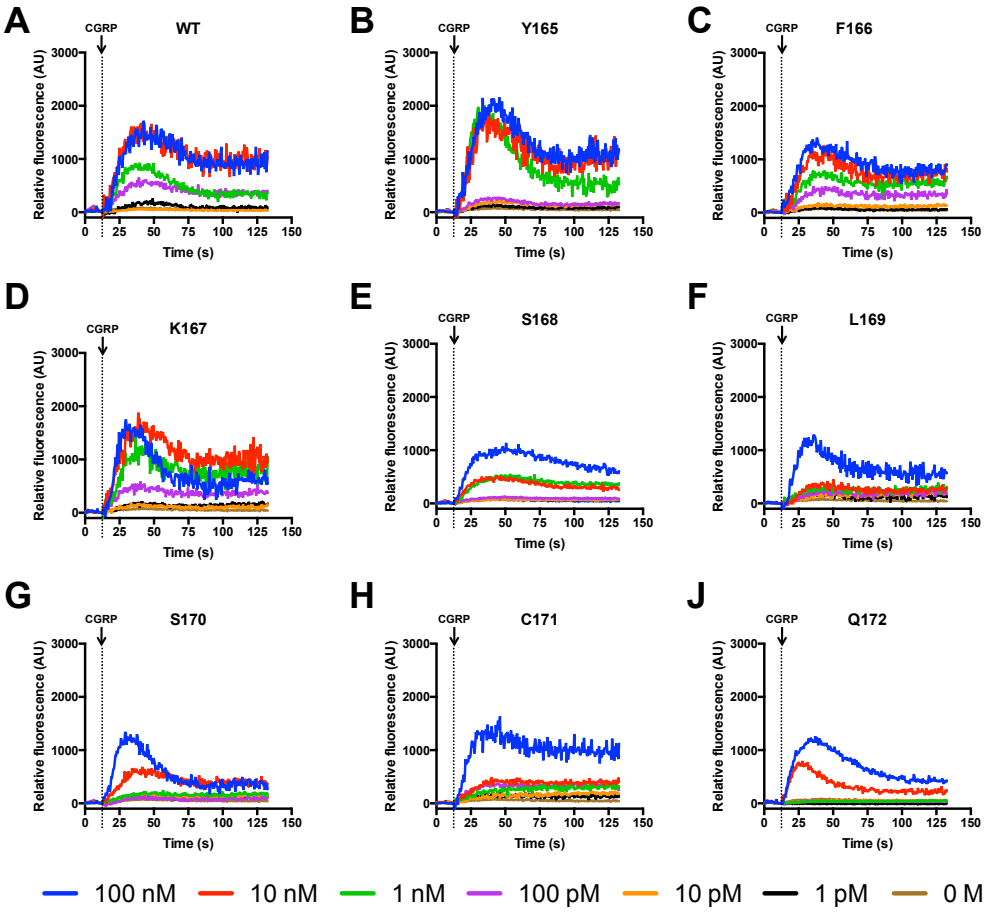

Figure 5.14: Effects of alanine scan upon mobilisation of $_{i}Ca^{2+}$.

HEK 293 cells, loaded with FLUO-4/AM, transfected with pIRES-RAMP1-SNAP-CLR for either WT CLR (A), Y165A (B), F166A (C), K167A (D), S168A (E), L169A (F), S170A (G), C171A (H) or Q172A (I), were stimulated with CGRP and increases in fluorescence measured. Data are expressed as fluorescence values relative to baseline, and are representative of the average response obtained from 3 replicates. Dotted line indicates point of CGRP injection.

In order to directly compare the effects of each mutation, the raw Ca^{2+} traces (Figure 5.14) were converted to dose-response curves (Figure 5.15). Normalising these relative to the maximal $_{i}Ca^{2+}$ response observed for stimulation with 100 μM ionomycin reduces variability due to differential dye loading and cell passage number. This data is then presented relative to the response observed for WT CLR, in order to ascertain the effects of alanine substitution. Through analysing these dose-response curves, two distinct populations of mutants can clearly be identifed: those with responses similar to WT (Y165-K167A) (Figure 5.15A-C, Table 5.10), and those displaying a reduction in potency (S168-C171A) (Figure 5.15D-H, Table 5.10). Concurrent with reductions in

potency, L169-C171A all display greatly reduced pKa values relative to WT (Table 5.10). Overall, it has been possible to identify that mutating ICL1 has profound effects upon CGRP-stimulated $_{i}Ca^{2+}$ mobilisation for S168-C171, whilst having minimal effects for Y165-K167 and Q172. This suggests that ICL1 plays roles in mediating $G\alpha_{q/11}$ signalling. It also indicates that residues at the start of ICL1 are more tolerant to alanine substitution (in terms of $_{i}Ca^{2+}$ mobilisation) and thus, those spanning ICL1 are more important in terms of mediating $G\alpha_{q/11}$ coupling.

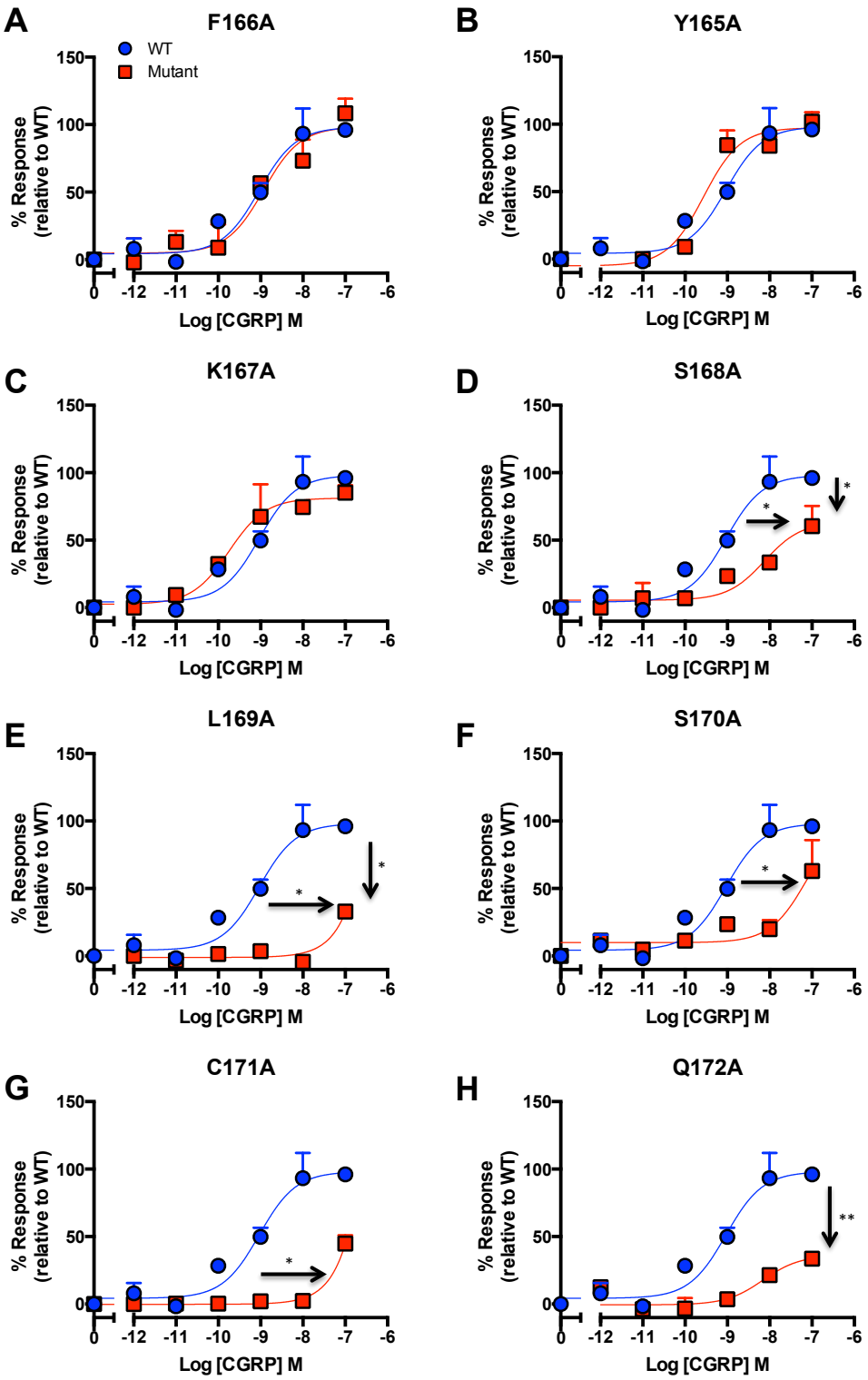

Figure 5.15: $_{i}Ca^{2+}$ mobilisation dose-response curves for the alanine scan of ICL1 (Y165-Q172) of CLR.

Mobilisation of $_{i}Ca^{2+}$ was measured, upon CGRP stimulation, in HEK 293 cells transfected with pIRES-RAMP1-SNAP-CLR for either WT CLR ● , or each mutant ■ : Y165A (A), K167A (B), S168A (C), L169A (D), S170A (E), C171A (F), Q172A (G). Data are expressed relative response produced by wild type CLR, ± SEM, of 3 replicates. Arrows indicate changes in pEC_{50} or E_{max}. Significance was calculated using a one-way ANOVA with Dunnet's post-test (*, $p < 0.05$, **, $p < 0.01$).

Table 5.10: Potency (pEC_{50}), affinity (pKa) and coupling efficacy (Log τ) values for $_{i}Ca^{2+}$ mobilisation in HEK 293 cells, transfected with pIRES-RAMP1-SNAP-CLR (WT, Y165-Q172A), upon CGRP stimulation.

	pEC_{50}[a]	E_{max}[b]	pKa[c]	Logτ[d]	n
WT	9.07±0.2	97.2±7.3	8.85±0.2	-0.33±0.04	3
Y165A	9.49±0.3	98.2±8.5	9.38±0.1	-0.28±0.03	3
F166A	9.03±0.3	97.3±9.7	8.76±0.2	0.32±0.05***	3
K167A	9.81±0.3	79.9±2.7	9.61±0.1*	-0.43±0.03	3
S168A	8.18±0.2*	61.7±9.1*	8.03±0.2*	-0.60±0.5	3
L169A	6.45±0.7*	40.2±15.0*	6.03±0.1***	0.21±0.03***	3
S170A	7.22±0.6*	94.9±18.4	6.95±0.3***	-0.31±0.0.7*	3
C171A	6.11±0.9*	59.4±17.5	6.18±0.2***	0.18±0.04***	3
Q172A	8.07±0.5	36.7±10.3**	8.10±0.2	-0.85±0.04***	3

Data ± SEM of n individual replicates.
[a] Negative logarithm of agonist concentration producing half-maximal response.
[b] Maximal response observed upon CGRP stimulation, as a percentage of that observed for wild type CLR.
[c] Negative logarithm of the equilibrium dissociation constant, as determined using the operational model of agonism (Black and Leff, 1983).
[d] Coupling efficacy parameter as determined using the operational model of agonism (Black and Leff, 1983).
Statistical difference between each mutant and wild type CLR was calculated using a one-way ANOVA with Dunnet's post-test (*, $p < 0.05$, **, $p < 0.01$, ***, $p < 0.001$).

In order to discern if mutation of Y165-Q172 to alanine has any effects upon the activation of ERK1/2, HEK 293 cells were transiently transfected with pIRES-RAMP1-SNAP-CLR (WT, Y165-Q172A). These cells were subsequently stimulated with CGRP, and levels of phospho-ERK1/2 measured. For WT CLR, it was observed that CGRP generates a fairly weak response (pEC_{50}: 7.35±0.3) (Figure 5.16, Table 5.11). Comparing this to the alanine mutants identified that whilst some display slight differences, none of these are significantly different from WT (Figure 5.16, Table 5.11). The only difference observed between each mutant and WT CLR is that Y165-K167A display lower efficacies (Log τ) (Table 5.11). It is thus concluded that mutation of residues Y165-Q172 had little effect upon the ability of RAMP1-CLR to activate ERK1/2, in a CGRP-dependent manner. Therefore, ICL1, potentially, plays no role in ERK1/2-mediated signalling.

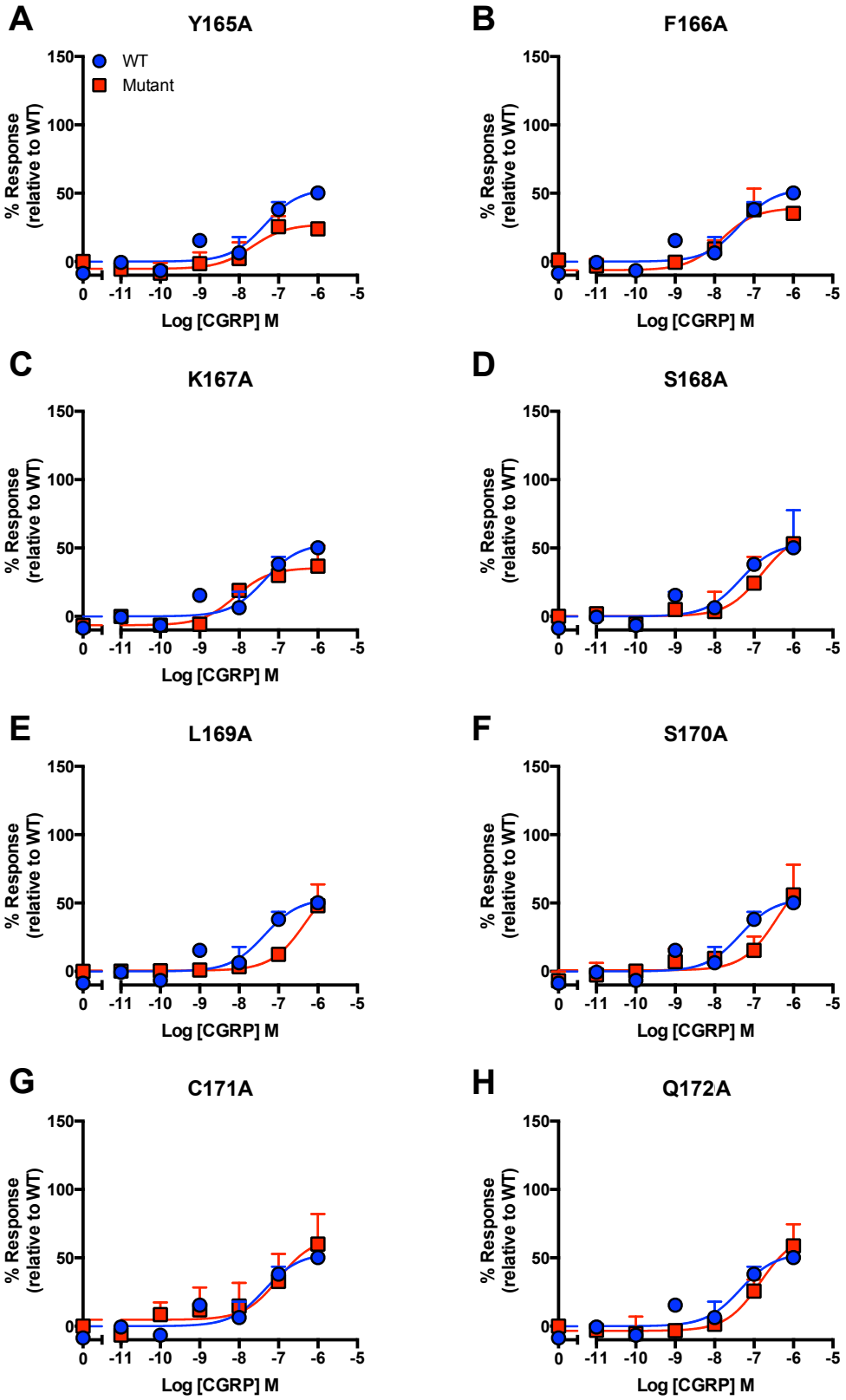

Figure 5.16: Activation of ERK1/2 for the alanine scan of ICL1 (Y165-Q172) of CLR.

Activation of ERK1/2 was measured, upon CGRP stimulation, in HEK 293 cells transfected with pIRES-RAMP1-SNAP-CLR for either: WT CLR, Y165A (A), F166A (B), K167A (C), S168A (D), L169A (E), S170A (F), C171A (G) or Q172A (H). Data represented as the percentage response obtained relative to WT CLR, ± SEM, of 3 replicates.

Table 5.11: Potency (pEC_{50}), affinity (pKa) and coupling efficacy (Log τ) values for ERK1/2 activation in HEK 293 cells, transfected with pIRES-RAMP1-SNAP-CLR (WT, Y165-Q172A), upon CGRP stimulation.

	pEC_{50}[a]	E_{max}[b]	pKa[c]	Logτ[d]	n
WT	7.35±0.3	100.1±19.2	6.49±0.4	-0.0037±0.1	2
Y165A	7.67±0.4	51.1±11.5	7.68±0.5	-0.70±0.1*	2
F166A	7.82±0.3	73.5±11.6	7.68±0.3	-0.56±0.08*	2
K167A	8.10±0.3	66.5±10.4	8.00±0.3	-0.59±0.08*	2
S168A	6.82±0.4	114.5±6.9	6.78±0.4	-0.35±0.2	2
L169A	6.71±0.3	110±24.2	6.51±0.3	-0.32±0.1	2
S170A	6.64±0.6	130±52.2	6.44±0.6	-0.24±0.3	2
C171A	7.00±0.5	85.1±22.5	6.78±0.6	-0.35±0.2	2
Q172A	6.84±0.3	126±21.3	6.69±0.3	-0.27±0.1	2

Data ± SEM of n individual replicates.
[a] Negative logarithm of agonist concentration producing half-maximal response.
[b] Maximal response observed upon CGRP stimulation, as a percentage of that observed for wild type CLR.
[c] Negative logarithm of the equilibrium dissociation constant, as determined using the operational model of agonism (Black and Leff, 1983).
[d] Coupling efficacy parameter as determined using the operational model of agonism (Black and Leff, 1983).
Statistical difference between each mutant and wild type CLR was calculated using a one-way ANOVA with Dunnet's post-test (*, $p < 0.05$).

5.10 Quantifying the effects of CLR ICL1 alanine mutations upon pathway bias

From the data obtained from the alanine scan of ICL1, effects upon cAMP production and $_{i}Ca^{2+}$ mobilisation were observed (Figures 5.13-15, Tables 5.9-10), whilst observing minimal effects upon ERK1/2 activation (Figure 5.16, Table 5.11). Through quantifying these differences in terms of pathway bias, as performed in Chapters 3 and 4, it was possible to elucidate the differing effects that each residue has upon influencing differential G protein signalling. It was also observed that RAMP1-CLR heterodimers stimulated with CGRP display ~100-fold bias towards preferentially signalling via $G\alpha_s$ and $G\alpha_q$, over activating ERK1/2 (Figure 5.17). As each residue in ICL1 was mutated to alanine, it was possible to observe decreases in the extent of this bias, to the point that L169A and C171A are equally biased towards $_{i}Ca^{2+}$ mobilisation and ERK1/2 activation (Figure 5.17). Comparing the extent of bias between cAMP production and $_{i}Ca^{2+}$ mobilisation for each mutant uncovered an interesting trend: Y165-K167A are all more biased towards $_{i}Ca^{2+}$ mobilisation, over cAMP production (relative to ERK1/2 activation) (Figure 5.17). This then switches to being more biased towards cAMP production for S168-Q172A (Figure 5.17). An identical trend is observed when analysing relative bias, using ERK1/2 and WT CLR as references (Figure 5.18). This identified that relative to WT CLR, each of the mutants are more biased towards ERK1/2 activation over the other studied pathways (Figure 5.18). However, Y165-K167A are still more biased to $_{i}Ca^{2+}$ mobilisation over cAMP, with this switching for S168-Q172A (Figure 5.18). What is thus observed is that residues at the base of (Y165), and close to, TM1 (F166-K167) potentially play roles in the determination of coupling to $G\alpha_s$. This manifests itself as a bias towards mobilising $_{i}Ca^{2+}$ when mutated to alanine, as these mutations have reduced the CLR's ability to influence cAMP production. In contrast, the residues across the face of ICL1 (S168-C171) and at the base of TM2 (Q172) appear to play roles in influencing $G\alpha_{q/11}$ coupling, manifesting itself as a bias towards

cAMP production, due to the disruptive effects of mutation upon the CLR's ability to mobilise $_{i}Ca^{2+}$. This work has therefore identified a potential role of ICL1 in the determination of G protein specificity for the CLR, which may begin to explain how biased agonism occurs at this receptor.

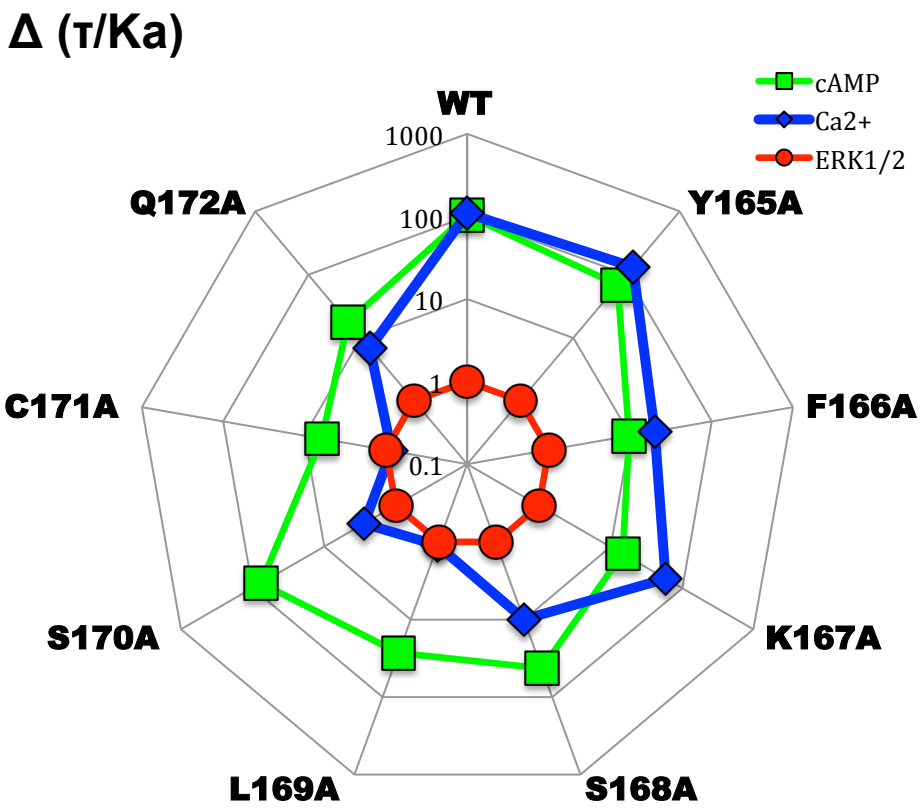

Figure 5.17: Quantification of pathway bias (Δ (τ/Ka)) for WT and Y165-Q172A CLR.

Pathway bias (Δ (τ/Ka)) between cAMP production, $_{i}Ca^{2+}$ mobilisation and ERK1/2 activation is shown for WT CLR, Y165A, F166A, K167A, S168A, L169A, S170A, C171A, Q172A, when co-expressed with RAMP 1 in HEK 293 cells, and stimulated with CGRP.

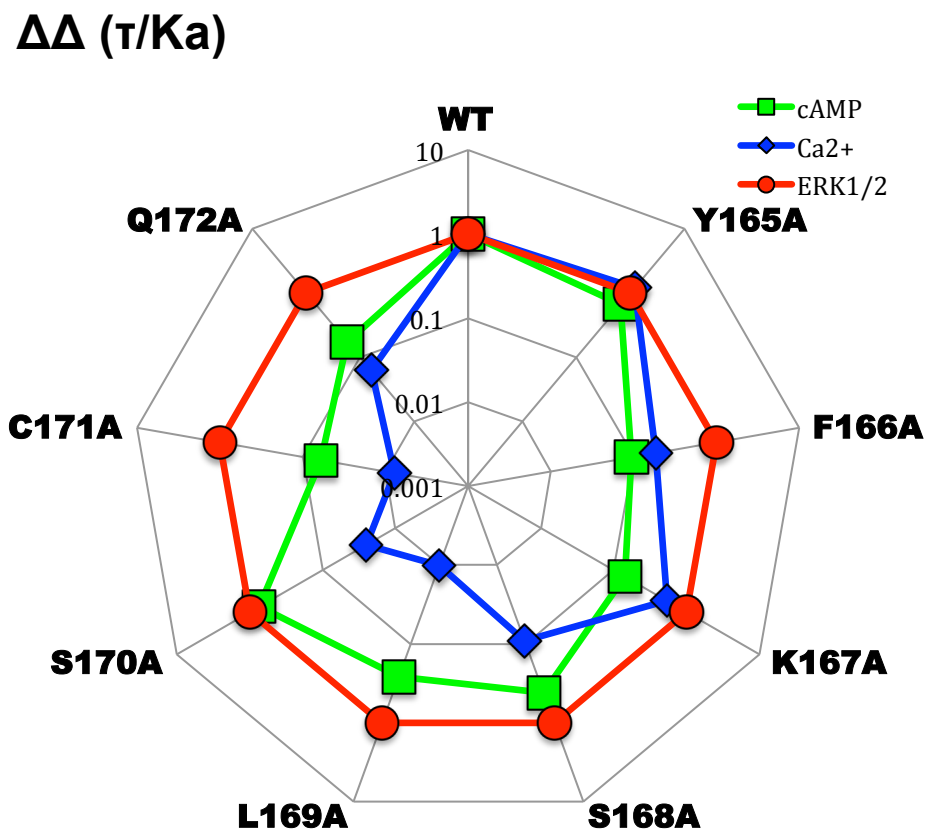

Figure 5.18: Relative pathway bias (ΔΔ (τ/Ka)) for WT and Y165-Q172A CLR.

Relative pathway bias (ΔΔ (τ/Ka)) between cAMP production, $_{i}Ca^{2+}$ mobilisation and ERK1/2 activation is shown for WT CLR, Y165A, F166A, K167A, S168A, L169A, S170A, C171A, Q172A, when co-expressed with RAMP 1 in HEK 293 cells, and stimulated with CGRP.

5.11 Summary

This chapter has attempted to investigate the role of ICL1 in RAMP1-CLR activation and signalling. In order to achieve this, a saturation mutagenesis approach was utilised, mutating each residue (Y165-Q172), in turn, to: alanine, glutamic acid, glycine, histidine, isoleucine and arginine. The effect of these substitutions upon CGRP-mediated signalling, were characterised, when each mutant was co-expressed with RAMP1. To achieve this, classical pharmacological analyses: cAMP accumulation (for all substitutions), $_{i}Ca^{2+}$ mobilisation and pERK1/2 assays (for alanine substitutions), were utilised, subsequently analysing their effects in terms of pathway bias.

As with previous studies (Bentrop *et al*, 1997, Wess *et al*, 1998), it was observed that mutating ICL1 has implications for cell surface expression of our receptor (Figure 5.7, Table 5.3). Interestingly, at some positions (Y165A, S168E, S168G, C171I) this actually results in an increase in expression, of between 10-50% over WT (Figure 5.7, Table 5.3). Some substitutions are well tolerated (F166A, S168A, S170A, F166E, F166H, S170H, Y165I, Y165R, K167R), with minimal impact upon expression (no greater than a 15% reduction) (Figure 5.7, Table 5.3). The most dramatic effects are observed for Q172H and L169R, with expressions of 10.05% and 4.35% that of WT, respectively (Figure 5.7, Table 5.3). Most other residues, except those specifically mentioned, tend to display levels of expression >30% that of WT (Figure 5.7, Table 5.3). Intriguingly, mutating L169 seems to be particularly susceptible to reducing expression, with all substitutions at this position resulting in reductions in expression of at least 66% (57.27% for isoleucine substitutions), relative to WT (Figure 5.7, Table 5.3). This residue is highly conserved amongst family B GPCRs (Figure 5.2); combined with the large reduction in cell surface expression we observe upon mutating this residue in the CLR, this suggests that a leucine at this position appears to play key roles in regulating expression. Whilst it is clear that reducing cell surface expression of each mutant will have effects upon signalling, it was still

possible to observe fairly robust responses for Q172H and L169R, these being the lowest expressed receptors (10.05% and 4.35%, respectively) (Figure 5.7, Table 5.3). The fact that signalling for these mutants can still be observed indicates the large extent of receptor reserve inherent in the system under study. Thus, whilst reducing expression will influence the observed results, this may potentially have minimal impact.

Whilst cell surface expression of the CLR was quantified in this study, no investigation into cell surface expression of RAMP1 was undertaken. It is possible that some effects upon expression of the CLR are due to modulating its ability to interact with RAMP1, although it would be expected that both CLR and RAMP1 expression would reduce in proportion to each other. However, it is likely that through mutating the CLR, potential effects upon its ability to interact with RAMP1 may occur, having consequences upon the CLR's ability to signal. It has previously been identified that the N-termini of RAMPs play roles in influencing ligand binding, whilst the C-termini influence downstream signalling (Udawela *et al*, 2006a); it is therefore plausible that by affecting the ability of the CLR to interact with RAMP1, there may be unknown effects upon these regions, and hence the CLR's ability to signal.

In terms of cAMP signalling, effects as diverse of those upon cell surface expression were observed, with substitutions at each position in ICL1 (Y165-Q172) having a wide range of effects: some being very tolerant to mutation, some having reduced activity or complete abolition of functionality, and others displaying a gain-of-function. It was identified that arginine substitution is particularly well tolerated at all positions: indeed, S168R results in an increase in potency of ~29 fold (Figure 5.12, Table 5.8). Interestingly, analysis of ICL1 of all family B GPCRs reveals that for all receptors, except the CLR, CT and CRF receptors, arginine (or positively charged lysine) is fairly well conserved at this position (Figure 5.2). This suggests a particularly key role for a positive charge at this position. Indeed, by introducing an arginine at this position an interaction with downstream signalling proteins, potentially Gβ, may have been

promoted. In the GLP-1R, H171, the equivalent residue to S168, has been observed to directly interact with D312 of Gβ via an electrostatic interaction (Zhang *et al*, 2017).

Substitution with glutamic acid within ICL1 is fairly detrimental upon CLR's signalling ability, suggesting that negatively charged residues aren't tolerated in this region; indeed, all WT residues here tend to be polar and uncharged (except K167). This may potentially be due to charge-charge repulsion from negatively charged phospholipids within the inner leaflet of the plasma membrane, or glutamic acids within H8 (Figures 5.3 and 5.4). Upon performing glycine substitutions, a mutation that is generally deleterious, slight gains of function for C171 and Q172 were observed (Figure 5.9, Table 5.5). This suggests that gaining flexibility in this region allows for easier activation of the CLR, by CGRP. Therefore, C171 and Q172 may possibly serve to hold the WT CLR in an inactive conformation, an ability that has been lost through gaining greater flexibility with glycine substitution. Indeed, this may be particularly true of C171, as this residue is universally conserved amongst family B GPCRs (Figure 5.2). Effects observed upon mutation of Q172 may also be explained by its influence upon the shape/positioning of TM2 and ICL2, and not solely due to effects upon ICL1. Mutation of Y165 is well tolerated for all residues, except glycine (Figure 5.8-5.13A). This may suggest that Y165 plays a role in 'anchoring' ICL1 in an optimal conformation for signalling. Through increasing flexibility of the peptide backbone at this position, it is plausible that ICL1 is allowed to 'swivel' and 'flex' more than in WT CLR, having detrimental effects upon its functionality.

Through the use of an alanine scanning approach, it was possible to differentially affect CGRP's ability to mediate cAMP production (Figure 5.13, Table 5.9), compared to its ability to mediate the mobilisation of $_{i}Ca^{2+}$ (Figure 5.14-15, Table 5.10). This data suggests that ICL1 plays differing roles in the determination of $G\alpha_{s}$-mediated signalling (shown through cAMP accumulation assays) and coupling to $G\alpha_{q/11}$ (shown via

$_{i}Ca^{2+}$ mobilisation assays). In contrast, mutating this region had minimal effect upon CGRP-mediated ERK1/2 activation (Figure 5.16, Table 5.11). As it has previously been shown that ERK1/2 activation can occur in a β-arrestin-dependent, G protein-independent, manner (Shenoy *et al*, 2006), it is plausible that CGRP-mediated ERK1/2 activation at RAMP1-CLR heterodimers occurs via β-arrestins. Thus, as mutating ICL1 has little effect upon ERK1/2 activation, it is possible that ICL1 plays no role in β-arrestin-mediated signalling. Indeed, β-arrestins have previously been shown to bind the phosphorylated C-terminus of GPCRs (Lohse *et al*, 1990, Gurevich *et al*, 1995). Thus, ICL1 appears to play roles in influencing G protein coupling and signalling, particularly for $G\alpha_s$ and $G\alpha_{q/11}$, but not ERK1/2 activation. This is particularly highlighted through analysis of the effects of each alanine substitution upon pathway bias (Figures 5.17-18). This indicated how residues at the base of TM1 and the start of ICL1 (Y165-K167) play roles in heavily influencing coupling to $G\alpha_s$, and hence cAMP production. In contrast, residues across the face of ICL1 (S168-C171) play roles in influencing $_{i}Ca^{2+}$ mobilisation, via $G\alpha_{q/11}$. Thus, it appears that these predominantly polar residues are important in $G\alpha_{q/11}$ coupling, whilst hydrophobic/positively charged residues (Y165-K167) at the start of ICL1 are required for $G\alpha_s$ coupling. Recent work by Flock and colleagues has identified the existence of a 'selectivity barcode' upon each individual G protein subtype, which is 'read' by GPCRs (Flock *et al*, 2017). This allows a given GPCR to specifically interact with only a given subset of G proteins, preventing aberrant G protein-GPCR coupling. These 'barcodes' have been identified to specifically interact with a GPCR via ICL 2 and 3 as well as TM 5 and 6 (Flock *et al*, 2017). Whilst their work does not specifically identify ICL1 as influencing specificity, it does provide a potential mechanism for its determination. It is plausible that ICL1 may play a similar, as yet, undefined role, or that by modulating ICL1, in the work presented in this chapter, unknown structural effects have occurred, resulting in rearrangements of ICL2/3 or TM5/6 which have affected the CLR's ability to read the 'selectivity barcodes' on $G\alpha_s$ or $G\alpha_{q/11}$.

By comparing the pharmacological data for cAMP production to the existing crystal structures for inactive GCGR and GLP-1R (Figure 5.4A-B), and in turn comparing these to the active GLP-1R (Figure 5.4C), it was possible to identify how ICL1 of family B GPCRs may potentially interact with H8. This may occur via charge-charge interactions between positively charged residues on ICL1 and glutamic acid residues within H8. Upon activation, ICL1 undergoes large conformational rearrangements (Figure 5.6B-C), and the ICL1-H8 interaction breaks, with these two regions moving apart (Figure 5.4B-C), allowing downstream signalling to occur. Therefore, this data suggests that ICL1 may, potentially, interact with H8 to hold family B GPCRs in an inactive state, as well as being a region that plays a role in determining G protein specificity, and also influencing bias (Figure 5.19).

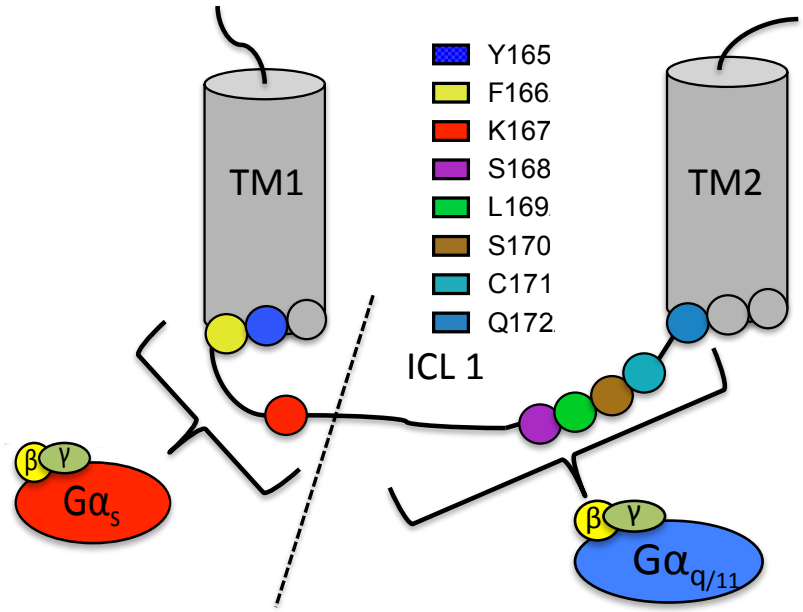

Figure 5.19: ICL1 of CLR plays roles in determining G protein specificity.

Analysis of pathway bias data (Figure 5.11-12) reveals differential roles for ICL1 in determining G protein specificity. Residues at the base of TM1 and start of ICL1 (Y165-K167) play roles in influencing $G\alpha_s$ coupling, whilst those across ICL1 (S168-Q172) more heavily influence $G\alpha_{q/11}$ coupling.

Chapter 6
Discussion

6.1 Overview

The phenomenon of biased agonism is becoming a much-studied subject. Many researchers, who work on GPCR-mediated signalling, are also investigating the extent of biased agonism. This allows for an informed approach to the development of new test compounds for the pharmaceutical industry. Through elucidating the extent of inherent bias exhibited by a GPCR's endogenous agonist(s), it is possible to understand, and appreciate, the full signalling repertoire of a target receptor. Alongside this, an in-depth knowledge of the effects following activation of each pathway provides the potential to develop pharmaceutical drugs that activate selected, beneficial pathways. Further, knowledge of biased agonism, exhibited by endogenous ligands, can be used to elucidate which activated pathways are responsible for unwanted, off-target side effects. A fine example of this being the μ-opioid receptor, with $G\alpha_{12}$ activation providing analgesia (Pradhan *et al*, 2010, 2012), whilst activation of β-arrestin-mediated signalling is responsible for most of the side effects associated with opioid treatment (Raehal *et al*, 2005). Such knowledge of bias has informed the development of drugs that preferentially activate $G\alpha_{12}$-mediated signalling pathways (Chen *et al*, 2013, DeWire *et al*, 2013), thereby providing pain relief, with more limited side effects. Thus, it is evident that knowledge of biased agonism allows for the informed development of novel compounds, with potentially enhanced therapeutic potential. Hence, knowledge of biased agonism may allow for increased: efficacy, safety and tolerance of novel drugs.

The work presented within this thesis has applied the study of biased agonism to three GPCRs: two from family A, namely the A_1R and $A_{2A}R$, and the prototypical RAMP-interacting GPCR of family B, the CLR.

Through completion of these investigations, a framework is provided, upon which further work can build, providing the potential for the development of adenosine receptor-targeting therapeutics. In addition, the mechanisms of action for different signalling pathways, mediated by the RAMP-CLR heterodimers have been identified, as well as quantifying biased agonism, and providing a potential structural mechanism for such a phenomenon.

6.2 Biased agonism of the A_1R: differential $G\alpha_{i/o}$ coupling?

In Chapter 3, work was presented pertaining to the investigation of A_1R agonists that had previously been designed (Figure 3.2) and published (Knight *et al*, 2016, Appendix 1). The work presented within this thesis relates to an in-depth, pharmacological characterisation of the active compounds developed from this study. Of these, Cmpds 5, 6, 16 and 18 had been found to display selectivity for the A_1R, over other AR subtypes (Knight *et al*, 2016, Appendix 1), whilst Cmpds 20 and 21 were non-selective AR agonists. For all of the investigated A_1R agonists it was possible to observe activation of the canonical, $G\alpha_{i/o}$-mediated signalling pathway, as evidenced by their ability to inhibit forskolin-stimulated cAMP production (Figure 3.4, Table 3.2). Upon analysis of the dose-response curves obtained from these experiments, it was observed that many were non-monotonic: at higher agonist concentrations, it was evident that the extent of inhibition actually started to decrease (Figure 3.4). Through the use of PTX pre-treatment it was identified that both prototypical and atypical agonists were able to mediate cAMP production (Figure 3.5, Table 3.3). This suggests that the upward inflections observed in cAMP inhibition dose-response curves are due to a switching of the A_1R from activating predominantly $G\alpha_{i/o}$-mediated to $G\alpha_s$-mediated signalling. Interestingly, the points of upward inflection in our cAMP inhibition dose-response curves closely correlate with the lowest agonist concentration able to mediate cAMP production. Coupling of the A_1R to $G\alpha_s$ has also

previously been reported in CHO-K1 cells stimulated with NECA or CCPA (Cordeaux *et al*, 2004, Baker and Hill, 2007, Gao and Jacobson, 2016), as well as HEK 293T cells stimulated with adenosine (Rittiner *et al*, 2012). Indeed, the potencies of the stimulating agonists in these published studies closely matches those observed in this thesis. However, most of the agonists, be they proto- or atypical, appear to be equipotent, with respect to activating $G\alpha_s$ signalling, with all being less potent compared to their ability to stimulate $G\alpha_{i/o}$ activation (Figure 3.4 and 3.5, Table 3.2 and 3.3). However, in contrast to most of the compounds, and previously published reports, this work identified one agonist, Cmpd 18, which is ~10-fold more potent than previously reported agonists (Cordeaux *et al*, 2004, Baker and Hill, 2007, Rittiner *et al*, 2012, Gao and Jacobson, 2016,). Thus, what has been observed is that a GPCR classically associated as being $G\alpha_{i/o}$-coupled is also able to couple to, and activate, $G\alpha_s$. There is, therefore, potential for experiments measuring A_1R-mediated cAMP inhibition to actually obtain results that are the function of the activation of two diametrically opposing signalling pathways.

In addition to an ability of the A_1R to modulate intracellular cAMP levels, an ability of our agonist to mediate: the mobilisation of ${}_iCa^{2+}$ was identified (Figure 3.6-7, Table 3.4). This investigation solely focused upon A_1R-mediated ${}_iCa^{2+}$mobilisation, which has previously been observed in DDT1MF-2 (hamster vas deferens smooth muscle) cells, which endogenously express the A_1R (Fredholm *et al*, 2013). Additionally, the A_1R can also mediate the influx of extracellular Ca^{2+} (Dickenson and Hill, 1993). It has also been observed that PTX pre-treatment results in total abolition of both A_1R-mediated intracellular and extracellular Ca^{2+} mobilisation (Dickenson and Hill, 1993, Gao and Jacobson, 2016). This indicates that the A_1R mediates both the mobilisation of ${}_iCa^{2+}$, and entry of extracellular Ca^{2+}, in $G\alpha_{i/o}$-dependent manner. It has also been reported that PLC activation can be mediated via Gβ/γ (Camps *et al*, 1992), resulting in ${}_iCa^{2+}$ mobilisation. This may also occur with the A_1R, as treatment with UBO-QIC results in diminished NECA-induced

mobilisation of $_{i}Ca^{2+}$, with no associated effects upon NECA-stimulated cAMP inhibition (Gao and Jacobson, 2016).

In addition to mediating Ca^{2+} signalling, the A_1R has also been reported to activate ERK1/2 (Husain *et al,* 2007, Migita *et al,* 2008, Jajoo *et* al, 2010, Baltos *et al*, 2016, Gao and Jacobson, 2016). Indeed, this may be an important pathway activated by the A_1R, as it, alongside Akt activation, has been reported to be cytoprotective (Baltos *et al*, 2016). A_1R-mediated ERK1/2 activation may also be responsible for the anti-inflammatory, -necrotic and -apoptotic actions of adenosine (Lee *et al*, 2004). Upon investigating the ability of the proto- and atypical agonists to activate this pathway, it was observed that all agonists displayed an ability to activate ERK1/2 (Figure 3.8, Table 3.5). However, most of these were also partial agonists, suggesting that they have a general propensity to activate other signalling pathways over ERK1/2 activation, a pathway seen to be sensitive to PTX treatment (Husain *et al*, 2007*,* Stewart *et al*, 2009, Gao and Jacobson, 2016).

It was observed that all of the agonists tested displayed an ability to differentially activate four signalling pathways: cAMP inhibition, cAMP production, $_{i}Ca^{2+}$ mobilisation and ERK1/2 activation (Figure 6.1). As each agonist displays differing abilities to activate these pathways, there is clear biased agonism occurring. What has been observed is that of the endogenous cognate agonists, adenosine is the only agonist found to be more biased toward activating the canonical $G\alpha_{i/o}$, cAMP inhibition pathway, over $G\alpha_{s}$, relative to NECA (Figure 3.9). Thus, it seems that only the natural agonist, adenosine, predominantly activates the classical A_1R signalling pathway, whilst all synthetic derivatives display a greater preference to mediating cAMP production, relative to NECA (Figure 3.9). However, through our development of atypical agonists, two have been developed, Cmpds 6 and 20, which display the greatest relative bias towards ERK1/2 activation (Figure 3.10). Indeed, most of the atypical agonists, with the exception of Cmpd 18, display bias towards ERK1/2 activation over cAMP inhibition, relative to NECA. AR-mediated ERK1/2

signalling has been reported to promote proliferation (Jacques-Silva *et al*, 2004, Migita *et al*, 2008). Specifically, A_1R-mediated ERK1/2 activation is cytoprotective (Baltos *et al*, 2016), as well as being able to promote neurite outgrowth in primary striatal neuronal precursor cells (Canals *et al*, 2005). There is, therefore, potential, that the agonists, along with CCPA, may be able to promote cell proliferation and survival, to greater extents than NECA.

Agonist	cAMP production	$_{i}Ca^{2+}$	ERK1/2
NECA	↓↓↓	↓↓	↓
Adenosine	↓↓↓	↓↓	↓↓
CCPA	↓↓↓	↓↓	↑
Cmpd 5	-	↑↑	↑↑
Cmpd 6	↓↓	↓	↑
Cmpd 16	-	-	↑
Cmpd 18	↓	-	↓
Cmpd 20	↓↓↓	↓↓↓	-
Cmpd 21	↓↓	↑	↑

Figure 6.1: A_1R agonists display differential abilities to activate differing signalling pathways, relative to cAMP inhibition.

The A_1R agonists tested in Chapter 3 display differing abilities to mediate the: production of cAMP, mobilisation of $_{i}Ca^{2+}$, or activation of ERK1/2, relative to their ability to mediate the inhibition of cAMP production. ↑/↓ indicates an increase/decrease in potency, relative to that observed for cAMP inhibition, whilst ' **–** ' indicates no difference. The number of arrows indicates the extent of change.

The fact that it was possible to observe differences between each agonist's ability to activate three pathways mediated via $G\alpha_{i/o}$ proteins is, in itself, interesting. It would be expected that a given agonist would

activate each pathway mediated by a single G protein, to similar extents. Thus, no bias would be observed between cAMP inhibition, $_{i}Ca^{2+}$ mobilisation, or ERK1/2 activation for the A_1R agonists. However, investigations into A_1R-mediated ERK1/2 activation have highlighted different abilities of A_1R agonists to specifically activate this pathway, via $G\alpha_{oa}$, $G\alpha_{ob}$, and $G\alpha_{i2}$ (Stewart *et al*, 2009). This study also highlighted how differing agonists have different efficacies, dependent upon the G protein being activated (Stewart *et al*, 2009). As it has also previously been shown, in yeast, that the A_1R can couple to GPA/$G\alpha_{i1/2}$ and GPA/$G\alpha_{i3}$ proteins (Stewart *et al*, 2009), it is potentially plausible that the A_1R is able to mediate its signalling via multiple $G\alpha_{i/o}$ isoforms. Thus, the apparent bias observed within Chapter 3 may arise due to each agonist mediating the activation of either: $G\alpha_{i1}$, $G\alpha_{i2}$, $G\alpha_{i3}$, $G\alpha_{oa}$ and/or $G\alpha_{ob}$. It is possible that these G proteins, or their associated Gβ/γ (in the case of Ca^{2+} signalling), are responsible for activating the differing downstream signalling pathways of the A_1R (Figure 6.2). It is also plausible that the agonists utilised in this study may have differing abilities to promote or reduce oligomerisation of the A_1R. This has been observed for the melatonin 1 and 2 receptors (Ayoub *et al*, 2002), and the dopamine D_2 receptor (Tabor *et al*, 2016). It is plausible that through modulating oligomerisation, there could be potential effects upon the A_1R's ability to mediate activation of the signalling pathways studied in Chapter 4.

In order to investigate differential $G\alpha_{i/o}$ coupling, the use of PTX-insensitive $G\alpha_{i/o}$ proteins, transfected into CHO-K1-A_1R cells, would be required. Following treatment with PTX, cAMP inhibition, $_{i}Ca^{2+}$ mobilisation as well as ERK1/2 activation, could be measured. Where responses are still observed, this would identify: the individual G proteins activated by each agonist, as well as which G proteins are responsible for mediating the various signalling pathways studied. Further, an investigation into the ability of the agonists to mediate Akt activation, and promote both proliferation and cell survival, would add further scope and depth to the characterisation of these compounds. This would also highlight if they may have any potential therapeutic benefits. Eventually,

study of these agonists could be moved into various mouse models of CVD, to determine their effects upon the cardiovascular system.

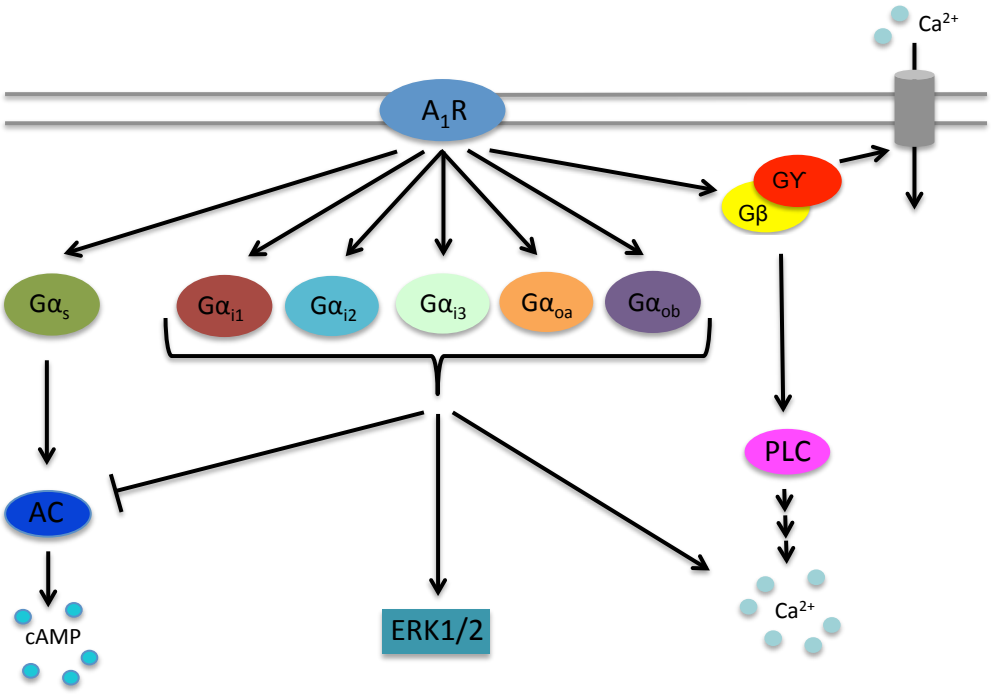

Figure 6.2: A_1R displays an ability to activate multiple downstream signalling proteins.

The A_1R can mediate the production of cAMP, via the activation of $G\alpha_s$, as well as mediating the inhibition of adenylate cyclase (AC) activity, via PTX-sensitive $G\alpha_{i/o}$ proteins. Further, $G\alpha_{i/o}$ protein activation can lead to the activation of ERK1/2 signalling, as well as the mobilisation of $_iCa^{2+}$. Increases in $[_iCa^{2+}]$ can also be brought about via the action of Gβγ, which can mediate the entry of extracellular Ca^{2+}, via regulating cell surface Ca^{2+} channels, in addition to directly activating PLC.

Overall, this work has identified how it is possible to utilise the structure of existing non-selective AR agonists as scaffolds upon which to build new AR agonists, some with improved selectivity. The recently solved structure of the A_1R has identified the existence of a secondary ligand binding pocket, as well as differences in ECL2, compared to the $A_{2A}R$ (Glukhova *et al*, 2017). These regions provide a possible route through which selectivity for the A_1R, over the $A_{2A}R$, may be developed. What is not known is how the selective agonists bind to the A_1R, and if they utilise this secondary pocket. However, by modulating specific R groups, it was possible to significantly alter each agonist's ability to activate differing signalling pathways all mediated by the A_1R, thereby having profound effects upon the extent of biased agonism exhibited at the A_1R. These agonists were not developed from a therapeutic perspective; initially, they were developed to provide scaffolds upon which fluorescent A_1R-

selective agonists could be developed. They do, however, hold potential therapeutic benefit in promoting cell survival and/or proliferation, as well as providing pharmacological tools to dissect the signalling pathways that are evident upon A_1R activation, as utilised here.

6.3 Triazoloquinazolines: $A_{2A}R$ agonists

The work relating to the $A_{2A}R$, presented within Chapter 3, required validation of the findings of an *in silico* screen performed by collaborators in the research group of Dr. A. Bender (University of Cambridge, UK). These compounds were identified from a screen looking for dual PDE10A inhibitors, and $A_{2A}R$ agonists. They are all known PDE10A inhibitors (Kheler *et al*, 2011), but their activity against the $A_{2A}R$ was unknown, asides *in silico* data suggesting they dock to the $A_{2A}R$.

The design rationale behind dual target agonists such as these is that they may provide some potential benefit in the treatment of various neurodegenerative diseases. Adenosine has long been known to play key roles in neuromodulation in the brain, particularly the $A_{2A}R$, which is highly enriched in medium spiny neurons of the striatum (Shearman and Weaver, 1997, Rosin *et al*, 1998). In Huntington's disease, the expression levels of the $A_{2A}R$ are aberrantly affected by mutant huntingtin protein (HTT), with expression further reducing with disease progression (Martinez-Mir *et al*, 1991, Chiang *et al*, 2005). However, the levels of $A_{2A}R$-mediated signalling appear not to be affected by this reduction (Varani *et al*, 2001, Chou *et al*, 2005). In spite of this, activation of the $A_{2A}R$, by CGS21680, in mouse models of Huntington's, has been observed to delay loss of motor coordination, and accumulation of HTT aggregates (Chou *et al*, 2005, Lin *et al*, 2013). Further, CGS21680 has been reported to significantly reduce caspase 3 activation (Chiu *et al*, 2015), thus providing a potential means of reducing neuronal death.

PDE10A is a dual cAMP-cGMP phosphodiesterase, being highly expressed in striatal medium spiny neurons (Fujishige *et al*, 1999, Coskran *et al*, 2006). In animal models of Huntington's disease, HTT has been observed to aberrantly affect the expression of PDE10A (Hu *et al*, 2004, Leuti *et al*, 2013), and it is thought that these effects may be detrimental for neuronal survival and correct basal ganglia function, via effects upon dopamine D1 and D2 signalling (Hebb *et al*, 2004, Giampà *et al*, 2009, 2010). Thus, there is a potential that targeting PDE10A may provide, some, potential therapeutic benefit in cases of Huntington's. There may also be potential for multi-target drugs, targeting both the $A_{2A}R$ and PDE10A. Thus, in Chapter 3, a classical pharmacological approach was utilised to validate our collaborators' *in silico* findings, with respect to TZQ test compounds' actions upon the $A_{2A}R$.

To identify the ability of the TZQ compounds to act as AR agonists, the yeast-screening platform (Brown *et al*, 2000) was utilised, which confirmed two important points: the test compounds did indeed display efficacy against the $A_{2A}R$; and some were selective for the $A_{2A}R$, over the A_1R and $A_{2B}R$. Validating these findings in CHO-K1-$A_{2A}R$ cells further identified that the test compounds were indeed active, as agonists, against the $A_{2A}R$. The main difference observed between yeast and mammalian findings was that TZQ 3 and 5 displayed much reduced potencies in CHO-K1 cells, compared to yeast, relative to the other TZQ compounds. Whilst the yeast system often displays reduced potencies, relative to those obtained from experiments in mammalian cells, it tends to faithfully recapitulate observed trends (Weston *et al*, 2015, 2016, Appendix 2, Knight *et al*, 2016, Appendix 1). One possible explanation for this lies in that, in these strains, chimeric yeast/human G proteins are utilised, which have had the final 5 C-terminal amino acids of the yeast Gα homologue, GPA1, replaced with the equivalent residues of each human Gα (Brown *et al*, 2000), which are known to be less specific (Dowell and Brown, 2002).

The experiments performed in yeast expressing the $A_{2A}R$ investigated coupling, and activation, of GPA1/$G\alpha_s$, as did those looking at the $A_{2B}R$. As this appears to be the G protein through which these two receptors modulate intracellular cAMP levels, these results can be taken as being fairly representative. However, where the A_1R has been investigated, GPA1/$G\alpha_{i1/2}$ was utilised. As $G\alpha_{i1}$ and $G\alpha_{i2}$ have identical C-termini, in respect to the final 5 residues, it is not possible to distinguish between these two G proteins in yeast. Likewise, as only the ability of the TZQ compounds to activate this chimeric G protein has been measured, a potential ability of them to signal via other G proteins, activated by the A_1R (Stewart *et al*, 2009), could be missed. Despite these limitations in both the system of choice, and approach, it was still possible to successfully identify the TZQ compounds as being agonists of the $A_{2A}R$. It was also possible to confirm their selectivity over other ARs, with the exception of the A_3R: unfortunately, to date, there have been no published accounts of functional expression of the A_3R in yeast, despite the work of others, including members of our own laboratory. Thus, to test for efficacy against the A_3R, cAMP inhibition assays were performed in CHO-K1-A_3R cells. This identified that only TZQ 4 was also an agonist of the A_3R. Thus, through a combinatorial approach, of utilising both yeast and mammalian systems, it was possible to identify a series of compounds, from the triazoloquinazoline chemical series, that acted as agonists against the ARs, with some being selective for the $A_{2A}R$. This is unsurprising as 9-chloro-2-(2-furanyl)[1,2,4]triazolo[1,5-*c*]quinazolin-5-amine (CGS15943), a triazoloquinazoline, has long been known to bind, non-selectively to the A_1, A_{2A}, and $A_{2B}R$ (Williams *et al*, 1987, Ongini *et al*, 1999). It has also been seen that by using CGS15943 as a scaffold, and modulating specific functional R groups, AR subtype selectivity can be achieved (Kim *et al*, 1996, 1998); a process, similar to that, which was performed for A_1R agonists (Knight *et al*, 2016, Appendix 1).

6.3.1 Triazoloquinazolines display bias toward ERK1/2-activation: potential therapeutic benefit?

The $A_{2A}R$ is able to mediate cAMP production; however, it also able to mediate ERK1/2 activation (Canals *et al*, 2005). As AR-mediated ERK1/2 activation is known to be beneficial for both cell survival and proliferation (Jacques-Silva *et al*, 2004, Migita *et al*, 2008, Baltos *et al*, 2016), as well as promoting neurite outgrowth, in primary striatal neuronal precursor cells (Canals *et* al, 2005), there was interest to determine the efficacy of the TZQ agonists at activating this pathway. It was observed that all, except TZQ 5, were able to mediate the activation of ERK1/2, albeit only upon stimulation with TZQ 3 at micromolar levels (Figure 3.14, Table 3.9). Comparisons of the responses observed, to those for cAMP production, identified that TZQ 1 and 2 displayed increased potencies for ERK1/2 activation (Figure 3.13, 3.14, Table 3.8, 3.9). It is interesting to note how, for the A_1R, ERK1/2 activation has been reported to occur in a PTX-sensitive, $G\alpha_{i/o}$-dependent manner (Husain *et al*, 2007*,* Stewart *et al*, 2009, Gao and Jacobson, 2016); however, the closely related $A_{2A}R$ is also able to activate ERK1/2, but no reports have been published of $G\alpha_{i/o}$ coupling to this GPCR. Thus, it appears that ERK1/2 activation is mediated, from the $A_{2A}R$, in a different manner, to that from the A_1R. It would be interesting to determine how activation of this pathway occurs for both receptors in greater depth, allowing us to understand how two receptors, with seemingly opposing actions, can activate the same signalling pathway.

Analysing the extent of pathway bias for both of these compounds, determined the extent of bias towards either cAMP production or ERK1/2 activation. This identified that all of the compounds, for which full dose-response curves could be fitter, are biased towards ERK1/2 activation (Figure 3.15). Indeed, so is the reference agonist CGS21680. There is therefore potential that these compounds may prove beneficial in promoting the survival of neuronal cells, through ERK-conferred

cytoprotective effects (Baltos *et al*, 2016), or ERK-induced proliferation (Jacques-Silva *et al*, 2004, Migita *et al*, 2008). Indeed, their ability to promote cAMP production may also prove beneficial, as PKA activity has been reported to be required for growth of striatal neuronal precursor cells (Canals *et al*, 2005). Thus, there is some potential for these compounds to be of benefit in some neurodegenerative diseases, with respect to their agonistic activity at the $A_{2A}R$, a receptor, along with the A_1R, that is known to be one of the main mediators of adenosine neuromodulation within the brain. Therefore, there is merit in characterising these compounds in primary striatal neuronal cells, and in investigating their direct effects upon cell survival and growth. In this system it would be important to understand the expression profiles of other GPCRs, primarily those that have been shown to dimerise with the $A_{2A}R$, such as the dopamine D_2 (Kamiya *et al*, 2003, Fuxe *et al*, 2005) and D_3 receptors (Torvinen *et al*, 2005), cannabinoid CB_1 receptor (Ferré *et al*, 2009) and glutamate $mGluR_5$ (Zezula and Freissmuth, 2008). The formation of heterodimers with any of these receptors may alter the signalling profile of the TZQ compounds identified in Chapter 3. Indeed, it is also possible that the triazoloquinazolines themselves may have an ability to promote/reduce dimerisation with other such GPCRs. The TZQ compounds do, however, provide good pharmacological tools, with which the signalling repertoire exhibited by the $A_{2A}R$ can be characterised, particularly TZQ 2 in investigating $A_{2A}R$-mediatd ERK1/2 activation.

To date, only the ability of the TZQ agonists to mediate cAMP accumulation and ERK1/2 activation, in an $A_{2A}R$-dependent manner, has been determined. There is also a need to test the ability of these compounds to mediate both: $_iCa^{2+}$ mobilisation, and Akt activation. Further, it would be interesting to determine the ability of these compounds to promote cell survival and proliferation, as well as to inhibit apoptosis. Additionally, an investigation into the effects of these compounds upon primary striatal neuronal cells, endogenously expressing the $A_{2A}R$ and PDE10A, would also add further depth to this investigation. There is also a need to determine if there are any

synergistic effects of the dual action of triazoloquinazolines upon the $A_{2A}R$ and PDE10A. Currently, it is not known whether PDE10A is expressed in the cell lines used in this thesis. To address this, qPCR would need to be utilised in order to quantify the expression levels of mRNA for each PDE isoform. Where cell lines express both PDE10A and $A_{2A}R$, the of use siRNA for PDE10A, and $A_{2A}R$ antagonists, both singularly, and in combination, would be required. This will allow elucidation of the effects of these compounds upon each target alone, and identify any synergy between targeting both PDE10A and the $A_{2A}R$. Having quantified the effects of the TZQ compounds upon PDE10A and the $A_{2A}R$, as well as associated signalling pathways, there may be potential to, eventually, move the compounds into an *in vivo* setting.

6.4 Biased agonism of the CLR: a role for RAMPs?

As observed for the A_1R and $A_{2A}R$, there is an inherent ability of GPCRs to activate multiple downstream signalling pathways, to differing extents. For family B GPCRs this is further modified, for some receptors, through the association of receptor activity-modifying proteins, which provide one mechanism whereby signalling from a single GPCR may be modulated. This is no more evident than with the prototypical RAMP-interacting receptor, the CLR. In Chapter 4, work was presented pertaining to the effects of RAMP interaction, upon the CLR's ability to mediate: cAMP production and inhibition; mobilisation of $_{i}Ca^{2+}$; as well as elucidating the mechanisms of action for these pathways (Figure 6.3). Ultimately, RAMP-mediated modulation of biased agonism was quantified for each agonist: CGRP, AM and AM2. In Chapter 5 this work was expanded, focusing upon RAMP1-CLR, identifying how the ICL1 region plays a role in influencing the G protein specificity of the CLR.

The CLR's ability to couple to, and signal through, $G\alpha_s$ has been well documented (Poyner *et al*, 2002, Hong *et al*, 2012), but signalling via other pathways has, until know, received much more limited investigation.

Indeed, of the work that has been published pertaining to $G\alpha_s$-mediated cAMP production, from the CLR, there is much variability in the established potencies of the three endogenous agonists: CGRP, AM and AM2 (Table 1.5) (Roh *et al*, 2004, Takei *et al*, 2004, Wunder *et al*, 2008, Holmes *et al*, 2013, Watkins *et al*, 2014). Such variability in measured responses is potentially due to the wide array of immortalised cell lines in which these experiments have been performed. In Chapter 4, a HEK 293 cell line, which, as we had previously established, lack expression of any functional RAMPs (Weston *et al*, 2015) was utilised. In this thesis, it was further established that this cell line also lacks expression of functional CLR (Figure 4.1).

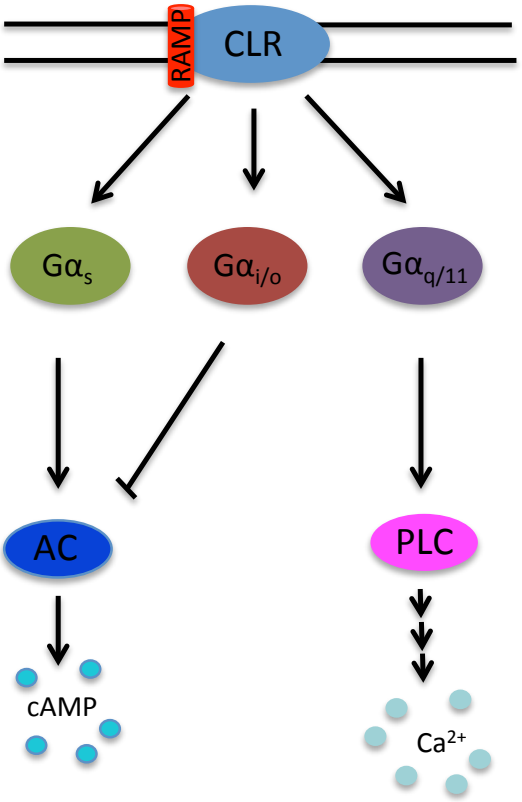

Figure 6.3: RAMP-CLR heterodimers couple to $G\alpha_s$, $G\alpha_{i/o}$ and $G\alpha_{q/11}$.

Each RAMP-CLR heterodimer displays an ability to couple to, and signal via: $G\alpha_s$, to elevate intracellular cAMP levels; $G\alpha_{i/o}$, to reduce cAMP levels, as well as $G\alpha_{q/11}$ to mediate the mobilisation of $_{i}Ca^{2+}$. All of these pathways can be activated by CGRP, AM or AM2, except the cognate ligand at each receptor (CGRP for RAMP1-CLR, and AM for RAMP2/3-CLR), which is unable to activate $G\alpha_{i/o}$-mediated signalling.

Having established a suitable cell line, it was identified that at RAMP1-CLR heterodimers, the three agonists: CGRP, AM and AM2, display a rank order of potency of CGRP > AM = AM2 (Figure 4.2A, Table 4.1). This was different to that observed with RAMP2- and RAMP3-CLR, where rank orders of: AM > CGRP > AM2 and AM = AM2 > CGRP, respectively were observed (Figures 4.2B-C, Table 4.1). These

observations are thus in broad agreement with those obtained from other studies (Roh *et al*, 2004, Takei *et al*, 2004, Wunder *et al*, 2008, Holmes *et al*, 2013, Watkins *et al*, 2014) (Table 1.5 for summary). Further to differing potencies at each RAMP-CLR heterodimer, it was observed that all three agonists affect the largest response with RAMP1-CLR, but, with the exception of AM at RAMP2-CLR, all other responses are greatly reduced (Figure 4.2, Table 4.1). This is in contrast to other published work, which suggests that CGRP, AM and AM2 all elicit responses of the same level (Hong *et al*, 2012); however, this work does have problems with regards to incomplete dose-response curves. Nevertheless, work in CHO cells has suggested that AM2 is a partial agonist at RAMP2-CLR heterodimers (Wunder *et al*, 2008). Therefore, what is observed in this thesis is, that for the same three peptide agonists: CGRP, AM and AM2, the RAMPs are able to modulate both the levels of response, and potency, at the same central GPCR, CLR, in terms of $G\alpha_s$-mediated cAMP accumulation.

In addition to $G\alpha_s$-mediated signalling, it has also been observed that there is potential for the CLR to couple to $G\alpha_{i/o}$ proteins (Kim, 1991, Wiley *et al*, 1992, Main *et al*, 1998, Disa *et al*, 2000, Kuwasako *et al*, 2010), but little follow up work has been performed. Therefore, as with previous studies, PTX was utilised to ablate any potential $G\alpha_{i/o}$-coupling to the CLR, and cAMP accumulation subsequently measured, in response to stimulation with either: CGRP, AM or AM2, at each RAMP-CLR heterodimer. This identified that all three agonists are able to couple to $G\alpha_{i/o}$, but in a RAMP-dependent manner. Crucially, it was observed that the cognate ligand at each RAMP-CLR heterodimer: CGRP for RAMP1-CLR, and AM for RAMP2/3-CLR, is unable to couple to $G\alpha_{i/o}$ (Figure 4.4 Table 4.2). Therefore, what was observed through investigating $G\alpha_{i/o}$ coupling is that the RAMPs, in addition to modulating the CLR's response to three agonists, are also able to modulate G protein coupling. This could have implications upon observed results from other systems. Where previous work has drawn conclusions about the CLR's ability to mediate-$G\alpha_s$ signalling, without consideration of potential $G\alpha_{i/o}$ effects, greatly misleading results could have be obtained. This is highlighted

through work performed in collaboration with Dr. Harriet Watkins: who performed identical experiments to those in Chapter 4, but in HEK 293S cells. From this, she obtained data suggesting that all agonists are, or near to, full agonists at each RAMP-CLR heterodimer (Weston *et al*, 2016, Appendix 2). These responses were subsequently found to be insensitive to PTX pre-treatment (Weston *et al*, 2016, Appendix 2). Through investigating the G protein content of HEK 293 versus HEK 293S cells, it was identified that HEK 293S cells have a greatly reduced expression of both $G\alpha_{i1}$ and $G\alpha_{i2}$ (Weston *et al*, 2016, Appendix 2). Therefore, it is plausible that the CLR is able to specifically couple to $G\alpha_{i1}$ and/or $G\alpha_{i2}$, as well as $G\alpha_{s}$. This ability of the CLR to couple to $G\alpha_{i/o}$ proteins may primarily be relevant in neuronal and electrically excitable cells, as it is these cell types for which PTX pre-treatment has been found to predominantly display effects upon the CLR (Kim *et* al, 1991, Disa *et al*, 2000, Walker *et al*, 2010). Indeed, some of these effects may influence the activity of various ion channels within the nervous system. What the work in this thesis has not identified is the specific $G\alpha_{i/o}$ proteins activated. In order to achieve this, it would be necessary to expand upon the PTX experiments, having transfected in PTX-insensitive G proteins. If effects upon E_{max} and/or potency, for a specific PTX-insensitive G protein, were observed, it would identify the specific $G\alpha_{i/o}$ proteins the CLR is able to couple to, as well as whether or not RAMPs possess the ability to modulate this.

As well as modulating intracellular cAMP levels, it was also observed that the CLR is able to mediate the mobilisation of ${}_{i}Ca^{2+}$. The investigations performed within Chapter 4 determined that $G\alpha_{q/11}$ is the direct mediator of ${}_{i}Ca^{2+}$ release brought about through activation of the CLR, by CGRP, AM and AM2. In addition, as with cAMP production, RAMPs modulate the specific response brought about by each agonist. However, AM2 always appears to bring about a small response, with an associated reduced efficacy. This suggests that AM2 may play a minor role in regulating Ca^{2+} signalling from the CLR. Previous studies have observed CLR-mediated mobilisation of ${}_{i}Ca^{2+}$ in alveolar epithelial cells and dorsal root ganglia, as

well as the trigeminal ganglia (Walker *et al*, 2010). This suggests that CLR-mediated $_{i}Ca^{2+}$ release may play essential roles in regulating airway function, as well as nociception. Additionally, AM stimulation has been seen to mediate Ca^{2+} release in bovine aortic endothelial cells, leading to elevation of cGMP levels, via the action of endothelial nitric oxide synthase (eNOS) (Shimekake *et al*, 1995). There is therefore the potential that AM may mediate vascular dilation. Thus, RAMP-CLR heterodimers may provide a novel target in the treatment of hypertension.

This study, into the signalling repertoire of RAMP-CLR heterodimers, lacks any investigation of the effect of RAMP association upon ERK1/2 activation, nor how this occurs for the CLR. To address this, experiments similar to those performed in Chapter 5 would be required, investigating ERK1/2 activation, in response to CGRP, AM and AM2 stimulation, at each RAMP-CLR heterodimer. Ultimately this would give a wider understanding of the fuller signalling repertoire of the CLR. Having determined this, it would then be interesting to determine if the pharmacology observed in HEK 293 cells is translatable to primary cell lines endogenously expressing both RAMP and CLR, such as human umbilical vein endothelial cells (HUVECs) (Aslam *et al*, 2012). Investigations in cell lines such as these would determine if the effects previously observed are cell type specific, or due to overexpression of both RAMP and CLR. Further, it would identify the role of RAMP-CLR signalling within the cardiovascular system.

Overall, Chapter 4 highlights the ability of the CLR to couple to: $G\alpha_{s}$, eliciting cAMP production; $G\alpha_{i/o}$, opposing the action of $G\alpha_{s}$; and $G\alpha_{q/11}$, facilitating the release of $_{i}Ca^{2+}$. It has also been observed how RAMPs differentially modulate the extent of response to each agonist, at these three pathways (Figure 4.14 and 4.15), potentially though direct RAMP-G protein interactions (Weston *et al*, 2016, Appendix 2). It has been seen that all ligands are predominantly biased towards modulating cellular levels of cAMP, with the exception of AM2 at RAMP2-CLR, and CGRP at RAMP3-CLR heterodimers. However, by removing the action of inhibitory

$G\alpha_{i/o}$ proteins, an increase in the extent of response for these two agonists, resulting in them becoming biased toward cAMP modulation (Figure 4.14B) is observed. The fact that the CLR is predominantly biased towards modulating cAMP levels suggests that cAMP is the main mechanism by which the CLR mediates its effects. This is further validated by studies using PKA inhibitors, such as H89, which suggest that the effects of CGRP are predominantly brought about via cAMP-dependent PKA signalling (Permpoonputtana *et al*, 2016). However, in OHS-4 osteosarcoma cells, CGRP is only able to mobilise $_{i}Ca^{2+}$, without increasing cAMP levels (Drissi *et al*, 1999). Therefore, the pathways activated by the CLR may, potentially, be dependent upon cell type (Wootten *et al*, 2013). What is clearly evident from quantifying bias of the three agonists (Figures 4.14 and 4.15) is that they exhibit distinct patterns, dependent upon the RAMP associated with CLR. Further to the action of RAMPs upon biased agonism of the CLR, there is a potential for both RAMPs and agonists to mediate oligomerisation of the CLR, either with itself, or, in the case of agonists, modulate RAMP-CLR oligomerisation. The ability of the GLP-1R to form homodimers has been identified, whilst disruption of this interaction results in a reduced ability to mediate cAMP production, $_{i}Ca^{2+}$ mobilisation, and ERK1/2 activation (Harikumar *et al*, 2012). Whilst this has not been investigated for the CLR, there is potential for a similar phenomenon to occur, which may influence biased agonism.

6.5 Biased agonism of the CLR: a role for ICL1?

In Chapter 5 it was observed that the ICL1 region of the CLR has implications upon downstream signalling, particularly that mediated via $G\alpha_{s}$ and $G\alpha_{q/11}$ (Figure 5.8-15, Table 5.4-10), but plays a limited role in influencing ERK1/2 activation (Figure 5.16, Table 5.11). As ICL1 mutations had clear effects upon known G protein-mediated signalling pathways, cAMP production and $G\alpha_{q/11}$-mediated $_{i}Ca^{2+}$ release (Weston *et al*, 2016), but not ERK1/2 activation, this lead to the proposal that CLR-

mediated ERK activation occurs in a G protein-independent manner. This could potentially be via β-arrestin-dependent mechanisms, as observed for other GPCRs (Shenoy and Lefkowitz, 2005 and 2011).

One interesting finding of the saturation mutagenesis study is that when S168 in the CLR was substituted for arginine, a significant gain-of-function was observed in terms of a greatly increased potency for CGRP (Figure 5.12D, Table 5.8). The equivalent residue within the GLP-1R, H171, has been observed to form an electrostatic interaction with D312 of the associated Gβ subunit (Zhang *et al*, 2017). Thus, in the S168R mutant of the CLR, a positive charge has been introduced, which may now serve an analogous function to H171 in the GLP-1R. Analysis of the amino acid sequence for all family B GPCRs identifies that positively charged residues (arginines and lysines) are highly conserved at this position (Figure 5.2), suggesting that this residue may play a universal role in interacting with Gβ. However, the CLR, CTR and CRF receptors all contain a serine in this position, suggesting that these receptors may potentially interact with Gβ through the formation of salt bridges. As S168R in the CLR results in a gain-of-function (Figure 5.12D, Table 5.8), it appears that electrostatic interactions with Gβ are more favourable. Similar interactions with Gβ have also been observed with residues within H8 (Zhang *et al*, 2017). Thus, there is the possibility that, upon receptor activation, the separation of ICL1-H8 not only allows a conformational change, to the active state, but also opens up an area where Gβ may interact with the GPCR. This may explain why, when S168 was mutated to glutamic acid, a reduction in signalling was observed (Figure 5.8D, Table 5.4): potentially due to charge-charge repulsion between ICL1 and the Gβ subunit. Such interactions between ICL1 and an associated G protein suggest that ICL1 of family B GPCRs may also play roles in helping to stabilise receptor-G protein interactions, and/or in influencing G protein specificity, though Gβ.

Analysis of the alanine scan data in terms of each mutation's effect upon the extent of bias exhibited between cAMP production, $_{i}Ca^{2+}$ mobilisation,

and ERK1/2 activation, revealed two distinct regions of ICL1 with differing effects upon signalling: the residues at the base of TM1 and start of ICL1 (Y165-K167) appear to predominantly influence $G\alpha_s$-mediated signalling, whilst those across ICL1 and the base of TM2 (S168-C171) predominantly influence $G\alpha_{q/11}$-mediated signalling (Figure 5.17-18). This suggests that ICL1 plays roles in influencing G protein specificity. Indeed, this is something that has previously been suggested (Wess, 1997, Swift *et al*, 2006). However, what has not been accounted for in this mutagenesis study is any effect upon CLR-RAMP interaction. Chapter 4 identified the key role of RAMPs in modulating biased agonism of the CLR. It is plausible that through mutating ICL1 of the CLR, the ability to interact with RAMP1 may have been affected, which may have unknown effects upon downstream signalling, and biased agonism. This is something that will need addressing in future follow up work. This study into $G\alpha_s$ and $G\alpha_{q/11}$ also lacks any indication of if, or how, this region of the CLR influences the $G\alpha_{i/o}$ pathway that was identified in Chapter 4. Therefore, it would be interesting to investigate how the mutations affect AM-mediated signalling, in both untreated and PTX-treated cells.

Whilst ICL3 is predominantly seen to be responsible for GPCR-G protein interactions (Taylor and Neubig, 1994, Liu *et al*, 1995 Cai *et al*, 2001, Itoh *et al*, 2001, Janz and Farrens, 2004), recent work by Flock *et al* has identified a 'selectivity barcode' upon G proteins, which determines if a G protein will interact with a given GPCR (Flock *et al*, 2017). It was identified that this 'barcode' is specifically read by a GPCR via interactions with ICL 2/3 as well as TM 5/6 (Flock *et al*, 2017). In addition, the work presented in Chapter 5 suggests that ICL1 may plays roles in influencing these interactions: either directly, through interacting with Gβ, influencing association of Gα, or through modulating the G protein-binding pocket, by modulating the positioning of TM2, and hence, ICL2 and the G protein binding pocket; something, which may be supported by the fact that pepducins, utilising different regions of different ICLs, can play roles in activating or inhibiting differential signalling pathways (Carr *et al*, 2014).

6.6 ICL1: a role in GPCR activation

In addition to a role in influencing bias at the CLR, the possibility of direct interactions between ICL1 and H8, which are broken upon receptor activation, was identified. Similar observations have been made within the protease-activated receptor 1 (PAR1), where a series of ionic and H-bonding interactions between TM7 and H8 have previously been observed (Swift *et al*, 2006). This TM7-H8-ICL1 network has been suggested to function in a coordinated manner to transfer ligand-induced signals to the associated G protein, particularly $G\alpha_q$ (Swift *et al*, 2006).

Direct interactions between E377 in H8 and K135 in ICL1 of the PAR1 have been observed, with similar interactions also occurring in many other family A GPCRs (Swift *et al*, 2006). The equivalent of E377, in family B GPCRs, is universally conserved (E388 in the CLR (Figure 5.3)), but the equivalent of K135 is a cysteine (C171 in the CLR), which is also conserved amongst all family B receptors (Figure 5.2). Analysis of the crystal structures for GCGR and the GLP-1R, identified that these residues (C171 and C174, respectively) are similarly positioned spatially (Figure 5.6A-B), and that, in the GLP-1R, this residue (C174) undergoes only a small amount of movement upon activation (Figure 5.6B-C). The work upon ICL1 of the CLR has suggested that this residue may play a role in stabilising the ICL1-TM2 junction, playing a structural role. As this residue is conserved amongst family B GPCRs, this residue may play similar roles across the whole family. Interestingly, conserved between all family B GPCRs is an arginine two positions up from C171, R173 in the CLR (Figure 5.2). Analysis of the existing structures for the GCGR and GLP-1R identified the possibility of an interaction between R173/176 (equivalent residues in the GCGR and GLP-1R, to the R173 in the CLR) and E406/408 (Figure 5.4A-B). These residues may serve an analogous function to the K135-E377 interaction in PAR1 (Swift *et al*, 2006).

Unlike PAR1, in all family B GPCRs, with the exception of the CLR, CTR and CRF receptors, a second glutamic acid is present within H8 (position 392, relative to the CLR (Figure 5.3)). Chapter 5 has highlighted a possible interaction between this glutamic acid in H8 and positively charged residues at the start of ICL1. Within the existing crystal structures for the GCGR and GLP-1R, in their inactive states, there is the possibility for an interaction between S167/K168, in the GCGR, as well as H171/R170, in the GLP-1R, with E410/412 (Figure 5.4A-B). Thus, there is the possibility that these residues, in family B GPCRs, form a second ICL1-H8 interaction, analogous to that played by K135-E377 in PAR1 (Swift *et al*, 2006). The fact that a glutamic acid at position 392 is absent in the CLR, CTR and CRF receptors (Figure 5.3) suggests that these receptors do not form this interaction. Therefore, in the majority of family B GPCRs, it is probable that two ICL1-H8 interactions occur, primarily, between positively charged residues on ICL1, and negatively charged glutamic acids within H8. However, for the CTR, CLR and CRF receptors, there may only be a single interaction between the equivalents of R173 and E388.

Upon activation of the rhodopsin receptor, ICL1 and H8 have been observed to move apart (Altenbach *et al*, 2001, Klein-Seetharaman *et al*, 2001). Likewise in the GLP-1R active structure (Figure 5.4C), a greater separation between ICL1 and H8, compared to the inactive structure is observed (Figure 5.4B). Concurrent with this are movements of R170 and H171 away from the axis of H8, along with a rotation of R176 away from E408 in H8 (Figure 5.4B-C). This suggests that breaking an ICL1-H8 interaction may be a step that is required to occur upon GPCR activation, for both families A and B. Within the μ-opioid receptor, movement of ICL1-H8 is observed to occur prior to movement of TMs 5 and 6 (Sounier *et al*, 2015), suggesting this may be an early, key, event in receptor activation.

Interestingly, the ICL regions of GPCRs have been utilised as a series of drugs that can act either as allosteric agonists or antagonists, depending

upon which ICL is used (Covic *et al*, 2001, Kuliopulos and Covic, 2003, Carr *et al*, 2014). These drugs, termed pepducins, consist of regions of either ICL1, 2, or 3, from a given GPCR, tethered to hydrophobic moieties, allowing cell penetration (Covic *et al*, 2001). The fact that these drugs can activate, or inhibit, orthosteric agonist-induced activation highlights how important the ICL regions of GPCRs are in both activation and signalling. Further, the work in Chapter 5 may also inform further upon how this drug class functions.

This work identifying ICL1 as a key region of the CLR in receptor activation and mediator of signalling has so far only focused upon Y165-Q172. As discussed, there is a potential for an ICL1-H8 interaction. To fully investigate this, mutants of H8 would have to be generated, particularly focusing upon the conserved glutamic acids, as well as introducing a second glutamic acid into H8 of the CLR, as per the majority of family B. Further, as R173 has been highlighted as a particularly key residue in forming an ICL1-H8 interaction, substitutions of this residue would be required, and experiments identical to those in Chapter 5 performed. To support the *in vitro* findings, molecular dynamics simulations would provide a greater understanding/explanation of the biological effects we observe for each mutation.

6.7 ICL1 influences cell surface expression

As has previously been observed, mutation of ICL1 has dramatic effects upon GPCR cell surface expression (Bentrop *et al*, 1997, Wess *et al*, 1998). A similar effect has been observed for the: α_{1B}-, α_{2B}-, and β_2-adrenergic receptors, as well as for the angiotensin II type 1 receptor (Duvernay *et al*, 2009). In these family A GPCRs, a conserved leucine residue within ICL1 (L48) was found to be required for export from the ER, and subsequent trafficking to the cell surface. Interestingly, analysis of the sequences of ICL1 for all family B GPCRs identifies an equally conserved leucine (Figure 5.2). Initial investigations into the cell surface

expression of our CLR mutants (performed by Heptares therapeutics), revealed that, when this residue (L169) is mutated, a reduction in surface expression of between ~66-95% that of WT was observed (Figure 5.7, Table 5.3). The only exception to this was where this residue is mutated to isoleucine, which instead exhibited a reduction of ~43% (Figure 5.7, Table 5.3). Thus, a similarly structured residue at this position can apparently rescue some reduced expression. It therefore seems that conserved leucines, in both family A and B GPCRs, may be key in regulating receptor expression. However, how this applies to the CLR, which absolutely requires RAMP association for trafficking (McLatchie *et al*, 1998), is unknown. In order to further determine a role of this residue upon cell surface expression further follow up experiments to the initial expression experiments, would be required.

6.8 Models of GPCR signalling – understanding bias

Many attempts have been made to model signalling from GPCRs, initially starting with the two-state model (Figure 1.7) which suggested that a GPCR exists in either inactive (R) or active (R*) states. It was believed that agonists served to shift the equilibrium of a system towards the R* state, thereby resulting in more active receptors and an increased signalling output. Whilst the two-state model may serve to explain relatively simple receptors activating only a single pathway, such as the neurotensin receptor (Mustain *et al*, 2011), it fails to recapitulate many of the behaviours observed at other GPCRs. For example, the two-state model fails to explain how one agonist can activate multiple differing pathways, with differing potencies and/or efficacies, such as what we observe within this thesis for the A_1R and $A_{2A}R$, as well as the CLR. Nor does it explain how differing receptor conformations have been observed for a given receptor, dependent upon the bound ligand (Swaminath *et al*, 2004, 2005). Further, this model fails to capture the effect of the associating G protein; indeed, differences in antagonist affinity have been

observed depending upon which Gα subunit is associated with the A_1R (Baker and Hill, 2007).

Attempts to redress these imperfections in the two-state model were made by De Lean and colleagues, who developed the ternary complex model (De Lean *et al*, 1980). This was then further refined to produce the extended ternary complex (ETC) model (Samama *et al*, 1993). Like the two state model, the ETC model allows for a receptor in both active and inactive conformations. However, it now allows for conversion between these states in the absence of an agonist, thus encapsulating constitutive activity. The ETC model also allows for a ligand binding a receptor, but not resulting in activation, thereby accounting for allosteric modulators, inverse agonists, and antagonists. The effect of G protein association with a GPCR is also encompassed, by allowing a G protein to interact with an active receptor, or a ligand-bound active receptor. One situation that the ETC model does not account for is the association of a G protein with an inactive receptor. Adding this to the ETC model yields the cubic ternary complex (CTC) model (Weiss *et al*, 1996). This model now allows for a receptor to be 'pre-coupled' to a GPCR in both inactive and active states, and for the activation of a receptor, through G protein association. The CTC model thus explains the differences in antagonist affinity for the A_1R in differing G protein bound states (Baker and Hill, 2007), and further encapsulates constitutive signalling.

In an attempt to further explain GPCR-mediated signalling and biased agonism, we further refined the cubic ternary complex model. We developed a model consisting of multiple CTC models, accounting for differing active conformations of a GPCR, as well as association of differing G proteins (Appendix 3). The ETC and CTC models, whilst accounting for G protein association, treat them all as one single entity, essentially a 'black box' that transduces signals. We separate this box into several parameters accounting for multiple G proteins. Likewise, we apply the same principle for multiple active receptor conformations. Our model thus allows for a single receptor to couple to, and activate, multiple

downstream signalling pathways, both in the presence and absence of an agonist, thus encapsulating constitutive activity. We utilised our multi-CTC model to account for two active receptor states and two associating G proteins. From this, we identify that a ligand acting as an agonist of one pathway also acts as an antagonist of the 2nd pathway, by reducing the number of receptors available to be activated for pathway 2. Our model is also able to account for differing receptor number, as well as temporal aspects of signalling output and how these influence perceived biased agonism (Herenbrink *et al*, 2016). Further, our model is novel in that it allows for receptor 'cross-states', whereby one given active receptor state can associate with any given G protein. We also apply parameters accounting for differing affinities of an agonist for active or inactive receptor states, as well as for G protein-free or -bound receptors. Through this we are able to produce a new method of quantifying biased agonism, accounting for factors not apparent in the operational model of pharmacological agonism (Black and Leff, 1983). By applying our multi-CTC model to data obtained in Chapter 3, relating to the abilities of NECA, Cmpds 6 and 20 to produce non-monotonic dose-response curves (Figure 3.4) due to their ability to activate both $G\alpha_{i/o}$ and $G\alpha_{s}$ (Figures 3.4 and 3.5, Table 3.2 and 3.3), we are fully able to recapitulate the observed *in vitro* responses. Thus, our model is able to successfully reproduce experimental data, and therefore provides one possible alternative method of both analysing, and quantifying, biased agonism of GPCRs.

6.9 Conclusion

The work presented within this thesis has further highlighted the extent of biased agonism and pathway bias at GPCRs in both families A and B. It has identified, and quantitated, the abilities of the A_1R and CLR to activate various signalling pathways, and how both can activate opposing pathways with respect to cAMP production. In addition, this work has identified the mechanism of RAMP-CLR mediated $_iCa^{2+}$ mobilisation to be $G\alpha_{q/11}$-mediated, and further shown the ability of RAMPs to modulate CLR-mediated signalling, with respect to both the efficacy of the stimulating agonist, and G protein specificity. Further, a role of ICL1 in influencing G protein specificity at the CLR has been identified, as well as identifying a potential ICL1-H8 interaction, which is broken upon receptor activation. In addition to uncovering mechanisms of signalling from the A_1R and CLR, this thesis has also identified and characterised both selective, and non-selective agonists of both the A_1 and $A_{2A}R$, which may pose, as yet undetermined, therapeutic benefit for various pathological states.

Appendix 1

Publication: Knight *et al*, 2016

This appendix contains:

Knight A, Hemmings JL, Winfield I, Leuenberger M, Frattini E, Frenguelli BG, Dowell SJ, Lochner M, Ladds G (**2016**). Discovery of novel adenosine receptor agonists that exhibit subtype selectivity. *J. Med. Chem.* (59):947-964.

Journal of Medicinal Chemistry

Article

pubs.acs.org/jmc

Discovery of Novel Adenosine Receptor Agonists That Exhibit Subtype Selectivity

Anthony Knight,[†,▽] Jennifer L. Hemmings,[‡,▽] Ian Winfield,[§,#] Michele Leuenberger,[‡] Eugenia Frattini,[#] Bruno G. Frenguelli,[∥] Simon J. Dowell,[⊥] Martin Lochner,[*,‡] and Graham Ladds[*,#]

[†]Systems Biology Doctoral Training Centre, University of Warwick, Coventry CV4 7AL, U.K.

[‡]Department of Chemistry and Biochemistry, University of Bern, 3012 Bern, Switzerland

[§]Division of Biomedical Cell Biology, Warwick Medical School, University of Warwick, Coventry CV4 7AL, U.K.

[∥]School of Life Sciences, University of Warwick, Coventry CV4 7AL, U.K.

[⊥]Department of Platform Technology and Science, GlaxoSmithKline, Hertfordshire SG1 2NY, U.K.

[#]Department of Pharmacology, University of Cambridge, Tennis Court Road, Cambridge CB2 1PD, U.K.

Supporting Information

ABSTRACT: A series of N^6-bicyclic and N^6-(2-hydroxy)-cyclopentyl derivatives of adenosine were synthesized as novel A_1R agonists and their A_1R/A_2R selectivity assessed using a simple yeast screening platform. We observed that the most selective, high potency ligands were achieved through N^6-adamantyl substitution in combination with 5′-*N*-ethylcarboxamido or 5′-hydroxymethyl groups. In addition, we determined that 5′-(2-fluoro)thiophenyl derivatives all failed to generate a signaling response despite showing an interaction with the A_1R. Some selected compounds were also tested on A_1R and A_3R in mammalian cells revealing that four of them are entirely A_1R-selective agonists. By using in silico homology modeling and ligand docking, we provide insight into their mechanisms of recognition and activation of the A_1R. We believe that given the broad tissue distribution, but contrasting signaling profiles, of adenosine receptor subtypes, these compounds might have therapeutic potential.

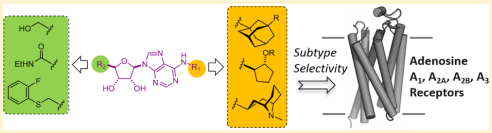

INTRODUCTION

Adenosine receptors (ARs) belong to the family of G protein-coupled receptors (GPCRs) and exist as four different subtypes, A_1, A_{2A}, A_{2B}, and A_3. All subtypes respond to the purinergic nucleoside adenosine, but they have a wide and varying tissue distribution. Many ARs have been linked to cardiovascular, respiratory, and inflammatory disorders.[1] Furthermore, in the central nervous system they have been implicated in acute pathological conditions such as epilepsy, hypoxia, and ischemia,[2,3] and chronic neurodegenerative disorders, such as Parkinson's, Alzheimer's, and Huntington's diseases.[4] In human cells, the A_1R and A_3R predominantly couple to the $G\alpha_i$ family of G proteins, inhibiting the production of cAMP, while the A_2R subtypes couple to the $G\alpha_s$ subunit, stimulating adenylate cyclase to elevate cAMP levels. Given their common ligands, diametrically opposed effects, and overlapping tissue distribution, the ARs have been the focus of extensive research to discover subtype selective ligands. However, limitations of mammalian systems can hinder the testing and development of these compounds. For instance, the A_1R can signal through the $G\alpha_{i1}$, $G\alpha_{i3}$, and $G\alpha_o$,[5] but it is currently difficult to differentiate between these effectors in an *in vivo* mammalian cell-based assay.

Most of the known AR agonists are based on the adenosine scaffold, and receptor subtype selectivity can be achieved by substituting the purine ring of the nucleoside at positions C-2 and/or N^6 with appropriate functional groups. For instance, substitution of the N^6-position with bulky cycloalkyl- and bicycloalkyl groups has resulted in A_1R-selective agonists.[6−10] Introduction of a wide range of N^6-substituents is conveniently achieved by nucleophilic aromatic substitution of the corresponding 6-chloro purine precursor with primary or secondary amines. The ribose moiety, in particular at the C-2′, C-3′, and C-5′ positions, has also been the subject of many modifications which can influence A_1R affinity, selectivity, and efficacy.[8,11,12] 5′-Carboxamido adenosine derivatives, such as the prototypical AR agonist 5′-*N*-ethylcarboxamidoadenosine (NECA), among many other examples, are known to be potent activators. More bulky groups, such as substituted 5′-thioaryl and 5′-oxoaryl moieties, have also been explored, and these studies have provided novel A_1R-selective and potent agonists.[13,14] In light of this, we designed a series of adenosine analogues that feature different cyclic and bicyclic substituents at the N^6 of the purine ring and various functional groups at the C-5′ of the ribose in order to assess the effect of these modifications on AR activity and subtype selectivity.

We[15−20] and others[5,21−23] have previously described the use of modified *Saccharomyces cerevisiae* strains containing chimeric (yeast-human) G protein alpha subunits to functionally couple

Received: September 10, 2015
Published: January 12, 2016

DOI: 10.1021/acs.jmedchem.5b01402
J. Med. Chem. 2016, 59, 947−964

Scheme 1. Synthesis of Adenosine Derivatives[a]

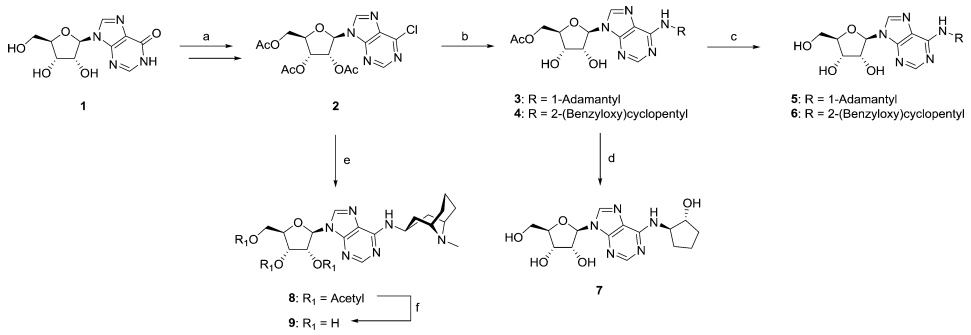

[a]Reagents and conditions: (a) procedures according to ref 29; (b) R-NH_2, Et_3N or DIPEA, EtOH, reflux, 18 h to 5 days (for specific conditions and yields see Experimental Section); (c) K_2CO_3, MeOH, rt, 3 h, 99%; (d) **4**, $Pd(OH)_2$, cyclohexene, ethanol, reflux, 18 h, 99%; (e) (1*R*,3*r*,5*S*)-9-methyl-9-azabicyclo[3.3.1]nonan-3-amine, DIPEA, EtOH, reflux, 18 h, 54%; (f) K_2CO_3, MeOH, rt, 3 h, 99%.

Scheme 2. Synthesis of Novel NECA Derivatives[a]

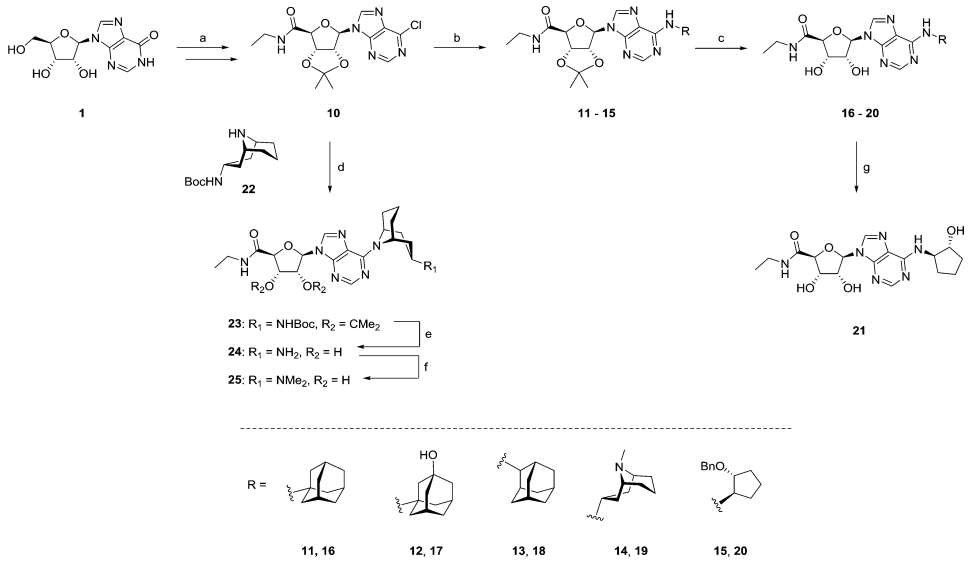

[a]Reagents and conditions: (a) procedures according to ref 32; (b) R-NH_2, Et_3N or DIPEA, EtOH, reflux, 18 h to 5 days (for specific conditions and yields see Experimental Section); (c) acetic acid, water, 80 °C, 18 h, 99%; (d) *tert*-butyl-9-azabicyclo[3.3.1]nonan-3-yl carbamate (**22**), DIPEA, EtOH, reflux, 18 h, 85%; (e) acetic acid, water, 80 °C, 18 h, 99%; (f) formic acid, formaldehyde (37% aq.), reflux, 18 h, 63%; (g) **20**, $Pd(OH)_2$, cyclohexene, ethanol, reflux, 18 h, 99%.

heterologously expressed GPCRs. Specifically, the chimeric G proteins enable mammalian GPCRs to functionally couple to the yeast-mating pathway. This pathway includes a reporter (*FUS1-lacZ*) gene providing a quantitative assay for GPCR activation.[16] The yeast platform provides a simple, affordable, and robust assay with which to identify novel GPCR ligands and their interactions with a single effector.[17,24,25] This system has also been established to study A_1R, $A_{2A}R$, and $A_{2B}R$ in a number of G protein backgrounds,[5,18,21−23] although evidence of functional couplings of the A_3R has not been reported.

In this study, we exploit the yeast system to characterize novel synthetic adenosine derivatives for their agonist activity against the A_1R, $A_{2A}R$, and $A_{2B}R$. We explored subtype selectivity further at the A_1R and A_3R in mammalian CHO-K1 cells for the compounds that were active against the A_1R in the yeast screen. Moreover, we use homology modeling and docking to gain insight into the binding of our agonists at the A_1R. Our yeast-based screen and mammalian cell assays have identified novel adenosine nucleosides exhibiting interesting A_1R selective profiles. Hence, they constitute valuable tool

DOI: 10.1021/acs.jmedchem.5b01402
J. Med. Chem. 2016, 59, 947−964

Scheme 3. Synthesis of CVT-3619 and New Derivatives[a]

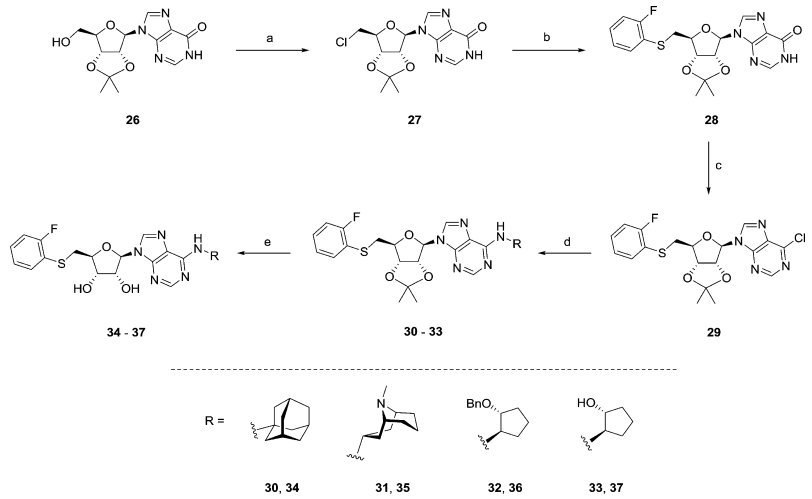

[a]Reagents and conditions: (a) CCl_4, PPh_3, DMF, rt, 18 h, 53%; (b) 2-fluorothiophenol, NaH, DMF, 0 °C to rt, 3 h, then chloride **27**, DMF, rt, 18 h, 48%; (c) $SOCl_2$, DMF, DCM, 50 °C, 5 h, 88%; (d) R-NH_2, Et_3N or DIPEA, EtOH, reflux, 18 h to 3 days (for specific conditions and yields see Experimental Section); (e) acetic acid, water, 80 °C, 18 h, 99%.

compounds for cellular studies and might have therapeutic potential.

RESULTS AND DISCUSSION

Chemistry. Known compounds **5**,[26] **6**,[27] and **7**[28] have previously been shown to be selective for the A_1R with respect to their binding affinity. These analogues were prepared for assessment using our yeast-based assay. Bulky bicyclic groups have been highlighted as beneficial for A_1R selectivity,[7−10] so we also prepared novel compound **9**. Intermediate **2** was required for efficient generation of the analogues (Scheme 1). This was synthesized according to the procedure adopted by Kotra et al.,[29] with minor experimental modifications.

Aromatic substitution of the N^6-chloro group with 1-adamantylamine or (1*R*,2*R*)-1-amino-2-benzyloxycyclopentane was carried out in the presence of triethylamine or Hünig's base. This resulted in partial deacetylation to give the monoacetylated products (**3** and **4**), which could be attributed to the use of excess base. The presence of the acetyl on the primary alcohol was confirmed using ^{1}H NMR and was then removed using potassium carbonate in methanol to give **5** and **6** in quantitative yield. The choice of base did not appear to have an effect on the reaction. Attempts to directly remove the benzyl group from **6** using hydrogenolysis returned unreacted starting material. However, treatment of monoprotected **4** with Pearlman's catalyst and cyclohexene afforded **7**. Interestingly, aromatic substitution with (1*R*,3*r*,5*S*)-9-methyl-9-azabicyclo-[3.3.1]nonan-3-amine (granatanamine) using less base did not result in deacetylation and afforded the expected product **8**. Deprotection was again carried out with potassium carbonate and methanol. Granatanamine was prepared according to a procedure previously developed in our group.[30]

Despite the widespread use of 5′-*N*-ethylcarboxamidoadenosine (NECA) as an A_1R agonist, we found that the analogous cyclopentyl (**21**) and adamantyl (**16**) congeners were novel compounds and to the best of our knowledge untested at the A_1R. This is possibly a consequence of the nonselective nature of NECA at the AR subtypes.[31] In this case, intermediate **10** was required to allow the generation of novel analogues (Scheme 2).

The amide building block **10** was prepared from **1** as previously reported by Middleton et al.[32] Displacement of the chloride in **10** with the appropriate amine in the presence of either Hünig's base or triethylamine gave intermediates **11**−**15**. This reaction proceeded with ease in refluxing ethanol overnight in the case of **13**−**15**; however, all 1-adamantyl analogues required 1 week at reflux to generate sufficient quantities of desired compounds. Interestingly, the 2-adamantylamine reaction was complete within 1 day. Acetonide deprotection was achieved by heating overnight in acetic acid and water to generate **16**−**20** with the quantitative yields observed. Removal of the benzyl protecting group from **20** with palladium hydroxide and cyclohexene to generate **21** proceeded in quantitative yield. We decided to prepare analogues **24** and **25** with the alternative bicyclic architecture to allow us to probe the necessity for a secondary amine at the adenine N^6 position. Chloride **10** was reacted with granatyl secondary amine **22**, which was prepared according to a literature protocol.[33] Like the adamantyl analogues, this reaction was very slow and required reflux for 1 week to generate sufficient quantities of the product to give **23**. Concomitant deprotection of the acetonide and Boc group occurred on treatment with acetic acid and water to give **24**. Dimethylamine **25** was then prepared using formic acid and formaldehyde.

Given the prior studies on CVT-3619 (**37**) showing that it is a specific partial agonist at the A_1R,[14] we prepared this compound for assessment using our yeast-based assay and planned to prepare new analogues with the 2-fluorothiophenol group at the C-5′ position of the ribose ring. In alignment with our strategy for adenosine and NECA analogues, we required

DOI: 10.1021/acs.jmedchem.5b01402
J. Med. Chem. 2016, 59, 947−964

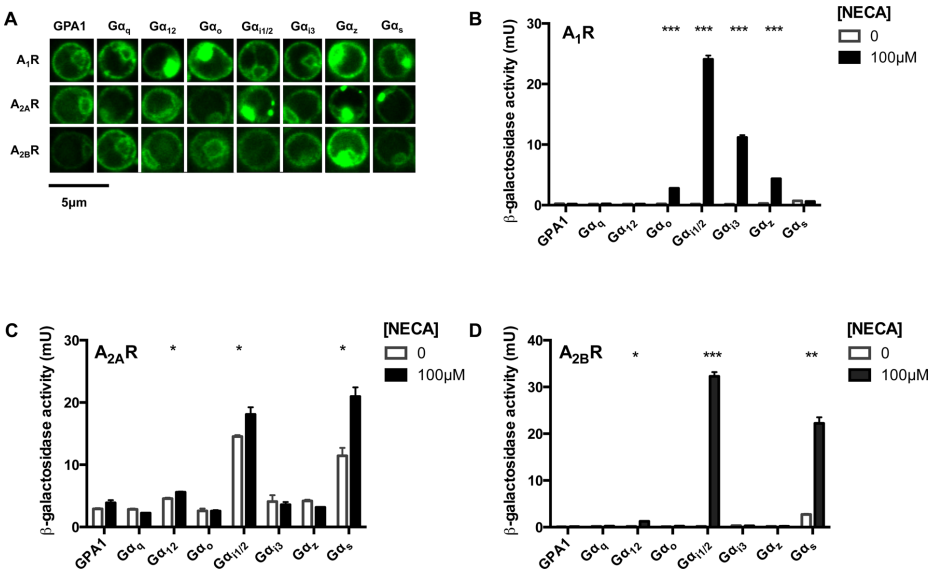

Figure 1. NECA-activated yeast-mating pathway via specific AR/Gα protein chimeras. (A) A C-terminal GFP tag was engineered onto the A_1R, A_{2A}R, and A_{2B}R, and expression at the plasma membrane was confirmed using fluorescence microscopy. Scale bar = 5 μm. (B–D) Yeast strains expressing the human (B) A_1R, (C) A_{2A}R, and (D) A_{2B}R were stimulated with 0 or 100 μM NECA for 16 h and assayed for the activation of the *FUS1-lacZ* reporter gene as previously described.[15−17,19] β-Galactosidase units (mU) are expressed as the ratio of *o*-nitrophenol product to cell density (determined colorimetrically; see Experimental Section). Data are the mean of 5 independent experiments ± SEM. Data were determined as significantly different from the nonligand response using Student's *t*-test where *, $p < 0.05$; **, $p < 0.01$; and ***, $p < 0.001$.

chloride **27**, which would allow efficient generation of analogues with various cyclic groups at the N^6 position of the adenine (Scheme 3). Primary chloride **27** was prepared from protected **26** using Appel conditions according to the previously reported procedure.[34] Treatment with 2-fluorothiophenol and sodium hydride gave **28** in 48% yield, and subsequent chlorination with our previously adopted conditions of thionyl chloride and DMF gave **29** in 88% yield. Introduction of the cyclic component was accomplished by reacting with the appropriate primary amine in the presence of DIPEA or triethylamine to give **30**–**33**. Again, the preparation of the adamantyl analogue required 1 week at reflux to obtain the product in sufficient yield. Initial attempts to directly remove the benzyl protecting group from **32** with palladium hydroxide and cyclohexene to generate **37** were unsuccessful. However, 6-chloropurine **29** reacted readily with (1*R*,2*R*)-2-aminocyclopentanol to generate the desired product directly. Acetonide deprotection with acetic acid and water at reflux generated final compounds **34**–**37** in excellent yields.

Biological Activity. We expressed all four AR subtypes, under the control of the constitutive *GAPDH* promoter, in a panel of transplant yeast strains engineered to contain chimeric Gα-subunits in which the 5 C-terminal amino acids of Gpa1p have been replaced with those of mammalian Gα_q, Gα_{12}, Gα_o, G$\alpha_{i1/2}$, Gα_{i3}, Gα_z, and Gα_s. Efficient trafficking of the A_1R, A_{2A}R, and A_{2B}R to the cell surface in yeast cells was confirmed using modified receptors engineered to contain a GFP fluorophore at the C-terminus (Figure 1A). NECA is a nonsubtype selective AR agonist and was used to determine through which Gα-subunits each receptor signaled. Yeast cells were exposed to 100 μM NECA for 16 h, and reporter gene activity (as measured through β-galactosidase production) was determined (Figure 1B–D).

Consistent with previous reports,[5,22] the A_1R generated significant ($p < 0.05$) responses in strains expressing G protein chimeras corresponding to Gα_o, Gα_{i1}, and Gα_{i3} (Figure 1B). In addition, we also report for the first time, functional coupling of the A_1R signaling through the GPA1/Gα_z transplant. Signaling was not observed via GPA1/Gα_q, GPA1/Gα_{12}, or GPA1/Gα_s or the unmodified Gpa1p ($n \geq 16$ isolates screened for functionality). Further, we observed that the A_{2A}R and A_{2B}R (Figure 1C and D) signaled through both GPA1/Gα_s and GPA1/Gα_{i1}, but we failed to identify any functional coupling for the A_3R in our panel of strains (Figure S1). Moreover, we report that the A_{2A}R displayed significantly elevated levels of ligand-independent signaling which is consistent with previous observations in yeast.[18] While we have observed that these GPCRs can couple to a number of different Gpa1p chimeras, we have chosen to focus on the ones that are widely reported to be the most physiologically relevant in mammalian cells. Consequently, the A_1R-GPA1/Gα_{i1}, A_{2A}R-GPA1/Gα_s, and A_{2B}R-GPA1/Gα_s strains were chosen for further compound characterization.

Subtype Selectivity of Adenosine Derivatives in Yeast. Having identified yeast strains that functionally express the A_1R, A_{2A}R, and A_{2B}R, we sought to validate their pharmacology in response to a range of agonists. Dose–response curves were determined for NECA, adenosine, 2-chloro-N^6-cyclopentyladenosine (CCPA), and CGS-21680 (Figure 2) using the yeast reporter assay. Sigmoidal dose–

DOI: 10.1021/acs.jmedchem.5b01402
J. Med. Chem. 2016, 59, 947−964

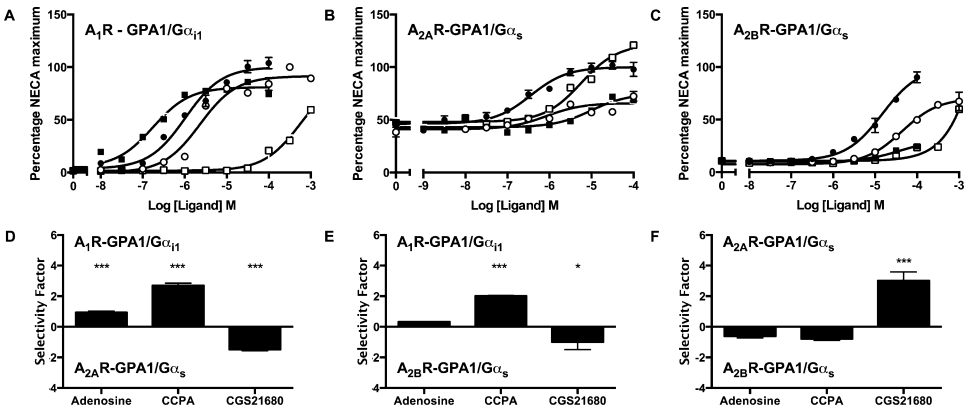

Figure 2. AR agonists display receptor subtype selectivity. Dose−response curves for various AR agonists were generated from yeast strains expressing (A) A_1R, (B) $A_{2A}R$, and (C) $A_{2B}R$ following stimulation for 16 h with (●) NECA, (○) adenosine, (■) CCPA, or (□) CGS-21680. Activation of the reporter gene was calculated and is expressed as the percentage of the maximum response achieved when cells were stimulated with the reference agonist NECA. (D−F) Receptor selectivity was calculated as the change in log (τ/K_A), relative to NECA, for the data in A−C. Data were determined as statistically different (**, $p < 0.01$; ***, $p < 0.001$) from NECA, using a one-way ANOVA with Bonferroni's post-test. All data are the mean of 5−8 independent experiments ± SEM.

response curves were observed allowing the maximum response (E_{max}) and potency (pEC_{50}) to be determined (Table 1). NECA, adenosine, and CCPA are full agonists at the A_1R (E_{max} compared with NECA by one-way ANOVA, $p > 0.05$) but have differing potencies (Table 1). This generates a rank order of potency for the ligands of CCPA > NECA > adenosine. CGS-21680 had a much lower potency than the other ligands (pEC_{50} = 3.2 ± 0.1) and failed to reach a maximal response. While the overall potency values are lower than observed in mammalian cells, the rank order of the ligands is conserved between yeast and mammalian systems.[35] Application of the operational model of pharmacological agonism[36] enabled calculation of the ligand binding affinity (pK_A) and efficacy (τ) (Table 2). In comparison to NECA, both adenosine and CCPA have a greater pK_A and a reduced τ.

We next sought to investigate the pharmacological properties of the $A_{2A}R$ expressed in our GPA1/$G\alpha_s$ expressing strains. Both CGS-21680 and NECA displayed strong agonism at the $A_{2A}R$, while adenosine and CCPA showed weak partial agonism (Figure 2B). Further, all ligands assayed display weak potency at the $A_{2B}R$ (rank ligand potencies, NECA > adenosine = CCPA ≫ CGS-21680), with CGS-21680 failing to generate a maximal response at the ligand concentrations assayed. Thus, in our strains, CGS-21680 would appear to be largely $A_{2A}R$ selective, and this is consistent with mammalian cell affinity data.[31,35]

We next sought to compare the selectivity/preference that ligands may possess for each of the ARs. Expression of the ARs in yeast generates a clean, robust assay, with no competing signaling machinery, so enabling the proportioning of receptor responses to individual signaling pathways. We have previously used the methods developed by Figuero et al.[37] to quantify ligand bias for receptors expressed in yeast.[19,20] Here, we report the adaptation of the equimolar method of comparison[37] to quantify ligand selectivity for a given receptor (see Experimental Section for more details). Since NECA is a full agonist for all three ARs expressed in yeast, it can be used as a reference ligand. By calculating the change in log (τ/K_A), for an agonist relative to NECA, for each AR subtype we have generated a quantitative means of comparing receptor selectivity for all our agonists (Figure 2D−F). Adenosine and CCPA are A_1R-selective but also preferentially activate $A_{2B}R$ over $A_{2A}R$. In contrast, CGS-21680 is A_2R subtype-selective with an overall preference for the $A_{2A}R$.

Bulkier N^6-adamantyl agonists have previously been shown to be A_1R selective with respect to binding affinity at rat receptors.[26] Therefore, we extended our studies to include novel AR agonists containing an adamantyl group. Compounds **5** and **16**−**18** were derived from adenosine and NECA, respectively (Schemes 1,2). These compounds appeared to be A_1R selective full agonists compared with NECA, with no significant response detected at the $A_{2A}R$ and $A_{2B}R$ ($p > 0.05$) (Figure 3A−C). However, **5** and **16**−**18** displayed reduced potency to the A_1R compared to that of their precursors and cyclopentyl variants (Table 1). Furthermore, pK_A values suggested that this might be a consequence of reduced ligand binding affinities (Table 2).

A_1R agonists derived from adenosine with substituted cyclopentyl groups at the adenine N^6 position have been reported previously (e.g., GR79236, *N*-[(1*S*,2*S*)-(2-hydroxy)-cyclopentyl]adenosine).[38] We found that N^6-cyclopentyl derivatives **6**, **7**, **20**, and **21** mainly signal through the A_1R, but for the latter two compounds, minimal responses were also detected at $A_{2A}R$ and $A_{2B}R$ (Table 1 and Figure 4).

Adenosine derivative **6** was highly A_1R-selective but failed to produce a maximal signal. In a patent in 2011,[27] **6** was described as an A_1R-selective agonist for reducing elevated intraocular pressure in the treatment of glaucoma or ocular hypertension, and this compound was assessed for selectivity with respect to binding affinity (K_i) at human subtypes A_1, A_{2A}, and A_3.[27] In accordance with our results, it was shown, using a radioligand displacement assay, that **6** binds with greater than 250-fold affinity at the A_1 over the A_{2A} subtype. In the yeast-based assays, the novel NECA analogues **20** and **21** have equal

DOI: 10.1021/acs.jmedchem.5b01402
J. Med. Chem. 2016, 59, 947−964

Table 1. Potency (pEC_{50}) and Maximal Response (E_{max}) of Reference Compounds and Synthetic Adenosine Derivatives at A_1R, $A_{2A}R$, and $A_{2B}R$ As Measured in Yeast[a]

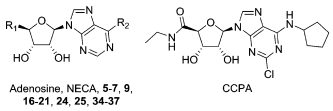

Adenosine, NECA, **5**-**7**, **9**, **16**-**21**, **24**, **25**, **34**-**37**

CCPA

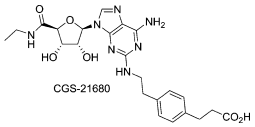

CGS-21680

Compd	R_1	R_2	A_1R		$A_{2A}R$		$A_{2B}R$	
			pEC_{50}[b]	E_{max}[c]	pEC_{50}[b]	E_{max}[c]	pEC_{50}[b]	E_{max}[c]
NECA	-CONHEt	$-NH_2$	6.0 ± 0.1	100 ± 2.4	6.47 ± 0.2	100 ± 2.0*	4.83 ± 0.1	100 ± 3.8
Adenosine	$-CH_2OH$	$-NH_2$	5.6 ± 0.1*	91.4 ± 2.8	5.24 ± 0.8	65.9 ± 1.7**	4.29 ± 0.1	70.4 ± 2.9**
CCPA	-	-	6.7 ± 0.1***	80.9 ± 2.2	5.00 ± 0.2	74.7 ± 4.9	4.14 ± 0.1	30.6 ± 2.0***
CGS-21680	-	-	3.2 ± 0.1***	91.3 ± 14.1	4.70 ± 0.1*	121.7 ± 4.1	2.20 ± 0.6***	59.1 ± 2.8***
5	$-CH_2OH$		4.8 ± 0.1***	98.5 ± 4.1	N.R.[d]		N.R.	
6	$-CH_2OH$		5.8 ± 0.1	89.8 ± 1.8	N.R.		N.R.	
7	$-CH_2OH$		6.2 ± 0.1	83.7 ± 4.4	N.R.		N.R.	
9	$-CH_2OH$		N.D.[e]		N.R.		N.R.	
16	-CONHEt		5.4 ± 0.0***	104.4 ± 1.3	N.R.		N.R.	
17	-CONHEt		4.0 ± 0.1***	100 ± 23.7	N.R.		N.R.	
18	-CONHEt		4.8 ± 0.0***	107.7 ± 3.0	N.R.		N.R.	
19	-CONHEt		N.D.		N.R.		N.R.	
20	-CONHEt		6.0 ± 0.1	99.3 ± 0.3	4.8 ± 0.3*	115.0 ± 13.0	3.9 ± 0.3	32.2 ± 11.4***
21	-CONHEt		6.5 ± 0.1**	99.0 ± 2.8	5.24 ± 0.3	77.7 ± 4.6	3.48 ± 0.3*	49.2 ± 0.4***
24	-CONHEt		N.R.		N.R.		N.R.	
25	-CONHEt		N.R.		N.R.		N.R.	
34			N.R.		N.D.		N.R.	
35			N.R.		N.R.		N.R.	
36			N.R.		N.R.		N.R.	
37			N.R.		N.R.		N.R.	

DOI: 10.1021/acs.jmedchem.5b01402
J. Med. Chem. 2016, 59, 947−964

Table 1. continued

[a]A_1R and A_2R receptors in GPA1/Gα_{i1} and GPA1/Gα_s yeast transplants, respectively. Values are the mean ± SEM from 5 to 8 independent repeats. Statistical significance compared to that of NECA (*, $p < 0.05$; **, $p < 0.01$; ***, $p < 0.001$) was determined by one-way ANOVA with Dunnett's post-test. [b]Negative logarithm of the agonist concentration required to induce a half-maximal response. [c]The maximal response to a ligand expressed as a percentage of that obtained for NECA. [d]N.R., no response. [e]N.D., not determined. Full dose−response curve was not feasible.

Table 2. Ligand Affinity (pK_A) and Efficacy ($\log \tau$) of Reference Compounds and Synthetic Adenosine Derivatives at A_1R, $A_{2A}R$, and $A_{2B}R$ expressed in Yeast[a]

	A_1R		$A_{2A}R$		$A_{2B}R$	
compd	pK_A[b]	$\log \tau$[c]	pK_A[b]	$\log \tau$[c]	pK_A[b]	$\log \tau$[c]
NECA	4.4 ± 0.1	1.5 ± 0.1	5.9 ± 0.2	0.5 ± 0.1	4.2 ± 0.1	0.6 ± 0.1
adenosine	4.6 ± 0.2	0.9 ± 0.1	5.6 ± 0.2	0.0 ± 0.3	3.8 ± 0.1	0.3 ± 0.1
CCPA	6.1 ± 0.1	0.6 ± 0.1	4.7 ± 0.3	−0.1 ± 0.1	4.4 ± 0.1	3.5 ± 0.1***
CGS-21680	2.1 ± 0.9*	1.1 ± 0.9	4.9 ± 0.1	−0.3 ± 0.0	3.4 ± 0.1	−0.2 ± 0.0
5	3.0 ± 1.1	1.8 ± 1.1	N.R.[d]		N.R.	
6	4.9 ± 0.1	0.5 ± 0.1	N.R.		N.R.	
7	5.5 ± 0.1	0.7 ± 0.1	N.R.		N.R.	
9	N.R.		N.R.		N.R.	
16	4.2 ± 0.3	1.2 ± 0.3	N.R.		N.R.	
17	3.5 ± 0.1	1.0 ± 0.1	N.R.		N.R.	
18	2.4 ± 0.1*	2.4 ± 0.0	N.R.		N.R.	
19	N.R.		N.R.		N.R.	
20	4.3 ± 0.5	1.6 ± 0.5	3.9 ± 0.7**	0.5 ± 0.5	3.5 ± 0.6	0.1 ± 0.5
21	4.8 ± 0.5	1.6 ± 0.5	4.6 ± 0.4	0.3 ± 0.1	4.2 ± 0.1	−0.2 ± 0.1
24	N.R.		N.R.		N.R.	
25	N.R.		N.R.		N.R.	
34	N.R.		N.D.[e]		N.R.	
35	N.R.		N.R.		N.R.	
36	N.R.		N.R.		N.R.	
37	N.R.		N.R.		N.R.	

[a]A_1R and A_2R in GPA1/Gα_{i1} and GPA1/Gα_s yeast transplants, respectively. Values are the mean ± SEM from 5 to 8 independent repeats. Statistical significance compared to that of NECA (*, $p < 0.05$; **, $p < 0.01$; ***, $p < 0.001$) was determined by one-way ANOVA with Dunnett's post-test. [b]Negative logarithm of the relative equilibrium disassociation constant for each compound generated through use of the operational model of agonism.[36] [c]The coupling efficiency parameter (τ), generated by comparison to NECA. [d]N.R., no response. [e]N.D., not determined. The full dose−response curve was not feasible.

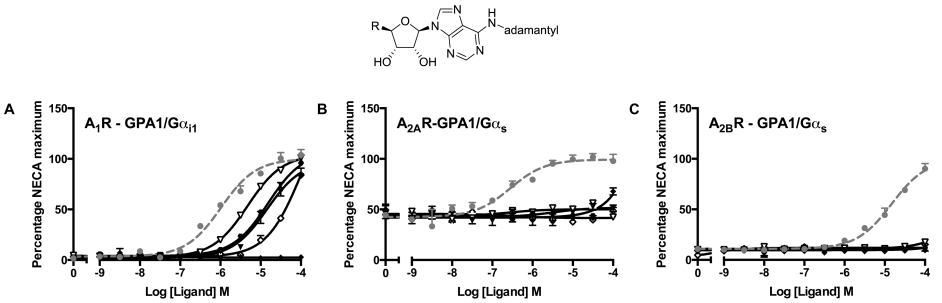

Figure 3. N^6-Adamantyl derivative selectivity at the human A_1R. Yeast strains expressing (A) A_1R, (B) $A_{2A}R$, and (C) $A_{2B}R$ were stimulated with N^6-adamantyl derivatives (▼) **5**, (▽) **16**, (◇) **17**, (●) **18**, and (◆) **34** for 16 h and reporter gene activity determined. Data are expressed as the percentage of the maximum response achieved when cells were stimulated with the reference agonist NECA (gray dotted line). All data are the mean of 5−8 independent experiments ± SEM.

or higher potency, respectively, than the parent compound NECA at the A_1R. However, in contrast to the N^6-cyclopentyl adenosine derivatives **6** and **7**, N^6-cyclopentyl NECA derivatives **20** and **21** are nonselective and signal through the A_1R, $A_{2A}R$, and $A_{2B}R$ (Table 1). Calculation of selectivity factors confirm that **21** preferentially signals $A_1R > A_{2B}R > A_{2A}R$.

As described above, the N^6-adamantyl derivatives only induced a detectable response in A_1R-expressing yeast strains, suggesting that bulky N^6-substituents promote total A_1R/A_2R selectivity. To explore this further, we created a series of ligands containing an N^6-azabicyclo (granatane) moiety. Compounds **9**, **19**, **24**, and **25** were screened for activity; however, no significant response was detected for these compounds via the

DOI: 10.1021/acs.jmedchem.5b01402
J. Med. Chem. 2016, 59, 947−964

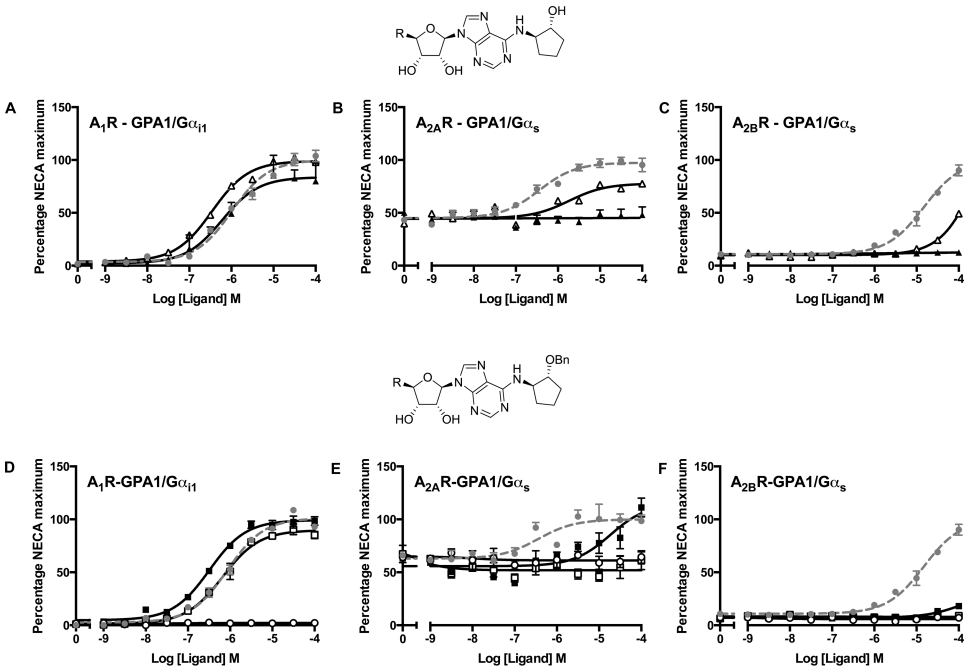

Figure 4. N^6-(2-Hydroxy)cyclopentyl derivatives of both adenosine and NECA display bias toward the A_1 receptor. Yeast strains expressing the A_1R (A and D), the $A_{2A}R$ (B and E), and the $A_{2B}R$ (C and F) were stimulated for 16 h with N^6-(2-hydroxy)cyclopentyl derivatives (▲) **7** and (Δ) **21** or N^6-(2-benzyloxy)cyclopentyl derivatives (□) **6**, (■) **20**, and (○) **36** and assayed for activation of the *FUS1> lacZ* reporter gene. Data are expressed as the percentage of the maximum response achieved when cells were stimulated with the reference agonist NECA (gray dotted line). Data are the mean of at least five independent experiments ± SEM.

A_1R, $A_{2A}R$, or $A_{2B}R$ ($p > 0.05$, one-way ANOVA). Some minimal response was observed for **9** and **19** at very high concentration (100 μM), but it was not feasible to generate full dose−response curves (Table 1).

Replacement of the 5′-ethyl carboxamide or 5′-hydroxy group with a 2-fluorothiophenyl moiety, as in adenosine analogues **34**−**37**, resulted in compounds that failed to produce any detectable response in the A_1R, $A_{2A}R$, and $A_{2B}R$ strains (Table 1). In fact, **34** was only able to activate the $A_{2A}R$ but at concentrations of greater than 100 μM. These results were somewhat surprising since the N^6-hydroxycyclopentyl congener **37** (CVT-3619, later named GS 9667) has previously been described as a selective, partial agonist of the A_1R, with reported K_i values of 113 nM and 1.1 μM when challenged with the antagonist [^{3}H]CPX, binding in hA_1R-expressing DDT$_1$MF-2, and CHO cells, respectively.[14] To determine if the lack of functional activity for **34**, **36**, and **37** in our yeast assays resulted from the compounds failing to cross the membrane, we performed a competition assay between **34**, **36**, and **37** and either NECA, adenosine, or CCPA at the A_1R (Figure S2).

In line with the previously reported data,[14] we confirmed **37** does appear to compete with all three ligands at the A_1R (pA_2 = 5.3 ± 0.4). Interestingly, despite the fact that **37** interacts with the A_1R, in our experimental system, it appears unable to induce a measurable response. It is worth noting that, A_1R agonist activity of **37** (CVT-3619) was previously demonstrated in rat adipocytes where it reduced cAMP content and consequently lipolysis,[14] although it is entirely possible that the observed response in these cell lines resulted from "off-target activation" of other receptors. Despite entering clinical trials where it was evaluated for its efficacy to lower lipids and thus improve glycemia, CVT-3619 (**37**) showed inadequate pharmacokinetics, and it was discontinued.[39] Furthermore, some recent studies suggest that the A_1R may not play a significant role in hepatic regulation of lipid metabolism.[40] Similar to **37**, close analogue **36** also acted as a competitive antagonist at A_1R (pA_2 = 6.4 ± 0.2, Figure S2), but **34** did not appear to bind to the A_1R at all.

Determining A_1R versus A_3R Selectivity in Mammalian Cells. Traditionally, many compounds that display selectivity for the A_1R compared to the A_2Rs frequently also display activity to the A_3R. However, as described previously, we were unable to obtain functional coupling of the A_3R to the yeast pheromone−response pathway (Figure S1). Thus, to provide a complete characterization of the A_1R-selective compounds isolated in the yeast screen, we utilized mammalian CHO-K1 cells transiently transfected with either the A_1R or the A_3R. CHO-K1 are an established cell line frequently used to assay the activity of adenosine receptors.[41,42] Both the A_1R and the A_3R couple to the inhibitory G protein family ($G\alpha_i$), thereby reducing the cellular concentration of cAMP.

DOI: 10.1021/acs.jmedchem.5b01402
J. Med. Chem. 2016, 59, 947−964

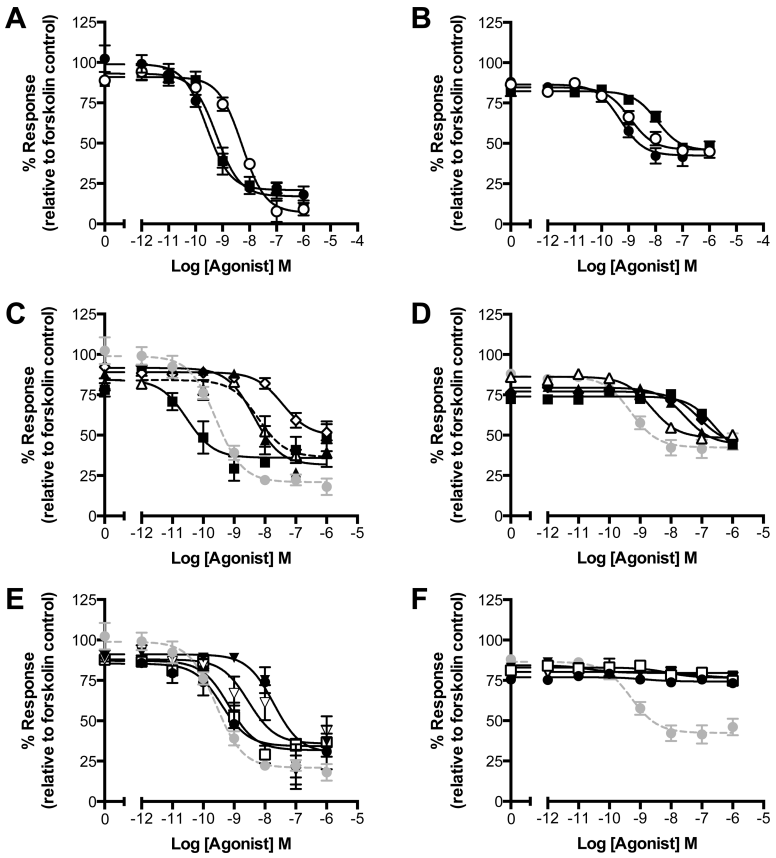

Figure 5. Determining the A_1R-selectivity of compounds isolated in the yeast screen against the A_1R and A_3R expressed in mammalian cells. CHO-K1 cells transiently transfected with A_1R (A, C, and E) or A_3R (B, D, and F) were stimulated with (●) NECA, (○) adenosine, (■) CCPA (A and B), or the compounds determined to be active at the A_1R from the yeast screen (▲) **7**, (◇) **17**, (■) **20**, (Δ) **21** (C and D) (▼) **5**, (□) **6**, (▽) **16**, and (●) **18** (E and F). In panels (C−F), the NECA dose-inhibition curve is shown as a gray dashed line with gray symbols. All cells were assayed for the inhibition of 10 μM forskolin-stimulated cAMP. Data are expressed as the percentage of the maximum response achieved when cells were stimulated with 10 μM forskolin. Data are the mean of 4−8 independent repeats ± SEM.

Using CHO-A_1R cells (CHO-K1 cells expressing the A_1R), we first confirmed that NECA, adenosine, and CCPA were able to inhibit forskolin-stimulated cAMP production (Figure 5A) generating pIC_{50} values (Table 3) equivalent to those previously reported.[41,42] Further, all compounds (**5**, **6**, **7**, **16**, **17**, **18**, **20**, and **21**) identified in yeast as eliciting a functional A_1R response displayed full agonist activity against the A_1R in the mammalian cells but with varying potencies (Figure 5B and Table 3). Significantly, when these compounds were assayed against the CHO-A_3R cells (Figure 5C and D, and Table 3), only **7**, **17**, **20**, and **21** were able to inhibit forskolin-stimulated cAMP production. Thus, taken together these data suggest that, at concentrations ≤1 μM, **5**, **6**, **16**, and **18** display A_1R-selectivity. Intriguingly, 2-adamantyl derivative **18** is almost as potent an agonist of A_1R as NECA but completely A_1R-selective.

Molecular Simulation of Agonist Docking into the A_1R. On the basis of the pharmacological experimental findings that most of our N^6-substituted 5′-*N*-ethylcarboxamido and 5′-hydroxymethyl derivatives activated the A_1R but that all of the 5′-(2-fluoro)thiophenyl derivatives failed to do so, we used a molecular modeling approach to dock all our synthetic adenosine derivatives into a homology model of the human A_1R. The recently solved crystal structure of the human A_{2A}R complexed with the agonist UK-432097 (PDB ID: 3QAK)[43] served as the template for this homology model. We reasoned that the bound agonist UK-432097 has a large N^6-substituent (Figure 6A) as is the case for our synthetic adenosine analogues.

In order to validate the utility of this A_{2A}R crystal structure as a template for generating the A_1R homology model, we docked compounds **20**, **21**, and **34**, which also showed activity at the A_{2A}R in our assays, into the A_{2A}R crystal structure. Indeed, the

DOI: 10.1021/acs.jmedchem.5b01402
J. Med. Chem. 2016, 59, 947−964

Table 3. Potency (pIC_{50}) and Response Range of Reference Ligands and Putative A_1R Selective Compounds at the A_1R and A_3R As Measured in Transfected CHO-K1 Cells[a]

	A_1R			A_3R		
compd	pIC_{50}[b]	response range[c]	n	pIC_{50}[b]	response range[c]	n
NECA	9.68 ± 0.16	−73.4 ± 5.8	6	9.31 ± 0.17	−44.1 ± 3.0	8
adenosine	8.63 ± 0.11*	−66.4 ± 3.7	6	8.94 ± 0.14	−38.7 ± 2.4	5
CCPA	9.30 ± 0.15	−71.4 ± 4.3	6	7.95 ± 0.13**	−46.6 ± 4.8	8
5	7.72 ± 0.20**	−61.0 ± 6.1	5	N.R.	N.R.	8
6	9.17 ± 0.15	−55.28 ± 3.6	4	N.R.	N.R.	6
7	8.36 ± 0.17*	−60.0 ± 4.4*	6	7.56 ± 0.11**	−35.1 ± 2.2	5
16	8.54 ± 0.3*	−52.15 ± 6.0*	6	N.R.	N.R.	6
17	7.43 ± 0.19	−39.3 ± 3.9**	4	7.1 ± 0.12**	−32.7 ± 2.2*	6
18	9.40 ± 0.34	−51.07 ± 7.9	6	N.R.	N.R.	6
20	10.53 ± 0.28*	−48.35 ± 5.6*	4	6.57 ± 0.15***	−38.0 ± 4.0	5
21	8.21 ± 0.2*	−47.67 ± 4.3*	4	8.64 ± 0.08	−37.9 ± 1.2	5

[a]Data are the mean ± SEM of *n* individual sets. Statistical significance compared to that of NECA (*, $p < 0.05$; **, $p < 0.01$; ***, $p < 0.001$) was determined by one-way ANOVA with Dunnett's post-test. [b]The negative logarithm of the agonist concentration required to produce a half-maximal response. [c]The response range of the agonists expressed as a percentage of total forskolin range (0−100%).

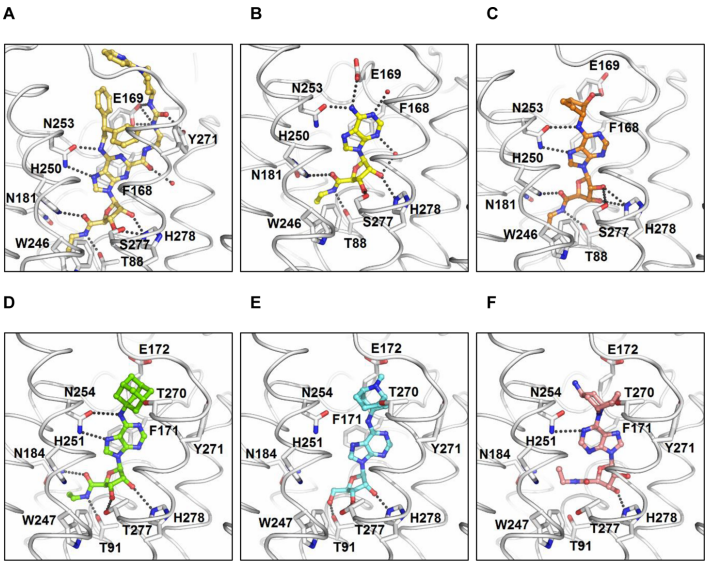

Figure 6. Docking of N^6-substituted adenosine derivatives into an A_1R homology model. (A) Crystal structures of human $A_{2A}R$ bound with agonist UK-432097 (gold, PDB ID: 3QAK) and (B) with agonist NECA (yellow, PDB ID: 2YDV) for comparison, indication key binding residues and interactions. Representative examples of proposed binding poses of N^6-substituted adenosine derivatives in the $A_{2A}R$ crystal structure and in the A_1R homology model. (C) **21** (orange) docked into $A_{2A}R$ crystal structure. (D) **16** (light green), (E) **9** (light blue) and (F) **24** (pink) docked into A_1R homology model. Black dotted lines represent potential hydrogen bonds. Numbering of residues in (A-C) according to P29274 ($hA_{2A}R$) and of homologous residues in (D-F) according to P30542 (hA_1R). Ballesteros-Weinstein (BW) numbering: T88 (A_{2A}), T91 (A_1): BW 3.36; F168 (A_{2A}), F171 (A_1): BW ECL2; E169 (A_{2A}), E172 (A_1): BW ECL2; N181 (A_{2A}), N184 (A_1): BW 5.42; W246 (A_{2A}), W247 (A_1): BW 6.48; H250 (A_{2A}), H251 (A_1): BW 6.52; N253 (A_{2A}), N254 (A_1): BW 6.55; T270 (A_1): BW 7.35; Y271 (A_{2A}), Y271 (A_1): BW 7.36; S277 (A_{2A}), T277 (A_1): BW 7.42; H278 (A_{2A}), H278 (A_1): BW 7.43. For activities of docked compounds see Table 1. Proposed binding poses for the remaining compounds are shown in (Figure S3).

proposed positions and side chain interactions for these compounds (Figure 6C and Figures S3A and S3B) are very similar to those of known agonists bound to the $A_{2A}R$ (Figure 6A and B).

Furthermore, after closely inspecting the crystal structures of the adenosine-, NECA- (Figure 6B), and UK-432097-bound (Figure 6A) human $A_{2A}R$ (PDB IDs: 2YDO, 2YDV, and 3QAK, respectively),[43,44] we would argue that hydrogen bond formation between the ligand and the homologous Thr-91$^{3.36}$, Asn-254$^{6.55}$, Thr-277$^{7.42}$, and His-278$^{7.43}$ (superscript: Ballesteros−Weinstein numbering[45]) in the A_1R is important to stabilize the active conformation of the receptor.[43,44] These residues are highly conserved across the AR family. Taking this into consideration (for details, see Experimental Section), the

DOI: 10.1021/acs.jmedchem.5b01402
J. Med. Chem. 2016, 59, 947−964

docking yielded ligand orientations for **5**-**7**, **16**-**18**, **20**, and **21** (Figure 6D and Figure S3C–I) that closely resemble the orientations of UK-432097- and NECA-bound to the human $A_{2A}R$ (Figure 6A and B). In this distinct position, the ribose moiety binds deeply into the binding pocket potentially forming hydrogen bonds with Thr-91$^{3.36}$, Asn-184$^{5.42}$, Thr-277$^{7.42}$, and His-278$^{7.43}$. The purine ring π-stacks against Phe-171^{ECL2} and can form hydrogen bonds with Asn-254$^{6.55}$, whereas the bulky N^6-substitutes are located near the exit of the binding pocket. We found experimentally that all of these compounds were agonists at the A_1R in our yeast-based functional assay. Intriguingly, **6** and **20** were docked before they were tested and based on our model predicted to be active agonists, which indeed was the case.

The predicted binding positions for granatane derivatives **9** and **19** are somewhat similar; however, the purine ring is further away from Asn-254$^{6.55}$ so that no hydrogen bonds are suggested (Figure 6E and Figure S3J). At very high concentration, **9** and **19** were able to partially activate the A_1R, but it was experimentally not possible to obtain full dose–response curves.

Docking of both inactive compounds **24** and **34** yielded binding positions where the purine ring adopts a *syn*-conformation with respect to the ribose (Figure 6F and Figure S3K). It is also noticeable that **24** is not in close contact with Trp-247$^{6.48}$, a residue which is highly conserved across the AR family and in a recent molecular dynamics simulation was shown to act as a conformational toggle switch in the receptor activation mechanism.[46] The docking simulations with adenosine derivatives **25** and **35**–**37**, all of which failed to activate the A_1R, did not return any binding positions for our model.

CONCLUSIONS

Herein, we report the synthesis of a series of adenosine derivatives that were modified at the N^6-position of the purine ring and the C-5′ positions of the ribose moiety. These compounds were evaluated using a yeast-based and mammalian cell-based assay for quantifying their AR subtype selectivity. Our biological data show that compounds bearing a granatane azabicyclic moiety at N^6 and/or a 5′-(2-fluorothiophenyl) substituent at the ribose fail to produce responses in A_1R, $A_{2A}R$ or $A_{2B}R$ cells. Conversely, N^6-adamantyl adenosine and NECA congeners were completely A_1R selective. Moreover, it emerged that N^6-(2-hydroxy)cyclopentyl and N^6-(2-benzyloxy)-cyclopentyl derivatives are potent agonists, preferentially activating A_1R over the other subtypes. It is worth noting that novel NECA derivative **20** exhibited higher potency and A_1R selectivity than its parent compound. Further, we present an A_1R homology model that corroborates our experimental findings. Notably, adenosine derivatives **5** and **6** and novel NECA analogues **16** and **18** are completely A_1R-selective, potent agonists. Therefore, they should represent useful tool compounds in purinergic signaling research and warrant further assessment of their therapeutic potential.

EXPERIMENTAL SECTION

General Chemistry. All reactions were performed under an inert argon atmosphere. Anhydrous tetrahydrofuran (THF), toluene, and dichloromethane (DCM) were obtained by filtration through a system of alumina columns under a positive pressure of argon. Anhydrous dimethylformamide (DMF) was purchased as dry over molecular sieves from Sigma-Aldrich. Solvents were evaporated under reduced pressure at approximately 45 °C using a Buchi Rotavapor or under high vacuum on a Schlenk line. Reagents were purchased from Sigma-Aldrich, Acros, Alfa Aesar, Fischer Scientific, or Hänseler and used without further purification. Reactions were monitored by thin layer chromatography (TLC) using aluminum sheets precoated with silica (Macherey-Nagel ALUGRAM Xtra SII, G/UV_{254}). Detection was under UV light source (λ_{max} 254 nm) or through staining with potassium permanganate solution (5%), vanillin spray, or ninhydrin, with subsequent heating. Flash column chromatography was carried out using silica gel from Sigma-Aldrich (pore size 60 Å, 230–400 mesh particle size) as the stationary phase.

Proton nuclear magnetic resonance spectra (^{1}H NMR) were recorded using a Bruker Avance 300 or an Avance II 400 spectrometer. Chemical shifts (δ_H) are reported in parts per million (ppm) and are referenced to the residual solvent peak. The order of citation in parentheses is (1) number of equivalent nuclei (by integration), (2) multiplicity, s (singlet), d (doublet), t (triplet), q (quartet), quint (quintet), m (multiplet) etc., (3) coupling constants (J) in Hertz (Hz), and (4) assignment. Carbon nuclear magnetic resonance spectra (^{13}C NMR) were recorded using a Bruker Avance 300 or an Avance II 400 spectrometer. Chemical shifts are quoted in parts per million (ppm) and are referenced to the residual solvent peak. The assignment is quoted in parentheses. COSY, HSQC, and DEPT were routinely used to assign peaks in ^{1}H and ^{13}C NMR spectra. Addition of D_2O was used to confirm the assignment of OH and NH peaks. Mass spectra and high resolution mass spectra (HRMS) were recorded on a ThermoScientific LTQ Orbitrap XL spectrometer consisting of a linear ion trap (LTQ) featuring a HCD collision cell, coupled to the Orbitrap mass analyzer, equipped with a nanoelectrospray ion source (NSI). MS and HRMS spectra were determined by the Mass Spectrometry Group at the Department of Chemistry and Biochemistry, University of Bern (PD Dr. S. Schürch).

The purity of the compounds was determined with UPLC-MS on a *Dionex* Ultimate 3000 using a reversed-phase column *Dionex* Acclain RSLC, 120C18, 3 × 50 mm, 2.2 μm, 120 Å pore size, flow 1.2 mL/min. The gradient used was 100%A to 100%D over 7 min, with A (water with 0.1% TFA) and D (10% H_2O/90% ACN+0.1% TFA). Purity was determined by total absorbance at 254 nm. All tested compounds were ≥95% pure, except **17** which was 94% pure.

Established Adenosine Agonists. 5′-*N*-Ethylcarboxamidoadenosine (NECA), 2-chloro-N^6-cyclopentyladenosine (CCPA), CGS-21680, 8-cyclopentyl-1,3-dipropylxanthine (DPCPX), and SLV-320 were purchased from R & D Systems (Bristol, UK). Where possible, compounds were prepared as 10 mM stocks in DMSO.

Chemical Synthesis. Intermediates **2**,[29] **10**,[32] **26**,[32] and **27**[34] were synthesized as described in the literature with only slight experimental modifications. (3-*endo*)-9-Methyl-9-azabicyclo[3.3.1]nonan-3-amine was synthesized as described previously by our group.[30] *tert*-Butyl-9-azabicyclo[3.3.1]nonan-3-ylcarbamate (**22**) was synthesized as described previously.[33] Intermediate **29**[47] is known but was obtained with different methodology. Intermediate **28** is a novel compound. Further details on the synthesis and characterization of these intermediates are available in the Supporting Information. 3-Amino-1-adamantanol and (1*R*,2*R*)-2-aminocyclopentanol hydrochloride were prepared as described in the Supporting Information.

*General Procedure A for the Synthesis of Intermediates **3**, **4**, **8**, **11**–**15**, **23**, and **30**–**33**.* The appropriate chloride was dissolved in ethanol (20 mL/mmol). The amine and triethylamine or DIPEA were then added, and the reaction mixture was refluxed until TLC analysis indicated completion. The solvent was removed in vacuo, and the resultant material was purified with column chromatography. The choice of base did not appear to have an effect on the yield or reaction time. In the case of compounds **4**, **8**, **13**–**15**, and **31**–**33**, the reaction was complete after 18 h, whereas sterically hindered **3**, **11**, **12**, **23**, and **30** required 5 days of refluxing at 120 °C to obtain sufficient amounts of product. In cases where the amine is a hydrochloride salt, this was first stirred for 20 min with the base, before the addition of the appropriate chloride in ethanol. For specific purification conditions, see individual compounds.

DOI: 10.1021/acs.jmedchem.5b01402
J. Med. Chem. 2016, 59, 947–964

*General Procedure B for the Synthesis of Compounds **16**–**20**, **24**, and **34**–**37**.* Acetonide protected compounds **11**–**15**, **23**, or **30**–**33** were dissolved in water and acetic acid and stirred at 80 °C overnight. The water was removed in vacuo, and the resultant crude material was purified with column chromatography.

*General Procedure C for the Synthesis of Compounds **7** and **21**.* Benzyl protected compounds **4** and **20** were dissolved in ethanol (8 mL/mmol). Cyclohexene and $Pd(OH)_2/C$ were added and refluxed at 100 °C until TLC indicated completion. The reaction mixture was allowed to cool to room temperature and filtered through Celite. The crude material was purified with column chromatography.

*General Procedure D for the Synthesis of Compounds **5**, **6** and **9**.* Acetyl protected compounds **3**, **4**, and **8** were dissolved in methanol (20 mL/mmol). Potassium carbonate was added and stirred vigorously for 3 h. The solvent was removed in vacuo, and the crude material was purified with column chromatography.

*6-N-(1-Adamantyl)-5′-O-acetyladenosine (**3**).* Compound**3** was synthesized according to general procedure A, using chloride **2** (0.2 g, 0.48 mmol), amantadine hydrochloride (0.14 g, 0.72 mmol), and DIPEA (0.84 mL, 4.80 mmol). After purification with column chromatography (methanol/DCM, 2–6%), monoacetylated **3** was obtained as a white solid as the major product (0.13 g, 62% yield). ^{1}H NMR (300 MHz, DMSO-d_6) δ 8.31 (1H, s, adenine H), 8.22 (1H, s, adenine H), 6.61 (1H, s, NH), 5.89 (1H, d, *J* 5.1, 1′-H), 5.56 (1H, d, *J* 5.7, 2′–OH), 5.37 (1H, d, *J* 5.4, 3′–OH), 4.67 (1H, dd, *J* 10.5, 5.2, 2′-H), 4.32 (1H, dd, *J* 11.8, 3.7, 5′-H*H*), 4.26 (1H, dd, *J* 10.5, 5.4, 3′-H), 4.16 (1H, dd, *J* 11.8, 6.1, 5′-*H*H), 4.07 (1H, m, 4′-H), 2.21 (6H, m, 6 × adamantyl H), 2.08 (3H, m, 3 × adamantyl H), 2.00 (3H, s, CH_3), 1.68 (6H, m, 6 × adamantyl H); ^{13}C NMR (100 MHz, DMSO-d_6) δ 170.1, 154.4, 151.9, 148.4, 139.5, 119.9, 87.9, 81.5, 72.8, 70.3, 63.9, 52.1, 41.0, 36.0, 29.0, 20.6; HRMS (ESI$^+$) *m*/*z* calcd for $C_{22}H_{30}N_5O_5$ $[MH]^+$ 444.2241, found 444.2229; purity UPLC-MS 99%, retention time = 2.92 min.

*6-N-((1R,2R)-2-(Benzyloxy)cyclopentyl)-5′-O-acetyladenosine (**4**).* Compound **4** was synthesized according to general procedure A, using chloride **2** (0.20 g, 0.48 mmol), (1*R*,2*R*)-1-amino-2-benzyloxycyclopentane (0.13 mL, 0.72 mmol), and triethylamine (0.19 mL, 1.34 mmol). After purification with column chromatography (methanol/DCM, 1–4%), monoacetylated product **4** was obtained as a pale yellow solid as the major product (0.12 g, 52% yield). ^{1}H NMR (300 MHz, DMSO-d_6) δ 8.34 (1H, s, adenine H), 8.25 (1H, br s, adenine H), 7.90 (1H, m, NH), 7.33–7.18 (5H, m, 5 × phenyl H), 5.93 (1H, d, *J* 5.1, 1′-H), 5.57 (1H, d, *J* 5.7, 2′–OH), 5.37 (1H, d, *J* 5.3, 3′–OH), 4.68 (1H, dd, *J* 10.4, 5.1, 2′-H), 4.63–4.51 (3H, m, *CH*$_2$Ph and 1-H), 4.33 (1H, dd, *J* 11.8, 3.6, 5′-*H*H), 4.27 (1H, dd, *J* 10.4, 5.3, 3′-H), 4.18 (1H, dd, *J* 11.8, 6.2, 5′-H*H*), 4.09 (1H, m, 4′-H), 4.01 (1H, m, 2-H), 2.13–1.90 (5H, m, 2 × cyclopentyl H and CH_3), 1.80–1.55 (4H, m, 4 × cyclopentyl H); ^{13}C NMR (100 MHz, DMSO-d_6) δ 170.1, 154.2, 152.5, 139.4, 138.9, 128.1, 127.3, 127.1, 114.5, 87.8, 84.1, 81.5, 72.9, 70.3, 70.1, 63.9, 56.4, 30.2, 21.4, 20.6; HRMS (ESI) calcd for $C_{24}H_{30}O_5N_6$ $[MH]^+$ 484.2191, found 484.2172; purity UPLC-MS 99%, retention time = 2.55 min.

*6-N-(1-Adamantyl)adenosine (**5**).*[48] Compound **5** was synthesized according to general procedure D, using **3** (0.03 g, 0.06 mmol) and potassium carbonate (0.005 g, 0.04 mmol). After purification with column chromatography (methanol/DCM, 4%), product **5** was obtained as a white solid (0.03 g, 99% yield). ^{1}H NMR (300 MHz, DMSO-d_6) δ 8.35 (1H, s, adenine H), 8.21 (1H, s, adenine H), 6.65 (1H, s, NH), 5.87 (1H, d, *J* 6.1, 1′-H), 5.44 (1H, d, *J* 6.1, 2′–OH), 5.37 (1H, dd, *J* 7.1, 4.6, 5′–OH), 5.19 (1H, d, *J* 4.6, 3′–OH), 4.62 (1H, dd, *J* 11.1, 6.1, 2′-H), 4.15 (1H, m, 3′-H), 3.97 (1H, m, 4′-H), 3.69 (1H, m, 5′-H*H*), 3.55 (1H, m, 5′*H*H), 2.23 (6H, m, 6 × adamantyl H), 2.10 (3H, m, 3 × adamantyl H), 1.69 (6H, m, 6 × adamantyl H); ^{13}C NMR (100 MHz, DMSO-d_6) δ 154.5, 151.6, 148.2, 139.6, 120.1, 88.0, 85.8, 73.4, 70.6, 61.6, 52.2, 41.0, 36.0, 29.0; HRMS (ESI$^+$) *m*/*z* calcd for $C_{20}H_{28}N_5O_4$ $[MH]^+$ 402.2136, found 402.2137; purity UPLC 99%, retention time = 2.66 min.

*6-N-((1R,2R)-2-(Benzyloxy)cyclopentyl)adenosine (**6**).*[49] Compound **6** was synthesized according to general procedure D, using **4** (0.01 g, 0.02 mmol) and potassium carbonate (0.01 g, 0.07 mmol). After purification with column chromatography (methanol/DCM, 2–3%), product **6** was obtained as a white solid (0.01 g, 99% yield). ^{1}H NMR (300 MHz, DMSO-d_6) δ 8.37 (1H, s, adenine H), 8.24 (1H, br s, adenine H), 7.94 (1H, m, NH), 7.33–7.19 (5H, m, 5 × phenyl H), 5.89 (1H, d, *J* 6.1, 1′-H), 5.46–5.37 (2H, m, 2′–OH and 5′–OH), 5.19 (1H, d, *J* 4.6, 3′–OH), 4.68–4.50 (4H, m, 1-H, 2′-H and *CH*$_2$Ph), 4.15 (1H, dd, *J* 7.8, 4.6, 3′-H), 4.05–3.94 (2H, m, 2-H and 4′-H), 3.68 (1H, dt, *J* 12.0, 4.1, 5′-*H*H), 3.56 (1H, m, 5′-H*H*), 2.14–1.89 (2H, m, 2 × cyclopentyl H), 1.77–1.56 (4H, m, 4 × cyclopentyl H); ^{13}C NMR (100 MHz, DMSO-d_6) δ 154.2, 152.2, 139.6, 138.9, 128.1, 127.3, 127.1, 87.9, 85.8, 84.1, 73.5, 70.6, 70.1, 61.6, 30.1, 21.4; HRMS (ESI) calcd for $C_{22}H_{28}O_5N_5$ $[MH]^+$ 442.2085, found 442.2097; purity UPLC-MS 98%, retention time = 2.30 min.

*6-N-((1R,2R)-2-(Hydroxy)cyclopentyl)adenosine (**7**).*[28] Compound **7** was synthesized according to general procedure C, using **4** (0.03 g, 0.06 mmol), cyclohexene (0.25 mL, 2.43 mmol), and $Pd(OH)_2/C$ (20 wt %, 0.01 g). After purification with column chromatography (methanol/DCM, 2–8%), product **7** was obtained as a white solid (0.02 g, 95% yield). Minor quantities of the monoacetylated product were also isolated. ^{1}H NMR (300 MHz, DMSO-d_6) δ 8.37 (1H, s, adenine H), 8.20 (1H, br s, adenine H), 7.74 (1H, d, *J* 6.8, NH), 5.89 (1H, d, *J* 6.1, 1′-H), 5.48–5.36 (2H, m, 2′–OH and 5′–OH), 5.19 (1H, d, *J* 4.6, 3′–OH), 4.87 (1H, m, 2-OH), 4.62 (1H, app. dd, *J* 11.3, 6.1, 2′-H), 4.29 (1H, br s, 1-H), 4.15 (1H, m, 3′-H), 4.06 (1H, m, 2-H), 3.97 (1H, m, 4′-H), 3.68 (1H, dt, *J* 11.9, 3.9, 5′-*H*H), 3.55 (1H, m, 5′-H*H*), 2.07 (1H, m, 1 × cyclopentyl H), 1.88 (1H, m, 1 × cyclopentyl H), 1.74–1.59 (2H, m, 2 × cyclopentyl H), 1.59–1.45 (2H, m, 2 × cyclopentyl H); ^{13}C NMR (100 MHz, DMSO-d_6) δ 154.7, 152.2, 139.6, 87.9, 85.9, 76.0, 73.5, 70.6, 61.6, 58.8, 32.3; HRMS (ESI) calcd for $C_{15}H_{22}O_5N_5$ $[MH]^+$ 352.1615, found 352.1616; purity UPLC-MS 99%, retention time = 1.46 min.

*Tri-O-acetyl-6-N-[(3-endo)-9-methyl-9-azabicyclo[3.3.1]non-3-yl]adenosine (**8**).* Compound **8** was synthesized according to general procedure A, using chloride **2** (0.3 g, 0.73 mmol), (3-*endo*)-9-methyl-9-azabicyclo[3.3.1]nonan-3-amine (0.45 g, 2.91 mmol), and DIPEA (0.15 mL, 0.88 mmol). After purification with column chromatography (methanol/DCM, 5–10%), product **8** was obtained as a white solid (0.21 g, 54% yield). ^{1}H NMR (400 MHz, MeOD-d_4) δ 8.30 (1H, br s, adenine H), 8.25 (1H, s, adenine H), 6.24 (1H, d, *J* 5.3, 1′-H), 6.03 (1H, t, *J* 5.3, 2′-H), 5.73 (1H, dd, *J* 5.3, 4.8, 3′-H), 4.83 (1H, br s, 3-H), 4.49–4.37 (3H, m, 4′-H and 5′-H$_2$), 3.44–3.42 (2H, m, 1- and 5-H), 2.77 (3H, s, NCH_3), 2.70–2.61 (2H, m, 2 × granatyl H), 2.20–2.03 (12H, m, 3 × CH_3 and 3 × granatyl H), 1.77–1.61 (3H, m, 3 × granatyl H), 1.43–1.40 (2H, m, 2 × granatyl H); ^{13}C NMR (100 MHz, MeOD-d_4) δ 172.2, 171.4, 171.2, 155.6, 154.3, 140.9, 87.9, 81.6, 74.3, 72.0, 64.2, 54.0, 41.7, 40.0, 32.6, 25.7, 20.6, 20.4, 20.2, 14.0; HRMS (ESI$^+$) *m*/*z* calcd for $C_{25}H_{35}N_6O_7$ 531.2562 $[MH]^+$, found 531.2553; purity UPLC-MS 96%, retention time = 2.14 min.

*6-N-[(3-endo)-9-Methyl-9-azabicyclo[3.3.1]non-3-yl]adenosine (**9**).* Compound **9** was synthesized according to general procedure D, using **8** (0.05 g, 0.10 mmol) and potassium carbonate (0.005 g, 0.03 mmol). The crude product was dissolved in acetone and passed through filtered paper to give **9** as a white solid (0.04 g, 99% yield). ^{1}H NMR (300 MHz, MeOH-d_4) δ 8.24 (1H, s, adenine H), 8.21 (1H, br s, adenine H), 5.95 (1H, d, *J* 6.5, 1′-H), 4.77 (1H, br s overlapping, 3-H), 4.74 (1H, dd, *J* 6.4, 5.2, 2′-H), 4.32 (1H, dd, *J* 5.1, 2.5, 3′-H), 4.17 (1H, app q, *J* 2.4, 4′-H), 3.89 (1H, dd, *J* 12.6, 2.4, 5′-*H*H), 3.74 (1H, dd, *J* 12.6, 2.6, 5′-H*H*), 3.13–3.10 (2H, m, 1- and 5-H), 2.60–2.50 (5H, m, NCH_3 and 2 × granatyl H), 2.16–1.98 (3H, m, 3 × granatyl H), 1.58–1.45 (3H, m, 3 × granatyl H), 1.16–1.12 (2H, m, 2 × granatyl H); ^{13}C NMR (100 MHz, MeOH-d_4) δ 153.7, 141.4, 128.5, 91.4, 88.3, 75.5, 72.7, 63.6, 52.7, 42.7, 40.8, 33.4, 25.8, 15.0; HRMS (ESI) calcd for $C_{19}H_{29}O_4N_6$ $[MH]^+$ 405.2245, found 405.2243; purity UPLC-MS 99%, retention time = 1.41 min.

*6-N-(1-Adamantyl)-5′-ethylamino-2′,3′-O-isopropylidene-5′-oxo-5′-deoxyadenosine (**11**).* Compound **11** was synthesized according to general procedure A, using chloride **10** (0.3 g, 0.82 mmol), amantadine hydrochloride (0.46 g, 2.45 mmol), and DIPEA (2.61 mL, 15.01 mmol). After purification with column chromatography (methanol/DCM, 2%), product **11** was obtained as a white solid

DOI: 10.1021/acs.jmedchem.5b01402
J. Med. Chem. 2016, 59, 947–964

(0.28 g, 72% yield). ^{1}H NMR (300 MHz, DMSO-d_6) δ 8.27 (1H, s, adenine H), 8.17 (1H, s, adenine H), 7.51 (1H, t, J 5.6, amide NH), 6.62 (1H, s, amine NH), 6.34 (1H, d, J 1.5, 1′-H), 5.41 (1H, dd, J 6.1, 1.5, 2′-H), 5.38 (1H, dd, J 6.1, 1.8, 3′-H), 4.53 (1H, d, J 1.8, 4′-H), 2.80 (2H, m, CH_2CH_3), 2.21 (6H, m, 6 × adamantyl H), 2.09 (3H, m, 3 × adamantyl H), 1.68 (6H, m, 6 × adamantyl H), 1.54 (3H, s, CH_3), 1.35 (3H, s, CH_3), 0.62 (3H, t, J 7.2, CH_2CH_3); ^{13}C NMR (100 MHz, DMSO-d_6) δ 168.1, 154.4, 151.8, 148.0, 139.9, 119.6, 112.9, 89.5, 85.8, 83.2, 83.0, 52.1, 41.0, 36.0, 33.0, 29.0, 26.7, 25.0, 13.8; HRMS (ESI$^+$) m/z calcd for $C_{25}H_{35}N_6O_4$ $[MH]^+$ 483.2714, found 483.2718.

*6-N-(3-Hydroxy-1-adamantyl)-5′-ethylamino-2′,3′-O-isopropylidene-5′-oxo-5′-deoxyadenosine (**12**).* Compound **12** was synthesized according to general procedure A, using chloride **10** (0.07 g, 0.19 mmol), 3-amino-1-adamantanol (0.05 g, 0.29 mmol), and triethylamine (0.5 mL, 3.6 mmol). After purification with column chromatography (methanol/DCM, 2−5%), product **12** was obtained as a white solid (0.07 g, 78% yield). ^{1}H NMR (300 MHz, DMSO-d_6) δ 8.26 (1H, s, adenine H), 8.16 (1H, s, adenine H), 7.49 (1H, t, J 5.6, amide NH), 6.74 (1H, s, amine NH), 6.33 (1H, d, J 1.1, 1′-H), 5.43−5.35 (2H, m, 2′-H and 3′-H), 4.53 (2H, s, 4′-H and OH), 2.81 (2H, m, CH_2CH_3), 2.18−2.01 (8H, m, 8 × adamantyl H), 1.65−1.43 (9H, m, 6 × adamantyl H and CH_3), 1.34 (3H, s, CH_3), 0.62 (3H, t, J 7.2, CH_2CH_3); ^{13}C NMR (100 MHz, DMSO-d_6) δ 168.1, 154.3, 151.7, 148.1, 140.0, 119.6, 112.9, 89.5, 85.6, 83.2, 83.0, 67.5, 54.6, 48.9, 44.2, 34.9, 33.0, 30.1, 26.7, 25.0, 13.8; HRMS (ESI$^+$) m/z calcd for $C_{25}H_{35}N_6O_5$ 499.2663 $[MH]^+$, found 499.2650; purity UPLC-MS 99%, retention time = 2.62 min.

*6-N-(2-Adamantyl)-5′-ethylamino-2′,3′-O-isopropylidene-5′-oxo-5′-deoxyadenosine (**13**).* Compound **13** was synthesized according to general procedure A, using chloride **10** (0.02 g, 0.06 mmol), 2-adamantylamine hydrochloride (0.03 g, 0.18 mmol), and DIPEA (0.05 mL, 0.27 mmol). After purification with column chromatography (methanol/DCM, 2%), product **13** was obtained as a white solid (0.02 g, 69% yield). ^{1}H NMR (300 MHz, DMSO-d_6) δ 8.29 (1H, s, adenine H), 8.17 (1H, br s, adenine H), 7.48 (1H, t, J 5.7, amide NH), 7.05 (1H, br s, NH), 6.34 (1H, s, 1′-H), 5.45−5.36 (2H, m, 2′- and 3′-H), 4.53 (1H, s, 4′-H), 4.36 (1H, br s, adamantyl H), 2.80 (2H, m, CH_2CH_3), 2.11−2.05 (4H, m, 4 × adamantyl H), 1.84 (6H, m, 6 × adamantyl H), 1.72 (2H, m, 2 × adamantyl H), 1.53−1.50 (5H, m, 2 × adamantyl H and CH_3), 1.34 (3H, s, CH_3), 0.59 (3H, t, J 7.2, CH_2CH_3); ^{13}C NMR (100 MHz, DMSO-d_6) δ 168.1, 154.1, 152.3, 140.3, 112.9, 89.5, 85.9, 83.2, 83.1, 37.1, 36.9, 36.8, 33.0, 30.9, 26.7, 26.6, 25.0, 13.8; HRMS (ESI) calculated for $C_{25}H_{35}N_6O_4$ $[MH]^+$ 483.2714, found 483.2707; purity UPLC-MS 94%, retention time = 3.12 min.

*6-N-[(3-endo)-9-Methyl-9-azabicyclo[3.3.1]non-3-yl]-5′-ethylamino-2′,3′-O-isopropylidene-5′-oxo-5′-deoxyadenosine (**14**).* Compound **14** was synthesized according to general procedure A, using chloride **10** (0.1 g, 0.27 mmol), (3-*endo*)-9-methyl-9-azabicyclo[3.3.1]-nonan-3-amine (0.17 g, 1.09 mmol), and DIPEA (0.06 mL, 0.33 mmol). After purification with column chromatography (methanol/DCM, 5−10%), product **14** was obtained as a white solid (0.11 g, 85% yield). ^{1}H NMR (300 MHz, MeOD-d_4) δ 8.21 (2H, m, 2 × adenine H), 6.35 (1H, d, J 1.0, 1′-H), 5.63 (1H, dd, J 6.1, 1.8, 3′-H), 5.51 (1H, m, 2′-H), 4.77 (1H, br s, 3-H), 4.64 (1H, d, J 1.7, 4′-H), 3.27−3.23 (1H, m, 1- and 5-H), 2.85 (2H, m, CH_2CH_3), 2.67−2.50 (5H, m, NCH_3 and 2 × granatyl H), 2.20−2.00 (3H, m, 3 × granatyl H), 1.65−1.51 (6H, m, CH_3 and 3 × granatyl H), 1.42 (3H, s, CH_3) 1.34−1.19 (2H, m, 2 × granatyl H), 0.63 (3H, t, J 7.3, CH_2CH_3); ^{13}C NMR (75 MHz, $CDCl_3$) 171.6, 155.6, 154.1, 142.0, 114.9, 92.4, 88.7, 85.3, 85.2, 53.3, 42.2, 40.4, 34.7, 33.1, 27.1, 25.8, 25.3, 14.6, 14.0; HRMS calculated for $C_{24}H_{36}O_4N_7$ $[MH]^+$ 486.2823, found 486.2810; purity UPLC-MS 99%, retention time = 1.97 min.

*6-N-((1R,2R)-2-(Benzyloxy)cyclopentyl)-5′-ethylamino-2′,3′-O-isopropylidene-5′-oxo-5′-deoxyadenosine (**15**).* Compound **15** was synthesized according to general procedure A, using chloride **10** (0.2 g, 0.54 mmol), (1*R*,2*R*)-1-amino-2-benzyloxycyclopentane (0.15 mL, 0.82 mmol), and triethylamine (0.21 mL, 1.51 mmol). Following the removal of the solvent from the reaction mixture, the residue was dissolved in ethyl acetate (100 mL) and washed with water (2 × 50 mL). The organic phase was then dried over anhydrous Na_2SO_4, and the solvent was removed in vacuo. After purification with column chromatography (methanol/DCM, 1−3%), product **15** was obtained as a pale yellow solid (0.22 g, 79% yield). ^{1}H NMR (300 MHz, DMSO-d_6) δ 8.27 (1H, s, adenine H), 8.20 (1H, br s, adenine H), 7.91 (1H, m, amine NH), 7.51 (1H, t, J 5.7, amide NH), 7.33−7.20 (5H, m, 5 × phenyl H), 6.34 (1H, s, 1′-H), 5.43−5.36 (2H, m, 2′- and 3′-H), 4.66−4.49 (4H, m, 4′-H, CH_2Ph and 1-H), 4.01 (1H, m, 2-H), 2.81 (2H, m, CH_2CH_3), 2.12−1.89 (2H, m, 2 × cyclopentyl H), 1.80−1.56 (4H, m, 4 × cyclopentyl H), 1.54 (3H, s, CH_3), 1.34 (3H, s, CH_3), 0.61 (3H, t, J 7.2, CH_2CH_3); ^{13}C NMR (100 MHz, DMSO-d_6) δ 168.1, 154.1, 152.4, 148.2, 139.9, 138.9, 128.1, 127.3, 127.1, 112.9, 89.5, 85.8, 84.0, 83.2, 83.1, 70.1, 56.4, 33.0, 30.2, 26.7, 25.0, 21.3, 13.8; HRMS (ESI) calculated for $C_{27}H_{35}O_5N_6$ $[MH]^+$ 523.2663, found 523.2649; purity UPLC-MS 99%, retention time = 3.08 min.

*6-N-(1-Adamantyl)-5′-ethylamino-5′-oxo-5′-deoxyadenosine (**16**).* Compound **16** was synthesized according to general procedure B, using **11** (0.10 g, 0.21 mmol), acetic acid (10 mL), and water (3 mL). After purification with column chromatography (methanol/DCM, 2−6%), product **16** was obtained as a white solid (0.09 g, 96% yield). ^{1}H NMR (300 MHz, DMSO-d_6) δ 8.89 (1H, t, J 5.5, amide NH), 8.39 (1H, s, adenine H), 8.27 (1H, s, adenine H), 6.77 (1H, s, amine NH), 5.95 (1H, d, J 7.7, 1′-H), 5.75 (1H, d, J 3.8, 3′−OH), 5.56 (1H, d, J 6.2, 2′−OH), 4.61 (1H, m, 2′-H), 4.30 (1H, d, J 1.2, 4′-H), 4.14 (1H, m, 3′-H), 3.22 (2H, m, CH_2CH_3), 2.23 (6H, m, 6 × adamantyl H), 2.09 (3H, m, 3 × adamantyl H), 1.68 (6H, m, 6 × adamantyl H), 1.08 (3H, t, J 7.2, CH_2CH_3); ^{13}C NMR (100 MHz, DMSO-d_6) δ 169.1, 154.6, 151.6, 148.0, 140.4, 120.4, 87.9, 84.7, 73.1, 71.9, 52.2, 41.0, 36.0, 33.2, 29.0, 14.7; IR [cm^{-1}] 3218, 2905, 2847, 1644; HRMS (ESI$^+$) m/z calcd for $C_{22}H_{31}N_6O_4$ $[MH]^+$ 443.2401, found 443.2393; purity UPLC 99%, retention time = 3.06 min.

*6-N-(3-Hydroxy-1-adamantyl)-5′-ethylamino-5′-oxo-5′-deoxyadenosine (**17**).* Compound **17** was synthesized according to general procedure B, using **12** (0.01 g, 0.02 mmol), acetic acid (3.6 mL), and water (1.2 mL). After purification with column chromatography (methanol/DCM, 1−5%), product **17** was obtained as a white solid (0.007 g, 78% yield). ^{1}H NMR (300 MHz, DMSO-d_6) δ 8.88 (1H, t, J 5.5, amide NH), 8.40 (1H, s, adenine H), 8.27 (1H, s, adenine H), 6.89 (1H, s, amine NH), 5.95 (1H, d, J 7.6, 1′-H), 5.74 (1H, d, J 4.2, 3′−OH), 5.57 (1H, d, J 6.4, 2′−OH), 4.61 (1H, m, 2′-H), 4.55 (1H, s, adamantyl OH), 4.30 (1H, d, J 1.2, 4′-H), 4.14 (1H, m, 3′-H), 3.21 (2H, m, CH_2CH_3), 2.20−2.05 (8H, m, 8 × adamantyl H), 1.66−1.43 (6H, m, 6 × adamantyl H), 1.08 (3H, t, J 7.2, CH_2CH_3); ^{13}C NMR (100 MHz, DMSO-d_6) δ 169.1, 154.5, 151.6, 148.0, 140.4, 120.3, 87.8, 84.7, 73.1, 72.0, 67.5, 54.7, 48.8, 44.2, 34.9, 33.3, 30.1, 14.7; HRMS (ESI$^+$) m/z calcd for $C_{22}H_{31}N_6O_5$ $[MH]^+$ 459.2350, found 459.2346; purity UPLC 94%, retention time = 2.18 min.

*6-N-(2-Adamantyl)-5′-ethylamino-5′-oxo-5′-deoxyadenosine (**18**).* Compound **18** was synthesized according to general procedure B, using **13** (0.02 g, 0.04 mmol), acetic acid (1.6 mL), and water (0.4 mL). After purification with column chromatography (methanol/DCM, 3−10%), product **18** was obtained as a white solid (0.02 g, 99% yield). ^{1}H NMR (300 MHz, DMSO-d_6) δ 8.86 (1H, m, amide NH), 8.43 (1H, s, adenine H), 8.27 (1H, s, adenine H), 7.15 (1H, br s, amine NH), 5.97 (1H, d, J 7.5, 1′-H), 5.74 (1H, d, J 4.3, 3′−OH), 5.54 (1H, d, J 6.4, 2′−OH), 4.62 (1H, m, 2′-H), 4.37 (1H, br s, adamantyl H), 4.30 (1H, d, J 1.4, 4′-H), 4.14 (1H, m, 3′-H), 3.21 (2H, m, CH_2CH_3), 2.13−2.08 (4H, m, 4 × adamantyl H), 1.85 (6H, m, 6 × adamantyl H), 1.73 (2H, m, 2 × adamantyl H), 1.56−1.52 (2H, m, 2 × adamantyl H), 1.08 (3H, t, J 7.2, CH_2CH_3); ^{13}C NMR (100 MHz, DMSO-d_6) δ 169.1, 154.3, 152.3, 140.6, 114.5, 87.8, 84.6, 73.1, 71.9, 37.2, 36.9, 33.3, 30.9, 26.8, 14.7; HRMS (ESI) calcd for $C_{22}H_{31}N_6O_4$ $[MH]^+$ 443.2401, found 443.2392; purity UPLC-MS 99%, retention time = 2.69 min.

*6-N-[(3-endo)-9-Methyl-9-azabicyclo[3.3.1]non-3-yl]-5′-ethylamino-5′-oxo-5′-deoxyadenosine (**19**).* Compound **19** was synthesized according to general procedure B, using **14** (0.03 g, 0.06 mmol), acetic acid (4.8 mL), and water (1.2 mL). After purification with column chromatography (methanol/DCM, 5−10%, with an additional 1% aqueous ammonia), product **19** was obtained as a white solid (0.03

DOI: 10.1021/acs.jmedchem.5b01402
J. Med. Chem. 2016, 59, 947−964

g, 99% yield). ^{1}H NMR (300 MHz, MeOD-d_4) δ 8.30 (1H, br s, adenine H), 8.27 (1H, s, adenine H), 6.01 (1H, d, J 7.7, 1′-H), 4.81 (1H partially behind solvent signal, m, 3-H), 4.75 (1H, dd, J 7.6, 4.8, 2′-H), 4.47 (1H, d, J 1.5, 4′-H), 4.31 (1H, dd, J 4.8, 1.4, 3′-H), 3.37 (2H, m, CH_2CH_3), 3.28 (2H partially behind solvent signal, m, 1-, and 5-H), 2.69−2.56 (5H, m, NCH_3 and 2 × granatyl H), 2.21−2.04 (3H, m, 3 × granatyl H), 1.68−1.56 (3H, m, 3 × granatyl H), 1.30 (2H, m, 2 × granatyl H), 1.21 (3H, t, J 7.3, CH_2CH_3); ^{13}C NMR (100 MHz, MeOD-d_4) δ 172.1, 155.8, 153.9, 142.1, 90.5, 86.5, 75.0, 73.4, 53.5, 42.1, 40.2, 35.1, 33.0, 25.7, 15.0, 14.4; HRMS (ESI) calcd for $C_{21}H_{32}N_7O_4$ $[MH]^+$ 446.2510, found 446.2523; purity UPLC-MS 99%, retention time = 1.62 min.

*6-N-((1R,2R)-2-(Benzyloxy)cyclopentyl)-5′-ethylamino-5′-oxo-5′-deoxyadenosine (**20**).* Compound **20** was synthesized according to general procedure B, using **15** (0.01 g, 0.02 mmol), acetic acid (1.6 mL), and water (0.4 mL). After purification with column chromatography (methanol/DCM, 2−4%), product **20** was obtained as a white solid (0.01 g, 99% yield). ^{1}H NMR (400 MHz, DMSO-d_6) δ 8.90 (1H, t, J 5.6, amide NH), 8.41 (1H, s, adenine H), 8.30 (1H, br s, adenine H), 8.03 (1H, m, amine NH), 7.33−7.20 (5H, m, 5 × phenyl H), 5.98 (1H, d, J 7.6, 1′-H), 5.73 (1H, d, J 4.3, 3′−OH), 5.53 (1H, d, J 6.5, 2′−OH), 4.67−4.53 (4H, m, 2′-H, CH_2Ph and 1-H), 4.32 (1H, d, J 1.5, 4′-H), 4.15 (1H, m, 3′-H), 4.03 (1H, m, 2-H), 3.23 (2H, m, CH_2CH_3), 2.08 (1H, m, 1 × cyclopentyl H), 1.96 (1H, m, 1 × cyclopentyl H), 1.79−1.60 (4H, m, 4 × cyclopentyl H), 1.09 (3H, t, J 7.2, CH_2CH_3); ^{13}C NMR (100 MHz, DMSO-d_6) δ 169.1, 154.3, 152.3, 140.4, 138.9, 128.1, 127.3, 127.1, 120.1, 87.8, 84.7, 84.1, 73.1, 72.0, 70.1, 56.4, 33.2, 30.2, 21.4, 14.7; HRMS (ESI) calcd for $C_{24}H_{31}O_5N_6$ $[MH]^+$ 483.2350, found 483.2339; purity UPLC-MS 98%, retention time = 2.59 min.

*6-N-((1R,2R)-2-(Hydroxy)cyclopentyl)-5′-ethylamino-5′-oxo-5′-deoxyadenosine (**21**).* Compound **21** was synthesized according to general procedure C, using **20** (0.08 g, 0.17 mmol), cyclohexene (0.66 mL, 6.55 mmol), and $Pd(OH)_2$/C (20 wt %, 0.02 g). After purification with column chromatography (methanol/DCM, 2−8%), product **21** was obtained as a white solid (0.07 g, 99% yield). ^{1}H NMR (300 MHz, DMSO-d_6) δ 8.91 (1H, t, J 5.4 Hz, amide NH), 8.41 (1H, s, adenine H), 8.26 (1H, br s, adenine H), 7.84 (1H, m, amine NH), 5.97 (1H, d, J 7.6, 1′-H), 5.75 (1H, d, J 4.3, 3′−OH), 5.55 (1H, d, J 6.5, 2′−OH), 4.86 (1H, m, 2-OH), 4.62 (1H, m, 2′-H), 4.31 (2H, m, 1-H and 4′-H), 4.14 (1H, m, 3′-H), 4.06 (1H, m, 2-H), 3.23 (2H, m, CH_2CH_3), 2.10 (1H, m, 1 × cyclopentyl H), 1.90 (1H, m, 1 × cyclopentyl H), 1.74−1.42 (4H, m, 4 × cyclopentyl H), 1.09 (3H, t, J 7.2, CH_2CH_3); ^{13}C NMR (100 MHz, DMSO-d_6) δ 169.1, 154.8, 152.2, 140.3, 87.8, 84.6, 76.0, 73.1, 72.0, 58.8, 33.3, 32.3, 20.4, 14.7; HRMS (ESI) calcd for $C_{17}H_{25}O_5N_6$ $[MH]^+$ 393.1881, found 393.1873; purity UPLC-MS 99%, retention time = 2.21 min.

*6-N-[(3-endo)-3-tert-Butyloxycarbonylamino-9-azabicyclo[3.3.1]-non-3-yl]-5′-ethylamino-2′,3′-O-isopropylidene-5′-oxo-5′-deoxyadenosine (**23**).* Compound **23** was synthesized according to general procedure A, using chloride **10** (0.03 g, 0.08 mmol), *tert*-butyl-9-azabicyclo[3.3.1]nonan-3-ylcarbamate (**22**) (0.04 g, 0.16 mmol), and triethylamine (0.41 mL, 2.94 mmol). Following the removal of the solvent from the reaction mixture, the residue was dissolved in ethyl acetate (100 mL) and washed with water (2 × 50 mL). The organic phase was then dried over anhydrous Na_2SO_4, and the solvent was removed in vacuo. After purification with column chromatography (methanol/DCM, 1−2%), product **23** was obtained as a pale yellow solid (0.03 g, 67% yield). ^{1}H NMR (300 MHz, MeOD-d_4) δ 8.18 (1H, s, adenine H), 8.13 (1H, m, adenine H), 6.33 (1H, s, 1′-H), 6.16 (1H, m, 1- or 5-H), 5.61 (1H, m, 2′-H), 5.49 (1H, m, 3′-H), 5.42 (1H, m, 1- or 5-H), 4.62 (1H, d, J 1.7, 4′-H), 3.29 (1H, m, granatyl H), 2.85 (2H, m, CH_2CH_3), 2.42−2.16 (3H, m, 3 × granatyl H), 1.79−1.34 (22H, m, 2 × CH_3, $-C(CH_3)_3$ and 7 × granatyl H), 0.66 (3H, dt, J 14.7, 7.2, CH_2CH_3); ^{13}C NMR (75 MHz, $CDCl_3$) 171.8, 155.4, 153.7, 140.6, 117.1, 115.0, 93.0, 88.9, 85.5, 85.3, 45.1, 44.1, 35.0, 33.6, 33.2, 32.5, 31.8, 30.9, 28.9, 27.2, 25.5, 15.0, 14.3; HRMS calculated for $C_{28}H_{42}O_6N_7$ $[MH]^+$ 572.3191, found 572.3187.

*6-N-[(3-endo)-3-Amino-9-azabicyclo[3.3.1]non-3-yl]-5′-ethylamino-5′-oxo-5′-deoxyadenosine (**24**).* Compound **24** was synthesized according to general procedure B, using **23** (0.02 g, 0.03 mmol), acetic acid (1.5 mL), and water (0.5 mL). The crude product was purified by prep-LC, with an eluent gradient of 100% A to 60% D in 40 min. The fractions were collected and dried by lyophilization, and product **24** was obtained as a white solid as the TFA salt (0.03 g, 99% yield). ^{1}H NMR (400 MHz, MeOD-d_4) δ 8.34 (1H, s, adenine H), 8.28 (1H, s, adenine H), 6.35 (1H, br s, 1- or 5-H), 6.03 (1H, d, J 7.6, 1′-H), 5.59 (1H, br s, 1- or 5-H), 4.74 (1H, dd, J 7.5, 4.8, 2′-H), 4.48 (1H, d, J 1.6, 4′-H), 4.30 (1H, dd, J 4.8, 1.5, 3′-H), 3.36 (2H, q, J 7.3, CH_2CH_3), 3.00 (1H, ddd, J 18.3, 12.2, 5.8, 3-H), 2.57 (2H, m, 2 × granatyl H), 2.18 (1H, m, 1 × granatyl H), 1.87−1.64 (7H, m, 7 × granatyl H), 1.20 (3H, t, J 7.3, CH_2CH_3); ^{13}C NMR (100 MHz, MeOD-d_4) δ 172.2, 155.2, 152.6, 150.7, 141.1, 121.8, 90.6, 86.4, 75.0, 73.5, 45.1, 35.1, 31.0, 15.0, 14.7; ^{19}F NMR (376 MHz, DMSO-d_6) δ −77.3; HRMS (ESI) calcd for $C_{20}H_{30}O_4N_7$ $[MH]^+$ 432.2354, found 432.2343; purity UPLC-MS 99%, retention time = 1.80 min.

*6-N-[(3-endo)-3-Aminodimethyl-9-azabicyclo[3.3.1]non-3-yl]-5′-ethylamino-5′-oxo-5′-deoxyadenosine (**25**).* Formic acid (0.02 mL) and formaldehyde (37% aq. solution, 0.04 mL) were added to **24** (0.01 g, 0.02 mmol) and stirred at 90 °C overnight. Additional formic acid (0.02 mL) and formaldehyde (37% aq. solution, 0.04 mL) were added and stirred at 105 °C for 3 h. The reaction mixture was allowed to cool to room temperature and made alkaline with 1 M NaOH solution. This was then thoroughly extracted with ethyl acetate (3 × 100 mL), and the combined organic extracts were washed with sat. aq. $NaHCO_3$ (50 mL), water (50 mL), and brine (50 mL), dried over anhydrous Na_2SO_4, and the solvent removed in vacuo to give **25** as white solid (0.006 g, 67% yield). ^{1}H NMR (300 MHz, MeOH-d_4) δ 8.27 (1H, s, adenine H), 8.21 (1H, s, adenine H), 6.26 (1H, br s, 1- or 5-H), 6.01 (1H, d, J 7.6, 1′-H), 5.49 (1H, br s, 1- or 5-H), 4.78 (1H, dd, J 7.7, 4.8, 2′-H), 4.46 (1H, d, J 1.4, 4′-H), 4.30 (1H, dd, J 4.8, 1.4, 3′-H), 3.38 (2H, m, CH_2CH_3), 2.45 (9H, m, 2 × CH_3 and 3 × granatyl H), 2.18 (1H, m, 1 × granatyl H), 1.77−1.58 (7H, m, 7 × granatyl H), 1.20 (3H, t, J 7.3, CH_2CH_3); ^{13}C NMR (100 MHz, DMSO-d_6) δ 172.1, 155.1, 153.3, 151.5, 140.8, 121.6, 90.4, 86.4, 75.0, 73.2, 58.6, 41.8, 35.1, 30.8, 15.1, 14.9; HRMS (ESI) calcd for $C_{22}H_{34}O_4N_7$ $[MH]^+$ 460.2667, found 460.2661; purity UPLC-MS 99%, retention time = 1.87 min.

*6-N-(1-Adamantyl)-5′-(2-fluorophenylthio)-2′,3′-O-isopropylidene-5′-deoxyadenosine (**30**).* Compound **30** was synthesized according to general procedure A, using chloride **29** (0.1 g, 0.23 mmol), amantadine hydrochloride (0.13 g, 0.69 mmol), and DIPEA (0.18 mL, 1.03 mmol). After purification with column chromatography (methanol/DCM, 0.5%), product **30** was obtained as a white solid (0.09 g, 69% yield). ^{1}H NMR (300 MHz, DMSO-d_6) δ 8.29 (1H, s, adenine H), 8.23 (1H, s, adenine H), 7.38 (1H, td, J 7.8, 1.6, Ar H), 7.31−7.07 (3H, m, 3 × Ar H), 6.67 (1H, s, amine NH), 6.17 (1H, d, J 2.2, 1′-H), 5.51 (1H, dd, J 6.2, 2.2, 2′-H), 5.05 (1H, dd, J 6.2, 2.7, 3′-H), 4.20 (1H, td, J 6.9, 2.5, 4′-H), 3.25 (2H overlapping with solvent signal, m, 5′-H_2), 2.22 (6H, m, 6 × adamantyl H), 2.09 (3H, m, 3 × adamantyl H), 1.75−1.63 (6H, m, 6 × adamantyl H), 1.49 (3H, s, CH_3), 1.31 (3H, s, CH_3); ^{13}C NMR (100 MHz, DMSO-d_6) δ 161.3, 158.9, 154.4, 151.9, 147.7, 139.8, 131.1, 128.5 (d, J 7.9), 124.9 (d, J 3.6), 121.8 (d, J 17.1), 119.9, 115.6 (d, J 21.9), 113.2, 89.5, 85.1, 83.4, 83.2, 52.2, 41.0, 36.0, 34.4, 29.0, 26.8, 25.1; ^{19}F NMR (376 MHz, DMSO-d_6) δ −110.4; HRMS (ESI^+) m/z calcd for $C_{29}H_{35}N_5O_3FS$ $[MH]^+$ 552.2439, found 552.2425.

*6-N-[(3-endo)-9-Methyl-9-azabicyclo[3.3.1]non-3-yl]-5′-(2-fluorophenylthio)-2′,3′-O-isopropylidene-5′-deoxyadenosine (**31**).* Compound **31** was synthesized according to general procedure A, using chloride **29** (0.1 g, 0.23 mmol), (3-*endo*)-9-methyl-9-azabicyclo[3.3.1]-nonan-3-amine (0.14 g, 0.92 mmol), and DIPEA (0.04 mL, 0.28 mmol). After purification with column chromatography (methanol/DCM, 5−10%), product **31** was obtained as a pale yellow solid (0.08 g, 61% yield). ^{1}H NMR (400 MHz, $CDCl_3$) δ 8.33 (1H, s, adenine H), 7.76 (1H, s, adenine H), 7.36 (1H, m, Ar H), 7.20 (1H, m, Ar H), 7.04−6.97 (2H, m, 2 × Ar H), 6.01 (1H, d, J 2.0, 1′-H), 5.54 (1H, dd, J 6.3, 1.9, 2′-H), 5.52 (1H overlapping with 2′-H signal, br s, NH), 5.10 (1H, dd, J 6.3, 2.8, 3′-H), 4.75 (1H, br s, 3-H), 4.37 (1H, td, J 7.2, 2.8, 4′-H), 3.25 (H, dd, J 13.7, 7.6, 5-H*H*), 3.17 (1H, dd, J 13.7, 6.5, 5-H*H*), 3.11 (2H, m, 1- and 5-H), 2.65−2.52 (2H, m, 2 × granatyl H),

DOI: 10.1021/acs.jmedchem.5b01402
J. Med. Chem. 2016, 59, 947−964

2.50 (3H, s, NCH_3), 2.04−1.91 (3H, m, 3 × granatyl H), 1.56 (3H, s, CH_3), 1.53 (1H, m, granatyl H), 1.37 (3H, s, CH_3), 1.35−1.29 (2H, m, 2 × granatyl H), 1.02 (2H, m, 2 × granatyl H); ^{13}C NMR (75 MHz, $CDCl_3$) 163.5, 160.2, 154.6, 153.5, 139.3, 133.3, 129.2 (d, *J* 8.0), 124.5 (d, *J* 3.8), 122.0 (d, *J* 17.5), 115.9 (d, *J* 22.5), 114.3, 91.3, 86.6, 84.2, 84.1, 51.4, 40.3, 36.2, 33.6, 27.1, 25.4, 24.2, 14.4; ^{19}F NMR (376 MHz, DMSO-d_6) δ −108.4; HRMS calculated for $C_{28}H_{36}O_3N_6FS$ $[MH]^+$ 555.2548, found 555.2548; purity UPLC-MS 93%, retention time = 2.88 min.

*6-N-((1R,2R)-2-(Benzyloxy)cyclopentyl)-5′-(2-fluorophenylthio)-2′,3′-O-isopropylidene-5′-deoxyadenosine (**32**).* Compound **32** was synthesized according to general procedure A, using chloride **29** (0.05 g, 0.11 mmol), (1*R*,2*R*)-1-amino-2-benzyloxycyclopentane (0.03 mL, 0.17 mmol), and triethylamine (0.04 mL, 0.31 mmol). After purification with column chromatography (methanol/DCM, 2%), product **32** was obtained as a sticky yellow oil (0.06 g, 99% yield). ^{1}H NMR (300 MHz, DMSO-d_6) δ 8.32 (1H, s, adenine H), 8.26 (1H, br s, adenine H), 7.96 (1H, m, amine NH), 7.39 (1H, td, *J* 7.8, 1.6, Ar H), 7.32−7.06 (8H, m, 8 × Ar H), 6.19 (1H, d, *J* 2.1, 1′-H), 5.51 (1H, dd, *J* 6.2, 2.1, 2′-H), 5.07 (1H, dd, *J* 6.2, 2.6, 3′-H), 4.67−4.47 (3H, m, 1-H and CH_2Ph), 4.21 (1H, td, *J* 7.1, 2.6, 4′-H), 4.01 (1H, m, 2-H), 3.25 (2H overlapping with solvent signal, m, 5′-H_2), 2.13−1.89 (2H, m, 2 × cyclopentyl H), 1.79−1.57 (4H, m, 4 × cyclopentyl H), 1.49 (3H, s, CH_3), 1.31 (3H, s, CH_3); ^{13}C NMR (100 MHz, DMSO-d_6) δ 161.3, 158.9, 154.2, 152.5, 147.9, 139.8, 138.9, 131.1, 128.5 (d, *J* 7.9), 128.1, 127.3, 127.1, 124.9 (d, *J* 3.5), 121.8 (d, *J* 17.1), 115.6 (d, *J* 22.0), 113.2, 89.4, 85.2, 84.0, 83.4, 83.2, 70.1, 56.5, 34.4, 30.1, 26.8, 25.1, 21.4; ^{19}F NMR (376 MHz, DMSO-d_6) δ −110.4; HRMS (ESI) calculated for $C_{31}H_{35}O_4N_5FS$ $[MH]^+$ 592.2388, found 592.2378; purity UPLC-MS 94%, retention time = 3.98 min.

*6-N-((1R,2R)-2-(Hydroxy)cyclopentyl)-5′-(2-fluorophenylthio)-2′,3′-O-isopropylidene-5′-deoxyadenosine (**33**).* Compound **33** was synthesized according to general procedure A using chloride **29** (0.05 g, 0.11 mmol), (1*R*,2*R*)-2-aminocyclopentanol hydrochloride (0.02 g, 0.14 mmol), and triethylamine (0.04 mL, 0.31 mmol). After purification with column chromatography (methanol/DCM, 2%), product **33** was obtained as a white solid (0.04 g, 73% yield). ^{1}H NMR (300 MHz, DMSO-d_6) δ 8.31 (1H, s, adenine H), 8.22 (1H, br s, adenine H), 7.76 (1H, m, NH), 7.39 (1H, td, *J* 7.8, 1.6, Ar H), 7.31−7.07 (3H, m, 3 × Ar H), 6.18 (1H, d, *J* 2.1, 1′-H), 5.51 (1H, dd, *J* 6.2, 2.1, 2′-H), 5.06 (1H, dd, *J* 6.2, 2.7, 3′-H), 4.86 (1H, m, 2-OH), 4.27 (1H, br s, 1-H), 4.21 (1H, td, *J* 7.1, 2.6, 4′-H), 4.06 (1H, m, 2-H), 3.26 (2H overlapping with solvent signal, m, 5′-H_2), 2.06 (1H, m, 1 × cyclopentyl H), 1.89 (1H, m, 1 × cyclopentyl H), 1.72−1.60 (2H, m, 2 × cyclopentyl H), 1.60−1.43 (5H, m, 2 × cyclopentyl H and CH_3), 1.32 (3H, s, CH_3); ^{13}C NMR (100 MHz, DMSO-d_6) δ 161.3, 158.9, 154.7, 152.5, 139.8, 131.1, 128.6 (d, *J* 7.9), 124.9 (d, *J* 3.5), 121.8 (d, *J* 17.1), 115.6 (d, *J* 22.0), 113.2, 89.5, 85.1, 83.4, 83.2, 76.0, 58.9, 34.4, 32.3, 26.8, 25.1, 20.4; ^{19}F NMR (376 MHz, DMSO-d_6) δ −110.4; HRMS (ESI) calculated for $C_{24}H_{29}O_4N_5FS$ $[MH]^+$ 502.1919, found 502.1912; purity UPLC-MS 99%, retention time = 3.14 min.

*6-N-(1-Adamantyl)-5′-(2-fluorophenylthio)-5′-deoxyadenosine (**34**).* Compound **34** was synthesized according to general procedure B, using **30** (0.01 g, 0.02 mmol), acetic acid (3.2 mL), and water (0.8 mL). After purification with column chromatography (methanol/DCM, 1−3%), product **34** was obtained as a white solid (0.004 g, 40% yield). ^{1}H NMR (400 MHz, DMSO-d_6) δ 8.32 (1H, s, adenine H), 8.21 (1H, s, adenine H), 7.46 (1H, td, *J* 7.8, 1.6, Ar H), 7.29−7.12 (3H, m, 3 × Ar H), 6.60 (1H, s, NH), 5.87 (1H, d, *J* 5.7, 1′-H), 5.51 (1H, d, *J* 6.1, 2′−OH), 5.37 (1H, d, *J* 5.0, 3′−OH), 4.82 (1H, dd, *J* 11.1, 5.7, 2′-H), 4.22 (1H, dd, *J* 8.7, 4.9, 3′-H), 4.00 (1H, m, 4′-H), 3.42 (1H, dd, *J* 13.8, 5.5, 5′-*H*H), 3.31 (1H overlapping with solvent signal, m, 5′-H*H*), 2.23 (6H, m, 6 × adamantyl H), 2.10 (3H, m, 3 × adamantyl H), 1.68 (6H, m, 6 × adamantyl H); ^{13}C NMR (100 MHz, DMSO-d_6) δ 161.1, 158.7, 154.4, 151.9, 148.5, 139.7, 130.5, 128.1 (d, *J* 7.9), 125.0 (d, *J* 3.4), 122.6 (d, *J* 17.1), 119.9, 115.5 (d, *J* 21.8), 87.7, 82.8, 72.7, 72.5, 52.1, 41.0, 36.0, 34.6, 29.0; ^{19}F NMR (376 MHz, DMSO-d_6) δ −110.78; HRMS (ESI^+) *m*/*z* calcd for $C_{26}H_{31}N_5O_3FS$ $[MH]^+$ 512.2126, found 512.2130.

*6-N-[(3-endo)-9-Methyl-9-azabicyclo[3.3.1]non-3-yl]-5′-(2-fluorophenylthio)-5′-deoxyadenosine (**35**).* Compound **35** was synthesized according to general procedure B, using **31** (0.01 g, 0.02 mmol), acetic acid (3.2 mL), and water (0.8 mL). After purification with column chromatography (methanol/DCM, 1−10%, with an additional 1% aqueous ammonia), product **35** was obtained as a white solid (0.005 g, 50% yield). ^{1}H NMR (400 MHz, MeOD-d_4) δ 8.24 (1H, s, adenine H), 8.17 (1H, s, adenine H), 7.45 (1H, m, Ar H), 7.21 (1H, m, Ar H), 7.07−7.01 (2H, m, 2 × Ar H), 5.95 (1H, d, *J* 5.2, 1′-H), 4.84 (1H, 2′-H under solvent signal as determined by COSY analysis), 4.83 (1H, br s, 3-H, partially hidden by solvent signal), 4.37 (1H, m, 3′-H), 4.20 (1H, m, 4′-H), 3.40 (2H, m, CH_2CH_3), 3.31 (2H, 1- and 5-H under solvent signal as determined by COSY analysis), 2.70−2.57 (5H, m, NCH_3 and 2 × granatyl H), 2.16−2.04 (3H, m, 3 × granatyl H), 1.69−1.59 (3H, m, 3 × granatyl H), 1.32−1.29 (2H, m, 2 × granatyl H); ^{13}C NMR (100 MHz, MeOD-d_4) δ 163.8, 155.6, 154.0, 140.9, 133.2, 129.7 (d, *J* 7.9), 125.7 (d, *J* 3.7), 116.5 (d, *J* 22.5), 90.1, 85.0, 74.7, 74.1, 53.7, 40.2, 36.5, 32.9, 25.7, 14.3, 7.6; ^{19}F NMR (376 MHz, DMSO-d_6) δ −111.5; HRMS (ESI^+) *m*/*z* calcd for $C_{25}H_{32}N_6O_3FS$ $[MH]^+$ 515.2235, found 515.2240; purity UPLC-MS 99%, retention time = 2.24 min.

*6-N-((1R,2R)-2-(Benzyloxy)cyclopentyl)-5′-(2-fluorophenylthio)-5′-deoxyadenosine (**36**).*[47] Compound **36** was synthesized according to general procedure B, using **32** (0.02 g, 0.03 mmol), acetic acid (3.2 mL), and water (0.8 mL). After purification with column chromatography (methanol/DCM, 1−3%), product **36** was obtained as a pale yellow solid (0.02 g, 99% yield). ^{1}H NMR (300 MHz, DMSO-d_6) δ 8.35 (1H, s, adenine H), 8.24 (1H, br s, adenine H), 7.89 (1H, m, amine NH), 7.46 (1H, m, Ar H), 7.33−7.10 (8H, m, 8 × Ar H), 5.90 (1H, d, *J* 5.6, 1′-H), 5.52 (1H, d, *J* 6.0, 2′−OH), 5.38 (1H, d, *J* 5.1, 3′−OH), 4.81 (1H, dd, *J* 11.1, 5.6, 2′-H), 4.68−4.50 (3H, m, 1-H and CH_2Ph), 4.21 (1H, dd, *J* 8.7, 4.8, 3′-H), 4.00−3.97 (2H, m, 4′-H and 2-H), 3.42 (1H, dd, *J* 13.8, 5.5, 5′-*H*H), 3.32 (1H overlapping with solvent signal, m, 5′-H*H*) 2.14−1.91 (2H, m, 2 × cyclopentyl H), 1.77−1.58 (4H, m, 4 × cyclopentyl H); ^{13}C NMR (100 MHz, DMSO-d_6) δ 161.1, 158.7, 154.2, 152.5, 139.6, 139.0, 130.5, 128.1, 128.0, 127.3, 127.1, 125.0 (d, *J* 3.4), 122.6 (d, *J* 17.2), 155.5 (d, *J* 21.9), 87.6, 84.1, 82.8, 72.7, 72.6, 70.1, 56.4, 34.6, 30.2, 21.4; ^{19}F NMR (376 MHz, DMSO-d_6) δ −110.8; HRMS (ESI) calcd for $C_{28}H_{31}O_4N_5FS$ $[MH]^+$ 552.2075, found 552.2071; purity UPLC-MS 99%, retention time = 3.14 min.

*6-N-((1R,2R)-2-(Hydroxy)cyclopentyl)-5′-(2-fluorophenylthio)-5′-deoxyadenosine (**37**).*[14] Compound **37** was synthesized according to general procedure B, using **33** (0.01 g, 0.02 mmol), acetic acid (3.2 mL), and water (0.8 mL). After purification with column chromatography (methanol/DCM, 1−5%), product **37** was obtained as a white solid (0.005 g, 56% yield). The O-acetylated product was also isolated in small quantities. ^{1}H NMR (300 MHz, DMSO-d_6) δ 8.34 (1H, s, adenine H), 8.21 (1H, br s, adenine H), 7.69 (1H, d, *J* 7.1, amine NH), 7.47 (1H, td, *J* 7.8, 1.6, Ar H), 7.31−7.10 (3H, m, 3 × Ar H), 5.89 (1H, d, *J* 5.7, 1′-H), 5.54 (1H, d, *J* 6.0, 2′−OH), 5.40 (1H, d, *J* 5.0, 3′−OH), 4.87 (1H, d, *J* 4.0, 2-OH), 4.80 (1H, dd, *J* 10.9, 5.6, 2′-H), 4.30 (1H, br s, 1-H), 4.21 (1H, dd, *J* 8.6, 4.7, 3′-H), 4.09−3.95 (2H, m, 4′-H and 2-H), 3.42 (1H, dd, *J* 13.7, 5.5, 5′-*H*H), 3.32 (1H, m, 5′-H*H*), 2.07 (1H, m, 1 × cyclopentyl H), 1.90 (1H, m, 1 × cyclopentyl H), 1.72−1.42 (4H, m, 4 × cyclopentyl H); ^{13}C NMR (100 MHz, DMSO-d_6) δ 161.1, 158.7, 154.6, 152.4, 139.6, 130.5 (d, *J* 1.7), 128.1 (d, *J* 7.9), 125.0 (d, *J* 3.4), 122.6 (d, *J* 17.1), 115.5 (d, *J* 21.8), 87.6, 82.8, 76.1, 72.7, 72.6, 58.8, 34.6, 32.3, 20.4; ^{19}F NMR (376 MHz, DMSO-d_6) δ −110.8; HRMS (ESI) calcd for $C_{21}H_{25}O_4N_5FS$ $[MH]^+$ 462.1606, found 462.1590; purity UPLC-MS 95%, retention time = 2.35 min.

Biology Materials. Yeast extract and yeast nitrogen base were purchased from Difco (Franklin Lakes, NJ). All other reagents were purchased from Sigma-Aldrich (St. Louis, MO).

Constructs and DNA Manipulation. p426-GPD-A_1R was kindly provided by Professor Arthur Christopoulos and Dr. Lauren May (Monash University, Australia). Mammalian expression vectors containing the A_1R, A_{2A}R, A_{2B}R, and A_3R were purchased from Missouri S&T cDNA Resource Center (http://cdna.org) (Rolla,

DOI: 10.1021/acs.jmedchem.5b01402
J. Med. Chem. 2016, 59, 947−964

MO). DNA manipulations were performed using standard techniques. Oligonucleotides were supplied by Invitrogen and PCR amplification performed using FastStart Taq polymerase (Roche Diagnostics, Burgess Hill, UK). All constructs generated by PCR were sequenced by GATC (GATC Biotech, London, UK) prior to use.

General Yeast Methods. General yeast procedures were performed as described previously.[16] Cells were routinely cultured in YPDA (yeast, peptone, dextrose, and adenine). Yeast transformations were achieved using the lithium acetate/single-stranded DNA/polyethylene glycol method as previously described.[50] Cells were selected for uracil biosynthesis and routinely cultured in synthetic dropout media lacking uracil (SD-URA).

Yeast Strain Construction. The production of the dual reporter strains expressing chimeras of five C-terminal amino acids of human $G\alpha$ protein with the yeast Gpa1p, 1−467 (GPA1/Gα) has been described previously.[16] Mammalian GPCRs were introduced into the yeast strains (MMY12, MMY14, MMY19, MMY22, MMY23, MMY25, and MMY28) using the p426-GPD expression plasmid. Positive isolates were selected upon their ability to generate β-galactosidase activity above the basal level when stimulated with 100 μM NECA. For chimeric strains that did not initially appear to functionally couple ($n \geq 16$ isolates) to the ARs, and expression and membrane localization were confirmed using fluorescence microscopy.

Yeast Reporter Gene Assay. Yeast cells were treated with compounds as described in Dowell and Brown.[16] Initially, cells were cultured overnight in SD-URA at 30 °C. Cells were diluted 1:10 in SD-URA and allowed to grow for 8 h at 30 °C. Finally, cell density was adjusted to an OD_{600} of 0.02 and treated with 1% (v/v) of the appropriate compound dissolved in DMSO in a 96-well plate for 16 h at 30 °C. For compounds dissolved in other solvents, the media were supplemented with 1% (v/v) DMSO prior to treatment. To compensate for an elevated basal signal, the $A_{2A}R$ was routinely cultured in SD-URA lacking histidine (SD-URA-HIS) and treatment media supplemented with 5 mM 3-amino-triazole. All strains used in this study contain the *lacZ* gene under the control of the pheromone-responsive *FUS1* promoter. To assess β-galactosidase activity, cells were lysed as previously described.[19,51−53] 2-Nitrophenyl β-D-galactopyranoside (ONPG) was used as a chromogenic substrate for β-galactosidase and detected by OD_{430}. Absorbance was measured using a Mithras LB940 microplate reader (Berthold Technologies, Harpenden, UK). The strains are Δ*far1* and are therefore incapable of cell cycle arrest induced by the pheromone-response. Consequently, these cells grow throughout treatment. To compensate for variability in cell number and bleed through from the chromogenic reporter, cell density was measured by OD_{620} and a response calculated as $(OD_{430}-OD_{620})/OD_{620}$.

Confocal Microscopy of Yeast. To visualize receptor expression C-terminal in-frame fusion constructs between the A_1R, $A_{2A}R$, and $A_{2B}R$ and GFP were generated using the two-step cloning method described by Ladds et al.[54] These receptors were expressed in yeast using the p426-GPD vector consistent with their untagged counterparts. Isolates were cultured for 24 h in SD-URA. One hundred microliters of cells was harvested by centrifugation, washed in PBS, and briefly sonicated. Cells were imaged using a True Confocal Scanner Leica TCS SP5 microscope (Leica Microsystems Ltd., Milton Keynes, UK) and were processed using ImageJ as described previously.[55]

Mammalian Cell Culture and Transfection. CHO-K1 cells, provided by Dr. Ewan St. John Smith (University of Cambridge), were routinely cultured in Hams-F12, supplemented with 10% fetal bovine serum (FBS), and maintained at 37 °C, in humidified air with 5% CO_2. Cells were transfected with 2 μg of DNA using FuGene 6 at a 3:1 (w/v) DNA/FuGene 6 ratio. Cells were harvested 48 h post-transfection for assaying.

cAMP Accumulation Assay. Transfected cells were washed with PBS and resuspended in stimulation buffer (PBS containing 0.1% BSA and 25 μM rolipram). Cells were seeded at 2500 cells per well in 384-well white Optiplates. Cells were then simultaneously incubated with 10 μM forskolin (to stimulate cAMP production) and adenosine receptors ligands (ranging between 1 μM to 10 pM) for 30 min at room temperature. Cells were then lysed, and the extent of cAMP accumulation measured using a LANCE cAMP Detection Kit (PerkinElmer). Plates were read using a Mithras LB 940 multimode plate reader (Berthold Technologies).

Data Analysis. Data were analyzed using Prism 6.0e (Graphpad Software, San Diego, CA). Concentration−response curves were fitted using the three-parameter logistic equation to obtain EC_{50} and E_{max}. Schild analysis was performed in Prism as described by Motulsky and Christopoulos.[56] Nonlinear regression of the operational model of pharmacological agonism[36] was used to obtain values for efficacy (log τ) and the equilibrium dissociation constant (log K_A). These values were then used to quantify signaling bias as the change in log (τ/K_A) relative to NECA.[37] We have used this method previously to enable the quantification of G protein bias,[19,20] but here, we have extended the analysis to include receptor selectivity. Since the receptors are expressed in the same cell background and NECA is a full potent agonist against all receptor subtypes, we reasoned that changes in log (τ/K_A) for a given ligand, relative to NECA for each AR, would provide a quantitative means of comparing receptor selectivity. Statistically significant differences were detected using one-way ANOVA with Bonferroni's or Dunnett's multiple comparison tests or Student's t tests as appropriate, and a probability (p) < 0.05 was considered significant.

Homology Modeling and Docking. The protein sequence of the human A_1R (accession number P30542) was aligned with an agonist (UK-432097)-bound human $A_{2A}R$ template (PDB ID: 3QAK) using PSI-Coffee[57] (Figure S4). MODELER v9.14[58] was used to build 500 models and the best model selected according to the inbuilt molecular probability function. The ligands were constructed ab initio in Chem3D Pro v14.0 (PerkinElmer, Waltham, MA) and energy-minimized using the included MM2 force field. For each ligand, a library of 200 conformers was generated using OMEGA v2.5 (OpenEye Scientific Software, Santa Fe, NM). FRED RECEPTOR v2.2.5 (OpenEye Scientific Software) was utilized to generate a docking template, whereas the binding site was defined as a box of V = 9486 Å^3 around the bound UK-432097 agonist. For predicting the binding poses, the ligands were docked into this binding site template using FRED v2.1 (OpenEye Scientific Software), which utilizes an exhaustive process to position and score all conformers of a ligand at all possible positions within the defined binding site. Binding poses that did not form a hydrogen bond with Thr-91$^{3.36}$, Asn-254$^{6.55}$, or Thr-277$^{7.42}$ were discarded (hA_1R numbering according to P30542; superscript, Ballesteros−Weinstein numbering[35]). Ten docking poses were generated for each ligand, ranked using the inbuilt Chemgauss3 scoring function, and visualized with PyMOL v1.7 (Schrödinger LLC, Portland, OR).

■ ASSOCIATED CONTENT

Supporting Information

The Supporting Information is available free of charge on the ACS Publications website at DOI: 10.1021/acs.jmedchem.5b01402.

Synthesis procedures and spectral data for synthetic intermediates, reproduction of ^{1}H and ^{13}C NMR spectra, purity assessment for final compounds, Schild analysis of compounds **36** and **37**, functional assessment of A_3R in yeast, and predicted docking poses for compounds (PDF)

■ AUTHOR INFORMATION

Corresponding Authors

*(M.L.) Phone: +41 31 631 3311. Fax: +41 31 631 4272. E-mail martin.lochner@dcb.unibe.ch.

*(G.L.) Phone: +44 1223 334020. Fax: +44 1223 334100. E-mail: grl30@cam.ac.uk.

DOI: 10.1021/acs.jmedchem.5b01402
J. Med. Chem. 2016, 59, 947−964

Author Contributions

[▽]A.K. and J.L.H. contributed equally to this work.

Notes

The authors declare no competing financial interest.

■ ACKNOWLEDGMENTS

This study was supported by the Swiss National Science Foundation (SNSF professorship PP00P2_123536 and PP00P2_146321 to M.L.), the BBSRC (to G.L., BB/G01227X/1 and BB/M00015X/1), an MRC Doctoral Training Partnership (to I.W. MR/J003964/1), and the EPSRC (to A.K., EP/GS00045/1).

■ ABBREVIATIONS USED

AR, adenosine receptor; A_1R, A_1 adenosine receptor; $A_{2A}R$, A_{2A} adenosine receptor; $A_{2B}R$, A_{2B} adenosine receptor; A_3R, A_3 adenosine receptor; CCPA, 2-chloro-N^6-cyclopentyladenosine; DIPEA, di-*iso*-propyl ethyl amine (Hünig's base); GAPDH, glyceraldehyde-3-phosphate dehydrogenase; Gpa1p, guanine nucleotide-binding protein alpha-1 subunit; NECA, 5′-*N*-ethylcarboxamidoadenosine

■ REFERENCES

(1) Sachdeva, S.; Gupta, M. Adenosine and its receptors as therapeutic targets: an overview. *Saudi Pharm. J.* **2013**, *21*, 245−253.
(2) Dale, N.; Frenguelli, B. G. Release of adenosine and ATP during ischemia and epilepsy. *Curr. Neuropharmacol.* **2009**, *7*, 160−179.
(3) Fredholm, B. B.; Chen, J.-F.; Cunha, R. A.; Svenningsson, P.; Vaugeois, J.-M. Adenosine and brain function. *Int. Rev. Neurobiol.* **2005**, *63*, 191−270.
(4) Chen, J.-F.; Sonsalla, P. K.; Pedata, F.; Melani, A.; Domenici, M. R.; Popoli, P.; Geiger, J.; Lopes, L. V.; de Mendonça, A. Adenosine A_{2A} receptors and brain injury: broad spectrum of neuroprotection, multifaceted actions and "fine tuning" modulation. *Prog. Neurobiol.* **2007**, *83*, 310−331.
(5) Stewart, G. D.; Valant, C.; Dowell, S. J.; Mijaljica, D.; Devenish, R. J.; Scammells, P. J.; Sexton, P. M.; Christopoulos, A. Determination of adenosine A_1 receptor agonist and antagonist pharmacology using *Saccharomyces cerevisiae*: implications for ligand screening and functional selectivity. *J. Pharmacol. Exp. Ther.* **2009**, *331*, 277−286.
(6) Nell, P. G.; Albrecht-Küpper, B. The adenosine A_1 receptor and its ligands. *Prog. Med. Chem.* **2009**, *47*, 163−201.
(7) Petrelli, R.; Torquati, I.; Kachler, S.; Luongo, L.; Maione, S.; Franchetti, P.; Grifantini, M.; Novellino, E.; Lavecchia, A.; Klotz, K.-N.; Cappellacci, L. 5′-*C*-Ethyl-tetrazolyl-N^6-substituted adenosine and 2-chloro-adenosine derivatives as highly potent dual acting A_1 adenosine receptor agonists and A_3 adenosine receptor antagonists. *J. Med. Chem.* **2015**, *58*, 2560−2566.
(8) Franchetti, P.; Cappellacci, L.; Vita, P.; Petrelli, R.; Lavecchia, A.; Kachler, S.; Klotz, K.-N.; Marabese, I.; Luongo, L.; Maione, S.; Grifantini, M. N^6-Cycloalkyl- and N^6-bicycloalkyl-C5′(C2′)-modified adenosine derivatives as high-affinity and selective agonists at the human A_1 adenosine receptor with antinociceptive effects in mice. *J. Med. Chem.* **2009**, *52*, 2393−2406.
(9) Ashton, T. D.; Aumann, K. M.; Baker, S. P.; Schiesser, C. H.; Scammells, P. J. Structure−activity relationships of adenosines with heterocyclic N^6-substituents. *Bioorg. Med. Chem. Lett.* **2007**, *17*, 6779−6784.
(10) Hutchinson, S. A.; Baker, S. P.; Scammells, P. J. Adenosine receptor ligands with oxygenated N^6-substituents. *Bioorg. Med. Chem. Lett.* **1999**, *9*, 933−936.
(11) Cappellacci, L.; Franchetti, P.; Pasqualini, M.; Petrelli, R.; Vita, P.; Lavecchia, A.; Novellino, E.; Costa, B.; Martini, C.; Klotz, K.-N.; Grifantini, M. Synthesis, biological evaluation, and molecular modeling of ribose-modified adenosine analogues as adenosine receptor agonists. *J. Med. Chem.* **2005**, *48*, 1550−1562.
(12) Cappellacci, L.; Franchetti, P.; Vita, P.; Petrelli, R.; Lavecchia, A.; Costa, B.; Spinetti, F.; Martini, C.; Klotz, K.-N.; Grifantini, M. 5′-Carbamoyl derivatives of 2′-*C*-methyl-purine nucleosides as selective A_1 adenosine receptor agonists: affinity, efficacy, and selectivity for A_1 receptor from different species. *Bioorg. Med. Chem.* **2008**, *16*, 336−353.
(13) Morrison, C. F.; Elzein, E.; Jiang, B.; Ibrahim, P. N.; Marquart, T.; Palle, V.; Shenk, K. D.; Varkhedkar, V.; Maa, T.; Wu, L.; Wu, Y.; Zeng, D.; Fong, I.; Lustig, D.; Leung, K.; Zablocki, J. A. Structure−affinity relationships of 5′-aromatic ethers and 5′-aromatic sulfides as partial A_1 adenosine agonists, potential supraventricular anti-arrhythmic agents. *Bioorg. Med. Chem. Lett.* **2004**, *14*, 3793−3797.
(14) Fatholahi, M.; Xiang, Y.; Wu, Y.; Li, Y.; Wu, L.; Dhalla, A. K.; Belardinelli, L.; Shryock, J. C. A novel partial agonist of the A_1-adenosine receptor and evidence of receptor homogeneity in adipocytes. *J. Pharmacol. Exp. Ther.* **2006**, *317*, 676−684.
(15) Brown, A. J.; Dyos, S. L.; Whiteway, M. S.; White, J. H. M.; Watson, M.-A. E. A.; Marzioch, M.; Clare, J. J.; Cousens, D. J.; Paddon, C.; Plumpton, C.; Romanos, M. A.; Dowell, S. J. Functional coupling of mammalian receptors to the yeast mating pathway using novel yeast/mammalian G protein α-subunit chimeras. *Yeast* **2000**, *16*, 11−22.
(16) Dowell, S. J.; Brown, A. J. Yeast assays for G-protein-coupled receptors. *Recept. Channels* **2002**, *8*, 343−352.
(17) Brown, A. J.; Goldsworthy, S. M.; Barnes, A. A.; Eilert, M. M.; Tcheang, L.; Daniels, D.; Muir, A. I.; Wigglesworth, M. J.; Kinghorn, I.; Fraser, N. J.; Pike, N. B.; Strum, J. C.; Steplewski, K. M.; Murdock, P. R.; Holder, J. C.; Marshall, F. H.; Szekeres, P. G.; Wilson, S.; Ignar, D. M.; Foord, S. M.; Wise, A.; Dowell, S. J. The orphan G protein-coupled receptors GPR41 and GPR43 are activated by propionate and other short chain carboxylic acids. *J. Biol. Chem.* **2003**, *278*, 11312−11319.
(18) Bertheleme, N.; Singh, S.; Dowell, S. J.; Hubbard, J.; Byrne, B. Loss of constitutive activity is correlated with increased thermostability of the human adenosine A_{2A} receptor. *Br. J. Pharmacol.* **2013**, *169*, 988−998.
(19) Weston, C.; Poyner, D.; Patel, V.; Dowell, S.; Ladds, G. Investigating G protein signalling bias at the glucagon-like peptide-1 receptor in yeast. *Br. J. Pharmacol.* **2014**, *171*, 3651−3665.
(20) Weston, C.; Lu, J.; Li, N.; Barkan, K.; Richards, G. O.; Roberts, D. J.; Skerry, T. M.; Poyner, D.; Pardamwar, M.; Reynolds, C. A.; Dowell, S. J.; Willars, G. B.; Ladds, G. Modulation of glucagon receptor pharmacology by receptor activity-modifying protein-2 (RAMP2). *J. Biol. Chem.* **2015**, *290*, 23009−23022.
(21) Peeters, M. C.; van Westen, G. J. P.; Guo, D.; Wisse, L. E.; Müller, C. E.; Beukers, M. W.; Ijzerman, A. P. GPCR structure and activation: an essential role for the first extracellular loop in activating the adenosine A_{2B} receptor. *FASEB J.* **2011**, *25*, 632−643.
(22) Peeters, M. C.; Wisse, L. E.; Dinaj, A.; Vroling, B.; Vriend, G.; Ijzerman, A. P. The role of the second and third extracellular loops of the adenosine A_1 receptor in activation and allosteric modulation. *Biochem. Pharmacol.* **2012**, *84*, 76−87.
(23) Liu, R.; Groenewoud, N. A.; Peeters, M.; Lenselink, E.; Ijzerman, A. A yeast screening method to decipher the interaction between the adenosine A_{2B} receptor and the C-terminus of different G protein α-subunits. *Purinergic Signalling* **2014**, *10*, 441−453.
(24) Ladds, G.; Goddard, A.; Davey, J. Functional analysis of heterologous GPCR signalling pathways in yeast. *Trends Biotechnol.* **2005**, *23*, 367−373.
(25) Brown, A. J.; Daniels, D. A.; Kassim, M.; Brown, S.; Haslam, C. P.; Terrell, V. R.; Brown, J.; Nichols, P. L.; Staton, P. C.; Wise, A.; Dowell, S. J. Pharmacology of GPR55 in yeast and identification of GSK494581A as a mixed-activity glycine transporter subtype 1 inhibitor and GPR55 agonist. *J. Pharmacol. Exp. Ther.* **2011**, *337*, 236−246.
(26) Gao, Z.-G.; Blaustein, J. B.; Gross, A. S.; Melman, N.; Jacobson, K. A. N^6-Substituted adenosine derivatives: selectivity, efficacy, and species differences at A_3 adenosine receptors. *Biochem. Pharmacol.* **2003**, *65*, 1675−1684.

DOI: 10.1021/acs.jmedchem.5b01402
J. Med. Chem. 2016, 59, 947−964

(27) Jagtap, P.; Andover, N. Adenosine Compounds and Their Use Thereof. WO2011/119919 A1, 2011.
(28) Knutsen, L. J. S.; Lau, J.; Petersen, H.; Thomsen, C.; Weis, J. U.; Shalmi, M.; Judge, M. E.; Hansen, A. J.; Sheardown, M. J. *N*-Substituted adenosines as novel neuroprotective A_1 agonists with diminished hypotensive effects. *J. Med. Chem.* **1999**, *42*, 3463−3477.
(29) Kotra, L. P.; Manouilov, K. K.; Cretton-Scott, E.; Sommadossi, J.-P.; Boudinot, F. D.; Schinazi, R. F.; Chu, C. K. Synthesis, biotransformation, and pharmacokinetic studies of 9-(β-D-arabinofuranosyl)-6-azidopurine: a prodrug for ara-A designed to utilize the azide reduction pathway. *J. Med. Chem.* **1996**, *39*, 5202−5207.
(30) Vernekar, S. K. V.; Hallaq, H. Y.; Clarkson, G.; Thompson, A. J.; Silvestri, L.; Lummis, S. C. R.; Lochner, M. Toward biophysical probes for the 5-HT_3 receptor: structure−activity relationship study of granisetron derivatives. *J. Med. Chem.* **2010**, *53*, 2324−2328.
(31) Gao, Z.-G.; Mamedova, L. K.; Chen, P.; Jacobson, K. A. 2-Substituted adenosine derivatives: affinity and efficacy at four subtypes of human adenosine receptors. *Biochem. Pharmacol.* **2004**, *68*, 1985−1993.
(32) Middleton, R. J.; Briddon, S. J.; Cordeaux, Y.; Yates, A. S.; Dale, C. L.; George, M. W.; Baker, J. G.; Hill, S. J.; Kellam, B. New fluorescent adenosine A_1-receptor agonists that allow quantification of ligand-receptor interactions in microdomains of single living cells. *J. Med. Chem.* **2007**, *50*, 782−793.
(33) Yang, Z.; Manning, D. D. 2-Alkylbenzoxazole Carboxamides as 5-HT_3 Modulators. US2008/0214601 A1, 2008.
(34) Verheyden, J. P. H.; Moffatt, J. G. Halo sugar nucleosides. III. Reactions for the chlorination and bromination of nucleoside hydroxyl groups. *J. Org. Chem.* **1972**, *37*, 2289−2299.
(35) Ijzerman, A. P.; Fredholm, B. B.; Jacobson, K. A.; Linden, J.; Müller, C. E. Adenosine Receptors: A1 Receptor. IUPHAR/BPS Guide to Pharmacology. Last modified on 23/07/2015.http://www.guidetopharmacology.org/GRAC/ObjectDisplayForward?objectId=18 (accessed on Aug 14, 2015).
(36) Black, J. W.; Leff, P. Operational models of pharmacological agonism. *Proc. R. Soc. London, Ser. B* **1983**, *220*, 141−162.
(37) Figueroa, K. W.; Griffin, M. T.; Ehlert, F. J. Selectivity of agonists for the active state of M1 to M4 muscarinic receptor subtypes. *J. Pharmacol. Exp. Ther.* **2009**, *328*, 331−342.
(38) Gurden, M. F.; Coates, J.; Ellis, F.; Evans, B.; Foster, M.; Hornby, E.; Kennedy, I.; Martin, D. P.; Strong, P.; Vardey, C. J.; Wheeldon, A. Functional characterization of three adenosine receptor types. *Br. J. Pharmacol.* **1993**, *109*, 693−698.
(39) Colca, J. R. Discontinued drugs 2011: endocrine and metabolic. *Expert Opin. Invest. Drugs* **2012**, *21*, 1619−1624.
(40) Yang, M.; Chu, R.; Chisholm, J. W.; Doege, H.; Belardinelli, L.; Dhalla, A. K. Adenosine A_1 receptors do not play a major role in the regulation of lipogenic gene expression in hepatocytes. *Eur. J. Pharmacol.* **2012**, *683*, 332−339.
(41) Cordeaux, Y.; Briddon, S. J.; Alexander, S. P. H.; Kellam, B.; Hill, S. J. Agonist-occupied A_3 adenosine receptors exist within heterogeneous complexes in membrane microdomains of individual living cells. *FASEB J.* **2008**, *22*, 850−860.
(42) Baker, J. G.; Hill, S. J. A comparison of the antagonist affinities for the G_i- and G_s-coupled states of the human adenosine A_1-receptor. *J. Pharmacol. Exp. Ther.* **2007**, *320*, 218−228.
(43) Xu, F.; Wu, H.; Katritch, V.; Han, G. W.; Jacobson, K. A.; Gao, Z.-G.; Cherezov, V.; Stevens, R. C. Structure of an agonist-bound human A_{2A} adenosine receptor. *Science* **2011**, *332*, 322−327.
(44) Lebon, G.; Warne, T.; Edwards, P. C.; Bennett, K.; Langmead, C. J.; Leslie, A. G. W.; Tate, C. G. Agonist-bound adenosine A_{2A} receptor structures reveal common features of GPCR activation. *Nature* **2011**, *474*, 521−525.
(45) Ballesteros, J. A.; Weinstein, H. Integrated Methods for the Construction of Three-Dimensional Models and Computational Probing of Structure-Function Relations in G Protein-Coupled Receptors. In *Methods in Neurosciences*; Stuart, C. S., Ed.; Academic Press: San Diego, CA, 1995; Vol. 25, pp 366−428.
(46) Yuan, S.; Hu, Z.; Filipek, S.; Vogel, H. W246$^{6.48}$ opens a gate for a continuous intrinsic water pathway during activation of the adenosine A_{2A} receptor. *Angew. Chem. Int. Ed.* **2015**, *54*, 556−559.
(47) Elfatih, E.; Prabha, I.; Venkata, P.; Vaibhav, V.; Zablocki, J. Partial and Full Agonists of A_1 Adenosine Receptors. US2005/0020532 A1, 2005.
(48) Hong, C. I.; Tritsch, G. L.; Mittelman, A.; Hebborn, P.; Chheda, G. B. Synthesis and antitumor activity of 5′-phosphates and cyclic 3′,5′-phosphates derived from biologically active nucleosides. *J. Med. Chem.* **1975**, *18*, 465−473.
(49) Zablocki, J.; Elfatih, E.; Organ, M.; Bilokin, Y.; Mayer, S.; Disanti, A.; Miller, S.; Kernast, P. Partial and Full Agonists of A_1 Receptors. US2006/0052330 A1, 2006.
(50) Gietz, R. D.; Schiestl, R. H. Microtiter plate transformation using the LiAc/SS carrier DNA/PEG method. *Nat. Protocols* **2007**, *2*, 35−37.
(51) Dohlman, H. G.; Apaniesk, D.; Chen, Y.; Song, J.; Nusskern, D. Inhibition of G-protein signaling by dominant gain-of-function mutations in Sst2p, a pheromone desensitization factor in *Saccharomyces cerevisiae*. *Mol. Cell. Biol.* **1995**, *15*, 3635−43.
(52) Didmon, M.; Davis, K.; Watson, P.; Ladds, G.; Broad, P.; Davey, J. Identifying regulators of pheromone signalling in the fission yeast *Schizosaccharomyces pombe*. *Curr. Genet.* **2002**, *41*, 241−253.
(53) Ladds, G.; Davis, K.; Hillhouse, E. W.; Davey, J. Modified yeast cells to investigate the coupling of G protein-coupled receptors to specific G proteins. *Mol. Microbiol.* **2003**, *47*, 781−792.
(54) Ladds, G.; Davis, K.; Das, A.; Davey, J. A constitutively active GPCR retains its G protein specificity and the ability to form dimers. *Mol. Microbiol.* **2005**, *55*, 482−497.
(55) Croft, W.; Hill, C.; McCann, E.; Bond, M.; Esparza-Franco, M.; Bennett, J.; Rand, D.; Davey, J.; Ladds, G. A physiologically required G protein-coupled receptor (GPCR)-regulator of G protein signaling (RGS) interaction that compartmentalizes RGS activity. *J. Biol. Chem.* **2013**, *288*, 27327−27342.
(56) Motulsky, H. A.; Christopoulos, A. *Fitting Models to Biological Data Using Linear and Nonlinear Regression: A Practical Guide to Curve Fitting*; Oxford University Press: New York, 2004.
(57) Notredame, C.; Higgins, D. G.; Heringa, J. T-coffee: a novel method for fast and accurate multiple sequence alignment. *J. Mol. Biol.* **2000**, *302*, 205−217.
(58) Webb, B.; Sali, A. Comparative Protein Structure Modeling Using MODELLER. In *Current Protocols in Bioinformatics*; John Wiley & Sons, Inc.: New York, 2002.

DOI: 10.1021/acs.jmedchem.5b01402
J. Med. Chem. 2016, 59, 947−964

Appendix 2

Publication: Weston *et al*, 2016

This appendix contains:

Weston C, Winfield I, Harris M, Hodgson R, Shah A, Dowell SJ, Mobarec JC, Woodcock DA, Reynolds CA, Poyner DR, Watkins HA, Ladds G (**2016**). Receptor activity-modifying protein-directed G protein signaling specificity for the calcitonin gene-related peptide family of receptors. *J. Biol. Chem.* (42):21925-21944.

and erratum:

Weston C, Winfield I, Harris M, Hodgson R, Shah A, Dowell SJ, Mobarec JC, Woodcock DA, Reynolds CA, Poyner DR, Watkins HA, Ladds G (**2016**). Receptor activity-modifying protein-directed G protein signaling specificity for the calcitonin gene-related peptide family of receptors. *J. Biol. Chem.* (49):25763.

⌘ *Author's Choice*

THE JOURNAL OF BIOLOGICAL CHEMISTRY VOL. 291, NO. 42, pp. 21925–21944, October 14, 2016

Receptor Activity-modifying Protein-directed G Protein Signaling Specificity for the Calcitonin Gene-related Peptide Family of Receptors*[S]

Received for publication, August 1, 2016, and in revised form, August 25, 2016 Published, JBC Papers in Press, August 26, 2016, DOI 10.1074/jbc.M116.751362

Cathryn Weston[‡1], Ian Winfield[‡§1], Matthew Harris[§], Rose Hodgson[‡], Archna Shah[‡], Simon J. Dowell[¶], Juan Carlos Mobarec[‖], David A. Woodlock[‖], Christopher A. Reynolds[‖], David R. Poyner[**], Harriet A. Watkins[‡‡], and Graham Ladds[§2]

*From the [‡]Division of Biomedical Cell Biology, Warwick Medical School, University of Warwick, Coventry, CV4 7AL, United Kingdom, the [§]Department of Pharmacology, University of Cambridge, Cambridge, CB2 1PD, United Kingdom, the [¶]Department of Platform Technology and Science, GlaxoSmithkline, Hertfordshire, SG1 2NY, United Kingdom, the [‖]School of Biological Sciences, University of Essex, Wivenhoe Park, Colchester, Essex, CO4 3SQ, United Kingdom, the **School of Life and Health Sciences, Aston University, Aston Triangle, Birmingham, B4 7ET, United Kingdom, and the [‡‡]School of Biological Sciences and Maurice Wilkins Centre for Molecular Biodiscovery, University of Auckland, Auckland 1010, New Zealand*

The calcitonin gene-related peptide (CGRP) family of G protein-coupled receptors (GPCRs) is formed through the association of the calcitonin receptor-like receptor (CLR) and one of three receptor activity-modifying proteins (RAMPs). Binding of one of the three peptide ligands, CGRP, adrenomedullin (AM), and intermedin/adrenomedullin 2 (AM2), is well known to result in a $G\alpha_s$-mediated increase in cAMP. Here we used modified yeast strains that couple receptor activation to cell growth, via chimeric yeast/$G\alpha$ subunits, and HEK-293 cells to characterize the effect of different RAMP and ligand combinations on this pathway. We not only demonstrate functional couplings to both $G\alpha_s$ and $G\alpha_q$ but also identify a $G\alpha_i$ component to CLR signaling in both yeast and HEK-293 cells, which is absent in HEK-293S cells. We show that the CGRP family of receptors displays both ligand- and RAMP-dependent signaling bias among the $G\alpha_s$, $G\alpha_i$, and $G\alpha_{q/11}$ pathways. The results are discussed in the context of RAMP interactions probed through molecular modeling and molecular dynamics simulations of the RAMP-GPCR-G protein complexes. This study further highlights the importance of RAMPs to CLR pharmacology and to bias in general, as well as identifying the importance of choosing an appropriate model system for the study of GPCR pharmacology.

Calcitonin gene-related peptide (CGRP),[3] adrenomedullin (AM), and adrenomedullin 2 (AM2, also known as intermedin) are members of the calcitonin peptide family (1). This family also includes calcitonin and amylin. CGRP, an extremely abundant neuropeptide, is widely distributed throughout the sensory nervous system. It is a very potent vasodilator released during neurogenic inflammation and is particularly implicated in the onset of migraine. It is also cardioprotective and is associated with both pro- and anti-inflammatory actions (2, 3). AM is produced by the vascular endothelium and has extensive effects on the cardiovascular system including stimulation of angiogenesis and the modulation of vascular tone (4–6). AM2 affects the vascular system in a similar manner to AM (7–9). Like CGRP, AM and AM2 are also cardioprotective, and their administration results in decreased blood pressure and increased speed of recovery from myocardial infarction (10, 11).

CGRP, AM, and AM2 activate three receptors that share a common class B G protein-coupled receptor (GPCR) subunit, the calcitonin receptor-like receptor (CLR) (12). In each receptor, CLR forms a heterodimer with receptor activity-modifying protein (RAMP) 1, 2, or 3. The formation of this heterodimer is obligatory for receptor function and efficient translocation of both subunits to the cell surface (13). Heterodimerization with RAMP1, RAMP2, or RAMP3 forms the CGRP, AM_1, or AM_2 receptor, respectively (13). The peptide ligands activate each receptor with differing potencies (1, 12).

Activation of all three CLR-based receptors by CGRP, AM, or AM2 generates increased cAMP production through coupling to the stimulatory G protein, $G\alpha_s$ (1, 12, 14). However, CGRP, AM, and AM2 can signal through other pathways (1, 15, 16). Several studies have indicated that the CGRP family of receptors can also couple to $G\alpha_{i/o}$ subunits, because their cAMP

* This work was supported by the National Heart Foundation of New Zealand (to H. A. W.), the School of Biological Sciences, University of Auckland seed fund (to H. A. W.), Grants BB/M00015X/1 (to G. L.), BB/M000176/1 (to D. R. P.), and BB/M006883/1 (to C. A. R.) from the BBSRC, BBSRC Doctoral Training Partnership Grant BB/JO14540/1 (to M. H.), MRC Doctoral Training Partnership MR/J003964/1 (to I. W.), the Warwick Impact Fund (to C. W. and G. L.), Grant RD13301 from the Warwick Research Development Fund (to C. W. and G. L.), and the Warwick Undergraduate Research Scholarship Scheme (to A. S. and R. H). The authors declare they have no conflicts of interest with the contents of this article.

[S] This article contains supplemental Movies 1 and 2.
[1] Both authors contributed equally to this work.
[2] To whom correspondence should be addressed: Dept. of Pharmacology, University of Cambridge, Tennis Court Rd., Cambridge, CB2 1PD, United Kingdom. Tel.: 44-1223-334020; E-mail: grl30@cam.ac.uk.

[3] The abbreviations used are: CGRP, calcitonin gene-related peptide; AM, adrenomedullin; GPCR, G protein-coupled receptor; CLR, calcitonin receptor-like receptor; RAMP, receptor activity-modifying protein; POPC, 1-palmitoyl-2-oleoyl-*sn*-glycero-3-phosphocholine; PTX, pertussis toxin; GLP, glucagon-like peptide; GCGR, glucagon receptor; TM, transmembrane; ANOVA, analysis of variance.

responses can be significantly increased through treatment with pertussis toxin (PTX), particularly in electrically excitable cells (17–20). The AM/AM_2 receptor cAMP signaling in HEK-293 cells has also been shown to be PTX-sensitive (21). The existing information on the stimulation of signaling by CGRP, AM, or AM2 other than through the $G\alpha_s$-cAMP pathway has been gained predominantly from physiological studies, and the relative signaling bias of CGRP, AM, and AM2 at the three CLR-based receptors, even for the cAMP pathway, remains to be determined.

The study of signaling bias *in vivo* is complicated by cross-talk from the wide range of signaling pathways present in certain cell lines or primary cell cultures. The *Saccharomyces cerevisiae* growth system (22) provides a robust assay that enables the examination of the coupling of a GPCR of choice to single G protein subunits. This is achieved through replacing the last five amino acids of the native yeast G protein with the corresponding sequence from the human G protein of choice (22, 23). This assay has recently been successfully employed to characterize the signaling pathways underlying glucagon-like peptide 1 (GLP-1) receptor response to GLP-1 and the many receptor agonist mimetics available (24, 25). Miret *et al*. (26) in 2002 very elegantly described the functional expression of the CLR with RAMP1 and RAMP2 in yeast. However, somewhat surprisingly, given the more recent interest in signaling bias, a further characterization of RAMP-CLR combinations in yeast has not been performed.

In this study we have utilized *S. cerevisiae* to express either RAMP1, -2, or -3 along with CLR to assess the coupling of the three CGRP family receptors to different human $G\alpha$ subunits upon stimulation with CGRP, AM, or AM2. We demonstrate that all members of the CGRP receptor family successfully couple to GPA1/$G\alpha_s$, GPA1/$G\alpha_i$, and GPA1/$G\alpha_q$ yeast chimeras and that the coupling preference of each receptor is dependent upon the stimulating ligand. The results obtained from the yeast system were verified in HEK-293 mammalian cell lines by the assessment of cAMP accumulation (which showed sensitivity to PTX) and mobilizations of intracellular calcium ($(Ca^{2+})_i$). The data confirm that RAMPs alter the ability of each peptide to couple to G proteins; they also indicate that the G proteins influence the rank order of agonist potency at the different receptors. For CGRP, AM, and AM2 this means that potent activation of what would not generally be considered their "normal" receptors can be observed when alternative downstream pathways, such as stimulation of $G\alpha_i$ or mobilizations of $(Ca^{2+})_i$, are considered.

Considerable understanding of class B GPCR structure, function, and dynamics has been gained (27), primarily through molecular dynamics simulations (28–33). Consequently, to gain insight into the possible mechanisms behind our experimental results, we used molecular modeling and molecular dynamics simulations of RAMP complexes with CLR and the glucagon receptor (GCGR) to suggest a mechanism whereby the C-terminal tail of the RAMPs may influence G protein bias at the CLR. Finally we demonstrate that care is required when selecting an appropriate mammalian cell line to use when investigating G protein bias, as analysis of a HEK-293S cell line failed to show $G\alpha_i$ coupling for any of the RAMP-CLR complexes, thus highlighting the fact that agonist bias can be directly influenced by the cellular background.

Results

$G\alpha_s$ Coupling of CLR-based Receptors—We co-expressed CLR under the control of the strong *PGK* promoter with RAMP1, RAMP2, or RAMP3 independently in a yeast strain containing a chimeric $G\alpha$ subunit in which the C-terminal five amino acids of GPA1 had been replaced with those of mammalian $G\alpha_s$, in order to study the coupling of the resultant receptors to a system expressing just a single G protein. Concentration-response curves were constructed for growth of *S. cerevisiae* for each RAMP-CLR combination (*i.e.* the CGRP, AM_1, and AM_2 receptors) using the agonists CGRP, AM, and AM2. When CLR was co-expressed with RAMP1, all three ligands appeared to generate an equivalent level of response but with differing potencies (Fig. 1*A* and Table 1). This generated a rank order of potency for the three ligands of CGRP > AM > AM2. Application of the operational model of pharmacological agonism (34) indicates that all three ligands exhibit similar efficacies (log τ) in yeast when CLR and RAMP1 are co-expressed (Fig. 1*D* and Table 1). RAMP2 co-expression with CLR generated a functional receptor (Fig. 1*B*) with rank ligand potencies of AM > AM2 = CGRP. AM2 appeared to behave as a partial agonist with a reduced log τ at the RAMP2-CLR heterodimer when compared with the other peptide agonists (Table 1). AM had a significantly higher efficacy ($p < 0.05$) than that displayed by CGRP. Expression of RAMP3 with CLR in *S. cerevisiae* generated a functional receptor where all three ligands activated GPA1/$G\alpha_s$-coupled signaling with similar potencies and efficacies (Fig. 1*C*).

We sought to confirm the pharmacology observed in the *S. cerevisiae* growth assay of the RAMP-CLR complexes in mammalian cell lines. For this we used HEK-293 cells that do not functionally express any RAMPs (25). Co-transfection of CLR and RAMP1 generated a rank order of ligand potency of CGRP ≫ AM = AM2. The rank order of ligand potency with co-transfection of CLR and RAMP2 was AM > CGRP ≫ AM2 and for CLR and RAMP3 was AM2 = AM > CGRP (Fig. 2 and Table 2). It is worth noting that, in our HEK-293 cells, only AM acted as a full agonist against the CLR when in complex with either RAMP2 or RAMP3. Overall the mammalian and yeast data showed similar results, with the most potent ligand at each receptor remaining the same in each case.

$G\alpha_i$ Coupling of CLR-based Receptors—To address the possibility that the CGRP family of receptors may couple not only to $G\alpha_s$ but also to other subunits, we returned to the *S. cerevisiae* growth assay. In this case the yeast strain used contained a chimeric GPA1/$G\alpha$ subunit including the last five residues of mammalian $G\alpha_i$. We once again constructed concentration-response curves for yeast growth to the three agonists, CGRP, AM, and AM2. The co-expression of CLR and RAMP1 resulted in similar potencies for CGRP, AM, and AM2 (Table 1); however, AM and AM2 displayed significantly increased efficacy relative to CGRP for the activation of GPA1/$G\alpha_i$ (Table 1 and Fig. 3, *A* and *D*). In contrast, when RAMP2 and CLR were co-transformed into the GPA1/$G\alpha_i$ yeast strain, the rank order of ligand potency for GPA1/$G\alpha_i$ yeast-based growth

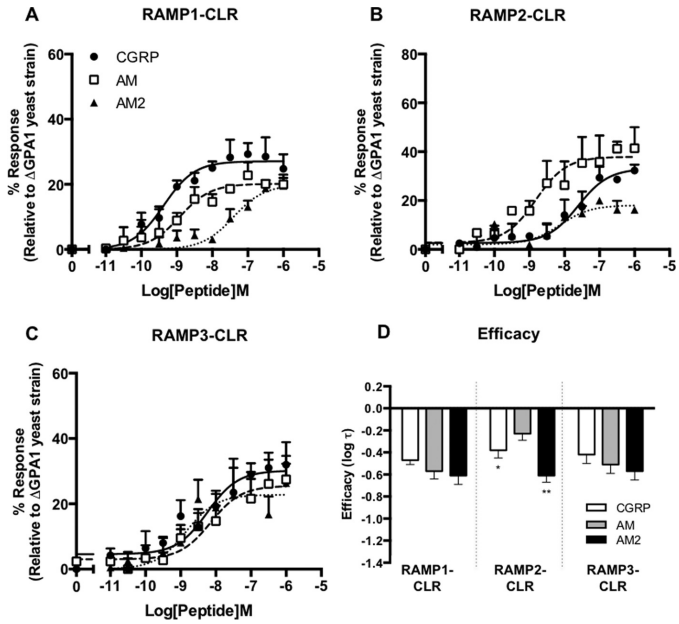

FIGURE 1. **Functional expression of CLR co-transformed with all three RAMPs in yeast cells.** Dose-response curves to CGRP, AM, and AM2 were constructed in yeast strains containing the GPA1/Gα_s chimera and expressing CLR with RAMP1 ($n = 6$) (*A*), RAMP2 ($n = 7$) (*B*), and RAMP3 ($n = 8$) (*C*). Reporter gene activity was determined following 20 h of stimulation with each ligand. Data are expressed as a percentage of the maximum response observed in yeast strain MMY11 (lacking GPA1) and are means ± S.E. of *n* individual data sets. *D*, *bar chart* showing the efficacy of each ligand for each RAMP-CLR combination as determined via application of the operational model of receptor agonism (see Ref. 34 and Table 1). Data were determined as statistically different from the cognate ligand for each receptor (*, $p < 0.05$; **, $p < 0.01$; ***, $p < 0.001$) using a one-way ANOVA with Bonferroni's post-test.

TABLE 1

Summary of pharmacological parameters for various ligands upon expression of the CLR with each RAMP in yeast strains containing GPA1/Gα_s, GPA1/Gα_i, or the GPA1/Gα_q chimera

Data are the mean ± S.E. of *n* individual data sets. Statistical significance compared with the cognate ligand (*, $p < 0.05$; **, $p < 0.01$; ***, $p < 0.001$; ****, $p < 0.0001$) for each receptor heterodimer (CGRP for RAMP1 + CLR and AM for CLR with either RAMP2 or RAMP3) was determined by one-way ANOVA with Dunnett's post-test.

	RAMP1-CLR			RAMP2-CLR			RAMP3-CLR		
	CGRP	AM	AM2	CGRP	AM	AM2	CGRP	AM	AM2
GPA1/Gα_s									
pEC_{50}[a]	9.35 ± 0.2*	8.80 ± 0.4***	7.22 ± 0.3***	7.60 ± 0.3*	8.82 ± 0.3*	8.05 ± 0.3*	8.24 ± 0.2	8.15 ± 0.4	8.85 ± 0.3
E_{max}[b]	27.10 ± 1.6*	20.39 ± 2.8***	20.65 ± 1.1***	30.34 ± 4.1	37.46 ± 3.5	19.90 ± 2.5***	30.17 ± 2.7	25.51 ± 3.6	22.80 ± 2.3
pK_α[c]	9.22 ± 0.2*	8.81 ± 0.3***	7.31 ± 0.3***	7.70 ± 0.3*	8.77 ± 0.3	8.10 ± 0.3	8.30 ± 0.3	8.10 ± 0.3	8.61 ± 0.4
log τ[d]	−0.43 ± 0.04	−0.59 ± 0.07*	−0.61 ± 0.08	−0.38 ± 0.08*	−0.23 ± 0.06	−0.61 ± 0.06**	−0.42 ± 0.08	−0.51 ± 0.08	−0.57 ± 0.08
n	6	6	6	7	7	7	8	8	8
GPA1/Gα_i									
pEC_{50}[a]	8.26 ± 0.5	8.38 ± 0.3 *	8.57 ± 0.2**	8.89 ± 0.2**	7.91 ± 0.2**	8.42 ± 0.5**	8.52 ± 0.2	7.89 ± 0.8	8.49 ± 0.2
E_{max}[b]	19.80 ± 3.0*	34.20 ± 3.7***	41.5 ± 3.3****	24.43 ± 1.7*	24.49 ± 2.0*	15.71 ± 2.5*	22.60 ± 1.8*	26.71 ± 1.8*	15.71 ± 2.1*
pK_α[c]	8.40 ± 0.5	8.20 ± 0.3**	8.24 ± 0.2	8.64 ± 0.2	7.75 ± 0.2	8.30 ± 0.5	8.37 ± 0.2	8.00 ± 0.2	8.30 ± 0.3
log τ[d]	−0.70 ± 0.1**	−0.33 ± 0.07**	−0.18 ± 0.1***	−0.50 ± 0.04**	−0.51 ± 0.05*	−0.89 ± 0.1**	−0.56 ± 0.06*	−0.50 ± 0.05*	−0.78 ± 0.07*
n	6	6	6	6	6	6	7	7	7
GPA1/Gα_q									
pEC_{50}[a]	7.53 ± 0.1	7.26 ± 0.2	7.99 ± 0.2	7.14 ± 0.2	7.93 ± 0.2	9.22 ± 0.4*	6.19 ± 0.5*	7.83 ± 0.2	6.76 ± 0.25
E_{max}[b]	26.50 ± 1.2	14.08 ± 1.2****	16.73 ± 1.1****	27.74 ± 2.3	29.03 ± 2.6	11.33 ± 1.3****	20.7 ± 4.2	25.56 ± 2.0	32.11 ± 3.7
pK_α[c]	27.40 ± 0.1	7.19 ± 0.2	7.91 ± 0.03	7.01 ± 0.2	7.78 ± 0.2	9.16 ± 0.4*	6.10 ± 0.6*	7.71 ± 0.2	6.60 ± 0.3
log τ[d]	−0.46 ± 0.03	−0.79 ± 0.04***	−0.70 ± 0.04***	−0.42 ± 0.05	−0.39 ± 0.05	−0.88 ± 0.08***	−0.63 ± 0.2	−0.48 ± 0.05	−0.34 ± 0.1
n	7	7	7	6	6	6	6	6	6

[a] The negative logarithm of the agonist concentration required to produce a half-maximal response.
[b] The maximal response to the ligand expressed as a percentage of that obtained from a yeast strain (MMY11) lacking GPA1.
[c] The negative logarithm of the equilibrium disassociation constant for each ligand generated through use of the operational model of agonism (34).
[d] Log τ is the coupling efficacy parameter of each ligand.

was CGRP > AM = AM2 (Table 1 and Fig. 3*B*). AM2 showed a significantly decreased efficacy compared with the other peptides (Table 1 and Fig. 3*D*). As with the RAMP1-CLR heterodimer, the combination of CLR and RAMP3 expressed in the GPA1/Gα_i strain resulted in similar potencies for CGRP, AM, and AM2 (Table 1 and Fig. 3*C*). However, AM2 displayed a significantly reduced efficacy when compared with AM (Table 1 and Fig. 3*D*).

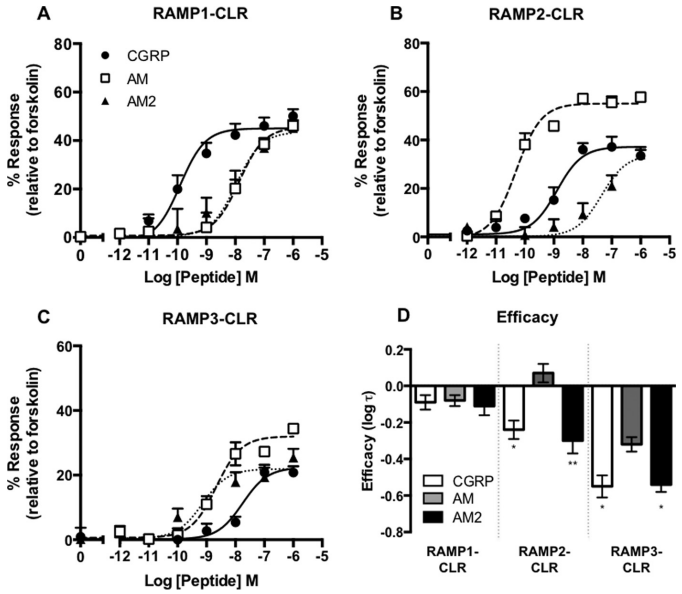

FIGURE 2. **Expression of CLR in combination with each RAMP generates functional $G\alpha_s$-coupled receptors in HEK-293 cells.** cAMP accumulation was determined in HEK-293 cells transiently transfected with the CLR and RAMP1 ($n = 11$) (*A*), RAMP2 ($n = 8$) (*B*), and RAMP3 ($n = 9$) (*C*) following 30-min stimulation with CGRP, AM, and AM2. Data are expressed as percentage of cAMP production, determined using 100 μM forskolin stimulation, and are means ± S.E. of *n* individual data sets. *D*, *bar* chart showing the efficacy of each ligand for each RAMP-CLR combination as determined via application of the operational model of receptor agonism (34). Data were determined as statistically different from the cognate ligand for each receptor (*, $p < 0.05$; **, $p < 0.01$) using one-way ANOVA with Bonferroni's post-test.

TABLE 2

Potency (pEC_{50}), affinity (pK_a) and coupling efficacy (log τ) values for cAMP production at the CLR co-expressed with each RAMP and stimulated with various agonists measured in HEK-293 cells

Data are the mean ± S.E. of *n* individual data sets. Statistical significance compared with the cognate ligand (*, $p < 0.05$; **, $p < 0.01$; ***, $p < 0.001$) for each receptor heterodimer (CGRP for RAMP1-CLR and AM for CLR with either RAMP2 or RAMP3) was determined by one-way ANOVA with Dunnett's post-test.

	RAMP1-CLR			RAMP2-CLR			RAMP3-CLR		
	CGRP	AM	AM2	CGRP	AM	AM2	CGRP	AM	AM2
pEC_{50}[a]	9.81 ± 0.20	7.92 ± 0.19**	7.93 ± 0.24**	8.97 ± 0.24***	10.35 ± 0.13	7.48 ± 0.23***	7.75 ± 0.3**	8.86 ± 0.14	9.14 ± 0.22**
E_{max}[b]	45.0 ± 2.2	45.2 ± 3.7	43.6 ± 4.2**	37.2 ± 2.4***	55.0 ± 1.7	34.1 ± 4.0**	22.3 ± 2.1**	32.1 ± 1.6	21.9 ± 1.7**
pK_a[c]	9.60 ± 0.18	7.64 ± 0.28**	7.76 ± 0.20**	8.71 ± 0.2**	9.95 ± 0.23	7.16 ± 0.24**	7.64 ± 0.26**	8.50 ± 0.19	9.00 ± 0.18**
log τ[d]	−0.08 ± 0.04	−0.08 ± 0.09**	−0.11 ± 0.06**	−0.23 ± 0.05***	0.09 ± 0.05	−0.29 ± 0.07**	−0.54 ± 0.06**	−0.33 ± 0.04	−0.56 ± 0.04**
n	11	11	11	8	8	8	9	9	9

[a] The negative logarithm of the agonist concentration required to produce a half-maximal response.
[b] The maximal response to the ligand expressed as a percentage of the maximal cAMP production as determined using 100 μM forskolin stimulation.
[c] The negative logarithm of the equilibrium disassociation constant for each ligand generated through use of the operational model of agonism (34).
[d] Log τ is the coupling efficacy parameter of each ligand.

In mammalian cells the $G\alpha_s$ and $G\alpha_i$ subunits act in opposition to regulate cAMP production. Therefore if a receptor can couple to both subunits in mammalian cells, the cAMP response measured is the result of a combination of the contribution from both pathways. Treatment of cells with PTX has been shown to uncouple receptors from the $G\alpha_i$ subunit and therefore remove any inhibition of cAMP production. We sought to confirm the apparent $G\alpha_s$-$G\alpha_i$ coupling bias exhibited by the different RAMP-CLR combinations in the yeast reporter strains by measuring cAMP production from transiently transfected mammalian cells following PTX treatment.

Pretreatment of HEK-293 cells co-expressing RAMP1 with the CLR resulted in little overall increase in CGRP-mediated cAMP production (Fig. 4*A*). However, a significant elevation in E_{max} was observed in the same PTX-treated, RAMP1-CLR-expressing cells when challenged with either AM or AM2 (Fig. 4 and Table 3), suggesting that a $G\alpha_i$ component for both of these ligands had been removed (Table 3). HEK-293 cells expressing CLR with either RAMP2 (Fig. 4*B*) or RAMP3 (Fig. 4*C*) displayed PTX-induced increases in E_{max} for cAMP accumulation following stimulation with both CGRP and AM2 (Table 3). However, for both combinations, the AM response appeared to be unaffected by PTX treatment, suggesting that little $G\alpha_i$ coupling was present. Indeed, it is worth noting, that the cognate ligand for each receptor (CGRP for RAMP1-CLR and AM for RAMP2-CLR or RAMP3-CLR) did not appear to display an

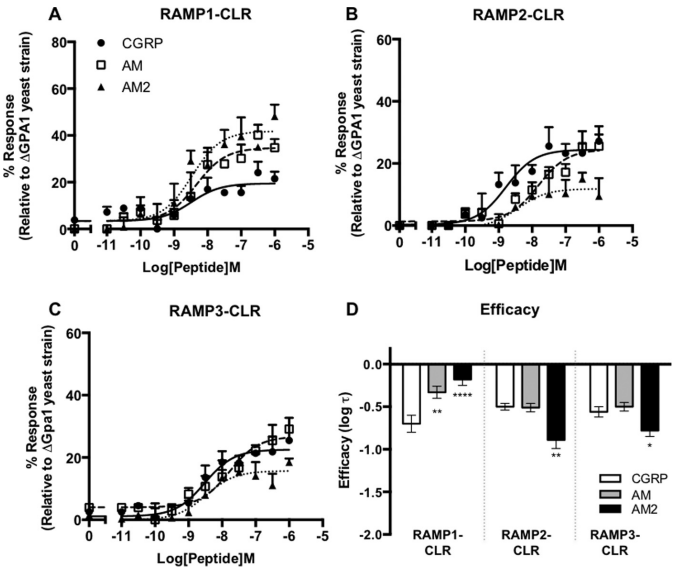

FIGURE 3. **Co-transformation of CLR with all three RAMPs in yeast cells generates receptors that couple functionally to the $G\alpha_i$ chimera.** Dose-response curves to CGRP, AM, and AM2 were constructed in yeast strains containing the GPA1/$G\alpha_i$ chimera and expressing CLR with RAMP1 ($n = 6$) (*A*), RAMP2 ($n = 6$) (*B*), and RAMP3 ($n = 7$) (*C*). Reporter gene activity was determined following 20 h of stimulation. All data are expressed as percentage of the maximum response observed in yeast strain MMY11 (lacking GPA1) and are means ± S.E. of *n* individual data sets. *D, bar* chart showing the efficacy of each ligand for each RAMP-CLR combination as determined via application of the operational model of receptor agonism (Ref. 34 and Table 1). Data were determined as statistically different from the cognate ligand for each receptor (*, $p < 0.05$; **, $p < 0.01$; ***, $p < 0.001$; ****, $p < 0.0001$) using a one-way ANOVA with Bonferroni's post-test.

increased E_{max} upon PTX treatment, suggesting limited $G\alpha_i$ components in these cases. Importantly, PTX treatment of untransfected HEK-293 cells did not result in a change in the overall levels of cAMP accumulation as determined by forskolin stimulation (untreated, 16.57 ± 2.5 pmol cell^{-1}; treated, 16.45 ± 2.4 pmol cell^{-1}), thereby confirming that the effects observed were specific to the RAMP-CLR combinations. Thus, there is abundant evidence that receptor and ligands can activate $G\alpha_i$ in a mammalian cell, albeit in a complex pattern.

Cell Line Variability in G Protein Expression—The HEK-293 human cell lineage has undergone a number of modifications (35). One such lineage, HEK-293S, was adapted for growth in suspension (36). Interestingly, HEK-293S lines have also been reported to lack expression of RAMPs and therefore provide an alternative background for investigating the modulation of GPCR signal transduction (37, 38). Given that previous reports suggest that some of the effects observed with RAMPs are cell type-dependent (37, 39), we utilized HEK-293S cells as an alternative cell line. Surprisingly, and in contrast to what was observed for HEK-293 cells, HEK-293S cells pretreated with PTX and co-expressing RAMP1, RAMP2, or RAMP3 with CLR failed to demonstrate any significant change in either potency or E_{max} when challenged with CGRP, AM, or AM2 (Fig. 5 and Table 4; compare with Fig. 4). These results suggest that in HEK-293S cells, the RAMP-CLR combinations display little $G\alpha_i$-mediated responses. This led us to speculate about the respective G protein content for the two cell lines. Using semi-quantitative RT-PCR we assessed the expression of 12 $G\alpha$ subunits (Fig. 6, *A* and *B*) in both mammalian cell lines. In the HEK-293 cells we were able to detect the expression of ten $G\alpha$ subunits, with a profile similar to that documented previously for these cells (40). Transcripts were not detectable for the $G\alpha_{14}$ or $G\alpha_{15}$ subunits. Interestingly, in comparison with the HEK-293 cells, the HEK-293S cells displayed significantly lower expression of two $G\alpha_i$ subunits (relative to GAPDH) but broadly similar levels of all others $G\alpha$ subunits. Furthermore, there was a much better correlation between the pEC_{50} values for the ligands on HEK-293 and HEK-293S cells when the former had been pretreated with PTX, to remove the $G\alpha_i$ component, suggesting that the differences in $G\alpha_i$ expression between the two cell lines have functional significance (Fig. 6*C*, $r = 0.80$ (95% confidence interval, 0.27–0.96) with PTX *versus* 0.52 (95% confidence interval, −0.22 to 0.89) without PTX; $p < 0.05$). Importantly, these data demonstrate the need for caution when choosing cells for assessing G protein-mediated signaling responses.

$G\alpha_{q/11}$ Coupling of CLR-based Receptors—To provide a complete investigation of the G protein coupling of the RAMP-CLR complexes, we extended our study to include the remaining nine GPA1/$G\alpha$ yeast chimera-expressing strains. Coupling with the RAMP-CLR heterodimers was observed only in one additional strain that representing $G\alpha_q$ (strain MMY89). Concentration-response curves were generated (Fig. 7, *A–C*, and Table 1), demonstrating that at RAMP1-CLR all three ligands displayed similar potencies, with CGRP being the most efficacious (log τ, Table 1) as expected for the cognate ligand at this

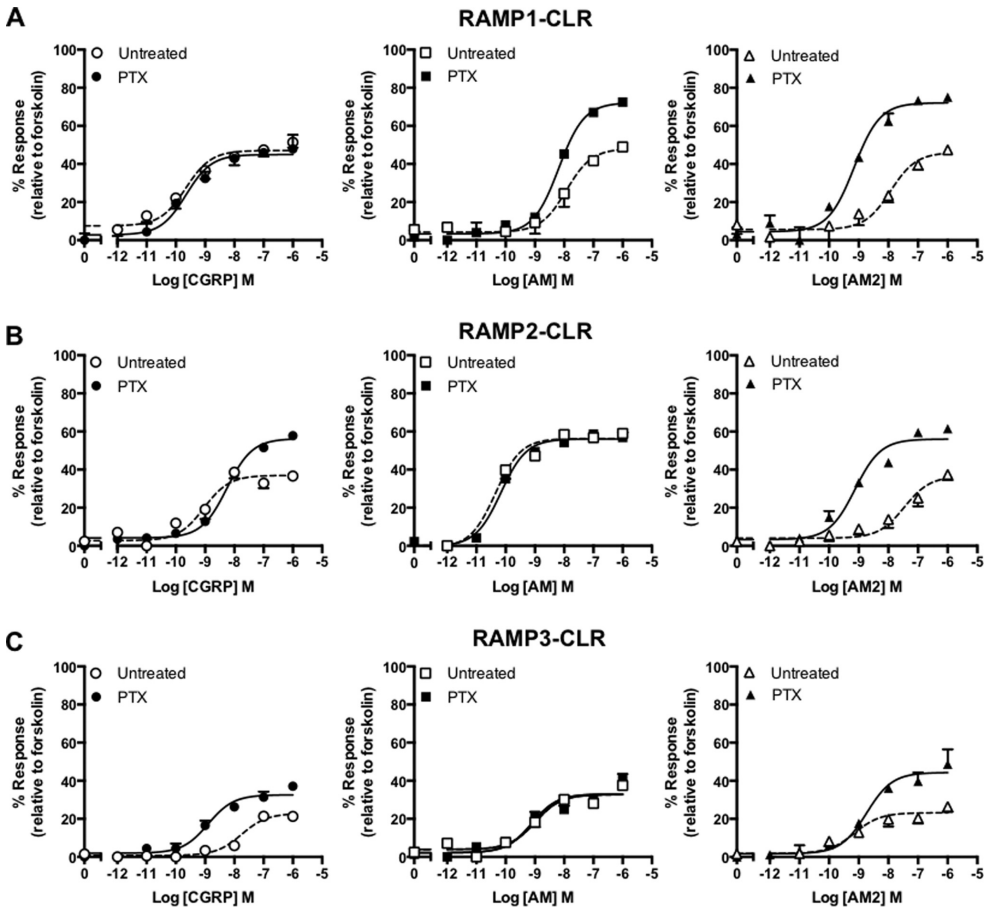

FIGURE 4. **CLR in combination with each RAMP generates receptors that display PTX-sensitive effects in response to ligand stimulation.** cAMP accumulation was determined in the presence (treated) and absence (untreated) of PTX from HEK-293 cells transiently transfected with CLR and RAMP1 ($n = 6$) (*A*), RAMP2 ($n = 5$) (*B*), and RAMP3 ($n = 5$) (*C*). Cells were stimulated for 30 min with CGRP, AM, and AM2. Data are expressed as percentage of the maximal cAMP production as determined using 100 μM forskolin stimulation in the presence of PTX and are means ± S.E. of *n* individual data sets.

receptor. AM2 is the most potent ligand when activating the RAMP2-CLR complex, having a reduced E_{max} and log τ relative to CGRP and AM (Table 1). With RAMP3-CLR, a rank order of ligand potency of AM > AM2 > CGRP was observed (Fig. 7*C* and Table 1), with all three ligands displaying broadly similar efficacies (Table 1).

Ligand-engendered G Protein Bias—To provide a means by which to determine the relative bias each agonist displays at each RAMP-CLR complex for the three different chimeric G proteins (in yeast), we calculated the bias factor (expressed as $\Delta\Delta(\tau/K_a)$) (41). For the RAMP1-CLR heterodimer, the values were calculated relative to CGRP, whereas when CLR was expressed with RAMP2 or RAMP3 the reference ligand was AM. In all cases the reference pathway used was GPA1/Gα_s (Fig. 7*E*). The bias plots demonstrated that at the RAMP1-CLR complex, AM2 showed a much greater bias toward signaling via GPA1/Gα_i and GPA1/Gα_q relative to CGRP, whereas AM showed a bias profile approximately equal to CGRP. With RAMP2-CLR, however, CGRP showed a much greater bias toward GPA1/Gα_i signaling over GPA1/Gα_s and GPA1/Gα_q, whereas AM2 was more biased toward GPA1/Gα_q. In the presence of RAMP3 all three ligands were equally biased toward GPA1/Gα_s and GPA1/Gα_i, but CGRP and AM were less biased toward GPA1/Gα_q signaling relative to AM2.

Activation of RAMP-CLR Complexes Leads to Mobilization of Intracellular Ca^{2+} in Mammalian Cells—To confirm our findings from *S. cerevisiae*, we again utilized HEK-293 cells transiently expressing the CLR in conjunction with each RAMP and measured the release of $(Ca^{2+})_i$ upon stimulation with CGRP, AM, and AM2. Although all three ligands resulted in calcium

TABLE 3

Potency (pEC_{50}), affinity (pK_a), and coupling efficacy (log τ) values for cAMP production at the CLR co-expressed with each RAMP, stimulated with various agonists measured in HEK-293 cells in the presence and absence of pertussis toxin

Data are the mean ± S.E. of *n* individual data sets. Statistical difference between PTX-treated and untreated cells was determined using Student's *t* test (*, $p < 0.05$; **, $p < 0.01$; ***, $p < 0.001$; ****, $p < 0.0001$).

	Untreated					Treated				
	pEC_{50}[a]	E_{max}[b]	pK_a[c]	log τ[d]	*n*	pEC_{50}[a]	E_{max}[b]	pK_a[c]	log τ[d]	*n*
RAMP1										
CGRP	9.66 ± 0.2	47.07 ± 2.2	9.43 ± 0.2	−0.11 ± 0.04	9	9.65 ± 0.2	44.95 ± 2.2	9.33 ± 0.3	−0.11 ± 0.07	6
AM	7.93 ± 0.2	48.06 ± 2.5	7.67 ± 0.2	−0.09 ± 0.05	9	8.14 ± 0.07	72.17 ± 1.7***	7.66 ± 0.2	− 0.36 ± 0.1**	6
AM2	7.93 ± 0.2	46.10 ± 4.1	7.70 ± 0.2	−0.11 ± 0.07	9	9.15 ± 0.1*0	72.15 ± 2.4***	8.56 ± 0.3	− 0.40 ± 0.1**	6
RAMP2										
CGRP	19.00 ± 0.2	36.97 ± 2.4	18.82 ± 0.2	−0.27 ± 0.05	9	18.25 ± 0.4	56.27 ± 1.4***	7.92 ± 0.2*	0 0.1 ± 0.06**	6
AM	10.35 ± 0.1	56.33 ± 1.6	10.00 ± 0.1	−0.07 ± 0.02	9	10.16 ± 0.07	56.07 ± 1.1	9.83 ± 0.2	0.07 ± 0.02	6
AM2	17.46 ± 0.2	36.61 ± 3.5	17.24 ± 0.2	−0.29 ± 0.07	9	19.13 ± 0.1**	56.05 ± 2.2***	8.84 ± 0.2**	00.1 ± 0.06*	6
RAMP3										
CGRP	7.75 ± 0.3	22.38 ± 2.6	7.64 ± 0.3	−0.54 ± 0.07	8	8.90 ± 0.1*	32.61 ± 1.5*	8.74 ± 0.2*	−0.29 ± 0.06	7
AM	8.98 ± 0.2	32.00 ± 1.5	8.83 ± 0.1	−0.33 ± 0.03	8	9.10 ± 0.2	35.95 ± 2.2	8.94 ± 0.2	−0.34 ± 0.05	7
AM2	9.10 ± 0.2	21.92 ± 1.7	9.08 ± 0.2	−0.51 ± 0.06	8	8.74 ± 0.2	44.35 ± 2.7****	8.43 ± 0.1*	−0.07 ± 0.07***	7

[a] The negative logarithm of the agonist concentration required to produce a half-maximal response.
[b] The maximal response to the ligand expressed as a percentage of the maximal cAMP production as determined using 100 μM forskolin stimulation in the presence of pertussis toxin treatment.
[c] The negative logarithm of the equilibrium disassociation constant for each ligand generated through use of the operational model of agonism (34).
[d] Log τ is the coupling efficacy parameter of each ligand.

mobilization at each RAMP-CLR complex (Fig. 8 and Table 5), these results differed slightly from that observed in *S. cerevisiae*. At both RAMP1 and RAMP2-CLR a rank order of ligand potency of CGRP = AM > AM2 was seen, whereas CGRP was the most efficacious ligand (Table 5). With RAMP3-CLR, both AM and AM2 were equipotent, with CGRP being the least potent agonist. Treatment with PTX was seen to have no effect upon the levels of calcium released in response to the three ligands, at any RAMP-CLR complex.

To confirm our yeast findings that the CLR can couple to $G\alpha_q$ and thereby promote $(Ca^{2+})_i$ mobilization in mammalian cells, we utilized the known selective $G\alpha_{q/11}$ inhibitor YM-254890 (42). Pretreatment with YM-254890 for 30 min prior to stimulation with AM and AM2 was sufficient to abolish all $(Ca^{2+})_i$ mobilization at all RAMP-CLR complexes. Furthermore, the response to CGRP at all three RAMP-CLR complexes was also considerably attenuated with $(Ca^{2+})_i$ release, being detected only when cells were stimulated with CGRP in the micromolar range. Similar data were obtained using HEK-293S cells (Table 5), suggesting that despite differences in $G\alpha_i$ content, the release of $(Ca^{2+})_i$ was consistent between the two cell types. These finding suggest that all three ligands are able to initiate calcium mobilization at all three RAMP-CLR complexes in a Gαq-dependent manner in both mammalian cell lines.

Pathway Bias at the RAMP-CLR Complexes—Through calculating the change in the ratio of $\log(\tau/K_a)$ between cAMP accumulation and the release of $(Ca^{2+})_i$, it is possible to determine the extent of signaling bias for a ligand (Fig. 9*A*). In HEK-293 cells all ligands showed cAMP bias over $(Ca^{2+})_i$, except for AM2 and CGRP at RAMP2-CLR and RAMP3-CLR, respectively. In contrast, in HEK-293S cells all ligands showed clear bias toward cAMP at each RAMP-CLR complex. Interestingly, treatment of HEK-293 cells with PTX generated bias profiles similar to that observed for HEK-293S cells (Fig. 9).

Further analysis of these bias factors relative to the cognate ligand at each RAMP-CLR complex (Fig. 9*B*) indicates that only AM2 displays bias toward cAMP at the RAMP1- and RAMP3-CLR complexes, whereas all other ligands display a preference to mobilize $(Ca^{2+})_i$. Again, this is slightly different than the bias profile for HEK-293S cells. At the RAMP1-CLR complex, AM is biased toward $(Ca^{2+})_i$, and AM2 is cAMP-biased. For RAMP2-CLR, CGRP is biased toward $(Ca^{2+})_i$ mobilization, whereas AM2 is neutral. At RAMP3-CLR all ligands are neutral and display no bias. As noted above, the inhibition of any signaling input from $G\alpha_i$ in HEK-293 cells via PTX treatment generates a relative bias profile comparable with that seen in HEK-293S cells. Thus, we show that not only do RAMPs play a significant role in modulating signaling bias but also that cellular G protein content can drastically modulate any perceived bias.

Molecular Modeling of CLR and GCGR in Complex with RAMPs—Our experimental data suggest that RAMPs may perform a critical role in modulating G protein coupling and bias. However, we do not as yet have any insight into the mechanism by which this may be achieved. To at least partially address this issue, we turned to the use of molecular modeling. We generated models of GCGR in complex with RAMP2 and CLR in complex with RAMP1. We used the GCGR system because it provides a reference system. The interaction between the peptide and the ligand is particularly well defined in the homologous GLP-1R system through reciprocal mutagenesis and photoaffinity labeling (28, 29); also we have shown that the interaction between GCGR and RAMP2 affects G protein bias (25). Models taken from the last step in the 500-ns trajectory show that in both cases, the C-terminal region of the RAMP resides in the vicinity of helix 8 (H8), the intracellular ends of TM6 and TM7, and the C-terminal region of $G\alpha_s$ (Fig. 10, *A* and *B*). There are differences in the orientation of the extracellular domain and the precise location of the RAMP transmembrane (TM) helix due to the dynamic nature of the systems, the longer "stalk" (the region between the extracellular domain and TM1) in GCGR, and the sequence differences between the receptors and between RAMP1 and RAMP2. There are no direct interactions between the RAMPs and the peptide ligands.

Analyses of the MD trajectories show that for GCGR and CLR, the C-terminal region of the RAMP approaches the C-ter-

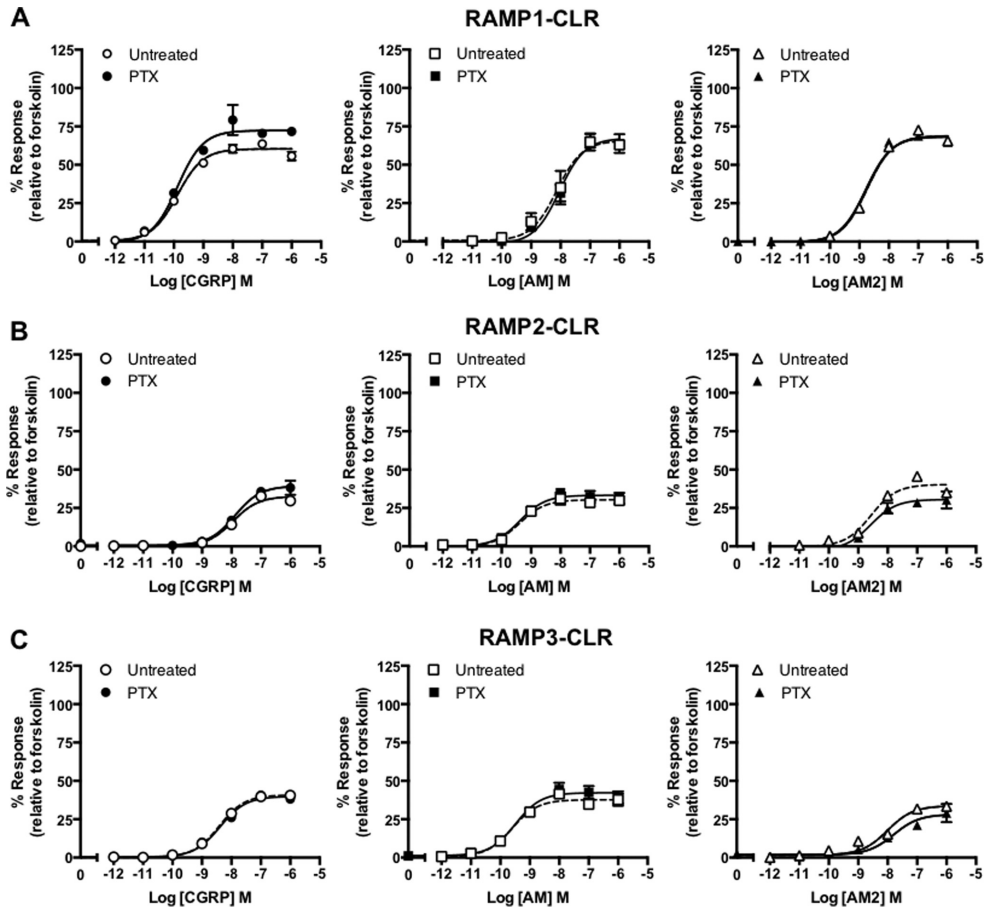

FIGURE 5. **RAMP-CLR responses appear PTX-insensitive when assayed using HEK-293S cells.** cAMP accumulation was determined in the presence (treated) and absence (untreated) of PTX from HEK-293S cells transiently transfected with CLR and RAMP1 ($n = 5$) (*A*), RAMP2 ($n = 5$) (*B*), and RAMP3 ($n = 5$) (*C*). Cells were stimulated for 30 min with CGRP, , and AM2. Data are expressed as percentage of the maximal cAMP production as determined using 100 μM forskolin stimulation in the presence of PTX and are means ± S.E. of *n* individual data sets.

minal peptide of the G protein within the first 100 ns (Fig. 10*C*). For GCGR the primary interaction is with the G protein, but there are also interactions with H8. For CLR the first part of the tail interacts with the G protein, whereas the tip of the tail interacts with H8; in both CLR and GCGR there are also interactions with the intracellular end of TM6. The interactions are driven by a combination of steric, hydrophobic, and electrostatic factors. Movies of both simulations are provided as supporting information (supplemental Movies 1 (RAMP2-GCGR-Gα_s) and 2 (RAMP1-CLR-Gα_s)).

The extracellular end of TM7 of GCGR moves inward under the influence of RAMP2. Analysis of the distances between the extracellular end of TM2 (Cα of residue Lys-205), TM7 (Cα of residue Gly-375), the RAMP2 linker (Cα of residue Val-145), and the peptide (Cα of residue Tyr-13) shows that the RAMP TM, TM7, and the peptide move as a collective unit toward TM2 (Fig. 11), indicating a mechanism whereby the peptide ligand can influence the RAMP and vice versa even in the absence of a direct interaction.

Discussion

The pharmacology of the CGRP family of receptors is relatively well characterized with respect to Gα_s coupling and the resultant accumulation of cAMP (1, 12). Gα_q and Gα_i coupling to these receptors, however, is less well characterized. Here we report the extension of the use of the *S. cerevisiae* system to investigate signaling bias in the CGRP family of receptors. These receptors are obligate heterodimers of the GPCR, namely CLR with one of three RAMPs. This dimerization adds an increased level of complexity to the system. We find that the

TABLE 4

Potency (pEC_{50}) and maximal response (E_{max}) for cAMP production at the CLR co-expressed with each RAMP stimulated with various agonists measured in HEK-293S cells in the presence or absence of pertussis toxin

Data are the mean ± S.E. of *n* individual data sets. No statistical difference was found between untreated and PTX-treated HEK-293S cells using Student's *t* test.

	Untreated			Treated		
	pEC_{50}[a]	E_{max}[b]	*n*	pEC_{50}[a]	E_{max}[b]	*n*
RAMP1						
CGRP	9.88 ± 0.1	59.98 ± 1.1	5	9.87 ± 0.1	72.92 ± 2.3	5
AM	8.13 ± 0.1	60.00 ± 3.1	5	8.03 ± 0.1	61.26 ± 2.6	5
AM2	8.74 ± 0.1	68.94 ± 1.2	5	8.78 ± 0.1	68.30 ± 1.6	5
RAMP2						
CGRP	8.00 ± 0.1	32.56 ± 1.0	5	7.88 ± 0.1	39.32 ± 1.7	5
AM	9.39 ± 0.1	30.34 ± 0.8	5	9.38 ± 0.1	33.28 ± 1.2	5
AM2	8.57 ± 0.1	40.30 ± 1.5	5	18.58 ± 0.16	30.52 ± 2.0	5
RAMP3						
CGRP	8.42 ± 0.1	40.84 ± 0.6	5	8.38 ± 0.1	39.84 ± 1.0	5
AM	9.63 ± 0.1	39.09 ± 1.2	5	9.49 ± 0.2	42.26 ± 1.6	5
AM2	8.01 ± 0.1	33.75 ± 1.5	5	7.79 ± 0.2	28.21 ± 2.4	5

[a] The negative logarithm of the agonist concentration required to produce a half-maximal response.

[b] The maximal response to the ligand expressed as a percentage of the maximal cAMP production as determined using 100 μM forskolin stimulation in the presence of PTX treatment.

RAMPs influence the G protein coupling in a ligand- and receptor-dependent manner, in some cases radically changing ligand selectivity.

When GPA1/$G\alpha_i$ coupling in the yeast system was compared with coupling to GPA1/$G\alpha_s$, markedly different responses were observed for each ligand. Most significantly, at all three receptors, the rank order of potency of the ligands was altered, either being reversed or with differences abolished. Efficacy calculations for each ligand in the presence of GPA1/$G\alpha_i$ also revealed G protein-directed changes in the activity of each ligand. AM2 displayed a much greater efficacy at the RAMP1-CLR heterodimer than AM, and surprisingly CGRP efficacy was greatly reduced. These data indicate that the ligands display a degree of G protein bias at each receptor; this was further supported through the construction of bias plots through calculation of $\Delta\Delta(\tau/K_A)$. The data contrast with the established potency profiles for $G\alpha_s$-coupled receptors observed in mammalian cells and also yeast. Although $G\alpha_s$ is recognized as the main signaling pathway activated by CLR-based receptors (15), the data illustrate that if $G\alpha_i$ or $G\alpha_q$ activation occurs, the conventional agonist potency ratios may lead to erroneous conclusions about the nature of the receptor. Caution should at least be taken when referring to these receptors, because it is clear that CGRP will preferentially activate the $G\alpha_s$-coupled CGRP receptor (RAMP1-CLR), but this is not the situation when the receptor is coupled to other G proteins. Indeed, this trend is observed for all receptors in this family, with AM being the preferential ligand for both the AM_1 (RAMP2-CLR) and AM_2 (RAMP3-CLR) receptors coupled to $G\alpha_s$ but not when $G\alpha_i$ coupled. To avoid confusion we have, for the most part, described these receptors as RAMP1/2/3-CLR in this study. A further point that arises from these observations is that the reversals in potency ratios that we observed suggest that differences in the ability of the peptides to penetrate the yeast cell wall are not a contributing factor to our observations.

Our data also shed new light on the comparative efficacies of CGRP, AM, and AM2 at the three receptors for $G\alpha_s$ coupling.

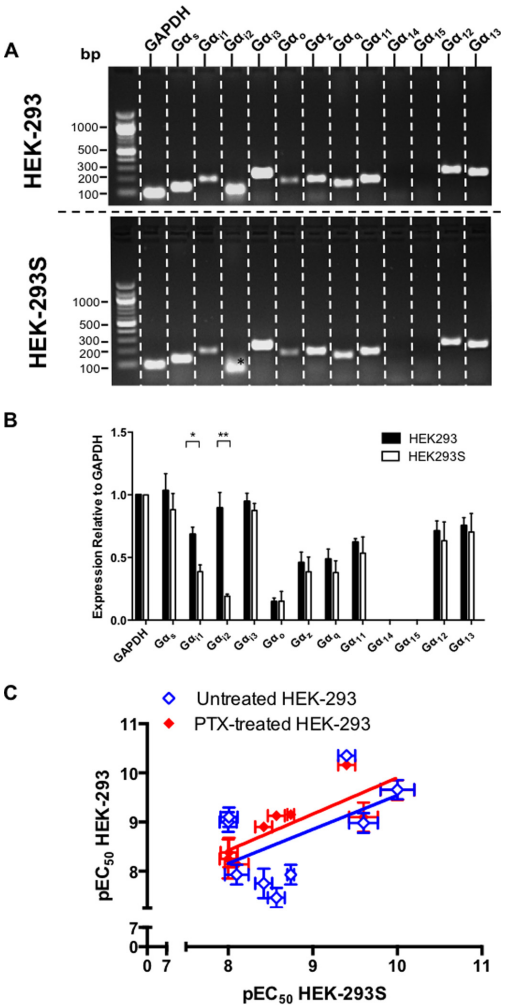

FIGURE 6. **Reduced $G\alpha_i$ expression in HEK-293S cell lines leads to PTX insensitivity.** *A*, expression profiles of Gα genes were assessed in HEK-293 and HEK-293S cells. RNA was extracted from cells and treated with DNase 1 to remove genomic DNA contamination. Gα gene expression was examined by RT-PCR using gene-specific primers. *, indicates a lack of detectable transcript for $G\alpha_{i2}$. The band shown is a nonspecific product as confirmed by DNA sequencing. *B*, semiquantitative expression (relative to GAPDH) for the Gα genes from *A* ($n = 4$). Statistical difference between HEK-293 and HEK-293S cells was determined using Student's *t* test: *, $p < 0.05$; **, $p < 0.01$. *C*, the correlation of log agonist potencies ± S.E. for CGRP, AM, and AM2 at RAMP-CLR combinations expressed in HEK-293S (Table 4) cells and HEK-293 cells either with (*red symbol*) or without (*blue symbol*) pretreatment with PTX (Table 3) was analyzed by a *scatter plot*, and Pearson's correlation coefficients (*r*) were calculated. A significant correlation was observed only between HEK-293S cells and HEK-293 cells pretreated with PTX.

Typically, they have been reported to show similar maximal responses, although there are issues with incomplete concentration-response curves (1). However, there is evidence for par-

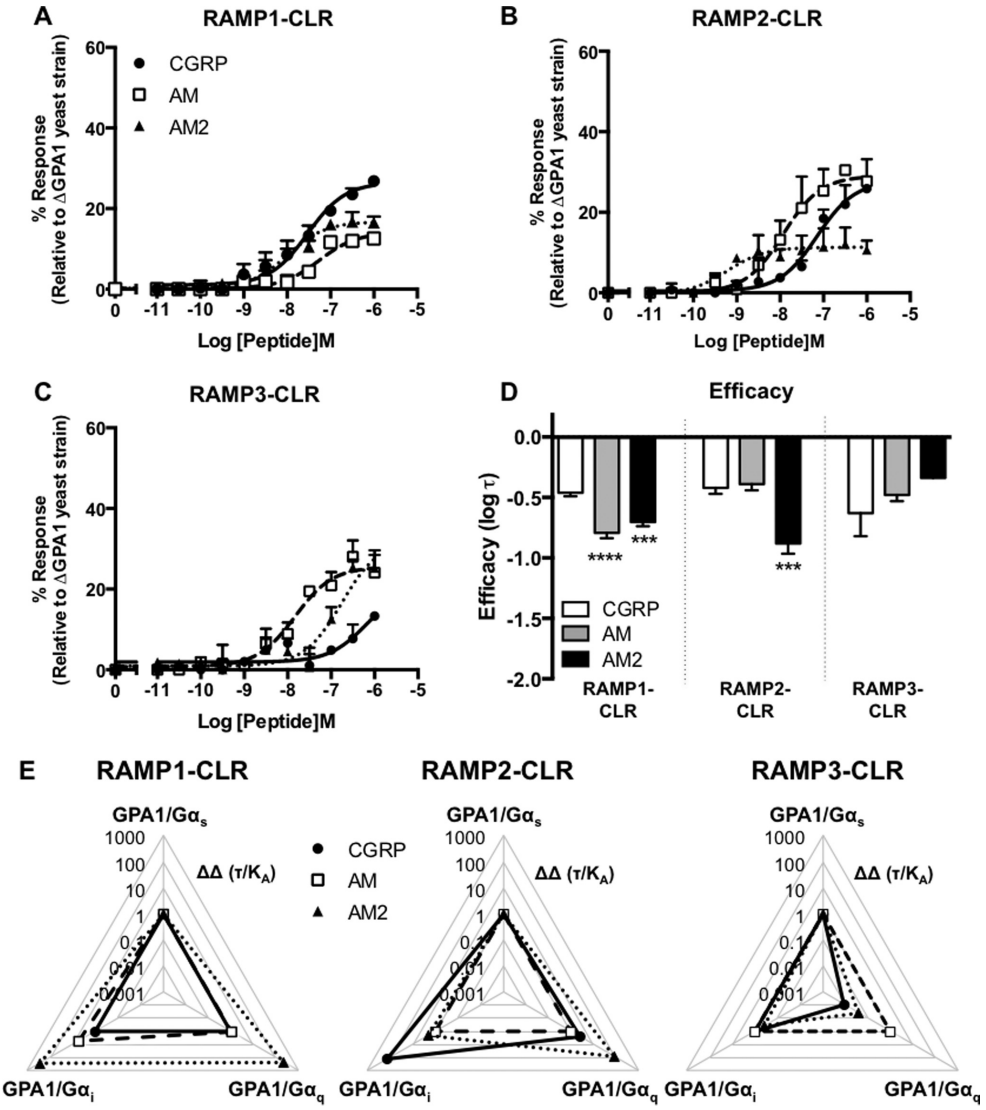

FIGURE 7. **Functional coupling of CLR co-transformed with all three RAMPs to the $G\alpha_q$ chimera.** Dose-response curves to CGRP, AM, and AM2 were constructed in yeast strains containing the GPA1/$G\alpha_q$ chimera and expressing CLR with RAMP1 ($n = 7$) (*A*), RAMP2 ($n = 6$) (*B*), and RAMP3 ($n = 7$) (*C*). Reporter gene activity was determined following 24-h stimulation. All data are expressed as percentage of the maximum response observed in yeast strain MMY11 and are means ± S.E. of *n* individual data sets. *D*, *Bar* chart showing the efficacy of each ligand for each RAMP-CLR combination at the $G\alpha_q$ chimera determined via application of the operational model of receptor agonism (Ref. 34 and Table 1). Data were determined as statistically different from the cognate ligand for each receptor (***, $p < 0.001$; ****, $p < 0.0001$) using one-way ANOVA with Bonferroni's post-test. *E*, signaling bias plots were calculated as $\Delta\Delta(\tau/K_a)$ values on a logarithmic scale for each ligand and for each chimera G protein for the three individual RAMP-CLR complexes. Determination of values requires normalization to a reference ligand (CGRP for RAMP1-CLR and AM for CLR with RAMP2 or RAMP3) and a reference pathway (in all cases, GPA1/$G\alpha_s$).

tial agonism of AM2 in CHO cells when RAMP2 is co-expressed with CLR (43). By its nature, the measurement of efficacy is very sensitive to the cell or tissue being studied as well as the experimental protocol. In this study, the use of the yeast assay enabled us to calculate the efficacy and potency values for each ligand-receptor combination for specific G protein sub-

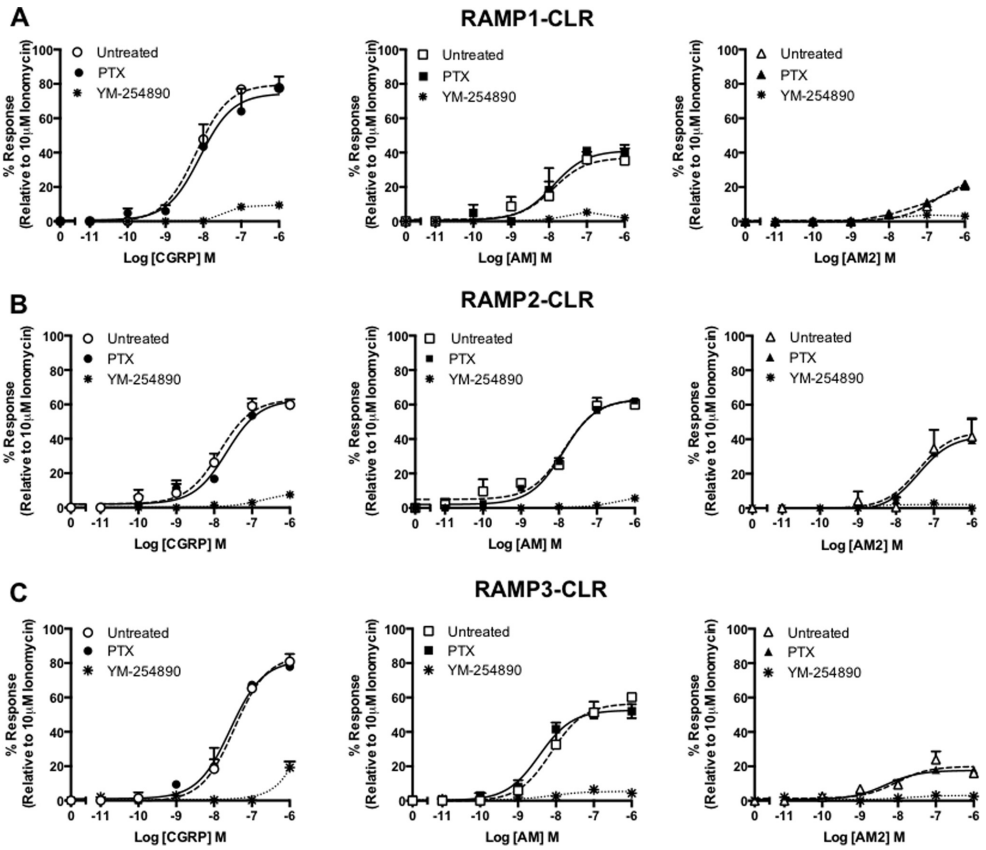

FIGURE 8. **CLR in combination with each RAMP generates receptors that mobilize $(Ca^{2+})_i$ release when expressed in HEK-293 cells.** $(Ca^{2+})_i$ mobilization was determined from HEK-293 cells transiently transfected with CLR and RAMP1 ($n = 5$) (*A*), RAMP2 ($n = 5$) (*B*), and RAMP3 ($n = 5$) (*C*). Cells were stimulated for 2 min with CGRP, AM, and AM2. Data are expressed as percentage of the maximal $(Ca^{2+})_i$ release as determined using 10 μM ionomycin. To determine the contribution made by different G proteins to the $(Ca^{2+})_i$ response, cells were preincubated with either PTX (to inhibit $G\alpha_i$) or YM-254890 (a selective $G\alpha_q$ inhibitor). All values are means ± S.E. of *n* individual data sets.

units without the complication of pathway cross-talk. Our data revealed that all ligands have similar efficacies in cells expressing the RAMP1-CLR combination coupled to GPA1/$G\alpha_s$. In contrast, AM has a significantly increased efficacy at the RAMP2-CLR heterodimer.

The relative potencies of the three peptides at the CGRP, AM_1, and AM_2 receptors that we observed in our current studies for $G\alpha_s$ coupling largely agree with previous observations (1 for review, 7–9, 43, and 44) (Table 2 and Fig. 12). Importantly when each receptor was expressed in *S. cerevisiae* strains, enabling us to measure the activation of GPA1/$G\alpha_s$, the rank potency order for the peptides fit the pattern observed in mammalian cells (Table 1 and Fig. 9), with the exception of CGRP, which displayed an unexpectedly high potency at the RAMP3-CLR heterodimer. These data indicate that, as with the GLP-1 and glucagon receptors, the yeast system is a valid model for studying G protein coupling to class B GPCRs. The comparable pharmacology of the three receptors demonstrates the value of the yeast system for assessment of the effect of complex formation by GPCRs and could be applied not only to dimerization of these receptors with RAMPs but also other modifying or downstream signaling proteins.

An important consideration is whether the $G\alpha_i$/$G\alpha_q$ coupling observed in yeast has any relevance to mammalian cell systems. The yeast strains express only chimeric G proteins (containing the C-terminal five amino acids of the human G protein), which are reported to be less specific when compared with equivalent G proteins expressed in mammalian cells (22). To establish the extent of $G\alpha_i$ coupling in HEK-293 cells, we investigated cAMP production before and after PTX treatment; the greater the enhancement of cAMP production following toxin addition, the greater the extent of $G\alpha_i$ coupling that the toxin inactivates. When compared with the coupling seen in yeast to GPA1/$G\alpha_i$, although the correlation is not exact, there

TABLE 5

Potency (pEC_{50}), affinity (pK_a), and coupling efficacy (log τ) values for $(Ca^{2+})_i$ mobilization at the CLR co-expressed with each RAMP stimulated with various agonists measured in HEK-293 and HEK-293S cells

Data are the mean ± S.E. of *n* individual data sets. Statistical significance compared with the cognate ligand (*, $p < 0.05$; **, $p < 0.01$; ***, $p < 0.001$; ****, $p < 0.0001$) for each receptor heterodimer (CGRP for RAMP1-CLR and AM for CLR with either RAMP2 or RAMP3) was determined by one-way ANOVA with Dunnett's post-test.

	HEK-293					HEK-293S				
	pEC_{50}[a]	E_{max}[b]	pK_a[c]	log τ[d]	*n*	pEC_{50}[a]	E_{max}[b]	pK_a[c]	log τ[d]	*n*
RAMP1										
CGRP	8.19 ± 0.1	79.68 ± 0.7	7.50 ± 0.1	0.60 ± 0.05	5	8.06 ± 0.1	67.64 ± 2.0	7.57 ± 0.1	0.32 ± 0.04	5
AM	7.90 ± 0.2	37.00 ± 3.5****	7.69 ± 0.4	−0.24 ± 0.10	5	7.63 ± 0.2	38.18 ± 3.8****	7.42 ± 0.2	−0.21 ± 0.07****	5
AM2	6.76 ± 0.2***	25.05 ± 2.4****	6.64 ± 0.1**	−0.48 ± 0.06**	5	6.94 ± 0.1***	33.28 ± 1.7****	6.76 ± 0.1**	−0.30 ± 0.03****	5
RAMP2										
CGRP	7.86 ± 0.1	63.20 ± 3.0	7.43 ± 0.1	0.54 ± 0.10	5	7.55 ± 0.3	55.35 ± 4.5	7.21 ± 0.3	0.07 ± 0.08	5
AM	7.86 ± 0.1	63.00 ± 1.8	7.45 ± 0.2	−0.19 ± 0.06	5	7.68 ± 0.2	52.26 ± 4.5	7.39 ± 0.2	0.03 ± 0.10	5
AM2	7.41 ± 0.4	44.41 ± 7.1*	7.15 ± 0.4	−0.10 ± 0.13**	5	7.42 ± 0.4	20.17 ± 2.8****	7.33 ± 0.2	−0.65 ± 0.13***	5
RAMP3										
CGRP	7.47 ± 0.2*	84.39 ± 8.5*	6.66 ± 0.4*	0.74 ± 0.26	5	7.51 ± 0.2	65.3 ± 4.7	7.07 ± 0.2**	0.24 ± 0.10*	5
AM	8.12 ± 0.1	56.69 ± 6.6	7.76 ± 0.3	0.13 ± 0.13	5	8.02 ± 0.2	44.3 ± 3.2	8.56 ± 0.2	−0.11 ± 0.06	5
AM2	8.05 ± 0.3	19.99 ± 2.4*	7.95 ± 0.3*	−0.63 ± 0.08*	5	7.44 ± 0.3	20.1 ± 4.3	7.35 ± 0.3**	−0.62 ± 0.07**	5

[a] The negative logarithm of the agonist concentration required to produce a half-maximal response.
[b] The maximal response to the ligand expressed as a percentage of the maximal $(Ca^{2+})_i$ release as determined using 10 μM ionomycin stimulation.
[c] The negative logarithm of the equilibrium disassociation constant for each ligand generated through use of the operational model of agonism (34).
[d] Log τ is the coupling efficacy parameter of each ligand.

is at least a measure of agreement between the HEK-293 and yeast data, suggesting that the latter may be a guide as to what could be seen in mammalian cells given the appropriate conditions. Comparing the relative bias plots for yeast and HEK-293 cells in Figs. 7 and 9 further emphasizes this correlation; the pattern shown for the two systems is broadly similar. As the effects of RAMPs on GPCR pharmacology are known to be sensitive to the cell line background (37, 42) and significant heterogeneity in PTX sensitivity of CGRP has been reported previously (20, 45), it would perhaps be surprising if the HEK-293 cells were a perfect match to yeast. Indeed, as we have shown (Fig. 6), in terms of the expression levels of $G\alpha_i$ subunits, two similar HEK-293 cell lines are, in fact, very different; HEK-239S cells appear to have a reduced level of $G\alpha_i$ expression compared with HEK-293 cells. When combined with our observation of the PTX sensitivity of the CLR response in HEK-293S cell lines, it becomes apparent that we need to carefully consider the G protein content of cell lines that we utilize when investigating G protein-mediated signaling bias.

Our results have demonstrated that the CGRP family of receptors can couple to $G\alpha_s$, $G\alpha_i$ and $G\alpha_q$ subunits. Further, using the yeast system we observed a ligand-dependent G protein coupling bias with each receptor, highlighting the ability of the yeast platform to uncover potential G protein bias for other GPCRs. Importantly, this ability is, at least partially, transferred into mammalian cells and provides an excellent starting point for subsequent investigations into both the extent to which this bias occurs in native mammalian cells and the molecular basis for the phenomenon. Any examination of the physiological significance of G protein promiscuity needs to consider the cellular background in which the CLR/RAMP receptor is expressed; we observed significant differences between our three cell hosts that depend, at least partly, on the G proteins they express (Fig. 13). Indeed, it is worth highlighting that, as a direct consequence of the reduced overall $G\alpha_i$ content in HEK-293S cells, all three ligands at the CGRP family of receptors display bias toward cAMP accumulation over $(Ca^{2+})_i$ release (Fig. 9). Coupling to $G\alpha_i$ (or possibly $G\alpha_o$) may be particularly relevant in neuronal and other electrically excitable cells where many (18, 19) of the effects of PTX on CGRP have been observed (reviewed in Ref. 15). In neuronal and other cells, the direct $G\alpha_i/G\alpha_o$ effects on ion channels may also be particularly significant. For example, there is the potential for a complex interplay between neuronally released CGRP and the AM or AM2 peptides released locally through cross-talk among all three CLR-based receptors, with the potential for the $G\alpha_i$ coupling to naturally limit excitation produced via $G\alpha_s$.

The role of $G\alpha_{q/11}$ coupling in mediating responses to CGRP, AM, and AM2 has not been well investigated; the few relevant studies have examined activation of protein kinase C or release of calcium from internal stores rather than directly studying $G\alpha_{q/11}$. For CGRP, a further complication is that it can also activate the amylin-1 receptor with high affinity (46), so it is not always clear that the observed effects are mediated via CLR. However, in HEK-293 cells, alveolar epithelial cells, dorsal root ganglia, and trigeminal ganglia, there is evidence for either release of intracellular calcium or activation of PKC alongside PKA activation (15). A similar pattern has been seen for AM in bovine aortic endothelial cells (47). Although evidence from PKA inhibitors such as H89 suggests that cAMP is the primary second messenger that mediates many effects of CGRP (48), there is the potential for spatial and temporal modulation of this primary signal via $(Ca^{2+})_i$, a possibility that remains to be explored.

By utilizing molecular models of two diverse class B GPCR systems, namely the RAMP1-CLR-CGRP and RAMP2-GCGR-glucagon systems, we have gained insight into signaling bias. We believe the simulations reported here are the first molecular dynamics simulations on RAMP-GPCR heterodimers. The interaction of the RAMP TM helix with TM6/TM7 is supported both by docking experiments on CLR (27) and by studies on the secretin-GLP-1 chimeric receptor (49); this interaction remains stable throughout both 500-ns simulations of the active receptors, with the RAMP retaining a straight helix through both simulations, despite the presence of proline(s). The interaction is primarily with TM7 and the N-terminal end of TM6. This provides some evidence that GCGR and CLR may interact with RAMP in a similar way. Despite the persistence

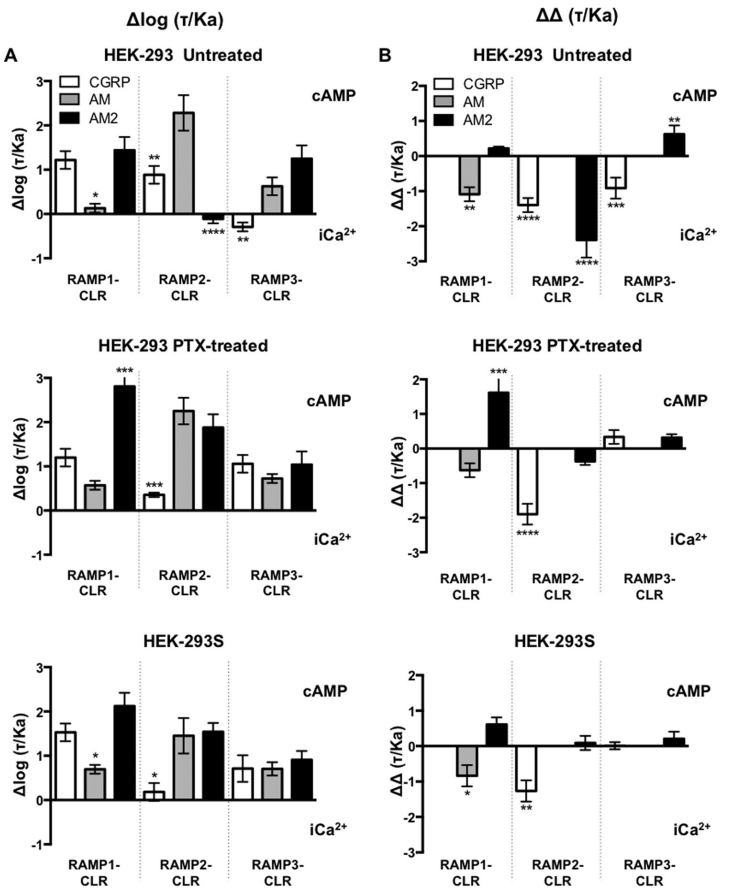

FIGURE 9. **Quantification of biased agonism at the three RAMP-CLR complexes.** *A*, normalized transduction coefficients, Δlog (τ/K_a), for cAMP accumulation and (Ca^{2+})$_i$ mobilization obtained for the three RAMP-CLR complexes upon stimulated with CGRP, AM, or AM2 in untreated HEK-293 cells, HEK-293 cells treated with PTX, and HEK-293S cells. *B*, relative bias factors, $\Delta\Delta(\tau/K_a)$, for cAMP accumulation and (Ca^{2+})$_i$ mobilization for the three individual RAMP-CLR complexes upon stimulated with CGRP, AM, or AM2 in untreated HEK-293 cells, HEK-293 cells treated with PTX, and HEK-293S cells. Determination of values requires normalization to a reference ligand (CGRP for RAMP1-CLR and AM for CLR with RAMP2 or RAMP3) and a reference pathway (in all cases cAMP accumulation). Data were determined as statistically different from the cognate ligand for each receptor (*, $p < 0.05$; **, $p < 0.01$; ***, $p < 0.001$; ****, $p < 0.0001$).

and stability of the TM interactions, the C terminus is quite flexible, sampling a wide region of space in both simulations. RAMP2 interacted primarily with the C terminus of $G\alpha_s$, whereas RAMP1 interacted primarily with H8 but also made contact with TM6 and most importantly $G\alpha_s$. These simulations therefore indicate that the RAMP could affect the bias shown in G protein coupling by CLR either by direct interaction and/or allosterically by altering the orientation of TM6 and TM7 or H8. These simulations were carried out on a model of the active receptor in complex with a C-terminal fragment of $G\alpha_s$ (Arg-374 to Leu-394). The C-terminal helix of $G\alpha_s$ sits above the face of the G protein. Models of RAMP2-GCGR in complex with the G protein heterotrimer indicated that the RAMP could also interact directly with residues around Gly-353 of $G\alpha_s$ (results not shown).

In addition, the allosteric effects of the RAMP linker may alter the extracellular face of the receptor (as seen in CLR with RAMP2 and RAMP3 (27)), and these effects could be transmitted to the intracellular end of the helix. In our simulations, we see some evidence for the top of TM7 moving in toward the TM bundle under pressure of the RAMP (Fig. 11) as part of a collective unit comprising TM7, the peptide, and the RAMP TM. This concerted movement provides a possible mechanism whereby the influence of the ligand can be conveyed to the RAMP and thereby affect the bias via interactions of the C terminus of the RAMP. The inward movement of the extracellular

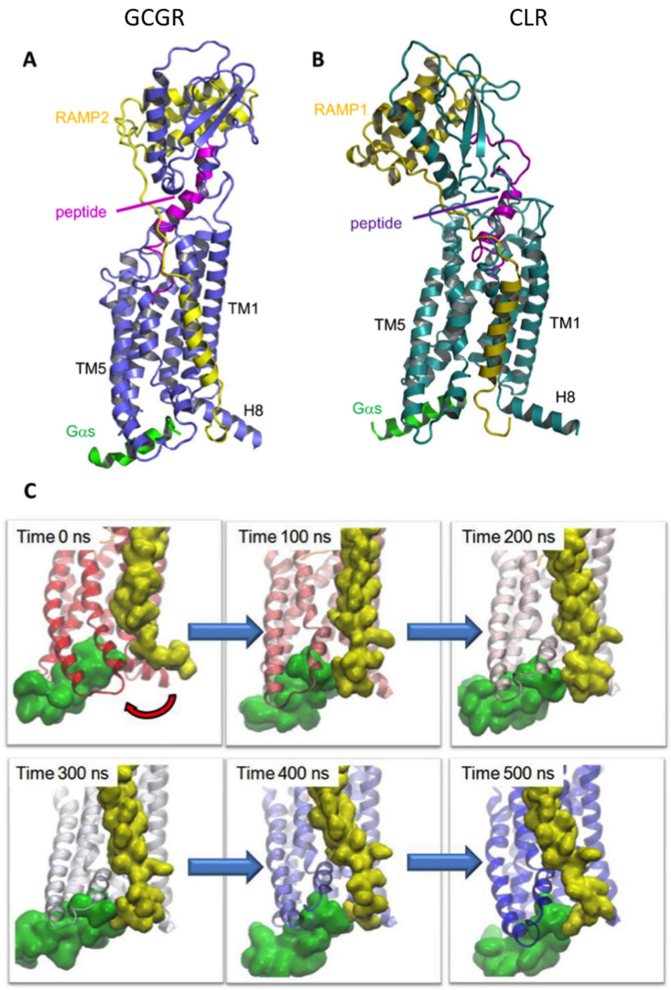

FIGURE 10. **Class B GPCR-RAMP heterodimeric models and molecular dynamics simulations.** Molecular models and dynamic simulation suggest that the C-terminal tail of RAMP1/2 (*olive*/*yellow*, when in complex with either GCGR (*A*, *blue*) or CLR (*B*, *teal*), interacts directly with the bound C-terminal of $G\alpha_s$ (*green*) and/or helix 8. The glucagon peptide agonist is shown in *magenta*, and CGRP is shown in *purple*. *C*, the RAMP2 C terminus approaches the $G\alpha_s$ (*red arrow*) during a molecular dynamics simulation of an active GCGR-RAMP2-glucagon complex. RAMP2 is shown in *yellow* and $G\alpha_s$ in *green*, and the GCGR is colored according to time progression from *red* (0 ns) to *blue* (500 ns).

end of TM7 has been linked explicitly to activation (50), but movement of TM6 and/or H8 under the influence of the RAMP may also affect bias and activation. Thus we suggest that RAMPs have the potential to interact allosterically with not only the GPCR but also the bound G protein. This leads to the possibility that, upon ligand binding, the RAMPs contribute to the G protein bias. To confirm this likelihood, we aim to extend this project to investigate all ligand-RAMP-CLR-G protein complexes and further elucidate the role that RAMPs play in modulating G protein coupling and bias at the CGRP family of receptors.

Finally, we suggest that this study has broader implications. Our results shown here are similar to those described for the GCGR (25) in that RAMPs alter the ability of peptides to stimulate different G proteins. However, as we have shown, significant pharmacological differences can be observed in differing recombinant cell lines and expression systems. These differences can be explained through several factors; these systems rely firstly upon overexpression of the receptor and chaperone proteins under study and secondly upon the cellular content of further downstream signaling proteins such as G proteins. It is therefore important that findings in systems such as those

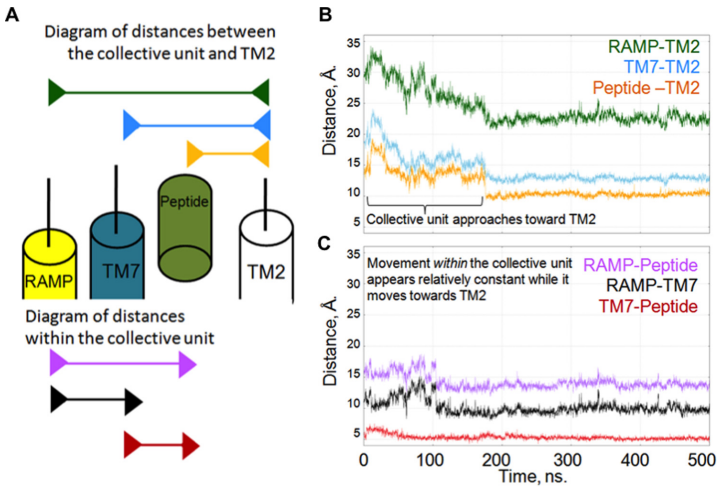

FIGURE 11. **The peptide agonist, the GPCR , and the RAMP TM helix move as a collective unit during molecular dynamics simulations.** *A*, schematic diagram of the distances between the members of the collective unit and TM2. *Top*, *arrow bars* indicate the following distances in order: RAMP2-TM2 (*green*), TM7-TM2 (*cyan*), and peptide-TM2 (*orange*). *Bottom*, *arrow bars* indicate the distances within the members of the collective unit in order: RAMP2-peptide (*purple*), RAMP-TM7 (*black*), and TM7-peptide (*red*). *B*, distances from each of the collective unit components (RAMP TM, TM7, and glucagon agonist) to TM2 (ordered as in *A*). These distances decrease in a similar manner, reflecting their concerted movement. *C*, distances between each of the collective unit components (RAMP, TM7, and glucagon agonist) (ordered as in *A*). These distances are relatively constant, reflecting their movement as a collective unit.

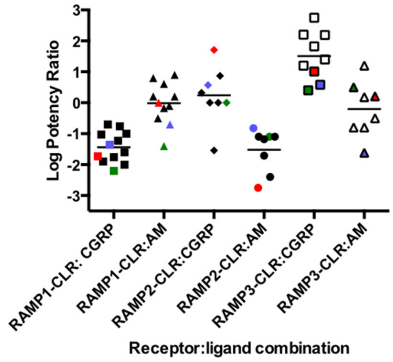

FIGURE 12. **Agonist potency ratios for CGRP, AM, and AM2 at the CLR in combination with each RAMP.** Log potency ratios (as measured by the accumulation of intracellular cAMP) are defined as log(EC_{50} AM2/EC_{50} agonist). Data are taken from Hong *et al.* (1) and others (43, 44). HEK-293 and HEK-293S cell data from the current study are shown in *red* and *blue*, respectively, and yeast $G\alpha_s$ coupling is shown in *green*.

explained here be further validated. This would be best achieved in cell lines endogenously expressing the GPCR and RAMP of interest. This is thus something that we aim to undertake as a follow-up to the work presented here for CLR-RAMP complexes. It is clear that there is a complex interplay among the ligand, the RAMP, and the CLR that alters G protein activation for these receptors. Further, our data presented here add to the growing wealth of literature suggesting that many ligands for class B GPCRs display either a $G\alpha_s$ or $G\alpha_i$ signaling preference. To date, this ligand-engendered bias has been observed for receptors binding corticotropin-releasing factor, urocortin 1, GLP-1, and glucagon (24, 25, 51). In the current study, the yeast growth assay system was able to provide a valuable indication of the potential of the CGRP family of receptors to couple to either $G\alpha_s$ or $G\alpha_i$ when stimulated by CGRP, AM, or AM2, allowing us to uncover novel G protein signaling preferences for each ligand. We therefore conclude that this system is a good platform from which to explore the effect of RAMP dimerization to other members of the class B GPCRs.

Experimental Procedures

Materials—Human (h) αCGRP, hAM, and hAM2 (1–47) were purchased from Bachem (Bubendorf, Switzerland) and made to 1 mM stocks in water containing 1% BSA. Yeast nitrogen base and yeast extract were purchased from Difco (Franklin Lakes, NJ). Fluorescein-di-β-D-glucopyranoside was purchased from Invitrogen. Forskolin was from Tocris Bioscience (Wiltshire, UK), and YM-254890 was supplied by Alpha Laboratories (Hampshire, UK). Both the ALPHAScreen and LANCE® cAMP detection assay kits and all reagents were from PerkinElmer Life Sciences.

Expression Constructs—To enable expression of the human CLR, we used either a previously described (25) Myc-tagged cDNA construct provided by Dr. Michel Bouvier (University of Montreal, Canada) or a human CLR with an N-terminal HA epitope tag. All human FLAG-tagged RAMPs were used as described previously (37).

Yeast Strain Construction and Assay—General yeast procedures were performed as described previously (22, 24). The human CLR was introduced into yeast cells under the control of the *PGK* promoter using a plasmid containing *ura3* (pDT-PGK). The three human RAMPs were introduced into yeast under the control of the *GAPDH* promoter using plasmids con-

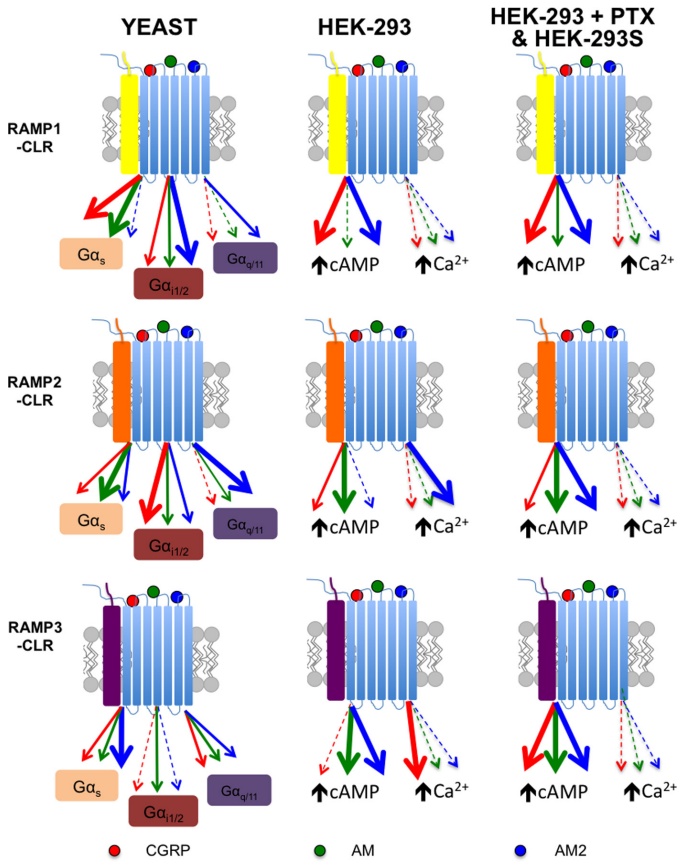

FIGURE 13. **A working model of biased agonism at the different RAMP-CLR complexes.** The individual RAMP-CLR complexes can bind the agonists CGRP (*red*), AM (*green*), and AM2 (*blue*) to activate different downstream chimeric GPA1/Gα subunits (in yeast) or promote increases in intracellular cAMP and/or mobilize release of $(Ca^{2+})_i$ (in HEK-293/HEK-293S cells). The *thickness* of the *lines* indicates the bias that each agonist displays for either the chimeric G protein or the specific downstream signaling cascade. The yeast system enabled the comparison of different individual G proteins ($G\alpha_s$, $G\alpha_{i1/2}$, and $G\alpha_q$), whereas in mammalian cells we investigated cAMP accumulation (± PTX) and elevation of $(Ca^{2+})_i$.

taining *leu2* (p425-GPD) (25). *S. cerevisiae* dual reporter strains expressing chimeras of yeast GPA1(1–467) (GPA1/Gα) with the five C-terminal amino acids of 11 human G proteins representing $G\alpha_s$, $G\alpha_{16}$, $G\alpha_q$, $G\alpha_o$, $G\alpha_{i1/2}$, $G\alpha_{i3}$, $G\alpha_z$, $G\alpha_{12}$, $G\alpha_{13}$, and $G\alpha_{14}$ (MMY84–MMY93) were used in this study (52). The human CLR and RAMPs were transformed into yeast cells (at a ratio of 1:1 to enable equal expression) using the lithium acetate/single-stranded DNA/polyethylene glycol method as described previously (53). Positive transformants were selected and maintained on synthetic dropout (SD) medium lacking both uracil and leucine (SD-Ura-Leu). Receptor signaling was measured using the yeast growth assay as described previously (24). Cell growth was initially performed in SD-Ura-Leu medium at 30 °C to select cells expressing only both plasmids. Cells were then cultured to remove basal activity in SD-Ura-Leu-His medium overnight at 30 °C and assayed using medium supplemented with fluorescein-di-β-D-glucopyranoside. A fluorescein signal was detected as an increase in fluorescence (excitation wavelength = 485 nm, emission wavelength = 535 nm) as a measure of growth. Different concentrations of ligand (0.01 nM–100 μM) were assayed using 96-well plates, and fluorescence was detected using a Tecan Infinite M200 microplate reader (Tecan Ultra Evolution, Reading, UK) or a Mithras LB 940 microplate reader (Berthold Technologies, Harpenden, UK) for 20 h. Positive isolates were selected for their ability to grow above basal level in SD-Ura-Leu-His medium, when stimulated with 10 μM CGRP or AM as appropriate for the RAMP-CLR complex being studied. Chimeric strains were deemed not to functionally couple when $n > 16$ isolates had been assayed and none showed growth above basal levels. In this study functional couplings were only observed for MMY84, MMY86, and MMY88 representing $G\alpha_s$, $G\alpha_{i1/2}$, and $G\alpha_q$, respectively.

Mammalian Cell Culture and Transfection—HEK-293 cells, provided by Dr. Jügen Müller (University of Aston), were cultured in DMEM supplemented with 10% heat-inactivated FBS and kept at 37 °C in a humidified 95% air, 5% CO_2 incubator. HEK-293S cells (a gift from AstraZeneca) were cultured in DMEM supplemented with 8% heat-inactivated FBS and kept at 37 °C in a humidified 95% air, 5% CO_2 incubator. HEK-293 cells were transfected with FuGENE 6 (Roche Applied Science) in accordance with the manufacturer's instructions using a 1:3 (w:v) DNA:FuGENE ratio and a 1:1 ratio of RAMP to CLR. HEK-293S cells were seeded into 96-well poly-D-lysine-coated plates at a density of 15,000 cells/well (determined using a Countess™ cell counter, Invitrogen) 1 day prior to transfection. HEK-293S cells were transiently transfected as described previously (38) using a 1:1 ratio of RAMP to CLR. The transfected cell lines were grown for 24–48 h prior to assaying. Where appropriate, PTX (200 ng/ml) was added to ADP-ribosylate $G\alpha_i$ for 16 h prior to assaying, thereby uncoupling receptor-mediated $G\alpha_i$-dependent inhibition of cAMP production.

cAMP Accumulation Assays—The transfected HEK-293 cells were washed in PBS, resuspended in stimulation buffer (PBS containing 0.1% BSA and 0.5 mM IBMX), and seeded at 2000 cells/well in 384-well white Optiplates. Ligands were added in the range of 1 pM to 1 mM, and cAMP accumulation was measured after 30 min of stimulation using a LANCE® cAMP detection kit (PerkinElmer Life Sciences). We had found previously that a 30-min stimulation was the optimum time for assaying cAMP accumulation for family B GPCRs (24, 25). Plates were read using a Mithras LB 940 multimode microplate reader (Berthold Technologies). HEK-293S cells were assayed for cAMP accumulation as described elsewhere (54). Values were converted to concentration using a cAMP standard curve performed in parallel.

Calcium Mobilization Assays—Transfected HEK-293 cells were grown to confluence in black, clear bottomed, 96-well plates. On the day of assay cells were washed with calcium-free Hanks' balanced salt solution and incubated for 1 h at room temperature in the presence of 10 μM Fluo-4/AM (Invitrogen) containing 2.5 mM probenecid. Cells were then washed followed by the addition of 100 μl of Ca^{2+}-free Hanks' balanced salt solution. Ligands were added robotically using a Mithras LB 940 multimode microplate reader in the range of 10 pM to 1 μM, and fluorescence was determined immediately post-injection with an excitation wavelength set to 485 nm and an emission wavelength set to 535 nm. Recordings were obtained every 0.5 s for 120 s. Peak magnitude was calculated using five-point smoothing followed by correction against background fluorescence. The peak was used to generate concentration-response curves and normalized relative to 10 μM ionomycin. To determine the role played by $G\alpha_{q/11}$ in $(Ca^{2+})_i$ mobilization, cells were pretreated (for 30 min) with 100 nM YM-254890, which inhibits $G\alpha_{q/11}$ signaling (42).

RT-PCR—RNA was extracted from HEK-293 and HEK-293S cells using a RNAqueous-4PCR kit (ThermoFisher Scientific) as per the manufacturer's protocol. All RNA samples were treated with DNase I to remove contaminating genomic DNA. Reverse transcription was performed using a QuantiTect reverse transcription kit (Qiagen, Manchester, UK). The PCR amplification was performed as described previously (55) using gene-specific primers to human $G\alpha$ subunits: $G\alpha_s$, forward (5′-CGACGACACTCCCGTCAAC-3′) and reverse (5′-CCCGGAGAGGGTACTTTTCCT-3′) (PrimerBank ID, 3297877a1 (56)); $G\alpha i_1$, forward (5′-TTAGGGCTATGGGGAGGTTGA-3′) and reverse (5′-GGTACTCTCGGGATCTGTTGAAA-3′) (PrimerBank ID, 156071490c1 (56)); $G\alpha i_2$, forward (5′-TACCGGGCGGTTGTCTACA-3′) and reverse (5′-GGGTCGGCAAAGTCGATCTG-3′) (PrimerBank ID, 261878574c1 (56)); $G\alpha i_3$, forward (5′-ATCGACCGCAACTTACGGG-3′) and reverse (5′-AGTCAATCTTTAGCCGTCCCA-3′) (PrimerBank ID, 169646784c1 (56)); Gαq, forward (5′-TGGGTCAGGATACTCTGATGAAG-3′) and reverse (5′-TGTGCATGAGCCTTATTGTGC-3′) (PrimerBank ID, 312176363c1 (56)); $G\alpha_{11}$, forward (5′-GGCTTCACCAAGCTCGTCTAC-3′) and reverse (5′-CACTGACGTACTGATGCTCG-3′) (PrimerBank ID, 115511048c1) (56)); $G\alpha_z$, forward (5′-GGTCCCGGAGAATTGACCG-3′) and reverse (5′-ATGAGGGGCTTGTACTCCTTG-3′) (PrimerBank ID, 45580725c1) (56)); $G\alpha_o$, forward (5′-GGAGCAAGGCGATTGAGAAAA-3′) and reverse (5′-GGCTTGTACTGTTTCACGTCT-3′) (PrimerBank ID, 162461737c1 (56)); $G\alpha_{12}$, forward (5′-CCGCGAGTTCGACCAGAAG-3′) and reverse (5′-TGATGCCAGAATCCCTCCAGA-3′) (PrimerBank ID, 42476110c1) (56)); $G\alpha_{13}$, forward (5′-CAGCAACGCAAGTCCAAGGA-3′) and reverse(5′-CCAGCACCCTCATACCTTTGA-3′) (PrimerBank ID, 215820623c1) (56)); $G\alpha_{14}$, forward (5′-GAGCGATGGACACGCTAAGG-3′) and reverse (5′-TCCTGTCGTAACACTCCTGGA-3′) (PrimerBank ID, 222418795c1 (56)); $G\alpha_{15}$, forward (5′-CCAGGACCCCTATAAAGTGACC-3′) and reverse (5′-GCTGAATCGAGCAGGTGGAAT-3′) (PrimerBank ID, 156104882c1 (56)); and *GAPDH*, forward (5′-AATGGGCAGCCGTTAGGAAA-3′) and reverse (5′-GCGCCCAATACGACCAAATC-3′). All products were resolved on a 2% agarose gel and imaged using a G:Box iChemi gel documentation system utilizing GeneTools analysis software (Syngene, Cambridge, UK), and densitometry was performed using GeneTools.

Molecular Modeling—Models of the GCGR in complex with RAMP2 and CLR in complex with RAMP1 were based on the previously reported models of GLP-1R in complex with GLP-1 and CLR in complex with RAMP2/3, respectively (27–29). These models were built using MODELLER 9.16 (57) from the GCGR and CRFR x-ray structures of the TM domain (58, 59), the x-ray structures of the extracellular domain (60, 61), and NMR structures of closely related peptides (62, 63). The helical region of the CGRP peptide was structurally aligned to the corresponding region in GLP-1 based on the sequence alignment (27) because the position of the GLP1 helix within GLP-1R is well defined by experimentation; the initial models are available as supporting information. The RAMP-GPCR complexes were placed in a hydrated POPC membrane using CHARMM GUI (64) to generate a system containing 20,482 and 28,013 TIP3P water molecules (65), as well as 183 and 243 lipid molecules for the RAMP2-GCGR and RAMP1-CLR heterodimers, respectively. The histidine protonation was determined using the PDB2PQR server (66). The AMBERSP99 force field parameters for the protein (67), and the lipid14 force field parameters for POPC (68, 69) were added using AmberTools (70). Molecular

dynamics simulations were run for 500 ns at 298 K using ACEMD (71).

Data Analysis—Data analysis for cAMP assays was performed in GraphPad Prism 6.0f (San Diego, CA). Data were fitted to obtain concentration-response curves using either the three-parameter logistic equation (for pEC_{50} values) or the operational model for partial agonism (34) to obtain values of efficacy (log τ) and the equilibrium dissociation constant (log K_a). These values were then used to quantify signaling bias as change in log (τ/K_a) relative to the natural cognate ligand for the respective receptor (41). We denoted these as CGRP for CLR with RAMP1 and AM for CLR with either RAMP2 or RAMP3. Statistical differences were analyzed using one-way ANOVA or Student's *t* test as appropriate with post hoc Bonferroni's or Dunnett's multiple comparisons, and $p < 0.05$ was considered significant. Correlations between pEC_{50} values for cAMP assays of HEK-293 and HEK-293S cells were assessed by scatter plot and Pearson's correlation coefficient (r). For RT-PCR, normalization to the internal standard GAPDH was performed to reduce variance and enable a comparison between different cell lines. To quantitate the ligand-dependent response in the yeast system, a strain lacking GPA1 (MMY11), grown in rich medium, was used as a standard (72). As GPA1 is not present in this strain, the $G\beta\gamma$ subunits are unregulated and free to signal, allowing us to determine the maximal response of our system. E_{max} values are reported as a percentage of this maximum response, and statistical analysis was performed on these data. For the mammalian cell-based assays, data analysis was carried out as for the yeast curves. To account for the day-to-day variation experienced from transient transfections, we used the maximal level of cAMP accumulation from cells in response to 100 μM forskolin stimulation as our reference and 10 μM ionomycin for $(Ca^{2+})_i$ assays. E_{max} values from these curves are reported as a percentage of these controls, and all statistical analysis has been performed on these data. Where appropriate the operational model for partial agonism (34) was used to obtain efficacy (log τ) and equilibrium disassociation constant (log K_a) values. In both cases, this normalization removes the variation due to differences in transfection or transformation but retains the variance for control values. The means of individual experiments were combined to generate the curves shown.

Author Contributions—C. W., H. A. W., and G. L. conceived and designed the research. C. W., A. S., and R. H. performed the yeast experiments, and I. W. and H. A. W. performed the mammalian assays. M. H. performed the RT-PCR. C. A. R., J. C. M., and D. A. W. carried out the computational chemistry, and S. J. D. provided yeast strains. C. W., D. R.P., H. A. W., J. C. M., C. A. R., and G. L. analyzed the data. C. W., D. R. P., H. A. W., J. C. M., C. A. R., and G. L. wrote the manuscript, and S. J. D. revised and edited the manuscript.

References

1. Hong, Y., Hay, D. L., Quirion, R., and Poyner, D. R. (2012) The pharmacology of adrenomedullin 2/intermedin. *Br. J. Pharmacol.* **166,** 110–120
2. Russell, F. A., King, R., Smillie, S. J., Kodji, X., and Brain, S. D. (2014) Calcitonin gene-related peptide: physiology and pathophysiology. *Physiol. Rev.* **94,** 1099–1142
3. Edvinsson, L., and Warfvinge, K. (2013) CGRP receptor antagonism and migraine therapy. *Curr. Protein Pept. Sci.* **14,** 386–392
4. Kato, J., and Kitamura, K. (2015) Bench-to-bedside pharmacology of adrenomedullin. *Eur. J. Pharmacol.* **764,** 140–148
5. Fritz-Six, K. L., Dunworth, W. P., Li, M., and Caron, K. M. (2008) Adrenomedullin signaling is necessary for murine lymphatic vascular development. *J. Clin. Invest.* **118,** 40–50
6. Ichikawa-Shindo, Y., Sakurai, T., Kamiyoshi, A., Kawate, H., Iinuma, N., Yoshizawa, T., Koyama, T., Fukuchi, J., Iimuro, S., Moriyama, N., Kawakami, H., Murata, T., Kangawa, K., Nagai, R., and Shindo, T. (2008) The GPCR modulator protein RAMP2 is essential for angiogenesis and vascular integrity. *J. Clin. Invest.* **118,** 29–39
7. Roh, J., Chang, C. L., Bhalla, A., Klein, C., and Hsu, S. Y. (2004) Intermedin is a calcitonin/calcitonin gene-related peptide family peptide acting through the calcitonin receptor-like receptor/receptor activity-modifying protein receptor complexes. *J. Biol. Chem.* **279,** 7264–7274
8. Holmes, D., Campbell, M., Harbinson, M., and Bell, D. (2013) Protective effects of intermedin on cardiovascular, pulmonary and renal diseases: comparison with adrenomedullin and CGRP. *Curr. Protein Pept. Sci.* **14,** 294–329
9. Takei, Y., Inoue, K., Ogoshi, M., Kawahara, T., Bannai, H., and Miyano, S. (2004) Identification of novel adrenomedullin in mammals: a potent cardiovascular and renal regulator. *FEBS Lett.* **556,** 53–58
10. Smillie, S. J., and Brain, S. D. (2011) Calcitonin gene-related peptide (CGRP) and its role in hypertension. *Neuropeptides* **45,** 93–104
11. Kataoka, Y., Miyazaki, S., Yasuda, S., Nagaya, N., Noguchi, T., Yamada, N., (2010) The first clinical pilot study of intravenous adrenomedullin administration in patients with acute myocardial infarction. *J. Cardiovasc. Pharmacol.* **56,** 413–419
12. Poyner, D. R., Sexton, P. M., Marshall, I., Smith, D. M., Quirion, R., Born, W., Muff, R., Fischer, J. A., and Foord, S. M. (2002) International Union of Pharmacology. XXXII. The mammalian calcitonin gene-related peptides, adrenomedullin, amylin, and calcitonin receptors. *Pharmacol. Rev.* **54,** 233–246
13. McLatchie, L. M.,, Fraser, N. J., Main, M. J., Wise, A., Brown, J., Thompson, N., Solari, R., Lee, M. G., and Foord, S. M.(1998) RAMPs regulate the transport and ligand specificity of the calcitonin-receptor-like receptor. *Nature* **393,** 333–339
14. Hay, D. L., Poyner, D. R., and Smith, D. M. (2003) Desensitisation of adrenomedullin and CGRP receptors. *Regul. Pept.* **112,** 139–145
15. Walker, C. S., Conner, A. C., Poyner, D. R., and Hay, D. L. (2010) Regulation of signal transduction by calcitonin gene-related peptide receptors. *Trends Pharmacol. Sci.* **31,** 476–483
16. Woolley, M. J., and Conner, A. C. (2013) Comparing the molecular pharmacology of CGRP and adrenomedullin. *Curr. Protein Pept. Sci.* **14,** 358–374
17. Wiley, J. W., Gross, R. A., and MacDonald, R. L. (1992) The peptide CGRP increases a high-threshold Ca^{2+} current in rat nodose neurones via a pertussis toxin-sensitive pathway. *J. Physiol.* **455,** 367–381
18. Disa, J., Parameswaran, N., Nambi, P., and Aiyar, N. (2000) Involvement of cAMP-dependent protein kinase and pertussis toxin-sensitive G-proteins in CGRP mediated JNK activation in human neuroblastoma cell line. *Neuropeptides* **34,** 229–233
19. Kim D .(1991) Calcitonin-gene-related peptide activates the muscarinic-gated K+ current in atrial cells. *Pflugers Arch.* **418,** 338–345
20. Main, M. J., Brown, J., Brown, S., Fraser, N. J., and Foord, S. M. (1998) The CGRP receptor can couple via pertussis toxin sensitive and insensitive G proteins. *FEBS Lett.* **441,** 6–10
21. Kuwasako, K., Kitamura, K., Nagata, S., Hikosaka, T., and Kato, J. (2010) Function of the cytoplasmic tail of human calcitonin receptor-like receptor in complex with receptor activity-modifying protein 2. *Biochem. Biophys. Res. Commun.* **392,** 380–385
22. Dowell, S. J., and Brown, A. J. (2002) Yeast assays for G-protein-coupled receptors. *Receptors Channels* **8,** 343–352
23. Ladds, G., Goddard, A., and Davey, J. (2005) Functional analysis of heterologous GPCR signalling pathways in yeast. *Trends Biotechnol.* **23,** 367–373

24. Weston, C., Poyner, D., Patel, V., Dowell, S., and Ladds, G. (2014) Investigating G protein signalling bias at the glucagon-like peptide-1 receptor in yeast. *Br. J. Pharmacol.* **171,** 3651–3665
25. Weston, C., Lu, J., Li, N., Barkan, K., Richards, G. O., Roberts, D. J., Skerry, T. M., Poyner, D., Pardamwar, M., Reynolds, C. A., Dowell, S. J., Willars, G. B., and Ladds, G. (2015) Modulation of glucagon receptor pharmacology by RAMP2. *J. Biol. Chem.* **290,** 23009–23022
26. Miret, J. J., Rakhilina, L., Silverman, L., and Oehlen, B. (2002) Functional expression of heteromeric calcitonin gene-related peptide and adrenomedullin receptors in yeast. *J. Biol. Chem.* **277,** 6881–6887
27. Watkins, H. A., Chakravarthy, M., Abhayawardana, R. S., Gingell, J. J., Garelja, M., Pardamwar, M., McElhinney, J. M., Lathbridge, A., Constantine, A., Harris, P. W., Yuen, T. Y., Brimble, M. A., Barwell, J., Poyner, D. R., Woolley, M. J., *et al.* (2016) Receptor activity-modifying proteins 2 and 3 generate adrenomedullin receptor subtypes with distinct molecular properties. *J. Biol. Chem.* **291,** 11657–11675
28. Wootten, D., Reynolds, C. A., Smith, K. J., Mobarec, J. C., Koole, C., Savage, E. E., Pabreja, K., Simms, J., Sridhar, R., Furness, S. G., Liu, M., Thompson, P. E., Miller, L. J., Christopoulos, A., and Sexton, P. M. (2016) The extracellular surface of the GLP-1 receptor is a molecular trigger for biased agonism. *Cell* **165,** 1632–1643
29. Wootten, D., Reynolds, C. A., Koole, C., Smith, K. J., Mobarec, J. C., Simms, J., Quon, T., Coudrat, T., Furness, S. G., Miller, L. J., Christopoulos, A., and Sexton, P. M. (2016) A hydrogen-bonded polar network in the core of the glucagon-like peptide-1 receptor is a fulcrum for biased agonism: lessons from Class B crystal structures. *Mol. Pharmacol.* **89,** 335–347
30. Yang, D., de Graaf, C., Yang, L., Song, G., Dai, A., Cai, X., Feng, Y., Reedtz-Runge, S., Hanson, M. A., Yang, H., Jiang, H., Stevens, R. C., and Wang, M. W. (2016) Structural determinants of binding the seven-transmembrane domain of the glucagon-like peptide-1 receptor (GLP-1R). *J. Biol. Chem.* **291,** 12991–13004
31. Yang, L., Yang, D., de Graaf, C., Moeller, A., West, G. M., Dharmarajan, V., Wang, C., Siu, F. Y., Song, G., Reedtz-Runge, S., Pascal, B. D., Wu, B., Potter, C. S., Zhou, H., Griffin, P. R., *et al.* (2015) Conformational states of the full-length glucagon receptor. *Nat. Commun.* **6,** 7859
32. Singh, R., Ahalawat, N., and Murarka, R. K. (2015) Activation of corticotropin-releasing factor 1 receptor: insights from molecular dynamics simulations. *J. Phys. Chem. B* **119,** 2806–2817
33. Li, Y., Sun, J., Li, D., and Lin, J. (2016) Activation and conformational dynamics of a class B G-protein-coupled glucagon receptor. *Phys. Chem. Chem. Phys.* **18,** 12642–12650
34. Black, J. W., and Leff, P. (1983) Operational models of pharmacological agonism. *Proc. R. Soc. Lond. B Biol. Sci.* **220,** 141–162
35. Lin, Y. C., Boone, M., Meuris, L., Lemmens, I., Van Roy, N., Soete, A., Reumers, J., Moisse, M., Plaisance, S., Drmanac, R., Chen, J., Speleman, F., Lambrechts, D., Van de Peer, Y., Tavernier, J., and Callewaert, N. (2014) Genome dynamics of the human embryonic kidney 293 lineage in response to cell biology manipulations. *Nat. Commun.* **5,** 4767
36. Stillman, B. W., and Gluzman, Y. (1985) Replication and supercoiling of simian virus 40 DNA in cell extracts from human cells. *Mol. Cell. Biol.* **5,** 2051–2060
37. Wootten, D., Lindmark, H., Kadmiel, M., Willcockson, H., Caron, K. M., Barwell, J., Drmota, T., and Poyner, D. R. (2013) Receptor activity modifying proteins (RAMPs) interact with the VPAC 2 receptor and CRF1 receptors and modulate their function. *Br. J. Pharmacol.* **168,** 822–834
38. Qi, T., Dong, M., Watkins, H. A., Wootten, D., Miller, L. J., and Hay, D. L. (2013) Receptor activity-modifying protein-dependent impairment of calcitonin receptor splice variant Δ(1–47) hCT((a)) function. *Br. J. Pharmacol.* **168,** 644–657
39. Hay, D. L., Walker, C. S., Gingell, J. J., Ladds, G., Reynolds, C. A., and Poyner, D. R. (2016) Receptor activity-modifying proteins: multifunctional G protein-coupled receptor accessory proteins. *Biochem. Soc. Trans.* **44,** 568–573
40. Atwood, B. K., Lopez, J., Wager-Miller, J., Mackie, K., and Straiker, A. (2011) Expression of G protein-coupled receptors and related proteins in HEK293, AtT20, BV2, and N18 cell lines as revealed by microarray analysis. *BMC Genomics* **12,** 14
41. Figueroa, K. W., Griffin, M. T., and Ehlert, F. J. (2009) Selectivity of agonists for the active state of M1 to M4 muscarinic receptor subtypes. *J. Pharmacol. Exp. Ther.* **328,** 331–342
42. Takasaki, J., Saito, T., Taniguchi, M., Kawasaki, T., Moritani, Y., Hayashi, K., and Kobori, M. (2004) A novel $G\alpha_q$/11-selective inhibitor. *J. Biol. Chem.* **279,** 47438–47445
43. Wunder, F., Rebmann, A., Geerts, A., and Kalthof, B. (2008) Pharmacological and kinetic characterization of adrenomedullin 1 and calcitonin gene-related peptide 1 receptor reporter cell lines. *Mol. Pharmacol.* **73,** 1235–1243
44. Watkins, H. A., Walker, C. S., Ly, K. N., Bailey, R. J., Barwell, J., Poyner, D. R., and Hay, D. L. (2014) Receptor activity-modifying protein-dependent effects of mutations in the calcitonin receptor-like receptor: implications for adrenomedullin and calcitonin gene-related peptide pharmacology. *Br. J. Pharmacol.* **171,** 772–788
45. Aiyar, N., Disa, J., Stadel, J. M., and Lysko, P. G. (1999) Calcitonin gene-related peptide receptor independently stimulates 3′,5′-cyclic adenosine monophosphate and Ca^{2+} signaling pathways. *Mol. Cell. Biochem.* **197,** 179–185
46. Christopoulos, G., Perry, K. J., Morfis, M., Tilakaratne, N., Gao, Y., Fraser, N. J., Main, M. J., Foord, S. M., and Sexton, P. M. (1999) Multiple amylin receptors arise from receptor activity-modifying protein interaction with the calcitonin receptor gene product. *Mol. Pharmacol.* **56,** 235–242
47. Shimekake, Y., Nagata, K., Ohta, S., Kambayashi, Y., Teraoka, H., Kitamura, K., Eto, T., Kangawa, K., and Matsuo, H. (1995) Adrenomedullin stimulates two signal transduction pathways, cAMP accumulation and Ca^{2+} mobilization, in bovine aortic endothelial cells. *J. Biol. Chem.* **270,** 4412–4417
48. Permpoonputtana, K., Porter, J. E., Govitrapong, P. (2016) Calcitonin gene-related peptide mediates an inflammatory response in Schwann cells via cAMP-dependent ERK signaling cascade. *Life Sci.* **144,** 19–25
49. Harikumar, K. G., Simms, J., Christopoulos, G., Sexton, P. M., and Miller, L. J. (2009) Molecular basis of association of receptor activity-modifying protein 3 with the family B G-protein-coupled secretin receptor. *Biochemistry* **48,** 11773–11785
50. Rasmussen, S. G., DeVree, B. T., Zou, Y., Kruse, A. C., Chung, K. Y., Kobilka, T. S., Thian, F. S., Chae, P. S., Pardon, E., Calinski, D., Mathiesen, J. M., Shah, S. T., Lyons, J. A., Caffrey, M., Gellman, S. H., *et al.* (2011) Crystal structure of the $\beta(2)$ adrenergic receptor-G_s protein complex. *Nature* **477,** 549–555
51. Ladds, G., Davis, K., Hillhouse, E. W., and Davey, J. (2003) Modified yeast cells to investigate the coupling of G protein-coupled receptors to specific G proteins. *Mol. Microbiol.* **47,** 781–792
52. Brown, A. J., Goldsworthy, S. M., Barnes, A. A., Eilert, M. M., Tcheang, L., Daniels, D., Muir, A. I., Wigglesworth, M. J., Kinghorn, I., Fraser, N. J., Pike, N. B., Strum, J. C., Steplewski, K. M., Murdock, P. R., Holder, J. C., *et al.* (2003) The orphan G protein-coupled receptors GPR41 and GPR43 are activated by propionate and other short chain carboxylic acids. *J. Biol. Chem.* **278,** 11312–11319
53. Gietz, R. D., and Schiestl, R. H. (2007) Quick and easy yeast transformation using the LiAc/SS carrier DNA/PEG method. *Nat. Protoc.* **2,** 35–37
54. Gingell, J. J., Qi, T., Bailey, R. J., and Hay, D. L. (2010) A key role for tryptophan 84 in receptor activity-modifying protein 1 in the amylin 1 receptor. *Peptides* **31,** 1400–1404
55. Ladds, G., Zervou, S., Vatish, M., Thornton, S., and Davey, J. (2009) Regulators of G protein signalling proteins in the human myometrium. *Eur. J. Pharmacol.* **610,** 23–28
56. Spandidos, A., Wang, X., Wang, H., and Seed, B. (2010) PrimerBank: a resource of human and mouse PCR primer pairs for gene expression detection and quantification. *Nucleic Acids Res.* **38,** D729–D799
57. Webb, B., and Sali, A. (2016) Comparative protein structure modeling using MODELLER. *Curr. Protoc. Bioinformatics* **54,** 5.6.1–5.6.37
58. Siu, F. Y., He, M., de Graaf, C., Han, G. W., Yang, D., Zhang, Z., Zhou, C., Xu, Q., Wacker, D., Joseph, J. S., Liu, W., Lau, J., Cherezov, V., Katritch, V., Wang, M. W., and Stevens, R. C. (2013) Structure of the human glucagon class B G-protein-coupled receptor. *Nature* **499,** 444–449

59. Hollenstein, K., Kean, J., Bortolato, A., Cheng, R. K., Doré, A. S., Jazayeri, A., Cooke, R. M., Weir, M., and Marshall, F. H. (2013) Structure of class B GPCR corticotropin-releasing factor receptor 1. *Nature* **499,** 438–443
60. Booe, J. M., Walker, C. S., Barwell, J., Kuteyi, G., Simms, J., Jamaluddin, M. A., Warner, M. L., Bill, R. M., Harris, P. W., Brimble, M. A., Poyner, D. R., Hay, D. L., and Pioszak, A. A. (2015) Structural basis for receptor activity-modifying protein-dependent selective peptide recognition by a G protein-coupled receptor. *Mol. Cell* **58,** 1040–1052
61. Koth, C. M., Murray, J. M., Mukund, S., Madjidi, A., Minn, A., Clarke, H. J., Wong, T., Chiang, V., Luis, E., Estevez, A., Rondon, J., Zhang, Y., Hötzel, I., and Allan, B. B. (2012) Molecular basis for negative regulation of the glucagon receptor. *Proc. Natl. Acad. Sci. U S A.* **109,** 14393–14398
62. Hoang, H. N., Song, K., Hill, T. A., Derksen, D. R., Edmonds, D. J., Kok, W. M., Limberakis, C., Liras, S., Loria, P. M., Mascitti, V., Mathiowetz, A. M., Mitchell, J. M., Piotrowski, D. W., Price, D. A., Stanton, R. V., *et al.* (2015) Short hydrophobic peptides with cyclic constraints are potent glucagon-like peptide-1 receptor (GLP-1R) agonists. *J. Med. Chem.* **58,** 4080–4085
63. Pérez-Castells, J., Martín-Santamaría, S., Nieto, L., Ramos, A., Martínez, A., Pascual-Teresa, Bd., and Jiménez-Barbero, J. (2012) Structure of micelle-bound adrenomedullin: a first step toward the analysis of its interactions with receptors and small molecules. *Biopolymers* **97,** 45–53
64. Jo, S., Kim, T., Iyer, V. G., and Im, W. (2008) CHARMM-GUI: a Web-based graphical user interface for CHARMM. *J. Comput. Chem.* **29,** 1859–1865
65. Jorgensen, W. L., Chandrasekhar, J., Madura, J. D., Impey, R. W., and Klein, M. L. (1983) Comparison of simple potential functions for simulating liquid water. *J. Chem. Phys.* **79,** 926–935
66. Dolinsky, T. J., Nielsen, J. E., McCammon, J. A., and Baker, N. A. (2004) PDB2PQR: an automated pipeline for the setup of Poisson-Boltzmann electrostatics calculations. *Nucleic Acids Res.* **32,** W665–W667
67. Hornak, V., Abel, R., Okur, A., Strockbine, B., Roitberg, A., and Simmerling, C. (2006) Comparison of multiple Amber force fields and development of improved protein backbone parameters. *Proteins* **65,** 712–725
68. Walker, R. C., Dickson, C. J., Madej, B. D., Skjevik, A. A., Betz, R. M., Teigen, K., and Gould, I. R. (2014) Amber lipid force field: Lipid14 and beyond, in *Abstracts of the 248th National Meeting of the American Chemical Society,* San Francisco, August 10–14, 2016, 163-COMP, American Chemical Society, Washington, DC
69. Dickson, C. J., Madej, B. D., Skjevik, A. A., Betz, R. M., Teigen, K., Gould, I. R., and Walker, R. C. (2014) Lipid14: the Amber lipid force field. *J. Chem. Theory Comput.* **10,** 865–879
70. Case, D. A., Betz, R. M., Botello-Smith, W., Cerutti, D. S., Cheatham, T. E., III, *et al.* (2016) *AMBER 2016*, University of California, San Francisco
71. Harvey, M. J., Giupponi, G., and Fabritiis, G. D. (2009) ACEMD: accelerating biomolecular dynamics in the microsecond time scale. *J. Chem. Theory Comput.* **5,** 1632–1639
72. Brown, A. J., Dyos, S. L., Whiteway, M. S., White, J. H., Watson, M. A., Marzioch, M., Clare, J. J., Cousens, D. J., Paddon, C., Plumpton, C., Romanos, M. A., and Dowell, S. J. (2000) Functional coupling of mammalian receptors to the yeast mating pathway using novel yeast/mammalian G protein α-subunit chimeras. *Yeast* **16,** 11–22

ADDITIONS AND CORRECTIONS

THE JOURNAL OF BIOLOGICAL CHEMISTRY VOL. 291, NO. 49, p. 25763, December 2, 2016

VOLUME 291 (2016) PAGES 21925–21944
DOI 10.1074/jbc.A116.751362

Receptor activity-modifying protein-directed G protein signaling specificity for the calcitonin gene-related peptide family of receptors.

Cathryn Weston, Ian Winfield, Matthew Harris, Rose Hodgson, Archna Shah, Simon J. Dowell, Juan Carlos Mobarec, David A. Woodcock, Christopher A. Reynolds, David R. Poyner, Harriet A. Watkins, and Graham Ladds

PAGES 21931 AND 21933:

There were some errors in Tables 3 and 4 whereby some data values were increased by the addition of 10 units to each data point. These errors have now been corrected and do not affect the results or conclusions of this work.

TABLE 3

Potency (pEC_{50}), affinity (pK_B) and coupling efficacy (log τ) values for cAMP production at the CLR co-expressed with each RAMP, stimulated with various agonists measured in HEK-293 cells in the presence and absence of pertussis toxin

Data are the mean ± S.E. of *n* individual data sets. Statistically different between PTX-treated and untreated was determined using Student's *t* test (*, $p < 0.05$; **, $p < 0.01$; ***, $p < 0.001$; and ****, $p < 0.0001$).

	Untreated					Treated				
	pEC_{50}[a]	E_{max}[b]	pK_a[c]	log τ[d]	*n*	pEC_{50}[a]	E_{max}[b]	pK_a[c]	log τ[d]	*n*
RAMP1										
CGRP	9.66 ± 0.2	47.07 ± 2.2	9.43 ± 0.2	−0.11 ± 0.04	9	9.65 ± 0.2	44.95 ± 2.2	9.33 ± 0.3	−0.11 ± 0.07	6
AM	7.93 ± 0.2	48.06 ± 2.5	7.67 ± 0.2	−0.09 ± 0.05	9	8.14 ± 0.07	72.17 ± 1.7***	7.66 ± 0.2	0.36 ± 0.1**	6
AM2	7.93 ± 0.2	46.10 ± 4.1	7.70 ± 0.2	−0.11 ± 0.07	9	9.15 ± 0.1*	72.15 ± 2.4***	8.56 ± 0.3	0.4 ± 0.1**	6
RAMP2										
CGRP	9.00 ± 0.2	36.97 ± 2.4	8.82 ± 0.2	−0.27 ± 0.05	9	8.25 ± 0.4	56.27 ± 1.4***	7.92 ± 0.2*	0 0.1 ± 0.06**	6
AM	10.35 ± 0.1	56.33 ± 1.6	10.00 ± 0.1	0.07 ± 0.02	9	10.16 ± 0.07	56.07 ± 1.1	9.83 ± 0.2	0.07 ± 0.02	6
AM2	7.46 ± 0.2	36.61 ± 3.5	7.24 ± 0.2	−0.29 ± 0.07	9	9.13 ± 0.1**	56.05 ± 2.2***	8.84 ± 0.2**	0.1 ± 0.06*	6
RAMP3										
CGRP	7.75 ± 0.3	22.38 ± 2.6	7.64 ± 0.3	−0.54 ± 0.07	8	8.90 ± 0.1*	32.61 ± 1.5*	8.74 ± 0.2*	−0.29 ± 0.06	7
AM	8.98 ± 0.2	32.00 ± 1.5	8.83 ± 0.1	−0.33 ± 0.03	8	9.10 ± 0.2	35.95 ± 2.2	8.94 ± 0.2	−0.34 ± 0.05	7
AM2	9.10 ± 0.2	21.92 ± 1.7	9.08 ± 0.2	−0.51 ± 0.06	8	8.74 ± 0.2	44.35 ± 2.7****	8.43 ± 0.1*	−0.07 ± 0.07***	7

[a] The negative logarithm of the agonist concentration required to produce a half-maximal response.
[b] The maximal response to the ligand expressed as a percentage of the maximal cAMP production as determined using 100 μM forskolin stimulation in the presence of pertussis toxin treatment.
[c] The negative logarithm of the equilibrium disassociation constant for each ligand generated through use of the operational model of agonism (34).
[d] Log τ is the coupling efficiency parameter of each ligand.

TABLE 4

Potency (pEC_{50}) and maximal response (E_{max}), for cAMP production at the CLR co-expressed with each RAMP, stimulated with various agonists measured in HEK-293S cells in the presence or absence of pertussis toxin

Data are the mean ± S.E. of *n* individual data sets. No statistical difference was found between untreated and PTX-treated HEK-293S cells using Student's *t* test.

	Untreated			Treated		
	pEC_{50}[a]	E_{max}[b]	*n*	pEC_{50}[a]	E_{max}[b]	*n*
RAMP1						
CGRP	9.88 ± 0.1	59.98 ± 1.1	5	9.87 ± 0.1	72.92 ± 2.3	5
AM	8.13 ± 0.1	60.00 ± 3.1	5	8.03 ± 0.1	61.26 ± 2.6	5
AM2	8.74 ± 0.1	68.94 ± 1.2	5	8.78 ± 0.1	68.30 ± 1.6	5
RAMP2						
CGRP	8.00 ± 0.1	32.56 ± 1.0	5	7.88 ± 0.1	39.32 ± 1.7	5
AM	9.39 ± 0.1	30.34 ± 0.8	5	9.38 ± 0.1	33.28 ± 1.2	5
AM2	8.57 ± 0.1	40.30 ± 1.5	5	8.58 ± 0.2	30.52 ± 2.0	5
RAMP3						
CGRP	8.42 ± 0.1	40.84 ± 0.6	5	8.38 ± 0.1	39.84 ± 1.0	5
AM	9.63 ± 0.1	39.09 ± 1.2	5	9.49 ± 0.2	42.26 ± 1.6	5
AM2	8.01 ± 0.1	33.75 ± 1.5	5	7.79 ± 0.2	28.21 ± 2.4	5

[a] The negative logarithm of the agonist concentration required to produce a half-maximal response.
[b] The maximal response to the ligand expressed as a percentage of the maximal cAMP production as determined using 100 μM forskolin stimulation in the presence of PTX treatment.

Authors are urged to introduce these corrections into any reprints they distribute. Secondary (abstract) services are urged to carry notice of these corrections as prominently as they carried the original abstracts.

Appendix 3

Manuscript: Bridge *et al*, 2017

This appendix contains:

Bridge LJ, Mead J, Frattini E, Winfield I, Ladds G (**2017**). Modelling and simulation of biased agonism dynamics at a G protein-coupled receptor. Submitted to: *J. Theor. Biol.*

Modelling and simulation of biased agonism dynamics at a G protein-coupled receptor

L. J. Bridge*[1], J. Mead[2], E. Frattini[2], I. Winfield[2,3] and G. Ladds*[2]

Abstract

Theoretical models of G protein-coupled receptor (GPCR) concentration-response relationships often assume an agonist producing a single functional response via a single active state of the receptor. These models have largely been analysed assuming steady-state conditions. There is now much experimental evidence to suggest that many GPCRs can exist in multiple receptor conformations and elicit numerous functional responses, with ligands having the potential to activate different signalling pathways to varying extents - a concept referred to as biased agonism, functional selectivity or pluri-dimensional efficacy. Moreover, recent experimental results indicate a clear possibility for time dependent bias, whereby an agonists bias with respect to different pathways may vary dynamically. Efforts towards understanding the implications of temporal bias by characterising and quantifying ligand effects on multiple pathways will clearly be aided by extending current equilibrium binding and biased activation models to include G protein-activation dynamics. Here, we present a new model of time-dependent biased agonism, based on ordinary differential equations for multiple cubic ternary activation models with G protein cycle dynamics. The model is generally applicable to systems with N^G G proteins and N^* active receptor states. Numerical simulations for $N^G = N^* = 2$ reveal new insights into the effects of system parameters (including cooperativities, and ligand and receptor concentrations) on bias dynamics, revealing new phenomena including the dynamic inter-conversion of bias direction. Further, we have fitted this model to 'wet' experimental data for two competing G proteins (G_i and G_s) that become activated upon stimulation of the adenosine A1 receptor with adenosine derivative compounds. We also show that our model can qualitatively describe the temporal dynamics of this competing G protein activation.

Keywords: *Mathematical pharmacology, G protein coupled receptors, receptor theory, biased signalling, ordinary differential equations.*

1 Introduction

Mathematical modelling and scientific computing are powerful tools for the analysis of cell signalling in pharmacology. "Analytical pharmacology", which has its roots in classical receptor theory and largely focuses on equilibrium cell responses to drugs, provides a vital theoretical basis which underpins drug classification and prediction of drug mechanism of action [19]. Much of the analysis has centered on assumptions of a single ligand binding a monomeric G protein-coupled receptor (GPCR), activating a single active state and coupling a single G protein. Concepts like allosterism, inverse agonism, oligomerisation and "biased signalling" are now widely accepted and have enhanced receptor theory towards better understanding of drug-receptor interactions and informed drug discovery [22]. GPCRs represent a target for perhaps up to half of all current drugs [48], and as such, development of the theory for ligand-GPCR interactions and their consequences is key.

Biased agonism is now a widely accepted phenomenon whereby a ligand may activate multiple different pathways at the same receptor, via multiple active conformations [44, 32, 16, 35]. Other terms for this phenomenon include *functional selectivity* and *pluri-dimensional efficacy*, while *receptor promiscuity* refers to the ability of a receptor to couple different G proteins with different affinities, via different active states. The possibility of multi-pathway activation may lead to a breakdown in the common classifications of ligands based on single active state theory [16], or errors in the interpretation of data using simple models [43]. Therefore, development of biased agonism theory has become an important field of pharmacological research.

[1]Department of Mathematics, Swansea University, Singleton Park, Swansea SA2 8PP. Email: l.bridge@swansea.ac.uk

[2]Department of Pharmacology, University of Cambridge , Tennis Court Road, Cambridge CB2 1PD, U.K.

[3]Division of Biomedical Sciences, Warwick Medical School, University of Warwick , Coventry CV4 7AL, U.K.

*corresponding authors

Biased signalling has implications for drug discovery, including the prospect of clinical selectivity and the potential of reduced side effects [41, 20, 18]. A schematic of biased agonism is shown in Figure 1.1, indicating possibility for a ligand to activate two (or more) G protein pathways at the same receptor, one of which may be a "target" therapeutic pathway, while the other may be an unwanted "side-effect" pathway (panel (b)). To understand, quantify and exploit the potential for biased agonism, theoretical models for such schematics are required.

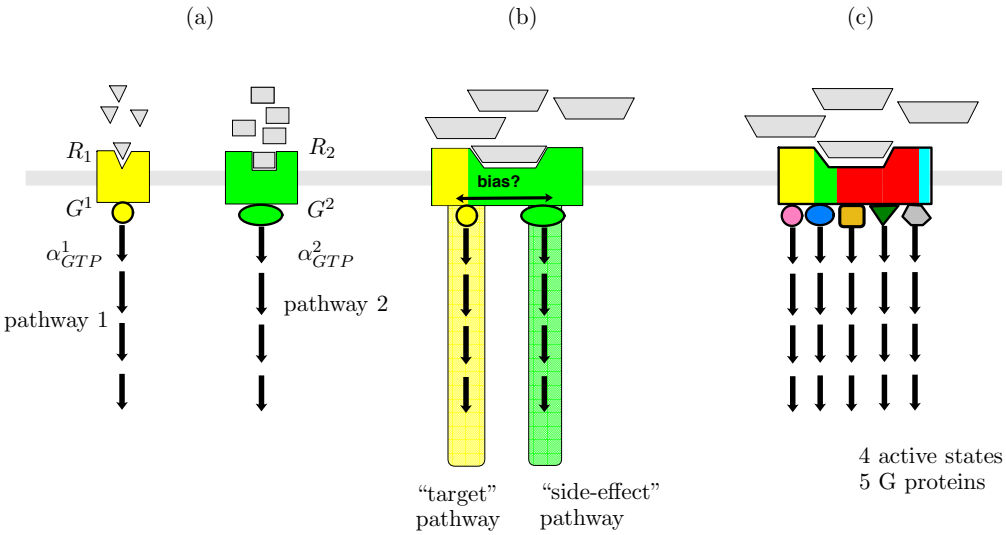

Figure 1.1: Pluri-dimensional efficacy and biased agonism at a GPCR. (a) A classical view of signalling - two different receptors, each bound and activated (to a single active conformation) by a specific ligand, and bound by a specific G protein. The activated G protein subunit α_{GTP} signals to a downstream pathway specific to the G protein. (b) A two-active-state, two-G protein biased signalling schematic. The receptor has two active states, and the proportion of receptors in either active state, and the inactive state, may be affected (biased) by a single ligand. Two different G proteins, specific to the active conformations, couple to the receptors and signal to two pathways. (c) Pluri-dimensional efficacy - multi-active receptor with multiple G proteins, not necessarily each specific to a single receptor conformation. Here we have $N^* = 4$ active states and $N^G = 5$ G proteins.

A two-active-state model of ligand binding and receptor activation at equilibrium was presented in [27]. This equilibrium model addressed the limitations of single-active-state theory which could not recapitulate different pathway potency and efficacy patterns at the same receptor. It was found that theoretically, an agonist may enrich one active receptor state at the expense of another, and pathway-dependent efficacy was observed in simulations. For an intact system, however, pathway-dependent potency (with active receptor as the pathway readout) was not possible. G protein coupling and activation were not explicitly modelled, but their importance for future modelling was acknowledged. Later equilibrium models included the binding of G proteins [38, 13], which give further scope for pathway-dependent pharmacology. An alternative model for biased agonism is given in [36], where downstream effects are modelled not explicitly via G protein binding, but by coupling the operational model of agonism [5] to active receptor stimuli. This model does not include constitutive activity of the receptors. Further equilibrium modelling for promiscuous coupling of receptors to multiple G proteins has been presented in [24, 43].

The direction and magnitude of a ligand's bias towards one pathway over another has largely been quantified using equilibrium assumptions and empirical models such as the operational model [34, 14, 21, 17]. A recent study [15] has highlighted the role of "kinetic context" in approaching such calculations, whereby the apparent bias of a ligand towards any given pathway may vary over time. Interpretation of experimental readouts in terms of bias must therefore take into account the signalling dynamics and associated timescales of the measured pathway. Thus, dynamic models of GPCR biased

signalling are proposed here to give new theoretical insights into the effects of biased agonists.

In [10], an ordinary differential equation (ODE) model for the dynamics of biased signalling at GPCRs is presented. The steady-state behaviour of the model is analysed, with particular attention paid to the effect of G protein, where the model output is active G protein. The dynamics are not examined in detail, but extensive analysis of GPCR signalling dynamics have been presented in [8, 47, 48], for mathematical models which also allow G proteins binding to inactive receptors, and constitutive receptor activity. In these models, the active G protein α subunit bound to guanisine triphosphate (α_{GTP}) is taken as a model readout which is representative of downstream signalling pathway activity.

In this paper we develop a new mathematical model for the dynamics of biased agonism at GPCRs. In Section 2, we formulate a general ODE model for the dynamics of a receptor which can activate multiple G protein-mediated pathways. The general model has receptor with N^* active conformations and N^G G proteins available for coupling, but our focus computationally (driven by [27]) throughout is the case $N^* = N^G = 2$. In Section 3, we present time course and concentration-response simulation results for our model, focusing on α_{GTP} dynamics. In particular, we highlight that our model has the propensity for agonist-inverse agonist interconversion both with respect to time and constitutive activity. A numerical analysis of the effects of multiple cooperativity factors is performed. In Section 4, we propose an heuristic method for quantifying dynamic bias, by way of bias factors, and show how these bias factors relate to our model parameters. It is shown that the bias rank order for a bank of ligands may change dynamically. In Section 5, we show that our model simulations fit well to new experimental data where biased agonism at the adenosine A_1 receptor is suspected. We conclude in Section 6 with a discussion of our main results, underlining our contribution to the biased signalling literature.

2 Model formulation

Here we formulate an ODE model for the dynamics of signalling for multi-active state GPCRs capable of binding multiple G proteins, in response to a single ligand binding. The model allows for a receptor which may have an inactive conformation R, or one of N^* active receptor conformations R^{*j}, for $j = 1, .., N^*$. Also, a receptor may couple to one of N^G G proteins G^θ, for $\theta = 1, .., N^G$. The model encompasses ligand binding, receptor activation, G protein binding and the G protein cycle, whereby the model output is activated G protein α_{GTP}, which signals to second messengers, and is therefore taken as an indicator of pathway response, as in [48, 47, 8].

2.1 A three-state (two active states) model

While the model is formulated for general N^G and N^*, we largely focus throughout on the case $N^* = N^G = 2$. A schematic for the transitions between 18 receptor states for this particular case is shown in Figure 2.1. R denotes inactive receptor, while R^{*j} $(j = 1, 2)$ denotes the j^{th} active state. Any species including L is a complex including ligand-bound receptor, while any species including G^θ $(\theta = 1, 2)$ is a complex including receptor coupled to the θ^{th} G protein. Double arrows represent the reversible binding and activation reactions between receptor states. As described in previous GPCR signalling studies (eg. [48, 47, 8]), a R^*G^θ or LR^*G^θ complex may dissociate and exchange GDP for GTP on the α subunit of the G protein, leading to the signalling *response* α^θ_{GTP} and the G protein cycle.

2.2 The (j, θ) receptor/G protein block

In order to formulate the ODE model for the schematic shown in Figure 2.1 (or, indeed, the general N^*, N^G-case), we consider the (j, θ) receptor/G protein block (where $j = 1, 2$ and $\theta = 1, 2$ for Figure 2.1). Each such block is seen to be a cubic ternary complex schema for activation of receptor from inactive state R to active state R^{*j}, with coupling to G protein G^θ [48]. In Figure 2.2, the equilibrium rate constants $K_\bullet$ and cooperativity factors μ, ν, ζ are labelled on each reversible reaction. For the individual kinetic rate constants and factors, we use lower case k, and subscripts $+$ and $-$ to

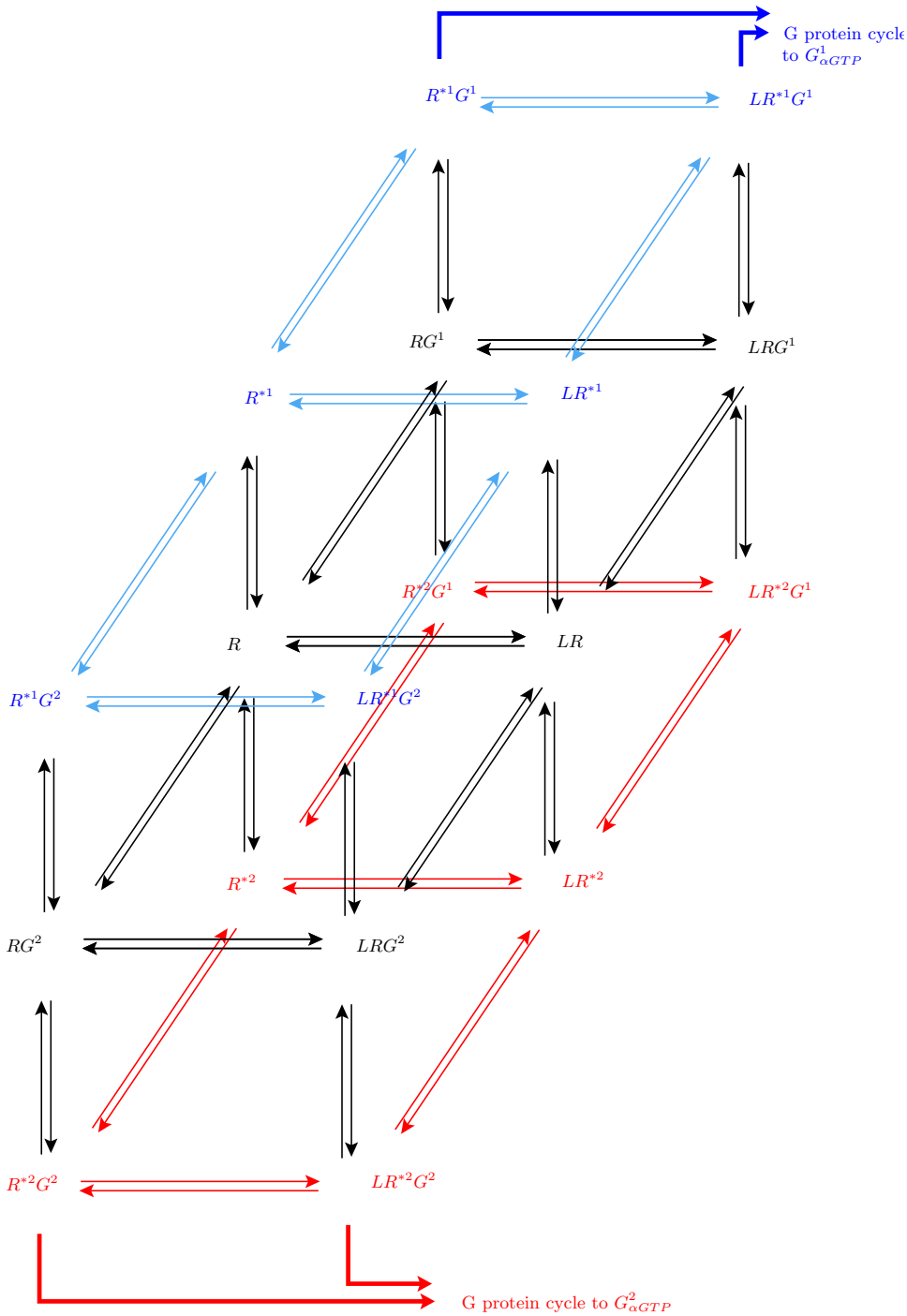

Figure 2.1: A multi-cubic ternary complex model schematic for biased signalling with two active receptor states and two G proteins.

denote the forward and backward reactions respectively. The descriptions of the rate constants and cooperativity factors are given in Table 2.1. The G protein cycle and α_{GTP} responses follow from dissociation of R^*G^θ and LR^*G^θ according to the following reactions (see [48]):

$$R^{*j}G^\theta \overset{k^{j,\theta}_{GTP+}}{\longrightarrow} R^{*j} + \alpha^\theta_{GTP} + \beta\gamma^\theta, \qquad LR^{*j}G^\theta \overset{\nu^\theta k^{j,\theta}_{GTP+}}{\longrightarrow} LR^{*j} + \alpha^\theta_{GTP} + \beta\gamma^\theta, \tag{2.1a}$$

$$\alpha^\theta_{GTP} \underset{k_{hyd-}}{\overset{k_{hyd+}}{\rightleftharpoons}} \alpha^\theta_{GDP}, \qquad \alpha^\theta_{GDP} + \beta\gamma^\theta \underset{k_{RA-}}{\overset{k_{RA+}}{\rightleftharpoons}} G^\theta. \tag{2.1b}$$

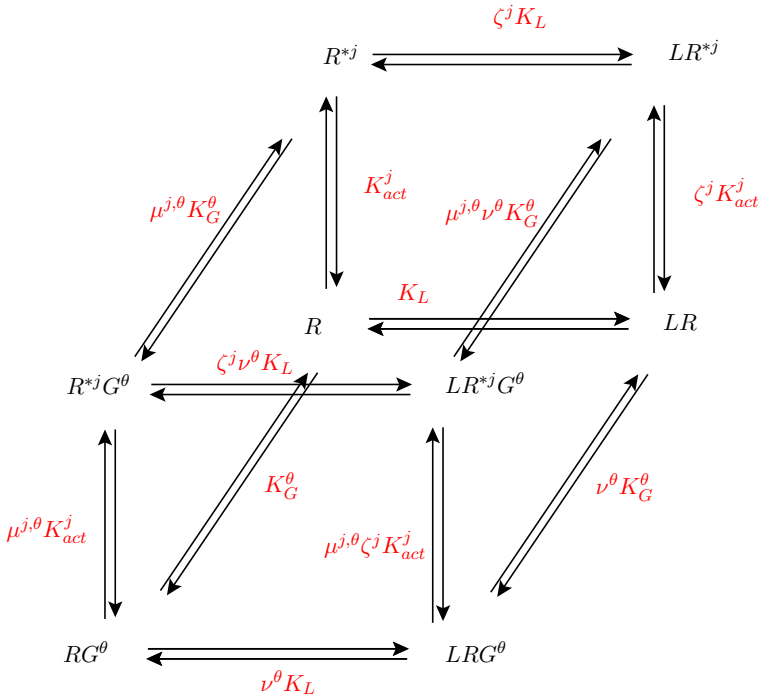

Figure 2.2: The (j,θ) receptor/G protein block of the multi-cubic ternary complex schematic, for ligand binding to, and activation of, receptor j, with coupling to G protein θ.

Table 2.1: Equilibrium rate constants and cooperativity factors for the (j,θ) block of the biased signalling schematic.

label	description of equilibrium constant
K_L	Association of ligand L and receptor R.
K^θ_G	Binding of G protein G^θ to receptor R.
K^j_{act}	Activation of receptor R to give active state R^{*j}.
$\mu^{j,\theta}$	Preference of G^θ for R^{*j} over R. Equally, the factor increase in propensity for $R \to R^{*j}$ activation when R is G^θ-bound.
ν^θ	Preference of L for RG^θ over R. Equally, the preference of G^θ for LR over R.
ζ^j	Preference of L for R^{*j} over R. Equally, the factor increase in propensity for $R \to R^{*j}$ activation when R is L-bound.

2.2.1 Governing equations

Suppose in general that a receptor has N^* distinct active states, and that each receptor may couple one of N^G distinct G proteins. Then applying Mass Action kinetics to our schematic and G protein cycle reactions gives a system of n nonlinear ODEs for the species concentrations, where

$$n = 3 + 2N^* + 6N^G + 2N^*N^G. \tag{2.2}$$

The first term here is given by species L, R and LR. The second term is given by active non-coupled receptor states R^{*j}, LR^{*j} and the third term corresponds to G protein not coupled to active receptor (G, RG, LRG, α^{θ}_{GTP}, $aGDP$, $\beta\gamma^{\theta}$). Finally, the number of active receptor/G protein complexes, $R^{*j}G^{\theta}$ and $LR^{*j}G^{\theta}$, is $2N^*N^G$, since we consider $j = 1, ..., N^*$ and $\theta = 1, ..., N^G$. If ligand concentration is considered constant, then we will not have an ODE for $[L]$ (so omitting equation (2.3b) below), and instead $n = 2\left(1 + N^* + 3N^G + N^*N^G\right)$.

$$\frac{d[R]}{dt} = k_{L-}[LR] - k_{L+}[L][R] + \sum_{j=1}^{N^*}\left(k^j_{act-}[R^{*j}] - k^j_{act+}[R]\right) + \sum_{\theta=1}^{N^G}\left(k^{\theta}_{G-}[RG^{\theta}] - k^{\theta}_{G+}[R][G^{\theta}]\right), \tag{2.3a}$$

$$\begin{aligned}\frac{d[L]}{dt} = {} & k_{L-}[LR] - k_{L+}[L][R] + \sum_{j=1}^{N^*}\left(\zeta^j_- k_{L-}[LR^{*j}] - \zeta^j_+ k_{L+}[L][R^{*j}]\right) \\ & + \sum_{\theta=1}^{N^G}\left(\nu^{\theta}_- k_{L-}[LRG^{\theta}] - \nu^{\theta}_+ k_{L+}[L][RG^{\theta}]\right) \\ & + \sum_{\theta=1}^{N^G}\sum_{j=1}^{N^*}\left(\zeta^j_-\nu^{\theta}_- k_{L-}[LR^{*j}G^{\theta}] - \zeta^j_+\nu^{\theta}_+ k_{L+}[L][R^{*j}G^{\theta}]\right),\end{aligned} \tag{2.3b}$$

$$\begin{aligned}\frac{d[LR]}{dt} = {} & k_{L+}[L][R] - k_{L-}[LR] + \sum_{j=1}^{N^*}\left(\zeta^j_- k^j_{act-}[LR^{*j}] - \zeta^j_+ k^j_{act+}[LR]\right) \\ & + \sum_{\theta=1}^{N^G}\left(\nu^{\theta}_- k^{\theta}_{G-}[LRG^{\theta}] - \nu^{\theta}_+ k^{\theta}_{G+}[LR][G^{\theta}]\right),\end{aligned} \tag{2.3c}$$

$$\begin{aligned}\frac{d[R^{*j}]}{dt} = {} & k^j_{act+}[R] - k^j_{act-}[R^{*j}] + \zeta^j_- k_{L-}[LR^{*j}] - \zeta^j_+ k_{L+}[L][R^{*j}] \\ & + \sum_{\theta=1}^{N^G}\left(\mu^{j,\theta}_- k^{\theta}_{G-}[R^{*j}G^{\theta}] - \mu^{j,\theta}_+ k^{\theta}_{G+}[R^{*j}][G^{\theta}]\right) + \sum_{\theta=1}^{N^G}\left(k^{j,\theta}_{GTP+}[R^{*j}G^{\theta}]\right), \qquad \text{for } j = 1, ..., N^*\end{aligned} \tag{2.3d}$$

$$\begin{aligned}\frac{d[LR^{*j}]}{dt} = {} & \zeta^j_+ k^j_{act+}[LR] - \zeta^j_- k^j_{act-}[LR^{*j}] + \zeta^j_+ k_{L+}[L][R^{*j}] - \zeta^j_- k_{L-}[LR^{*j}] \\ & + \sum_{\theta=1}^{N^G}\left(\mu^{j,\theta}_-\nu^{\theta}_- k^{\theta}_{G-}[LR^{*j}G^{\theta}] - \mu^{j,\theta}_+\nu^{\theta}_+ k^{\theta}_{G+}[LR^{*j}][G^{\theta}]\right) + \sum_{\theta=1}^{N^G}\left(\nu^{\theta}_- k^{j,\theta}_{GTP+}[LR^{*j}G^{\theta}]\right), \qquad \text{for } j = 1, ..\end{aligned} \tag{2.3e}$$

$$\begin{aligned}\frac{d[RG^{\theta}]}{dt} = {} & k^{\theta}_{G+}[R][G^{\theta}] - k^{\theta}_{G-}[RG^{\theta}] + \nu^{\theta}_- k_{L-}[LRG^{\theta}] - \nu^{\theta}_+ k_{L+}[L][RG^{\theta}] \\ & + \sum_{j=1}^{N^*}\left(\mu^{j,\theta}_- k^j_{act-}[R^{*j}G^{\theta}] - \mu^{j,\theta}_+ k^j_{act+}[RG^{\theta}]\right), \qquad \text{for } \theta = 1, ..., N^G,\end{aligned} \tag{2.3f}$$

$$\frac{d[LRG^{\theta}]}{dt} = \nu^{\theta}_+ k^{\theta}_{G+}[LR][G^{\theta}] - \nu^{\theta}_- k^{\theta}_{G-}[LRG^{\theta}] + \nu^{\theta}_+ k_{L+}[L][RG^{\theta}] - \nu^{\theta}_- k_{L-}[LRG^{\theta}]$$

$$+\sum_{j=1}^{N^*}\Big(\mu_-^{j,\theta}\zeta_-^j k_{act-}^j[LR^{*j}G^\theta]-\mu_+^{j,\theta}\zeta_+^j k_{act+}^j[LRG^\theta]\Big), \qquad \text{for } \theta=1,...,N^G, \tag{2.3g}$$

$$\begin{aligned}\frac{d[R^{*j}G^\theta]}{dt} &= \mu_+^{j,\theta}k_{G+}^\theta[R^{*j}][G^\theta]-\mu_-^{j,\theta}k_{G-}^\theta[R^{*j}G^\theta]+\zeta_-^j\nu_-^\theta k_{L-}[LR^{*j}G^\theta]-\zeta_+^j\nu_+^\theta k_{L+}[L][R^{*j}G^\theta]\\ &+\mu_+^{j,\theta}k_{act+}^j[RG^\theta]-\mu_-^{j,\theta}k_{act-}^j[R^{*j}G^\theta]\\ &-k_{GTP+}^{j,\theta}[R^{*j}G^\theta] \qquad \text{for } j=1,...,N^* \text{ and } \theta=1,...,N^G,\end{aligned} \tag{2.3h}$$

$$\begin{aligned}\frac{d[LR^{*j}G^\theta]}{dt} &= \mu_+^{j,\theta}\nu_+^\theta k_{G+}^\theta[LR^{*j}][G^\theta]-\mu_-^{j,\theta}\nu_-^\theta k_{G-}^\theta[LR^{*j}G^\theta]+\zeta_+^j\nu_+^\theta k_{L+}[L][R^{*j}G^\theta]-\zeta_-^j\nu_-^\theta k_{L-}[LR^{*j}G^\theta]\\ &+\mu_+^{j,\theta}\zeta_+^j k_{act+}^j[LRG^\theta]-\mu_-^{j,\theta}\zeta_-^j k_{act-}^j[LR^{*j}G^\theta]\\ &-\nu_-^\theta k_{GTP+}^{j,\theta}[LR^{*j}G^\theta] \qquad \text{for } j=1,...,N^* \text{ and } \theta=1,...,N^G,\end{aligned} \tag{2.3i}$$

$$\begin{aligned}\frac{d[G^\theta]}{dt} &= k_{G-}^\theta[RG^\theta]-k_{G+}^\theta[R][G^\theta]\ +\ \nu_-^\theta k_{G-}^\theta[LRG^\theta]-\nu_+^\theta k_{G+}^\theta[LR][G^\theta]\\ &+k_{GRA+}^\theta[\alpha_{GDP}^\theta][\beta\gamma^\theta]-k_{GRA-}^\theta[G^\theta]\\ &+\sum_{j=1}^{N^*}\Big(\mu_-^{j,\theta}k_{G-}^\theta[R^{*j}G^\theta]-\mu_+^{j,\theta}k_{G+}^\theta[R^{*j}][G^\theta]\Big)\\ &+\sum_{j=1}^{N^*}\Big(\mu_-^{j,\theta}\nu_-^\theta k_{G-}^\theta[LR^{*j}G^\theta]-\mu_+^{j,\theta}\nu_+^\theta k_{G+}^\theta[LR^{*j}][G^\theta]\Big), \qquad \text{for } \theta=1,...,N^G,\end{aligned} \tag{2.3j}$$

$$\frac{d[\alpha_{GDP}^\theta]}{dt} = k_{hyd+}^\theta[\alpha_{GTP}^\theta]-k_{hyd-}^\theta[\alpha_{GDP}^\theta]+k_{GRA-}^\theta[G^\theta]-k_{GRA+}^\theta[\alpha_{GDP}^\theta][\beta\gamma^\theta], \qquad \text{for } \theta=1,...,N^G, \tag{2.3k}$$

$$\begin{aligned}\frac{d[\beta\gamma^\theta]}{dt} &= k_{GRA-}^\theta[G^\theta]-k_{GRA+}^\theta[\alpha_{GDP}^\theta][\beta\gamma^\theta]\\ &+\sum_{j=1}^{N^*}\Big(k_{GTP+}^{j,\theta}[R^{*j}G^\theta]+\nu_-^\theta k_{GTP+}^{j,\theta}[LR^{*j}G^\theta]\Big), \qquad \text{for } \theta=1,...,N^G,\end{aligned} \tag{2.3l}$$

$$\begin{aligned}\frac{d[\alpha_{GTP}^\theta]}{dt} &= k_{hyd-}^\theta[\alpha_{GDP}^\theta]-k_{hyd+}^\theta[\alpha_{GTP}^\theta]\\ &+\sum_{j=1}^{N^*}\Big(k_{GTP+}^{j,\theta}[R^{*j}G^\theta]+\nu_-^\theta k_{GTP+}^{j,\theta}[LR^{*j}G^\theta]\Big), \qquad \text{for } \theta=1,...,N^G.\end{aligned} \tag{2.3m}$$

For the model "outputs", or downstream responses of the system to an input ligand concentration, we take the concentrations $[\alpha_{GTP}^\theta]$ for $\theta=1,...,N^G$, as we consider these as indicators of downstream activity in signalling pathways as in [7, 8]. For our computational results, we will consider the case with two G proteins and two active receptor states, such that $N^*=N^G=2$, and our model has 18 receptor states and 8 non-receptor-bound G protein species ($2\times(G+\alpha_{GTP}+\alpha_{GDP}+\beta\gamma)$). Taking ligand concentration constant (as in previous studies), the system (2.3) in this case consists of 26 ODEs.

Initial conditions for our simulations have $[R]_{t=0}=R_{tot}$ (the total receptor concentration), $[G^\theta]_{t=0}=G_{tot}^\theta$ (the total concentration for each G protein), and all other species zero at $t=0$.

3 Simulation results

Here we present numerical results (for α_{GTP}^θ concentrations) which illustrate the variety of dynamic behaviour which is possible for a system of two active states and two-G proteins. These results are

intended to demonstrate potential dynamics rather than provide exhaustive or accurate predictions for any particular receptors or ligands. For all simulations, we first compute the system with $[L] = 0$ for a long time (10^8 seconds) to allow the system to come to a steady-state equilibrium before the addition of ligand, and all parameters except those explicitly stated are maintained at the values in Table A.1.

3.1 Time Courses

3.1.1 Ligand is an agonist for both pathways

By varying the values of ζ^1 and ζ^2 , the preference of the ligand for a receptor in the respective active state over the inactive receptor state, we vary the efficacy with respect to the G protein pathways 1 and 2 respectively. In Figure 3.1, we show time courses of the responses to a ligand which is an equilibrium agonist for both pathways, for a range of concentrations. Three different ligand concentrations are used, and the α^{θ}_{GTP} responses for $\theta = 1, 2$ are shown. The higher efficacy with respect R^{*1} gives an increased response, and we note the peak-plateau dynamics. With increased ligand concentration, we see a higher α^{θ}_{GTP} response for both pathways, both at peak and plateau (end-point). Further, the peak timing is reduced with increased ligand concentration, in keeping with previous single active state studies [48, 7].

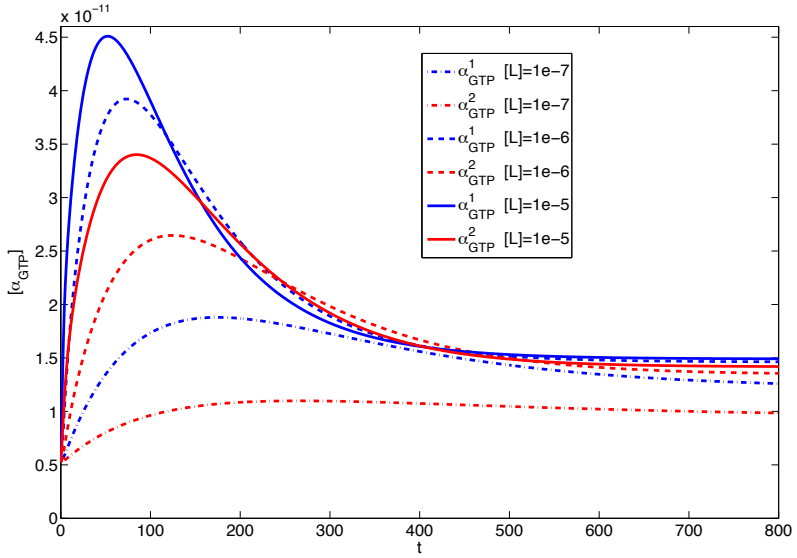

Figure 3.1: Graph showing the α^{θ}_{GTP} response (M) against time (in seconds) of two competing pathways with $\zeta^1_+ = 1000$ and $\zeta^2_+ = 100$ after the addition of $[L] = 10^{-7},\ 10^{-6},$ and10^{-5}M. Here, $\zeta^2_+ = 200$.

3.1.2 Ligand is agonist for one pathway and antagonist for the other

Neutral antagonists may be used as competitive ligands to endogenous agonists. Mathematical modelling of agonist-antagonist competition at a single active state GPCR has been considered in [8]. Within our two-active state model, we may simulate the dynamics of a system for which a given ligand is an agonist for one pathway but an antagonist for the other. In Figure 3.2, we show α_{GTP} and receptor time courses for this scenario, for a ligand which is an (equilibrium) agonist for pathway 1 ($\zeta^1_+ = 1000$, $\zeta^1_- = 1$) and an (equilibrium) antagonist for pathway 2 ($\zeta^2_+ = 1$, $\zeta^2_- = 1$), over a range of ligand concentrations. We note the peak-plateau α^1_{GTP} dynamics, and the nearly neutral effect on α^2_{GTP} dynamics. However, closer inspection of $[\alpha^2_{GTP}]$ reveals that the ligand in fact has an inverse

agonist effect on pathway 2. Since the ligand is an agonist for pathway 1, its effect on overall receptor activation is an increase in pathway 1 active states, given by

$$R^{*1}_{tot} = [R^{*1}] + [LR^{*1}] + [R^{*1}G^1] + [LR^{*1}G^1], \tag{3.1}$$

and a corresponding decrease in pathway 2 active states and free inactive receptor states, given, respectively, by

$$R^{*2}_{tot} = [R^{*2}] + [LR^{*2}] + [R^{*2}G^2] + [LR^{*2}G^2], \tag{3.2}$$

and

$$R^{\text{inactive}}_{tot} = [R] + [LR] + [RG^1] + [LRG^1] + [RG^2] + [LRG^2]. \tag{3.3}$$

Upon ligand addition, there are, therefore, fewer receptors available to activate pathway 2, giving a decrease in $[\alpha^2_{GTP}]$, and the inverse agonist effect of the "antagonist". For $[L] = 10^{-7}$M, we also see the undershoot α_{GTP} response previously reported for inverse agonists [7]. We note that a true neutral antagonist effect with constant $[\alpha^2_{GTP}]$ would be seen if we considered pathway 2 as an "isolated pathway" (see [27]) by setting $k^1_{act+} = 0$.

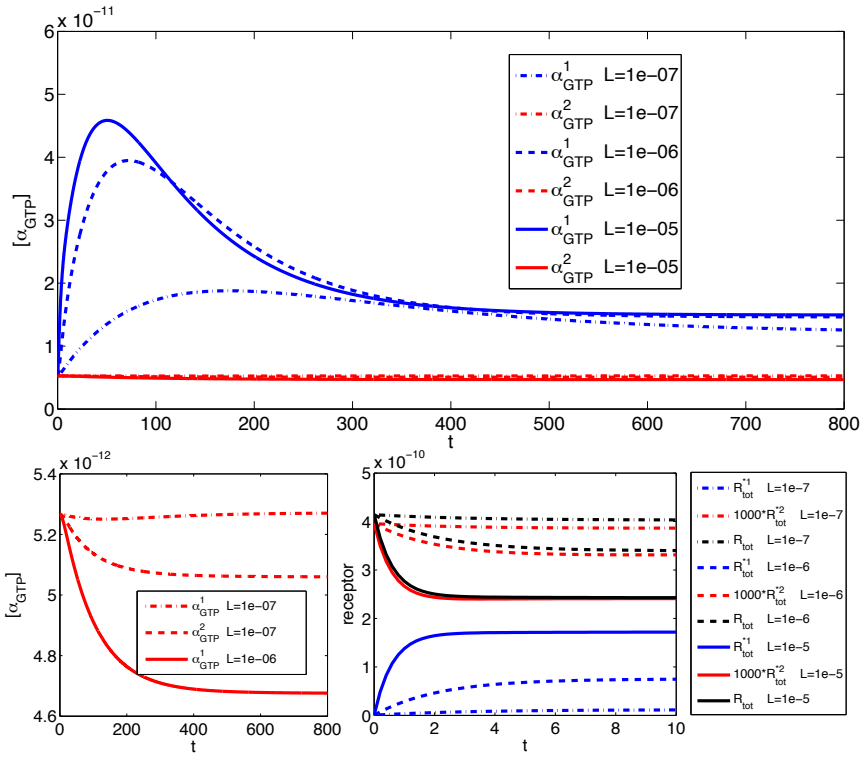

Figure 3.2: The α^{θ}_{GTP} response (M) against time (in seconds) for two pathways with $\zeta^1_+ = 1000$ and $\zeta^2_+ = 1$ after the addition of $[L] = 10^{-7}$, 10^{-6}, 10^{-5}M so that the ligand is an agonist for pathway 1 and an antagonist for pathway 2. Receptor concentrations are given in the bottom right panel. Here, $\zeta^1_+ = 1$.

3.1.3 Ligand is agonist for one pathway and inverse agonist for the other

Having seen apparent inverse agonist activity in the biased system for a ligand which would neutrally antagonise an isolated pathway, we now turn attention to a ligand which is a true inverse agonist for one pathway in the biased system, and an agonist for the other. In Figure 3.3, we show α_{GTP} time courses for this scenario, for a ligand which is an (equilibrium) agonist for pathway 1 ($\zeta^1_+ = 100$, $\zeta^1_- = 1$) and an (equilibrium) inverse agonist for pathway 2 ($\zeta^2_+ = 0.01$, $\zeta^2_- = 1$), over a range of

ligand concentrations. These simulations are for a system with increased R^{*2} constitutive activity, to represent conditions under which inverse agonism may be detectable. We note the peak-plateau α^1_{GTP} dynamics, and drop-off in α^2_{GTP} level. Further, we observe "undershoot" dynamics in the inversely agonised pathway, which may be seen in a single-active state system [7]. An interesting feature here is that while increasing ligand concentration decreases α^1_{GTP} peak time as before, this is accompanied by an increase in α^2_{GTP} peak time.

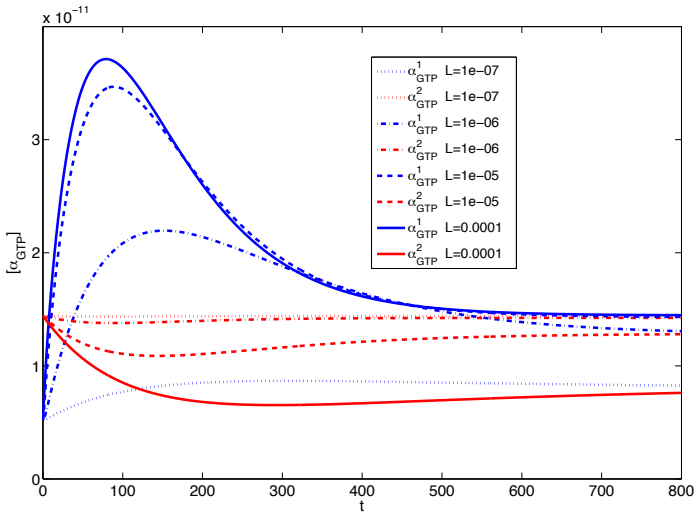

Figure 3.3: Graph showing the α^{θ}_{GTP} response (M) against time (s) after the addition of a range of ligand concentrations, where the ligand is an agonist for pathway 1 and an inverse agonist for pathway 2. Here, $\zeta^1_+ = 100$, $\zeta^2_+ = 0.01$, $k^2_{act-} = 10$.

3.1.4 Time course surfaces

In order to summarise the effect that efficacy parameter ζ has on a system, in Figure 3.4 we show summary time course surfaces for $[L] = 10^{-5}$M, where we vary ζ^1_+ over a spectrum of efficacy ranging from strong inverse agonist to strong agonist, while keeping all other parameters fixed. We clearly see that the stronger L is an agonist for pathway 1, the lesser its effect on pathway 2. When L is an agonist for both pathways, the peak-plateau dynamic response is clear for both α^1_{GTP} and α^2_{GTP}, but increasing agonist strength for pathway 1, the pathway 2 response drops off. Similarly, for a pathway 2 antagonist, the α^2_{GTP} dynamic response varies from apparent antagonism to inverse agonism with increasing ζ^1_+. Also, for a pathway 2 inverse agonist, the magnitude of α^2_{GTP} inverse agonism increases with ζ^1_+.

3.1.5 Observed agonist effect is system-dependent - constitutive activity and inter-conversion

A feature of the equilibrium three-state model in [27] is that a ligand's effect on a pathway can change qualitatively from agonist to inverse agonist, depending on the system-specific level of constitutive activity in that pathway. This so-called "inter-conversion" of ligand effect is demonstrated at steady-state in [27], with respect to active receptor states. In Figure 3.5, we show the effects of increasing the constitutive activity in pathway 2 by decreasing k^2_{act-}. With low constitutive activity ($k^2_{act-} = 100$), the time courses for $\alpha^{1,2}_{GTP}$ are indistinguishable. As pathway 2 constitutive activity is increased, it is clear that pathway 2 basal α_{GTP} increases at the expense of pathway 1 basal α_{GTP}, similarly to the active receptor trend in [27, 37]. The agonist effect on α^2_{GTP} becomes less pronounced with decreased

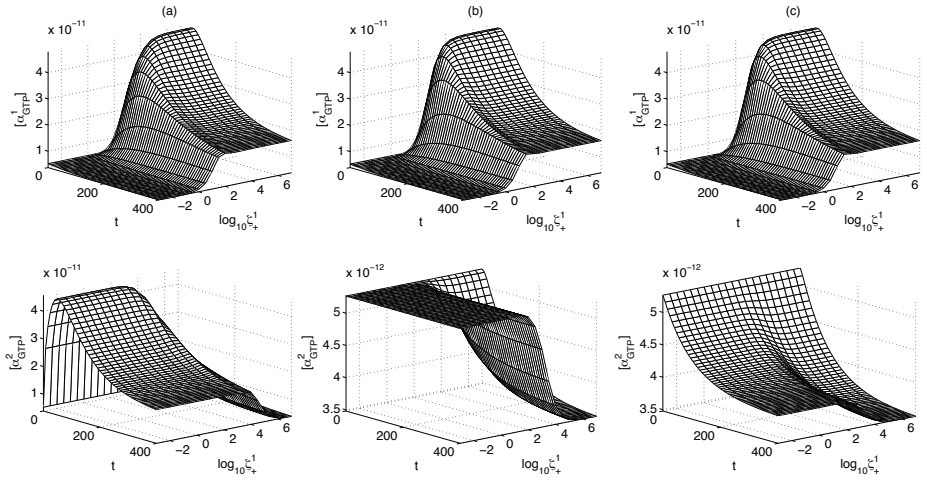

Figure 3.4: Time course surfaces for α^{θ}_{GTP} response (M) dynamically changing for system with varying agonist efficacy parameter ζ^1_+, acting under a ligand concentration of $10^{-5}M$. Column (a): $\zeta^2_+ = 1000$; column (b): $\zeta^2_+ = 1$; column (c): $\zeta^2_+ = 0.001$.

k^2_{act-}, as the G protein response is largely effected via the basal activity, but the ligand remains a pathway 2 agonist. In contrast, with high activation of pathway 2 ($k^2_{act-} = 1$), the long-time α^1_{GTP} response decreases with "agonist" concentration, so that the ligand is now having an apparent inverse agonist effect, despite its isolated pathway classification as an agonist. It is also worth noting that for ($k^2_{act-} = 10$), we observe non-monotonicity in the peak and plateau α^1_{GTP} as functions of $[L]$. Thus non-monotonic concentration-response curves may result from multi-active state receptors with varying constitutive activity levels.

3.1.6 Observed agonist effect may be time-dependent: G protein cycle and dynamic inter-conversion

With our new model, we are able to examine the α^{θ}_{GTP} dynamics under variation of constitutive receptor activation. In the final plot of Figure 3.5, we see the phenomenon of *dynamic inter-conversion* between agonist and inverse agonist action. The ligand is an agonist for both pathways under equilibrium classification, but after initially displaying a typical agonist response, α^1_{GTP} eventually drops below basal levels in an apparent inverse agonist response. The dynamic peak response to agonism occurs as in previous simulations [48]. The below basal long-time level is a result of G protein cycle dynamics on active receptor equilibration. As α^1_{GTP} is inactivated and G^1 reassociates, any new free receptors resulting from LRG complex dissociation are pulled towards a pathway 2 dominant equilibrium, and the receptor pool for G^1 activation decreases below basal level.

3.2 Concentration-response relationships

3.2.1 Peak and plateau responses with varying ligand activation efficacy and constitutive receptor activity

The ligand concentration-dependent features which summarise the α_{GTP} equilibrium and dynamic behaviour may be summarised using conventional concentration-response curves. In Figure 3.6, we show concentration response curves for both pathways, where the measured responses are the peak and plateau α_{GTP} levels. The non-monotonicity first noted in subsection 3.1.5 is clearly a possibility. For a ligand which agonises both pathways, with high constitutive activity in one pathway, the plateau response in the other pathway is non-monotonic. The peak concentration-response curve is yet more

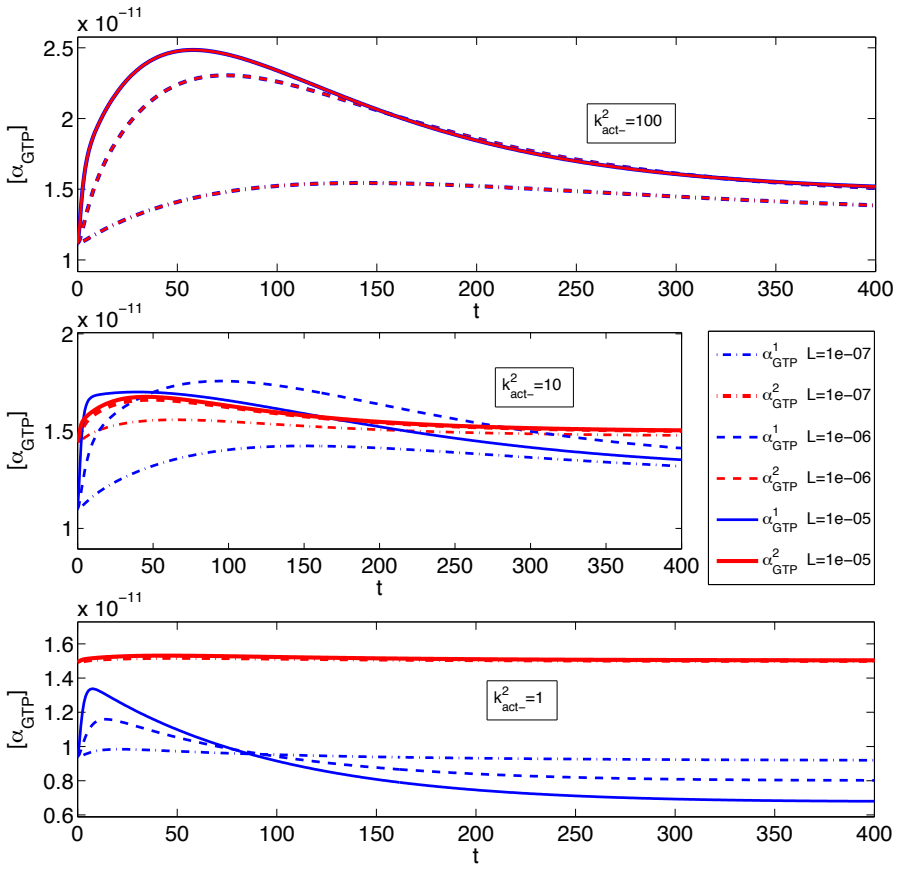

Figure 3.5: Time courses for α^{θ}_{GTP} response (M) dynamically changing for systems with differing constitutive receptor activation level in pathway 2, varying k^2_{act-}. Here, $\zeta^1_+ = \zeta^2_+ = 100$, $k^1_{act-} = 100$, $k^2_{act-} = 100$.

complex; it is also non-monotonic, with a biphasic structure. We remark that biased agonism together with constitutive activity in our new model for α_{GTP} response is a mechanism by which non-monotonic concentration-response relationships can occur. Such behaviour cannot be observed for three-state models [27, 37] where the "readout" is a particular active receptor fraction.

Further demonstration of the dynamic and concentration-dependent features of the system is given in Figure 3.7, where we clearly see decreasing peak timing for both pathways where the ligand is an agonist for both, but an increasing trough time at the pathway for which the ligand is an inverse agonist.

3.2.2 Effect of total receptor number on concentration-response

The total concentration of receptor can considerably affect the appearance of bias in a system [34]. In Figure 3.8, we investigate the effect of differing receptor expression by examining concentration-response curves for two pathways being agonised by a ligand (L_1) with different efficacies ($\zeta^1_+ = 1000$ and $\zeta^2_+ = 100$) at a range of receptor concentrations R_{tot} (from $4.15 \times 10^{-11} M$ to $4.15 \times 10^{-8} M$). As R_{tot} is decreased, we observe both a rightward shift of the curves (increased EC_{50}), together with a drop in the maximal responses, for both the peak and plateau values of α_{GTP}.

Whilst overall efficacy depends partly on the preference of the ligand for an active rather than

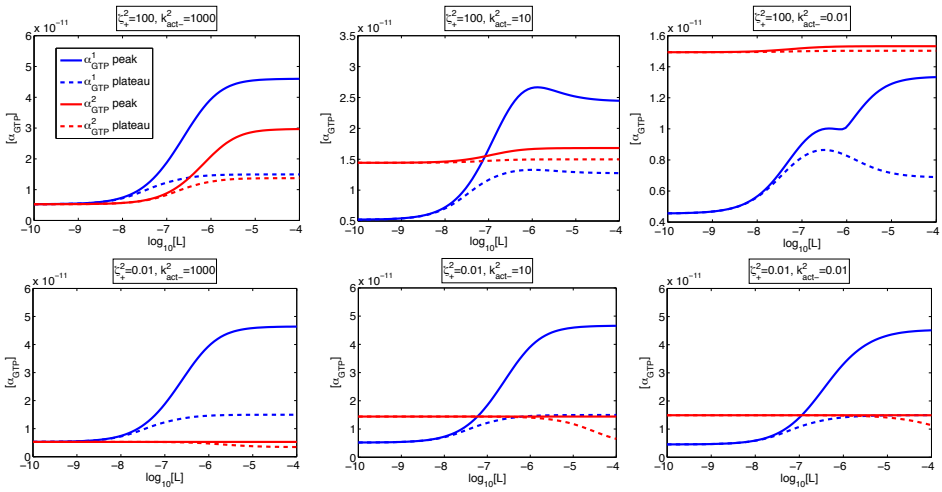

Figure 3.6: Concentration-response curves (α^{θ}_{GTP} concentration against ligand concentration) where the ligand is an agonist for both pathways ($\zeta^1_+ = 1000$, $\zeta^1_- = 1$, $\zeta^2_+ = 100$, $\zeta^2_- = 1$, top row) and agonist for pathway 1 but an inverse agonist for pathway 2 ($\zeta^1_+ = 1000$, $\zeta^1_- = 1$, $\zeta^2_+ = 0.01$, $\zeta^2_- = 1$, bottom row). Constitutive activity for pathway 2 is low ($k^2_{act-} = 1000$, left column), medium ($k^2_{act-} = 10$, middle column), and high ($k^2_{act-} = 1$, left column). Here, $\zeta^2_+ = 100$.

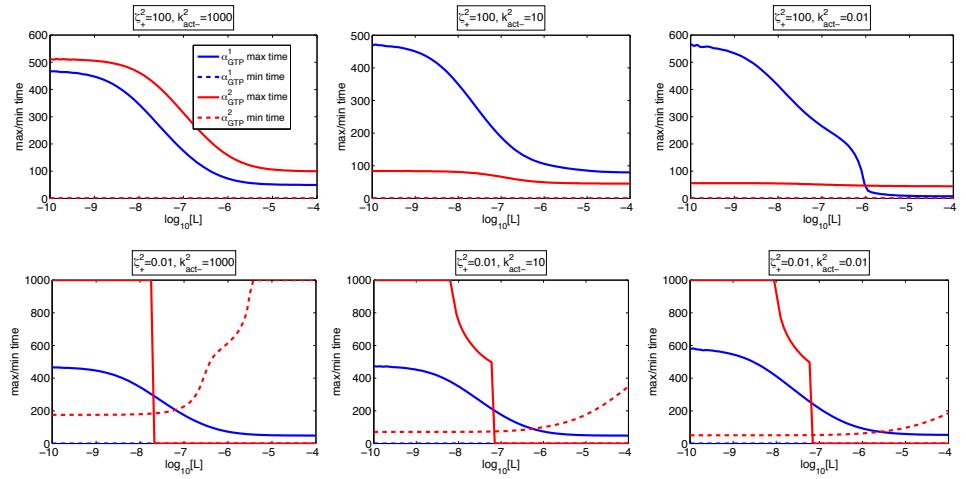

Figure 3.7: Concentration-response curves (α^{θ}_{GTP} maximum and minimum timing against ligand concentration) where the ligand is an agonist for both pathways ($\zeta^1_+ = 1000$, $\zeta^1_- = 1$, $\zeta^2_+ = 100$, $\zeta^2_- = 1$, top row) and agonist for pathway 1 but an inverse agonist for pathway 2 ($\zeta^1_+ = 1000$, $\zeta^1_- = 1$, $\zeta^2_+ = 0.01$, $\zeta^2_- = 1$, bottom row). Constitutive activity for pathway 2 is low ($k^2_{act-} = 1000$, left column), medium ($k^2_{act-} = 10$, middle column), and high ($k^2_{act-} = 1$, left column). Here, $\zeta^2_+ = 100$.

inactive receptor (controlled through variation of the ζ parameters), it is important to note that it can also depend on the preference of a ligand-bound receptor for each of the G proteins (mediated by the ν parameters). In the case of a system in which the ligand-dependent parameters affecting efficacy are chosen so as to counteract each other ($\zeta^1_+ = 2000$, $\zeta^2_+ = 100$, $\nu^1_+ = 1$, $\nu^2_+ = 25$), we see that (Figure 3.9) not only the magnitude of the preference for one pathway, but even the direction

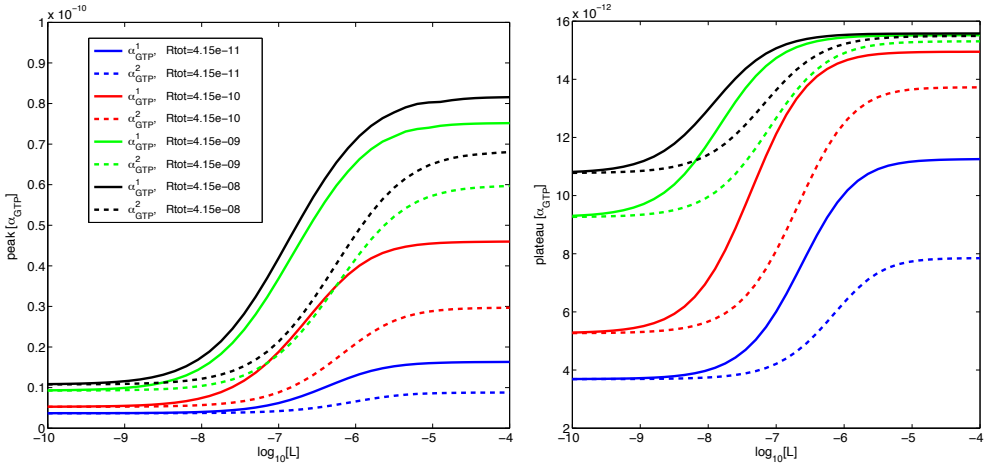

Figure 3.8: Concentration-response curves for peak and plateau α_{GTP} for two pathways being agonised by L_1, a ligand with different efficacies for the two pathways ($\zeta_+^1 = 1000$ and $\zeta_+^2 = 100$), under varying receptor concentrations.

(in terms of which pathway experiences the higher response) can be affected by a changing receptor concentration. In this case, peak α_{GTP} exhibits a change in direction, while plateau level does not.

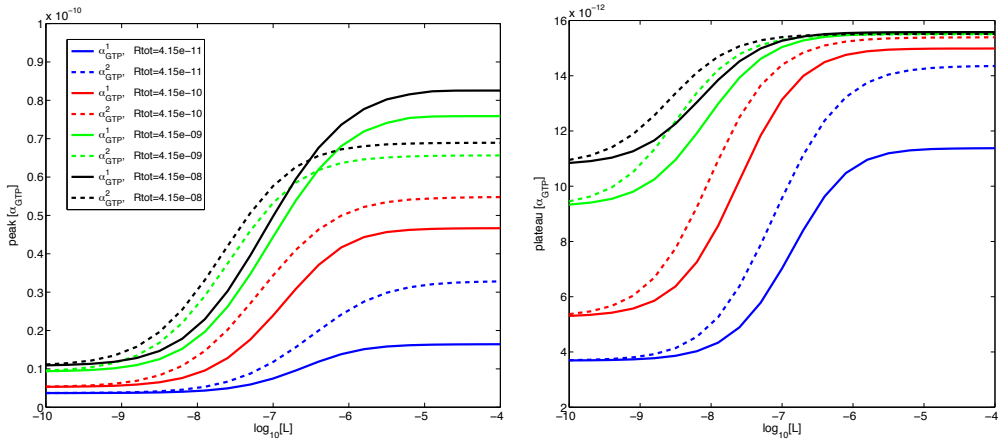

Figure 3.9: Concentration-response curves for two pathways being agonised by L_2, a ligand with parameters $\zeta_+^1 = 2000$, $\zeta_+^2 = 100$, $\nu_+^1 = 1$, $\nu_+^2 = 25$, vary under changing receptor concentrations.

3.3 Response surfaces

Parameter sensitivity and concentration-response relations may be conveniently summarised using response surfaces which show the effects of varying two system parameters [6, 48, 8]. We now use this method to show the sensitivity of simulated response ($\alpha_{GTP}^{1,2}$ peak and plateau) to variations in system parameters, in particular the microaffinity coefficients ζ, ν and μ.

3.3.1 Effect of ζ - the possibility of biphasic relationships

In Figure 3.10, we see the effect of varying ζ^1_+ and ζ^2_+ for a fixed ligand concentration. The reciprocal effects on the two G protein pathways mediated by the competing receptor states are clear. As ζ^1_+ is increased, both peak and plateau α^1_{GTP} increase, accompanied by decreases in α^2_{GTP}. Furthermore, it is clear that biphasic relationships are possible.

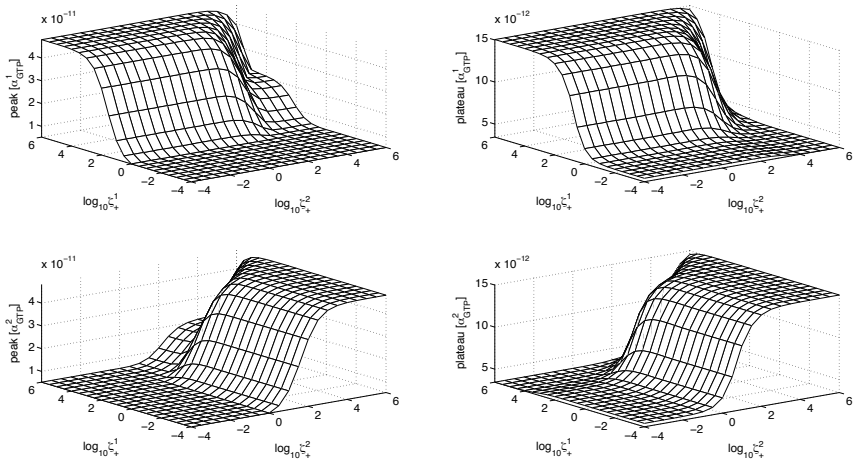

Figure 3.10: Response surfaces for varying ligand efficacy, for fixed ligand concentration $[L] = 10^{-5}$M. Parameters ζ^1_+ and ζ^2_+ are varied through the spectrum of efficacy for each receptor active state.

3.3.2 Effect of G protein non-specificity and receptor "cross-states"

Thus far in our computations, we have focussed on systems in which the two G proteins are each specific to a particular active receptor conformation. By setting $\mu^{1,1} = 1, \mu^{2,2} = 1, \mu^{1,2} = 0, \mu^{2,1} = 0$, we have simulated systems whereby G protein 1 can neither activate a pre-coupled receptor towards R^{*2}, nor bind to R^{*2}, and vice-versa. It is a novel aspect that our model allows receptor "cross-states", where there is not exclusive specificity of each G protein for one particular active receptor state. We see in Figure 3.11 the effects of non-exclusive specificity and accessibility of these cross states on the α_{GTP} responses. The general trend is that with all cross states signalling (with $k^{j,\theta}_{GTP} = 1, \forall\theta$), increasing μ_{21} gives a decreased peak α^1_{GTP} and slight increase in plateau α^1_{GTP}.

Our model allows for variation in specificity of not only the G proteins for each receptor conformation, but also the propensity for G protein cycling with respect to these active states, controlled by $k^{j,\theta}_{GTP+}$. With cross states which do not signal (with $k^{j,\theta}_{GTP} = 0$ for $j \neq \theta$), increasing μ_{12} now gives a decreased peak and plateau α^2_{GTP} as the general trend, with non-monotonicity, which may be explained by considering the effects on basal conditions. Further explanation and discussion of these effects is given in Appendix B.

3.3.3 Effect of ν, the preference of ligand for specific G protein-coupled receptor

The microaffinity constant ν^θ controls the preference of ligand for RG^θ over R. The effect of varying ν^θ is as expected, in that increasing ν^θ increases both peak and plateau α^θ_{GTP} (see Figure C.1 in Appendix C).

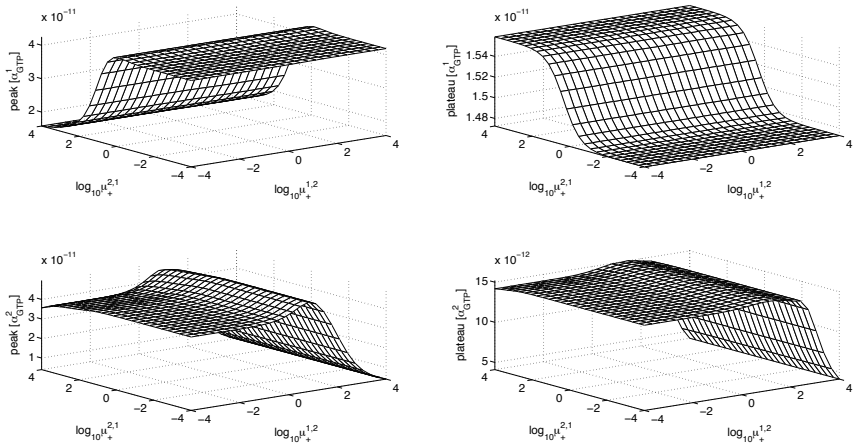

Figure 3.11: Response surfaces for varying ligand accessibility of receptor cross states for fixed ligand concentration $[L] = 10^{-5}$M.

4 Detecting and quantifying bias

A *balanced agonist* is one which signals with equal efficacy to available downstream pathways, whereas a *biased agonist* has different efficacies for signalling to different pathways [34]. There is a need to detect and quantify the level of bias towards one pathway over another, considering that physiologically and clinically, certain pathways represent therapeutic targets while others are "side effect" pathways [14]. Here, we employ current quantification methods for the level of ligand bias within our two-pathway system.

4.1 Bias factors and the Operational Model

The operational model of agonism [5] provides a standardised and widely adopted method for estimating ligand affinity and "operational efficacy" parameters from functional response data in the form of hyperbolic concentration-response curves. Briefly, for a single downstream readout E resulting from ligand concentration $[A]$ at a receptor,

$$E([A]) = E_{max}\frac{\tau[A]}{K_D + (\tau+1)[A]}, \tag{4.1}$$

where E_{max} is the maximum response of the system, K_D is the ligand's equilibrium dissociation constant, and τ is a measure of ligand efficacy, in particular measuring the propensity of the ligand *and the system* to yield a response. A modified form of the model is sometimes used to account for nonzero basal responses [39], namely

$$E([A]) = \text{basal} + (E_{max} - \text{basal})\frac{\tau[A]}{K_D + (\tau+1)[A]}. \tag{4.2}$$

Further generalisation of this model is possible by introducing a Hill coefficient to the signal transduction sub-model [5, 39]. Recently, the operational model has been used to quantify the level of bias in systems exhibiting multi-dimensional efficacy (ie. the activation of multiple pathways at a single receptor). Bias is typically defined with respect to a reference ligand, and "bias factors" are computed using fitted values of τ [34] or both τ and K_D [20, 17, 14]. Here, we follow the transduction coefficients method [20] by defining a transduction coefficient for a ligand A at a given pathway as

$$\mathbb{T}_A = \log_{10}\left(\frac{\tau}{K_D}\right)_{\text{lig}A}. \tag{4.3}$$

The difference in transduction coefficients for two ligands A and B is usually written in $\Delta\log$ notation, with

$$\begin{aligned}\Delta\log_{10}\left(\frac{\tau}{K_D}\right)_{\text{lig}A-\text{lig}B} &= \Delta\mathbb{T}_{A-B} \;=\; \mathbb{T}_A-\mathbb{T}_B \\ &= \log_{10}\left(\frac{\tau}{K_D}\right)_{\text{lig}A}-\log_{10}\left(\frac{\tau}{K_D}\right)_{\text{lig}B} \;=\; \log_{10}\left(\frac{\tau}{K_D}\Big|_A\;\frac{K_D}{\tau}\Big|_B\right). \end{aligned} \tag{4.4}$$

The *relative bias factor* for a ligand A, relative to ligand B, for pathway 1 over pathway 2, is usually defined by first calculating its logarithm, written in $\Delta\Delta\log$ notation as

$$\begin{aligned}\log_{10}\text{bias}^{1-2}_{A-B} = \Delta\Delta\log_{10}\left(\frac{\tau}{K_D}\right)^{\text{path1}-\text{path2}}_{\text{lig}A-\text{lig}B} &= \Delta\mathbb{T}^{\text{path1}}_{A-B}-\Delta\mathbb{T}^{\text{path2}}_{A-B} \\ = \log_{10}\left(\frac{\tau}{K_D}\Big|^{\text{path1}}_A\;\frac{K_D}{\tau}\Big|^{\text{path1}}_B\;\frac{K_D}{\tau}\Big|^{\text{path2}}_A\;\frac{\tau}{K_D}\Big|^{\text{path2}}_B\right), \end{aligned} \tag{4.5}$$

so that

$$\text{bias}^{1-2}_{A-B} = \frac{\tau}{K_D}\Big|^{\text{path1}}_A\;\frac{K_D}{\tau}\Big|^{\text{path1}}_B\;\frac{K_D}{\tau}\Big|^{\text{path2}}_A\;\frac{\tau}{K_D}\Big|^{\text{path2}}_B. \tag{4.6}$$

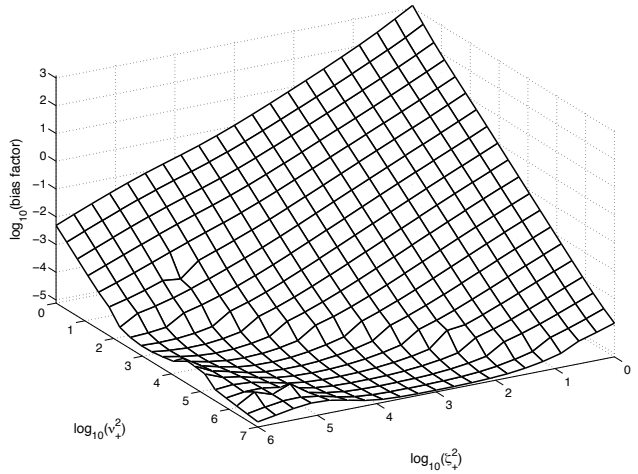

Figure 4.1: Bias factor surface for fixed ligand 1 parameters, varying ligand 2 parameters ζ_2 and ν_2. Bias factor bias^{1-2}_A represents the bias for pathway 1 over pathway 2 signalling. Here, $k_{L+}=10^5$, $k^1_{act+}=k^2_{act+}=0.05$, and $k^1_{hyd-}=k^2_{hyd-}=10^{-8}$.

4.2 Bias factor's dependence on ζ and ν

The bias factor, $\text{bias}^{1-2}_A=\frac{\tau}{K_D}\Big|^{\text{path1}}_A\;\frac{K_D}{\tau}\Big|^{\text{path2}}_A$, is a standard measure of a ligand's bias for effecting a response in pathway 1 over pathway 2. While this is defined in terms of the parameters τ and K_D which are fitted to the semi-mechanistic operational model, rather than explicitly in terms of the parameters in our new α_{GTP} model, we expect correlations between the bias factor and ligand-specific parameters in our model. In particular, when α_{GTP} is measured at equilibrium and taken as the response E, we expect, on the whole, bias factor should increase with decreased ζ_2 and ν_2, which control a ligand's effect on R^{*2} activation and G^2 coupling to the receptor. In Figure 4.1, we show the bias factor bias^{1-2}_A for a bank of ligands generated by varying ζ^2_+ and ν^2_+, while keeping all other

parameters fixed. The correlation is clear. The overall trend is the expected increase in bias_A^{1-2} with decreasing ζ_+^2 and ν_+^2, while the relationship is approximately a power law over much of the parameter space shown.

4.3 Kinetic context and dynamic bias factors

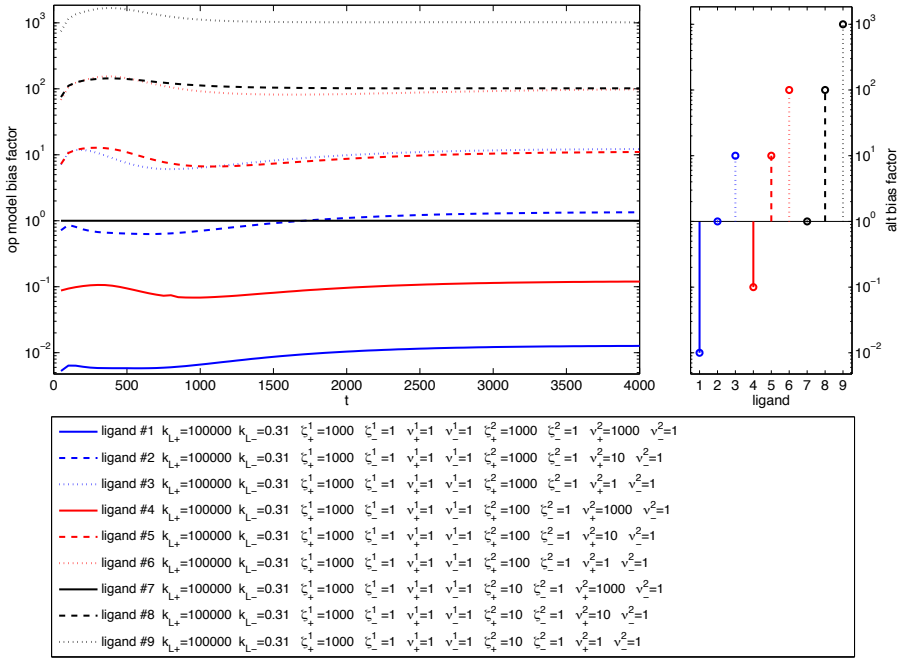

Figure 4.2: Bias factor dynamics for a bank of nine ligands. The operational model bias factor bias_A^{1-2} represents the bias for pathway 1 over pathway 2 signalling is shown for each time point, and the alternative bias factor is shown in the right hand panel. Reference ligand is ligand 7, a strong agonist for pathway 1. Here, $k_{L+} = 10^5$, $k_{act+}^1 = k_{act+}^2 = 0.05$, $k_{hyd-}^1 = k_{hyd-}^2 = 10^{-8}$ and $k_{RA-}^1 = k_{RA-}^2 = 1.3 \times 10^{-4}$.

It has recently been demonstrated that binding, activation and signalling dynamics may significantly affect bias measurements, and hence the classification of biased ligands, and that "kinetic context" is an important consideration in the quantification of bias [15]. Although bias calculations based on the operational model implicitly assume equilibrium conditions, this method is shown to be an effective and simple heuristic approach to investigating and quantifying dynamic bias in [15]. In Figure 4.2, we show bias factor time courses for a bank of ligands, generated by constructing a concentration-response curve for each ligand at each time point, then fitting each of these curves to the operational model (using optimisation routines in MATLAB). Here, the bias factor is calculated with respect to the reference ligand (ligand 7), and we see that the long-time bias factor $\text{bias}_{A-ref}^{1-2}$ indeed increases with decreased ζ_+^2 and/or ν_+^2. We also plot, in the right hand panel, an alternative bias factor based on our model parameters, specifically

$$\text{alt-bias}_{A-ref}^{1-2} = \frac{\frac{k_{L+,A}}{k_{L-,A}}\left(\frac{\nu_A^1\zeta_A^1}{\nu_A^2\zeta_A^2}\right)}{\frac{k_{L+,ref}}{k_{L-,ref}}\left(\frac{\nu_{ref}^1\zeta_{ref}^1}{\nu_{ref}^2\zeta_{ref}^2}\right)}, \tag{4.7}$$

which should also indicate ligand bias. We note the excellent agreement between the dynamic bias factors from operational model fitting and our alternative bias factor. Dynamically, there is the

possibility of a change of order of bias factors, and this phenomenon is even more marked for the bank of ligands shown in Figure 4.3. Clearly, the order of bias factors may change dynamically, so the classification of ligands requires consideration of kinetic context, as described in [15].

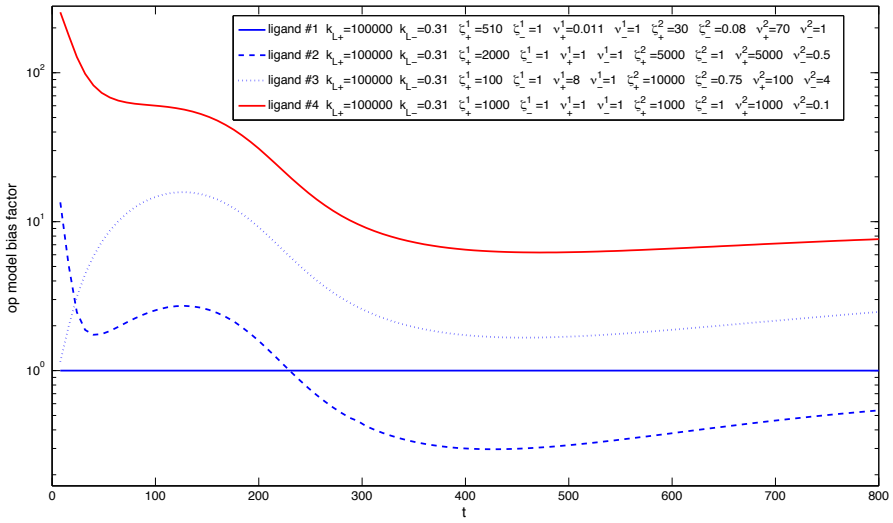

Figure 4.3: Bias factor dynamics for a bank of four ligands. Bias factor bias_A^{1-2} represents the bias for pathway 1 over pathway 2 signalling. Here, $k_{L+} = 10^5$, $k^1_{act+} = k^2_{act+} = 0.01$, $k^1_{hyd-} = k^2_{hyd-} = 10^{-8}$ and $k^1_{RA-} = k^2_{RA-} = 1.3 \times 10^{-4}$.

5 Fitting to a model of downstream functional antagonism via biased signalling

Our model outputs thus far have been the α_{GTP} levels of the two G proteins in the system, which represent responses downstream of ligand binding, and may correspond to a downstream functional experimental readout. We now consider whether our model can be used to explain, and fit to, experimental end point data in a system where biased agonism is suspected.

5.1 Experimental method

The adenosine A_1 receptor (A_1R) is well known for mediating the protective effects of adenosine in the heart [12, 31]. How these effects are brought about is not fully understood, as the A_1R is able to couple to multiple signalling pathways [3]. This makes interpretation of physiological effects difficult to attribute to an individual, signalling pathway. While the A_1R is a predominantly Gi-coupled receptor, which inhibits the accumulation of the second messenger, cyclic adenosine monophosphate (cAMP), it has been observed that at higher agonist concentrations, the levels of cAMP begin to rise again producing a non-monotonic response profile. This accumulation of cAMP arises through the ability of the A_1R to switch its G protein coupling and now promote activation of Gs [11, 2]. The extent to which an individual agonist either inhibits or stimulates cAMP production at the A_1R may vary.

To obtain data to enable fitting of our models, experiments were performed using Chinese hamster ovary-K1 (CHO-K1) cells stably expressing the A_1 receptor, treated with a range of concentrations of a single agonist each time, and the effect on intracellular concentration of cAMP determined (see Appendix D and [45, 23, 46] for details). In particular, the experiments were carried out for three different agonists individually, namely 5'(N-ethyl carboxamido) adenosine (NECA), and two test compounds which bind the A_1R, denoted here as Compound 6 (Cmpd6) and Compound 20 (Cmpd20) ([23]). The

measured response was the accumulated cAMP concentration in the presence of the phosphodiesterase (PDE) inhibitor rolipram, which blocks cAMP degradation.

For each concentration of each agonist, two experiments were performed. Firstly, intact (wild-type) cells were used, which allow for coupling and activation of both G_i and G_s proteins to the A_1R, thereby allowing activation of both the G_i pathway which inhibits cAMP production via an increased $\alpha_{GTP,i}$ signal, and the G_s pathway which stimulates cAMP production via an increased $\alpha_{GTP,s}$ signal. For these cells, the recorded response is the percentage inhibition of cAMP when compared with cells treated with forskolin (which promotes maximal stimulation of cAMP production [4]). The second experimental condition is for cells that have been treated with pertussis toxin (PTX), which both inhibits binding of G_i to its receptor and blocks its signal transduction, thereby locking α_i in its inactive, GDP-bound state [30]. For these cells, the recorded response is the percentage stimulation of cAMP when compared with forskolin-stimulated cells. Time courses of cAMP were not recorded, and the signalling readout in each case is taken at the endpoint of the experiment ($t = 1800$s).

Further details of the experiments are given in Appendix D.

5.2 Experimental results

In Figure 5.1, we show the experimental cAMP endpoint signals in response to three ligands individually in turn (NECA, Cmpd6 and Cmpd20) for the two different experimental conditions. For wild-type cells the log concentration response curves *for the inhibition of cAMP* show non-monotonic behaviour with a downturn at higher concentrations, whereas the log concentration response curves *for the production of cAMP* in PTX-treated cells show, with the exception of one data point for the NECA experiment, monotonic behaviour. By blocking the inhibitory pathway, we largely see "standard" monotonic behaviour, which suggests that the non-monotonic wild-type response results from crosstalk between the inhibitory and stimulatory pathways. Since in each case a single ligand has been introduced, we hypothesise that the target receptor may exhibit biased agonist effects, via two active conformations, one of which is specific to the G_i protein and the other to the G_s protein.

5.3 Modelling considerations

Since the data shown in Figure 5.1 are hypothesised to result from biased agonism with competition between two activated G protein pathways, we now seek to fit our model to the data, in order to add support to this hypothesis and understand the possible underlying mechanisms.

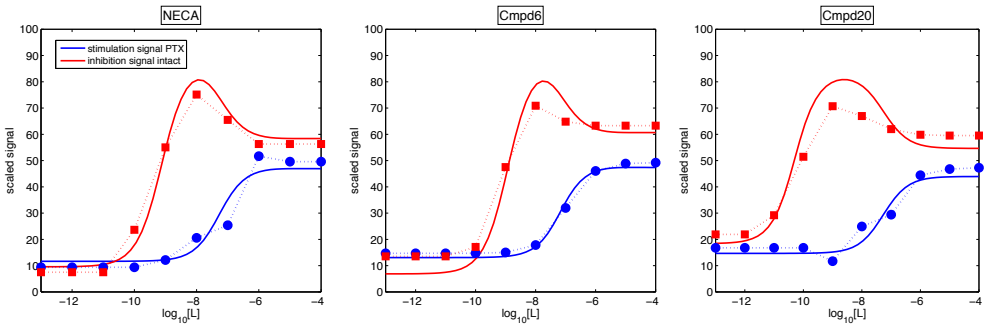

Figure 5.1: Using the model of biased agonism with functional antagonism at level of α_{GTP} to fit cAMP readouts ($\text{signal}_{\text{stim}}(1800)$ and $\text{signal}_{\text{inhib}}(1800)$) for three different ligands (NECA, Cmpd6 and Cmpd20). Experimental data points are given (red squares with dashed lines for percentage cAMP inhibition for wild-type cells, blue circles with dashed lines for percentage cAMP production in PTX-treated cells, each compared with forskolin-treated cells which give maximal cAMP response) for end point readouts over a range of ligand concentrations. Solid curves are the fitted log concentration response curves for our model.

Within our modelling framework, we let G^1 and G^2 represent the G_s and G_i proteins respectively. We simulate the PTX effect of blocking G_i binding and activation by setting $k^2_{G+} = k^{22}_{GTP+} = k^2_{GRA-} =$

0. Since cAMP is produced in response to G_s activation [4, 25], for a simple, minimal model of cAMP levels in PTX-treated cells, with blocked cAMP degradation, we take the cAMP production rate proportional to $\alpha_{GTP,s}$ levels, so that $\frac{d[cAMP]}{dt} \propto \alpha_{GTP,s}$, and hence the stimulation signal is given by

$$\text{signal}_{\text{stim}}(t) = \int_0^t C_s[\alpha_{GTP,s}](t)\, dt \;=\; \int_0^t C_s[\alpha^1_{GTP}(t)]\, dt, \tag{5.1}$$

where C_s is a constant.

For the wild-type cells in which both stimulatory and inhibitory cAMP pathways are intact, we require a model for crosstalk between G_i and G_s pathways. Here we use a simple "functional antagonism" model for the competing effects of these pathways. Functional antagonism refers to the response of a cell in which signalling via one pathway is antagonised by signalling via another pathway, and simple theoretical models have been presented which are based on differences between pathway signals [28, 42, 26]. Here, we use such a model where $\alpha_{GTP,s}$ and $\alpha_{GTP,i}$ are stimuli to the cAMP stimulatory and inhibitory pathways respectively, and the cAMP production rate is simply a scaled difference between the two α_{GTP} levels. The inhibition signal is then given by

$$\text{signal}_{\text{inhib}}(t) = \int_0^t C_i[\alpha_{GTP,i}](t) - C_s[\alpha_{GTP,s}](t)\, dt \;=\; \int_0^t C_i[\alpha^2_{GTP}](t) - C_s[\alpha^1_{GTP}](t)\, dt, \tag{5.2}$$

where C_i is a constant, and C_s is the constant as in (5.1). Since functionally opposite signalling can result in non-monotonic concentration-response curves with downturns ([42, 33]) such as those seen in the cAMP inhibition curves in Figure 5.1, our biased agonism model augmented by the simple functional readout models (5.1) and (5.2) may be able to recapitulate the experimental data, at least qualitatively. We proceed to employ parameter estimation methods to pursue a fit to the concentration-response curves for each ligand.

5.4 Parameter estimation

We fit the experimental data to the model given by (2.3) with $N^* = N^G = 2$, together with (5.1) and (5.2), where simulations are first run to a time of 10^8 seconds with $[L] = 0$, to pre-equilibrate the system before ligand addition. For each ligand, the experimental data for the intact and PTX cells were fitted simultaneously, using optimisation algorithms to minimise the squared error between simulation and data points. The methods used were the trust region algorithm implemented in PottersWheel [29], followed by a genetic algorithm routine implemented in MATLAB [1]. A subset of the kinetic parameters were varied; for each reversible reaction, we fixed one rate constant (typically for the reverse reaction), and allowed one rate constant to float. Further, we consider systems where the active receptor cross states are inaccessible, such that $\mu^{j,\theta} = k^{j,\theta}_{GTP+} = 0$ are fixed for $j \neq \theta$, since these have been shown to largely have little effect. Fitted parameters for the NECA data set were used as initial parameter guesses for Cmpd6 and Cmpd20, to speed up the overall fitting for Cthese compounds. For each ligand, the model can clearly fit the data very well qualitatively. In Figure 5.1,

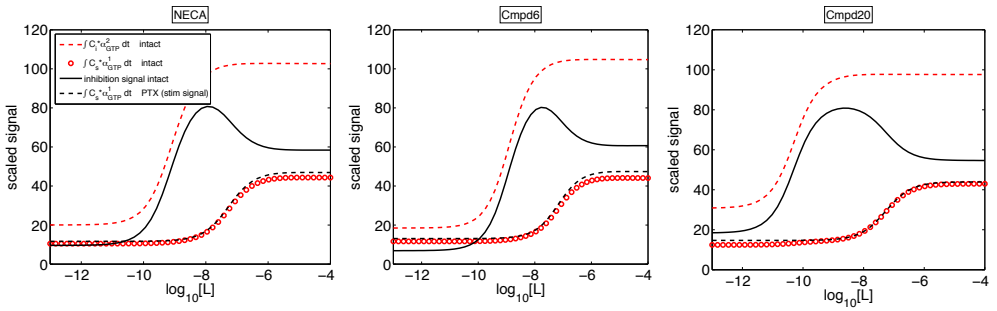

Figure 5.2: Log concentration response curves for $\int \alpha^1_{GTP}\, dt$ and $\int \alpha^2_{GTP}\, dt$ levels using fitted parameter values.

we see that the model fit for the stimulation curve is monotonic, with maximal and basal signals, and

EC_{50} values in good agreement with the data. Further, the fitted inhibition curve in each case is non-monotonic, with the concentration which gives the peak value in good agreement with the data. The basal, peak and plateau levels are in good agreement with the data, and the model recapitulates the differences in peak "spread" between the three ligands. Values for the fitted parameters are given in Table E.1.

In Figure 5.2, simulations from the fitted parameter sets for each ligand show the $\int \alpha_{GTP}$ contributions to the overall measured signal for both cell types. In each case, the stimulatory responses for the intact cells and the PTX cells are almost indistinguishable, and while the individual $\int \alpha_{GTP}$ curves are monotonic, the difference between them for the intact cells is not.

Having estimated parameters which fit the experimental data (taken at a single time point $t = 1800$s), we may now simulate the underlying α_{GTP} dynamics up to this time point. In Figure 5.3, we show time courses for $\alpha_{GTP,i}$ and $\alpha_{GTP,s}$ levels, using the NECA-fitted parameters. With the ligand being an agonist for both G protein pathways, the peak-plateau α_{GTP} dynamics are clear, and consistent with the temporal characteristics observed in our earlier numerical simulations. Peak values are monotonic with $[L]$, with α^1_{GTP} peaking later than α^2_{GTP}. We conclude that our model

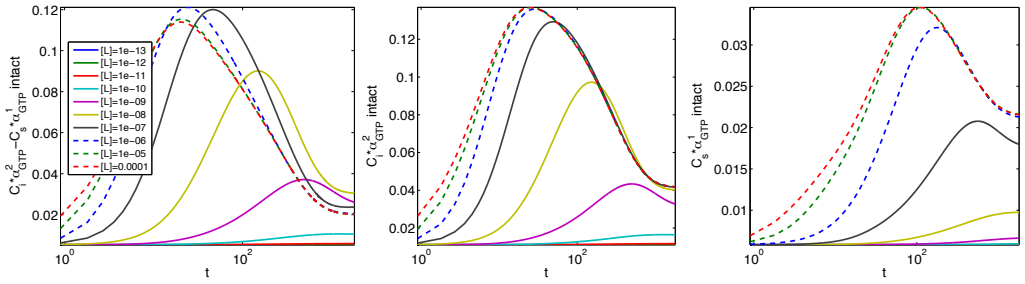

Figure 5.3: Underlying $\alpha_{GTP,i}$ and $\alpha_{GTP,s}$ dynamics for NECA-fitted parameters, for a range of agonist concentrations. Time is on a logarithmic scale to clearly show the peak-plateau time scales.

recapitulates, and fits to, experimental data well in the cases shown, therefore adding support to the biased agonism conjecture for the experiments discussed, and validating our model. Our functional model for cAMP production is very simple, comprising a linear combination of $\alpha_{GTP,i}$ and $\alpha_{GTP,s}$. It is reasonable to expect that a more detailed model of cAMP signalling with more degrees of freedom would result in an even better fit to the data.

6 Discussion

Biased agonism is now a widely accepted phenomenon for signalling via GPCRs [44, 20], and exploiting this is a potential route to developing novel therapeutics [20, 18]. Theoretical (mathematical) models are key tools towards understanding biased signalling, and have previously been presented for equilibrium conditions [27, 38]. These models have enabled a foundation biased agonism theory to be established, largely at the level of receptor activation. For functional readouts downstream of the receptor, further detail has been added at the level of G protein binding [13], and simple empirical models for pathway signalling [36]. In this paper, we have developed a new model for biased agonism which includes the detail of G protein activation via a cubic ternary complex/G protein cycle model, with α_{GTP} as a readout, and serving as an indicator/proxy of pathway activity. This model is general in terms of the number of active receptor conformations and G proteins, and also that it is not specific to any particular pathway; it can thus be used to model biased signalling at any GPCR, and detailed further signalling components can be added downstream of α_{GTP} to model particular pathways as desired. Potentially, our model could provide a foundation for simulating single-ligand multi-pathway dynamics, such as recent experimental work revealing dynamic biased signalling behaviour at the dopamine D_2 receptor [15].

An important advance in the present study is the analysis of signalling dynamics as predicted by our model. The role of kinetic context in the investigation of biased agonism has recently been highlighted [15] and, as such, a model and method for analysing dynamics represents a timely contribution to the literature. A number of dynamic features have been observed here, including the apparent inverse agonist effect of an "antagonist", dynamic inter-conversion of agonist effect, and the time-dependence of bias factor order. Non-monotonic concentration-response relationships for endpoint signals are possible from our model, for both a single α_{GTP} readout within a two-pathway system, and downstream crosstalk between two α_{GTP} signals.

The current standard method for quantifying bias from experimental data uses parameters fitted to the equilibrium operational model of agonism [5, 21]. Calculating bias factors using this empirical model applied to timecourse data shows the dynamic nature of bias [15], and our model and computations have reproduced this phenomenon. We propose that such analysis may provide important new insights into, and quantitative characterisation of, experimental timecourse results. The use of operational model appears to be the current state-of-the-art in bias quantification, but it has a number of limitations: it is empirical rather than mechanistic, it does not consider dynamics, and it does not account for constitutive activity [41]. An alternative model which includes constitutive activity is given in [40], but this equilibrium model has yet to be fully explored with respect to biased signalling. While beyond the scope of our current work, a valuable future investigation will focus on further formulation and definition of dynamic bias factors, including constitutive activity.

We have shown our model to be capable of reproducing endpoint trends in experimental data for cAMP levels in response to ligands at the A_1R receptor, through multi-pathway ($\alpha_{GTP,s}$ and $\alpha_{GTP,i}$) signalling with functionally opposite downstream signals. This endpoint analysis has resulted in parameterisations of the model which then predict the underlying α_{GTP} dynamics, qualitatively consistent with our earlier agonist-induced simulations. This validation of our model allows us to propose its use for further study of downstream signalling, and fitting to time-course data when it becomes available. For example, for any future dynamic cAMP experimental readouts, our simple functional models (5.1)-(5.2) can be used to fit to time-courses, with better fits expected by letting a greater number of parameters float, or using a more detailed cAMP model (eg. [25]). The simulation and fitting in the current work also clearly shows that single-ligand multi-pathway activation at a single receptor provides a mechanism for non-monotonic concentration-response relations either for α_{GTP} itself or for downstream signals, by way functional antagonism. While functional signalling experiments often results in monotonic concentration-response curves, relationships with downturns at high concentrations are not uncommon [9, 49, 33], and the current work provides a plausible mechanistic model for understanding such results in systems where multi-pathway signalling via a single receptor is possible.

The mathematical work here represents a theoretical framework for further study of the potential benefits of developing biased agonists as therapeutics. The multidimensionality of GPCR signalling now constitutes a new paradigm in drug discovery, and the potential benefits of new understanding of multi-pathway signalling lie in the development of "functionally selective" drugs which preserve efficacy in target pathways, while minimising activation of unwanted side-effect pathways at the same receptor [35]. Further mechanistic modelling encompassing G protein binding and activation, downstream signalling, dynamics and complexity of the level we have studied here is acknowledged as a potentially very valuable advance towards such drug discovery goals [44, 41].

Acknowledgements
This study was supported by the BBSRC (to G.L., BB/M00015X/2; to J.M., a Research Experience Placement award) and an MRC Doctoral Training Partnership (to I.W. MR/J003964/1). Predictive mOdelling for hEalthcare through MathS (POEMS) network funding by EPSRC supported LJB's travel to Cambridge.

A Parameter values

In Table A.1, we give a base parameter set for all computations. Any variations from this parameter set are shown in figure titles and captions.

Table A.1: Parameter values for 2 G protein, 2 active receptor state model.

label	meaning	cell or ligand specific	value	units	source
k_{L+}	Ligand binding rate	Ligand	9.40E+04	$M^{-1}s^{-1}$	Bridge et al (2010)
k_{Lm}	Ligand unbinding rate	Ligand	3.10E-01	s^{-1}	”
k^1_{act+}	Receptor activation rate to R^{*1}	Cell	1.00E+00	s^{-1}	”
k^1_{act-}	Receptor deactivation rate from R^{*1}	Cell	1.00E+03	s^{-1}	”
k^2_{act+}	Receptor activation rate to R^{*2}	Cell	1.00E+00	s^{-1}	”
k^2_{act-}	Receptor deactivation rate from R^{*2}	Cell	1.00E+03	s^{-1}	”
k^1_{G+}	G protein 1 binding rate	Cell	1.00E+08	$M^{-1}s^{-1}$	”
k^1_{G-}	G protein 1 unbinding rate	Cell	1.00E-01	s^{-1}	”
k^2_{G+}	G protein 2 binding rate	Cell	1.00E+08	$M^{-1}s^{-1}$	”
k^2_{G-}	G protein 2 unbinding rate	Cell	1.00E-01	s^{-1}	”
k^1_{GRA+}	G protein 1 reassociation rate	Cell	7.00E+05	$M^{-1}s^{-1}$	”
k^1_{GRA-}	G protein 1 dissociation rate	Cell	1.30E-03	s^{-1}	”
k^2_{GRA+}	G protein 2 reassociation rate	Cell	7.00E+05	$M^{-1}s^{-1}$	”
k^2_{GRA-}	G protein 2 dissociation rate	Cell	1.30E-03	s^{-1}	”
k^1_{hyd+}	Hydrolysis rate of $G\alpha^1_{GTP}$	Cell	1.00E-02	s^{-1}	”
k^1_{hyd-}	Exchange rate of GTP for GDP at G^1_α	Cell	1.00E-04	s^{-1}	”
k^2_{hyd+}	Hydrolysis rate of $G\alpha^2_{GTP}$	Cell	1.00E-02	s^{-1}	”
k^2_{hyd-}	Exchange rate of GTP for GDP at G^2_α	Cell	1.00E-04	s^{-1}	”
$k^{1,1}_{GTP+}$	$R^{*1}G^1$ dissociation rate	Cell	1.00E+00	s^{-1}	”
$k^{1,2}_{GTP+}$	$R^{*1}G^2$ dissociation rate	Cell	1.00E+00	s^{-1}	”
$k^{2,1}_{GTP+}$	$R^{*2}G^1$ dissociation rate	Cell	1.00E+00	s^{-1}	”
$k^{2,2}_{GTP+}$	$R^{*2}G^2$ dissociation rate	Cell	1.00E+00	s^{-1}	”
ν^θ_+	Forward cooperativity factor for ligand binding a G^θ bound receptor	Ligand	1.00E+00		”
ν^θ_-	Backward cooperativity factor for ligand binding a G^θ bound receptor	Ligand	1.00E+00		”
ζ^j_+	Forward cooperativity factor for ligand-bound R^j activation	Ligand	1.00E+03		”
ζ^j_-	Backward cooperativity factor for ligand-bound R^j activation	Ligand	1.00E+00		”
$\mu^{j,\theta}_+$	Forward cooperativity factor for G^θ-bound R^j activation	Cell	1.00E+00 ($j=\theta$), 0 ($j\neq\theta$)		”
$\mu^{j,\theta}_-$	Backward cooperativity factor for G^θ-bound R^j activation	Cell	1.00E+00		”
R_{tot}	Total receptor concentration	Cell	4.15E-10	M	”
G^1_{tot}	Total G^1 concentration	Cell	4.15E-10	M	”
G^2_{tot}	Total G^2 concentration	Cell	4.15E-10	M	”
L_{tot}	Total Ligand concentration	Ligand	1.00E+07	M	”

B Receptor cross states

In Figure B.1, we show simulated time courses for α_{GTP}, under variation of receptor cross state activation and accessibility. In the top row, we allow activation of both G proteins by either active state (by setting $k^{j,\theta}_{GTP} = 1\ \forall j, \theta$), and vary the propensity for G protein binding to the active states by varying $\mu^{1,2}_{+}$. With $\mu^{2,1}_{+} = 0.001$ (so that there is very little $R^{*2}G^1$, top left plot), as $\mu^{1,2}_{+}$ increases, basal α^2_{GTP} increases due to increased signalling via pre-coupled $R^{*1}G^2$. Also there is a slight increase in plateau α^2_{GTP}. In this case, the perhaps unexpected trend in the peak response, whereby peak α^2_{GTP} does not increase with $\mu^{1,2}_{+}$, is due to the fact that for large $\mu^{1,2}_{+}$, the basal conditions are "near equilibrium", and the peak may increase or decrease with increased $\mu^{1,2}_{+}$. The α^1_{GTP} equilibrium and dynamics are not significantly affected by changes in $\mu^{1,2}_{+}$. Performing the same simulations with $\mu^{2,1}_{+} = 1000$ (top right plot), α^1_{GTP} dynamics are again largely unaffected by the variation in $\mu^{1,2}_{+}$, but this time the system is closer to equilibrium and α^1_{GTP} has a lower peak than for $\mu^{2,1}_{+} = 0.001$.

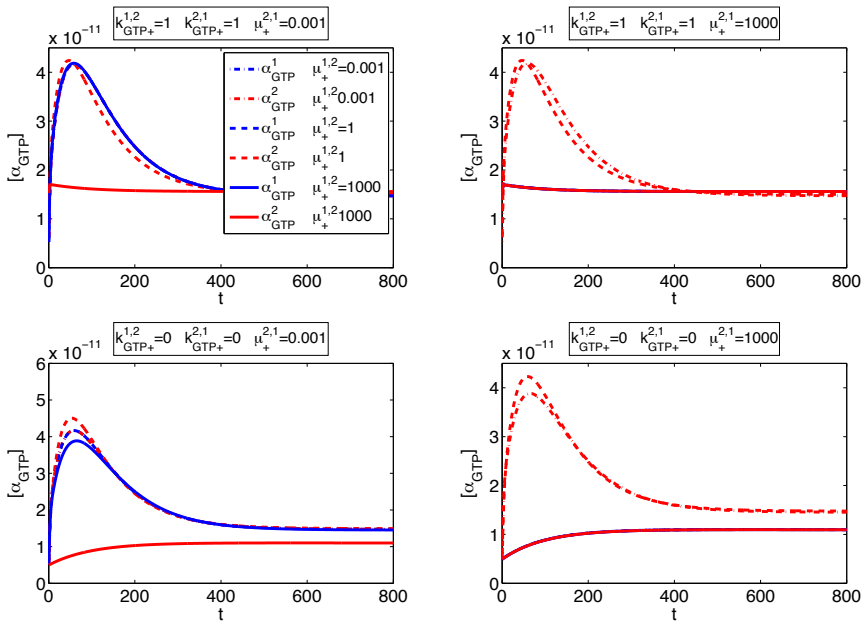

Figure B.1: Time courses for varying agonist accessibility of receptor cross states. Here, $[L] = 10^{-5}$M.

In the case where cross states are accessible in the G protein binding sense, but there is specificity with respect to g protein activation (so $k^{1,2}_{GTP} = k^{1,2}_{GTP} = 0$), for increasing $\mu^{1,2}_{+}$, we now have more of G^2 trapped in a non-signalling complex $R^{*1}G^2$, giving reduced basal and equilibrium α^2_{GTP}. The basal and equilibrium levels are monotonic with $\mu^{1,2}_{+}$, but the peak levels are not. For $\mu^{2,1}_{+} = 0.001$, as $\mu^{1,2}_{+}$ increases, more R^{*1} is trapped in non-signalling complexes, so there is less $R^{*1}G^1$ available to signal, resulting in a lower α^1_{GTP}. For $\mu^{2,1}_{+} = 1000$, we see the same trends, but with lower $\alpha^{1,2}_{GTP}$ signals, since there is more non-signalling $R^{*2}G^1$.

C Effect of ν

In Figure C.1, we show that the effect of varying ν^θ (the microaffinity constant ν^θ that controls the preference of ligand for RG^θ over R) is as expected; increasing ν^θ increases both peak and plateau α^θ_{GTP}.

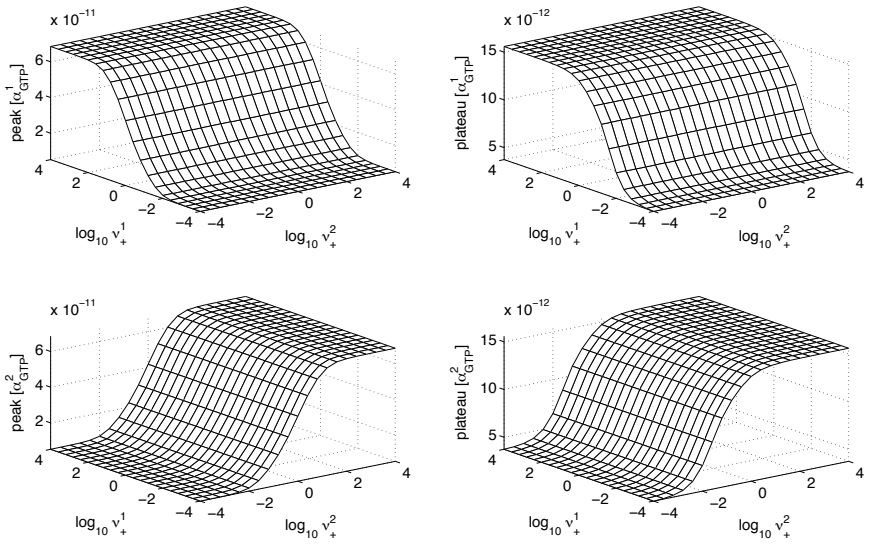

Figure C.1: Response surfaces for varying $\nu_+^{1,2}$, with expected monotonic relationships. Here, $[L] = 10^{-5}$M.

D Further experimental detail for cAMP experiments

CHO-K1 cells, expressing the A_1R were routinely grown in Hams F-12 media (supplemented with 10% FBS), at 37°C, in a humidified atmosphere, containing 5% CO2. Where Gs assays were performed, cells were pre-treated, for 16-18 hours with 200 ng/ml PTX. Upon day of assay, cells were harvested and brought to single cells suspension using trypsin (containing 0.05 EDTA). Cells were washed and resuspended in stimulation buffer (PBS containing 0.1% BSA and 25 μM rolipram). Cells were seeded onto 384-well, white, optiplates and stimulated with either agonist alone, or co-stimulated with agonist and 10 M forskolin, for 30 minutes. cAMP levels were then detected using a LANCE®cAMP detection kit (PerkinElmer, Boston, MA), and plates read using a LB 940 multimode microplate reader (Berthold technologies, Germany) (excitation: 340 nm, emission: 665 nm).

E Parameter estimates for cAMP experiments

In Table E.1, we show parameter estimates for the experimental data shown in Figure 5.1. Inspection of the values shows that ligand-dependent parameter values vary over orders of magnitude across the three experiments, while cell-only parameter value estimates are all within an order of magnitude of each other, as expected. Also, our estimates for the G protein totals are consistent with the observation that in most membranes, the amount of G_i protein exceeds the amount of G_s

References

[1] Matlab. The MathWorks Inc.

[2] J. G. Baker and S. J. Hill. A comparison of the antagonist affinities for the gi-and gs-coupled states of the human adenosine a1-receptor. *Journal of Pharmacology and Experimental Therapeutics*, 320(1):218–228, 2007.

[3] J.-A. Baltos, K. J. Gregory, P. J. White, P. M. Sexton, A. Christopoulos, and L. T. May. Quantification of adenosine a 1 receptor biased agonism: implications for drug discovery. *Biochemical pharmacology*, 99:101–112, 2016.

[4] G. J. Barritt. *Communication within animal cells*. Oxford University Press, 1992.

Table E.1: Parameter estimates for fitting biased agonism with functional antagonism model to cAMP data (see Figure 5.1).

Parameter	Cmpd6	Cmpd20	NECA
k_{L+}	1.20E+04	7.49E+03	1.52E+04
ζ_+^1	4.47E+03	1.52E+02	4.55E+03
ζ_+^2	2.70E+04	7.00E+03	2.54E+04
ν_+^1	5.82E-01	1.22E+01	5.82E-01
ν_+^2	6.00E+00	2.54E+02	8.36E+00
k_{act+}^1	8.80E-01	1.44E+00	9.32E-01
k_{act+}^2	6.47E-01	1.40E+00	5.94E-01
k_{G+}^1	6.34E+08	5.69E+08	6.55E+08
k_{G+}^2	2.89E+09	3.72E+09	2.36E+09
k_{GRA+}^1	7.55E+05	7.99E+05	7.63E+05
k_{GRA+}^2	4.10E+05	3.50E+05	3.28E+05
k_{hyd+}^1	2.42E-03	4.40E-03	2.42E-03
k_{hyd+}^2	3.20E-03	3.00E-03	3.30E-03
$k_{GTP+}^{1,1}$	1.90E-01	2.01E-01	1.75E-01
$k_{GTP+}^{2,2}$	1.87E-01	2.27E-01	1.87E-01
$\mu_+^{1,1}$	1.28E+00	2.16E+00	1.28E+00
$\mu_+^{2,2}$	8.60E-01	8.50E-01	8.60E-01
R_{tot}	4.15E-10	4.15E-10	4.15E-10
G_{tot}^1	3.79E-10	4.80E-10	4.49E-10
G_{tot}^2	8.22E-10	7.20E-10	8.28E-10
C_s	4.30E+08	4.36E+08	3.24E+08
C_i	4.40E+08	5.30E+08	4.99E+08

[5] J. Black and P. Leff. Operational models of pharmacological agonism. *Proceedings of the Royal Society of London B: Biological Sciences*, 220(1219):141–162, 1983.

[6] S. J. Bornheimer, M. R. Maurya, M. G. Farquhar, and S. Subramaniam. Computational modeling reveals how interplay between components of a gtpase-cycle module regulates signal transduction. *Proceedings of the National Academy of Sciences of the United States of America*, 101(45):15899–15904, 2004.

[7] L. Bridge. Modeling and simulation of inverse agonism dynamics. *Methods in enzymology*, 485:559–582, 2009.

[8] L. Bridge, J. King, S. Hill, and M. Owen. Mathematical modelling of signalling in a two-ligand g-protein coupled receptor system: Agonist–antagonist competition. *Mathematical biosciences*, 223(2):115–132, 2010.

[9] E. J. Calabrese and L. A. Baldwin. Hormesis: U-shaped dose responses and their centrality in toxicology. *Trends in Pharmacological Sciences*, 22(6):285–291, 2001.

[10] C. Chen, Y. Cordeaux, S. Hill, and J. King. Modelling of signalling via g-protein coupled receptors: pathway-dependent agonist potency and efficacy. *Bulletin of mathematical biology*, 65(5):933–958, 2003.

[11] Y. Cordeaux, A. P. IJzerman, and S. J. Hill. Coupling of the human a1 adenosine receptor to different heterotrimeric g proteins: evidence for agonist-specific g protein activation. *British journal of pharmacology*, 143(6):705–714, 2004.

[12] M. Donato and R. J. Gelpi. Adenosine and cardioprotection during reperfusionan overview. In *Biochemistry of Hypertrophy and Heart Failure*, pages 153–159. Springer, 2003.

[13] F. J. Ehlert. On the analysis of ligand-directed signaling at g protein-coupled receptors. *Naunyn-Schmiedeberg's archives of pharmacology*, 377(4-6):549–577, 2008.

[14] J. Gundry, R. Glenn, P. Alagesan, and S. Rajagopal. A practical guide to approaching biased agonism at g protein coupled receptors. *Frontiers in Neuroscience*, 11, 2017.

[15] C. K. Herenbrink, D. A. Sykes, P. Donthamsetti, M. Canals, T. Coudrat, J. Shonberg, P. J. Scammells, B. Capuano, P. M. Sexton, S. J. Charlton, et al. The role of kinetic context in apparent biased agonism at gpcrs. *Nature communications*, 7, 2016.

[16] T. Kenakin. Functional selectivity and biased receptor signaling. *Journal of Pharmacology and Experimental Therapeutics*, 336(2):296–302, 2011.

[17] T. Kenakin. What is pharmacological affinity? relevance to biased agonism and antagonism. *Trends in pharmacological sciences*, 35(9):434–441, 2014.

[18] T. Kenakin. The effective application of biased signaling to new drug discovery. *Molecular pharmacology*, 88(6):1055–1061, 2015.

[19] T. Kenakin and A. Christopoulos. Analytical pharmacology: the impact of numbers on pharmacology. *Trends in pharmacological sciences*, 32(4):189–196, 2011.

[20] T. Kenakin and A. Christopoulos. Signalling bias in new drug discovery: detection, quantification and therapeutic impact. *Nature reviews Drug discovery*, 12(3):205–216, 2013.

[21] T. Kenakin, C. Watson, V. Muniz-Medina, A. Christopoulos, and S. Novick. A simple method for quantifying functional selectivity and agonist bias. *ACS chemical neuroscience*, 3(3):193, 2012.

[22] T. Kenakin and M. Williams. Defining and characterizing drug/compound function. *Biochemical pharmacology*, 87(1):40–63, 2014.

[23] A. Knight, J. L. Hemmings, I. Winfield, M. Leuenberger, E. Frattini, B. G. Frenguelli, S. J. Dowell, M. Lochner, and G. Ladds. Discovery of novel adenosine receptor agonists that exhibit subtype selectivity. *Journal of medicinal chemistry*, 59(3):947–964, 2016.

[24] J. P. Kukkonen, J. Näsman, and K. E. Åkerman. Modelling of promiscuous receptor–gi/gs-protein coupling and effector response. *Trends in pharmacological sciences*, 22(12):616–622, 2001.

[25] R. Leander and A. Friedman. Modulation of the camp response by g\ alpha _i and g\ beta\ gamma: A computational study of g protein signaling in immune cells. *Bulletin of mathematical biology*, 76(6):1352–1375, 2014.

[26] P. Leff, G. Martin, and J. Morse. Application of the operational model of agonism to establish conditions when functional antagonism may be used to estimate agonist dissociation constants. *British journal of pharmacology*, 85(3):655–663, 1985.

[27] P. Leff, C. Scaramellini, C. Law, and K. McKechnie. A three-state receptor model of agonist action. *Trends in pharmacological sciences*, 18(10):355–362, 1997.

[28] D. MACKAY. An analysis of functional antagonism and synergism. *British journal of pharmacology*, 73(1):127–134, 1981.

[29] T. Maiwald and J. Timmer. Dynamical modeling and multi-experiment fitting with potterswheel. *Bioinformatics*, 24(18):2037–2043, 2008.

[30] S. Mangmool and H. Kurose. Gi/o protein-dependent and-independent actions of pertussis toxin (ptx). *Toxins*, 3(7):884–899, 2011.

[31] T. Minamino. Cardioprotection from ischemia/reperfusion injury. *Circulation journal*, 76(5):1074–1082, 2012.

[32] H. O. Onaran, S. Rajagopal, and T. Costa. What is biased efficacy? defining the relationship between intrinsic efficacy and free energy coupling. *Trends in pharmacological sciences*, 35(12):639–647, 2014.

[33] V. PliSka. Models to explain dose-response relationships that exhibit a downturn phase. *Trends in pharmacological sciences*, 15(6):178–181, 1994.

[34] S. Rajagopal, S. Ahn, D. H. Rominger, W. Gowen-MacDonald, C. M. Lam, S. M. DeWire, J. D. Violin, and R. J. Lefkowitz. Quantifying ligand bias at seven-transmembrane receptors. *Molecular pharmacology*, 80(3):367–377, 2011.

[35] Z. Rankovic, T. F. Brust, and L. M. Bohn. Biased agonism: An emerging paradigm in gpcr drug discovery. *Bioorganic & medicinal chemistry letters*, 26(2):241–250, 2016.

[36] D. Roche, D. Gil, and J. Giraldo. Multiple active receptor conformation, agonist efficacy and maximum effect of the system: the conformation-based operational model of agonism. *Drug discovery today*, 18(7):365–371, 2013.

[37] C. Scaramellini and P. Leff. A three-state receptor model: Predictions of multiple agonist pharmacology for the same receptor typea. *Annals of the New York Academy of Sciences*, 861(1):97–103, 1998.

[38] C. Scaramellini and P. Leff. Theoretical implications of receptor coupling to multiple g proteins based on analysis of a three-state model. *Methods in enzymology*, 343:17–29, 2002.

[39] J. Shonberg, L. Lopez, P. J. Scammells, A. Christopoulos, B. Capuano, and J. R. Lane. Biased agonism at g protein-coupled receptors: The promise and the challengesa medicinal chemistry perspective. *Medicinal research reviews*, 34(6):1286–1330, 2014.

[40] R. Slack and D. Hall. Development of operational models of receptor activation including constitutive receptor activity and their use to determine the efficacy of the chemokine ccl17 at the cc chemokine receptor ccr4. *British journal of pharmacology*, 166(6):1774–1792, 2012.

[41] L. A. Stott, D. A. Hall, and N. D. Holliday. Unravelling intrinsic efficacy and ligand bias at g protein coupled receptors: A practical guide to assessing functional data. *Biochemical pharmacology*, pages 1–12, 2015.

[42] E. Szabadi. A model of two functionally antagonistic receptor populations activated by the same agonist. *Journal of theoretical biology*, 69(1):101–112, 1977.

[43] S. Tuček, P. Michal, and V. Vlachová. Modelling the consequences of receptor–g-protein promiscuity. *Trends in pharmacological sciences*, 23(4):171–176, 2002.

[44] J. D. Urban, W. P. Clarke, M. Von Zastrow, D. E. Nichols, B. Kobilka, H. Weinstein, J. A. Javitch, B. L. Roth, A. Christopoulos, P. M. Sexton, et al. Functional selectivity and classical concepts of quantitative pharmacology. *Journal of Pharmacology and Experimental Therapeutics*, 320(1):1–13, 2007.

[45] C. Weston, J. Lu, N. Li, K. Barkan, G. O. Richards, D. J. Roberts, T. M. Skerry, D. Poyner, M. Pardamwar, C. A. Reynolds, et al. Modulation of glucagon receptor pharmacology by receptor activity-modifying protein-2 (ramp2). *Journal of Biological Chemistry*, 290(38):23009–23022, 2015.

[46] C. Weston, I. Winfield, M. Harris, R. Hodgson, A. Shah, S. J. Dowell, J. C. Mobarec, D. A. Woodlock, C. A. Reynolds, D. R. Poyner, et al. Receptor activity-modifying protein-directed g protein signaling specificity for the calcitonin gene-related peptide family of receptors. *Journal of Biological Chemistry*, 291(42):21925–21944, 2016.

[47] P. Woodroffe, L. Bridge, J. King, C. Chen, and S. Hill. Modelling of the activation of g-protein coupled receptors: drug free constitutive receptor activity. *Journal of mathematical biology*, 60(3):313–346, 2010.

[48] P. Woodroffe, L. Bridge, J. King, and S. Hill. Modelling the activation of g-protein coupled receptors by a single drug. *Mathematical biosciences*, 219(1):32–55, 2009.

[49] X.-W. Zhu, S.-S. Liu, L.-T. Qin, F. Chen, and H.-L. Liu. Modeling non-monotonic dose–response relationships: Model evaluation and hormetic quantities exploration. *Ecotoxicology and environmental safety*, 89:130–136, 2013.

Chapter 7
Bibliography

Ahmad A, Ahmad S, Glover L, Miller SM, Shannon JM, Guo X, Franklin WA, Bridges JP, Schaack JB, Colgan SP, White CW (**2009**). Adenosine A2A receptor is a unique angiogenic target of HIF2alpha in pulmonary endothelial cells. *Proc. Natl. Acad. Sci. USA.* (106):10684-10689.

Albrandt K, Brady EM, Moore CX, Mull E, Sierzega ME, Beaumont K (**1995**). Molecular cloning and functional expression of a third isoform of the human calcitonin receptor and partial characterization of the calcitonin receptor gene. *Endocrinology.* (136):5377-5384.

Allard B, Beavis PA, Darcy PK, Stagg J (**2016**). Immunosuppressive effects of adenosine in cancer. *Curr. Opin. Pharmacol.* (29):7-16.

Altenbach C, Klein-Seetharaman J, Cai K, Khorana HG, Hubbell WL (**2001**). Structure and function in rhodopsin: Mapping light-dependent changes in distance between residue 316 in helix 8 and residues in the sequence 60-75, covering the cytoplasmic end of helices TM1 and TM2 and their connection loop CL1. *Biochemistry*. (40):15493-15500.

Ammon-Treiber S, Höllt V (**2005**). Morphine-induced changes of gene expression in the brain. *Addict. Biol.* (10):81-89.

Armour SL, Foord S, Kenakin T, Chen WJ (**1999**)**.** Pharmacological characterization of receptor-activity-modifying proteins (RAMPs) and the human calcitonin receptor. *J. Pharmacol. Toxicol. Methods.* (42):217-224.

Ashton TD, Aumann KM, Baker SP, Schiesser CH and Scammells PJ (**2007**). Structure−activity relationships of adenosines with heterocyclic N^6-substituents. *Bioorg. Med. Chem. Lett*. (17):6779-6784.

Aslam M, Pfeil U, Gündüz D, Rafiq A, Kummer W, Piper HM, Noll T (**2012**). Intermedin (adrenomedullin2) stabilises the endothelial barrier and antagonises thrombin-induced barrier failure in endothelial cell monolayers. *Br. J. Pharmacol.* (165):208-222.

Avlani VA, Gregory KJ, Morton CJ, Parker MW, Sexton PM, Christopoulos A (**2007**). Critical role the second extracellular loop in the binding of both orthosteric and allosteric G protein-coupled receptor ligands. *J. Biol. Chem.* (282):25677-25686.

Ayoub MA, Couturier C, Lucas-Meunier E, Angers S, Fossier P, Bouvier M, Jockers R (**2002**). Monitoring of ligand-independent dimerization and ligand-induced conformational changes of melatonin receptors in living cells by bioluminescence resonance energy transfer. *J. Biol. Chem.* (277):21522-21528.

Baggio LL, Drucker DJ (**2007**). Biology of incretins: GLP-1 and GIP. *Gastroenerology.* (132):2131-2157.

Bailey RJ, Walker CS, Ferner AH, Loomes KM, Prijic G, Halim A, Whiting L, Phillips ARJ, Hay DL (**2012**). Pharmacological characterization of rat amylin receptors: implications for the identification of amylin receptor subtypes. *Br. J. Pharmacol.* (166):151-167.

Baker JG, Hill SJ (**2007**). A comparison of the antagonist affinities for the G_i- and G_s-coupled states of the human adenosine receptor. *J. Pharmacol. Exp. Ther.* (320):218-228.

Ballestteros JS, Jensen AD, Liapakis G, Rasmussen SG, Shi L, Gether U, Javitch JA (**2001**). Activation of the beta 2-adrenergic receptor involves disruption of an ionic lock between the cytoplasmic ends of transmembrane segments 3 and 6. *J. Biol. Chem.* (276):29171-29177.

Baltos JA, Gregory KJ, White PJ, Sexton PM, Christopoulos A, May LT (**2016**). Quantification of adenosine A(1) receptor biased agonism: Implications for drug discovery. *Biochem. Pharmacol*. (99):101-112.

Baraldi PG, Cacciari B, Romagnoli R, Spalluto G, Monopoli A, Ongini E, Varani K, Borea PA (**2002**). 7-Substituted 5-amino-2-(2-furyl)pyrazolo[4,3-e]-1,2,4-triazolo[1,5-c]pyrimidines as A2A adenosine receptor antagonists: a study on the importance of modifications at the side chain on the activity and solubility. *J. Med. Chem.* (45):115-126.

Baraldi PG, Fruttarolo F, Tabrizi MA, Preti D, Romagnoli R, El-Kashef H, Moorman A, Varani K, Gessi S, Merighi S, Borea PA (**2003**). Design, synthesis, and biological evaluation of C9- and C2-substituted pyrazolo[4,3-e]-1,2,4-triazolo[1,5-c]pyrimidines as new A2A and A3 adenosine receptor antagonists. *J. Med. Chem.* (46):1229-1241.

Belardinelli L, Shryock JC, Song Y, Wang D, Srinivas M (**1995**). Ionic basis of the electrophysiological actions of adenosine on cardiomyocytes. *FASEB. J.* (9):359-365.

Benovic JL, Pike LJ, Cerione RA, Staniszewski C, Yoshimasa T, Codina J, Caron MG, Lefkowitz RJ (**1985**). Phosphorylation of the mammalian beta-adrenergic receptor by cyclic AMP-dependent protein kinase, regulation of the rate of receptor phosphorylation and dephosphorylation by agonist occupancy and effects on coupling of the receptor to the stimulatory guanine nucleotide regulatory protein. *J. Biol. Chem.* (260):7094-7101.

Bentrop J, Schwab K, Pak WL, Paulsen R (**1997**). Site-directed mutagenesis of highly conserved amino acids in the first cytoplasmic loop of the drosophila Rh1 opsin blocks rhodopsin synthesis in the nascent state. *EMBO J.* (16):1600-1609.

Bertheleme N, Singh S, Dowell SJ, Hubbard J, Byrne B (**2013**). Loss of constitutive activity is correlated with increased thermostability of the human adenosine A2A receptor. *Br. J. Pharmacol.* (169):988-998.

Birnbaumer L. Abramowitz J, Brown AM (**1990**)**.** Receptor-effector coupling by G proteins. *Biochem. Biophys. Acta.* (1031):163-224.

Black JW, Leff P (**1983**)**.** Operational models of pharmacological agonsim. *Proc. R. Soc. Lond. B. Biol. Sci.* (220):141-162.

Bockaert J, Pin JP (**1999**). Molecular tinkering of G protein-coupled receptors: an evolutionary success. *EMBO J.* (18):1723-1729.

Borea PA, Varani K, Vincenzi F, Baraldi PG, Tabrrizi MA, Merighi S, Gessi S (**2015**). The A_3 adenosine receptor: history and perspectives. *Pharmacol. Rev.* (67):74-102.

Bos JL, Rehmann H, Wittinghofer A (**2007**). GEFs and GAPs: critical elements in the control of small G proteins. *Cell*. (129):867-877.

Branca C, Wisely EV, Hartman LK, Caccamo A, Oddo S (**2014**). Administration of a selective β2 adrenergic receptor antagonist exacerbates neuropathology and cognitive deficits in a mouse model of Alzheimer's disease. *Neurobiol. Aging.* (35):2726-2735.

Bristow MR (**2000**). β-Adrenergic receptor blockade in chronic heart failure. *Circulation*. (101):558-569.

Broselid S, Berg KA, Chavera TA, Khan R, Clarke WP, Olde B, Leeb-Lundberg LM (**2014**). G protein-coupled receptor 30 (GPR30) forms a plasma membrane complex with membrane-associated guanylate kinases (MAGUKs) and protein kinase a-anchoring protein 5 (AKAP5) that constitutively inhibits cAMP production. *J. Biol. Chem.* (289):22117-22127.

Brown AJ, Dyos SL, Whiteway MS, White JHM, Watson M-A, Marzioch M, Clare JJ, Cousens DJ, Paddon C, Plumpton C, Romanos MA, Dowell SJ (**2000**)**.** Functional coupling of mammalian receptors to the yeast mating pathway using novel yeast/mammalian G protein α-subunit chimeras. *Yeast.* (16):11-22.

Brown AJ, Goldsworthy SM, Barnes AA, Eilert MM, Tcheang L, Daniels D, Muir AI, Wigglesworth MJ, Kinghorn I, Fraser NJ, Pike NB, Strum JC, Steplewski KM, Murdock PR, Holder JC, Marshall FH, Szekeres PG, Wilson S, Ignar DM, Foord SM, Wise A, Dowell SJ (**2003**)**.** The orphan G protein-coupled receptors GPR41 and GPR43 are activated by propionate and other short chain carboxylic acids. *J. Biol. Chem.* (278):11312-11319.

Burtey A, Schmid EM, Ford MGJ, Rapport JZ, Scott MGH, Marullo S, Simon SM, McMahon HT, Benmerah A (**2007**). The conserved isoleucine-valine-phenylalanine motif couples activation state and endocytic functions of β-arrestins. *Traffic.* (8):914-931.

Cai K, Itoh Y, Khorana FC (**2001**). Mapping of contact sites in complex formation between transducing and light-activated rhodopsin by covalent crosslinking: use of a photoactivatable reagent. *Proc. Natl. Acad. Sci. USA.* (98):4877-4882.

Camps M, Hou C, Sidiropoulos D, Stock JB, Jakobs KH, Giershick P (**1992**). Stimulation of phospholipase C by guanine-nucleotide binding protein βγ subunits. *Eur. J. Biochem*. (206):821-831.

Canals M, Angulo E, Casadó V, Canela EI, Mallol J, Viñals, Staines W, Tinner B, Hillion J, Agnati L, Fuxe K, Ferré S, Lluis C, Franco R (**2005**). Molecular mechanisms involved in the adenosine A_1 and A_{2A} receptor-induced neuronal differentiation in neuroblastoma cells and striatal primary cultures. *J. Neurochem*. (92):337-348.

Carpenter B, Nehmé R, Warne T, Leseli AGW, Tate CG (**2016**). Structure of the adenosine A_{2A} receptor bound to an engineered G protein. *Nature.* (536):104-107.

Carr III R, Du Y, Quoyer J, Panettieri Jr RA, Janz JM, Bouvier M, Kobilka BK, Benovic JL (**2014**). Development and characterization of pepducins as G_s-biased allosteric agonists. *J. Biol. Chem.* (289):35668-35684.

Carroll RC, Peralta EG (**1998**). The m3 muscarinic acetylcholine receptor differentially regulates calcium influx and release through modulation of monovalent cation channels. *EMBO J* (11):3036-3044.

Casadó V, Barrondo S, Spasic M, Callado LF, Mallol J, Canela E, Lluís C, Mena J, Cortés A, Sallés J, Franco R (**2010**). Gi protein coupling to adenosine A1-A2A receptor heteromers in human brain caudate nucleus. *J. Neurochem.* (114):972-980.

Cekic C, Sag D, Li Y, Theodorescu D, Strieter RM, Linden J (**2012**). Adenosine A2B receptor blockade slows growth of bladder and breast tumours. *J. Immunol.* (188):198-205.

Cerione RA, Codina J, Benovic JL, Lefkowitz RJ, Birnbaumer L, Caron MG (**1984**). The mammalian β_2-adrenergic receptor: reconstitution of functional interactions between pure receptor and pure stimulatory binding protein of the adenylate cyclase system. *Biochemistry.* (23):4519-4525.

Chang CL, Roh J, Hsu SY (**2004**). Intermedin, a novel calcitonin family peptide that exists in teleosts as well as in mammals: a comparison with other calcitonin/intermedin family peptides in vertebrates. *Peptides.* (25):1633–1642.

Chappe V, Irvine T, Liao J, Evangelidis A, Hanrahan JW (**2005**). Phosphorylation of CFTR by PKA promotes binding of the regulatory domain. *EMBO. J.* (24):2730-2740.

Chen JF, Sonsalla PK, Pedata F, Melani A, Domenici, MR, Popoli P, Geiger J, Lopes LV, deMendonça A (**2007**). Adenosine A_{2A} receptors and brain injury: broad spectrum of neuroprotection, multifaceted actions and “fine tuning” modulation. *Prog. Neurobiol*. (83):310−331.

Chen XT, Pitis P, Liu G, Yuan C, Gotchev D, Cowan CL, Rominger DH, Koblish M, Dewire SM, Crombie AL, Violin JD, Yamashita DS (**2013**). Structure-activity relationships and discovery of a G protein biased μ opioid receptor ligand, [(3-methoxythiophen-2-yl)methyl] ({2-[(9R)-9-(pyridine-2-yl)-6oxaspiro-[4,5]decan-9-yl]ethyl})amine (TRV130), for the treatment of acute severe pain. *J. Med. Chem.* (56):8019-8031.

Cheong SL, Frederico S, Venkatesan G, Mandel AL, Shao YM, Moro S, Spallut, Pastorin G (**2013**). The A_3 Adenosine receptor as multifaceted therapeutic target: Pharmacology, Medicinal chemistry and in silico approaches. *Med Res Rev.* (33):235-335.

Chiang MC, Lee YC, Huang CL, Chern Y (**2005**). cAMP-response element-binding protein contributes to suppression of the A2A adenosine receptor promoter by mutant Huntingtin with expanded polyglutamine residues. *J. Biol. Chem.* (280):14331-14340.

Chiu FL, Lin JT, Chuang CY, Chien T, Chen CM, Chen KH, Hsiao HY, Lin YS, Chern Y, Kuo HC (**2015**). Elucidating the role of the A_{2A} adenosine receptor in neurodegeneration using neurons derived from Huntington’s disease iPSCs. *Hum. Mol. Genet.* (24):6066-6079.

Chou SY, Lee YC, Chen HM, Chiang MC, Lai HL, Chang HH, Wu YC, Sun CN, Chien CL, Lin YS, Wang SC, Tung YY, Chang C, Chern Y (**2005**). CGS21680 attenuates symptoms of Huntington’s disease in a transgenic mouse model. *J. Neurochem.* (93):310-320.

Christalli G, Lambertucci C, Taffi S, Vittori S, Volpini R (**2003**). Medicinal chemistry of adenosine A2A receptor agonists. *Curr. Top. Med. Chem.* (3):387-401.

Christopoulos A, Christopoulos G, Morfis M, Udawela M, Laburthe M, Couvineau A, Kuwasako K, Tilakaratne N, Sexton PM (**2003**)**.** Novel receptor partners and function of receptor activity-modifying proteins. *J. Biol. Chem.* (278):3293-3297.

Ciruela F, Casadó V, Rodrigues RJ, Luján R, Burgueño J, Canals M, Borycz J, Rebola N, Goldberg SR, Mallol J, Cortés A, Canela EL, López-Giménez JF, Milligan G, Lluis C, Cunha RA, Ferré S, Franco R (**2006**). Presynaptic control of striatal glutamatergic neurotransmission by adenosine A1-A2A receptor heteromers. *J. Neurosci.* (26):2080-2087.

Clapham DE, Neer EJ (**1997**)**.** G protein beta gamma subunits. *Annu. Rev. Pharmacol. Toxicol.* (37):167-203.

Conner M, Hicks MR, Dafforn T, Knowles TJ, Ludwig C, Staddon S, Overduin M, Günther UL, Thorne J, Wheatley M, Poyner DR, Conner AC (**2008**). Functional and biophysical analysis of the C-terminus of the CGRP-receptor; a family B GPCR. *Biochemistry.* (47):8434-8444.

Cordeaux Y, Briddon SJ, Megson AE, McDonnell J, Dickenson JM, Hill SJ (**2000**). Influence of receptor number on functional responses elicited by agonists acting at the human adenosine A1 receptor: evidence for signaling pathway dependent changes in agonist potency and relative intrinsic activity. *Mol. Pharmacol.* (58):1075–1084.

Cordeaux Y, Ijzerman AP, Hill SJ (**2004**). Coupling of the human A1 Adenosine receptor to different heterotrimeric G-proteins; evidence for agonist-specific G protein activation. *Br. J. Pharmacol.* (143):705–714.

Correl CC, McKittrick BA (**2014**). Biased ligand modulation of seven transmembrane receptors (7TMRs): functional implications for drug discovery. *J. Med. Chem.* (57):6887-6896.

Coskran TM, Morton D, Menniti FS, Adamowicz WO, Kleiman RJ, Ryan AM, Strick CA, Schmidt CJ, Stephenson DT (**2006**). Immunohistochemical localization of phosphodiesterase 10A in multiple mammalian species. *J. Histochem. Cytochem.* (54):1205-1213.

Covic L, Gresser AL, Talavera J, Swift S, Kuliopulos A (**2001**). Activation and inhibition of G protein-coupled receptors by cell-penetrating membrane-tethered peptide. *Proc. Natl. Acad. Sci. USA.* (99):643-648.

Cueille C, Pidoux E, de Vernejoul MC, Ventura-Clapier R, Garel JM (**2002**). Increased myocardial expression of RAMP1 and RAMP3 in rats with chronic heart failure. *Biochem. Biophys. Res. Commun.* (294):340–346.

Dale N, Frenguelli BG (**2009**). Release of adenosine and ATP during ischemia and epilepsy. *Curr. Neuropharmacol.* (7):160−179.

Davenport AP, Alexander SP, Sharman JL, Pawson AJ, Benson HE, Monaghan AE, Liew WC, Mpamhanga CP, Bonner TI, Neubig RR, Pin JP, Spedding M, Harmar AJ (**2013**). International Union of Basic and Clinical Pharmacology. LXXXVIII. G protein-coupled receptor list: recommendations for new pairings with cognate ligands. *Pharmacol. Rev.* (65):967-986.

DeFea KA (**2011**). Beta-arrestins as regulator of signal termination and transduction: How do they determine what to scaffold? *Cell. Sig.* (23):621-629.

De Lean A, Stadel JM, Lefkowitz RJ (**1980**). A ternary complex model explains the agonist-specific binding properties of adenylate cyclase coupled β-adrenergic receptor. *J. Biol. Chem.* (225):7108-7117.

Desi AJ, Roberts DJ, Richards GO, Skerry TM (**2014**). Role of receptor activity modifying protein 1 in function of the calcium sensing receptor in the human TT thyroid carcinoma cell line. *PLoS One.* (9):e85237.

Desmet CJ, Gallenne T, Prieur A, Reyal F, Visser NL, Wittner BS, Smit MA, Geiger TR, Laoukili J, Iskit S, Rodenko B, Zwart W, Evers B, Horling H, Ajouaou A, Zevenhoven J, van Vilet M, Ramaswarmy S, Wessels LFA, Peeper DS (**2013**). Identification of a pharmacologically tractable Fra1/ADORA2B axis promoting breast cancer metastasis. *Proc. Natl. Acad. Sci. USA.* (110):5139-5144.

DeWire SM, Yamashita DS, Rominger DH, Liu G, Cowan CL, Graczyk TM, Chen XT, Pitis PM, Gotchev D, Yuan C, Koblish M, Lark MW, Violin JD (**2013**). A G protein-biased ligand at the μ-opioid receptor is potentially analgesic with reduced gastrointestinal and respiratory dysfunction compared with morphine. *J. Pharmacol. Exp. Ther.* (344):708-717.

Dhalla AK, Wong MY, Wang WQ, Biaggioni I, Belardinelli L (**2006**). Tachycardia caused by A2A adenosine receptor agonists is mediated by direct sympathoexcitation in awake rats. *J. Pharmacol. Exp. Ther.* (316):695-702.

Dickenson JM, Hill SJ (**1993**). Adenosine A1-receptor stimulated increases in intracellular calcium the smooth muscle cell line, DDT1MF-2. *Br. J. Pharmacol.* (108):85-92.

Dickerson IM (**2010**). The CGRP-receptor component protein: A regulator for CLR :151-perspectives (Hay, D.L. and Dickerson, I.M., eds), 59–73, Springer.

Dionisotti S, Ferrara S, Molta C, Zocchi C, Ongini E (**1998**). Labeling of A2A adenosine receptors in human platelets by use of the new nonxanthine antagonist radioligand [3H]SCH 58261. *J. Pharmacol Exp. Ther.* (278):1209-1214.

Disa J, Parameswaran N, Nambi P, Aiyar N (**2000**). Involvement of cAMP-dependent protein kinase and pertussis toxin-sensitive G-proteins in CGRP mediated JNK activation in human neuroblastoma cell line. *Neuropeptides.* (34):229-233.

Dohlman HG, Apaniesk D, Chen Y, Song J, Nusskern D (**1995**). Inhibition of G-protein signaling by dominant gain-of-function mutations in Sst2p, a pheromone desensitization factor in *Saccharomyces cerevisiae. Mol. Cell. Biol.* (15):3635-3643.

Doronin S, Shumay H, Wang Yu, Malbon CC (**2002**). Akt mediates sequestration of the beta(2)-adrenergic receptor in response to insulin. *J. Biol. Chem.* (277):15124-15131.

Dowell SJ, Brown AJ (**2002**). Yeast assays for G protein-coupled receptors. *In:* Leifert WR. G Protein-coupled receptors in drug discovery. Humana Press. (552):213-229.

Drissi H, Lieberherr M, Hott M, Marie PJ, Lasmoles F (**1999**). Calcitonin gene-related peptide (CGRP) increases intracellular free Ca2+ concentrations but not cyclic AMP formation in CGRP receptor-positive osteosarcoma cells (OHS-4). *Cytokine.* (11):200-207.

Dumas EO, Pollack GM (**2008**). Opioid tolerance development: A pharmacokinetic/pharmacodynamics perspective. *AAPS. J.* (10):537-550.

Duvernay MT, Dong C, Zhang X, Robitaille M, Hébert TE, Wu G (**2009**). A single conserved leucine residue on the first intracellular loop regulates ER export of G protein-coupled receptors. *Traffic.* (10):552-566.

Fenalti G, Giguere PM, Katritch V, Huang X-P, Thompson AA, Cherezov VM Roth BL, Stevens RC (**2014**). Molecular control of δ-opioid receptor signalling. *Nature.* (50):191–196.

Ferré S, Ciruela F, Borycz J, Solinas M, Quarta D, Antoniou K, Quiroz C, Justinova Z, Lluis C, Franco R, Goldberg SR (**2008**). Adenosine A1-A2A receptor heteromers: new targets for caffeine in the brain. *Front. Biosci.* (13):2391-2399.

Ferré S, Goldberg SR, Lluis C, Franco R (**2009**). Looking for the role of cannabinoid receptor heteromers in striatal function. *Neuropharmacol.* (56):226-234.

Figueroa KW, Griffin MT, Ehlert FJ (**2009**). Selectivity of agonists for the active state of M1 to M4 muscarinic receptor subtypes. *J. Pharmacol. Exp. Ther.* (328):331-342.

Flock T, Hauser AS, Lund N, Gloriam DE, Balaji S, Babu MM (**2017**). Selectivity determinants of GPCR-G-protein binding. *Nature.* (545):317-322.

Fossetta J, Jackson J, Deno G, Fan X, Du XK, Bober L, Soude-Bermejo A, de Bouteiller O, Caux C, Lunn C, Lundell D, Palmer RK (**2003**). Pharmacological analysis of calcium responses mediated by the A3 adenosine receptor in monocyte-derived dendritic cells and recombinant cells. *Mol. Pharmacol.* (63):342-350.

Franchetti P, Cappellacci L, Vita P, Petrelli R, Lavecchia A, Kachler S, Klotz KN, Marabese I, Luongo L, Maione S, Grifantini M (**2009**). N^6-Cycloalkyl- and N^6-bicycloalkyl-C5′(C2′)-modified adenosine derivatives as high-affinity and selective agonists at the human A_1 adenosine receptor with antinociceptive effects in mice. *J. Med. Chem*. (52):2393−2406.

Franco R, Ferré S, Agnati L, Torvinen M, Ginés S, Hillion J, Casadó V, Liedó P, Zoli M, Lluis C, Fuxe K (**2000**). Evidence for adenosine/dopamine receptor interactions: indications for heteromization. *Neuropsychopharmacology*. (23):S50-59.

Fredholm BB, Chen JF, Cunha R, Svenningsson P, Vaugeois JM (**2005**). Adenosine and brain function. *Int. Rev. Neurobiol.* (63):191−270.

Fredholm BB, Ijzerman AP, Jacobson KA, Linden J, and Müller, CE (**2011**). International Union of Basic and Clinical Pharmacology. LXXXI. Nomenclature and classification of adenosine receptors–an update. *Pharmacol. Rev.* (63):1–34.

Fredholm BB, Assender JW, Irenius E, Kodama N, Saito N (**2013**). Synergistic effects of adenosine A1 and P2Y receptor stimulation on calcium mobilization and PKC translocation in DDT1 MF-2 cells. *Cell. Mol. Neurobiol*. (23):379–400.

Fredriksson R, Langerström MC, Lundin LG, Schiöth HB (**2003**). The G-protein-coupled receptors in the human genome form five main families. Phylogenetic analysis, Paralogon groups and fingerprints. *Mol. Pharmacol.* (63):1256-1272.

Fujishige K, Kotera J, Michibata H, Yuasa K, Takebayashi S, Okumura K, Omori K (**1999**). Cloning and characterization of a novel human phosphodiesterase that hydrolyzes both cAMP and cGMP (PDE10A). *J. Biol. Chem.* (274):18438-18445.

Furness SG, Wootten D, Christopoulos A, Sexton PM (**2012**). Consequences of splice variation on Secretin family G protein-coupled receptor function. *Br. J. Pharmacol.* (166):98-109.

Fuxe K, Ferré S, Canals M, Torvinen M, Terasmaa A, Marcellinio D, Goldberg SR, Staines W, Jacobsen KX, Lluis C, Woods AS, Agnati LF, Franco R (**2005**). Adenosine A2A and dopamine D2 heteromeric receptor complexes and their function. *J. Mol. Neurosci.* (26):209-220.

Gao ZG, Jacobson KA (**2016**). On the selectivity of the Gaq inhibitor UBO-QIC: A comparison with the Gai inhibitor pertussis toxin. *Biochem. Pharmacol.* (107):59-66.

Garland SL (**2013**). Are GPCRs still a source of new targets? *J. Biomol. Screen.* (18):279-288.

Gautam N, Downes GB, Yank K, Kisselev I (**1998**). The G-protein βγ complex. *Cell. Signal.* (10):447-455.

Gee KR, Brown KA, Chen WN, Bishop-Stewart J, Gray D, Johnson I (**2000**). Chemical and physiological characterization of fluo-4 Ca(2+)-indicator dyes. *Cell Calcium* (27):97-106.

Giampà C, Patassini S, Borreca A, Laurenti D, Marullo F, Bernardi G, Menniti FS, Fusco FR (**2009**). Phosphodiesterase 10 inhibition reduces striatal excitotoxicity in the quinolinic acid model of Huntington's disease. *Neurobiol. Dis.* (34):450-456.

Giampà C, Laurenti D, Anzilotti S, Bernardi G, Menniti FS, Fusco FR (**2010**). Inhibition of the striatal specific phophodiesterase PDE10A ameliorates striatal and cortical pathology in R6/2 mouse model of Huntington's disease. *PLoS One.* (5):e13417.

Gingell JJ, Burns ER, Hay DL (**2014**). Activity of pramlintide, rat and human amylin but not Aβ1-42 at human amylin receptors. *Endocrinology*. (155):21-26.

Glukhova A, Thai DM, Nguyen AT, Vecchio EA, Jörg M, Scammells PJ, May LT, Sexton PM, Christopoulos A (**2017**). Structure of the Adenosine A_1 receptor reveals the basis for subtype selectivity. *Cell*. (168):867-877.

Gurevich VV, Dion SB, Onorato JJ, Ptasdienski J, Kim CM, Sterne-Marr R, Hosey MM, Benovi JL (**1995**). Arrestin interactions with G protein-coupled receptors. *J. Biol. Chem.* (270):720-731.

Hack SP, Christie MJ (**2003**). Adaptations in adenosine signaling in drug dependence: therapeutic implications. *Curr. Rev. Neurobiol.* (15):235-274.

Haeusler D, Grassinger L, Fuchshuber F, Horleinsberger WJ, Hoftberger R, Leisser I, Girschele F, Shanab K, Spreitzer H, Gerdenitsch W, Hacker M, Wadsak W, Mitterhauser M (**2015**). Hide and seek: a comparative autoradiographic in vitro investigation of the adenosine A_3 receptor. *Eur. J. Nucl. Med. Mol. Imag.* (42):928-939.

Hager MV, Clydesdale, Gellman SH, Sexton PM, Wootten D (**2017**). Characterization of signal bias at the GLP-1 receptor induced by backbone modification of GLP-1. *Biochem. Pharmacol.* (136):99-108.

Hammarberg C, Schulte G, Fredholm BB (**2003**). Evidence for functional adenosine A3 receptors in microglia cells. *J. Neurochem.* (86):1051-1054.

Harikumar KG, Simms J, Christopoulos G, Sexton PM, Miller LJ (**2009**). Molecular basis of association of receptor activity-modifying protein 3 with family B G protein-coupled secretin receptor. *Biochemistry*. (48):11773-11785.

Harikumar KG, Wootten D, Pinon DI, Koole C, Ball AM, Furness SGB, Graham B, Dong M, Christopoulos A, Miller LJ, Sexton PM (**2012**). Glucagon-like peptide-1 receptor dimerization differentially regulates agonist signaling but does not affect small molecule allostery. *Proc. Natl. Acad. USA.* (109):18607-18612.

Hasakó G, Csóka B, Németh ZH, Vizi ES, Pacher P (**2009**). A(2B) adenosine receptors in immunity and inflammation. *Trends. Immunol.* (30):263-270.

Hay DL, Poyner DR, Smith DM (**2003**). Desensitisation of adrenomedullin and CGRP receptors. *Regul. Pept*. (112):139-145.

Hay DL, Christopoulos G, Christopoulos A, Poyner DR, Sexton PM (**2005**). Pharmacological discrimination of Calcitonin Receptor: Receptor Activity-Modifying Protein Complexes. *Mol. Pharmacol.* (67):1655-1665.

He C, Yan X, Zhang T, Mirshahi T, Jin T, Huang A, Logothetis DE (**2002**). Identification of critical residues controlling G protein-gated inwardly rectifying K+ channel activity through interactions with the beta gamma subunits of G proteins. *J. Biol. Chem.* (277):6088-6096.

Hebb AL, Robertson HA, Denovan-Wright EM (**2004**). Striatal phophodiesterase mRNA and protein levels are reduced in Huntington's disease transgenic mice prior to the onset of motor symptoms. *Neuroscience.* (123):967-981.

Hepler JR, Gilman AG (**1992**). G proteins. *Trends. Biochem. Sci.* (17):383-387.

Herenbrink CK, Sykes DA, Donthamsetti P, Canals M, Coudrat T, Shonberg J, Scammells PJ, Capuano B, Sexton PM, Charlton SJ, Javitch JA, Christopoulos A, Lane RJ (**2016**). The role of kinetic context in apparent biased agonism at GPCRs. *Nat. Commun.* (7):10842.

Herlitze S, Garcia DE, Mackie K, Hille B, Scheuer T, Catterall WA (**1996**). Modulation of Ca2+ channels by G-protein beta gamma subunits. *Nature.* (380):258-262.

Hilairet S, Foord SM, Marshall FH, Bouvier M (**2001a**). Protein–protein interaction and not glycosylation determines the binding selectivity of heterodimers between the calcitonin receptor-like receptor and the receptor activity-modifying proteins. *J. Biol. Chem*. (276):29575-29581.

Hilairet S, Belanger C, Bertrand J, Laperriere A, Foord SM, Bouvier M (**2001b**). Agonist-promoted internalization of a ternary complex between calcitonin receptor-like receptor (CRLR), receptor activity-modifying protein 1 (RAMP1) and beta-arrestin. *J. Biol. Chem*. (276):42182-42190.

Hill SJ (**2006**). G-protein-coupled receptors: past, present and future. *Br. J. Pharmacol.* (147):S27-37.

Hill SJ, May LT, Kellam B, Woolard J (**2014**). Allosteric interactions at adenosine A(1) and A(3) receptors: new insights into the role of small molecules and receptor dimerization. *Br. J. Pharmacol.* (171):1102-1113.

Hirata T, Kakizuka A, Ushikubi F, Fuse I, Okuma M, Narumiya S (**1994**). Arg60 to Leu mutation of the human thromboxane A2 receptor in a dominantly inherited bleeding disorder. *J. Clin. Invest.* (94):1662-1667.

Hirsch JA, Schubert C, Gurevich VV, Singler PB (**1999**). The 2.8 A crystal structure of visual arrestin: a model for arrestin's regulation. *Cell.* (97):257-269.

Hochhauser E, Leshem D, Kaminski O, Cheporko Y, Vidne BA, Shainberg A (**2007**). The protective effect of prior ischemia reperfusion adenosine A1 or A3 receptor activation in the normal and hypertrophied heart. *Interact. Cardiovasc. Thorac. Surg.* (6):363-368.

Hoffman G, Garrison TR, Dohlman, HG (**2002**). Analysis of RGS proteins in Saccharomyces cerevisiae. *Methods. Enzymol*. (344):617-631.

Hollenstein K, Kean J, Bortolato A Cheng RK, Doré AS, Jazayeri A, Cooke RM, Weir M, Marshal FH (**2013**). Structure of class b GPCR corticotropin-releasing factor receptor 1. *Nature.* (499):438-443.

Holmes D, Campbell M, Harbinson M, Bell D (**2013**). Protective effects of intermedin on cardiovascular, pulmonary and renal disease: comparison with adrenomedullin and CGRP. *Curr. Protein. Pept. Sci.* (14):294-329.

Hong Y, Hay DL, Quirion R, Poyner DR (**2012**). The pharmacology of adrenomedullin 2/intermedin. *Br. J. Pharmacol.* (116):110-120.

Hu H, McCaw EA, Hebb AL, Gomez GT, Denovan-Wright EM (**2004**). Mutant huntingtin affects the rate of transcription of striatum-specific isoforms of phosphodiesterase 10A. *Eur. J. Neurosci.* (20):3351-3363.

Huang C, Miller RT (**2007**). The calcium-sensing receptor and its interacting proteins. *J. Cell. Mol. Med.* (11):923-934.

Huang CL, Slesinger PA, Casey PJ, Jan YN, Jan LY (**1995**)**.** Evidence that direct binding of G beta gamma to the GIRK1 G protein-gated inwardly rectifying K+ channel is important for channel activation. *Neuron.* (15):1133-1143.

Huang L, Zhou JG, Zhang Y, Wang F, Wang Y, Liu DH, Li XJ, Jin SH, Bai YJ, Ma H (**2017**). Opioid-induced constipation relief of fixed-ratio combination prolonged-release oxycodone/naloxone compared with oxycodone and morphine for chronic non-malignant pain: A systematic review and meta-analysis of randomized controlled trials. *J. Pain. Symptom. Manage.* Doi: 10.1016/j.jpainsymman.2017.07.025.

Huang LJ, Taylor SS (**1998**). Dissecting cAMP binding domain A in the R^1 α subunit of cAMP-dependent protein kinase. *J. Biol. Chem.* (273):26739-26746.

Huang W, Manglik A, Venkatakrishnan AJ, Laeremans T, Feinberg EN, Sanborn AL, Kato HE, Livingston KE, Thorsen TS, Kling RC, Granier S, Gmeiner P, Husbands SM, Traynor JR, Weis WI, Steyaert, Dror RO, Kobilka BK (**2015**). Structural insights into μ-opioid receptor activation. *Nature.* (524):315-321.

Husmann K, Sexton PM, Fischer JA, Born W (**2000**). Mouse receptor- activity-modifying proteins 1, -2 and -3: amino acid sequence, expression and function. *Mol. Cell. Endocrinol.* (162):35-43.

Hussain S, Shearer TW, Crossin CE (**2007**). Mechanisms linking adenosine A1 receptors and extracellular signal-regulated kinase 1/2 activation in human trabecular meshwork cells. *J. Pharmacol. Exp. Ther.* (320):258-265.

Hutchinson SA, Baker SP, Scammells PJ (**1999**). Adenosine receptor ligands with oxygenated N^6-substituents. *Bioorg. Med. Chem. Lett.* (9):933-936.

Hwa J, Garriga P, Liu X, Khorana HG (**1997**). Structure and function in rhodopsin: packing of the helices in the transmembrane domain and folding to a tertiary structure in the intradiscal domain are coupled. *Proc. Natl. Acad. Sci. USA.* (94):10571-10576.

Iannone R, Miele L, Maiolino P, Pinto A, Morello S (**2013**). Blockade of A2b adenosine receptor reduces tumour growth and immune suppression mediated by myeloid-derived suppressor cells in a mouse model of melanoma. *Neoplasia.* (15):1400-1409.

Ibrisimovic E, Drobny H, Yang Q, Höfer T, Boehm S, Nanoff C, Schicker K (**2012**). Constitutive activity of the A2A adenosine receptor and compartmentalised cyclic AMP signalling fine-tune noradrenaline release. *Purinergic. Signal.* (8):677-692.

Itoh Y, Cai K, Khorana HG (**2001**). Mapping of contact sites in complex formation between light-activated rhodopsin and transducing by covalent crosslinking: use of a chemically preactivated reagent. *Proc. Natl. Acad. Sci. USA.* (98):4883-4887.

Iwami G, Kawabe J, Ebina T, Cannon PJ, Homey CJ, Ishikawa Y (**1995**). Regulation of adenylyl cyclase by Protein Kinase A. *J. Biol. Chem.* (270):12481-12484.

Jacobson KA, Gao ZG (**2006**). Adenosine receptors as therapeutic targets. *Nat. Rev. Drug. Discov.* (5):247-264.

Jacobson KA (**2009**). Introduction to adenosine receptors as therapeutic targets. *Handb. Exp. Pharmacol.* (193):1-24.

Jacques-Silva MC, Barnardi A, Rodnight R, Lenz G (**2004**). ERK, PKC and PI3K/Akt pathways mediate extracellular ATP and adenosine-induced proliferation of U138-MG human glioma cell line. *Oncology*. (67):450-459.

Jajoo S, Mukherjea D, Kumar S, Sheth A, Kaur T, Rybak LP, Ramkumar V (**2010**). Role of β-arrestin1/ERK MAP kinase pathway in regulating adenosine A_1 receptor desensitization and recovery. *Am. J. Physiol. Cell. Physiol.* (298):56-65.

Janes K, Symons-Liguori AM, Jacobson KA, Salvemini D (**2016**). Identification of A3 adenosine receptor agonists as novel non-narcotic analgesics. *Br. J. Pharmacol.* (173):1253-1267.

Janz JM, Farrens DL (**2004**). Rhodopsin activation exposes a key hydrophobic binding site for the transducing alpha-subunit C terminus. *J. Biol. Chem*. (279):29767-29773.

Jazayeri A, Rappas M, Brown AJH, Kean J, Errey JC, Robertson NJ, Fiez-Vandal C, Andrews SP, Congreve M, Bortolata A, Mason JS, Baig AH, Teobald I, Doré AS, Weir M, Cooke RM, Marshall FH (**2017**). Crystal structure of the GLP-1 receptor bound to a peptide agonist. *Nature.* (546):254-258.

Joost P, Methner A (**2002**). Phylogenetic analysis of 277 G protein-coupled receptors as a tool for the prediction of orphan receptor ligands. *Genome. Biol.* (3):RESEARCH 0063.

Kamiya T, Saitoh O, Yoshioka K, Nakata H (**2003**). Oligomerization of adenosine A2A and dopamine D2 receptors in living cells. *Biochem. Biophys. Res. Commun.* (306):544-549.

Kang DS, Kern RC, Puthenveedu MA, von Zastrow M, Williams JC, Benovic JL (**2009**). Structure of an arrestin2-clatrin complex reveals a novel clathrin binding domain that modulates receptor trafficking. *J. Biol. Chem.* (284):29860-29872.

Kang Y, Zhou E, Gao X, He Y, Liu W, Ishchenko A, Barty A, White TA, Yefanov O, Han GW, Xu Q, de Waal PW, Ke J, Tan MHE, Zhang C, Moeller A, West GM, Pascal BD, van Eps, N, Caro LN, Vishnivetskiy SA, Lee RJ, Sunio-Powell KM, Gu X, Pal K Ma j, Zhi X, Boutet S, Williams GJ, Messerschmidt M, Gati C, Zatsepin NA, Wang D, James D, Basu S, Roy-Chowdhury S, Conrad CE, Coe J, Liu H, Lisova S, Kupitz C, Grotjohann I, Fromme R, Jiang Y, Tan M, Yang H, Li J, Wang M, Zheng Z, Li D, Howe N, Zhao Y, Standfuss J, Diederichs K, Dong Y, Potter CS, Carragher B, Caffert M, Jiang H, Chapman HN, Spence JCH, Fromme P, Weierstall U, Ernst OP, Katritch V, Gurevich VV, Griffin PR, Hubbell WL, Stevens RC, Cherezov V, Melcher K, Xu HE (**2015**). Crystal structure of rhodopsin bound to arrestin by femtosecond X-ray laser. *Nature.* (523):561-567.

Karoor V, Malbon CC (**1996**). Insulin-like growth factor receptor-1 stimulates phosphorylation of the beta2-adrenergic receptor in vivo on sites distinct from those phosphorylated in response to insulin. *J. Biol. Chem.* (271):29347-29351.

Karoor V, Wang L, Wang HY, Malbon CC (**1998**). Insulin stimulates sequestration of beta-adrenergic receptors and enhanced association of beta-adrenergic receptors with grb2 via tyrosine 350. *J. Biol. Chem.* (273):33035-33041.

Kehler J, Ritzen A, Lannggård M, Petersen SL, Farah MM, Bundgaard C, Christoffersen CT, Nielsen J, Kilburn JP (**2011**). Triazoloquinazolines as a novel class of phosphodiesterase 10A (PDE10A) inhibitors. *Bioorg. Med. Chem. Lett.* (21):3738-3742.

Kenakin T (**2004**). Principles: receptor theory in pharmacology. *Trends. Pharmacol. Sci.* (25):186-192.

Kenakin T, Watson C, Muniz-Medina, Christopoulos A, Novick S (**2012**). A simple method for quantifying functional selectivity and agonist bias. *ACS. Chem. Neurosci.* (3):193-203.

Kieffer TJ, McIntosh CG, Pederson RA (**1995**). Degradation of glucose-dependent insulinotropic polypeptide and truncated glucagon-like peptide 1 in vitro and in vivo by dipeptidyl peptidase IV. *Endocrincology*. (136):3585-3596.

Kim D (**1991**). Calcitonin-gene-related-peptide activates the muscarinic gated K^+ current in atrial cells. *Pflugers. Arch.* (418):338-345.

Kim YC, Ji XD, Jacobson KA (**1996**). Derivatives of the triazoloquinazolines adenosine antagonist (CGS15943) are selective for the human A_3 receptor subtype. *J. Med. Chem*. (39):4142-4148.

Kim YC, de Zwart M, Chang L, Moro S, von Frijtag Drabbe Künzel JK, Melman N, IJzerman AP, Jacobson KA (**1998**). Derivatives of the triazoloquinazoline adenosine antagonist (CGS15943) having high potency at the human A_{2B} and A_3 receptor subtypes. *J. Med. Chem*. (41):2835-2845.

Kim YM, Benovic JL (**2002**). Differential role of arrestin-2 interaction with clathrin and adaptor protein 2 in G protein-coupled receptor trafficking. *J. Biol. Chem.* (277):30760-30768.

Klein-Seetharaman J, Hwa J, Cai K, Altenbach C, Hubbell WL, Khorana HG (**2001**). Probing the dark state tertiary structure in the cytoplasmic domain of rhodopsin: Proximities between amino acids deduced from spontaneous disulfide bond formation between cys316 and engineered cysteines in cytoplasmic loop 1. *Biochemistry*. (40):12472-12478.

Kleinau G, Jaeschke H, Worth CL, Mueller S, Gonzalez J, Paschke R, Krause G (**2010**). Principles and determinants of the G protein coupling by the Rhodopsin-like thyrotropin receptor. *PLoS One.* (5):e9745.

Knight A, Hemmings JL, Winfield I, Leuenberger M, Frattini E, Frenguelli BG, Dowell SJ, Lochner M, Ladds G (**2016**). Discovery of novel adenosine receptor agonists that exhibit subtype selectivity. *J. Med. Chem.* (59):947-964.

Kobilka BK, Deupi X (**2007**). Conformational complexity of G-protein-coupled receptors. *Trends. Pharmacol. Sci.* (28):397-406.

Koole C, Wootten D, Simms J, Valant C, Sridhar R, Woodman OL, Miller LJ, Summers J, Christopoulos A, Sexton PM (**2010**). Allosteric ligands of the glucagon-like peptide 1 receptor (GLP-1R) differentially modulate endogenous and exogenous peptide responses in a pathway-selective manner: Implications for drug screening. *Mol. Pharmacol*. (78):456–465.

Kranenberg O, Moolenaar WH (**2001**). Ras-MAP kinase signaling by lysophospatidic acid and other G protein-coupled receptor agonists. *Oncogene*. (20):1540-1546.

Krishnan A, Sällamn M, Almén R, Fredriksson R, Schiöth HB (**2012**). The origin of GPCRs: identification of mammalian like Rhodopsin, Adhesion, Glutamate and Frizzled GPCRs in fungi. *PLoS One.* (7):e29817.

Krupnick JG, Goodman OB, Keen Jr. JH, Benovic JL (**1997**). Arrestin/clathrin interaction, Localization of the clathrin binding domain of nonvisual arrestins to the carboxy terminus. *J. Biol. Chem.* (272):15011-15016.

Kruse AC, Ring AM, Manglik A, Hu J, Hu K, Eitel K, Hübner H, Pardon E, Valant C, Sexton PM, Christopoulos A, Felder CC, Gmeiner P, Steyaert J, Weis WI, Garcia KC, Wess J, Kobilka BK (**2013**). Activation and allosteric modulation of a muscarinic acetylcholine receptor. *Nature.* (504):101-106.

Kuliopulos A, Covic L (**2003**). Blocking receptors on the inside: pepducin-based intervention of PAR signaling and thrombosis. *Life. Sci.* (74):255-262.

Kull B, Svenningsson P, Fredholm BB (**2000**). Adenosine A_{2A} receptors are co-localized with and activate G_{olf} in rat striatum. *Mol. Pharmacol*. (58):771-777.

Kuwasako K, Shimekake Y, Masuda M, Nakahara K, Yoshida T, Kitaura M, Kitamura K, Eto T, Sakata T (**2000**). Visualization of the calcitonin receptor-like receptor and its receptor activity-modifying proteins during internalization and recycling. *J. Biol. Chem.* (275):29602–29609.

Kuwasako K, Kitamura K, Nagoshi Y, Eto T (**2003**). Novel calcitonin-(8-32)-sensitive adrenomedullin receptors derived from co-expression of calcitonin receptor with receptor activity-modifying proteins. *Biochem. Biophys. Res. Commun.* (301):460-464.

Kuwasako K, Cao YN, Nagoshi Y, Tsuruda T, Kitamura K, Eto T (**2004**). Characterization of the human calcitonin gene-related peptide receptor subtypes associated with receptor activity-modifying proteins. *Mol. Pharmacol.* (65):207-213.

Kuwasako K, Cao Y-N, Chu C-P, Iwatsubo S, Eto T, Kitamura K (**2006**). Functions of the cytoplasmic tails of the human receptor activity-modifying protein components of calcitonin gene-related peptide and adrenomedullin receptors. *J. Biol. Chem.* (281):7205–7213.

Kuwasako K, Kitamura K, Nagata S, Hikosaka T, Kato J (**2010**). Function of the cytoplasmic tail of human calcitonin receptor-like receptor in complex with receptor activity-modifying protein 2. *Biochem. Biophys. Res. Commun.* (392):380-385.

Ladds G, Davis K, Das A, Davey J (**2005a**). A constitutively active GPCR retains its G protein specificity and the ability to form dimers. *Mol. Microbiol.* (55):482-497.

Ladds G, Goddard A, Davey J (**2005b**). Functional analysis of heterologous GPCR signalling pathways in yeast. *Trends. Biotechnol.* (23):367-373.

Lambright DG, Noel JP, Hamm HE, Siegler PB (**1994**). Structural determinants for activation of the alpha-subunit of a heterotrimeric G protein. *Nature*. (369):612-628.

Langley JN (**1905**). On the reaction of cells and of nerve-endings to certain poisons chiefly as regards the reaction of striated muscle to nicotine and to curari. *J. Physiol.* (33):374-413.

Laporte SA, Oakley RH, Zhang J, Holt JA, Ferguson SS, Caron MG, Barak LS (**1999**). The β2-adrenergic receptor/beta-arrestin complex recruits the clathrin adaptor AP-2 during endocytosis. *Proc. Natl. Acad. Sci. USA.* (96):3712-3717.

Laporte SA, Oakley RH, Holt JA, Barak LS, Caron MG (**2000**). The interaction of β-arrestin with the AP-2 adapter is required for the clustering of β2-adrenergic receptor into clathrin-coated pits. *J. Biol. Chem.* (275):23120-23126.

Lebon G, Warne T, Edwards PC, Bennett K, Langmead CJ, Leslie AGW, Tate CG (**2011**). Agonist-bound adenosine A2A receptor structures reveal common features of GPCR activation. *Nature*. (474):521-525.

Lee CF, Chern Y (**2014**). Adenosine receptors and Huntington's disease. *Int. Rev. Neurobiol.* (119):195-232.

Lee HT, Gallos G, Nasr SH, Emala CW (**2004**). A1 adenosine activation inhibits inflammation, necrosis and apoptosis after renal ischemia-reperfusion injury in mice. *J. Am. Soc. Nephrol.* (15):102-111.

Lefkowitz RJ, Hausdorff WP, Caron MG (**1990**). Role of phosphorylation in desentization of the beta-adrenoceptor. *Trends. Pharmacol. Sci.* (11):190-194.

Lefkowitz RJ (**2005**). Transduction of receptor signals by β-arrestins. *Science.* (308):512-517.

Lei Q, Jones MB, Talley EM, Garrison JC, Bayliss DA (**2003**). Molecular mechanisms mediating inhibition of G protein-coupled inwardly rectifying K^+ channels. *Mol. Cells.* (15):1-9.

Lenhart OM, Broselid S, Barrick CJ, Leeb-Lundberg LMF, Caron KM (**2013**). G-protein coupled receptor 30 interacts with receptor activity modifying protein 3 and confers sex-dependent cardioprotection. *J. Mol. Endocrinol*. (51):191-202.

Leuthauser K, Gujer R, Aldecoa A, McKinney RA, Muff R, Fischer JA, Born W (**2000**). Receptor-activity-modifying protein 1 forms heterodimers with two G-protein-coupled receptors to define ligand recognition. *Biochem. J.* (351): 347-351.

Leuti A, Laurenti D, Giampà C, Montagna E, Dato C, Anzilotti S, Melone MA, Bernardi G, Fusco FR (**2013**). Phosphodiesterase 10A (PDE10A) localization in the R6/2 mouse model of Huntington's disease. *Neurobiol. Dis.* (52):104-116.

Lin JT, Chang WC, Chen HM, Lai HL, Chen CY, Tao MH, Chern Y (**2013**). Regulation of feedback between protein kinase A and the proteasome system worsens Huntington's disease. *Mol. Cell. Biol.* (33):1073-1084.

Linden J, Thai T, Figler H, Jin X, Robeva AS (**1999**). Characterization of the human A(2B) adenosine receptors: radioligand binding, western blotting and coupling to G(q) in human embryonic kidney 293 cells and HMC-1 mast cells. *Mol. Pharmacol*. (65):705-713.

Liu B, Wu D (**2003**). The first inner loop of endothelin receptor type B is necessary for specific coupling to $G\alpha_{13}$. *J. Biol. Chem.* (278):2384-2387.

Liu J, Conklon BR, Blin N, Yun J, Wess J (**1995**). Identification of a receptor G-protein contact site critical for signaling specificity and G-protein activation. *Proc. Natl. Acad. Sci. USA.* (92):11642-11646.

Logothetis DE, Kurachi Y, Galper J, Neer EJ, Clapham DE (**1987**). The βγ subunity of GTP-binding proteins activate the muscarininc K+ channel in heart. *Nature.* (325):321-326.

Lohse MJ, Benovic JL, Codina J, Caron MG, Lefkowitz RJ (**1990**). β-arrestin: a protein that regulates β-adrenergic receptor function. *Science.* (248):1547-1550.

Lohse MJ (**2010**). Dimerization in GPCR mobility and signaling. *Curr. Opin. Pharmacol.* (10):53-58.

Lüscher C, Slesinger PA (**2010**) Emerging roles for G protein-gated inwardly rectifying potassium (GIRK) channels in health and disease. *Nature. Rev. Neurosci.* (11):301-315.

Lynge J, Hellsten Y (**2000**). Distribution of adenosine A1, A2A and A2B receptors in human skeletal muscle. *Acta. Physiol. Scand.* (169):283-290.

Main MJ, Brown J, Brown S, Fraser NJ, Foord SM (**1998**). The CGRP receptor can couple via pertussis toxin sensitive and insensitive G proteins. *FEBS. Lett.* (441):6-10.

Marcellino D, Carriba P, Filip M, Borgkvist A, Frankowska M, Beelido I, Tanganelli S, Müller CE, Fisone G, Lluis C, Agnati LF, Franco R, Fuxe K (**2008**). Antagonistic cannabinoid CB1/dopamine D2 receptor interactions in striatal CB1/D2 heteromers. A combined neurochemical and behavioural analysis. *Neuropharmacol.* (54):815-823.

Marchese A, Paing MM, Temple BRS, Trejo J (**2008**). G protein-coupled receptor sorting to endosomes and lysosomes. *Ann. Rev. Pharmacol. Toxicol.* (48):601-629.

Martinez-Mir MI, Probst A, Palacios JM (**1991**). Adenosine A2 receptors: selective localization in the human basal ganglia and alterations with disease. *Neuroscience*. (42):697-706.

Massie BM, O'Connor CM, Metra M, Ponikowski P, Teerlink JR, Cotter G, Weatherley BD, Cleland JG, Givertz MM, Voors A, DeLucca P, Mansoor GA, Salerno CM, Bloomfield DM, Dittrich HC, PROTECT investigators and committees (**2010**). Rolofylline, an adenosine A1-receptor antagonist, in acute heart failure. *N. Eng. J. Med.* (363):1419-1428.

McCudden CR, Hains MD, Kimple RJ, Siderovski DP, Willard FS (**2005**). G-protein signalling: back to the future. *Cell. Mol. Life. Sci.* (62):551-577.

McLatchie LM, Fraser NJ, Main MJ, Wise A, Brown J, Thompson N, Solari R, Lee MG, Foord SM (**1998**). RAMPs regulate the transport and ligand specificity of the calcitonin-receptor-like receptor. *Nature.* (393):333–339.

Mehta PK, Griendling KK (**2007**). Angiotensin II cell signaling: physiological and pathological effects in the cardiovascular system. *Am. J. Physiol.* (292):C82-97.

Mentlein R, Gallwitz B, Schmidt WE (**1993**). Dipeptidyl-peptidase IV hydrolyses gastric inhibitory polypeptide, glucagon-like peptide-1(7-36)amide, peptide histidine methionine and is responsible for their degradation in human serum. *Eur. J. Biochem.* (214):829-835.

Migita H, Kominami K, Higashida M, Maruyama R, Tuchida N, McDonald F, Shimada F, Sakurada K (**2008**). Activation of adenosine A_1 receptor-induced neural stem cell proliferation via MEK/ERK and Akt signaling pathways. *J. Neurosci. Res.* (86):2820-2828.

Mika D, Leroy J, Vandecasteele G, Fischmeister R (**2012**). PDEs create local domains of cAMP signaling. *J. Mol. Cell. Cardiol.* (52):323-329.

Milde M, Rinne A, Wunder F, Engelhardt S, Bünemann M (**2013**). Dynamics of Gαi1 interaction with type 5 adenylate cyclase reveal the molecular basis for high sensitivity of Gi-mediated inhibition of cAMP production. *Biochem. J.* (454):515-523.

Milligan G, Canal M, Pediani JD, Ellis J, Lopez-Gimenez JF (**2007**). The role of GPCR dimerisation/oligmerisation in receptor signalling. *Ernst Schering. Found. Symp. Proc.* (2):145-162.

Milligan G (**2009**). G protein-coupled receptor hetero-dimerization: contribution to pharmacology and function. *Br. J. Pharmacol.* (158):5-14.

Mittal D, Sinha D, Barakauskas D, Young A, Kalimutho M, Stannard K, Caramia F, Haibe-Kains B, Stagg J, Khanna KK, Loi S, Smyth MJ (**2016**). Adenosine A2B receptor expression on cancer cells promotes metastasis. *Cancer. Res.* (76):4372-4382.

Morelli M, Di Paolo T, Wardas J, Calan F, Xiao D, Schwarzschild MA (**2007**). Role of adenosine A2A receptors in parkinsonian motor impairment and l-DOPA-induced motor complications. *Prog. Neurobiol.* (83):293-309.

Morello S, Miele L (**2014**). Targeting the adenosine A2b receptor in the tumor microenvironment overcomes local immunosuppression by myeloid-derived suppressor cells. *Oncoimmunology.* (14):3e27989.

Morfis M, Tilakarante N, Furness SG, Christopoulos G, Werry TD, Christopoulos A, Sexton PM (**2008**). Receptor Activity-Modifying Proteins Differentially Modulate the G Protein-Coupling Efficiency of Amylin Receptors. *Endocrinology.* (11):5423-5431.

Mustain WC, Rychahou PG, Evers BM (**2011**). The role of neurotensin in physiologic and pathologic processes. *Curr. Opin. Endocrinol. Diabetes. Obes.* (18):75-82.

Nag K, Kato A, Nakada T, Hoshijima K, Mistry AC, Takei Y, Hirose S (**2006**). Molecular and functional characterization of adrenomedullin receptors in pufferfish. *Am. J. Physiol. Regul. Integr. Comp. Physiol*. (290):R467-R478.

Nell PG, Albrecht-Küpper B (**2009**). The adenosine A_1 receptor and its ligands. *Prog. Med. Chem*. (47):163−201.

Ntantie E, Gonyo P, Lorimer EL, Hauser AD, Schuld N, McAllister D, Kalyanaraman B, Dwinell MB, Auchampach JA, Williams CL (**2013**). An adenosine-mediated signalling pathways suppresses prenylation of the GTPase Rap1B and promotes cell scattering. *Sci. Signal.* (6):ra39.

Ochaion A, Bar-Yehuda S, Cohen S, Barer F, Patoka R, Amital H, Reitblat T, Reitblat A, Ophir J, Konfino I, Chower Y, Ben-Horin S, Fishman P (**2009**). The anti-inflammatory target A(3) adenosine receptor is over-expressed in rheumatoid arthritis, psoriasis and Crohn's disease. *Cell. Immunol.* (258):115-122.

Ohta A, Gorelik E, Prasad SJ, Ronchese F, Lukashev D, Wong MK, Huang X, Caldwell S, Liu K, Smith P, Chen JF, Jackson EK, Apasov S, Abrams S, Sitkovsky M (**2006**). A2A adenosine receptor protects tumours from antitumor T cells. *Proc. Natl. Acad. Sci. USA.* (103):13132-13137.

Olah ME, Jacobson KA, Stiles GL (**1994**). Role of the second extracellular loop of adenosine receptors in agonist and antagonist binding. Analysis of chimeric A1/A3 adenosine receptors. *J. Biol. Chem*. (269):24692-24698.

Oliveira RF, Terrin A, Di Benedetto G, Cannon RC, Koh W, Kim M, Zaccolo M, Blackwell KT (**2010**). The role of type 4 phosphodiesterases in generating microdomains of cAMP: large scale stochastic simulations. *PLoS One.* (5):e11725.

Ongini E, Dionisotti S, Gessi S, Irenius E, Fredholm BB (**1999**). Comparison of CGS15943, ZM 241385 and SCH 58261 as anatagonists at the human adenosine receptors. *Naunyn. Schmiedebergs. Arch. Pharmacol.* (359):7-10.

Ongini E, Monopoli A, Cacciari B, Baraldi PG (**2001**). Selective adenosine A2A receptor antagonists. *Farmaco.* (56):87-90.

Paing MM, Temple BRS, Trejo J (**2004**). A tyrosine-based sorting signal regulates intracellular trafficking of protease-activated receptor-1: multiple mechanisms for agonist-induced G protein-coupled receptor internalization. *J. Biol. Chem.* (279):21938-21947.

Palczewski K, Kumasaka T, Hori T, Behnke CA, Motoshima H, Fox BA, Le Trong I, Okada T, Stenkamp RE, Yamamoto M, Miyano M (**2000**). Crystal structure of rhodopsin: a G protein-coupled receptor. *Science.* (289):739-745.

Peleg S, Varon D, Ivanina T, Dessauer CW, Dascal N (**2002**). G(alpha)(i) controls the gating of the G protein-activated K(+) channel, GIRK. *Neuron*. (33):87-99.

Perez P, Rincón SA (**2010**). Rho GTPases: regulation of cell polarity and growth in yeasts. *Biochem. J.* (426):243-253.

Permpoonputtana K, Porter JE, Govitrapong P (**2016**). Calcitonin gene-related-peptide mediates an inflammatory response in Schwann cells via cAMP-dependent ERK signalling cascade. *Life. Sci.* (144):19-25.

Peterfreund RA, MacCollin M, Gusella J, Fink JS (**1996**). Characterization and expression of the human A2a adenosine receptor gene. *J. Neurochem.* (66):362-368.

Petrelli R, Torquati I, Kachler S, Luongo L, Maione S, Franchetti P, Grifantini M, Novellino E, Lavecchia A, Klotz KN, Cappellacci L (**2015**). 5′-C-Ethyl-tetrazolyl-N^6-substituted adenosine and 2-chloro-adenosine derivatives as highly potent dual acting A_1 adenosine receptor agonists and A_3 adenosine receptor antagonists. *J. Med. Chem*. (58):2560−2566.

Pierce KL, Luttrell LM, Lefkowitz RJ (**2001**). New mechanisms in heptahelical receptor signaling to mitogen activated Protein Kinase Cascades. *Oncogene*. (20):1532-1539.

Pradhan AA, Walwyn W, Nozaki C, Filliol D, Erbs E, Matifas A, Evans C, Kieffer BL (**2010**). Ligand-directed trafficking of the μ-opioid receptor in vivo: two paths toward analgesic tolerance. *Neurosci. J.* (30):16459-16468.

Pradhan AA, Smith ML, Kieffer BL, Evans CJ (**2012**). Ligand-directed signaling within the opioid receptor family. *Br. J. Pharmacol.* (167):960-969.

Poyner DR, Sexton PM, Marshal I, Smith DM, Quirion R, Born W, Muff R, Fischer JA, Foord SM (**2002**). International union of pharmacology. XXXII. The Mammalian Calcitonin Gene-Related Peptides, Adrenomedullin, Amylin and Calcitonin receptors. *Pharmacol. Rev.* (54):233-246.

Qi T, Ly K, Poyner DR, Christopoulos G, Sexton PM, Hay DL (**2011**). Structure-function analysis of amino acid 74 of human RAMP1 and RAMP3 and its role in peptide interactions with adrenomedullin and calcitonin gene-related peptide receptors. *Peptides.* (32):1060-1067.

Qi YF, Shi YR, Bu DF, Pang YZ, Tang CS (**2003**)**.** Changes of adrenomedullin and receptor activity modifying protein 2 (RAMP2) in myocardium and aorta in rats with isoproterenol-induced myocardial ischemia. *Peptides.* (24):463–468.

Qin CX, May LT, Li R, Cao N, Rosli S, Deo M, Alexander AE, Horlock D, Bourke JE, Yang YH, Stewart AG, Kaye DM, Du XJ, Sexton PM, Christopoulos A, Gao XM, Ritchie RH (**2017**). Small-molecule-biased formyl peptide receptor agonist compound 17b protects against myocardial ischemia-reperfusion injury in mice. *Nature. Commun*. (8):14232-14245.

Raehal KM, Walker JK, Bohn LM (**2005**). Morphine side effects in β-arresin 2 knockout mice. *J. Pharmacol. Exp. Ther.* (314):1195-1201.

Rajagopal S, Ahn S, Rominger DH, Gowen-MacDonald W, Lam CW, Dewire SM, Violin JD, Lefkowitz RJ (**2011**). Quantifying ligand bias at seven-transmembrane receptors. *Mol. Pharmacol.* (80):367:377.

Randazzo PA, Kahn RA (**1994**). GTP hydrolysis by ADP-ribosylation factor is dependent on both an ADP-ribosylation factor GTPase-activating protein and acids phospholipids. *J. Biol. Chem.* (269):10758-10763.

Rawal N, Wattwil M (**1984**). Respiratory depression after epidural morphine-an experimental and clinical study. *Anesth. Analg.* (63):8-14.

Rich TC, Fagan KA, Tse TE, Schaack J, Cooper DM, Karpen JW (**2001**). A uniform extracellular stimulus triggers distinct cAMP signals in different compartments of a simple cell. *Proc. Natl. Acad. Sci. USA.* (98):13049-13054.

Rich TC, Xin W, Methats C, Hassell KA, Pigott LA, Le X, Karpen JW, Conti M (**2007**). Cellular mechanisms underlying prostaglandin-induced transient cAMP signals near the plasma membrane of HEK-293 cells. *Am. J. Physio. Cell. Physiol.* (292):C319-C331.

Rittiner JE, Korboukh I, Hull-Ryde EA, Jin J, Janzen WP, Frye SV, Zylka MJ (**2012**). AMP is an Adenosine A_1 receptor agonist. *J. Biol. Chem.* (287):5301-5309.

Rivero-Müller A, Jonas KC, Hanyaloglu AC, Huhtaniemi I (**2013**). Di/oligomerization of GPCRs - mechanisms and functional significance. *Prog. Mol. Biol. Tnsl. Sci.* (117):163-185.

Robeiro JA, Sebastiao AM (**2010**). Caffeine and adenosine. *J. Alzheimers. Dis.* (20):S1-15.

Roh J, Chang CL, Bhalla A, Klein C, Hsu SY (**2004**). Intermedin is a calcitonin/calcitonin gene-related peptide family peptide acting through the calcitonin receptor-like receptor/receptor activity modifying protein receptor complexes. *J. Biol. Chem.* (279):7264-7274.

Rosin DL, Robeva A, Woodard RL, Guyenet PG, Linden J (**1998**). Immunohistochemical localization of adenosine A2A receptors in the rat central nervous system. *J. Comp. Neurol*. (401):163-186.

Rozenfeld R Devi LA (**2010**). Exploring a role for the heteromerization in GPCR signaling specificity. *Biochem. J.* (433):11-18.

Ru F, Surdenikova L, Bronzmanova M, Kollarik M (**2011**). Adenosine-induced activation of esophageal nociceptors. *Am. J. Physiol. Gastointest. Liver. Physiol.* (300):G485-493.

Rui L (**2014**). Energy metabolism in the liver. *Compr. Physiol.* (4):177-197.

Russo AF (**2015**). Calcitonin gene-related peptide (CGRP): a new target for migraine. *Ann. Rev. Pharmacol. Toxicol.* (55):533-552.

Sacarselli M, Donaldson JG (**2009**). Constitutive internalization of G protein-coupled receptors and G proteins via clathrin-independent endocytosis. *J. Biol. Chem.* (284):3577-3585.

Sachdeva S, Gupta M (**2013**). Adenosine and its receptors as therapeutic targets: an overview. *Saudi Pharm. J*. (21):245-253.

Samama P, Cotecchia S, Costa T, Lefkowitz RJ (**1993**). A mutation induced active state of the β_2-adrenergic receptor: Extending the ternary complex model. *J. Biol. Chem.* (268): 4625-4636.

Schmid EM, Ford MG, Burtey A, Praefcke GJ, Peak-Chew SY, Mills IG, Benmerah A, McMahon HT (**2006**). Role of the AP2 β-appendage hub in recruiting partners for clathrin-coated vesicle assembly. *PLoS Biol.* (4):1532-1548.

Schulte G, Fredholm BB (**2000**). Human adenosine A(1), A(2A), A(2B) and A(3) receptors expressed in Chinese hamster ovary cells all mediate the phosphorylation of extracellular-regulated kinase 1/2. *Mol. Pharmacol.* (58):477-482.

Seino S, Shibasaki T (**2005**). PKA-dependent and PKA-independent pathways for cAMP-regulated exocytosis. *Physiol. Rev.* (85):1303-1342.

Sexton PM, Albiston A, Morfis M, Tilakaratne N (**2001**). Receptor activity modifying proteins. *Cell. Signal*. (13):73–82.

Sexton PM, Poyner DR, Simms J, Christopoulos A, Hay DL (**2009**). Modulating receptor function through RAMPs: can they represent drug targets in themselves? *Drug. Discov. Today.* (14):413-419.

Shah SZA, Zhao D, Khan SH, Yang L (**2015**). Regulatory mechanisms of endoplasmic reticulum resident IP3 receptors. *J. Mol. Neurosci.* (56):938-948.

Sharma R, Engemann S, Sahota P, Thakkar MM (**2010**). Role of adenosine and wake-promoting basal forebrain in insomnia and associated sleep disruptions caused by ethanol dependence. *J. Neurochem*. (115):782–794.

Shearman LP, Weaver DR (**1997**). [125I]4-aminobenzyl-5'-N-methylcarboxamidoadenosine ((125I)AB-MECA) labels multiple adenosine receptor subtypes in rat brain. *Brain. Res.* (745):10-20.

Shenoy SK, Lefkowitz RJ (**2005**). Receptor regulation: beta-arrestin moves up a notch. *Nat. Cell. Biol.* (7):1159-1161.

Shenoy SK, Drake MT, Nelso CD, Houtz DA, Xiao K, Madabushi S, Reiter E, Premont RT, Lichtarge O, Lefkowitz RJ (**2006**). Beta-arrestin-dependent, G protein-independent ERK1/2 activation by the beta2 adrenergic receptor. *J. Biol. Chem.* (281):1267-1273.

Shenoy SK, Lefkowitz RJ (**2011**). β-arrestin-mediated receptor trafficking and signal transduction. *Trends. Pharmacol. Sci.* (32):521-533.

Shihoya W, Nishizawa T, Okuta A, Tani K, Dohmae N, Fujiyoshi Y, Doi T (**2016**). Activation mechanism of endothelin ETB receptor by endothelin-1. *Nature*. (537):363-368.

Shimekake Y, Nagat K, Ohta S, Kambayashi Y, Teraoka H, Kitamura K, Eto T, Kangawa K, Matsuo H (**1995**). Adrenomedullin stimulates two signal transduction pathways, cAMP accumulation and Ca^{2+} mobilization, in bovine aortic endothelial cells. *J. Biol. Chem.* (270):4412-4417.

Shin HK, Park SN, Hong KW (**2000**). Implications of adenosine A2A receptors in hypotension-induced vasodilation and cerebral blood flow autoregulation in rat pial arteries. *Life. Sci.* (67):1435-1445.

Shneyvays V, Zinman T, Shainberg A (**2004**). Analysis of calcium responses mediated by the A3 adenosine receptor in cultured newborn cardiac myocytes. *Cell. Calcium.* (36):387-396.

Siu FY, He M, de Graff C, Han GW, Yang D, Zhang Z, Zhou C, Xu Q, Wacker D, Joseph JS, Liu W, Lau J, Cherezov V, Katritch V, Wang MW, Stevens RC (**2013**). Structure of the class B human glucagon G protein coupled receptor. *Nature.* (499):444-449.

Sloop KW, Michael MD, Moyers JS (**2005**). Glucagon as a target for the treatment of type 2 diabetes. *Expert. Opin. Ther. Targets.* (9):593-600.

Sondek J, Bohm A, Lambright DG, Hamm HE, Sigler PB (**1996**). Crystal structure of a G-protein beta gamma dimer at 2.1A resolution. *Nature*. (379):369-374.

Song G, Yang D, Wang Y, de Graaf C, Zhou Q, Jiang S, Liu K, Cai X, Dai A, Lin G, Liu D, Wu F, Wu Y, Zhao S, Ye L, Han GW, Lau J, Wu B, Hanson MA, Liu ZJ, Wang MW, Stevens RC (**2017**). Human GLP-1 receptor transmembrane domain structure in complex with allosteric modulators. *Nature.* (546):312-315.

Sorrentino C, Miele L, Porta A, Pinto A, Morello S (**2015**). Myeloid-derived suppressor cells contribute to A2B adenosine receptor-induced VEGF production and angiogenesis in a mouse melanoma model. *Oncotarget.* (6):27478-27489.

Sounier R, Mas C, Steyaert J, Laeremans T, Mangalik A, Huang W, Konilka BK, Déméné H, Granier S (**2015**). Propagation of conformational changes during μ-opioid receptor activation. *Nature.* (524):375-378.

Srinivasan S, Lubrano-Berthelier C, Govaerts C, Picard F, Santiago P, Conklin BR, Vaisse C (**2004**). Constitutive activity of the melanocortin-4 receptor is maintained by its N-terminal domain and plays a role in energy homeostasis in humans. *J. Clin. Invest.* (114):1158-1164.

Stauss DP, Strachan RT, Manglik A, Pani B, Kahsai AW, KIM TH, Wingler LM, Ahn A, Chatterjee A, Masoudi A, Kruse AC, Pardon E, Steyaert J, Weis WI, Prosser RS, Kobilka BK, Coast T, Lefkowitz RJ (**2016**). Allosteric nanobodies reveal the dynamic range and diverse mechanisms of G-protein-coupled receptor activation. *Nature.* (535):448-452.

Stewart GD, Valant C, Dowell SJ, Mijaljica D, Devenish RJ, Scammells PJ, Sexton PM, Christopoulos A (**2009**). Determination of adenosine A1 receptor agonist and antagonist pharmacology using Saccharomyces cerevisiae: implications for ligand screening and functional selectivity. *J. Pharmacol. Exp. Ther.* (331): 277-286.

Sullivan GW (**2003**). Adenosine A2A receptor agonists as anti-inflammatory agents. *Curr. Opin. Investig. Drugs.* (4):131-1319.

Swaminath G, Xiang Y, Lee T-W, Steenhuis J, Parnot C, Kobilka BK (**2004**)**.** Sequential binding of agonists to the b2 adrenoceptor. Kinetic evidence for intermediate conformational states. *J. Biol. Chem.* (279):686–691.

Swaminath G, Deupi X, Lee T-W, Zhu W, Thian FS, Kobilka TS, Kobilka BK (**2005**). Probing the b2 adrenoceptor binding site with catechol reveals differences in binding and activation by agonists and partial agonists. *J. Biol. Chem*. (280):22165–22171.

Swift S, Leger AJ, Talavera J, Zhang L, Bohm A, Kuliopulos A (**2006**). Role of the PAR1 receptor 8^{th} helix in signaling. The 7-8-1 receptor activation mechanism. *J. Biol. Chem.* (281):4109-4116.

Tabor A, Weisenburger S, Banerjee A, Purkayastha N, Kaindl JM, Hübner H, Wei L, Grömer TW, Kornhuber J, Tschammer N, Birdsall NJM, Mashanov GI, Sandoghdar V, Gmeiner P (**2016**). Visualization and ligand-induced modulation of dopamine receptor dimerization at the single molecule level. *Sci. Rep.* (12):33233.

Takasaki J, Saito T, Taniguchi M, Kawasaki T, Moritani Y, Hayashi K, Kobori M (**2004**). A novel $G\alpha_{q/11}$ inhibitor. *J. Biol. Chem.* (279):47438-47445.

Takei Y, Inoue K, Ogoshi M, Kawahara T, Bannai H, Miyano S (**2004**). Identification of novel adrenomedullin in mammals: a potent cardiovascular and renal regulator. *FEBS. Lett.* (556): 53–58.

Tansey JT, Huml AM, Vogt R, Davis KE, Jones JM, Fraser KA, Brasaemle DL, Kimmel AR, Londos C (**2003**). Functional studies on native and mutated forms of perilipins: a role in protein kinase A-mediated lipolysis of triacylglycerols. *J. Biol. Chem.* (278):8401-8406.

Taylor JM, Neubig RR (**1994**). Peptides as probes for G-protein signal transducing. *Cell. Signal.* (6):841-849.

Terrin A, Di Benedetto G, Pertegato V, Cheung YF, Baillie G, Lynch MJ, Elvassore N, Prinz A, Herberg FW, Houslay MD, Zaccolo M (**2006**). PGE(1) stimulation of HEK293 cells generates multiple contiguous domains with different [cAMP]: role of compartmentalized phosphodiesterases. *J. Cell. Biol.* (175):441-451.

Thomas III TA, Dragas-Graonic S, Holmes R, Perez HD (**1995**). Signal transduction by the formyl peptide receptor. *J. Biol. Chem.* (270):28010-28013.

Torvinen M, Marcellino D, Canals M, Agnati LF, Lluis C, Franco R, Fuxe K (**2005**). Adenosine A2A receptor and dopamine D3 receptor interactions: evidence of functional A2A/D3 heteromeric complexes. *Mol. Pharmacol.* (67):400-407.

Totsune K, Takahashi K, Mackenzie HS, Murakami O, Arihara Z, Sone M, Mouri T, Renner BM, Ito S (**2000**)**.** Increased gene expression of adrenomedullin and adrenomedullin-receptor complexes, receptor-activity modifying protein (RAMP)2 and calcitonin-receptor-like receptor (CRLR) in the hearts of rats with congestive heart failure. *Clin. Sci.* (99):541–546.

Tyers M, Futcher B (**1993**). Far1 and Fus3 link the mating pheromone signal transduction pathway to three G1-phase Cdc28 kinase complexes. *Mol. Cell Biol.* (13):5659-5669.

Udawela M, Hay DL, Sexton P (**2004**). The receptor activity modifying family of G protein coupled receptor accessory proteins. *Semin. Cell. Dev. Biol.* (15): 299-308.

Udawela M, Christopoulos G, Morfis M, Christopoulos A, Ye S, Tilikarate N, Sexton PM (**2006a**). A critical role for the short intracellular C terminus in receptor activity-modifying protein function. *Mol. Pharmacol*. (70):1750-1760.

Udawela M, Christopoulos G, Tilakaratne N, Christopoulos A, Albiston A, Sexton P (**2006b**). Distinct Receptor Activity-Modifying Protein domains differentially modulate interaction with calcitonin receptors. *Mol. Pharmacol.* (69):1984-1989.

van Eps N, Caro LN, Morizumi T, Ernst OP (**2015**). Characterizing rhodopsin signaling by EPR spectroscopy: from structure to dynamics. *Photochem. Photobiol. Sci.* (14):1586-1597.

Varani K, Rigamonti D, Sipione S, Camurri A, Borea PA, Cattabeni F, Abbracchio MP, Cattaneo E (**2001**). Abberent amplification of A_{2A} receptor signaling in striatal cells expressing mutant huntingtin. *FASAB. J.* (15):1245-1247.

Venter JC, Adams MD, Myers EW, Li PW, Mural RJ, Sutton GG, Smith HO, Yandell M, Evans CA, Holt RA, Gocayne JD, Amanatides P, Ballew RM, Huson DH, Wortman, JR, Zhang Q, Kodira CD, Zheng XH, Chen L, Skupski M, Subramanian G, Thomas PD, Zhang J, Gabor Miklos GL, Nelson C, Broder S, Clark AG, Nadeau J, McKusick VA, Zinder N, Levine AJ, Roberts RJ, Simon M, Slayman C, Hunkapiller M, Bolanos R, Delcher A, Dew I, Fasulo D, Flanigan M, Florea L, Halpern A, Hannenhalli S, Kravitz S, Levy S, Mobarry C, Reinert K, Remington K, Abu-Threideh J, Beasley E, Biddick K, Bonazzi V, Brandon R, Cargill M, Chandramouilswaran I, Charlab R, Chaturvedi K, Deng Z, Di Francesco V, Dunn P, Eilbeck K, Evangelista C, Gabrielian AE, Gan W, Ge W, Gong F, Gu Z, Guan P, Heiman TJ, Higgins ME. Ji RR, KeZ, Ketchum KA, Lai Z, Lei Y, Li Z, Li J, Liang Y, Lin X, Lu F, Merkulov GV, Milshina N, Moore HM, Naik AK, Narayan VA, Neelam B, Nusskern D, Rusch DB, Salzberg S, Shao W, Shue B, Sun J, Wang Z, Wang A, Wang X, Wang J, Wei M, Wildes R, Xiao C, Yan C, Yao A, Ye J, Zhang M, Zhang W, Zhang H, Zhao Q, Zheng L, Zhong F, Zhong W, Zhu S, Zhao S, Gilbert D, Baumhueter S, Spier G, Carter C, Cravchik A, Woodage T, Ali F, An H, Awe A, Baldwin D, Baden H, Baumstead M, Barrow I, beeson K, Busam D, Carver A, Center A, Cheng ML, Curry L, Danaher S, Davenport L, Desilets R, Dietz S, Dodson K, Doup L, Ferriera S, Garg N, Gluecksmann A,

Hart B, Haynes J, Haynes C, Heiner C, Hladun S, Hostin D, Houck J, Howland T, Ibegwam C, Johnson J, Kalush F, Kline L, Koduru S, Love A, Mann F, May D, McCawley S, McIntosh T, McMullen I, Moy M, Moy L, Murphy B, Nelson K, Pfannkock C, Pratts E, Puri V, Qureshi H, Reardon M, Rodriguez R, Rogers YH, Romblad D, Ruhfel B, Scott R, Sitter C, Smallwood M, Stewart E, String R, Suh E, Thomas R, Tint HH, Tse S, Vech C, Wang G, Wetter J, Williams S, Williams M, Windsor S, Winn-Deen E, Wolfe K, Zaverl J, Zaveri K, April JF, Guigó R, Cambell MJ, Sjolander KV, Karlak B, Kejariwal A, Mi H, Lazareva B, Hatton T, Narechania A, Diemer K, Muruganujan A, Guo N, Sato S, Bafna V, Istrail S, Lippert R, Schwartz R, Walenz B, Yooseph S, Allen D, Basu A, Baxendale J, Blick L, Caminha M, Carnes-Stine J, Caulk P, Chiang YH, Coyne M, Dahlke C, Mays A, Dombroski M, Donnelly M, Ely D, Esparham S, Fosier C, Gire H, Glanowski S, Glasser K, Glodek A, Gorokhov M, Graham K, Gropman B, Harris M, Heil J, Handerson S, Hoover J, Jennings D, Jordan C, Jordan J, Kasha J, Kagan L, Kraft C, Levitsky A, Lewis M, Liu X, Lopez J, Ma D, Majoros W, McDaniel J, Murphy S, Newman M, Nguyen T, Nguyen N, Nodell M, Pan S, Peck J, Peterson M, Rowe W, Sanders R, Scott J, Simpson M, Smith T, Sprague A, Stockwell T, Turner R, Venter E, Wen M, Wu D, Wu M, Xia A, Zandieh A, Zhu X (**2001**). The sequence of the human genome. *Science*. (291):1304-1351.

Vilardaga JP, Jean-Alphonse FG, Gardella TJ (**2014**). Endosomal generation of cAMP in GPCR signaling. *Nat. Chem. Biol.* (10):700-706.

Villar-Menéndez I, Díaz-Sánchez S, Blanch M, Albasanz JL, Pereira-Veiga T, Monje A, Planchat LM, Ferrer I, Martín M, Barrachina M (**2014**). Reduced striatal adenosine A2A receptor levels define a molecular subgroup of schizophrenia. *J. Psychiatr. Res.* (51):49-59.

Violin JD, Crombie AL, Soergel DG, Lark MW (**2014**). Biased ligands at G-protein-coupled receptors: promise and progress. *Trends. Pharmacol. Sci.* (35):308-316.

Vohra S, Taddese B, Conner AC, Poyner DR, Hay DL, Barwell J, Reeves PJ, Upton GJG, Reynolds CA (**2013**). Similarity between class A and class B G-protein-coupled receptors exemplified through calcitonin gene-related peptide receptor modeling and mutagenesis studies. *J. R. Soc. Interface.* (10):20120846.

Wacker D, Wang C, Katrich V, Hon GW, Huang X-P, Vardy E, McCorvy JD, Jiang Y, Chu M, Siu FY, Liu W, Xu HE, Cherezov V, Roth BL, Stevens RC (**2013**). Structural features for functional selectivity at serotonin receptors. *Science* (340):615-619.

Walker CS, Conner AC, Poyner DR, Hay DL (**2010**). Regulation of signal transduction by calcitonin gene-related peptide receptors. *Trends. Pharmacol. Sci.* (31):476-483.

Walker CS, Eftekhari S, Bower RL, Wilderman A, Insel PA, Edvinsson L, Waldvogel HJ, Jamaluddin MA, Risso AF, Hay DL (**2015**). A second trigeminal CGRP receptor: function and expression of the AMY_1 receptor. *Ann. Clin. Transl. Neurol.* (6):595-608.

Wang Z, Ma W, Chabot JG, Quirion R (**2009**). Cell-type specific activation of p38 and ERK mediates calcitonin gene-related peptide involvement in tolerance to morphine-induced analgesia. *FASEB. J*. (23):2576–2586.

Watkins HA, Walker CS, Ly KN, Bailey RJ, Barwell J, Poyner DR, Hay DL (**2014**). Receptor activity-modifying protein-dependent effects of mutations in the calcitonin receptor-like receptor: implications for adrenomedullin and calcitonin gene-related peptide pharmacology. *Br. J. Pharmacol.* (177):772-788.

Wei Q, Costanzi S, Balasubramnian R, Gao ZG, Jacobson KA (**2013**). A2B adenosine receptor blockade inhibits growth of prostate cancer cells. *Purinergic. Signal.* (9):271-280.

Weiss JM, Morgan PH, Lutz MW, Kenakin TP (**1996**). The cubic ternary complex receptor-occupancy model I. model description. *J. Theor. Biol.* (178):151-167.

Weiss SM, Benwell K, Cliffe IA, Gillespie RJ, Knight AR, Lerpiniere J, Misra A, Pratt RM, Revell D, Upton R, Dourish CT (**2003**). Discovery of nonxanthine adenosine A2A receptor antagonists for the treatment of Parkinson's disease. *Neurology*. (61):S101-106.

Wess J (**1997**). G-protein-coupled receptors: molecular mechanisms involved in receptor activation and selectivity of G-protein recognition. *FASEB. J.* (11):346–354.

Wess J (**1998**). Molecular basis of receptor/G-protein-coupling selectivity. *Pharmacol. Ther.* (80):231-264.

Wess J, Han SJ, Kim SK, Jacobson KA, Li JH (**2008**). Conformational changes involved in G-protein-coupled-receptor activation. *Trends. Pharmacol. Sci.* (29):616-625.

West GM, Chien YET, Katritch V, Gatchalian J, Chalmers MJ, Stevens RC, Griffin PR (**2011**). Ligand-dependent perturbation of the conformational ensemble for the GPCR beta2 adrenergic receptor revealed by HDX. *Structure.* (19):1424-1432.

West RE, Moss J, Vaughan N, Liu T, Liu TY (**1985**). Pertussis toxin catalyzed ADP-ribosylation of transducin. Cysteine 347 is the ADP-ribose acceptor site. *J. Biol. Chem.* (260):14428-14430.

Weston C, Poyner D, Patel V, Dowell S, Ladds G (**2014**). Investigating G protein signalling bias at the glucagon-like peptide-1 receptor in yeast. *Br. J. Pharmacol.* (171):3651-3665.

Weston C, Lu J, Li N, Barkan K, Richards GO, Roberts DJ, Skerry TM, Poyner D, Pardamwar M, Reynolds CA, Dowell SJ, Willars GB, Ladds G (**2015**). Modulation of glucagon receptor pharmacology by RAMP2. *J. Biol. Chem.* (290):23009-23022.

Weston C, Winfield I, Harris M, Hodgson R, Shah A, Dowell SJ, Mobarec JC, Woodcock DA, Reynolds CA, Poyner DR, Watkins HA, Ladds G (**2016**). Receptor activity-modifying protein-directed G protein signaling specificity for the calcitonin gene-related peptide family of receptors. *J. Biol. Chem.* (42):21925-21944.

Wettschureck N, Offermanns S (**2005**). Mammalian G proteins and their cell type specific functions. *Physiol. Rev.* (85):1159-1204.

Wiley JW, Gross RA, MacDonald RL (**1992**). The peptide CGRP increases a high-threshold Ca^{2+} current in rat nodose neurons via a pertussis toxin-sensitive pathway. *J. Physiol*. (455):367-381.

Williams M, Francis J, Ghai G, Braunwalder A, Psychoyos S, Stone GA, Cash WD (**1987**). Biochemical characterization of the triazoloquinazolines, CGS15943, a novel, non-xanthine adenosine antagonist. *J. Pharmacol. Exp. Ther.* (241):415-420.

Woolley MJ, Conner AC (**2013**). Comparing the molecular pharmacology of CGRP and adrenomedullin. *Curr. Protein. Pept. Sci.* (14):358-374.

Wootten D, Lindmark H, Kadmiel M, Willcockson H, Caron KM, Barwell J, Drmota T, Poyner DR (**2013**). Receptor activity modifying proteins (RAMPs) interact with the VPAC2 receptor and CRF1 receptors and modulate their function. *Br. J. Pharmacol.* (168):822-834.

Wootten D, Reynolds CA, Koole C, Smith KJ, Mobarec JC, Simms J, Quon T, Coudrat T, Furness SG, Miller LJ, Christopoulos A, Sexton PM (**2016**). A hydrogen-bonded polar network in the core of the glucagon-like peptide-1 receptor is a fulcrum for biased agonism: lessons from class b crystal structure. *Mol. Pharmacol.* (89):335-347.

Wu V, Yang M, McRoberts JA, Ren J, Seensalu R, Zeng N, Dagrag M, Birnbaumer M, Walsh JH (**1997**). First intracellular loop of the human cholecystokinin-A receptor is essential for cyclic AMP signaling in transfected HEK-293 cells. *J. Biol. Chem.* (272):9037-9042.

Wunder F, Rebmann A, Geerts A, Kalthof B (**2008**). Pharmacological and kinetic characterization of adrenomedullin 1 and calcitonin gene-related peptide 1 receptor reporter cell lines. *Mol. Pharmacol.* (73):1235–1243.

Xu F, Wu H, Katritch V, Han GW, Jacobson KA, Gao ZG, Cherezov V, Stevens RC (**2011**). Structure of an agonist-bound human A2A adenosine receptor. *Science*. (332):322-327.

Xu Y, Xie X (**2009**). Glucagon receptor mediates calcium signaling by coupling to G alpha q/11 and G alpha i/o in HEK293 cells. *J. Recept. Signal. Transduct. Res.* (6):318-325.

Yabe D, Seino Y (**2011**). Two incretin hormones glp-1 and gip: comparison of their actions in insulin secretion and cell preservation. *Prog. Biophys. Mol. Biol.* (107):248-256.

Yang Y, Shi Y, Guo S, Zhang S, Cui N, Shi W, Zhu D, Jiang C (**2008**). PKA-dependent activation of the vascular smooth muscle isoform of K_{ATP} channels by vasoactive intestinal polypeptide and its effect on relaxation of the mesenteric resistance artery. *Biochim. Biophys. Acta.* (1778):88-96.

Yatani A, Tamja Y, Green SA (**1999**). Coupling of beta-adrenergic receptors to cardiac L-type Ca^{2+} channels: preferential coupling of the beta1 versus beta2 receptor subtype and evidence for PKA-independent activation of the channel. *Cell. Signal.* (5):337-342.

Yu J, Polgar P, Lubinsky D, Gupta M, Wang L, Mierke D, Taylor L (**2005**). Coulombic and hydrophobic interactions in the first intracellular loop are vital for Bradykinin B2 receptor ligand binding and consequent signal transduction. *Biochemistry.* (44):5295-5306.

Yu XJ, Li CY, Xu YH, Chen LM, Zhou CL (**2009**). Calcitonin gene-related peptide increases proliferation of human HaCaT keratinocytes by activation of MAP kinases. *Cell Biol. Int*. (33):1144–1148.

Zaccolo M, Pozzan T (**2002**). Discrete microdomains with high concentrations of cAMP in stimulated rat neonatal cardiac myocytes. *Science.* (295):1711-1715.

Zezula J, Freissmuth M (**2008**). The A(2A)-adenosine receptor: a GPCR with unique features? *Br. J. Pharmacol.* (153):S184-190.

Zhang H, Qiao A, Yang D, Yang L, Dai A, de Graaf C, Reedtz-Runge S, Dharmarajan V, Zhang H, Han GW, Grant TD, Sierra RG, Weierstall U, Nelson G, Liu W, Wu Y, Ma L, Cai X, Lin G, Wu X, Geng Z, Dong Y, Song G, Griffin PR, Lau J, Cherezov V, Yang H, Hanson MA, Stevens RC, Zhao Q, Jiang H, Wang MW, Wu B (**2017**). Structure of the full-length glucagon class B G-protein-coupled receptor. *Nature.* (546):259-264.

Zhang M, Hu H, Zhang X, Lu W, Lim J, Eysteinsson T, Jacobson KA, Laties AM, Mitchell CH (**2010**). The A_3 adenosine receptor attenuates the calcium rise triggered by NMDA receptors in retinal ganglion cells. *Neurochem. Int.* (56):35-41.

Zhang Y, Sun B, Feng D, Hu H, Chu M, Qu Q, Tarrasch JT, Li S, Kobilka TS, Kobilka BK, Skiniotis (**2017**). Cryo-EM structure of the activated GLP-1 receptor in complex with a G protein. *Nature.* (546):248-253.

Zhao ZQ, Nakanishi K, McGee DS, Tan P, Vinten-Johansen J (**1994**). A_1 receptor mediated myocardial infarct size reduction by endogenous adenosine is exerted primarily during ischemia. *Cardiovasc. Res.* (28):270-279.